

Chiral Iron-N₄-Complexes for Asymmetric C-H Aminations

A DISSERTATION

In

Chemistry

Presented to the Faculties of Philipps-Universität Marburg in Partial Fulfillment
of the Requirements for the Degree of Doctor of Science

(Dr. rer. nat.)

Xiang Shen

Hubei, P. R. China

Marburg/Lahn 2022

Die vorliegende Dissertation entstand in der Zeit von September 2018 bis März 2022 am Fachbereich Chemie der Philipps-Universität Marburg unter der Betreuung von Herrn Prof. Dr. Eric Meggers.

Vom Fachbereich Chemie der Philipps-Universität Marburg (Hochschulkennziffer: 1180) als Dissertation am _____ angenommen.

Erstgutachter:	Prof. Dr. Eric Meggers
Zweitgutachter:	Prof. Dr. Armin Geyer
weitere Mitglieder Prüfungskommission:	Prof. Dr. Jörg Sundermeyer Prof. Dr. Bernhard Roling

Tag der mündlichen Prüfung: _____

Acknowledgements

It's really a wonderful life experience to study and get my Ph.D degree in the Meggers group at Philipps-Universität Marburg. I would like to thank everybody who helped and supported me over the past few years.

I would like to firstly thank my supervisor Prof. Dr. Meggers, for his kind help, teachment, and supervision over Ph.D. studies. It's not only the scientific attitude from him deeply impressed me but also his patience, warm heart and wisdom. During the past few years, he taught me a lot of the scientific skills and supervised me for solving a lot of problems occurred during my research progress. Next, I am grateful to my master supervisor, Prof. Lei Gong, for introducing me to the academic research and for his constant support and encouragement.

Besides, I also own my appreciation to Prof. Geyer, Prof. Sundermeyer and Prof. Roling for referring my thesis and being the defense committee.

I would like to thank all of my collogues in the Meggers group as well as the collaborators from the department and other institutes. Thanks a lot to Dr. Lili Zhang, Ina Pinnschmidt, Marcel Hemming for their kind help. Thanks a lot to Weici Xu, Xiaoqiang Huang, Jie Qing, Qiao Ma, Guanghui Wang, Long Li, Yuqi Tan, Zijun, Zhou, Peng Xiong, Chenhao Zhang, Yubiao Hong, Tianjiao Cui, Erik Winterling, Yvonne Grell, Philipp Steinlandt, Xin Nie, Lifang Zhao, Nemrud Demirel, Bing Zhou, Dominik Baran, Tim Ohlenburger for their helpful suggestions and cooperation for my research progress. I want to thank my dear mates Zijun Zhou and Chenhao Zhang independently for their endless support and encouragement for me when I felt very sad, without you guys I would be lost. Thanks a lot to my friend Marcel Hemming, you are the source of everyday's happiness, I like you so much! Thanks a lot to Dr. Klaus Harms, Radostan Riedel and Sergei Ivlev for the measurement and analysis of all single crystals. Thanks a lot to Dr. Xiulan Xie for the professional analysis of NMR spectra. Thanks a lot to Philipp Steinlandt for translating the abstract into german version and his humor everyday! Many thanks to Yvonne Grell for defense advice! Thanks a lot for Erik's help with lab instruments. Thanks a lot to all of the former group members.

At last, I would like to appreciate my beloved families for their constant support and endless encouragement! Best wishes for all of my beloved families, friends and my future career!

Publications and Poster Presentations

Publications:

1. Xiang Shen, Marcel Hemming, Zijun Zhou, Sergei Ivlev, Eric Meggers, Chiral α,α -Disubstituted α -Amino Acids by Enantioconvergent Iron-Catalyzed 1,3-Migratory Nitrene Insertion. *To be submitted*.
2. Chengxi Ye*, Xiang Shen*, Shuming Chen, Eric Meggers, Stereocontrolled 1,3-Nitrogen Migration to Access Chiral α -Amino Acids. *Nat. Chem.* **2022**, accepted for publication.
(*Equal contribution)
3. Zijun Zhou, Yuqi Tan, Xiang Shen, Sergei Ivlev, Eric Meggers, Catalytic Enantioselective Synthesis of β -Amino Alcohols via Nitrene Insertion. *Sci. China Chem.* **2020**, *64*, 452.
4. Guanghui Wang, Zijun Zhou, Xiang Shen, Sergei Ivlev, Eric Meggers, Asymmetric Catalysis with a Chiral-at-Osmium Complex. *Chem. Commun.* **2020**, *56*, 7714.

Abstract

Due to iron's low toxicity and abundance on Earth, chiral inexpensive metallic iron catalysts have gained great attention. There are still no examples of the direct use of simple and readily available chiral iron catalysts to catalyze the activation of C-H bonds to enantioselectively form C-N bonds. This thesis is based on the enantioselective catalytic amination of challenging secondary and tertiary C-H bonds via chiral N₄ iron catalysts. At the same time, the enantioselective amination produces a series of unnatural α -amino acids. A novel approach for synthesizing α -amino acids is disclosed.

In the first two sections, a series of chiral N₄ iron catalysts were synthesized and successfully applied to asymmetric secondary C-H bonds amination reactions. Our method employs abundant and easily accessible carboxylic acids as starting materials, which are connected to a nitrogenation reagent, followed by a highly regio- and enantioselective iron-catalyzed C(sp³)-H amination. This straightforward method displays a broad scope, providing rapid access to optically active α -amino acids with aryl, allyl, and alkyl side chains, and also permits stereocontrolled late-stage amination of carboxylic acid-containing drugs and natural products.

In the third section, A straightforward two-step synthesis of non-racemic α,α -disubstituted α -amino acids by an enantioconvergent 1,3-migratory nitrene C(sp³)-H insertion is reported. Readily available racemic α -branched carboxylic acids are DCC/EDCI-coupled to provide racemic azanyl esters which undergo a rearrangement into non-racemic *N*-Troc-protected α,α -disubstituted α -amino acids catalyzed by an easy to store and robust chiral iron catalyst. α,α -Disubstituted α -amino acids with one aryl group in α -position are provided in yields of up to 99% and with up to 88% ee. Selected examples demonstrate that recrystallization can improve the enantiomeric excess to 99% ee.

Zusammenfassung

Aufgrund der geringen Toxizität und des hohen Vorkommens von Eisen auf der Erde haben günstige und chirale Eisen-basierte Katalysatoren viel Aufmerksamkeit auf sich gezogen. Jedoch gibt es noch keine Beispiele für die direkte Verwendung einfacher und leicht erhältlicher chiraler Eisenkatalysatoren für die Aktivierung von C-H-Bindungen, um enantioselektiv C-N-Bindungen zu bilden. Diese Arbeit thematisiert die enantioselektive, katalytische Aminierung von anspruchsvollen sekundären und tertiären C-H-Bindungen mittels chiraler N₄-Eisenkatalysatoren, wobei diese Reaktion den Zugang zu einer Reihe unnatürlicher α -Aminosäuren ermöglicht. Dies stellt einen neuen Ansatz zur Darstellung solcher α -Aminosäuren dar.

In den ersten Abschnitt wurde eine Reihe von chiralen, N₄-Eisenkatalysatoren synthetisiert und erfolgreich auf die asymmetrische Aminierungsreaktion sekundärer C-H-Bindungen angewandt. Unsere Methode verwendet einfach zugängliche Carbonsäuren als Substrate, die zunächst mit einem Nitrogenierungs-Reagenz umgesetzt und anschließend in einer hoch regio- und enantioselektiven, Eisen-katalysierten C(sp³)-H-Aminierung eingesetzt wurden. Diese unkomplizierte Methode zeigt einen sehr breiten Anwendungsbereich, einen schnellen Zugang zu optisch aktiven α -Aminosäuren mit Aryl, Allyl- und Alkylseitenketten und ermöglicht ebenfalls die stereoselektive *late-stage* Aminierung von Carbonsäure-haltigen Arzneimitteln und Naturstoffen.

Im dritten Abschnitt wird über eine unkomplizierte zweistufige Synthese von nicht-racemischen α,α -disubstituierten α -Aminosäuren durch eine enantiokonvergente, 1,3-migratorische Nitren-C(sp³)-H-Insertion berichtet. Leicht verfügbare, racemische, α -verzweigte Carbonsäuren werden DCC/EDCI-gekuppelt, um racemische Azanylester bereitzustellen, die eine Umlagerung in nicht-racemische, *N*-Troc-geschützte α,α -disubstituierte Aminosäuren eingehen, katalysiert durch einen einfach zu lagernden und robusten chiralen Eisenkatalysator. α,α -Disubstituierte Aminosäuren mit einer Arylgruppe in α -Position können in Ausbeuten von bis zu 99% und mit bis zu 88% *ee* dargestellt werden. Ausgewählte Beispiele zeigen, dass durch Umkristallisation der Enantiomerenüberschuß auf 99% *ee* verbessert werden kann.

Table of Contents

Acknowledgements.....	V
Publications and Poster Presentations.....	VII
Abstract.....	IX
Zusammenfassung.....	XI
Table of Contents.....	XIII
Chapter 1: Theoretical Part.....	1
1.1 Introduction.....	1
1.2 Background of N4 Iron Complexes	2
1.2.1 Heme Enzyme	2
1.2.2 Iron Porphyrin	3
1.2.3 N4 Iron Complexes	4
1.3 Enantioselective C-N Bond Formation Catalyzed by Chiral Iron Catalyst	15
1.3.1 Iron-Catalyzed Asymmetric Azidation of β -Keto Esters and Oxindoles.....	16
1.3.2 Iron-Catalyzed Asymmetric Carboazidation of Styrenes	17
1.3.3 Iron-Catalyzed Asymmetric Intramolecular Aminohydroxylation of Indoles.....	20
1.3.4 Iron-Catalyzed Asymmetric Aminohydroxylation and Aminofluorination of Olefins	21
1.3.5 Iron-Heme Enzyme-Catalyzed Asymmetric Aziridination.....	22
1.3.6 Iron-Heme Enzyme-Catalyzed Asymmetric Aminohydroxylation.....	22
1.3.7 Iron-Heme Enzyme-Catalyzed Asymmetric Intermolecular Benzylic C-H Amination	23
1.3.8 Iron-Heme Enzyme-Catalyzed Asymmetric Amination of Primary, Secondary and Tertiary C(sp ³)-H Bonds	24
1.3.9 Iron-Heme Enzyme-Catalyzed Benzylic and Allylic C(sp ³)-H Bonds.....	25
1.3.10 Iron-Heme Enzyme-Catalyzed Benzylic C(sp ³)-H Bonds	26
1.4 Aim of Thesis	26
1.4.1 Synthesis of New N4 Chiral Iron Complexes	27
1.4.2 Apply N4 Iron Complexes in Asymmetric Intramolecular C-H Aminations.....	28
Chapter 2: Results and Discussion.....	32
2.1 Synthesis of Chiral N4 Iron Catalysts.....	32
2.1.1 Synthesis of Modified Chiral N4 Iron Catalysts	32
2.1.2 Gram-Scale Synthesis of (<i>R,R</i>)-FeBIP.....	34
2.1.3 Crystal Structure of (<i>R,R</i>)-FeBIP.....	35
2.1.4 Conclusions	35
2.2 Asymmetric Amination of Secondary C-H Bonds Catalyzed by Chiral N4 Iron Catalysts	37
2.1.1 Research Background and Reaction Design.....	37
2.1.2 Initial Experiments and Reaction Development.....	38

2.1.3 Substrate Scope	41
2.1.4 Mechanism Proposal	42
2.1.5 Conclusions	43
2.3 Enantioconvergent Tertiary C-H Bonds Amination Catalyzed by Chiral N4 Iron Catalysts	45
2.3.1 Research Background and Reaction Design.....	45
2.3.2 Initial Experiments and Reaction Development.....	47
2.3.3 Substrate Scope	50
2.3.4 Additional Experiments.....	52
2.3.5 Mechanism Proposal	54
2.2.6 Conclusions	54
Chapter 3: Summary and Outlook	57
3.1 Summary	57
3.2 Outlook	59
Chapter 4: Experimental Part.....	61
4.1 Materials and Methods.....	61
4.2 Synthesis of Chiral N4 Iron Catalysts.....	63
4.2.1 Synthesis of Ligands	63
4.2.2 Synthesis of Catalysts.....	70
4.2.3 Single Crystal X-Ray Diffraction	76
4.3 Asymmetric Amination of Secondary C-H Bonds Catalyzed by Chiral N4 Iron Catalysts	80
4.3.1 Synthesis of Substrates.....	80
4.3.2 Asymmetric Amination of Secondary CH Bonds Catalyzed by Chiral N4 Iron Catalysts...	87
4.3.3 Experimental and Characterization Data of New Products	88
4.3.4 Determining the Absolute Configuration of the α -Amino Acids.....	96
4.4 Enantioconvergent Tertiary C-H Bonds Amination Catalyzed by Chiral N4 Iron Catalysts	99
4.4.1 Synthesis of Carboxylic Acids.....	99
4.4.2 Synthesis of Substrates.....	104
4.4.3 Catalytic Enantioconvergent C(sp ³)-H Aminations	119
4.3.4 Experimental and Characterization Data of the Products.....	121
4.4.5 Large-Scale Reactions and Mechanistic Study.....	138
4.4.6 Single Crystal X-Ray Analysis of Compound (<i>S</i>)- 5q	148
Chapter 5: Appendices	151
5.1 List of Abbreviations	151
5.2 List of Figures.....	154
5.3 List of Tables	156

5.4 List of New N4 Iron Complexes.....	158
5.5 List of New Organic Compounds	159
5.6 Enantiomeric Excess for Catalytic Reactions.....	163
5.7 List of NMR Spectra of New Compounds	211
Statement.....	330
Curriculum Vitae.....	331

Chapter 1: Theoretical Part

1.1 Introduction

There is high current interest in developing homogeneous catalysts from earth abundant metals rather than previously dominant noble metals because earth rich metals are much cheaper, usually have less impact on health and the environment, and are expected to achieve a reaction mechanism different from noble metal catalysis.¹ Among the abundant metals on earth, iron is a particularly non-toxic metal. It has a very high content in the earth's crust and its chemical properties are very attractive, such as a variety of accessible oxidation states and rich coordination chemistry. Therefore, it is not surprising that iron is widely used in nature, such as part of proteins and enzymes. Chemists have adopted this strategy, and iron-catalyzed reactions in organic synthesis have gained great relevance in the past two decades. Concerning asymmetric iron catalysis, a large number of chiral iron complexes have been reported to catalyze asymmetric conversion, including asymmetric hydrogenation, asymmetric oxidation and asymmetric carbene or nitrene transfer reactions, but there are still challenges in catalytic performance and new catalytic mechanisms.²

Enantioselective C-N bond formation is of utmost importance due to its presence in natural products and bioactive molecules that have numerous applications in the pharmaceutical, agrochemical and fine chemical industries.³ Over the decades, enormous success has been achieved in the transition metal-catalyzed C-N bond-forming reactions, which played a vital role in the syntheses of nitrogen-containing natural and unnatural compounds.⁴ Most prominent enantioselective C-N bond formation reactions include: Azidation of C-H and C=C bonds and Amination of C-H and C=C bonds (**Figure 1**).⁵ All the above enantioselective C-N bond-forming reactions have been studied in great detail. However, the drawbacks of most of these catalysts are either very expensive or toxic. Therefore, the scientists shifted their attention to a cheaper and greener option and considered iron as one of the alternatives.

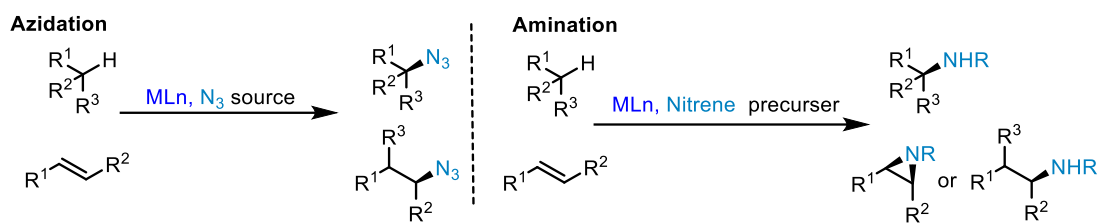


Figure 1. Construction of C-N bonds by enantioselective azidation and amination.

1.2 Background of N4 Iron Complexes

N4 ligands refer to ligands containing four nitrogen atoms and participate in coordination. The earliest related research is about P450.⁶ One of them is the structure of porphyrin chelated with ferric ions.⁷ Because of its excellent catalytic activity, it has attracted wide attention. Then some scientists began to study the catalytic activity of porphyrin metal catalysts and found that they were also useful in oxidation, carbene and nitrene insertion.⁸ Because the synthesis and modification of porphyrins are not very simple, new porphyrin ligands containing N4 have been designed and synthesized in the past two decades. There are also many catalytic applications of the catalysts synthesized from them. Especially the catalytic application of N4 iron catalyst (**Figure 2**).⁹

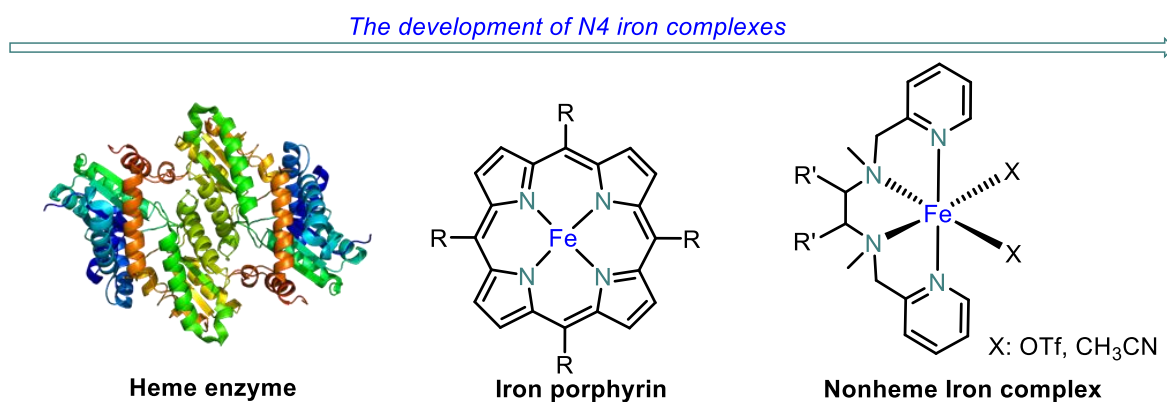


Figure 2. The development of N4 iron complexes.

1.2.1 Heme Enzyme

The cytochromes P450 constitute a large family of cysteine-heme enzymes, are present in all forms of life (plants, bacteria, and mammals), and play a key role in the oxidative transformation of endogenous and exogenous molecules. The total number of members of the cytochrome P450 family is increasing rapidly.¹⁰ In all these cysteine-heme enzymes, the prosthetic group is constituted of an iron (III) protoporphyrin covalently linked to the protein by the sulfur atom of a proximal cysteine ligand. These enzymes are potent oxidants that are able to catalyze the hydroxylation of

saturated C-H bonds, the epoxidation of double bonds, the oxidation of heteroatoms, dealkylation reactions, oxidations of aromatics, and so on. Two main mechanisms have been proposed and discussed depending on the nature of the substrate and on the enzyme itself: a cage-controlled radical mechanism (the “oxygen rebound” mechanism) or a concerted mechanism without formation of a radical intermediate based on the use of ultrafast “radical clocks” (**Figure 3**).¹¹

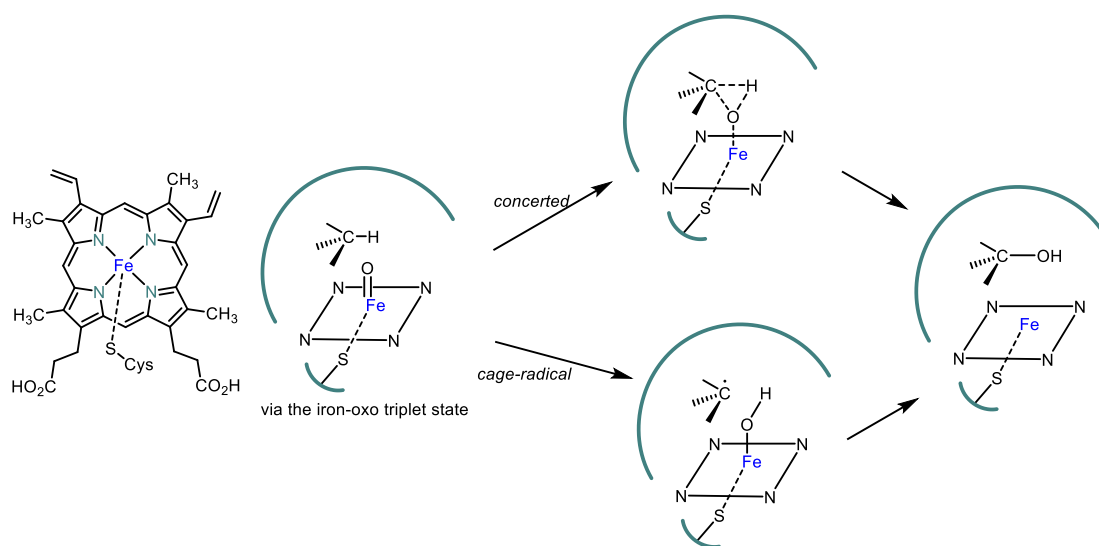


Figure 3. Prosthetic of cysteinato-heme enzymes and two possible reaction pathways in hydroxylation reactions catalyzed by P450 enzymes.

1.2.2 Iron Porphyrin

The selective, non-directed oxidations of unactivated hydrocarbons by cytochrome P-450 enzymes stimulated interest in developing chemical model systems. Well-defined iron catalysts with heme ligands that can be tuned were extensively explored as models for cytochrome P450 to catalyze aliphatic C-H hydroxylations (**Figure 4**). Based on this principle, the Groves group reported a series of iron-catalyzed hydrocarbon hydroxylation efforts from 1979 to the 1980s. Unfortunately, aliphatic C-H oxidation reactions with Iron (III) porphyrin catalyst is very low yielding, requiring solvent quantities of hydrocarbon substrate. Site-selectivities for hydroxylation were investigated with electronically biased substrates and shown to be minimal in the iron porphyrin systems, strong evidence exists that free radical processes operate contemporaneously with more selective metal(oxo) chemistry. Aliphatic C-H hydroxylations and epoxidations are not stereoretentive, leading to long-lived carbon-centred radicals that can open cyclopropane rings (**Figure 4B**).¹²

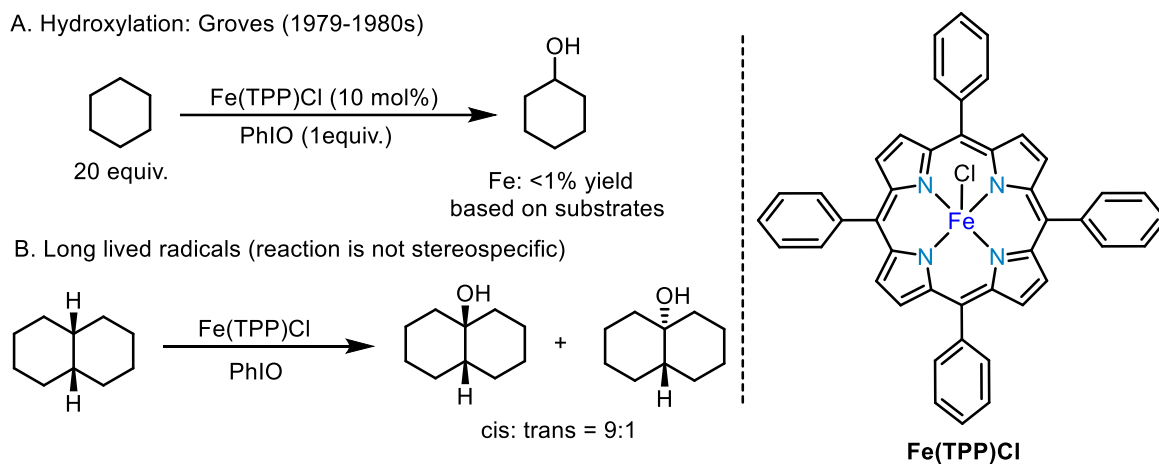


Figure 4. Aliphatic hydroxylation catalyzed by Iron (III) porphyrin.

1.2.3 N4 Iron Complexes

In the 1990s, well-defined pyridine/amine linked non-heme iron complexes began to appear in the form of small molecular functional mimics for non-heme iron oxidase. The polydentate amine ligands tris(2-pyridylmethyl)amine (TPA)¹³ and N,N'-dimethyl-N,N'-bis(2-pyridylmethyl)ethylene-1,2-diamine (MEP)¹⁴ and others¹⁵ were introduced and complexed with iron salts to furnish both monomeric and dimeric iron complexes that showed C-H hydroxylation activity with cyclohexane. Preparatively, these systems did not distinguish themselves from the previous state-of-the-art: reactions were run with large excesses of the substrate and afforded trace yields of oxidized products. However, mechanistically these systems appeared to be distinct. Most significantly, hydroxylations of cis-1,2 dimethyl cyclohexane were stereospecific, with no observed trans-alcohol. Labelling experiments with H₂O¹⁸ showed that the iron-bound oxidant generated from H₂O₂ was able to exchange with water, suggestive of an iron(oxo) intermediate (**Figure 5**).¹⁶

In the oxidation reaction, the Fe (MEP) complexes exhibited higher catalytic activity than those of Fe (TPA). Additionally, the MEP ligand has a strong σ -donating character via the bidentate tertiary amine ligation and a symmetrical, modular structure that allows electronic and steric structure-activity relationships to be evaluated in a synthetically straightforward way. In 2001, the Jacobson group discovered that [Fe(II)(MEP)(CH₃CN)₂](SbF₆)₂ is a preparatively useful catalyst with H₂O₂ for epoxidations of terminal olefins (**Figure 5**).¹⁷ Albeit a much lower energy process than aliphatic C-H oxidation, this discovery represented the first time a non-heme iron oxidation system had been rendered preparatively useful.

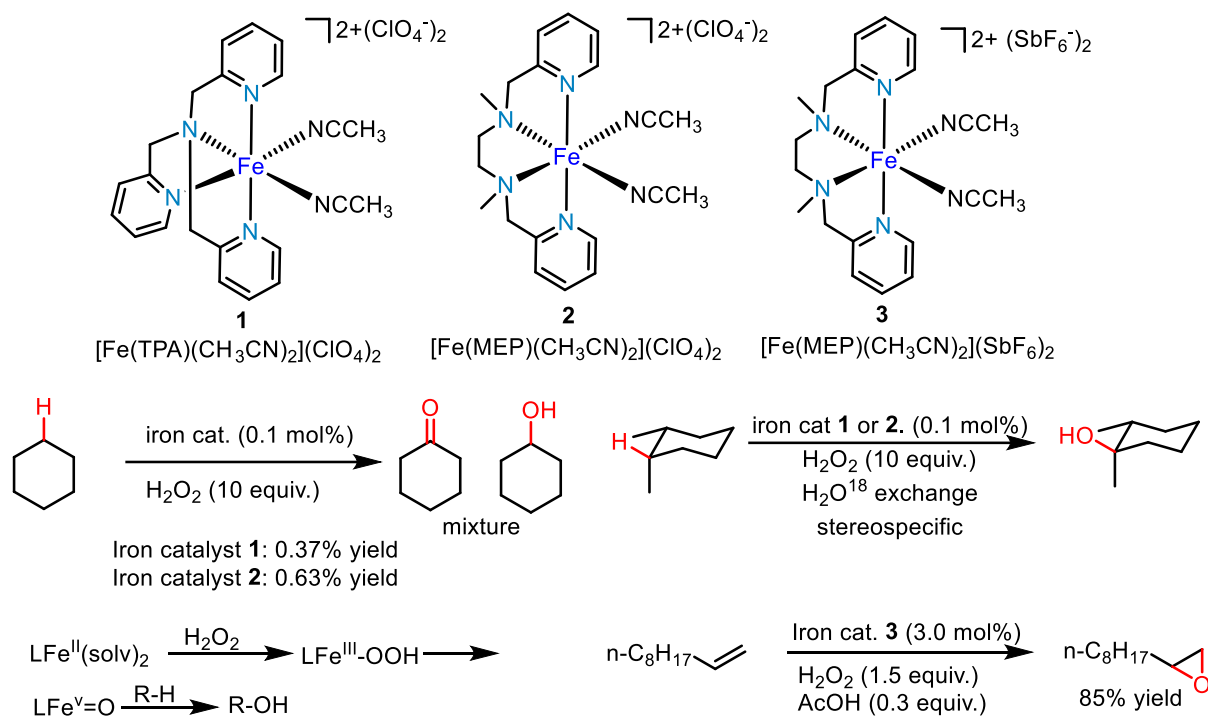


Figure 5. Aliphatic C–H hydroxylation and the epoxidation of terminal olefins catalyzed by N4 Fe complexes.

A breakthrough was made by the White group in 2007 when the MEP system was strategically altered to enable the first preparative, undirected C–H hydroxylation of aliphatic compounds. Increasing the σ -donation of the amine ligands and simultaneously rigidifying the ligand would result in improvements in selectivity. After significant experimentation, exchanging the ethylene diamine backbone with pyrrolidine rings ultimately furnished Fe (PDP) catalyst ($[Fe(II)(PDP)(CH_3CN)_2](SbF_6)_2$) **4** that afforded a significant improvement in selectivity for C–H hydroxylation (90%). This complex uses hydrogen peroxide (H_2O_2) to oxidize a variety of substrates. It realized the extraordinary potential of nonactivated sp^3 C–H bond oxidation in organic synthesis with both high activity and predictable selectivity. Predictable selectivity is entirely based on the electronic and spatial properties of C–H bonds, and directional groups are not required. It is worth mentioning that the hydroxylation of hydrocarbon bonds of complex natural products can also be realized in their catalytic system (**Figure 6A**).¹⁸ In 2013 the same group first demonstrated this with the discovery of catalyst $Fe(CF_3PDP)$ **5**. Site-selectivities could be predictably altered in aliphatic C–H oxidations with no changes made to the substrate or the reaction (**Figure 6B**).¹⁹

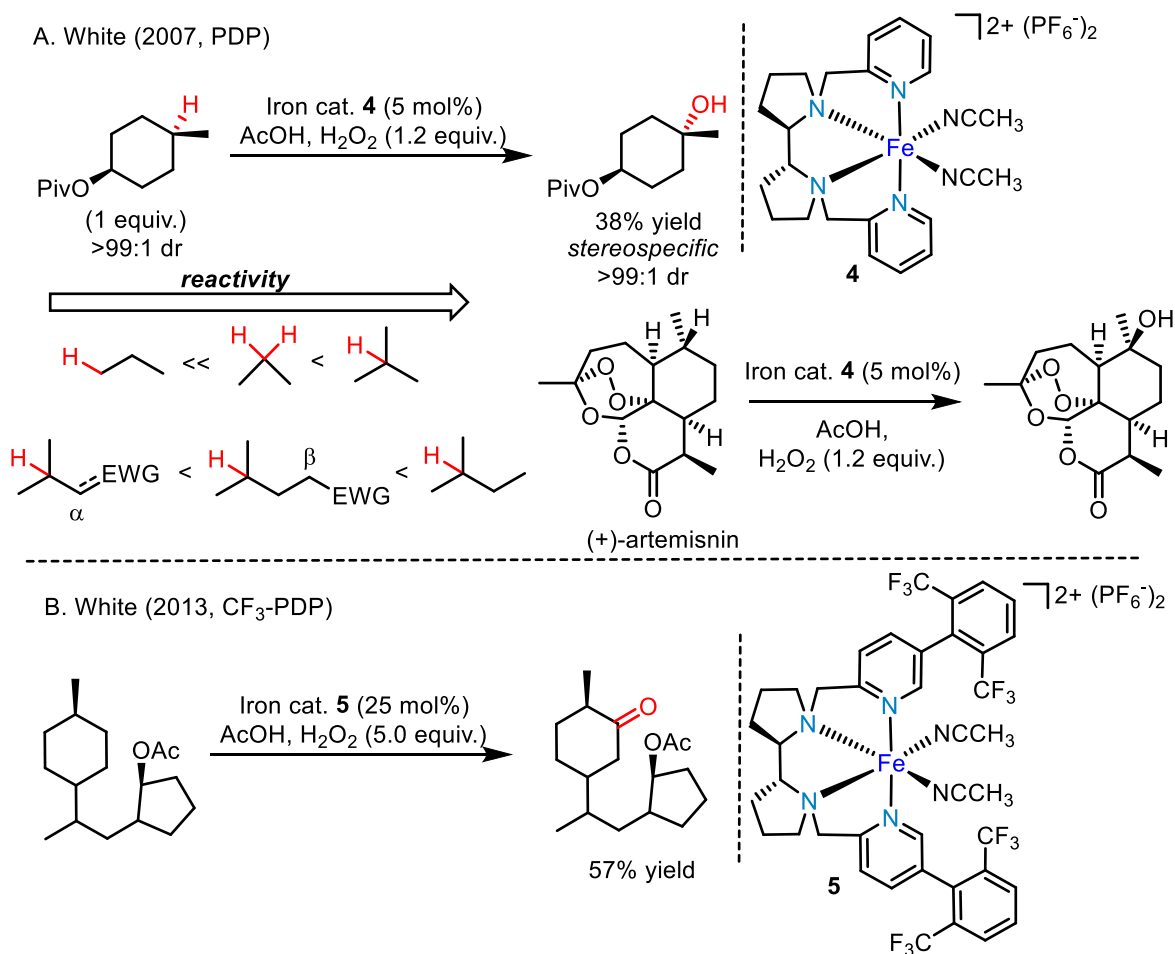


Figure 6. Useful aliphatic C–H oxidation reaction catalyzed by N4 Iron complex **4** and **5**.

In 2013, Costas with co-workers studied the asymmetric epoxidation of olefins with H₂O₂, catalyzed by aminopyridine iron complexes containing various substituents R¹, R² and R³ at the pyridine rings of the PDP ligand. The obtained catalytic epoxidation efficiency and enantioselectivity (up to 99%) were found to be strongly dependent on the electron-donating nature of the pyridine moieties. Complexes containing more electron-donating substituents at the pyridine rings exhibited higher enantioselectivities. Thus, **9** and **10** (**Figure 7A**) were identified as the best catalysts in the series. Complex **9**, which showed the highest olefin epoxidation enantioselectivity exhibited remarkable efficiency and enantioselectivity even at very low loading (3 mol%) of the carboxylic acid additive. For some substrates, (*S*)-Ibuprofen is the best additive that acts as an additive (**Figure 7B**). The authors assumed that electron-donating substituents in complexes **9** and **10** attenuated the electrophilicity of the corresponding oxoiron(V) intermediate, thus enhancing its enantioselectivity. And they proposed a possible mechanism.²⁰ The original mechanism proposed by Que and co-workers for the Fe-catalyzed AcOH-assisted epoxidation of olefins with H₂O₂ involves the intermediacy of

oxocarboxylate-iron(V) species Ib (**Figure 7C**) as the oxygen atom delivering agent. Species Ib is formed via acid-assisted heterolytic cleavage of the O–O bond in a Fe^{III}(OOH)-(HOAc) (Ia) precursor.²¹ Experimental spectroscopic evidence in favour of this mechanistic scenario has been also provided by Talsi, Bryliakov, and co-workers,²² and further computational support for the formation and oxidative competence of these species has been built by Rajaraman et al. in a study of the *ortho*-hydroxylation of aromatic compounds by non-heme Fe complexes.²³

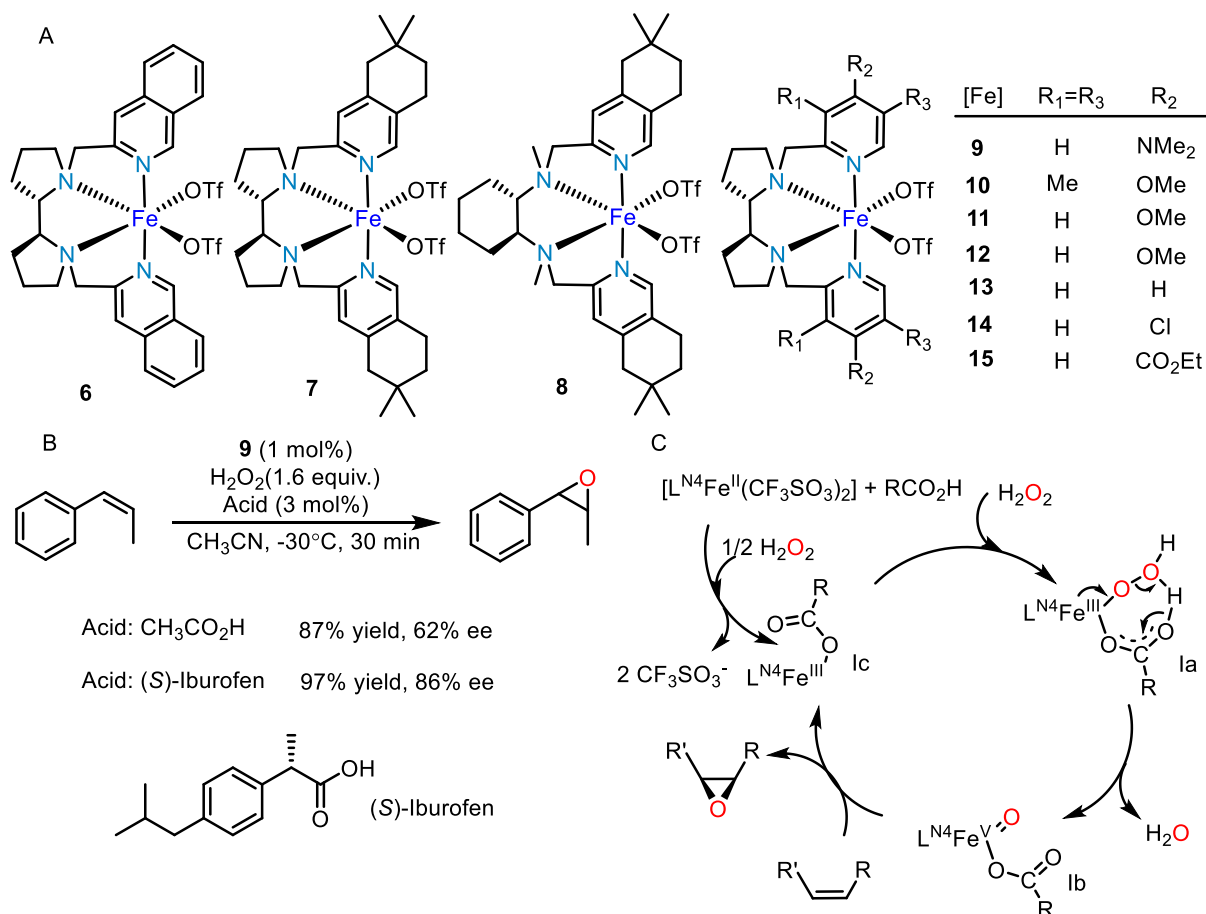


Figure 7. Asymmetric epoxidation with H₂O₂ by manipulating the electronic properties of non-heme Iron catalysts.

For the epoxidation of double bonds, some other N4 ligand catalysts have been reported. Back to 2011, the Yamamoto group reported the combination of Fe(OTf)₂ and novel phenanthroline ligands which enables the catalytic asymmetric epoxidation of acyclic β,β-disubstituted enones. The reaction provides highly enantioenriched α,β-epoxyketones (up to 92% ee) that can be further converted to functionalized β-ketoaldehydes with an all-carbon quaternary centre (**Figure 8A**).²⁴ The same year, the Sun group reported a new N4 iron complex **17** which can achieve the epoxidation of chalone and provide the product with up to 90% yield and 87% ee (**Figure 8B**).²⁵ And in 2012, the Sun group

reported another type N₄ iron complexes **19** and **20** which can catalyze the epoxidation of multisubstituted enones. The substrates scope is broad and ee value up to 98% (**Figure 8C**).²⁶ In 2015, the Gao group reported an in situ formed porphyrin-inspired iron complex **21-28** which can catalyze the asymmetric epoxidation of di- and trisubstituted enones. This reaction provides highly enantioenriched α,β -epoxyketones (up to 99% ee) (**Figure 8D**).²⁷ And all mechanisms for these reactions are similar to previously described.

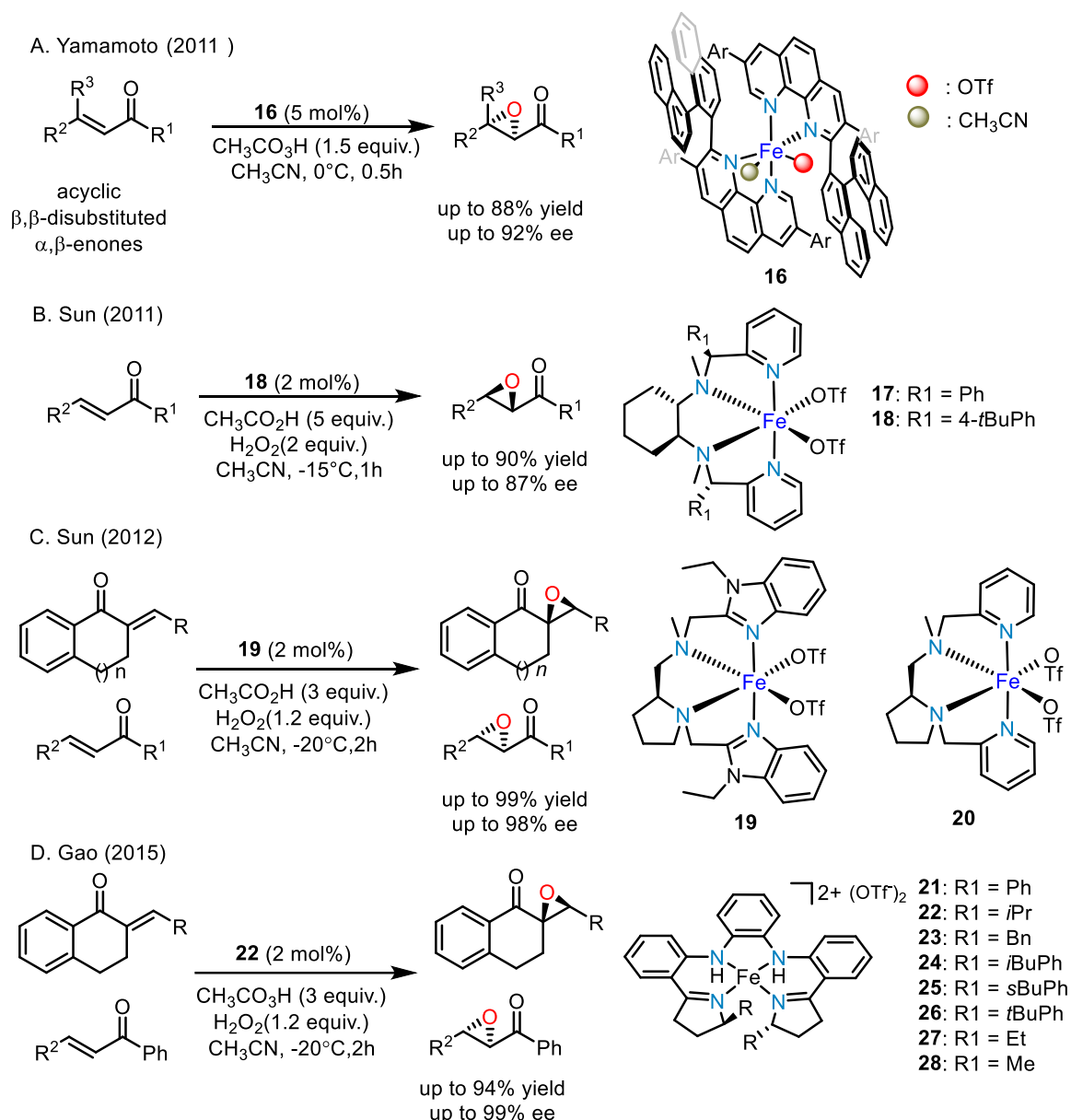


Figure 8. The epoxidation of double bonds catalyzed by N₄ iron catalysts.

In 2016, the Costas group reported that iron complexes with C₁-symmetric tetradentate N-based ligand catalyzed the asymmetric epoxidation of cyclic enones and cyclohexene ketones with aqueous hydrogen peroxide (**Figure 9B**). This catalytic system can provide the corresponding epoxides in good

to excellent yields and enantioselectivities (up to 99% yield, and 95% ee) under mild conditions and in short reaction time. Evidence is provided that reactions involve an electrophilic oxidant, and this element is employed in performing site-selective epoxidation of enones containing two alkene sites (**Figure 9C**). They think the design of C1 symmetric complexes where the electronic and steric properties of distinct heterocycles are combined constitutes a novel idea in the design of this class of catalysts. Screening different combinations of ligands, they found the best one **33**, a TIPS-substituted pyridine and a benzimidazole ring. (**Figure 9A**).²⁸

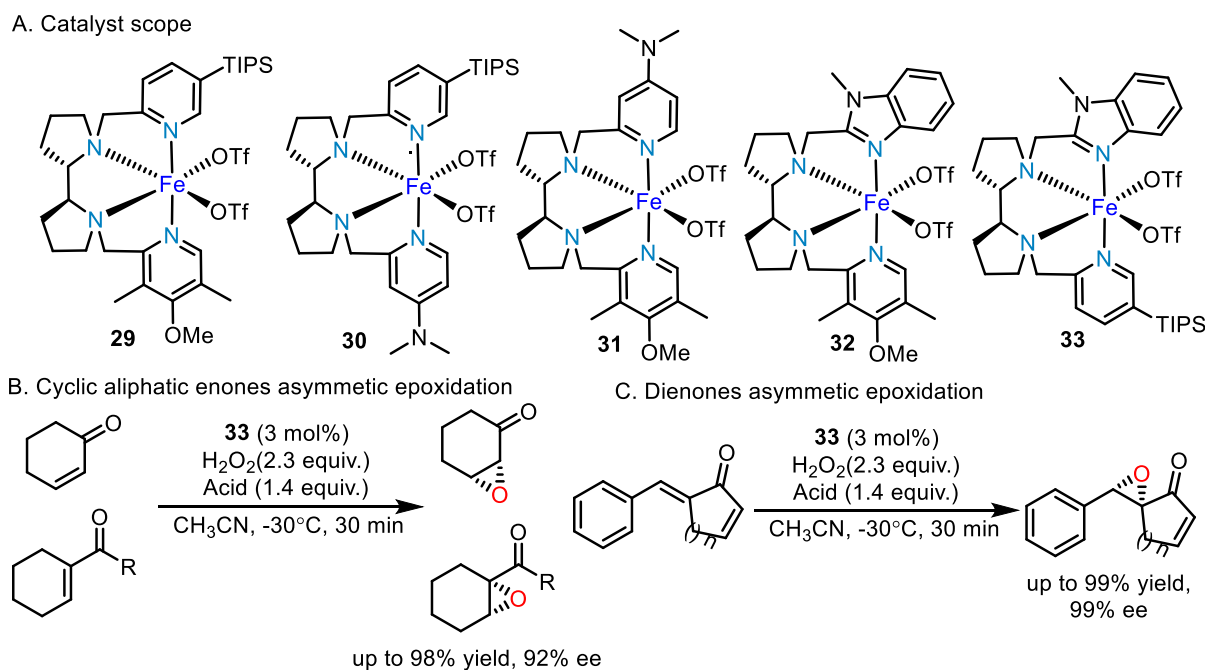


Figure 9. The asymmetric epoxidation of cyclic enones and cyclohexene ketones catalyzed by N4 iron catalysts.

Back to 2007, Collins and coworkers reported another new N4 iron complex **34** which have proven to be an efficient catalyst in the decomposition of numerous pollutants by hydrogen peroxide. This is the first synthesis of the oxoiron(V) complex. The reaction of **34** with *m*-CPBA in *n*-butyronitrile at -60°C yielded a deep green complex, identified as **35** by EPR, EXAFS and ESI-MS studies (**Figure 10A**).²⁹ In 2014, Gupta and coworkers reported another two similar complexes **36** and **37**. The latter one can catalyze the epoxidation of cyclohexane. However, its reaction condition is room temperature and the oxidants are sodium hypochlorite or *m*-CPBA. Their catalytic reaction can be carried out in a catalytic manner with modest yields and turnover numbers (**Figure 10B**).³⁰

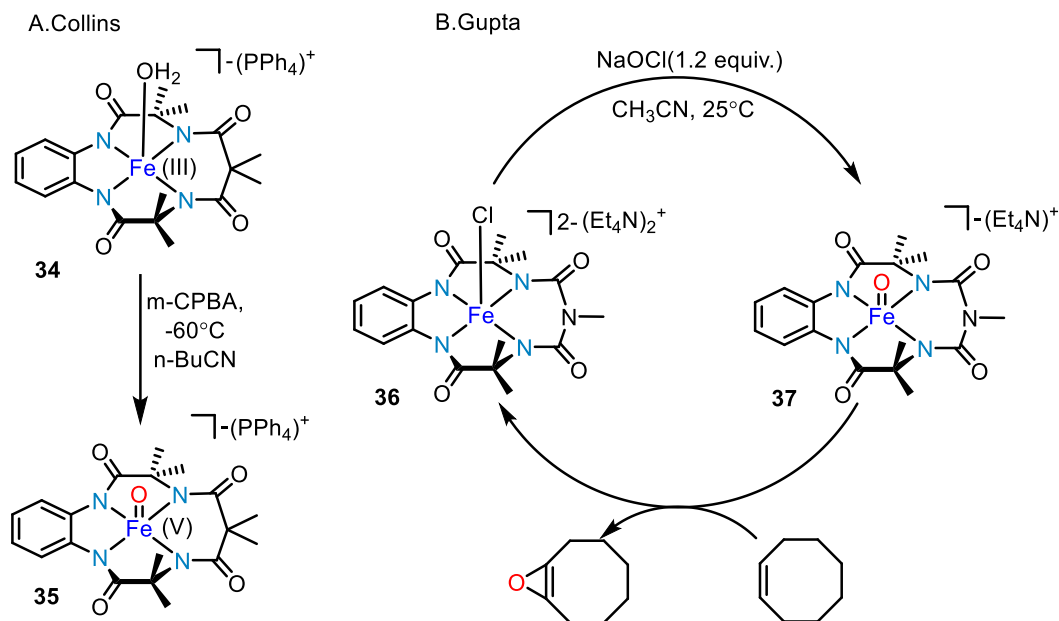


Figure 10. The synthesis of oxoiron(V) complexes.

In 2010, the Che group reported the **38**-catalyzed *cis*-dihydroxylation of a variety of alkenes, particularly electron-deficient ones, by oxone with high *cis*-diol selectivity (**Figure 11A**).³¹ In 2011, Costas and coworkers reported the **39**-catalyzed hydroxylation of alkanes and the *cis*-dihydroxylation of alkenes using H_2O_2 as oxidant. The hydroxylation of *cis*-1,2-dimethylcyclohexane is stereospecific and affords a racemic mixture of (1*R*,2*R*)-dimethylcyclohexanol and (1*S*,2*S*)-dimethylcyclohexanol. Similarly, oxidation of *cis*-2-heptene by **39** is *syn*-stereospecific and affords a 2:1 racemic mixture of 95% erythro-heptane-2,3-diol and 2-butyl-3-methyloxirane (97% *cis*). When the catalytic reactions were performed in the presence of H_2^{18}O , the oxidized products exhibited a correspondingly large content of ^{18}O . alcohols (1*R*,2*R*)-dimethylcyclohexanol and (1*S*,2*S*)-dimethylcyclohexanol were 76+3% ^{18}O -labelled, but erythro-diol was 84+3% $^{16}\text{O}^{18}\text{O}$ -labelled, which provided evidence that one of the two oxygen atoms in the major part of the diol derived from H_2O (**Figure 11B**).³² In 2015, Costas and coworkers reported another complex **40** which can react with peracetic acid at cryogenic temperatures and form the iron species **41**. This one also proves to be sensitive to the strength of the C-H bond, polar effects, and steric constraints, and therefore it bears the characteristics of a selective C-H hydroxylating agent (**Figure 11C**).³³ All three N4 iron catalysts are involved in subsequent reactions by forming iron (V) oxygen intermediates under the corresponding oxidation conditions.

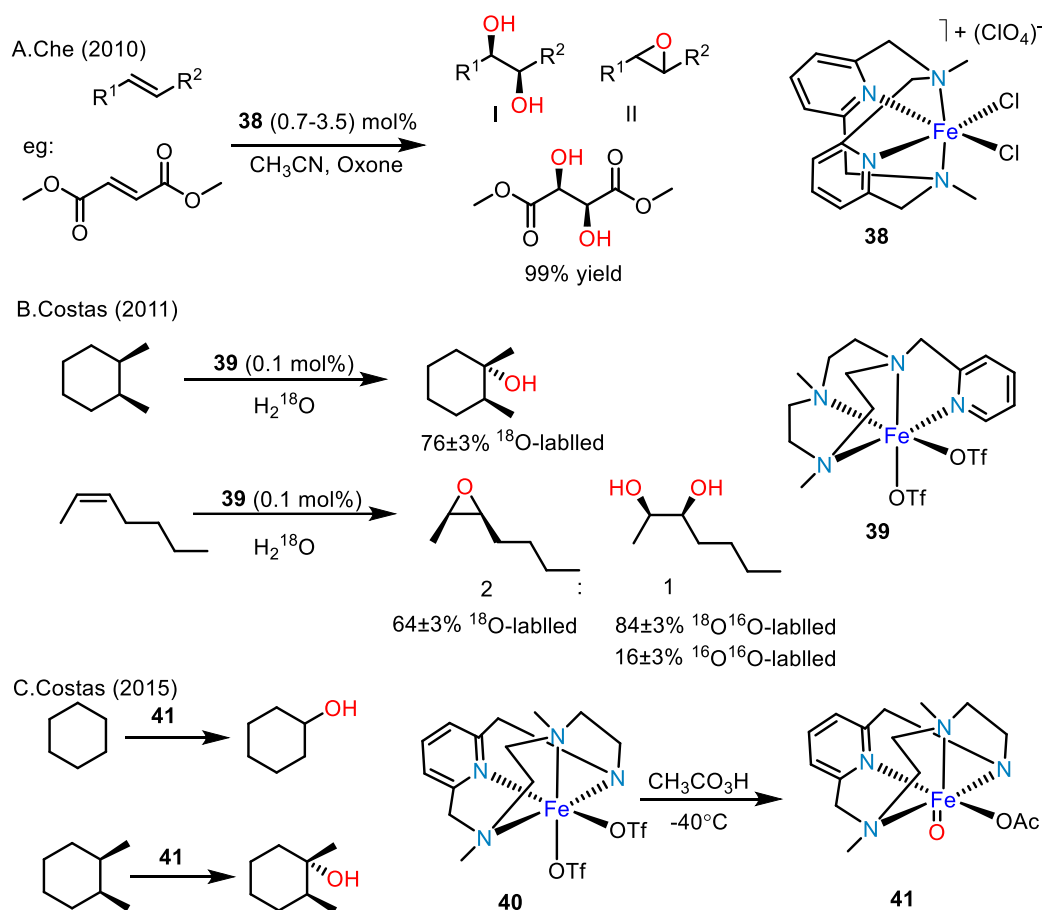
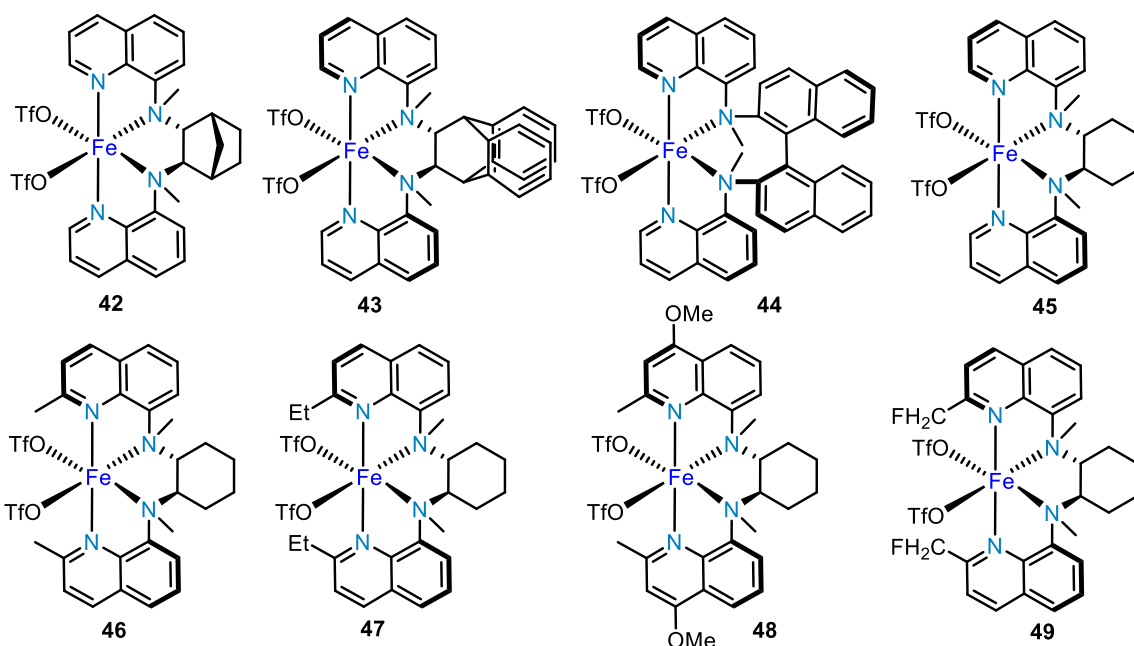


Figure 11. Different N4 iron complexes catalysis.

In 2016, the Che group reported the synthesis of new complexes able to catalyze the H_2O_2 -mediated *cis*-dihydroxylation of alkenes with excellent results in terms of stereoselectivity.³⁴ Among the different ligands tested, complex **46** (**Figure 12A**) was particularly selective towards the formation of *cis*-diols and brought to an ee higher than 90% in the oxidation of various (*E*)-alkenes, both electron-rich and electron-deficient, reaching 99.8% ee with methyl (*E*)-cinnamate. Lower enantioselectivities were obtained with (*Z*)-alkenes (**Figure 12B**).

A. Complexes scope



B.

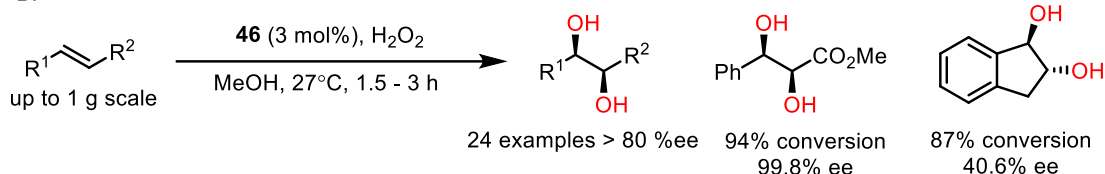


Figure 12. *cis*-dihydroxylation of olefins catalyzed by N4 iron complex **46**.

In 2019 complex **50** was also reported to work as a catalyst for the asymmetric epoxidation of a wide scope of alkenes with good enantioselectivity, but generally with slightly lower activity than other complexes already mentioned.³⁵ *cis*- β -Methyl styrene was also employed as a substrate and the conditions for catalysis were used as reported earlier, to enable direct comparison of **50** with related Fe (II) complexes (**Figure 13A**).³⁶ Under catalytic conditions, complex **50** oxidized *cis*- β -methyl styrenes to form the epoxide with 60% yield and an ee of 43% (**Figure 13B**). In organic synthesis, the trisubstituted cyclic α,β -epoxyketones are resourceful intermediates because of the presence of a chiral quaternary carbon centre.³⁷ The development of an iron catalyst for the enantioselective construction of such quaternary carbon centres coordinated to an oxygen atom is still highly attractive.³⁸ Using tetralone derivatives as substrates for this type of reaction, They obtained good yields of trisubstituted α,β -epoxyketones with quaternary carbon centres with excellent enantioselectivities (up to 97%, **Figure 13C**). Furthermore, the epoxidation of α,β -unsaturated ketones was evaluated. For chalcone and its derivatives, a higher epoxide yield and ee (up to 97%) were obtained with 2-eha than AcOH as the auxiliary carboxylic acid.

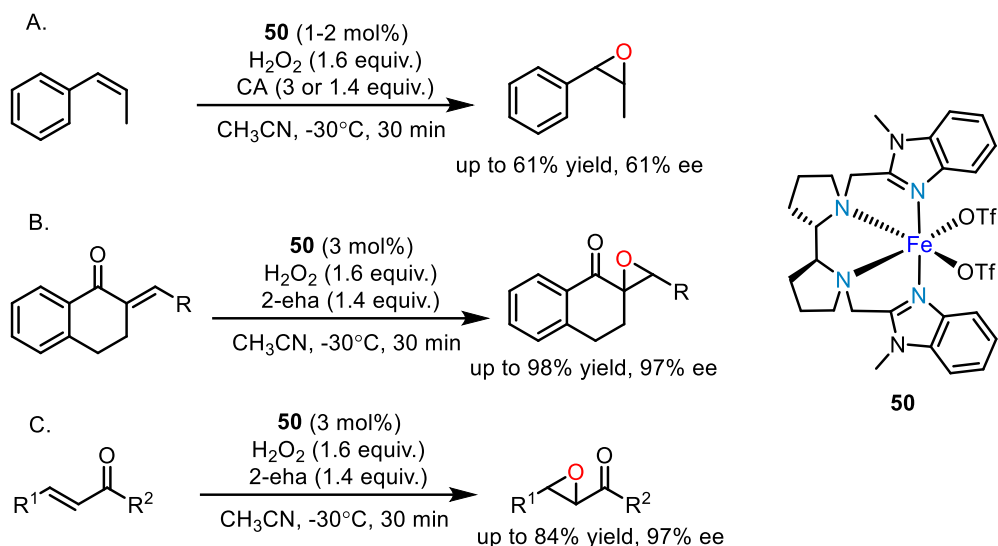


Figure 13. Highly enantioselective epoxidation of olefins catalyzed by N4 complex **50**.

In 2020, Che reported a protocol for the enantioselective alkylation of pyrroles, indoles and N,N-disubstituted anilines catalyzed by the N4 iron complex **51-53** (**Figure 14A**): the tetradentate ligand binds iron generating a Δ -*cis*- β configuration, thanks to the (*R,R*)-diaminocyclohexane backbone. Complex **53** was able to catalyze the conjugate addition of substituted indoles to α,β -unsaturated 2-acyl imidazoles, leading to the products of alkylation on positions 1, 2 or 3 of indole, but always with good yields and enantioselectivity ranging from 71.5% up to >99% (**Figure 14B**). High yields and excellent ee values were also obtained in the alkylation of pyrroles and anilines (**Figure 14C**).³⁹

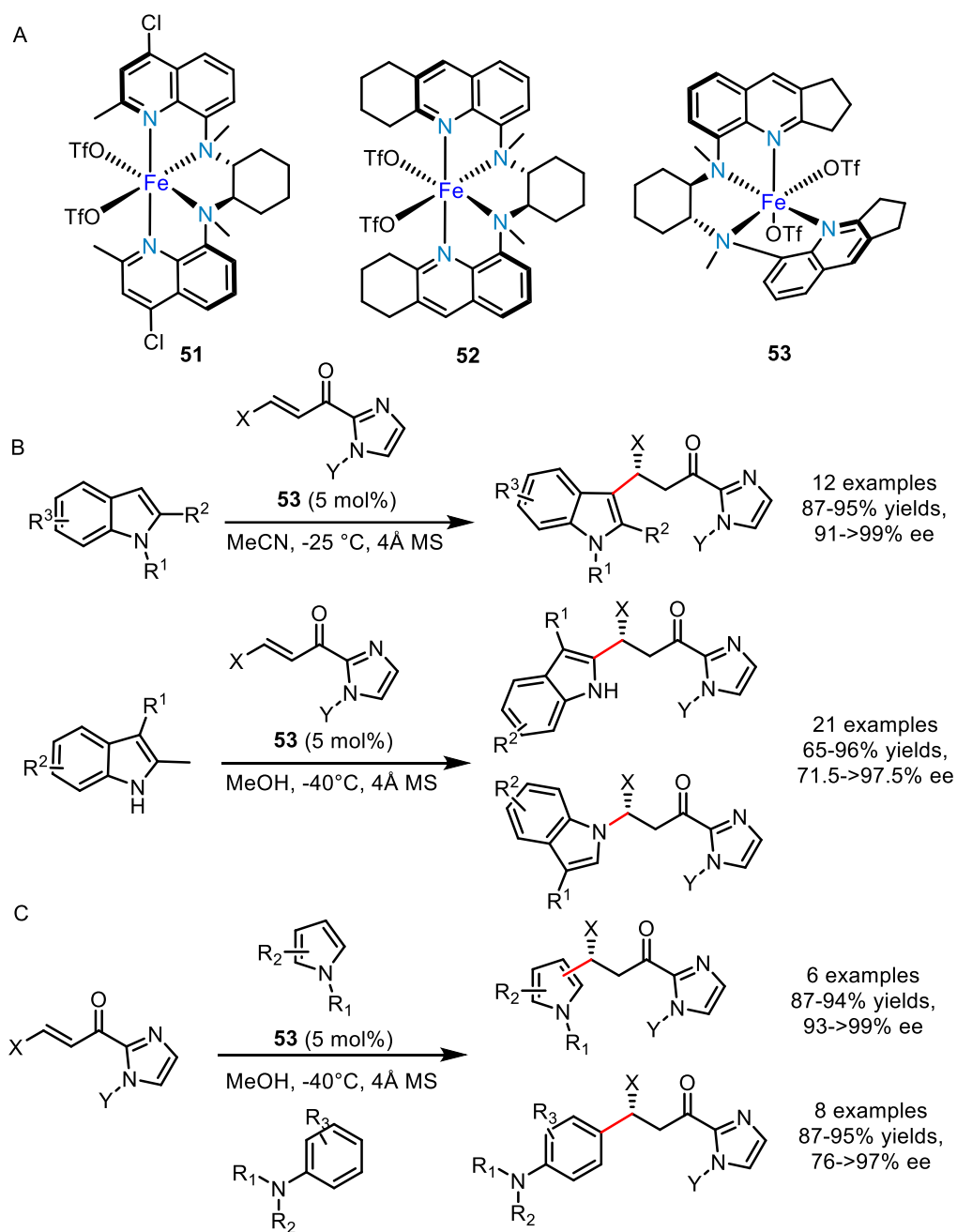


Figure 14. Alkylation of indoles, pyrroles and N,N-disubstituted anilines catalyzed by N4 Iron complex **53**.

1.3 Enantioselective C-N Bond Formation Catalyzed by Chiral Iron Catalyst

As described previously, the most prominent enantioselective C-N bond formation reactions catalyzed by iron complexes include azidation of C-H and C=C bonds and the amination of C-H and C=C bonds.

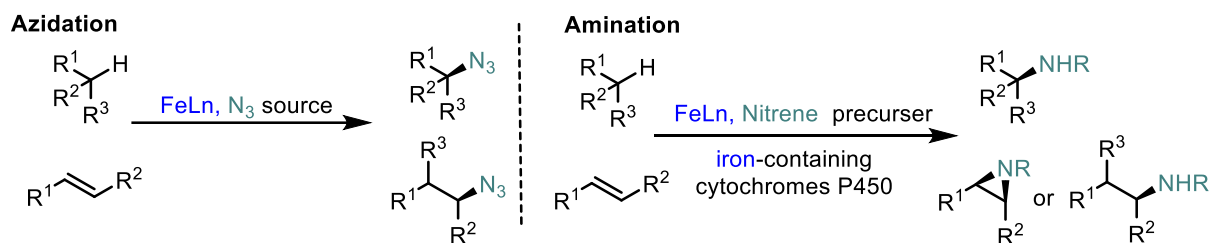


Figure 15. Azidation and amination catalyzed by iron complexes or iron-containing cytochromes P450.

It is noteworthy that there are two major ways to introduce C-N bonds into organic molecules through nitrene transfer (NT): the NR can add to a C=C bond (aziridination; **Figure 16** right) or insert into a C-H bond (amination). Although numerous examples of racemic NT promoted by a variety of transition metals are known, the development of general enantioselective reactions has been substantially more challenging. A simplified mechanism of transition-metal-mediated NT (**Figure 16** left) involves the initial reaction of a metal catalyst ML_n with a nitrene precursor RN=LG (where LG denotes a leaving group such as PhI, N₂ or CO₂) to give a metal-nitrene RNML_n. This reactive intermediate can engage a C=C bond to form an aziridine or insert into a C-H bond to generate an amine product. Depending on the electronic structure of the nitrene species, the reaction can occur through either a concerted or a stepwise pathway. The metal-nitrene intermediate typically exists in either a singlet or a triplet electronic ground state. Singlet metal nitrenes generally perform NT through concerted pathways involving asynchronous transition states. In contrast, triplet nitrene complexes afford radical intermediates by H-atom transfer or radical addition to the alkene, followed by radical recombination.⁴⁰

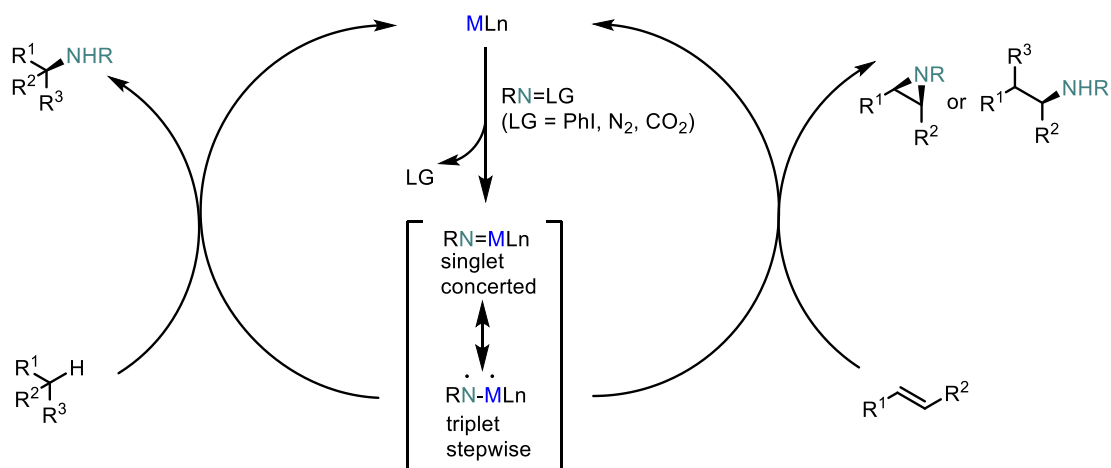


Figure 16. A simplified mechanism of transition-metal-mediated C=C aziridination or C-H amination or through nitrene transfer.

1.3.1 Iron-Catalyzed Asymmetric Azidation of β -Keto Esters and Oxindoles

In 2013, the first example of enantioselective Fe-catalyzed azidations of cyclic β -keto ester and oxindoles using a readily available and stable azidoiodinane as an N_3 -transfer reagent was reported by Gade and co-workers in high yields with up to 93% ee (**Figure A**).⁴¹ The reaction was catalyzed by the combination of boxmi-iron (II) chloride complex and silver carboxylate. The solvent of the reaction also plays an important role in achieving enantioselectivity and diethylether was found to be the best. Silver benzoates with an electron-withdrawing group were most suitable for the reaction e.g. silver 4-nitrobenzoate provided the highest enantioselectivity. Both electron-rich and -poor indanones and substituted cyclopentenone derivatives were converted to the corresponding azo product in high yields with high enantioselectivity. A bulky ester such as *tert*-butyl substituent is essential for enantioselectivity. Cyclic six-membered-ring beta-keto ester was also successfully employed in the process but with moderate enantioselectivity. The methodology was successfully extended to azidation of 3-aryloxindoles, wherein catalyst was prepared in situ from iron (II) propionate and the boxmi ligand (**Figure B**).

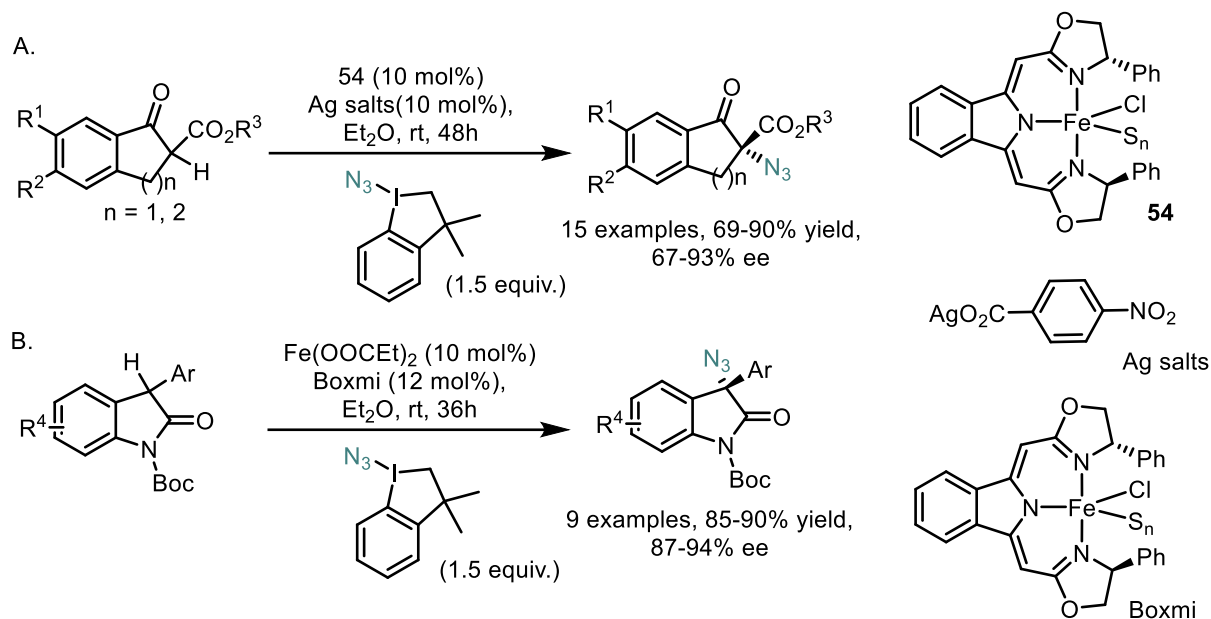


Figure 17. Enantioselective C-N coupling reaction between β -ketoesters and oxindoles catalyzed by Fe complex.

1.3.2 Iron-Catalyzed Asymmetric Carboazidation of Styrenes

In 2020, the Bao group reported the iron-catalysed enantioselective carboazidation of styrenes.⁴² This reaction proceeds through a carbon radical addition to double bond and the following group transfer of azido group from Fe (III)-N₃ species to benzylic radical (**Figure 18A**). The stereo-control on the radical centre is realized via the synergistic effects of van der Waals and π interactions in the rigid chiral space created by the tridentate chiral NON-pincer ligand and iron salt (**Figure 18B**). In their work, styrene with one or more substituents on the phenyl ring was examined and were found to provide the corresponding products with good to high yields and high enantiomeric ratios. Both electron-donating groups, such as methyl or methoxy, and electron-withdrawing groups, including F, Cl, Br, NO₂, are tolerated. And inexpensive industrial chemical feedstocks such as CBr₄, CHI₃, CHBr₃, CBrCl₃ and other commercially available carbon sources such as fluoroalkyl bromides or iodides all react effectively to afford the desired products. Finally, total of 67 substrates were catalyzed by this catalytic system and provided the desired product with up to 87% yield and 97:3 e.r. (**Figure 18C**).

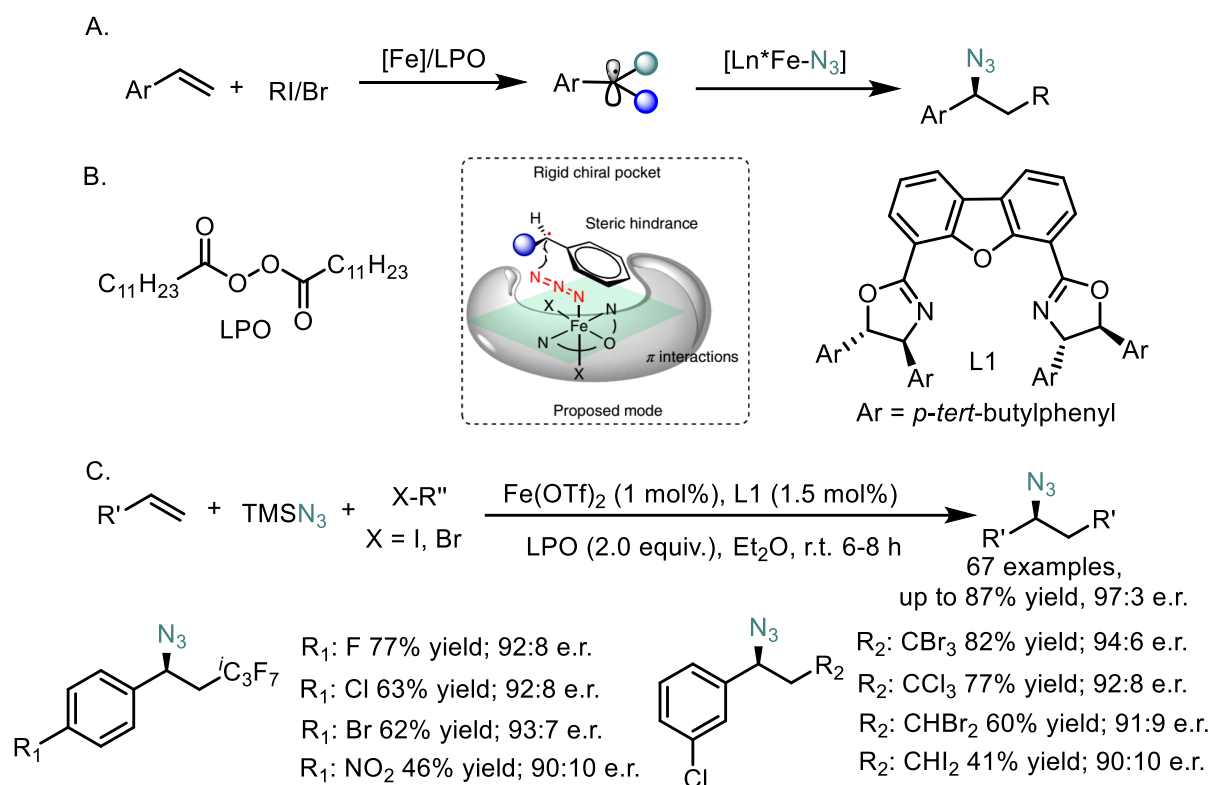


Figure 18. Iron-catalysed asymmetric carboazidation of styrenes.

In 2021, the Bao group reported the first iron-catalyzed radical asymmetric aminoazidation and diazidation of styrenes.⁴³ The reaction proceeds under mild reaction conditions, with low catalyst loading and broad styrene scope. For aminoazidation, most substrates are catalyzed by the combination of Fe (OTf)₂ and L1. Several substrates are catalyzed by the combination of Fe (OTf)₂ and L2. Most of the reactions were performed with L1 or L2, and it was found that L1 afforded products with better enantioselectivity in most cases except for reactions not forming products. Electron-donating groups such as methoxyl, methyl, isopropyl or *n*-octyl, and electron-withdrawing groups, including F, Cl, Br, CF₃, or CHF₂ are all tolerated. When vinyl and allyl/alkynyl groups are present in the same molecule the aminoazidation occurs selectively at the vinyl group, affording the desired product (**Figure 19A**). For diazidation of alkenes, they found the chiral iron catalyst is suitable for disubstituted and trisubstituted styrenes and produce the otherwise inaccessible chiral diazidation products (**Figure 19B**). For these two reactions, total of 54 examples were provided with up to 98% yield and 98.5:1.5 e.r.

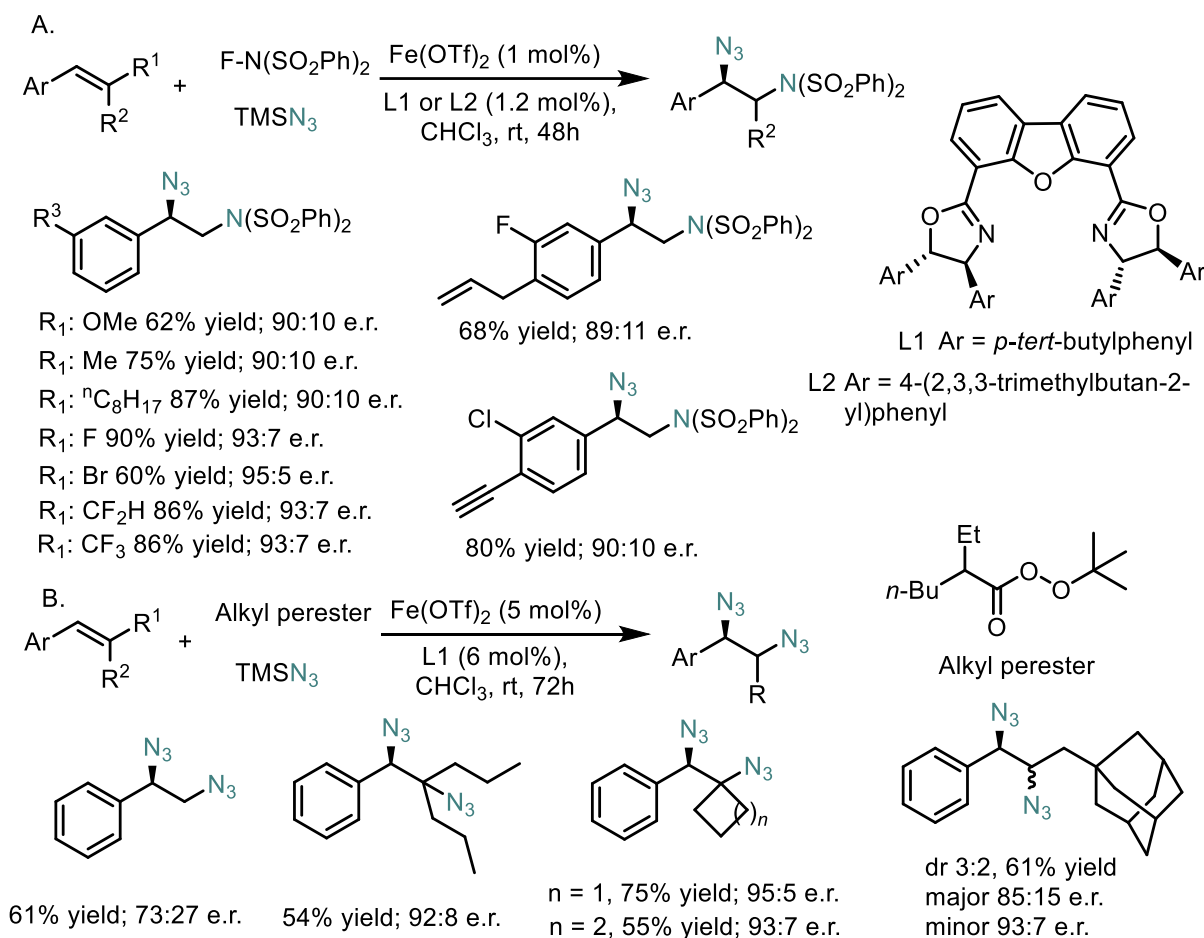


Figure 19. Iron-catalyzed radical asymmetric aminoazidation and diazidation of styrenes.

In 2021, the Feng group disclosed an efficient enantioselective radical carboazidation and diazidation of α,β -unsaturated ketones and amides catalyzed by chiral $\text{N,N}'$ -dioxide/ Fe(OTf)_2 complexes.⁴⁴ A series of substituted olefins are converted into corresponding olefins α -azido carbonyl derivatives have good enantioselectivity and are conducive to the preparation of chiral compounds α -amino ketones, ortho amino alcohols and ortho diamines. they studied the substrate range of ketene in asymmetric reaction, trifluoromethyl azide reaction. Using Togni reagent and TMSN_3 as reaction partners, a variety of α -aryl α,β -unsaturated ketones transfer the corresponding molecules smoothly β -trifluoromethyl- α -azido can obtain good enantioselectivity. In general, alkenones with substituted benzoyl groups have good tolerance, good yield (68%-88%), and high enantioselectivity (96.5:3.5-98:2). It should be noted that other commercial carbon sources, such as fluoroalkyl iodine, are suitable carbon partners. With the assistance of lauryl peroxide, the required adducts are transported in the ratio of 94:6 e.r. and 93.5:6.5 e.r. In addition, alkyl peroxides can also be oxidized as an ideal carbon source for alkyl azide, respectively. Methyl peroxide and ethyl peroxide also participated in the reaction, providing methyl product in the ratio of 93.5:6.5 e.r. and ethyl product in

the ratio of 87:13 e.r., respectively. The corresponding alkyl peroxides can generate a series of primary alkyl radicals with various functional substituents such as chlorine and esters, and provide related products with good yields at medium to good enantiomeric ratios (**Figure 20A**). And for diazidation, an array of α,β -unsaturated ketones with various substituents on the α -phenyl ring were all amenable in diazidation (75:25-91.5:8.5 e.r.)(**Figure 20B**).

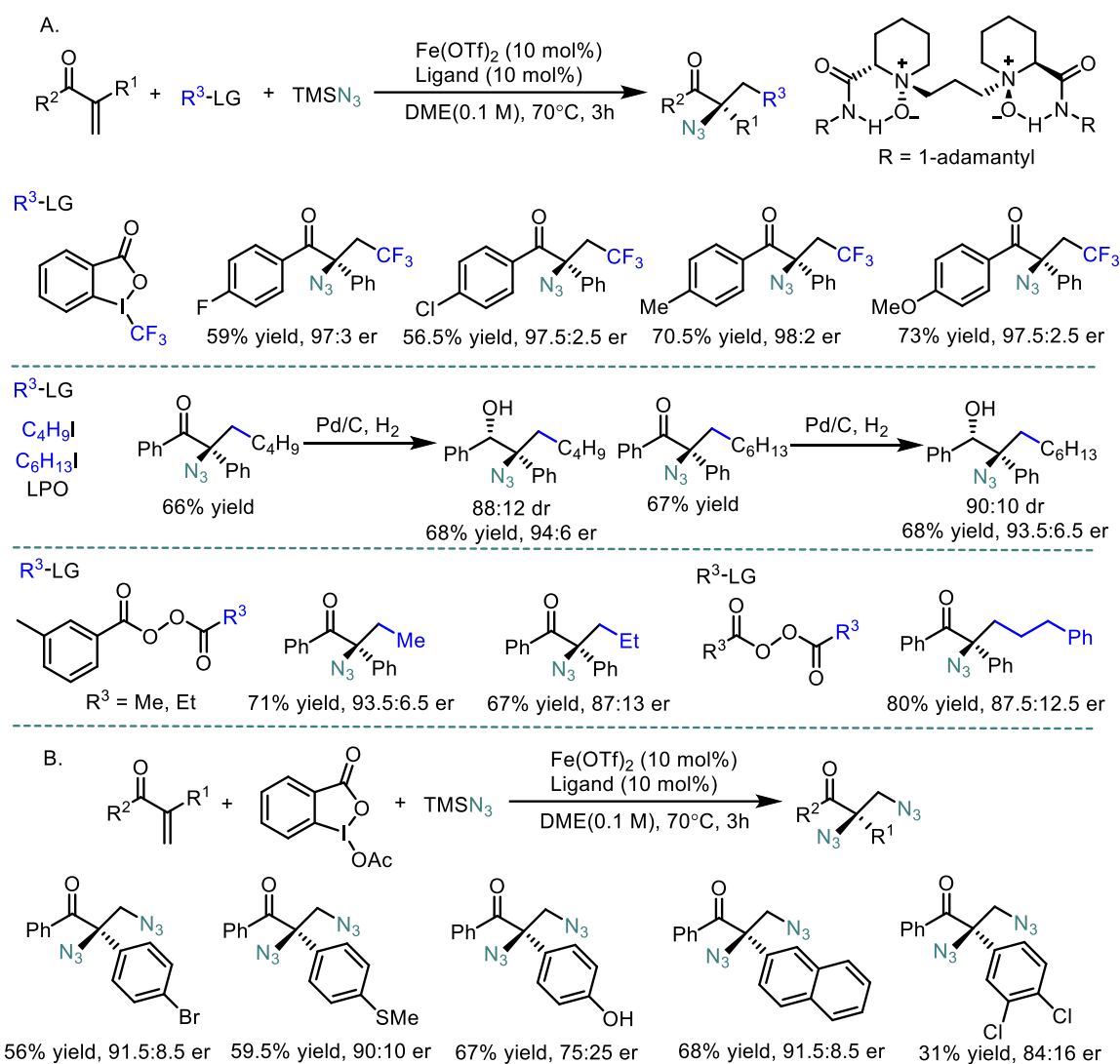


Figure 20. Iron-catalyzed enantioselective radical carboazidation and diazidation of α,β -Unsaturated Carbonyl Compounds.

1.3.3 Iron-Catalyzed Asymmetric Intramolecular Aminohydroxylation of Indoles

In 2013, the Xu group disclosed iron (II)-catalyzed asymmetric intramolecular aminohydroxylation of indoles.⁴⁵ In this reaction, the iron catalyst transfers the N and O groups of hydroxylamine to various indoles (dr > 20:1, ee up to 99%). Simple product derivatization provides enantiomerically enriched forms of aminohydroxyindole and aminoindolanes (**Figure 21**). They

applied the optimized reaction conditions to various substituted indoles. And observed that 5-methylindole is an excellent substrate for Fe (OAc)₂ catalyzed asymmetric amino hydroxylation. They also found that 6-methyl substituent, bromine substituent and chlorine substituent were well tolerated in the asymmetric amino hydroxylation of indole catalyzed by Fe (OAc)₂, which provided a multipurpose method for further research. Further studies showed that 6-phenylindole was an excellent substrate for Fe (OTf)₂ catalyzed asymmetric ammonia hydroxylation (91% ee), and 7-methylindole participated in Fe (OAc)₂ catalyzed asymmetric ammonia hydroxylation with acceptable ee (88% ee). However, they observed that the ee of amino hydroxylation of 4-bromoindole was significantly lower than that of other substrates (74% ee), suggesting that 4-H may be important for asymmetric induction.

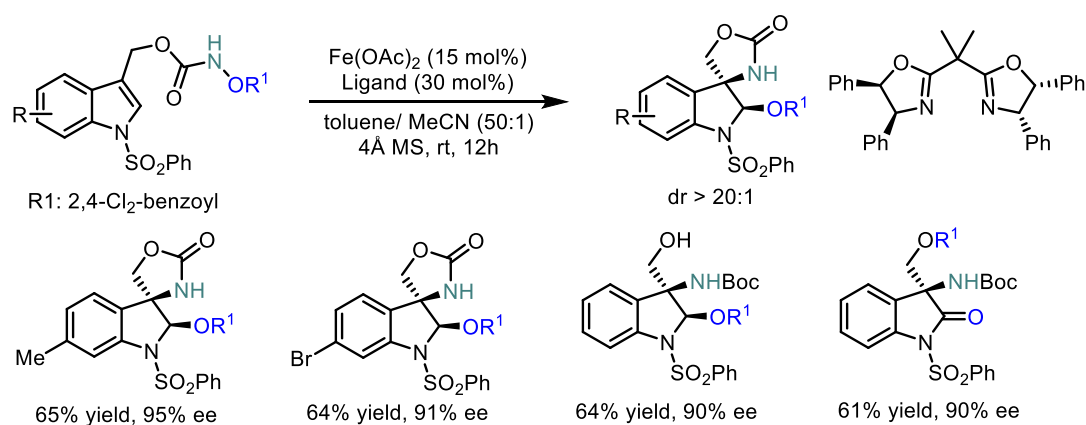


Figure 21. Iron(II)-catalyzed asymmetric intramolecular aminohydroxylation of indoles.

1.3.4 Iron-Catalyzed Asymmetric Aminohydroxylation and Aminofluorination of Olefins

In 2016, Xu and colleagues reported that the PyBOX ligand effectively supports a Fe centre to enable enantioselective intermolecular aminoxygenation and aminofluorination of indene.⁴⁶ Control experiments suggest the presence of a carbon centred radical intermediate generated through radical addition of a putative Fe–nitrene. This mechanism differs from the classical aziridination ring-opening pathway because the radical intermediate is proposed to be oxidized by the resulting high-valent Fe (III) intermediate through single-electron transfer to generate a carbocation, which subsequently combines with either BzO⁻ or F⁻ (**Figure 22**).

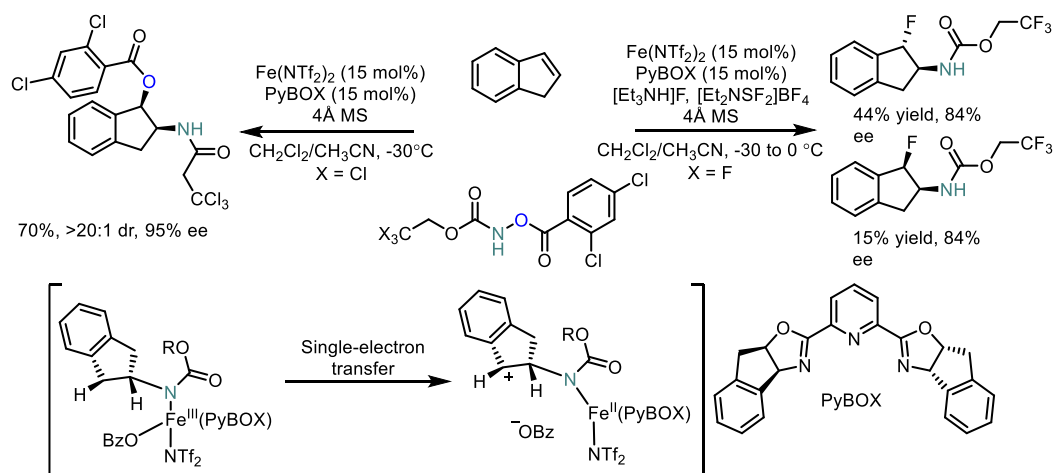


Figure 22. Enantioselective intermolecular aminoxygenation and aminofluorination of indene.

1.3.5 Iron-Heme Enzyme-Catalyzed Asymmetric Aziridination

Since the structures of iron carbene ($\text{Fe}=\text{C}(\text{R}^1)(\text{R}^2)$) and iron nitrene ($\text{Fe}=\text{NR}$) are similar to those of iron oxide ($\text{Fe}=\text{O}$) intermediates involved in the catalytic oxidation of cytochrome P450, Arnold and coworkers used synthetic carbene and nitrobenzene precursors never encountered in biological systems and reused P450 to catalyze unknown reactions in nature.⁴⁷ So, they tried different nitrene transfer reactions. In 2015, they disclosed that P411s could catalyze the asymmetric aziridination of styrene derivatives using tosyl azide as the nitrene source.⁴⁸ They found that evolved enzymes can suppress the reduction of azide. The final variant P I263F A328V L437V allows the preparation of a series of enantiomerically enriched aziridines from electron-rich and electrically neutral styrene. Due to their weakened nucleophilicity, electron-deficient styrene is a less effective substrate under these conditions (**Figure 23**).

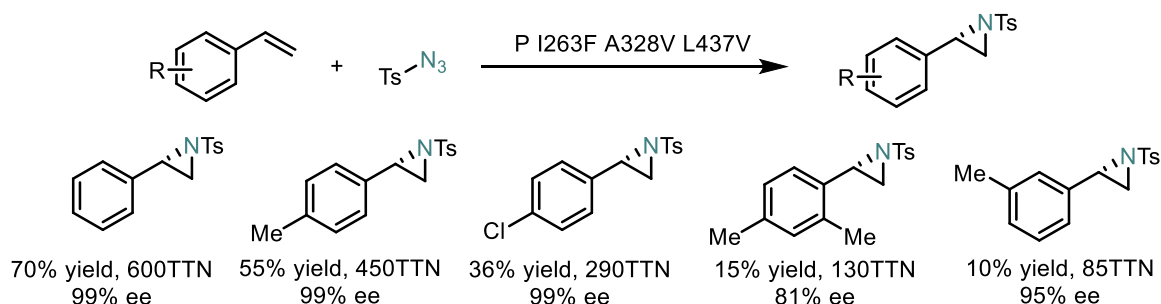


Figure 23. Iron-heme enzyme-catalyzed asymmetric aziridination.

1.3.6 Iron-Heme Enzyme-Catalyzed Asymmetric Aminohydroxylation

In 2019, Arnold and coworkers found that the transfer of unprotected nitrene to styrenes afforded amino alcohols as the final product when they used wild-type Rma cytochrome c as the catalyst.⁴⁹ They

proposed this due to the rapid ring-opening of the unprotected aziridine under the reaction conditions. Starting from Rma cyt *c*, active site engineering provides a " TQL " variant, a highly active biocatalyst for asymmetric amino hydroxylation of various styrene (including electron-deficient styrene). Further mechanism studies showed that the hydrolysis of unprotected enantiopure aziridine is enantiospecific. This finding suggests that the enantiomerically enriched aziridine formed by the enzyme may be the precursor of 1,2-aminoalcohol products (**Figure 24**).

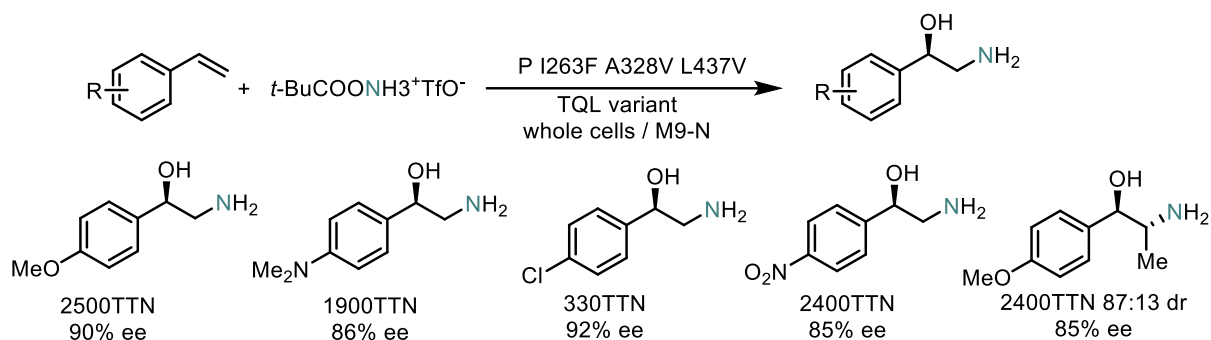
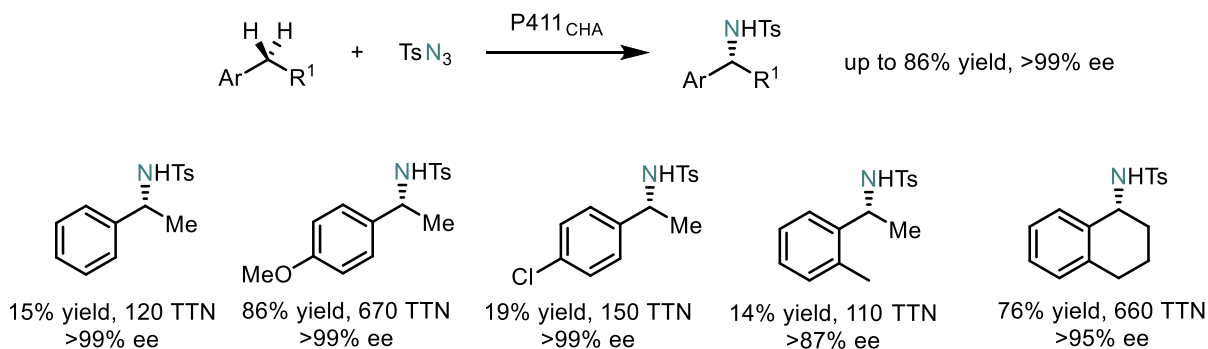


Figure 24. Iron-heme enzyme-catalyzed asymmetric aminohydroxylation.

1.3.7 Iron-Heme Enzyme-Catalyzed Asymmetric Intermolecular Benzylic C-H Amination

In 2017, the Arnold group successfully applied their chiral iron-porphyrin based enzymatic catalyst system in asymmetric intermolecular C-H amination of benzylic C-H bonds.⁵⁰ The chiral amides were obtained in up to >99% ee and up to 86% yield. Based on the manifold, they proposed the catalytic cycle for intermolecular amination shown in (**Figure 25**) First, reduction of the ferric state of the haem cofactor, with electrons derived from NADPH, gives the ferrous state. Reaction with a nitrene source, here tosyl azide (TsN_3), then provides the putative iron nitrenoid. Subsequent reaction of this intermediate with an alkane such as 4-ethylanisole would deliver the C-H amination product benzylic amine and regenerate the ferrous state of the catalyst. A competing process observed in P411-catalysed nitrene transfer is the reduction of the nitrenoid, generating the undesired by-product *p*-toluenesulfonamide. the targeted C-H bond is necessarily present in the enzyme active site when the reactive nitrenoid is formed, biasing productive C-H amination over the deleterious nitrenoid reduction pathway.



Proposed mechanism:

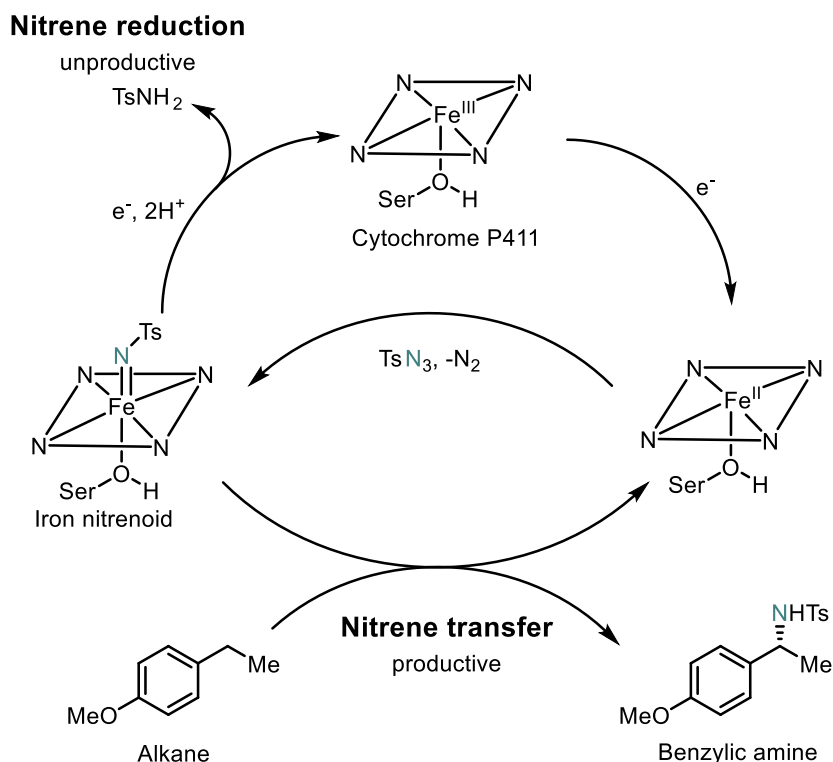


Figure 25. Iron-heme enzyme-catalyzed intermolecular benzylic C–H amidation.

1.3.8 Iron-Heme Enzyme-Catalyzed Asymmetric Amination of Primary, Secondary and Tertiary C(sp³)-H Bonds

In 2019, the Arnold group reported the intramolecular C-H amidation of sulfamoyl azide as a model system. They demonstrated that all three modes of enantioinduction could be achieved using P411 catalysts.⁵¹ The amidation of secondary C(sp³)-H bonds, primary C(sp³)-H bonds are two of three modes, and the third one is enantioconvergent tertiary C-H amidations via a putative stereoablative hydrogen atom transfer (HAT)/stereoselective rebound mechanism (**Figure 26**).

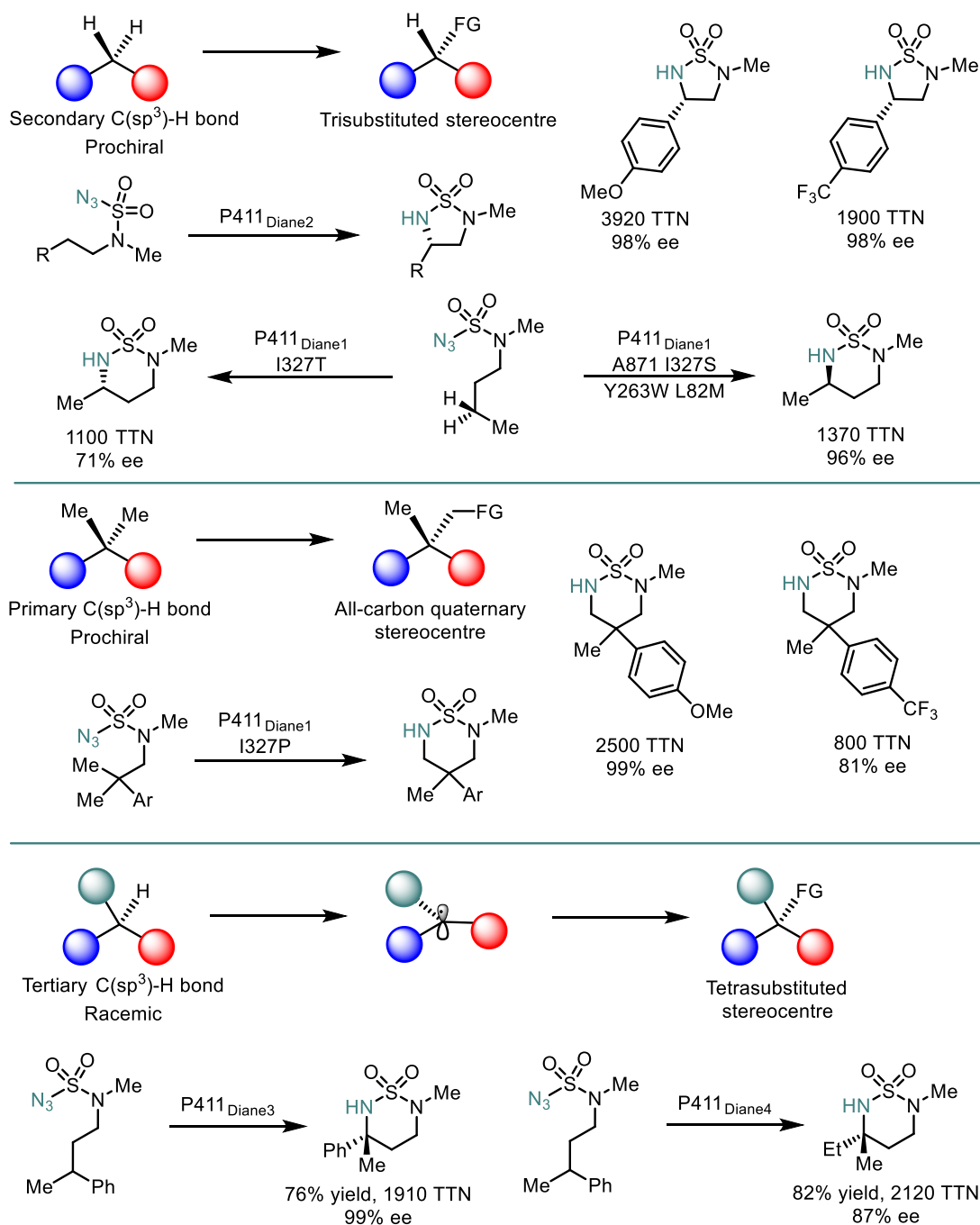


Figure 26. Iron-heme enzyme-catalyzed asymmetric amidation of primary, secondary, and tertiary C(sp³)-H bonds.

1.3.9 Iron-Heme Enzyme-Catalyzed Benzylic and Allylic C(sp³)-H Bonds

Even more exciting, in 2020, the Arnold group reported the asymmetric primary C-H aminations at both benzylic and allylic C-H bonds provided desired chiral amines in up to 3930 TTN and 96% ee.⁵² Variant P411APA chemoselectively aminates the allylic C-H bond, leaving the olefin moiety completely untouched. This chemoselectivity is orthogonal to the Rma cyt c TQL variant previously engineered for olefin aminohydroxylation. With P411BPA and P411APA, an array of easily available hydrocarbon starting

materials could be converted into value-added primary amines (**Figure 27**).

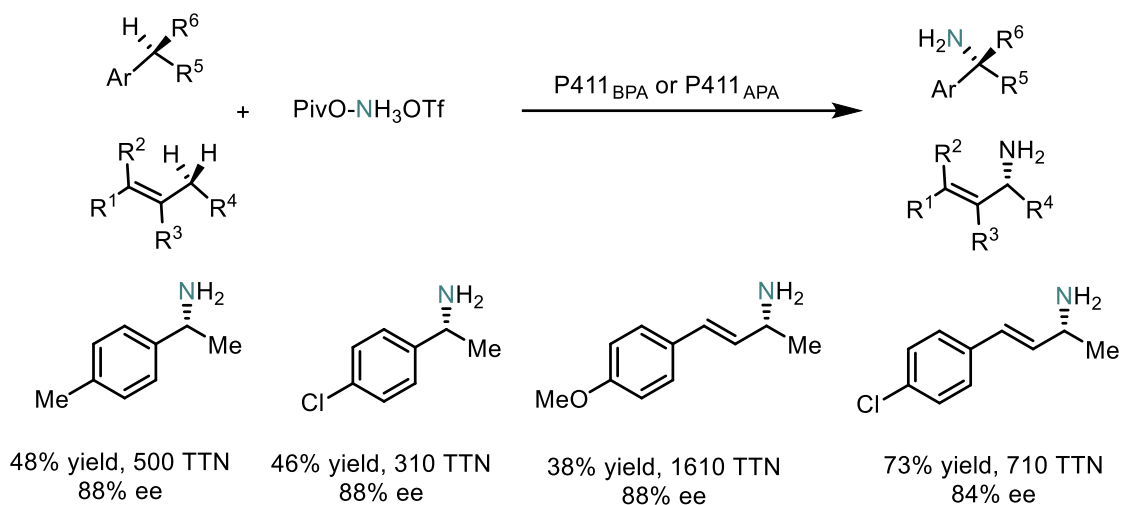


Figure 27. Iron-heme enzyme-catalyzed asymmetric amination of benzylic and allylic C(sp³)-H bonds.

1.3.10 Iron-Heme Enzyme-Catalyzed Benzylic C(sp³)-H Bonds

Subsequently, the Arnold group disclosed a biocatalytic, intermolecular benzylic C-H amidation reaction operating at mild and scalable conditions.⁵³ With hydroxamate esters as nitrene precursors, feedstock aromatic compounds can be converted to chiral amides with excellent enantioselectivity (up to >99% ee) and high yields (up to 87%) (**Figure 28**).

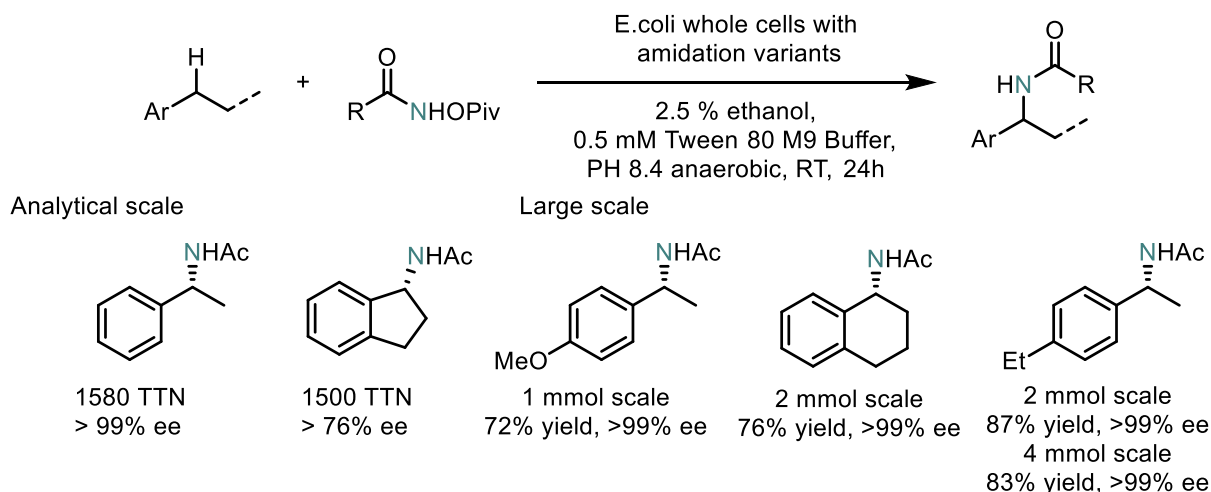


Figure 28. Biocatalytic, intermolecular C-H bond amination for enantioenriched amides.

1.4 Aim of Thesis

Based on the previous literature review, the activation of direct C-H bonds is still the most challenging direction among the current methods for the construction of chiral C-N bonds. Direct enantioselective C-H bond functionalization remains a difficult task due to the high dissociation energy and the ubiquity of C-H

bonds in organic substrates.⁵⁴ In this endeavour, the reported, efficient catalysts that are based on non-precious metals such as iron remains sparse. When compared to precious metals, non-precious metals as exemplified by iron are usually earth-abundant and relatively more biocompatible. The development of Fe catalysis can be linked to the preparation of biomimetic Fe complexes with the catalytic activity that could match that of heme and/or non-heme enzymes. Especially in the application of enantioselective C–H bonds functionalization.

Iron-catalyzed C-H bond asymmetric amination

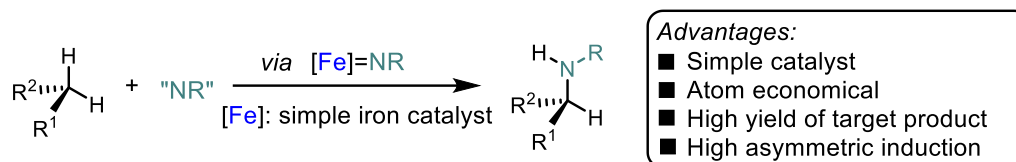


Figure 29. Iron-catalyzed C-H bond asymmetric amination.

Some N4 Iron complexes have been reported and can be applied in efficient asymmetric catalysis as demonstrated for enantioselective epoxidations, cis-dihydroxylation of alkenes and simple Michael addition reactions. It is worth mentioning that this catalyst has never been used for enantioselective catalysis of C-N bonds formation, especially the enantioselective amination of C-H bonds. Therefore, we envisioned that N4 Iron complexes might also catalyze asymmetric C-H amination reactions.

1.4.1 Synthesis of New N4 Chiral Iron Complexes

N4 ligands have been easy to synthesize during the last two decades and they can coordinate with a variety of metals (Mn, Fe, Co), especially iron. N4 ligands are typically prepared by electrophilic substitution from diamines and nitrogen-containing heterocycles. The chiral ligand can be also synthesized if the diamine is chiral. In addition, the leaving groups in the complexes now prepared from N4 ligands are primarily acetonitrile and triflate. The goal of this thesis is to develop novel catalysts with leaving groups other than acetonitrile and triflate.

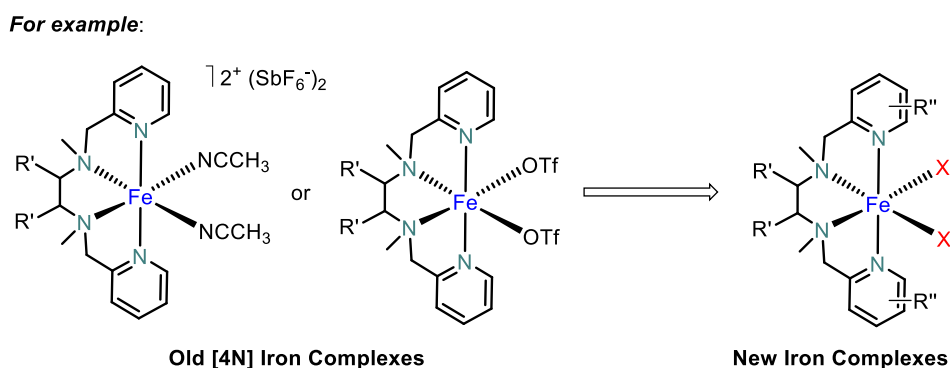


Figure 30. New N4 iron complexes design.

1.4.2 Apply N4 Iron Complexes in Asymmetric Intramolecular C-H Aminations

Transition-metal catalysed asymmetric C-H aminations are a major topic in organic synthesis nowadays. Despite various efforts which have been put into this research area, there are still some challenges that need to be solved in this field. For example, the development of less expensive and more easily available transition metal catalysts is a significant scientific endeavour. In this thesis, we intend to lay the foundation for iron-catalyzed enantioselective amination and establish the basis for further research.

Reference

- (a) P. Chirik, R. Morris, *Acc. Chem. Res.* **2015**, *48*, 2495; (b) M. Beller, *Chem. Rev.* **2019**, *119*, 2089.
- (a) R. Shang, L. Ilies, E. Nakamura, *Chem. Rev.* **2017**, *117*, 9086; (b) Y. Liu, T. You, H. X. Wang, Z. Tang, C. Y. Zhou, C. M. Che, *Chem. Soc. Rev.* **2020**, *49*, 5310.
- (a) R. Hili, A. Yudin, *Nat. Chem. Biol.* **2006**, *2*, 284; (b) G. Evano, N. Blanchard, M. Toumi, *Chem. Rev.* **2008**, *108*, 3054.
- (a) K. Shin, H. Kim, S. Chang, *Acc. Chem. Res.* **2015**, *48*, 1040; (b) J. Senra, L. Aguiar, A. Simas, *Curr. Org. Synth.* **2011**, *8*, 53.
- (a) S. K. Ghorai, V. G. Gopalsamuthiram, A. M. Jawalekar, R. E. Patre, S. Pal, *Tetrahedron* **2017**, *73*, 1769; (b) M. Ju, J. M. Schomaker, *Nat. Rev. Chem.* **2021**, *5*, 580.
- I. C. Gunsalus, T. C. Pederson, S. G. Sligar, *Annu. Rev. Biochem.* **1975**, *44*, 377.
- F. P. Guengerich, *Chem. Res. Toxicol.* **2001**, *14*, 611.
- Y. Yang, F. H. Arnold, *Acc. Chem. Res.* **2021**, *54*, 1209.
- (a) Y. Liu, T. You, H. X. Wang, Z. Tang, C. Y. Zhou, C. M. Che, *Chem. Soc. Rev.* **2020**, *49*, 5310.
(b) G. M. Fusi, S. Gazzola, U. Piarulli, *Adv. Synth. Catal.* **2021**, *363*, 1.
- P. R. Ortiz de Montellano, J. J. De Voss, *Nat. Prod. Rep.* **2002**, *19*, 477.

11. B. Meunier, S.P. De Visser, S. Shaik, *Chem. Rev.* **2004**, *104*, 3947.
12. (a) J. T. Groves, T. E. Nemo, R. S. Myers, *J. Am. Chem. Soc.* **1979**, *101*, 1032; (b) J. T. Groves, T. E. Nemo, *J. Am. Chem. Soc.* **1983**, *105*, 6243.
13. R. A. Leising, R. E. Norman, L., Jr. Que, *Inorg. Chem.* **1990**, *29*, 2553.
14. T. Okuno, S. Ito, S. Ohba, Y. Nishida, *J. Chem. Soc., Dalton Trans.* **1997**, 3547.
15. M. E. de Vries, R. M. La Crois, G. Roelfes, H. Kooijman, A. L. Spek, R. Hage, B. L. Feringa, *Chem. Commun.* **1997**, 1549.
16. C. Kim, K. Chen, J. Kim, L., Jr. Que, *J. Am. Chem. Soc.* **1997**, *119*, 5964.
17. M. C. White, A. G. Doyle, E. N. Jacobsen, *J. Am. Chem. Soc.* **2001**, *123*, 7194.
18. M. S. Chen, M. C. White, *Science* **2007**, *318*, 783.
19. P. E. Gormisky, M. C. White, *J. Am. Chem. Soc.* **2013**, *135*, 14052.
20. O. Cussó, I. Garcia-Bosch, X. Ribas, J. Lloret-Fillol, M. Costas, *J. Am. Chem. Soc.* **2013**, *135*, 14871.
21. R. Mas-Balleste, L., Jr. Que, *J. Am. Chem. Soc.* **2007**, *129*, 15964.
22. (a) O. Y. Lyakin, K. P. vBryliakov, G. J. P. Britovsek, E. P. Talsi, *J. Am. Chem. Soc.* **2009**, *131*, 10798. (b) O. Y. Lyakin, K. P. Bryliakov, E. P. Talsi, *Inorg. Chem.* **2011**, *50*, 5526.
23. A. Ansari, A. Kaushik, G. Rajaraman, *J. Am. Chem. Soc.* **2013**, *135*, 4235.
24. Y. Nishikawa, H. Yamamoto, *J. Am. Chem. Soc.* **2011**, *133*, 8432.
25. M. Wu, C.X. Miao, S. Wang, X. Hu, C. Xia, F. E. Kuhn, W. Sun, *Adv. Synth. Catal.* **2011**, *353*, 3014.
26. B. Wang, S. Wang, C. Xia, W. Sun, *Chem. Eur. J.* **2012**, *18*, 7332.
27. W. Dai, G. Li, B. Chen, L. Wang, S. Gao, *Org. Lett.* **2015**, *17*, 904.
28. O. Cusso, M. Cianfanelli, X. Ribas, R. J. Klein Gebbink, M. Costas, *J. Am. Chem. Soc.* **2016**, *138*, 2732.
29. F.T. de Oliveira, A. Chanda, D. Banerjee, X. Shan, S. Mondal, L., Jr. Que, E.L. Bominaar, E. Münck, T.J. Collins, *Science* **2007**, *315*, 835.
30. M. Ghosh, K.K. Singh, C. Panda, A. Weitz, M.P. Hendrich, T.J. Collins, B.B. Dhar, S. Sen Gupta, *J. Am. Chem. Soc.* **2014**, *136*, 9524.
31. T.W.S. Chow, E.L.M. Wong, Z. Guo, Y. Liu, J.S. Huang, C.M. Che, *J. Am. Chem. Soc.* **2010**, *132*, 13229.

32. I. Prat, J.S. Mathieson, M. Güell, X. Ribas, J.M. Luis, L. Cronin, M. Costas, *Nat. Chem.* **2011**, *3*, 788.
33. J. Serrano-Plana, W.N. Oloo, L. Acosta-Rueda, K.K. Meier, B. Verdejo, E. García-España, M.G. Basallote, E. Münck, L. Jr., Que, A. Company, M. Costas, *J. Am. Chem. Soc.* **2015**, *37*, 15833.
34. C. Zang, Y. Liu, Z.-J. Xu, C.-W. Tse, X. Guan, J. Wei, J.- S. Huang, C.-M. Che, *Angew. Chem. Int. Ed.* **2016**, *55*, 10253.
35. M. Mitra, O. Cusso, S. S. Bhat, M. Sun, M. Cianfanelli, M. Costas, E. Nordlander, *Dalton Trans.* **2019**, *48*, 6123.
36. O. Cusso, I. Garcia-Bosch, X. Ribas, J. Lloret-Fillol and M. Costas, *J. Am. Chem. Soc.* **2013**, *135*, 1487.
37. (a) K. Fuji, *Chem. Rev.* **1993**, *93*, 2037; (b) E. J. Corey and A. Guzman-Perez, *Angew. Chem. Int. Ed.* **1998**, *37*, 388; (c) B. M. Wang and Y. Q. Tu, *Acc. Chem. Res.* **2011**, *44*, 1207.
38. (a) B. Wang, S. Wang, C. Xia and W. Sun, *Chem. Eur. J.* **2012**, *18*, 7332; (b) E. J. Corey and F.-Y. Zhang, *Org. Lett.* **1999**, *1*, 1287; (c) Y. Liu, B. A. Provencher, K. J. Bartelsoand, L. Deng, *Chem. Sci.* **2011**, *2*, 1301.
39. J. Wei, B. Cao, C.W. Tse, X.Y. Chang, C.Y. Zhou, C. M. Che, *Chem. Sci.* **2020**, *11*, 684.
40. (a) S. Fantauzzi, A. Caselli, E. Gallo, *Dalton Trans.* **2009**, *2009*, 5434; (b) D. N. Zalatan, J. Du Bois, *Top. Curr. Chem.* **2009**, *292*, 347; (c) H. M. Davies, J. Du Bois, J. Q. Yu, *Chem. Soc. Rev.* **2011**, *40*, 1855; (d) G. Dequirez, V. Pons, P. Dauban, *Angew. Chem. Int. Ed.* **2012**, *51*, 7384; (e) Y. Park, Y. Kim, S. Chang, *Chem. Rev.* **2017**, *117*, 9247.
41. Q.H. Deng, T. Bleith, H. Wadepohl, L.H. Gade, *J. Am. Chem. Soc.* **2013**, *135*, 5356.
42. L. Ge, H. Zhou, M.-F. Chiou, H. Jiang, W. Jian, C. Ye, X. Li, X. Zhu, H. Xiong, Y. Li, L. Song, X. Zhang, H. Bao, *Nat. Catal.* **2020**, *4*, 28.
43. D. Lv, Q. Sun, H. Zhou, L. Ge, Y. Qu, T. Li, X. Ma, Y. Li, H. Bao, *Angew. Chem. Int. Ed.* **2021**, *60*, 12455.
44. W. Liu, M. Pu, J. He, T. Zhang, S. Dong, X. Liu, Y. D. Wu, X. Feng, *J. Am. Chem. Soc.* **2021**, *143*, 11856
45. Y. Q. Zhang, Y. A. Yuan, G. S. Liu, H. Xu, *Org. Lett.* **2013**, *15*, 3910.
46. (a) D. F. Lu, C. L. Zhu, J. D. Sears, H. Xu, *J. Am. Chem. Soc.* **2016**, *138*, 11360; (b) C. L. Zhu, D. F. Lu, J. D. Sears, Z. X. Jia, H. Xu, *Synthesis* **2016**, *48*, 3031.

47. Y. Yang, F. H. Arnold, *Acc. Chem. Res.* **2021**, *54*, 1209.
48. C. C. Farwell, R. K. Zhang, J. A. McIntosh, T. K. Hyster, F. H. Arnold, *ACS Cent. Sci.* **2015**, *1*, 89.
49. I. Cho, C. K. Prier, Z. J. Jia, R. K. Zhang, T. Görbe, F. H. Arnold, *Angew. Chem. Int. Ed.* **2019**, *58*, 3138.
50. C. K. Prier, R. K. Zhang, A. R. Buller, S. Brinkmann-Chen, F. H. Arnold, *Nat. Chem.* **2017**, *9*, 629.
51. Y. Yang, I. Cho, X. Qi, P. Liu, F. H. Arnold, *Nat. Chem.* **2019**, *11*, 987.
52. Z. J. Jia, S. Gao, F. H. Arnold, *J. Am. Chem. Soc.* **2020**, *142*, 10279.
53. S. V. Athavale, S. Gao, Z. Liu, S. C. Mallojjala, J. S. Hirschi, F. H. Arnold, *Angew. Chem. Int. Ed.* **2021**, *60*, 24864.
54. K. M. van Vliet, B. de Bruin, *ACS. Catal.* **2020**, *10*, 4751.

Chapter 2: Results and Discussion

2.1 Synthesis of Chiral N4 Iron Catalysts

As described in the introduction, chiral N4 iron catalysts are not currently used to catalyze the direct construction of C-N transformations from C-H bonds. Besides, according to published work from Que Jr group, White group and Costas group, the iron complexes of N4 ligands will go through high valence Fe (IV) oxo intermediates in the reaction process of catalyzing C-H bond oxidation or carbon-carbon double bond epoxidation and carbon-carbon double bond hydroxylation.¹ Inspired by this active reaction Fe (IV) oxo intermediate, we imagined whether iron catalysts with N4 ligands would form Fe nitrene intermediates. If it can be formed, then the N4 iron catalyst can achieve C-H amination. In addition, our group has successfully developed a series of enantioselective C-H aminations and enantioselective difunctionalization of double bonds catalyzed by chiral-at-metal ruthenium catalysts in the past 4 years.² It is worth mentioning that excellent enantioselectivity control can be achieved in all ruthenium-catalyzed C-H amination reactions. The structure of the N4 iron catalyst is similar to that of the ruthenium catalyst, so we envision that the N4 iron catalyst might also achieve good chirality control in the process of catalyzing C-H amination. With this background and idea in mind, we will present the synthesis of a series of N4 iron catalysts in this chapter.

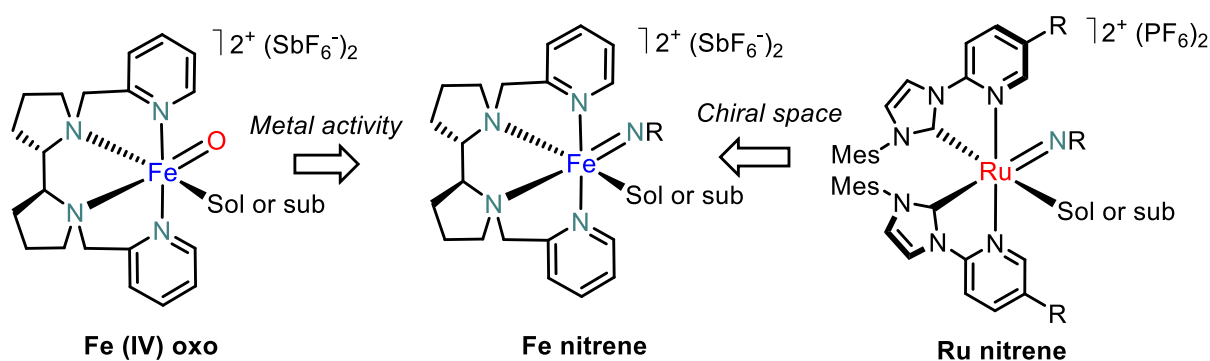


Figure 31. Proposal for N4 iron nitrene intermediates.

2.1.1 Synthesis of Modified Chiral N4 Iron Catalysts

The chiral N4 iron catalyst design went back to related chiral rigidifying pyrrolidine complexes first reported by White.^{1a} We synthesized two types of chiral N4 complexes, the first of which uses acetonitrile as the leaving group. A compound containing chlorine atoms as the leaving group is the second kind. The synthesis of the first of these categories is straightforward and follows the procedure described in the literature. The synthesis of a chiral ligand is the initial stage. To generate a chlorinated complex, the ligand is ligated 1:1 with an iron salt. After dissolving the chlorinated complex in acetonitrile, 2 equivalents of AgSbF₆ are added to form the acetonitrile coordination complex, with hexafluoroantimonate as the counterion. Four pyridine-class catalysts were synthesized. There have been three of these recorded.^{1a, 1b, 3} Benzimidazole-class catalysts are the other kind. There has been one of these reported.⁴ To improve the chiral control of the C-H amination process, we introduced a

large steric hindrance *tert*-butyl group and electron-withdrawing bromine to the benzimidazole ring based on steric hindrance and electronic effects. **Fe2-Fe5** yields range from 37% to 89%. **Fe6-Fe8** yields range from 58% to 83%. **Fe2**,^{1a} **Fe3**,³ **Fe5**^{1b} and **Fe6**⁴ have been reported.

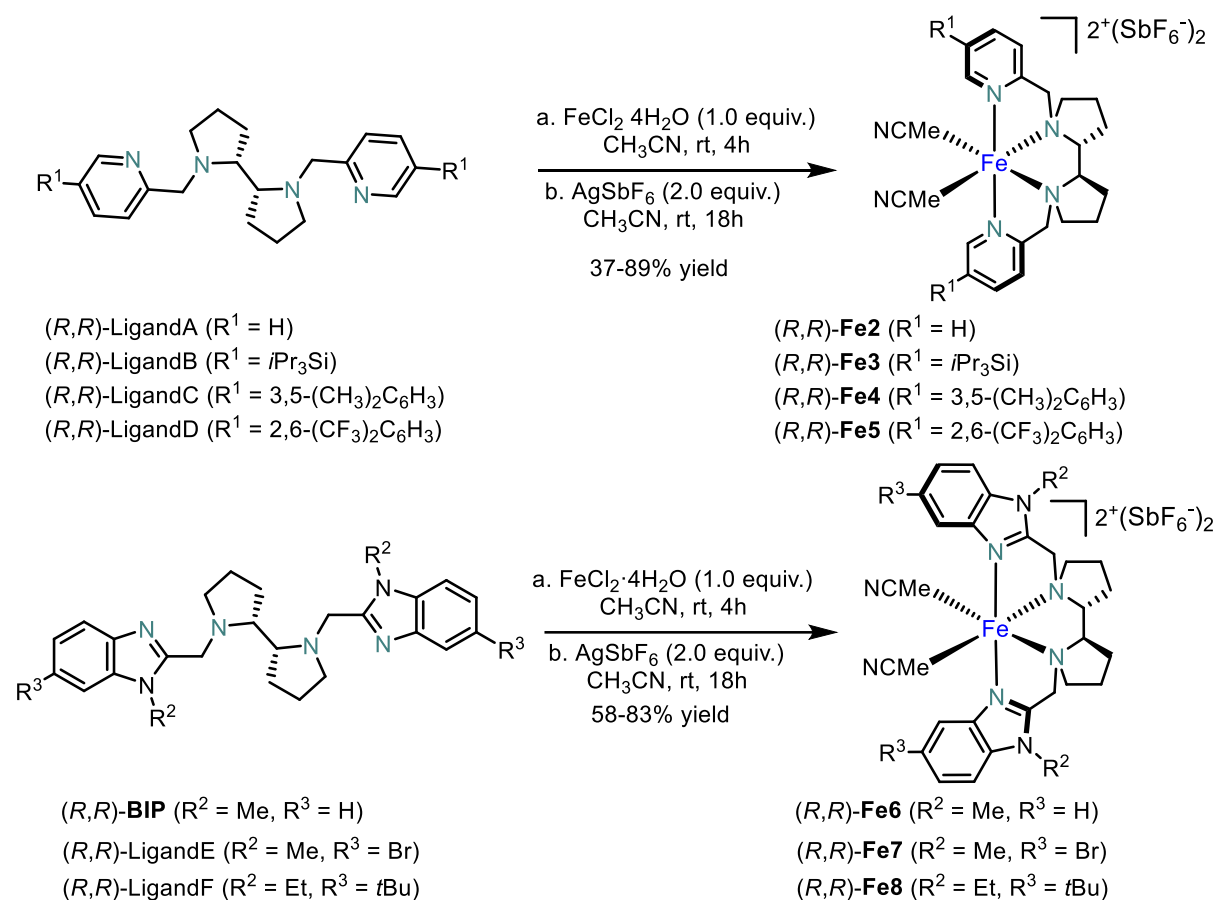


Figure 32. The synthesis of N4 iron complexes.

In our synthesis of acetonitrile complexes, we need to first synthesize complexes where the leaving group is chloride. We attempted to evaluate the activity of chiral iron complexes with a chloride leaving group because no one has previously disclosed their direct application. When we tested the catalytic activity of this complex, it was found to be very good. It is worth mentioning that this finding opened a new door for us. Firstly, the synthesis of such complexes where the leaving group is chloride is much easier without the addition of expensive silver salts to remove the chloride. Secondly, such complexes are more stable and we do not have to worry about loss of activity in the air. And in our thoughts, the ideal catalyst has always been one with excellent stability and catalytic activity. In the process of validating our idea, we first synthesized (R,R) -**BIP** with a 93% yield. To expand our catalyst library, we then synthesized (R) -**Fe8** and (R,R) -**Fe9** with 94% and 89% yields, respectively. Comparing the synthetic yields of the acetonitrile complex and the complex with chloride as the leaving group, the latter gives a much higher yield than the former.

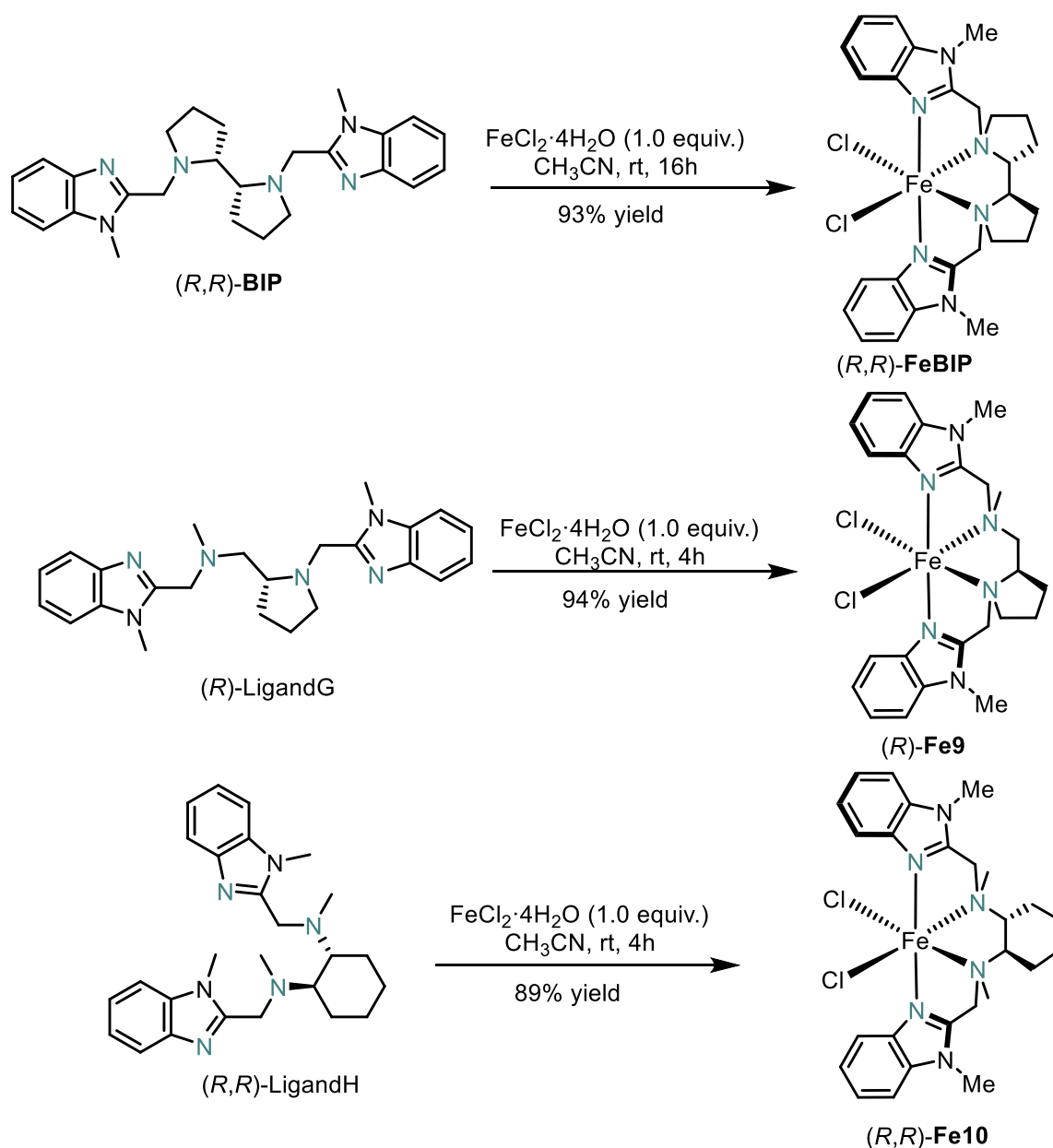


Figure 33. Synthesis of N4 iron chloride complexes.

2.1.2 Gram-Scale Synthesis of (*R,R*)-**FeBIP**

To a stirred solution of the ligand (*R,R*)-**BIP** (990 mg, 2.3 mmol, 1.05 equiv.) in 13 mL CH₃CN under N₂ atmosphere was added FeCl₂·4H₂O (437 mg, 2.2 mmol, 1 equiv.) in one portion. A yellow precipitate was formed within several seconds. The reaction mixture was stirred for 16 hours at room temperature before being diluted with diethyl ether (40 mL). The slurry was transferred into a centrifuge tube, and the solid material was separated by centrifugation and was washed with a mixed solvent of CH₃CN/diethyl ether (v/v = 1/2.5) for three times (3 x 35 mL in total). The solid was dried under nitrogen flow to afford (*R,R*)-[Fe(**BIP**)]Cl₂ as a yellow powder (1.14 g, 2.1 mmol, 93% yield).

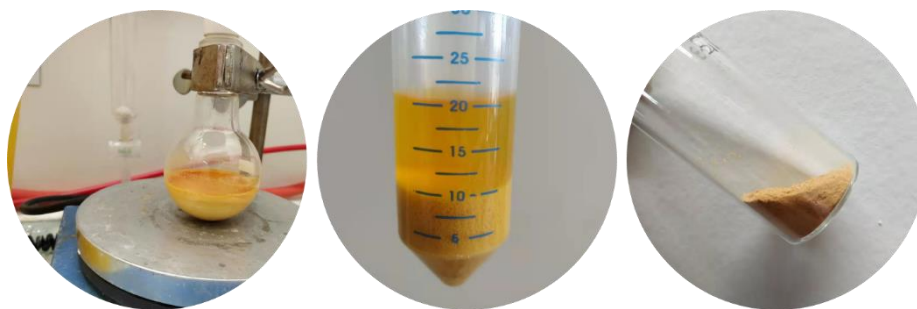


Figure 34. Synthesis of (R,R) -FeBIP.

2.1.3 Crystal Structure of (R,R) -FeBIP

For all but the reported catalysts, we have determined the structure of the complexes by elemental analysis and mass spectrometry. Secondly, to prove whether the BIP iron complex structure was correct, we tried a number of methods, eventually by first dissolving the BIP iron complex in DMF followed by a slow dropwise addition of tetrahydrofuran or ethyl acetate. It is then left to stand overnight and colourless yellow crystals are found to precipitate in the solution. The resulting crystal structure also reveals that the BIP ligand stereochemistry is (R,R) and the iron center stereochemistry is Δ .

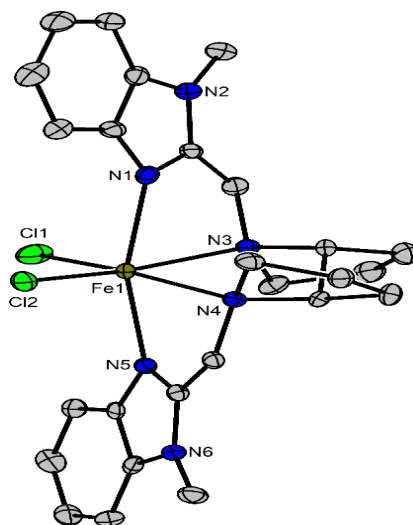


Figure 35. Crystal structure of (R,R) -FeBIP.

2.1.4 Conclusions

Two kinds of chiral N4 iron catalysts were synthesised in this chapter. The first type is a complex with acetonitrile as the leaving group, while the second type is a complex with chloride as the leaving group. Complexes with chloride as the leaving group are easier to synthesize and more stable. Furthermore, BIP complexes can be produced in gram scale yields of up to 93%. (R,R) -FeBIP complex crystals were also obtained. The stereochemistry of the crystal structure is consistent with the theoretical results.

References

1. (a) M. S. Chen, M. C. White, *Science* **2007**, *318*, 783; (b) P. E. Gormisky, M. C. White, *J. Am.*

- Chem. Soc.* **2013**, *135*, 14052; (c) O. Cussó, I. Garcia-Bosch, X. Ribas, J. Lloret-Fillol, M. Costas, *J. Am. Chem. Soc.* **2013**, *135*, 14871; (d) R. Mas-Balleste, L., Jr. Que, *J. Am. Chem. Soc.* **2007**, *129*, 15964.
2. (a) J. Qin, Z. Zhou, T. Cui, M. Hemming, E. Meggers, *Chem. Sci.* **2019**, *10*, 3202; (b) Z. Zhou, S. Chen, J. Qin, X. Nie, X. Zheng, K. Harms, R. Riedel, K. N. Houk, E. Meggers, *Angew. Chem. Int. Ed.* **2019**, *58*, 1088; (c) Z. Zhou, S. Chen, Y. Hong, E. Winterling, Y. Tan, M. Hemming, K. Harms, K. N. Houk, E. Meggers, *J. Am. Chem. Soc.* **2019**, *141*, 19048; (d) Z. Zhou, Y. Tan, T. Yamahira, S. Ivlev, X. Xie, R. Riedel, M. Hemming, M. Kimura, E. Meggers, *Chem* **2020**, *6*, 2024; (e) Y. Tan, S. Chen, Z. Zhou, Y. Hong, S. Ivlev, K. N. Houk, E. Meggers, *Angew Chem Int Ed.* **2020**, *59*, 21706; (f) Y. Tan, F. Han, M. Hemming, J. Wang, K. Harms, X. Xie, E. Meggers, *Org Lett*, **2020**, *22*, 6653; (g) Z. Zhou, Y. Tan, X. Shen, S. Ivlev, E. Meggers, *Sci. China Chem.* **2021**, *64*, 452.
3. S. Mina F, S. K. Ayer, J. L. Roizen, *J. Org. Chem.* **2018**, *83*, 5072.
4. M. Mainak, O. Cusso, S. S. Bhat, M.-Z. Sun, M. Cianfanelli, M. Costas, E. Nordlander, *Dalton Trans.* **2019**, *48*, 6123.

2.2 Asymmetric Amination of Secondary C-H Bonds Catalyzed by Chiral N4 Iron Catalysts

2.1.1 Research Background and Reaction Design

Asymmetric C-H bond amination via nitrene insertion is an attractive method for the synthesis of nitrogen-containing chiral organic compounds.¹ This method allows the direct installation of amino groups into the molecular backbone, avoiding tedious multi-step functional group conversions. Due to the high activity of free nitrene,² there may be problems of low selectivity and low yield when used directly for synthesis. Thus, the feasibility of efficient C-H bond amination via nitrene insertion often relies on the use of metal catalysts to mediate a nitrene transfer process by which metal-bound nitrene species can be generated, rather than free nitrene, and as a reactive intermediate to facilitate functionalization of C-H bonds. The exploration of metallic catalysts for C-H bond amination has led to the development of efficient rhodium-, ruthenium-, cobalt-, and copper-based metal catalysts with high regioselectivity for metal-catalyzed C-H bond amination. With which metal-catalyzed C-H bond amination reactions with high regio- and stereo-selectivity have been achieved.³ Following this progress, there has also been strong interest in developing chiral iron catalysts for the amination of C-H bonds, since the earth-abundance and biocompatibility characteristics of iron make iron complexes ideal candidates for economical and environmentally friendly catalysts.⁴ Moreover, iron, as a typical 3d metal, forms versatile complexes that show useful reactivity of bond-cleavage and -formation, e.g. oxidative addition, reductive elimination, σ -bond metathesis, single-electron transfer, and group-transfer.⁵

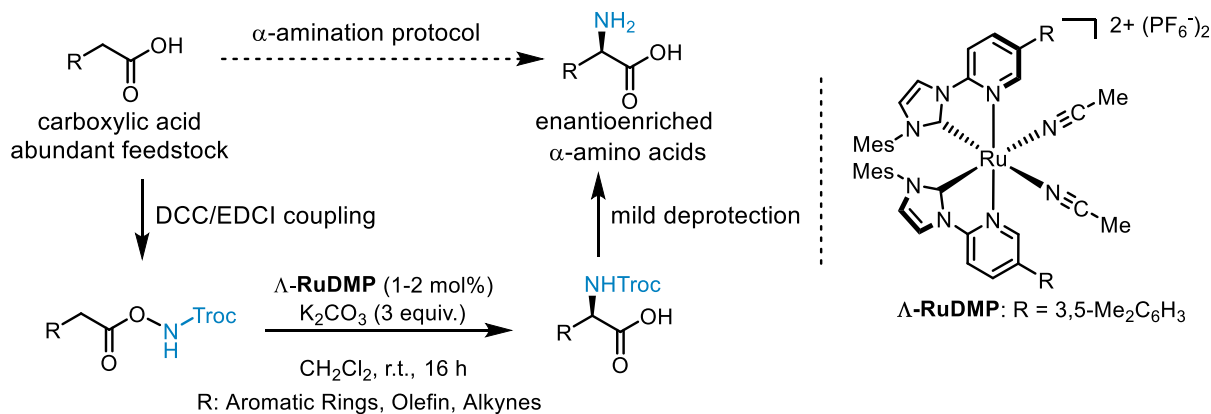
Previously, Chen-Xi Ye, a PhD student in the Meggers group, developed a ruthenium-catalyzed enantioselective synthesis of chiral α -amino acids by nitrene C(sp³)-H insertion (**Figure 36**).⁶ The method is based on a unique stereocontrolled 1,3-nitrogen shift from one carboxylic acid oxygen to the α -carbon. Although chiral-at-ruthenium catalysts can catalyze this type of reaction and obtain a wide variety of aryl, alkenyl, and alkynyl substituted amino acids with good yield and good ee value, more challenging alkyl substrates C-H cannot provide good results. On the other hand, in addition to ruthenium catalysts, we have also been pursuing cheaper and more efficient iron catalysts. Although a range of work has been reported on the activation of alkyl C-H bonds,⁷ iron-catalyzed activation of asymmetric alkyl C-H remains a highly desirable direction worthy of further investigation.

a.) Desirable features for enantioselective C-H functionalization methods

- (1) Avoiding noble metals
- (2) Cheap, nontoxic and easy available catalyst
- (3) Functionalization of non-activated C(sp³)-H bonds

b.) Developed by Meggers group

Chenxi's work



c.) This work: Efficient enantioselective C-H amination with simple N4 iron catalyst

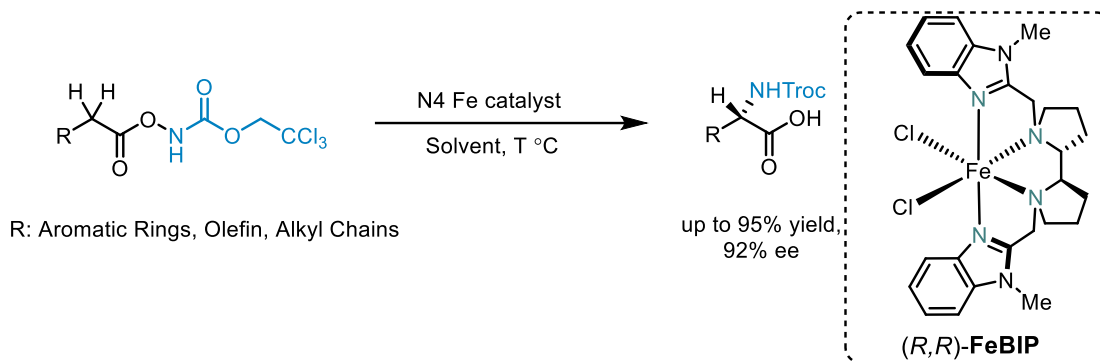


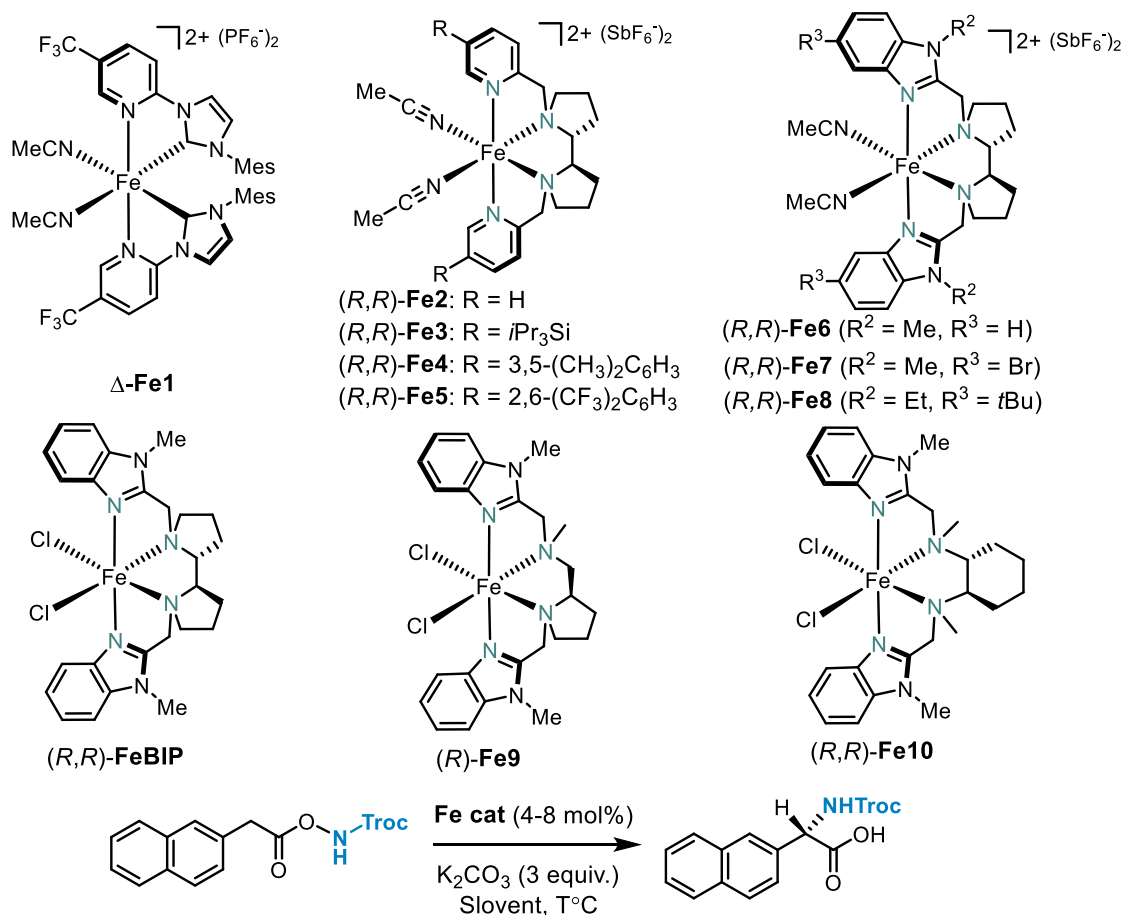
Figure 36. Previous reports and this design for asymmetric amination by N₄ iron catalysis.

2.1.2 Initial Experiments and Reaction Development

We commenced our study with readily available 2-naphthaleneacetic acid which was subjected to a dicyclohexylcarbodiimid (DCC)-coupling with 2,2,2-trichloroethoxycarbonyl (Troc)-N-protected hydroxylamine (TrocNHOH) to provide the azanyl ester **1a**. The azanyl ester **1a** was used as a model substrate for an iron-catalyzed asymmetric amination of secondary C-H bonds.

We firstly investigated the catalytic properties of the chiral-at-iron complex **Fe1**⁸ which was synthesized by our former group member Yubiao Hong and found that **Fe1** displayed low catalytic activity for the secondary C-H amidation of azanyl ester **2a**. And when we tested the activity of **Fe2**, we were surprised to find that it could catalyse the reaction and give 99% of the product, although the ee was only 11%. In order to further improve the chiral purity of the products, the iron complexes **Fe3-Fe5** with different substituents were screened. Although high yields were obtained from 95% to 97%, ee did not improve much, in the range of 14% to 45%. Revealingly, when we replaced the pyridyl with N-methylbenzimidazole moieties **Fe6**, the Troc-protected amino acid (*S*)-**2a** was obtained

in 95% yield with 82% ee (entry 5), and we also tried substituted N-methylbenzimidazole moieties **Fe7-Fe8**, which can provide (*S*)-**1a** in 90% yield with 74% ee and 93% yield with 59% ee, respectively. Interestingly, the bis-benzimidazole complex (*R,R*)-**FeBIP**, in which chlorides are used as labile monodentate ligands instead of the much more common acetonitriles or triflates, afforded further improved results with 96% yield and with 81% ee (entry 7). Exchanging the 2,2'-bipyrrolidine backbone with proline-derived 2-pyrrolidinemethaneamine ((*R*)-**Fe9**) or cyclohexane-1,2-diamine ((*R,R*)-**Fe10**) provided inferior results (entries 10 and 11), thus revealing the advantage of using a rigidified chiral backbone. And we also screened different solvents, such as DCE and TCE. When the solvent is TCE, the desired product (*S*)-**2a** was provided in 91% yield with 83% ee. In addition, when the reaction temperature was decreased to 0 °C, we were able to obtain (*S*)-**2a** 93% yield and 89% ee after 40 hours of reaction. Finally, we increased the amount of catalyst from 4 mol% to 8 mol% and obtained (*S*)-**2a** in 96% yield with 90% ee.

Table 1. Initial experiments and optimization.^a

Entry	Catalyst	Cat. Loading (mol%)	Solvent	T (°C)	t (h)	Yield (%) ^b	ee (%) ^c
1	Δ -Fe1	4	DCM	rt	16	trace	N.D.
2	(R,R) -Fe2	4	DCM	rt	16	99	11
3	(R,R) -Fe3	4	DCM	rt	16	95	14
4	(R,R) -Fe4	4	DCM	rt	16	96	45
5	(R,R) -Fe5	4	DCM	rt	16	97	15
6	(R,R) -Fe6	4	DCM	rt	16	95	82
7	(R,R) -Fe7	4	DCM	rt	16	90	74
8	(R,R) -Fe8	4	DCM	rt	16	93	59
9	(R,R) -FeBIP	4	DCM	rt	16	96	81
10	(R) -Fe9	4	DCM	rt	16	95	80
11	(R,R) -Fe10	4	DCM	rt	16	94	68
12	(R,R) -FeBIP	4	DCE	rt	16	89	81
13	(R,R) -FeBIP	4	TCE	rt	16	91	83
14	(R,R) -FeBIP	4	TCE	0	40	93	89
15	(R,R) -FeBIP	8	TCE	0	40	96	90

[a] All reactions were performed with 0.1 mmol of substrate **1a** in solvent (1.0 mL) under an atmosphere of nitrogen. [b] All yields refer to isolated products after column chromatography. [c] Enantiomeric excess determined by HPLC analysis of the isolated products on a chiral stationary phase.

2.1.3 Substrate Scope

With the optimized catalyst and reaction conditions in hand, we performed a substrate scope. we screened substrates for this reaction. The phenyl substrates were well tolerated and provided a 95% yield with 91% ee (**2b**). Electron-withdrawing trifluoromethyl in the para-position of phenyl moiety provided 72% yield with 92% ee (**2c**). An electron-donating methoxy group in the para-position of the phenyl moiety gave a 95% yield with 90% ee (**2d**). The substrate with phenyl allylic C-H afforded reduced yield and ee value. Replacing the phenyl allylic moiety with phenyl propargylic provided a lower yield and ee value. We think this is because the alkyne group may be coordinated with iron. It is worth noting that our chiral iron catalysts can also catalyze when confronted with the more challenging C-H bonds. Substrates with primary (**2g-2n**), secondary (**2o**), and tertiary (**2p**) aliphatic side chains underwent amination in 48-75% yield and with 85-92% ee. The method is also suitable for the late-stage amination of more complex molecules. Azanyl ester formation followed by iron-catalyzed stereocontrolled 1,3-nitrogen shift converted lithocholic acid to amino acid **2q** (77% yield, 23:1 dr).

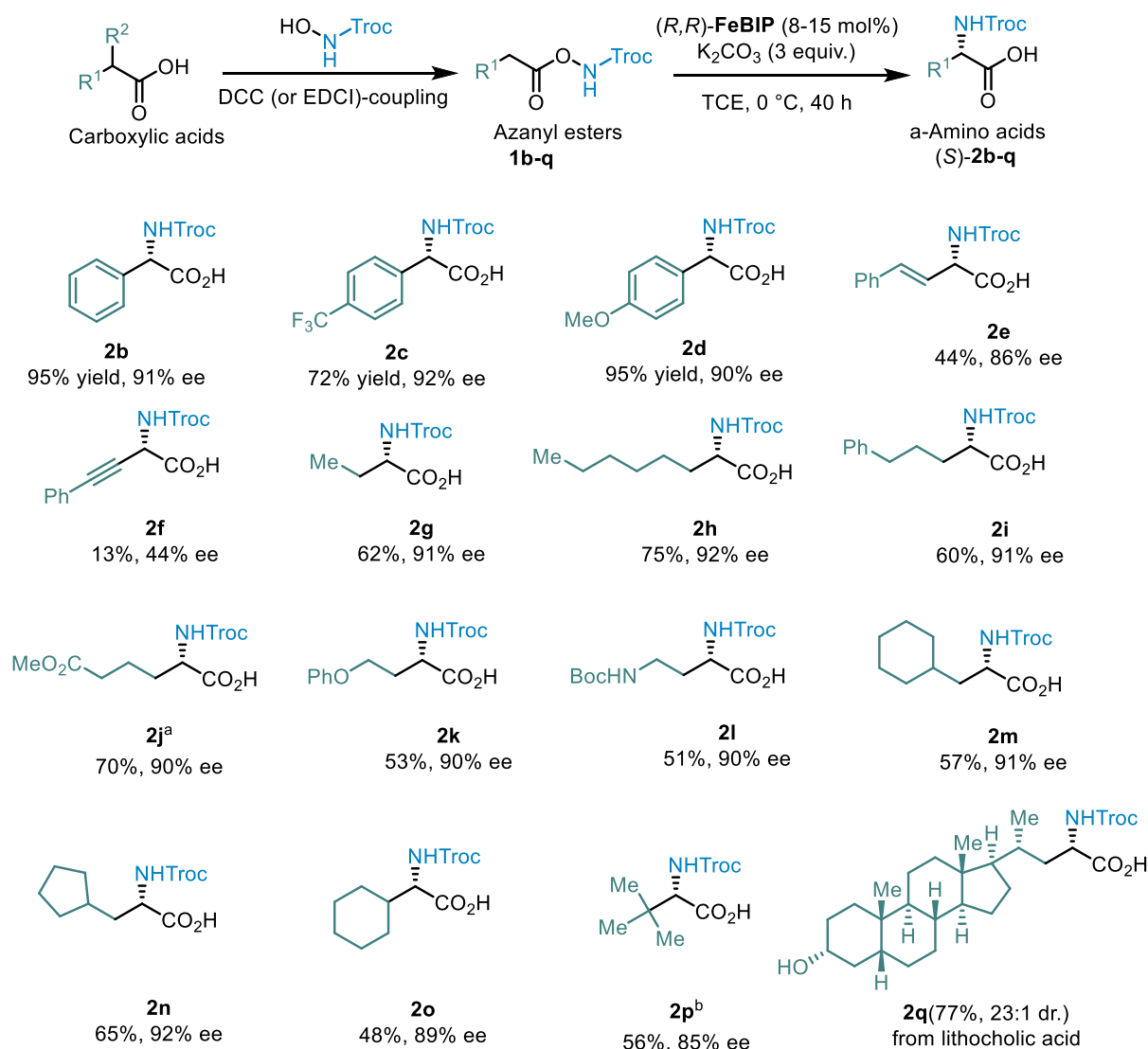


Figure 37. Reaction conditions: reactions were carried out with (*R,R*)-FeBIP (8-15 mol%), K₂CO₃ (3 equiv.) and 1,1,2,2-tetrachloroethane (TCE, 0.1 M) at 0 °C for 40 h. Enantiomeric excess (ee) values were determined by HPLC analysis (see Supplementary Information section 5 for full details). ^aIsolated after conversion to the methyl ester. ^bReaction performed at room temperature (25 °C) for 16 h.

2.1.4 Mechanism Proposal

A simplified mechanism proposal based on the DFT calculations and control experiments of ruthenium discussed before⁶ is shown in **Figure 38**. The azanyl ester substrate is first activated by N–O cleavage to provide intermediate **A** (corresponding to intermediate **IV** in **Figure 38**) after deprotonation. A subsequent hydrogen atom transfer then affords the diradical **B** (corresponding to intermediate **V** in **Figure 38**), followed by a rapid radical rebound to yield the chelate complex **C** (corresponding to intermediate **VI** in **Figure 38**). Protonation of the carboxylate induces product dissociation and concludes the catalytic cycle. The net result of the N–O bond fragmentation and subsequent stepwise C–H insertion is an asymmetric 1,3-nitrogen shift to provide non-racemic chiral α-amino acids.

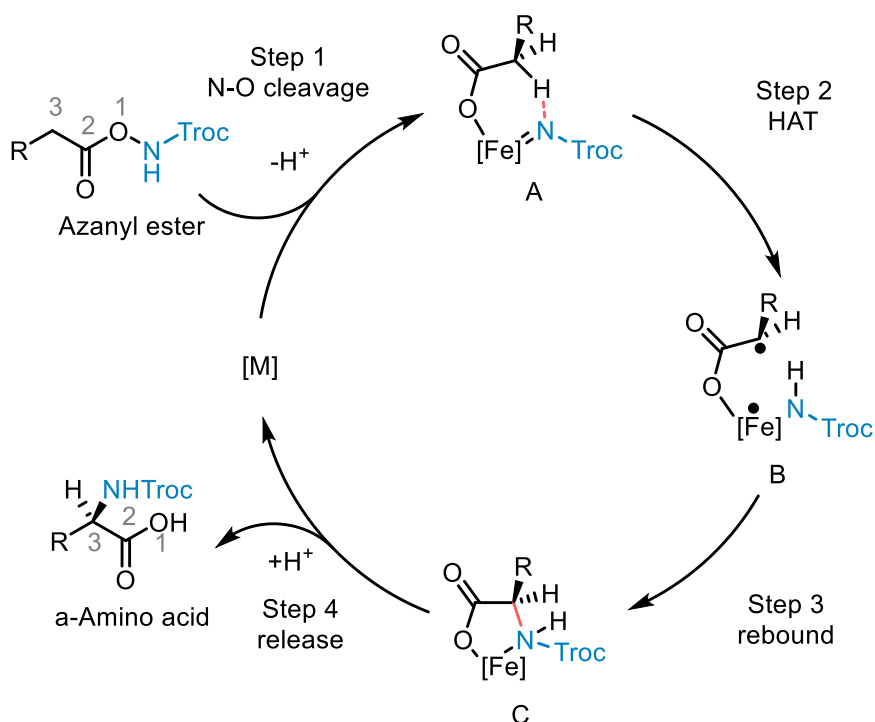


Figure 38. Proposed mechanism.

2.1.5 Conclusions

In conclusion, based on the previously work of our group, we reported the catalytic enantioselective synthesis of chiral α -amino acids by chiral N4 iron catalyzed nitrene $C(sp^3)$ -H insertion. Chiral N4 iron catalysis provided a good scope, enabling rapid access to optically active α -amino acids with aryl, allyl, and non-activated alkyl side chains. The good functional group tolerance of this method also permits the enantioselective late-stage amination of carboxylic acid-containing drugs and natural products. The Troc-protected amino acids obtained through this protocol can be used directly in synthesis with the Troc group being selectively removable under mild conditions via a reductive Grob fragmentation.⁹ This strategy will expedite the synthesis of unnatural α -amino acids, which are important building blocks of peptidomimetic drugs, as well as engineered proteins and enzymes with modulated properties.¹⁰

References

- (a) *Amino Group Chemistry – From Synthesis to the Life Sciences*, Ed.: Ricci, A., Wiley-VCH, Weinheim, **2008**; (b) *Modern Amination Methods*, Ed.: A. Ricci, Wiley-VCH, Weinheim, **2000**; (c) E. Tosi, R. M. de Figueiredo, J. M. Campagne, *Catalysts* **2021**, *11*; (d) M. Ju, J. M. Schomaker, *Nat. Rev. Chem.* **2021**, *5*, 580.
- (a) *Nitrenes*, Ed.: W. Lwowski, Interscience, New York, **1970**; (b) *Reactive Intermediates*, Ed.: C. Wentrup, Wiley, New York, **1984**.
- (a) P. Muller, C. Fruit, *Chem. Rev.* **2003**, *103*, 2905; (b) H. M. L. Davies, J. R. Manning, *Nature* **2008**, *451*, 417; (c) M. M. Diaz-Requejo, P. J. Perez, *Chem. Rev.* **2008**, *108*, 3379; (d) T. G.

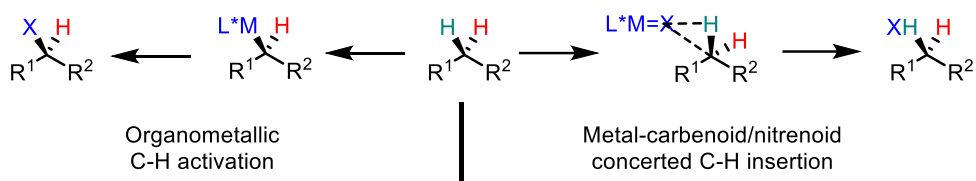
- Driver, *Org. Biomol. Chem.* **2010**, *8*, 3831; (e) R. T. Gephart, T. H. Warren, *Organometallics* **2012**, *31*, 7728; (f) J. L. Roizen, M. E. Harvey, Du Bois, J. *Acc. Chem. Res.* **2012**, *45*, 911; (g) Xiong, T.; Zhang, Q. *Chem. Soc. Rev.* **2016**, *45*, 3069; (h) B. Darses, R. Rodrigues, L. Neuville, M. Mazurais, P. Dauban, *Chem. Commun.* **2017**, *53*, 493; (i) C.J. Yang, C. Zhang, Q.-S. Gu, J.-H. Fang, X.-L. Su, L. Ye, Y. Sun, Y. Tian, Z.-L. Li, X.-Y. Liu, *Nat. Catal.* **2020**, *3*, 539.
- (a) J. W. Morgan, E. Anders, *Proc. Natl. Acad. Sci.* **1980**, *77*, 6973; (b) G. Papanikolaou, K. Pantopoulos, *Toxicol. Appl. Pharmacol.* **2005**, *202*, 199; (c) P. A. Frey, G. H. Reed, *ACS Chem. Biol.* **2012**, *7*, 1477; (d) A. C. Dlouhy, C. E. Outten, In *Metallomics and the Cell*, Guest Ed.: L. Banci, Vol. 12 of “Metal Ions in Life Sciences”, Eds. Series: A. Sigel, H. Sigel, R. K. O. Sigel, Springer Science and Business Media B. V, Dordrecht, Netherlands, **2013**, pp. 241.
 - (a) J. W. Morgan, E. Anders, *Proc. Natl. Acad. Sci.* **1980**, *77*, 6973; (b) G. Papanikolaou, K. Pantopoulos, *Toxicol. Appl. Pharmacol.* **2005**, *202*, 199; (c) P. A. Frey, G. H. Reed, *ACS Chem. Biol.* **2012**, *7*, 1477; (d) A. C. Dlouhy, C. E. Outten, In *Metallomics and the Cell*, Guest Ed.: L. Banci, Vol. 12 of “Metal Ions in Life Sciences”, Eds. Series: A. Sigel, H. Sigel, R. K. O. Sigel, Springer Science and Business Media B. V, Dordrecht, Netherlands, **2013**, pp. 241.
 - C.-X. Ye, X. Shen, S.-M. Chen, E. Meggers, *Nat. Chem.* **2022** accepted for publication.
 - J. He, M. Wasa, K. S. L. Chan, Q. Shao, J. Q. Yu, *Chem. Rev.* **2017**, *117*, 8754.
 - Y. Hong, L. Jarrige, K. Harms, E. Meggers, *J. Am. Chem. Soc.* **2019**, *141*, 4569.
 - A. Isidro-Llobet, M. Álvarez, F. Albericio, *Chem. Rev.* **2009**, *109*, 2455.
 - (a) M. A. T. Blaskovich, *J. Med. Chem.* **2016**, *59*, 10807; (b) F. Agostini, J. S. Völler, B. Kokschi, C. G. Acevedo-Rocha, V. Kubyshkin, N. Budisa, *Angew. Chem. Int. Ed.* **2017**, *56*, 9680; (c) I. Drienovská, G. Roelfes, *Nat. Catal.* **2020**, *3*, 193.

2.3 Enantioconvergent Tertiary C-H Bonds Amination Catalyzed by Chiral N4 Iron Catalysts

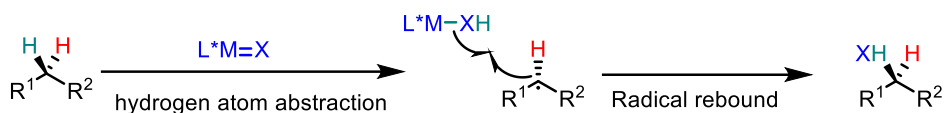
2.3.1 Research Background and Reaction Design

Direct asymmetric transformations of racemic tertiary C(sp³)-H bonds (pK_a>25)¹ remain a challenging area, particularly for enantioconvergent ones theoretically leading to highly enantioenriched products in 100% yield,² although enantioconvergent substitution reactions of racemic tertiary alkyl electrophiles are emerging as a powerful synthetic strategy to access quaternary stereocentres.³ In this regard, Arnold et al. achieved the first highly enantioconvergent tertiary C-H amination process using enzymatic catalysis.⁴ There have also been successive reports of work on enantiomeric convergent amination by Liu et al.⁵ and Peter Zhang et al.⁶ The issue for the lagging development of such a procedure stems mostly from the mechanistic constraint inherent in earlier enantioselective C-H functionalization methods: partial or total chirality retention (**Figure 39C**). Specifically, C-H activation catalysed by a transition metal and coordinated metal-carbenoid/nitrenoid C-H insertion have only achieved stereospecific conversions (**Figure 39A**),^{7,8} whereas hydroxylation by metal oxo species⁹ is hindered by partial or complete chirality retention (**Figure 39B**).¹⁰ As a result, these solutions are often more suited to kinetic resolution, which provides at best a 50% yield (**Figure 39C**, left). The explanation for chirality retention in non-constrained settings stems from the typically quick radical rebound (RR) step, which appears to be kinetically connected to the initial hydrogen atom abstraction (HAA) step. As a result, the resultant C-H functionalization products inherit chirality to varying degrees (**Figure 39B**).^{10c,10d} As a result, the commonly accepted transition-metal-catalyzed enantioselective C-H functionalization methods appear to limit efficient enantioconvergent conversions of racemic tertiary C(sp³)-H bonds (**Figure 39C**).

A. Organometallic C-H activation and metal-carbenoid/nitrenoid concerted C-H insertion



B. Metal-oxo/carbenoid/nitrenoid/stepwise C-H insertion



C. Challenge for enantioconvergent functionalization of tertiary aliphatic C-H

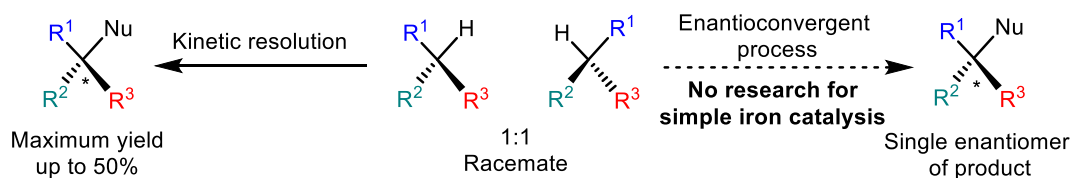


Figure 39. Design of catalytic enantioconvergent tertiary C (sp^3)-H functionalization. An Organometallic C–H activation and metal-carbenoid/nitrenoid concerted C–H insertion lead to stereospecific functionalization. B, Coupled HAA and radical rebound for metal-oxo-mediated C–H functionalization and stepwise metal-carbenoid/ nitrenoid C–H insertion tend to result in partial or complete chirality retention due to the commonly fast radical rebound. C, Reported C–H functionalization catalysed by a transition metal is amenable only to kinetic resolution, but not yet to enantioconvergent transformations, due to the chirality retention problem.

Seeking to address this challenge, we became interested in developing new methods with chiral N4 iron catalysis to provide a general platform for enantioconvergent reactions of racemic tertiary C(sp^3)-H bonds. Previously, we reported a stereocontrolled 1,3-nitrogen rearrangement via 1,3-migratory nitrene insertion as a strategy for highly regioselective and stereoselective C(sp^3)-H aminations to access chiral α -amino acids. Here we now report an application of this stereocontrolled 1,3-nitrogen migration to the iron-catalyzed ¹¹ enantioconvergent synthesis of α,α -disubstituted α -amino acids from racemic α -branched carboxylic acid feedstock molecules in two steps (**Figure 40**).

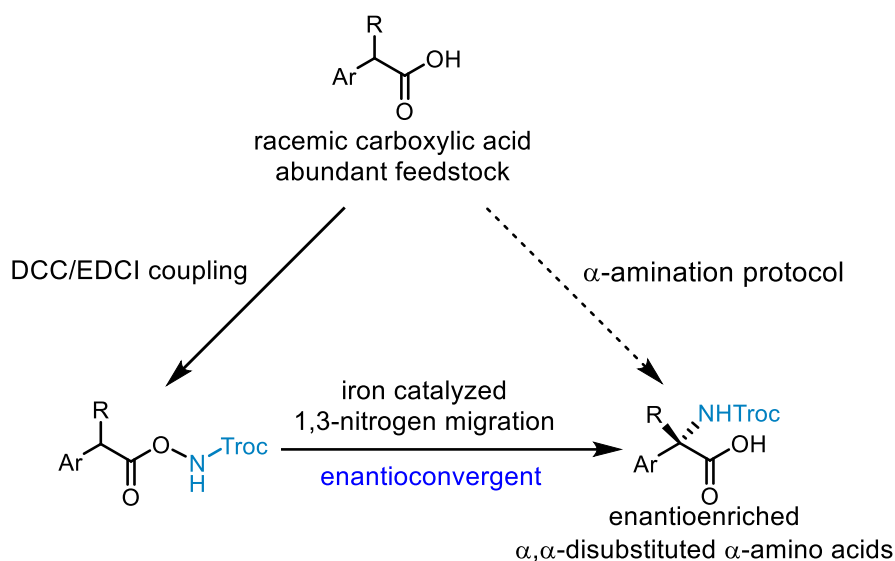


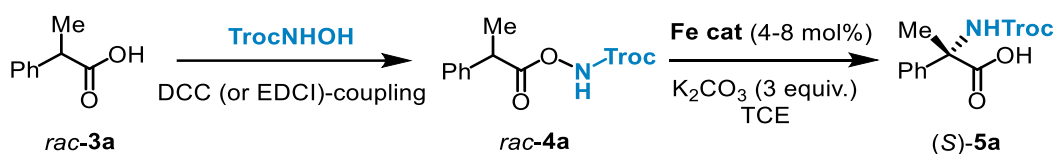
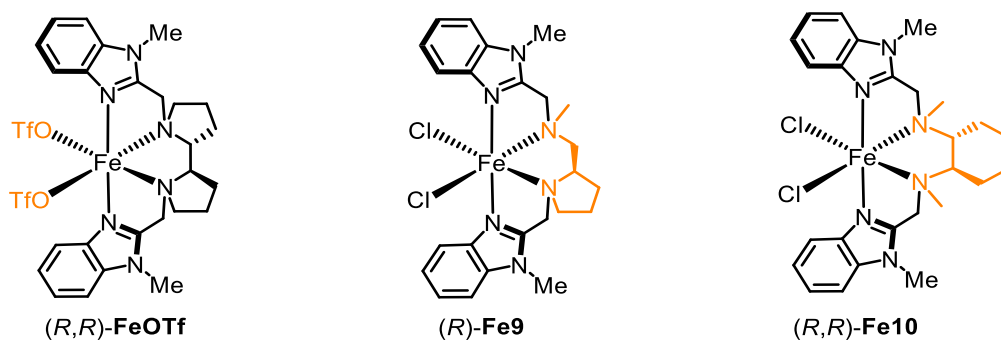
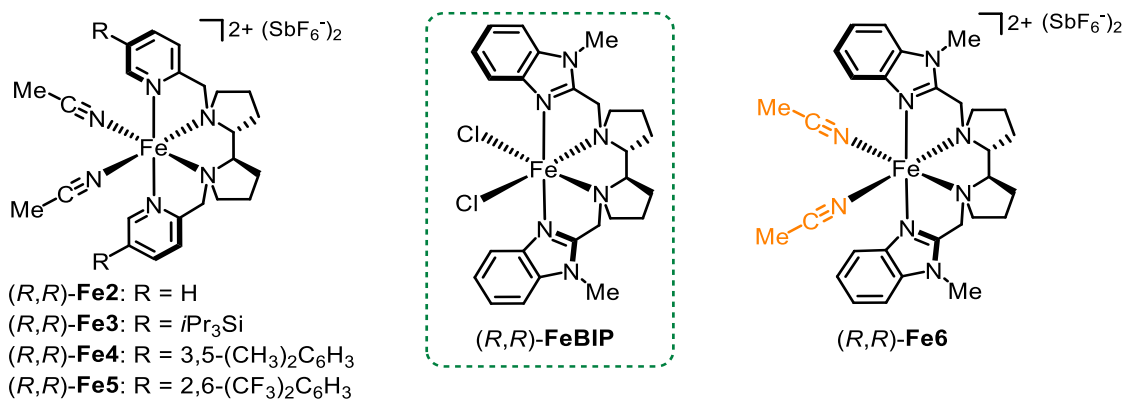
Figure 40. Iron-catalyzed enantioconvergent synthesis of α,α -disubstituted α -amino acids by 1,3-nitrogen migration.

2.3.2 Initial Experiments and Reaction Development

Initial experiments and optimization. We commenced our study with readily available racemic 2-phenylpropionic acid (*rac*-**3a**) which was subjected to a dicyclohexylcarbodiimid (DCC)-coupling with 2,2,2-trichloroethoxycarbonyl (Troc)-N-protected hydroxylamine (TrocNHOH) to provide the racemic azanyl ester *rac*-**4a**. The azanyl ester *rac*-**4a** was used as a model substrate for an iron-catalyzed enantioconvergent 1,3-nitrogen migration.

We firstly investigated the catalytic properties of the **Fe2**. In the presence of K_2CO_3 (3 equivalents), *rac*-**4a** was converted to the Troc-protected amino acid (*S*)-**5a** after 18 hours at room temperature in only 63% yield and with disappointing 22% ee (Table 1, entry 1). In order to further improve the chiral purity of the products, the iron complexes **Fe3-Fe5** were screened. the yields were obtained from 17% to 30%, ee did not improve much, in the range of 21% to 30%. (entries 2-4). Revealingly, when we tested iron complex (*R,R*)-**Fe6**, the Troc-protected amino acid (*S*)-**5a** was obtained in 94% yield with 76% ee (entry 5). Replacing the MeCN ligands with triflate anions, deriving at iron complex (*R,R*)-**FeOTf**,¹² a slightly improved yield and enantioselectivity were observed (entry 6). Interestingly, the bis-benzimidazole complex (*R,R*)-**FeBIP**, afforded further improved results with 96% yield and with 79% ee (entry 7). ((*R*)-**Fe8**) and ((*R,R*)-**Fe9**) provided inferior results (entries 8 and 9). Finally, we investigated the influence of temperature on the enantioselectivity of the 1,3-nitrogen migration with (*R,R*)-**FeBIP** for which the catalyst loading was increased to 8 mol% to counterbalance the reduced reaction rate. Accordingly, at 0 °C and -10 °C the

enantioselectivity increased to 83% and 84% ee, respectively (entries 10 and 11). For further studies, 0 °C was chosen as the optimal reaction temperature with a compromise out of reaction rate and enantioselectivity. In summary, we developed a chiral N4 iron catalyzed enantioconvergent conversion of the racemic azanyl ester *rac*-**4a** to enantioenriched α -amino acid (*S*)-**5a**.

Table 2. Initial experiments and optimization.^a

Entry	Catalyst	Cat. Loading (mol%)	T (°C)	Time (h)	Yield (%) ^b	ee (%) ^c
1	(<i>R,R</i>)- Fe2	4	rt	18	63	22
2	(<i>R,R</i>)- Fe3	4	rt	18	70	30
3	(<i>R,R</i>)- Fe4	4	rt	18	61	25
4	(<i>R,R</i>)- Fe5	4	rt	18	17	21
5	(<i>R,R</i>)- Fe6	4	rt	18	94	76
6	(<i>R,R</i>)- FeOTf	4	rt	18	95	77
7	(<i>R,R</i>)- FeBIP	4	rt	18	96	79
8	(<i>R</i>)- Fe9	4	rt	18	97	76
9	(<i>R,R</i>)- Fe10	4	rt	18	85	65
10	(<i>R,R</i>)- FeBIP	8	0	40	91	83
11	(<i>R,R</i>)- FeBIP	8	-10	40	89	84

[a] All reactions were performed with 0.1 mmol of racemic substrate **3a** in 1,1,2,2-tetrachloroethane (TCE) (1.0 mL) under an atmosphere of nitrogen. [b] All yields refer to isolated products after column chromatography. [c] Enantiomeric excess determined by HPLC analysis of the isolated products on a chiral stationary phase.

2.3.3 Substrate Scope

Having favorable reaction conditions identified, we next investigated the scope for this enantioconvergent C(sp³)-H amination (**Figure 41**). Starting from the initial 2-phenylpropionic acid azanyl ester substrate **4a**, we found that substituents in the para-position of the phenyl moiety are well tolerated, including alkyl groups (methyl, tert-butyl, isobutyl), electron-withdrawing substituents (F, Cl, Br, CF₃), and a methylsulfide, providing the α,α -disubstituted α -amino acids **5b-5i** in 62-96% yield and with satisfactory 80-87% ee. A para-methoxy substituent is an exception and afforded the α -amino acid **5j** in 97% yield and with a reduced 56% ee. Instead, a phenoxy substituent in meta-position of the phenyl moiety provided better results with 82% yield and 77% ee (**5k**). Likewise, a benzoyl substituent in meta-position afforded α -amino acid **5l** with 85% yield and 82% ee. Two substituents in the phenyl ring were also well accommodated as demonstrated for the α -amino acids **5n-5p** (63-76% yield, 68-83% ee). Replacing the phenyl moiety with a 2-naphthyl group provided the α -amino acid **5q** in 90% yield and with 84% ee. On a larger scale (1.0 mmol), the naphthyl α -amino acid **5q** was obtained in 88% yield and with 79% ee. The enantiomeric excess could be increased to 99% ee with a single recrystallization. Introducing a methoxy substituent into the 2-naphthyl moiety provided the α -amino acid **5r** with excellent 99% yield but just 64% ee, thus reinforcing that electron-donating groups reduce the enantioselectivity. Heteroaromatic moieties in the α -position are also suitable for the new method, including a thiophene (**5s**, 94% yield, 83% ee) and a quinoline (**5t**, 86% yield, 70% ee). However, the carbazole-containing α -amino acid **5u** was only isolated in 26% yield with 72% ee. Next, we evaluated the replacement of the methyl substituent in 2-phenylpropionic acid azanyl ester **4a** with other alkyl groups. Accordingly, replacing the methyl with an ethyl, *n*-propyl, or *n*-hexyl group provided the respective α,α -disubstituted α -amino acids **25-27** in 85-91% yield and with 82-83% ee. Secondary alkyl groups are also enabled for this method. For example, α -amino acids with isopropyl (**5y**), cyclopentyl (**5z**), or cyclohexyl (**5za**) groups were obtained in 44-88% yield and 82-88% ee. The tetrahydronaphthalene α -amino acid **5zb** was provided in 56% yield and with 68% ee, while the steroid-functionalized α -amino acid **5zc** was afforded in 41% yield and with 90:10 dr. The products **5zd** and **5ze** reveal an important limitation for the introduced method, namely that an aromatic moiety in α -position is a requirement for obtaining a significant enantiomeric excess in the course of the 1,3-nitrogen migration. Finally, it is worth noting that the enantiopurities of the Troc-protected α,α -disubstituted α -amino acids can be increased by simple crystallization. For

example, when the iron-catalyzed 1,3-nitrogen migration was executed on a 1 mmol scale and followed by a crystallization step in EtOAc/*n*-hexane, the amino acids **5d**, **5n** and **5q** were obtained in yields of 53%, 63% and 64% over the two steps, respectively, and all with 99% ee.

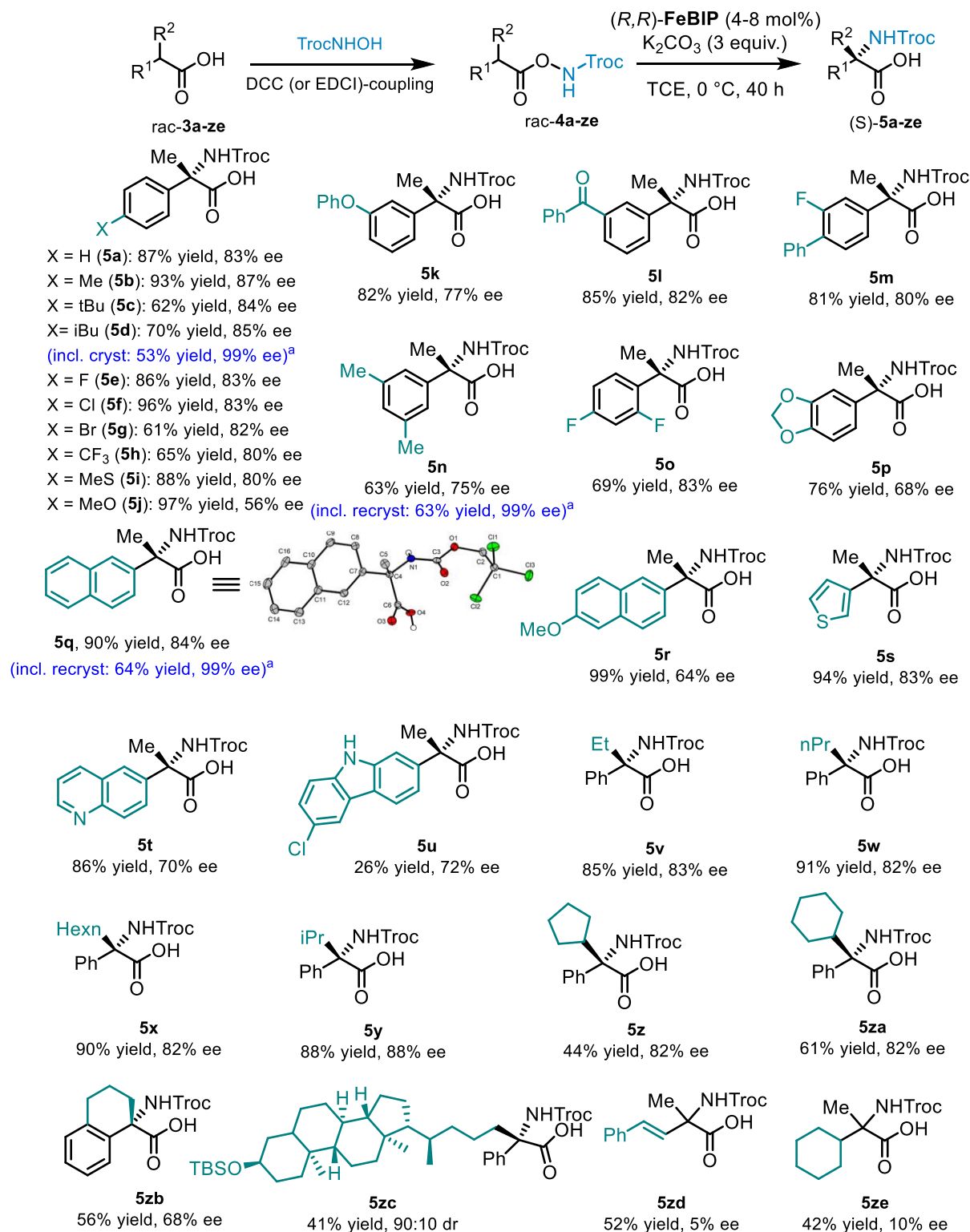


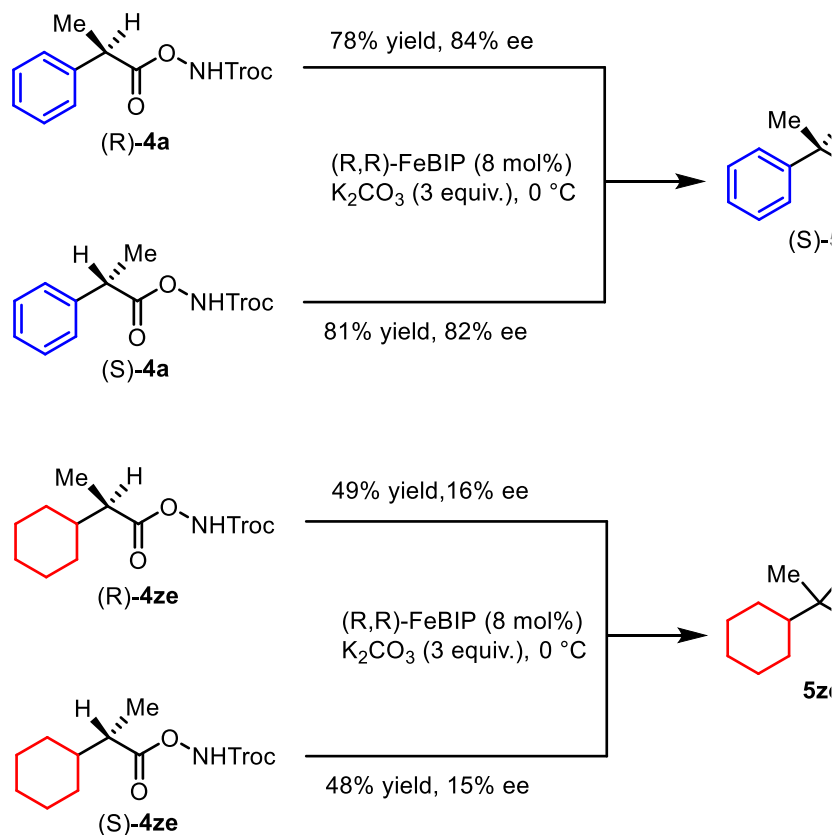
Figure 41. Substrate scope. Standard conditions: Racemic substrates (0.20 mmol), catalyst (8.0 mol%) and K₂CO₃ (0.6 mmol) in 1,1,2,2-tetrachloroethane (2.0 ml) under argon at 0 °C for 40 h. Isolated yields

are shown. ^a Increased scale with 1.0 mmol of the substrate.

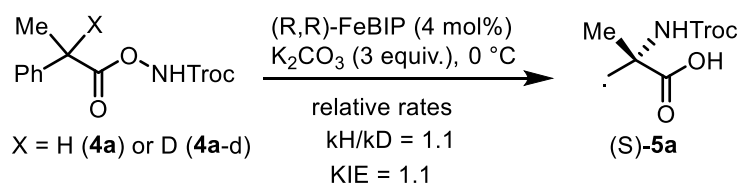
2.3.4 Additional Experiments

To obtain insight into the stereodiscriminating step, the azanyl esters (*R*)-**4a** and (*S*)-**4a**, derived from (*R*)- or (*S*)-2-phenylpropionic acid, respectively, were used as enantiomerically pure substrates instead of their racemate (**Figure 42a**). Using our standard reaction conditions, (*S*)-**5a** was formed with almost identical yields and ee values irrespective of starting from *R*-configured, *S*-configured, or racemic substrate, suggesting a radical mechanism in which the final C-N bond formation must be the stereodetermining step. Interestingly, when we instead performed the iron-catalyzed 1,3-nitrogen migration with the azanyl ester **4ze**, in which the phenyl moiety of substrate **4a** is replaced with a cyclohexyl moiety, almost racemic amino acid **5ze** was obtained, regardless of whether the reaction was performed with racemic, *R*- or *S*-configured substrate **4ze**. These experiments provide insight into the requirement of the aromatic moiety in α -position for achieving enantioconvergence, which is apparently not associated with a stabilization of the intermediate radical but rather the asymmetric induction itself. A kinetic isotope effect (KIE) of 1.1 also reveals that the C-H bond cleavage is not the rate-determining step in the catalytic cycle (**Figure 42b**). Finally, it is worth noting that this enantioconvergent C(sp³)-H amination to access enantiomerically enriched α,α -disubstituted α -amino acids are not suitable for chiral-at-ruthenium catalysts, which were demonstrated to be suitable for accessing α -monosubstituted α -amino acids by nitrene-mediated 1,3-nitrogen migration (**Figure 42c**).

a) Conversion of enantiomerically pure substrates



b) Kinetic isotope effect



c) Comparison with Ru-catalyzed 1,3-nitrogen migration

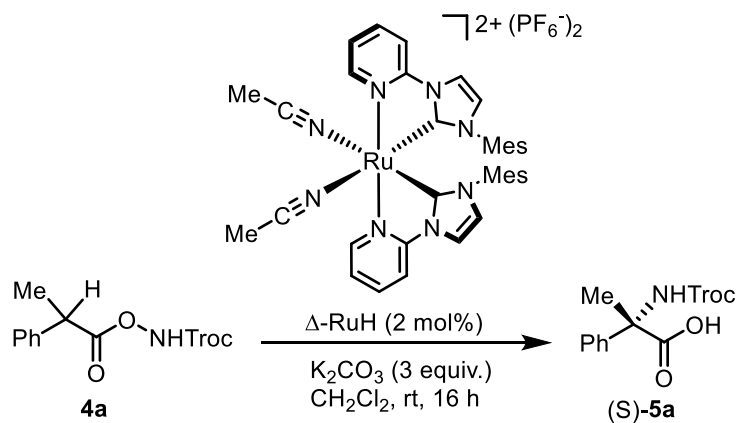


Figure 42. Additional experiments.

2.3.5 Mechanism Proposal

The catalytic cycle starts with a base- and iron-induced heterolytic cleavage of the N-O bond of the racemic azanyl ester to generate a nitrene and carboxylate which are both bound to the same iron center (**Figure 43**, intermediate **I**). Since the azanyl ester substrate is used as a racemic mixture, the iron nitrene intermediate forms as a mixture of the two diastereomers **Ia** and **Ib**. This is followed by hydrogen atom transfer (HAT) from the α -position of the carboxylate to the nitrene, thereby generating the diradical intermediates **IIa** and **IIb**, which have a sufficient long lifetime to be in equilibrium with each other. The subsequent C-N bond formation constitutes the stereodetermining step in the catalytic cycle, generating a single diastereomer **III**. A high stereodiscrimination in this step is only observed with an aryl substituent in α -position and this can be rationalized with a favorable stacking of the aryl group to one benzimidazole moiety in intermediated **IIa** but not **IIb**. Finally, protonation of the carboxylate then induces the dissociation of the amino acid from the iron catalyst and regenerates the iron catalyst for another catalytic cycle.

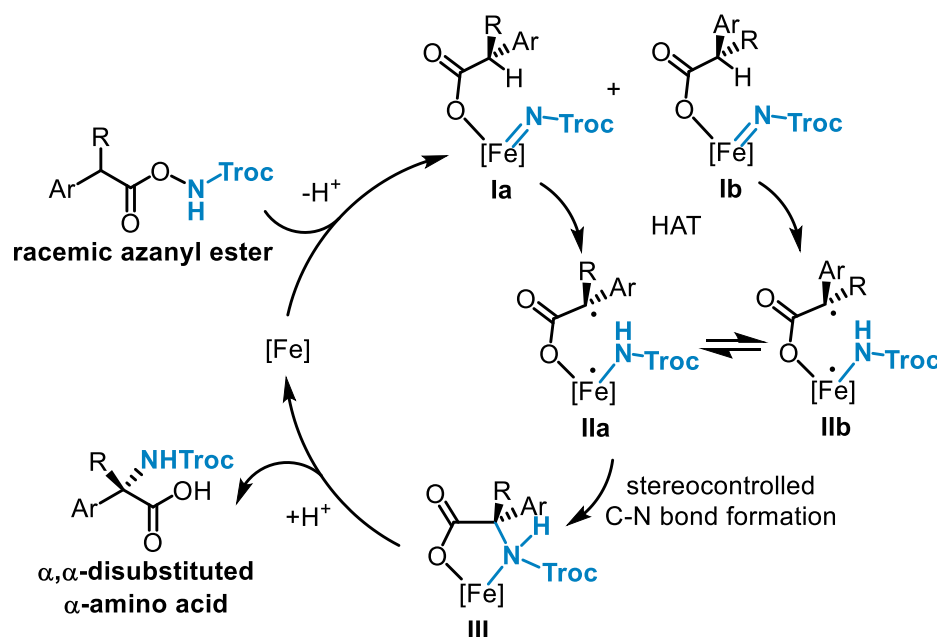


Figure 43. Proposed mechanism.

2.2.6 Conclusions

In summary, we have described a strategy for direct enantioconvergent tertiary $C(sp^3)$ -H amination starting from readily available racemic azanyl esters with a simple chiral N4 iron catalysis. The mechanistic blueprint consisting of sequential HAT and stereocontrolled C-N bond formation.

And the enantioenriched α,α -disubstituted α -amino acids can be provided by this powerful and straightforward method. Some of the products can be obtained as >99% ee by recrystallisation.

References

1. (a) C. G. Newton, S. G. Wang, C. C. Oliveira, N. Cramer, *Chem. Rev.* **2017**, *117*, 8908; (b) T. G. Saint-Denis, R. Y. Zhu, G. Chen, Q. F. Wu, J. Q. Yu, *Science* **2018**, *359*, 4798.
2. (a) V. Bhat, E. R. Welin, X. Guo, B. M. Stoltz, *Chem. Rev.* **2017**, *117*, 4528; (b) J. Choi, G. C. Fu, *Science* **2017**, *356*, 7230.
3. (a) Q. M. Kainz, C. D. Matier, A. Bartoszewicz, S. L. Zultanski, J. C. Peters, G. C. Fu, *Science* **2016**, *351*, 681; (b) A. E. Wendlandt, P. Vangal, E. N. Jacobsen, *Nature* **2018**, *556*, 447; (c) Z. Wang, H. Yin, G. C. Fu, *Nature* **2018**, *563*, 379; (d) X. Zhang, J. Ren, S. M. Tan, D. Tan, R. Lee, C. H. Tan, *Science*, **2019**, *363*, 400.
4. Y. Yang, I. Cho, X. Qi, P. Liu, F. H. Arnold, *Nat. Chem.* **2019**, *11*, 987.
5. C. J. Yang, C. Zhang, Q. S. Gu, J. H. Fang, X. L. Su, L. Ye, Y. Sun, Y. Tian, Z. L. Li, X. Y. Liu, *Nat. Catal.* **2020**, *3*, 539.
6. K. Lang, C. Li, I. Kim, X. P. Zhang, *J. Am. Chem. Soc.* **2020**, *142*, 20902.
7. (a) C. G. Newton, S. G. Wang, C. C. Oliveira, N. Cramer, *Chem. Rev.* **2017**, *117*, 8908; (b) T. G. Saint-Denis, R. Y. Zhu, G. Chen, Q. F. Wu, J. Q. Yu, *Science* **2018**, *359*, 4798.
8. (a) H. M. L. Davies, J. R. Manning, *Nature* **2008**, *451*, 417; (b) C. M. Che, V. K. Y. Lo, C. Y. Zhou, J. S. Huang, *Chem. Soc. Rev.* **2011**, *40*, 1950; (c) J. L. Roizen, M. E. Harvey, J. du Bois, *Acc. Chem. Res.* **2012**, *45*, 911; (d) H. M. L. Davies, K. Liao, *Nat. Rev. Chem.* **2019**, *3*, 347.
9. (a) M. Costas, M. P. Mehn, M. P. Jensen, L. Que, *Chem. Rev.* **2004**, *104*, 939; (b) L. Que, W. B. Tolman, *Nature* **2008**, *455*, 333; (c) O. Giorgio, C. Olaf, C. Miquel, *Chem. Asian J.* **2016**, *11*, 3148; (d) M. Milan, M. Bietti, M. Costas, *Chem. Commun.* **2018**, *54*, 9559; (e) M. C. White, J. Zhao, *J. Am. Chem. Soc.* **2018**, *140*, 13988; (f) W. Sun, Q. Sun, *Acc. Chem. Res.* **2019**, *52*, 2370.
10. (a) H. Lu, X. P. Zhang, *Chem. Soc. Rev.* **2011**, *40*, 1899; (b) J. C. Lewis, P. S. Coelho, F. H. Arnold, *Chem. Soc. Rev.* **2011**, *40*, 2003; (c) M. Milan, M. Bietti, M. Costas, *Chem. Commun.* **2018**, *54*, 9559; (d) Y. Wang, X. Wen, X. Cui, X. P. Zhang, *J. Am. Chem. Soc.* **2018**, *140*, 4792.
11. For reviews on iron-catalyzed C-H aminations, see (a) L. Zhang, L. Deng, *Chin. Sci. Bull.* **2012**, *57*, 2352; (b) S. K. Ghorai, V. G. Gopalsamuthiram, A. M. Jawalekar, R. E. Patre, S. Pal, *Tetrahedron* **2017**, *73*, 1769; (c) P. Wang, L. Deng, *Chin. J. Chem.* **2018**, *36*, 1222; (d) Y. Liu, T.

- You, T.-T. Wang, C.-M. Che, *Tetrahedron* **2019**, *75*, 130607; (e) B. Plietker, A. Röske, *Catal. Sci. Technol.* **2019**, *9*, 4188; (f) Y. Liu, T. You, H.-X. Wang, Z. Tang, C.-Y. Zhou, C.-M. Che, *Chem. Soc. Rev.* **2020**, *49*, 5310.
12. M. Mainak, O. Cusso, S. S. Bhat, M.-Z. Sun, M. Cianfanelli, M. Costas, E. Nordlander, *Dalton Trans.* **2019**, *48*, 6123.

Chapter 3: Summary and Outlook

3.1 Summary

A simple, convenient, and easy-to-synthesize chiral N₄ iron catalyst was identified and successfully applied to the formation of C-N bonds by asymmetric C-H amination. The simple N₄ iron catalyst enables rapid access to optically active α -amino acids with aryl and non-activated alkyl side chains, including α,α -disubstituted amino acids by enantioconvergent C-H amination.

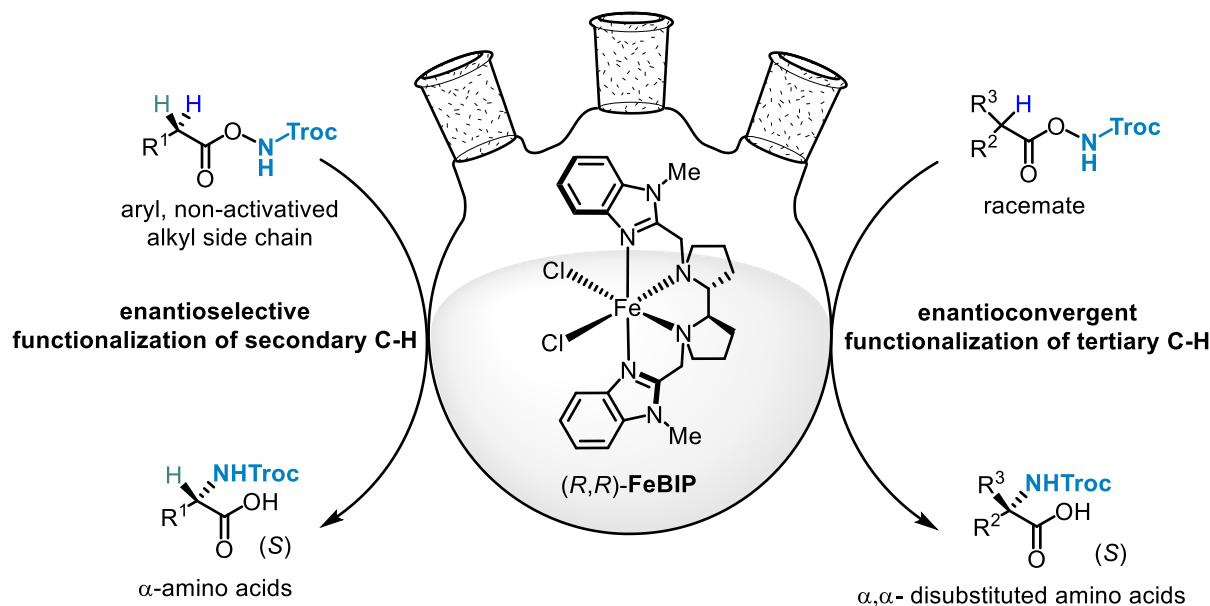


Figure 44. An overview of the key results of this thesis.

1) Asymmetric Amination of Secondary C-H Bonds Catalyzed by Chiral N₄ Iron Catalysts

Based on the previous work of our group, the enantioselective synthesis of α -amino acids by nitrene $C(sp^3)$ -H insertion with chiral N₄ iron catalysts was developed. The method is based on a unique stereocontrolled 1,3-nitrogen shift from one carboxylic acid oxygen to the α -carbon. Our method employs abundant and easily accessible carboxylic acids as starting materials. Chiral N₄ iron catalysis provides a broad scope, enabling rapid access to optically active α -amino acids with aryl, allyl, and non-activated alkyl side chains. The high functional group tolerance of this method also permits the enantioselective late-stage amination of carboxylic acid-containing drugs and natural products.

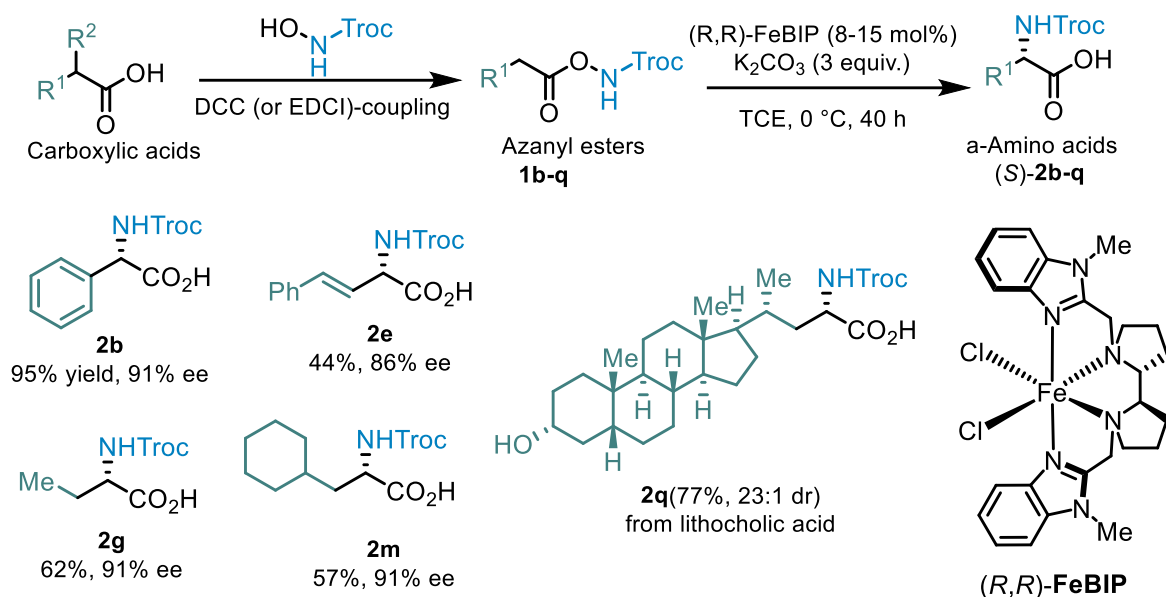


Figure 45. Asymmetric amination of secondary C-H bonds catalyzed by chiral N4 iron catalysts.

2) Enantioconvergent Tertiary C-H Bonds Amination Catalyzed by Chiral N4 Iron Catalysts

A powerful and straightforward method for the asymmetric synthesis of chiral α,α -disubstituted α -amino acids based on an enantioconvergent 1,3-migratory nitrene C(sp³)-H insertion was developed. Readily available racemic feedstock carboxylic acids are converted in a DCC/EDCI-coupling step into racemic azanyl esters which rearrange to enantioenriched α,α -disubstituted α -amino acids. The 1,3-migratory nitrene insertion is catalyzed by a robust chiral iron complex which is insensitive to air and humidity. Some of the products can be obtained as >99% ee by recrystallisation.

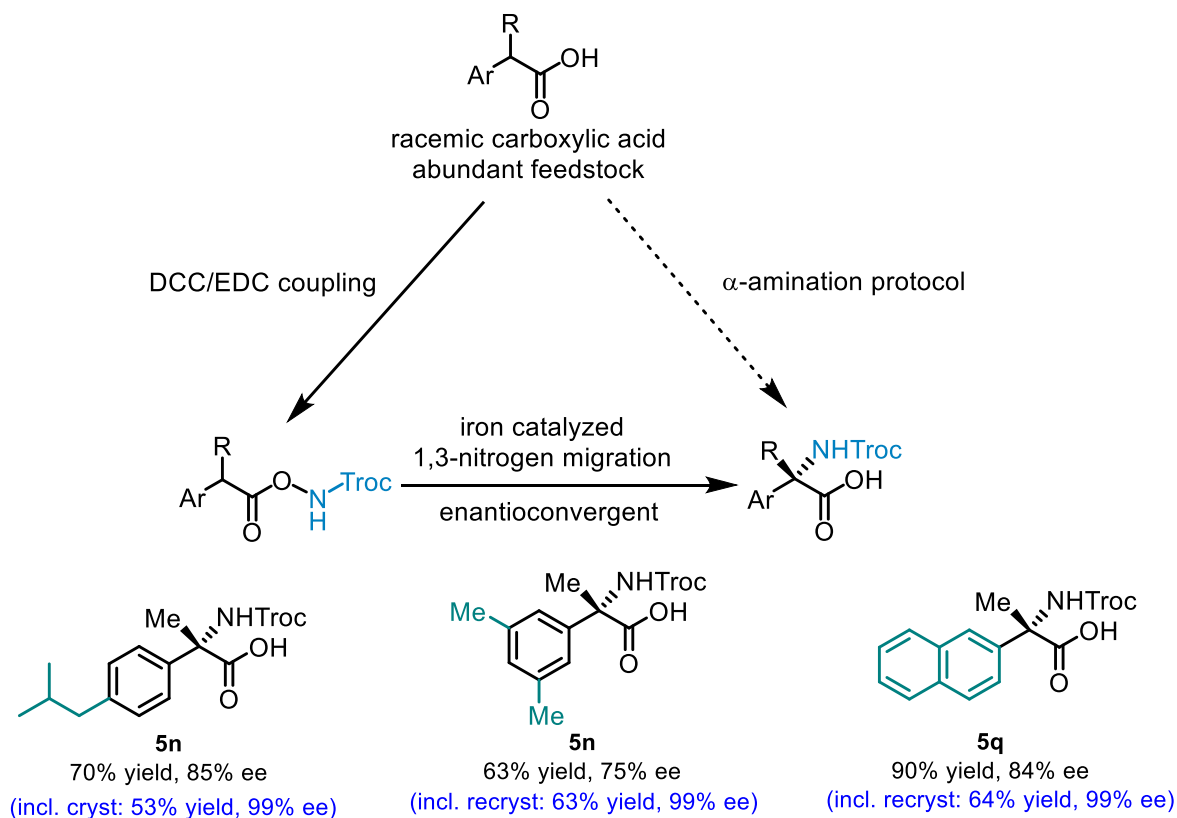


Figure 46. Enantioconvergent tertiary C-H bonds amination catalyzed by chiral N4 iron catalysts.

3.2 Outlook

Considering, the simplicity, stability and ease of synthesis of chiral N4 iron catalysts and the diverse synthetic applications of C-H amination products to drugs, natural products, chiral ligands, and chiral catalysts, it would be an extremely valuable direction if chiral N4 iron catalysts could be applied to other C-H amination reactions.

1) Expanding new substrate for enantiomeric convergence process

Since enantiomeric convergence allows one enantiomer of high chiral purity to be obtained directly from the racemic compound, it greatly accelerates the process of obtaining non-racemic compounds. Therefore enantiomeric convergence has been a direction of great interest to chemists. Based on our research work, we found that chiral N4 iron catalysts can achieve enantiomeric convergence very well, so it is also worthwhile to continue exploring the direction of designing new substrates suitable for enantiomeric convergence.

2) Exploiting asymmetric intermolecular C-H amination reactions

Compared with asymmetric intramolecular C-H amination reactions, the asymmetric intermolecular version is more direct for the synthesis of chiral amines. Usually, intramolecular

amination reactions start with the synthesis of suitable reaction precursors, while intermolecular amination reactions can be avoided. Secondly, the cyclic N-heterocycles obtained by intramolecular amination reactions require further ring opening to give the final chiral amine. The pervasiveness of the functional groups can be problematic due to the ring-opening conditions. But intermolecular amination reactions can avoid this and it gives direct and fast access to chiral amines. This would be a landmark discovery if a suitable reaction precursor could be found for the intermolecular asymmetric amination reaction in combination with chiral N₄ iron as a catalyst.

Chapter 4: Experimental Part

4.1 Materials and Methods

All reactions were carried out under an atmosphere of nitrogen with magnetic stirring. The catalysis reactions were performed using standard Schlenk glassware techniques.

Solvents and Reagents

Solvents were distilled under nitrogen from calcium hydride (CH_2Cl_2 , CH_3CN) or sodium/benzophenone (Et_2O , THF and toluene). Super-dry solvents, such as 1,1,2,2-tetrachloroethane (from Acros) and DMF (from Sigma Aldrich) were purchased from commercial available source and used directly without further drying. All reagents purchased from Acros, Alfa Aesar, Sigma Aldrich, TCI, ChemPur, Merck and Fluorochem were used without any further purifications.

Chromatographic Methods

The course of the reactions and the column chromatographic elution were monitored by thin-layer chromatography (TLC) [Macherey-Nagel (ALUGRAM®Xtra Sil G/UV254)]. Flash column chromatography was performed with silica gel from Merck (particle size 0.040-0.063 mm).

Nuclear Magnetic Resonance Spectroscopy (NMR)

^1H NMR, proton decoupled ^{13}C NMR, and proton coupled ^{19}F NMR spectra were recorded on Bruker Avance 300 system (^1H NMR: 300 MHz and 500 MHz, ^{13}C NMR: 75 MHz and 125 MHz, ^{19}F NMR: 282 MHz) spectrometers at ambient temperature. Chemical shifts are given in ppm on the δ scale, and were determined after calibration to the residual signals of the solvents, which were used as an internal standard. NMR standards were used are as follows: ^1H NMR spectroscopy: $\delta = 7.26$ ppm (CDCl_3), $\delta = 5.32$ ppm (CD_2Cl_2), $\delta = 2.50$ ppm ($\text{DMSO-}d_6$), $\delta = 3.31$ ppm (CD_3OD); ^{13}C -NMR spectroscopy: $\delta = 77.0$ ppm (CDCl_3), $\delta = 53.8$ ppm (CD_2Cl_2), $\delta = 118.26$, 1.32 ppm (CD_3CN), $\delta = 206.26$, $\delta = 39.52$ ppm ($\text{DMSO-}d_6$), $\delta = 49.0$ ppm (CD_3OD). ^{19}F NMR spectroscopy: $\delta = 0$ ppm (CFCl_3). The characteristic signals were specified from the low field to high field with the chemical shifts (δ in ppm). ^1H NMR spectra peak multiplicities indicated as singlet (s), doublet (d), doublet of doublet (dd), doublet of doublet of doublet (ddd), triplet (t), doublet of triplet (dt), quartet (q), multiplet (m). The

coupling constant J indicated in hertz (Hz).

High-Performance Liquid Chromatography (HPLC)

Chiral HPLC was performed with an Agilent 1200 Series, Agilent 1260 Series HPLC System or Shimadzu Lc-2030c. All the HPLC conditions were detailed in the individual procedures. The type of the columns, mobile phase and the flow rate were specified in the individual procedures.

Infrared Spectroscopy (IR)

IR measurements were recorded on a Bruker Alpha-P FT-IR spectrometer. The absorption bands were indicated a wave numbers ν (cm^{-1}). All substances were measured as films or solids.

Mass Spectrometry (MS)

High-resolution mass spectra were recorded on a Bruker En Apex Ultra 7.0 TFF-MS instrument using ESI or APCI or FD technique. Ionic masses are given in units of m/z for the isotopes with the highest natural abundance.

Crystal Structure Analysis

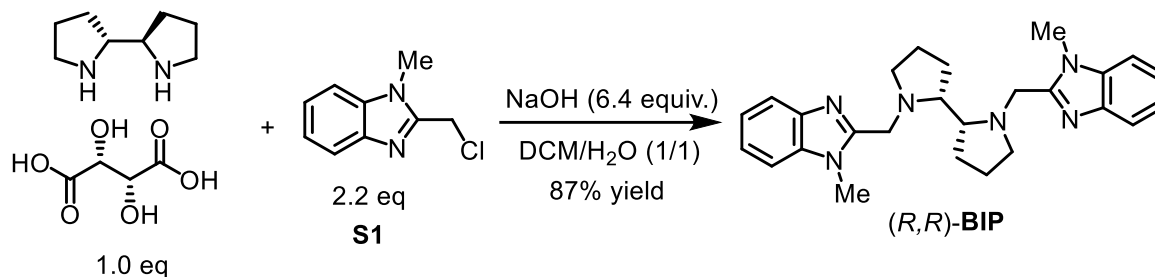
Crystal X-ray measurements and the crystal structure analysis were carried out by Dr. Klaus Harms (Chemistry Department, Philipps University of Marburg) and Sergei Ivlev (Chemistry Department, Philipps University of Marburg). X-ray data were collected with a Bruker 3 circuit D8 Quest diffractometer with MoK α radiation (microfocus tube with multilayer optics) and Photon 100 CMOS detector. Scaling and absorption correction was performed by using the SADABS software package of Bruker. Structures were solved using direct methods in SHELXS and refined using the full matrix least squares procedure in SHELXL-2013 or SHELXL-2014. The Flack parameter is a factor used to estimate the absolute configuration of the compounds. Disorder of PF₆ ions, solvent molecules or methylene groups was refined using restraints for both the geometry and the anisotropic displacement factors.

Optical Rotation Polarimeter

Optical rotations were measured on a Krüss P8000-T or Perkin-Elmer 241 polarimeter with $[\alpha]_D^{22}$ or $[\alpha]_D^{25}$ values reported in degrees with concentrations reported in g/100 mL.

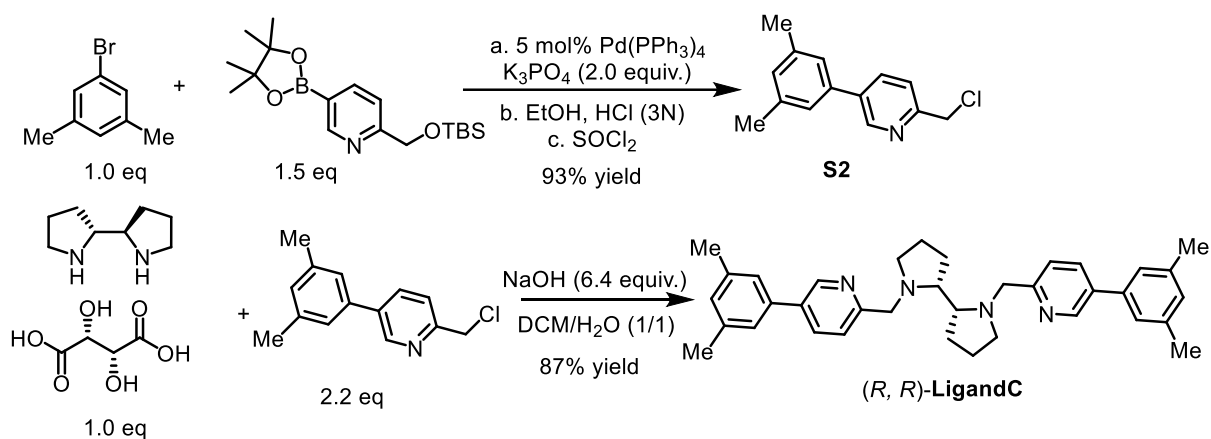
4.2 Synthesis of Chiral N4 Iron Catalysts

4.2.1 Synthesis of Ligands



Synthesis of *(R,R)*-BIP: Ligand **S1** was synthesized following a literature procedure.¹ Accordingly, a round bottomed flask was charged with a stir bar, 2-(chloromethyl)-1-methyl-1H-benzo[d]imidazole (1057.0 mg, 5.87 mmol, 2.2 equiv.), *(R,R)*-2,2'-bispyrrolidine/L-tartaric acid (918.3 mg, 2.67 mmol, 1.0 equiv.), NaOH (683.5 mg, 17.09 mmol, 6.4 equiv.) and 1:1 CH₂Cl₂:H₂O (11.2 mL) and the reaction was stirred vigorously at room temperature for 16 h. The reaction was diluted with 1M NaOH and CH₂Cl₂. The layers were separated and the aqueous layer was extracted with CH₂Cl₂ (5 x). The combined organic layers were dried (K₂CO₃), filtered and concentrated. Purification by flash chromatography on silica eluting with 5% MeOH/CH₂Cl₂ with 1% NH₄OH afforded the crude ligand, which was partitioned between CH₂Cl₂ and 1 M NaOH. The layers were separated and the aqueous layer was extracted with CH₂Cl₂ (5 x). This extraction removes traces of water and NH₄OH from the column conditions. The combined organic layers were dried (K₂CO₃), filtered and concentrated to afford the title compound (1002.0 mg, 2.34 mmol, 87 % yield) as a yellow powder.

(R,R)-**BIP**: ¹H NMR (300 MHz, CDCl₃) δ 1.50–1.93 (m, 8H), 2.15–2.51 (m, 2H), 2.62–2.80 (m, 2H), 2.80–3.00 (m, 2H), 3.53–3.75 (m, 2H), 3.80 (s, 6H), 4.24 (d, *J* = 13.4 Hz, 2H), 7.17–7.34 (m, 6H), 7.65–7.78 (m, 2H). ¹³C NMR (75 MHz, CDCl₃) δ 152.48, 142.31, 136.26, 122.54, 121.96, 119.71, 109.09, 65.45, 55.64, 52.59, 30.01, 26.41, 24.14. **IR (film):** ν (cm⁻¹) 2954, 2807, 1615, 1513, 1438, 1399, 1287, 1116, 860, 739, 524, 436. **HRMS (ESI, *m/z*)** calcd. for [C₂₂H₂₉N₆]⁺ [(M + H)⁺]: 429.2761, found: 429.2761.



Synthesis of S2: A 25 mL round bottomed flask fitted with a rubber septum was charged with a stir bar, Pd(PPh₃)₄ (289.0 mg, 0.25 mmol, 5 mol %), 1-bromo-3,5-bis(trimethyl)benzene (925.0 mg, 5.0 mmol, 1.0 equiv.) and K₃PO₄ (2.12 g, 10.0 mmol, 2.0 equiv.). The flask was evacuated and backfilled with N₂ (x3). Toluene (9.0 mL) and degassed deionized water (0.9 mL) were added followed by 2-(((*tert*-butyl)dimethylsilyloxy)methyl)-5-(4,4,5,5-tetramethyl-1,3,2-dioxaborolan-2-yl)pyridine (2.6 g, 7.5 mmol, 1.5 equiv.). The rubber septum was quickly replaced with a yellow polyethylene cap and secured with electrical tape. The reaction was heated at 100 °C in an oil bath for 16 h, at which time it was allowed to cool to room temperature and quenched with water (10 mL). The layers were separated and the aqueous layer was extracted with CH₂Cl₂ (3x10 mL). The combined organic layers were dried (Na₂SO₄), filtered and concentrated. Purification by flash chromatography on silica (~300 mL) eluting with 5% EtOAc/hexanes afforded the title compound in approximately 69% yield with some minor impurities resulting from protideborination of the pinacol borane. The product was taken on to subsequent synthetic steps during the course of which, the impurities were removed.

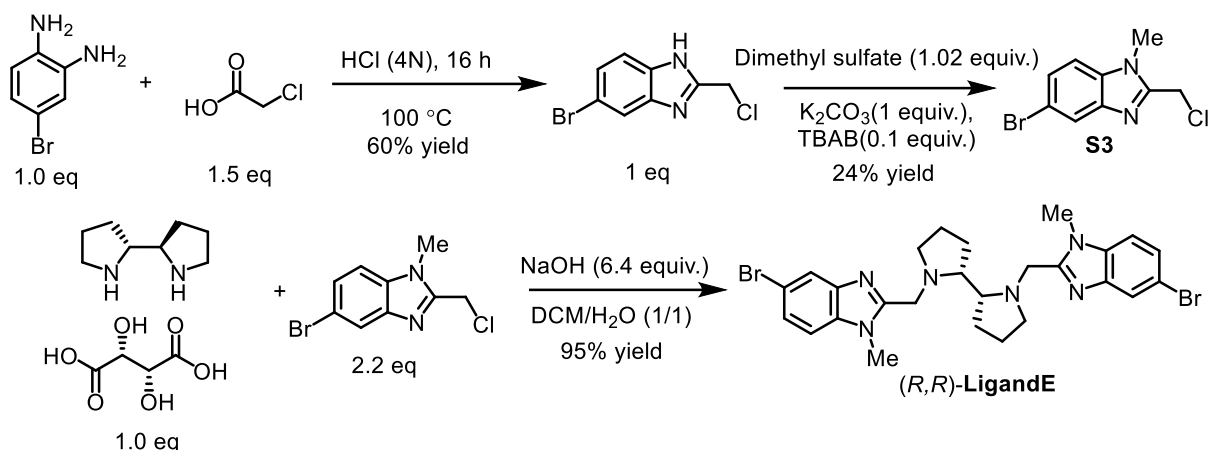
Then 2-(((*tert*-butyl)dimethylsilyloxy)methyl)-5-(3,5-dimethylphenyl)pyridine (1.13 g, 3.45 mmol, 1.0 equiv.) was dissolved in EtOH (3.5 mL) and 3N HCl (3.5 mL). The reaction was stirred vigorously for 3 h, quenched to neutral pH with saturated NaHCO₃, and diluted with CH₂Cl₂. The layers were separated and the aqueous layer was extracted with CH₂Cl₂ (x3). The combined organic layers were dried (Na₂SO₄), filtered and concentrated to give a crude solid. The solid was dissolved in CH₂Cl₂ (17 mL) and SOCl₂ (2.5 mL, 4.1 g, 34 mmol, 10.0 equiv.) was added dropwise. The reaction was stirred 16 h and quenched to neutral pH with saturated NaHCO₃. The layers were separated and the aqueous layer was extracted with CH₂Cl₂ (x3). The combined organic layers were dried (Na₂SO₄), filtered and

concentrated. Purification by flash chromatography on silica eluting with 5% EtOAc/*n*-hexanes afforded the title compound **S2** (749.0 mg, 3.24 mmol, 93% yield) as a red solid.

S2: $^1\text{H NMR}$ (300 MHz, CDCl_3) δ 8.78 (s, 1H), 7.88 (dd, $J = 8.1, 2.3$ Hz, 1H), 7.51 (d, $J = 8.1$ Hz, 1H), 7.19 (s, 2H), 7.06 (s, 1H), 4.73 (s, 2H), 2.40 (s, 6H). $^{13}\text{C NMR}$ (75 MHz, CDCl_3) δ 155.23, 148.10, 138.89, 137.41, 136.49, 135.54, 130.51, 125.18, 122.79, 46.75, 21.51. **IR (film):** ν (cm^{-1}) 3005, 2916, 1637, 1603, 1465, 842, 693, 639, 571, 463. **HRMS (ESI, m/z)** calcd. for $[\text{C}_{22}\text{H}_{29}\text{N}_6]^+ [(M + H)^+]$: 232.0888, found: 232.0888.

Synthesis of (*R,R*)-LigandC: A round bottomed flask was charged with a stir bar, 2-(chloromethyl)-5-(3,5-dimethylphenyl)pyridine (406.6 mg, 1.76 mmol, 2.2 equiv.), (*R,R*)-2,2'-bispyrrolidine/*L*-tartaric acid (275.0 mg, 0.8 mmol, 1.0 equiv.), NaOH (205.0 mg, 5.1 mmol, 6.4 equiv.) and 1:1 CH_2Cl_2 : H_2O (3.4 mL) and the reaction was stirred vigorously at room temperature for 16 h. The reaction was diluted with 1M NaOH and CH_2Cl_2 . The layers were separated and the aqueous layer was extracted with CH_2Cl_2 (x5). The combined organic layers were dried (K_2CO_3), filtered and concentrated. Purification by flash chromatography on silica eluting with 5% MeOH/ CH_2Cl_2 with 1% NH_4OH afforded the crude ligand, which was partitioned between CH_2Cl_2 and 1 M NaOH. The layers were separated and the aqueous layer was extracted with CH_2Cl_2 (x5). This extraction removes traces of water and NH_4OH from the column conditions. The combined organic layers were dried (K_2CO_3), filtered and concentrated to afford the title compound (370 mg, 0.70 mmol, 87 % yield) as a red oil.

(*R,R*)-LigandC: $^1\text{H NMR}$ (300 MHz, CDCl_3) δ 8.69 (d, $J = 1.6$ Hz, 2H), 7.77 (dd, $J = 8.1, 2.4$ Hz, 2H), 7.46 (d, $J = 8.1$ Hz, 2H), 7.14 (s, 4H), 7.02 (s, 2H), 4.31 (m, 2H), 3.64 (m, 2H), 3.09 (m, 2H), 2.92 (m, 2H), 2.37 (m, 14H), 1.81–1.72 (m, 8H). $^{13}\text{C NMR}$ (75 MHz, CDCl_3) δ 147.39, 138.67, 138.02, 135.05, 134.91, 129.58, 125.05, 122.67, 65.99, 61.03, 55.40, 26.51, 23.76, 21.47. **IR (film):** ν (cm^{-1}) 2959, 2914, 1602, 1488, 1361, 1116, 1025, 836, 731, 698, 636, 589, 459. **HRMS (ESI, m/z)** calcd. for $[\text{C}_{36}\text{H}_{43}\text{N}_4]^+ [(M + H)^+]$: 531.3482, found: 531.3498.



Synthesis of S3: A round bottomed flask was charged with a stir bar, 4-bromobenzene-1,2-diamine (1.87 g, 10 mmol, 1.0 equiv.), 2-chloroacetic acid (1.42 g, 15 mmol, 1.5 equiv.), HCl (4N, 10 mL) and the reaction was refluxed at 100 °C for 16 h. After that, the resulting solution was cooled to room temperature and then cooling to 0 °C neutralized with solid NaHCO_3 . Then the aqueous solution was extracted with ethyl acetate (50 mL x 3). The combined organic layers were washed with water, dried with MgSO_4 and concentrated under *vacuo*. The resulting residue was purified by flash column chromatography on silica gel (*n*-hexane: EtOAc = 5:1 to 2:1) to provide product (1.46 g, 6.0 mmol, 60%) as solid.

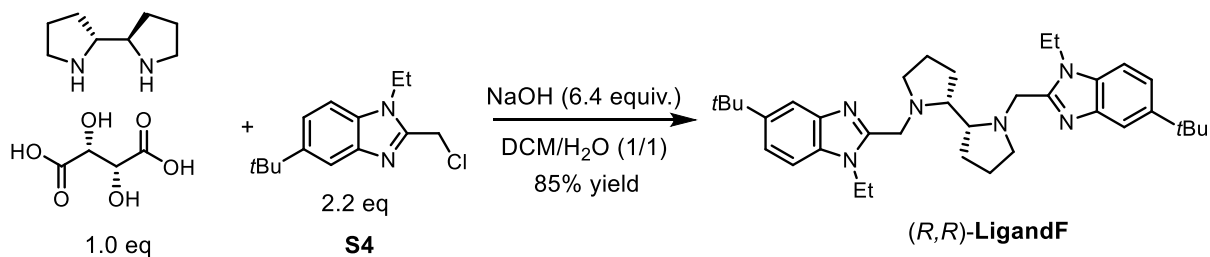
Then, a round bottomed flask was charged with a stir bar, 5-bromo-2-(chloromethyl)-1H-benzimidazole (1.46 g, 6.0 mmol, 1.0 equiv.), K_2CO_3 (0.922 g, 6.6 mmol, 1.1 equiv.), TBAB (193 mg, 0.6 mmol, 0.1 equiv.). After stirring for 5 minutes, dimethyl sulfate (580 μL , 6.12 mmol, 1.02 equiv.) was added dropwise. The reaction mixture was stirred at room temperature for 4 h. After that, water (4 mL) was added. The aqueous solution was extracted with ethyl acetate (20 mL x 4). The combined organic layers were washed with saturated brine, dried with MgSO_4 and concentrated under *vacuo*. The resulting residue was purified by flash column chromatography on silica gel (DCM: CH_3CN = 15:1 to 5:1) to provide product (0.37 g, 1.44 mmol, 24%) as a white solid.

S3: $^1\text{H NMR}$ (300 MHz, CDCl_3) δ 7.87 (d, J = 1.5 Hz, 1H), 7.40 (dd, J = 8.6, 1.8 Hz, 1H), 7.19 (d, J = 8.6 Hz, 1H), 4.80 (s, 2H), 3.83 (s, 3H). $^{13}\text{C NMR}$ (75 MHz, CDCl_3) δ 150.21, 143.44, 135.23, 126.77, 123.17, 115.71, 110.85, 36.71, 30.53. **IR (film):** ν (cm^{-1}) 3036, 1507, 1420, 1393, 1322, 1127, 1095,

867, 798, 747, 711, 644, 593, 437. **HRMS (ESI, m/z)** calcd. for $[C_9H_9BrClN_2]^+ [(M + H)^+]$: 258.9632, found: 258.9639.

Synthesis of (*R,R*)-LigandE: A round bottomed flask was charged with a stir bar, 5-bromo-2-(chloromethyl)-1-methyl-1H-benzo[d]imidazole (227.0 mg, 0.88 mmol, 2.2 equiv.), (*R,R*)-2,2'-bispyrrolidine/L-tartaric acid (138.0 mg, 0.4 mmol, 1.0 equiv.), NaOH (102.4 mg, 2.56 mmol, 6.4 equiv.) and 1:1 $CH_2Cl_2:H_2O$ (1.6 mL) and the reaction was stirred vigorously at room temperature for 16 h. The reaction was diluted with 1M NaOH and CH_2Cl_2 . The layers were separated and the aqueous layer was extracted with CH_2Cl_2 (x5). The combined organic layers were dried (K_2CO_3), filtered and concentrated. Purification by flash chromatography on silica eluting with 5% MeOH/ CH_2Cl_2 with 1% NH_4OH afforded the crude ligand, which was partitioned between CH_2Cl_2 and 1 M NaOH. The layers were separated and the aqueous layer was extracted with CH_2Cl_2 (x5). This extraction removes traces of water and NH_4OH from the column conditions. The combined organic layers were dried (K_2CO_3), filtered and concentrated to afford the title compound (220 mg, 0.38 mmol, 95 % yield) as a yellow powder.

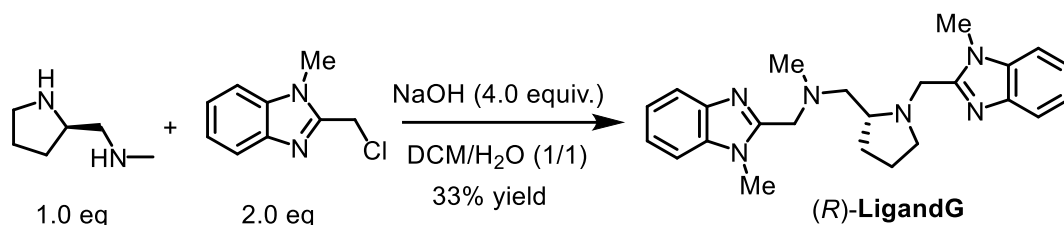
(*R,R*)-LigandE: 1H NMR (300 MHz, $CDCl_3$) δ 7.82 (d, $J = 1.8$ Hz, 2H), 7.33 (dd, $J = 8.6, 1.8$ Hz, 2H), 7.10 (d, $J = 8.5$ Hz, 2H), 4.22 (d, $J = 13.7$ Hz, 2H), 3.73 (s, 6H), 3.63 (d, $J = 13.7$ Hz, 2H), 2.86 (m, 2H), 2.73–2.67 (m, 2H), 2.31 (m, 2H), 1.82–1.60 (m, 8H). ^{13}C NMR (75 MHz, $CDCl_3$) δ 153.72, 143.60, 135.19, 125.56, 122.47, 114.92, 110.32, 65.73, 55.75, 52.59, 30.15, 26.54, 24.12. **IR (film):** ν (cm^{-1}) 2951, 2803, 1511, 1468, 1420, 1394, 1321, 791, 732, 589, 529, 470. **HRMS (ESI, m/z)** calcd. for $[C_{26}H_{31}Br_2N_6]^+ [(M + H)^+]$: 585.0971, found: 585.0971.



Synthesis of (*R,R*)-LigandF: According to the literature,² we synthesized **S4**. A round bottomed flask was charged with a stir bar, 5-(*tert*-butyl)-2-(chloromethyl)-1-ethyl-1H-benzo[d]imidazole (330.0 mg, 1.32 mmol, 2.2 equiv.), (*R,R*)-2,2'-bispyrrolidine/L-tartaric acid (207.0 mg, 0.6 mmol, 1.0 equiv.),

NaOH (153.6 mg, 3.84 mmol, 6.4 equiv.) and 1:1 CH₂Cl₂:H₂O (2.6 mL) and the reaction was stirred vigorously at room temperature for 16 h. The reaction was diluted with 1M NaOH and CH₂Cl₂. The layers were separated and the aqueous layer was extracted with CH₂Cl₂ (x5). The combined organic layers were dried (K₂CO₃), filtered and concentrated. Purification by flash chromatography on silica eluting with 5% MeOH/CH₂Cl₂ with 1% NH₄OH afforded the crude ligand, which was partitioned between CH₂Cl₂ and 1 M NaOH. The layers were separated and the aqueous layer was extracted with CH₂Cl₂ (x5). This extraction removes traces of water and NH₄OH from the column conditions. The combined organic layers were dried (K₂CO₃), filtered and concentrated to afford the title compound (288 mg, 0.51 mmol, 85 % yield) as a yellow powder.

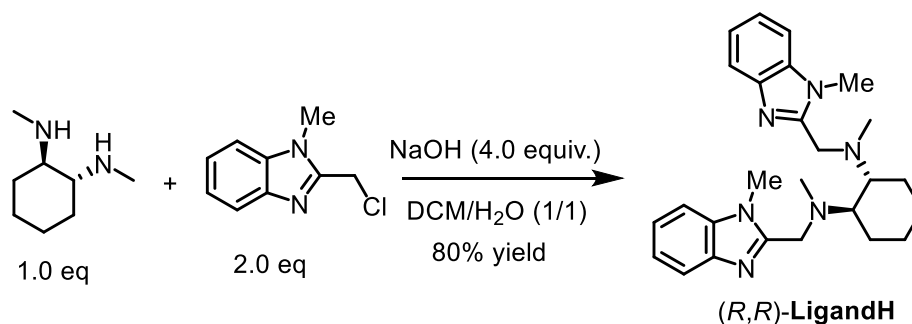
(R,R)-LigandF: ¹H NMR (300 MHz, CDCl₃) δ 7.76 (d, *J* = 1.7 Hz, 2H), 7.35 (dd, *J* = 8.5, 1.8 Hz, 2H), 7.27 (d, *J* = 7.8 Hz, 2H), 4.41 – 4.14 (m, 6H), 3.68 (d, *J* = 12.8 Hz, 2H), 2.95 – 2.84 (m, 2H), 2.79 (m, 2H), 2.37 (m, 2H), 1.94 – 1.52 (m, 8H), 1.40 (m, 24H). ¹³C NMR (75 MHz, CDCl₃) δ 151.82, 145.28, 142.58, 133.23, 120.56, 116.14, 108.74, 65.18, 55.38, 52.67, 38.86, 34.87, 32.01, 26.15, 24.08, 15.21. **IR (film):** ν (cm⁻¹) 2958, 2869, 1486, 1445, 1280, 1202, 1116, 905, 799, 728, 640, 405. **HRMS (ESI, *m/z*)** calcd. for [C₃₆H₅₃N₆]⁺ [(M + H)⁺]: 569.4326, found: 569.4326.



Synthesis of (R,R)-LigandG: A round bottomed flask was charged with a stir bar, 2-(chloromethyl)-1-methyl-1H-benzimidazole (360.0 mg, 2.0 mmol, 2.0 equiv.), (*R*)-*N*-methyl-1-(pyrrolidin-2-yl)methanamine (114.0 mg, 1.0 mmol, 1.0 equiv.), NaOH (160.0 mg, 4.0 mmol, 4.0 equiv.) and 1:1 CH₂Cl₂:H₂O (4.0 mL) and the reaction was stirred vigorously at room temperature for 16 h. The reaction was diluted with 1M NaOH and CH₂Cl₂. The layers were separated and the aqueous layer was extracted with CH₂Cl₂ (5 x). The combined organic layers were dried (K₂CO₃), filtered and concentrated. Purification by flash chromatography on silica eluting with 5% MeOH/CH₂Cl₂ with 1% NH₄OH afforded the crude ligand, which was partitioned between CH₂Cl₂ and 1 M NaOH. The layers were separated and the aqueous layer was extracted with CH₂Cl₂ (5 x). This extraction removes traces of water and NH₄OH from the column conditions. The combined

organic layers were dried (K_2CO_3), filtered and concentrated to afford the title compound (134.0 mg, 0.33 mmol, 33 % yield) as a yellow solid.

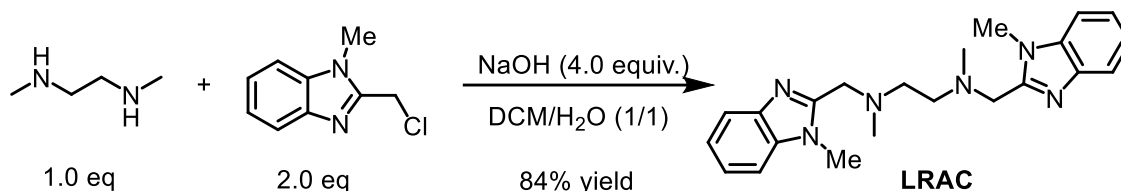
(R)-LigandG: 1H NMR (300 MHz, $CDCl_3$) δ 7.77 – 7.64 (m, 2H), 7.33 – 7.16 (m, 6H), 4.29 (d, J = 13.3 Hz, 1H), 3.81 (s, 3H), 3.80 – 3.68 (m, 3H), 3.66 (s, 3H), 2.83 – 2.69 (m, 2H), 2.59 – 2.47 (m, 1H), 2.46 – 2.29 (m, 2H), 2.27 (s, 3H), 2.07 – 1.89 (m, 1H), 1.71 – 1.42 (m, 3H). ^{13}C NMR (75 MHz, $CDCl_3$) δ 152.40, 151.88, 142.34, 142.32, 136.40, 136.31, 122.71, 122.51, 122.04, 121.92, 119.74, 119.64, 109.20, 109.16, 62.76, 62.27, 56.19, 55.04, 52.54, 43.40, 30.51, 30.19, 30.01, 22.73. **IR (film):** ν (cm^{-1}) 2948, 1434, 1455, 1398, 1363, 1004, 970, 739, 663, 548, 434. **HRMS (ESI, m/z)** calcd. for $[C_{24}H_{31}N_6]^+$ [(M + H) $^+$]: 403.2605, found: 403.2605.



(R,R)-LigandH: A round bottomed flask was charged with a stir bar, 2-(chloromethyl)-1-methyl-1H-benzimidazole (302.0 mg, 2.0 mmol, 2.0 equiv.), (1R,2R)-N,N'-dimethylcyclohexane-1,2-diamine (119.0 mg, 0.84 mmol, 1.0 equiv.), NaOH (134.0 mg, 3.36 mmol, 4.0 equiv.) and 1:1 $CH_2Cl_2:H_2O$ (3.2 mL) and the reaction was stirred vigorously at room temperature for 16 h. The reaction was diluted with 1M NaOH and CH_2Cl_2 . The layers were separated and the aqueous layer was extracted with CH_2Cl_2 (5 x). The combined organic layers were dried (K_2CO_3), filtered and concentrated. Purification by flash chromatography on silica eluting with 5% MeOH/ CH_2Cl_2 with 1% NH_4OH afforded the crude ligand, which was partitioned between CH_2Cl_2 and 1 M NaOH. The layers were separated and the aqueous layer was extracted with CH_2Cl_2 (5 x). This extraction removes traces of water and NH_4OH from the column conditions. The combined organic layers were dried (K_2CO_3), filtered and concentrated to afford the title compound (287.0 mg, 0.79 mmol, 80 % yield) as a yellow powder.

(R,R)-LigandH: 1H NMR (300 MHz, $CDCl_3$) δ 7.76 – 7.67 (m, 2H), 7.32 – 7.17 (m, 6H), 3.96 (s, 4H), 3.79 (s, 6H), 2.80 – 2.63 (m, 2H), 2.15 (s, 6H), 2.07 – 1.98 (m, 2H), 1.83 – 1.75 (m, 2H), 1.35 – 1.10

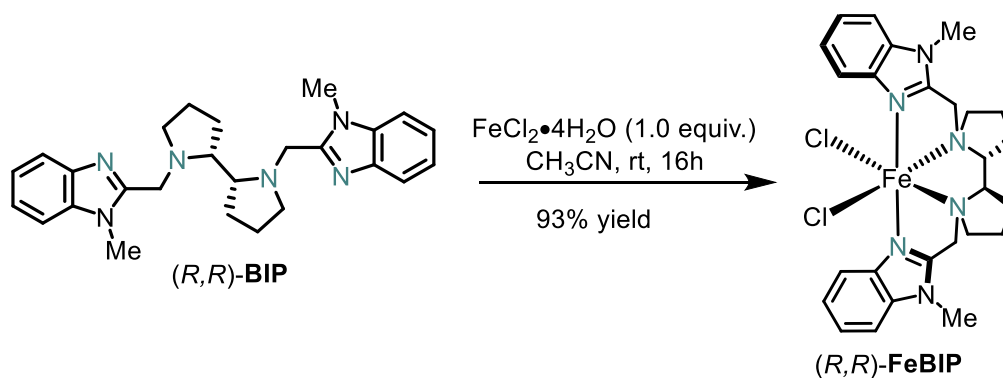
(m, 4H). ^{13}C NMR (75 MHz, CDCl_3) δ 152.60, 142.40, 136.48, 122.58, 121.94, 119.69, 109.21, 62.90, 51.79, 35.99, 30.03, 25.68, 24.16. **IR (film)**: ν (cm^{-1}) 2929, 2846, 1512, 1470, 1329, 1116, 872, 727, 574, 537, 463. **HRMS (ESI, m/z)** calcd. for $[\text{C}_{26}\text{H}_{35}\text{N}_6]^+ [(M + H)^+]$: 431.2918, found: 431.2918.



Synthesis of LRAC: A round bottomed flask was charged with a stir bar, 2-(chloromethyl)-1-methyl-1H-benzimidazole (216.0 mg, 1.2 mmol, 2.0 equiv.), N,N'-dimethyl-1,2-ethanediamine (52.9 mg, 0.6 mmol, 1.0 equiv.), NaOH (96 mg, 2.4 mmol, 4.0 equiv.) and $\text{CH}_2\text{Cl}_2:\text{H}_2\text{O}$ (1:1, 3.4 mL). The reaction was stirred vigorously at room temperature for 16 h. The reaction was diluted with NaOH (1 M) and CH_2Cl_2 . The layers were separated and the aqueous layer was extracted with CH_2Cl_2 (5 x). The combined organic layers were dried (K_2CO_3), filtered and concentrated. Purification by flash chromatography on silica eluting with 5% MeOH/ CH_2Cl_2 with 1% NH_4OH afforded the ligand **LRAC** (191.1 mg, 0.51 mmol, 84% yield) as a yellow solid.

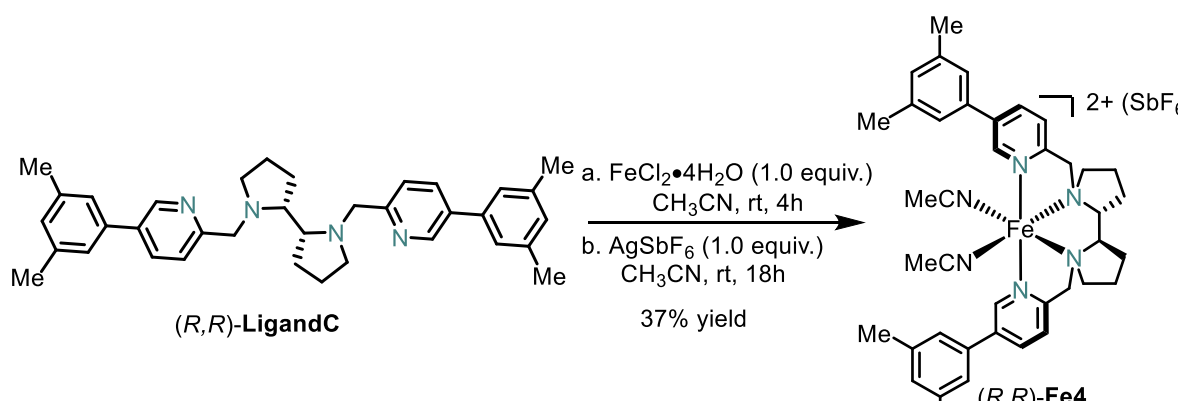
LRAC: ^1H NMR (300 MHz, CDCl_3) δ 7.81–7.69 (m, 2H), 7.33–7.19 (m, 6H), 3.81 (s, 4H), 3.76 (s, 6H), 2.65 (s, 4H), 2.27 (s, 6H). ^{13}C NMR (75 MHz, CDCl_3) δ 151.85, 142.34, 136.42, 122.62, 121.97, 119.71, 109.19, 55.61, 55.40, 42.79, 30.07. **IR (film)**: ν (cm^{-1}) 2954, 2842, 1514, 1350, 1171, 845, 739, 644, 538, 442, 413. **HRMS (ESI, m/z)** calcd. for $[\text{C}_{22}\text{H}_{29}\text{N}_6]^+ [(M + H)^+]$: 377.2448; found: 377.2448.

4.2.2 Synthesis of Catalysts



Synthesis of (*R,R*)-FeBIP: To a stirred solution of the ligand (*R,R*)-**BIP** (990 mg, 2.3 mmol, 1.05 equiv.) in 13 mL CH₃CN under N₂ atmosphere was added FeCl₂•4H₂O (437 mg, 2.2 mmol, 1.0 equiv.) in one portion. A yellow precipitate was formed within several seconds. The reaction mixture was stirred for 16 hours at room temperature before being diluted with diethyl ether (40 mL). The slurry was transferred into a centrifuge tube, and the solid material was separated by centrifugation and was washed with a mixed solvent of CH₃CN/diethyl ether (v/v = 1/2.5) for three times (3 x 35 mL in total). The solid was dried under nitrogen flow to afford (*R,R*)-[Fe(**BIP**)]Cl₂ as a yellow powder (1.14 g, 2.1 mmol, 93% yield). Single crystals formed in mixture of DMF/THF or DMF/ethyl acetate.

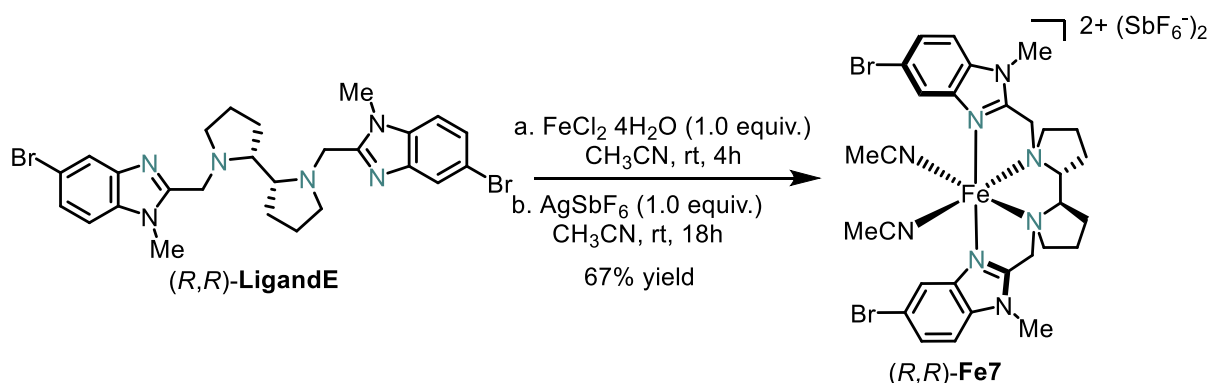
(*R,R*)-**FeBIP**: **HRMS (ESI, *m/z*)** calcd for [C₂₆H₃₂ClFeN₆]⁺ [(M - Cl)⁺]: 519.1726; found: 519.1722; **elemental analysis** calcd for [C₂₆H₃₂Cl₂FeN₆•2H₂O]: C, 52.81; H, 6.14; N, 14.21; found: C, 52.90; H, 5.82; N, 14.17.



Synthesis of (*R,R*)-Fe4: To a stirred solution of the ligand (*R,R*)-**LigandC** (132.6 mg, 0.25 mmol, 1.0 equiv.) in 1.4 mL CH₃CN under N₂ atmosphere was added FeCl₂•4H₂O (49.7 mg, 0.25 mmol, 1.0 equiv.) in one portion. A yellow precipitate was formed within several seconds. The reaction mixture was stirred for 4 hours at room temperature before being diluted with diethyl ether (3.5 mL). The slurry was transferred into a centrifuge tube, and the solid material was separated by centrifugation and was washed with a mixed solvent of CH₃CN/diethyl ether (v/v = 1/2.5) for three times (3 x 3.5 mL in total). The solid was dried under nitrogen flow to afford [Fe(*R,R*)-**LigandC**]Cl₂ as an orange solid (68.8 mg, 0.25 mmol, 42% yield): **HRMS (ESI, *m/z*)** calc'd [C₃₆H₄₂ClFeN₄]⁺ [(M - Cl)⁺]: 621.2442, found 621.2443.

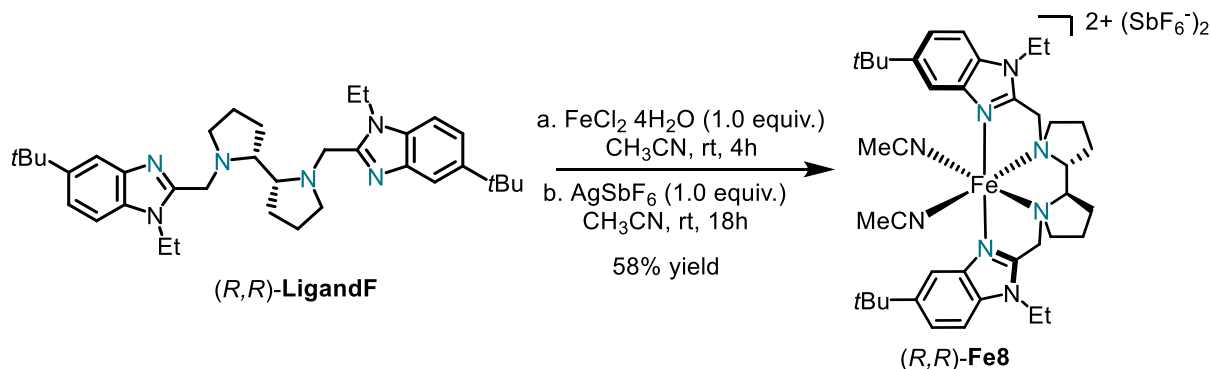
A flame dried 10 mL flask was charged with 60.9 mg of solid $[\text{Fe}(\text{R,R})\text{-LigandC}]\text{Cl}_2$ (0.093 mmol, 1.0 equiv.) suspended in CH_3CN (1.17 mL) under nitrogen. Silver hexafluoroantimonate (AgSbF_6 , 63.8 mg, 0.19 mmol, 2.0 equiv.) was weighed under an inert argon atmosphere and then added to the vigorously stirred heterogeneous mixture. The flask was covered with aluminum foil to protect the silver salts from light. After 18 hours, the reaction was filtered through Celite and concentrated under vacuum. The solid was redissolved in CH_3CN , filtered through a $0.22\mu\text{m}$ syringe filter, and concentrated. The residue was redissolved in CH_3CN and the filtration/concentration procedure was repeated two more times to ensure no silver salts remained. The brown solid obtained was dried under a nitrogen flow to yield $(\text{R,R})\text{-Fe4}$ (92.9 mg, 0.082 mmol, 88% yield).

$(\text{R,R})\text{-Fe4}$: HRMS (ESI, m/z) calcd for $[\text{C}_{38}\text{H}_{45}\text{F}_6\text{FeN}_5\text{Sb}]^+ [(\text{M}-(\text{CH}_3\text{CN})_2\text{SbF}_6)^-]$: 821.1696; found: 821.1695; elemental analysis calcd for $[\text{C}_{40}\text{H}_{48}\text{F}_{12}\text{FeN}_6\text{Sb}_2]$: C, 42.14; H, 4.24; N, 7.37; found: C, 41.38; H, 4.51; N, 5.64.



A flame dried 10 mL flask was charged with 60.9 mg of solid $[\text{Fe}(\text{R,R})\text{-LigandE}]\text{Cl}_2$ (0.093 mmol, 1.0 equiv.) suspended in CH_3CN (1.1 mL) under nitrogen. Silver hexafluoroantimonate (AgSbF_6 , 61.0 mg, 0.18 mmol, 2.0 equiv.) was weighed under an inert argon atmosphere and then added to the vigorously stirred heterogeneous mixture. The flask was covered with aluminum foil to protect the silver salts from light. After 18 hours, the reaction was filtered through Celite and concentrated under vacuum. The solid was redissolved in CH_3CN , filtered through a $0.22\mu\text{m}$ syringe filter, and concentrated. The residue was redissolved in CH_3CN and the filtration/concentration procedure was repeated two more times to ensure no silver salts remained. The brown solid obtained was dried under a nitrogen flow to yield $(\text{R,R})\text{-Fe7}$ (80.0 mg, 0.067 mmol, 76% yield).

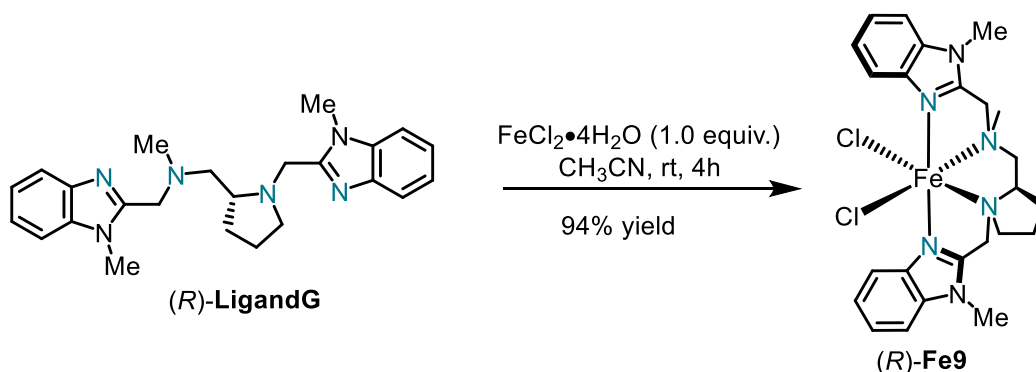
(*R,R*)-Fe7: HRMS (ESI, *m/z*) calcd for $[\text{C}_{26}\text{H}_{30}\text{Br}_2\text{F}_6\text{FeN}_6\text{Sb}]^+ [(\text{M}-(\text{CH}_3\text{CN})_2-(\text{SbF}_6))^-]^+$: 874.9190; found: 874.9199; **elemental analysis** calcd for $[\text{C}_{30}\text{H}_{36}\text{Br}_2\text{F}_{12}\text{FeN}_8\text{Sb}_2]$: C, 30.13; H, 3.03; N, 9.37; found: C, 29.98; H, 3.59; N, 10.18.



Synthesis of (*R,R*)-Fe8: To a stirred solution of the ligand (*R,R*)-**LigandF** (142.1 mg, 0.25 mmol, 1.0 equiv.) in 1.5 mL CH_3CN under N_2 atmosphere was added $\text{FeCl}_2 \cdot 4\text{H}_2\text{O}$ (49.7 mg, 0.25 mmol, 1.0 equiv.) in one portion. A yellow precipitate was formed within several seconds. The reaction mixture was stirred for 4 hours at room temperature before being diluted with diethyl ether (15 mL). The slurry was transferred into a centrifuge tube, and the solid material was separated by centrifugation and was washed with a mixed solvent of CH_3CN /diethyl ether ($v/v = 1/9$) for three times (3×3 mL in total). The solid was dried under nitrogen flow to afford $[\text{Fe}(\text{R,R})\text{-LigandF}](\text{Cl})_2$ as dark brown solid (127.0 mg, 0.18 mmol, 72% yield): HRMS (ESI) *m/z* calc'd $[\text{C}_{36}\text{H}_{52}\text{ClFeN}_6]^+ [\text{M-Cl}]^+$: 659.3286, found 659.3285.

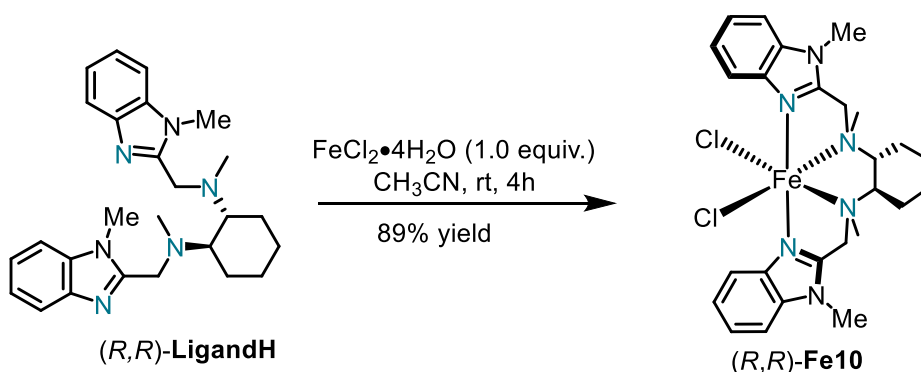
A flame dried 10 mL flask was charged with 59.4 mg of solid $[\text{Fe}(\text{R,R})\text{-LigandF}](\text{Cl})_2$ (0.085 mmol, 1.0 equiv.) suspended in CH_3CN (1.1 mL) under nitrogen. Silver hexafluoroantimonate (AgSbF_6 , 58.8 mg, 0.17 mmol, 2.0 equiv.) was weighed under an inert argon atmosphere and then added to the vigorously stirred heterogeneous mixture. The flask was covered with aluminum foil to protect the silver salts from light. After 18 hours, the reaction was filtered through Celite and concentrated under vacuum. The solid was redissolved in CH_3CN , filtered through a $0.22\mu\text{m}$ syringe filter, and concentrated. The residue was redissolved in CH_3CN and the filtration/concentration procedure was repeated two more times to ensure no silver salts remained. The brown solid obtained was dried under a nitrogen flow to yield (*R,R*)-**Fe8** (80.0 mg, 0.068 mmol, 80% yield).

(*R,R*)-Fe8: HRMS (ESI, m/z) calcd for $[C_{36}H_{52}F_6FeN_6Sb]^+ [(M-(CH_3CN)_2-(SbF_6))^+]$: 859.2545; found: 859.2539; **elemental analysis** calcd for $[C_{22}H_{28}Cl_2FeN_6]$: C, 40.77; H, 4.96; N, 9.51; found: C, 41.40; H, 4.29; N, 10.95.



Synthesis of (*R*)-Fe9: To a stirred solution of the ligand (*R*)-LigandH (80.4 mg, 0.2 mmol, 1.0 equiv.) in 1.1 mL CH_3CN under N_2 atmosphere was added $FeCl_2 \cdot 4H_2O$ (39.8 mg, 0.2 mmol, 1.0 equiv.) in one portion. A yellow precipitate was formed within several seconds. The reaction mixture was stirred for 4 hours at room temperature before being diluted with diethyl ether (3.3 mL). The slurry was transferred into a centrifuge tube, and the solid material was separated by centrifugation and was washed with a mixed solvent of CH_3CN /diethyl ether ($v/v = 1/3$) for three times (3 x 4 mL in total). The solid was dried under nitrogen flow to afford (*R*)-Fe9 as light yellow solid (99.0 mg, 0.19 mmol, 94% yield).

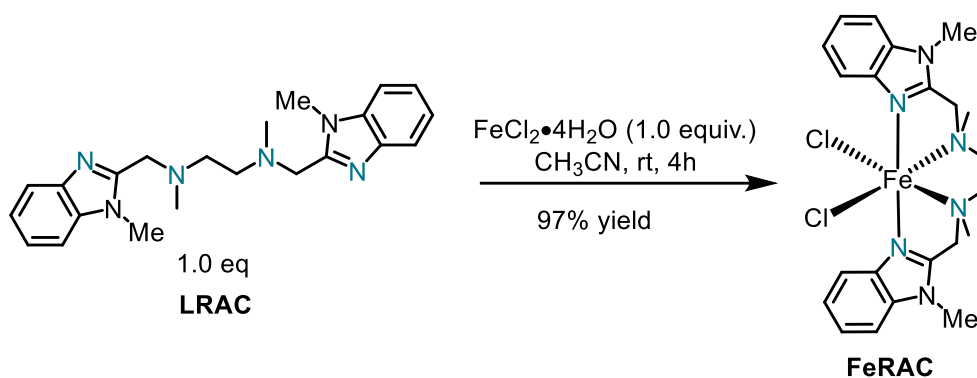
(*R*)-Fe9: HRMS (ESI, m/z) calcd for $[C_{24}H_{30}ClFeN_6]^+ [(M - Cl)^+]$: 493.1564; found: 493.1565; **elemental analysis** calcd for $[C_{24}H_{30}Cl_2FeN_6 \cdot H_2O]$: C, 52.67; H, 5.89; N, 15.36; found: C, 52.63; H, 5.71; N, 15.30.



Synthesis of (*R,R*)-Fe10: To a stirred solution of the ligand (*R,R*)-LigandH (130.9 mg, 0.3 mmol, 1.0 equiv.) in 1.8 mL CH_3CN under N_2 atmosphere was added $FeCl_2 \cdot 4H_2O$ (59.6 mg, 0.3 mmol, 1.0

equiv.) in one portion. A dark yellow brown precipitate was formed within several seconds. The reaction mixture was stirred for 4 hours at room temperature before being diluted with diethyl ether (5.4 mL). The slurry was transferred into a centrifuge tube, and the solid material was separated by centrifugation and was washed with a mixed solvent of CH₃CN/diethyl ether (v/v = 1/3) for three times (3 x 4 mL in total). The solid was dried under nitrogen flow to afford (*R,R*)-**Fe10** as a brown powder (148.0 mg, 0.27 mmol, 89% yield).

(*R,R*)-Fe10: HRMS (ESI, *m/z*) calcd for [C₂₆H₃₄ClFeN₆]⁺ [(M - Cl)⁺]: 521.1877; found: 521.1878; **elemental analysis** calcd for [C₂₆H₃₄Cl₂FeN₆•3H₂O]: C, 51.08; H, 6.59; N, 13.75; found: C, 51.12; H, 5.68; N, 13.75.



Synthesis of FeRAC: To a stirred solution of the ligand LRAC (94.1 mg, 0.25 mmol, 1.0 equiv.) in 1.4 mL CH₃CN under N₂ atmosphere was added FeCl₂•4H₂O (49.7 mg, 0.25 mmol, 1.0 equiv.) in one portion. A yellow precipitate was formed within several seconds. The reaction mixture was stirred for 4 hours at room temperature before being diluted with diethyl ether (3.5 mL). The slurry was transferred into a centrifuge tube, and the solid material was separated by centrifugation and was washed with a mixed solvent of CH₃CN/diethyl ether (v/v = 1/2.5) for three times (3 x 3.5 mL in total). The solid was dried under nitrogen flow to afford **FeRAC** as a yellow solid (112.0 mg, 0.24 mmol, 97% yield).

FeRAC: HRMS (ESI, *m/z*) calcd for [C₂₂H₂₈ClFeN₆]⁺ [(M - Cl)⁺]: 467.1413; found: 467.1415; **elemental analysis** calcd for [C₂₂H₂₈Cl₂FeN₆•3H₂O]: C, 47.41; H, 6.15; N, 15.08; found: C, 46.98; 5.59; N, 15.18.

4.2.3 Single Crystal X-Ray Diffraction

Crystallography of compound (*R,R*)-FeBIP: Single crystals of (*R,R*)-FeBIP were obtained by slow diffusion from the solution in DMF layered with EtOAc at room temperature. A suitable crystal of $C_{26}H_{32}Cl_2FeN_6 \cdot C_3H_7NO$ was selected under inert oil and mounted using a MiTeGen loop. Data collection and analysis was performed by Dr. Ivlev (Department of Chemistry). Intensity data of the crystal were recorded with a D8 Quest diffractometer (Bruker AXS). The instrument was operated with Mo-K α radiation (0.71073 Å, microfocus source) and equipped with a PHOTON III C14 detector. Evaluation, integration and reduction of the diffraction data was carried out using the Bruker APEX 3 software suite.³ Multi-scan and numerical absorption corrections were applied using the SADABS program.^{4,5} The structure was solved using dual-space methods (SHELXT-2018/2) and refined against F^2 (SHELXL-2018/3 using ShelXle interface).⁶⁻⁸ The measured crystal was found to be pseudo-merohedrally twinned and was refined with the SHELXL instruction TWIN 1 0 0 0 -1 0 -1 0 -1. All non-hydrogen atoms were refined with anisotropic displacement parameters. The hydrogen atoms were refined using the “riding model” approach with isotropic displacement parameters 1.2 times (1.5 times for terminal methyl groups) of that of the preceding carbon atom. Two of the three DMF solvent molecules were found to be disordered and were refined accordingly using the DSR plugin⁹ implemented in ShelXle. CCDC 2126462 contains the supplementary crystallographic data for this paper. These data can be obtained free of charge from The Cambridge Crystallographic Data Centre via www.ccdc.cam.ac.uk/structures.

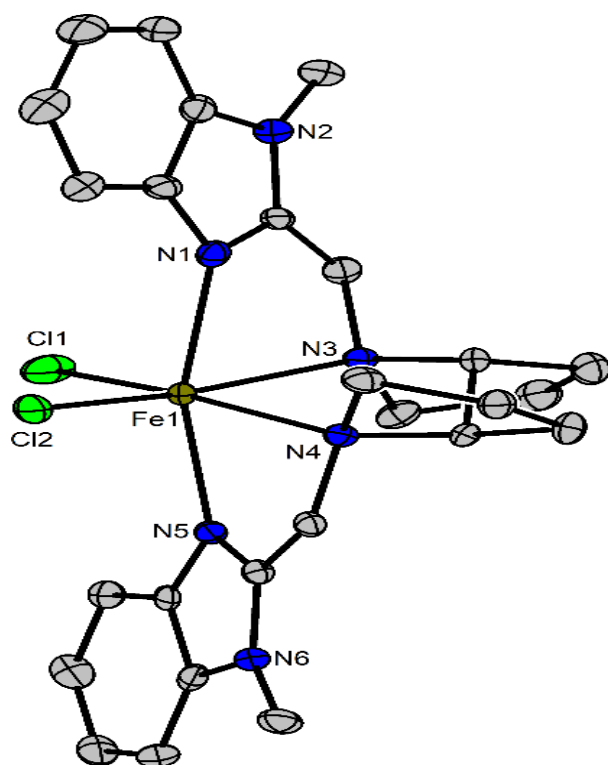


Figure 47. Crystal structure of *(R,R)*-FeBIP. Only one symmetry-independent molecule is shown. Only the hydrogen atoms at the stereocenters are shown. Displacement ellipsoids are shown at 50 % probability level at 100 K. The hydrogen atoms are shown with arbitrary radii.

Table 3. Selected crystallographic data and details of the structure determination for (*R,R*)-**FeBIP**.

Identification code	SI134
Empirical formula	C ₂₉ H ₃₉ Cl ₂ FeN ₇ O
Molar mass / g·mol⁻¹	628.42
Space group (No.)	<i>P</i> 2 ₁ (4)
<i>a</i> / Å	12.6513(5)
<i>b</i> / Å	22.0873(8)
<i>c</i> / Å	17.0272(6)
β / °	111.7740(10)
<i>V</i> / Å³	4418.5(3)
<i>Z</i>	6
$\rho_{calc.}$ / g·cm⁻³	1.417
μ / mm⁻¹	0.730
Color	yellow
Crystal habitus	block
Crystal size / mm³	0.182 x 0.133 x 0.112
<i>T</i> / K	100
λ / Å	0.71073 (Mo-K α)
θ range / °	2.249 to 28.368
Range of Miller indices	-16 ≤ <i>h</i> ≤ 16 -29 ≤ <i>k</i> ≤ 29 -22 ≤ <i>l</i> ≤ 22
Absorption correction	multi-scan and numerical
<i>T</i>_{min}, <i>T</i>_{max}	0.8781, 0.9633
<i>R</i>_{int}, <i>R</i>_{σ}	0.0526, 0.0385
Completeness of the data set	0.999
No. of measured reflections	132218
No. of independent reflections	21950
No. of parameters	1190
No. of restraints	289
<i>S</i> (all data)	1.028
<i>R</i>(<i>F</i>) (<i>I</i> ≥ 2σ(<i>I</i>), all data)	0.0292, 0.0297
<i>wR</i>(<i>F</i>²) (<i>I</i> ≥ 2σ(<i>I</i>), all data)	0.0668, 0.0671
Extinction coefficient	not refined
Flack parameter <i>x</i>	-0.003(4)
$\Delta\rho_{max}$, $\Delta\rho_{min}$ / e·Å⁻³	0.443, -0.250

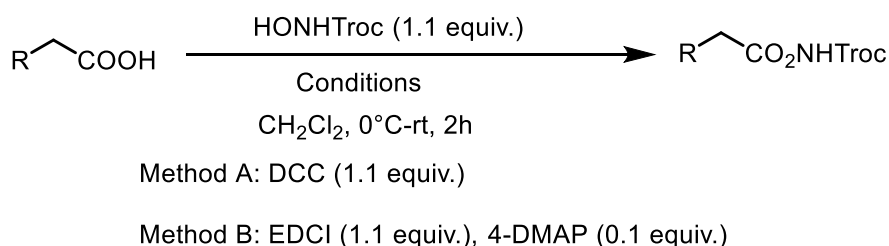
Reference

1. M. Mainak, O. Cusso, S. S. Bhat, M.-Z. Sun, M. Cianfanelli, M. Costas, E. Nordlander, *Dalton Trans.* **2019**, 48, 6123.

2. K. Zhang, L. Q. Lu, Y. Jia, Y. Wang, F. D. Lu, F. Pan, W. J. Xiao, *Angew. Chem. Int. Ed.* **2019**, *58*, 13375.
3. *APEX3*, Bruker AXS Inc., Madison, Wisconsin, USA, **2018**.
4. *SADABS*, Bruker AXS Inc., Madison, Wisconsin, USA, **2016**.
5. L. Krause, R. Herbst-Irmer, G. M. Sheldrick, D. Stalke, *J. Appl. Crystallogr.* **2015**, *48*, 3.
6. G. M. Sheldrick, *Acta Crystallogr., Sect. A: Found. Adv.* **2015**, *71*, 3.
7. G. M. Sheldrick, *Acta Crystallogr., Sect. C: Struct. Chem.* **2015**, *71*, 3.
8. C. B. Hübschle, G. M. Sheldrick, B. Dittrich, *J. Appl. Crystallogr.* **2011**, *44*, 1281.
9. D. Kratzert, I. Krossing, *J. Appl. Crystallogr.* **2018**, *51*, 928.

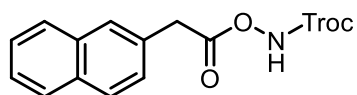
4.3 Asymmetric Amination of Secondary C-H Bonds Catalyzed by Chiral N4 Iron Catalysts

4.3.1 Synthesis of Substrates

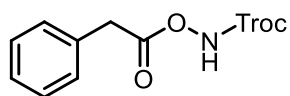


Method A: To a solution of carboxylic acid (1.0 equiv.) and *N*-protected hydroxylamine (1.1 equiv.) in dichloromethane (0.2 M) at 0 °C was added DCC (1.1 equiv.) in one portion. The reaction mixture was warmed to room temperature and was stirred for 2 hours. After completion, the reaction mixture was filtered and washed with dichloromethane. After being concentrated under reduced pressure, the residue was purified by chromatography on silica gel using indicated solvent as the eluent.

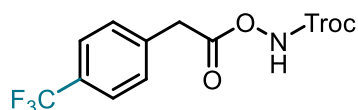
Method B: To a solution of carboxylic acid (1.0 equiv.), 4-DMAP (0.1 equiv.) and *N*-protected hydroxylamine (1.1 equiv.) in dichloromethane (0.2 M) at 0 °C was added EDCI (1.1 equiv.) in one portion. The reaction mixture was warmed to room temperature and was stirred for 1 hour. After completion, water was added, and the mixture was extracted with EtOAc for three times. The combined organic layer was washed with brine and was dried over anhydrous sodium sulfate. After filtration, the solvent was evaporated under reduced pressure, and the residue was purified by chromatography on silica gel using indicated solvent as the eluent.

2,2,2-Trichloroethyl (2-(naphthalen-2-yl)acetoxy)carbamate (**1a**)

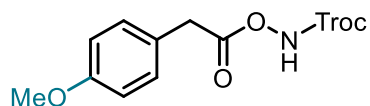
DCC coupling of 2-(naphthalen-2-yl)acetic acid with TrocNHOH gave 2,2,2-trichloroethyl (2-(naphthalen-2-yl)acetoxy)carbamate (**1a**) as a white solid (chromatography on silica gel, eluent: EtOAc/*n*-hexane = 1/8): **IR** (film) ν_{max} : 3322, 1749, 1445, 1206, 1098, 807, 719 cm^{-1} . **¹H NMR** (300 MHz, CDCl_3) δ 3.96 (s, 2H), 4.79 (s, 2H), 7.39–7.45 (m, 1H), 7.45–7.54 (m, 2H), 7.74–7.79 (m, 1H), 7.79–7.88 (m, 3H), 8.27–8.41 (br, 1H). **¹³C NMR** (75 MHz, CDCl_3) δ 38.8, 75.3, 94.5, 126.4, 126.6, 127.1, 127.8, 127.9, 128.5, 128.8, 129.4, 132.8, 133.6, 154.6, 170.4. **HRMS** calcd for $[\text{C}_{15}\text{H}_{12}\text{Cl}_3\text{NO}_4\text{Na}]^+ [(M + \text{Na})^+]$: 397.9724; found: 397.9734.

2,2,2-Trichloroethyl (2-phenylacetoxy)carbamate (1b)

DCC coupling of 2-phenylacetic acid with TrocNHOH gave 2,2,2-Trichloroethyl (2-phenylacetoxy)carbamate (**1b**) as a white solid (chromatography on silica gel, eluent: EtOAc/*n*-hexane = 1/10): **IR** (film) ν_{\max} : 3224, 1761, 1463, 1229, 1119, 712 cm^{-1} . **$^1\text{H NMR}$** (300 MHz, CDCl_3) δ 3.81 (s, 2H), 4.79 (s, 2H), 7.27–7.40 (m, 5H), 8.24–8.33 (br, 1H). **$^{13}\text{C NMR}$** (75 MHz, CDCl_3) δ 38.6, 75.3, 94.5, 127.9, 129.0, 129.4, 132.0, 154.6, 170.4. **HRMS** calcd for $[\text{C}_{11}\text{H}_{10}\text{Cl}_3\text{NO}_4\text{Na}]^+$ [(M + Na) $^+$]: 347.9568; found: 347.9571.

2,2,2-Trichloroethyl (2-(4-(trifluoromethyl)phenyl)acetoxy)carbamate (1c)

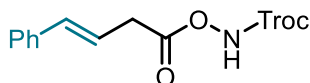
DCC coupling of 2-(4-(trifluoromethyl)phenyl)acetic acid with TrocNHOH gave 2,2,2-trichloroethyl (2-(4-(trifluoromethyl)-phenyl)acetoxy)carbamate (**1c**) as a colorless oil (chromatography on silica gel, eluent: EtOAc/*n*-hexane = 1/10): **IR** (film) ν_{\max} : 3182, 1725, 1322, 1117, 1062 cm^{-1} . **$^1\text{H NMR}$** (300 MHz, CDCl_3) δ 3.87 (s, 2H), 4.79 (s, 2H), 7.40–7.49 (m, 2H), 7.57–7.66 (m, 2H), 8.29–8.41 (br, 1H). **$^{13}\text{C NMR}$** (75 MHz, CDCl_3) δ 38.3, 75.4, 94.4, 124.1 (q, $J = 272.4$ Hz), 126.0 (q, $J = 3.8$ Hz), 129.9, 130.4 (q, $J = 32.8$ Hz), 135.9, 154.6, 169.7. **$^{19}\text{F NMR}$** (282 MHz, CDCl_3) δ -63.2. **HRMS** calcd for $[\text{C}_{12}\text{H}_9\text{Cl}_3\text{F}_3\text{NO}_4\text{Na}]^+$ [(M + Na) $^+$]: 415.9441; found: 415.9455.

2,2,2-Trichloroethyl (2-(4-methoxyphenyl)acetoxy)carbamate (1d)

DCC coupling of 2-(4-methoxyphenyl)acetic acid with TrocNHOH gave 2,2,2-trichloroethyl (2-(4-methoxyphenyl)acetoxy)carbamate (**1d**) as a colorless oil (chromatography on silica gel, eluent: EtOAc/*n*-hexane = 1/6): **IR** (film) ν_{\max} : 3264, 1752, 1511, 1244, 1114, 1087, 717 cm^{-1} . **$^1\text{H NMR}$** (300 MHz, CDCl_3) δ 3.74 (s, 2H), 3.80 (s, 3H), 4.79 (s, 2H), 6.82–6.93 (m, 2H), 7.19–7.26 (m, 2H),

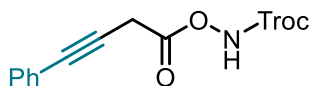
8.24–8.41 (br, 1H). ^{13}C NMR (75 MHz, CDCl_3) δ 37.7, 55.4, 75.3, 94.5, 114.4, 123.9, 130.5, 154.6, 159.3, 170.7. HRMS calcd for $[\text{C}_{12}\text{H}_{12}\text{Cl}_3\text{NO}_5\text{Na}]^+$ $[(\text{M} + \text{Na})^+]$: 377.9673; found: 377.9676.

2,2,2-Trichloroethyl (*E*)-((4-phenylbut-3-enoyl)oxy)carbamate [(*E*)-1e]



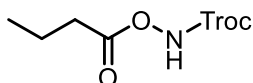
DCC coupling of (*E*)-4-phenylbut-3-enoic acid with TrocNHOH gave 2,2,2-Trichloroethyl (*E*)-((4-phenylbut-3-enoyl)oxy)carbamate (*E*)-1e as a light yellow oil (chromatography on silica gel, eluent: EtOAc/*n*-hexane = 1/10): IR (film) ν_{max} : 3187, 1799, 1721, 1514, 1263, 1138, 1079, 719 cm^{-1} . ^1H NMR (300 MHz, CDCl_3) δ 3.43 (dd, $J = 7.0, 1.3$ Hz, 2H), 4.81 (s, 2H), 6.25 (dt, $J = 15.9, 7.0$ Hz, 1H), 6.58 (dt, $J = 15.9, 1.3$ Hz, 1H), 7.21–7.44 (m, 5H), 8.31–8.45 (br, 1H). ^{13}C NMR (75 MHz, CDCl_3) δ 35.7, 75.3, 94.5, 119.2, 126.6, 128.1, 128.8, 135.2, 136.4, 154.6, 170.4. HRMS calcd for $[\text{C}_{13}\text{H}_{12}\text{Cl}_3\text{NO}_4\text{Na}]^+$ $[(\text{M} + \text{Na})^+]$: 373.9724; found: 373.9731.

2,2,2-Trichloroethyl ((4-phenylbut-3-ynoyl)oxy)carbamate (1f)



DCC coupling of 4-phenylbut-3-ynoic acid with TrocNHOH gave 2,2,2-trichloroethyl ((4-phenylbut-3-ynoyl)oxy)carbamate (1f) as a colorless oil (chromatography on silica gel, eluent: EtOAc/*n*-hexane = 1/10): IR (film) ν_{max} : 3204, 1758, 1132, 719 cm^{-1} . ^1H NMR (300 MHz, CDCl_3) δ 3.71 (s, 2H), 4.82 (s, 2H), 7.27–7.36 (m, 3H), 7.39–7.51 (m, 2H), 8.32–8.52 (br, 1H). ^{13}C NMR (75 MHz, CDCl_3) δ 24.6, 75.4, 78.6, 84.6, 94.4, 122.5, 128.4, 128.7, 132.0, 154.5, 167.3. HRMS calcd for $[\text{C}_{13}\text{H}_{10}\text{Cl}_3\text{NO}_4\text{Na}]^+$ $[(\text{M} + \text{Na})^+]$: 371.9568; found: 371.9575.

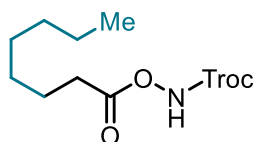
2,2,2-Trichloroethyl (butyryloxy)carbamate (1g)



DCC coupling of butyric acid with TrocNHOH gave 2,2,2-trichloroethyl (butyryloxy)carbamate (1g) as a colorless oil (chromatography on silica gel, eluent: EtOAc/*n*-hexane = 1/12): IR (film) ν_{max} : 3278, 2967, 1749, 1228, 1119, 719 cm^{-1} . ^1H NMR (300 MHz, CDCl_3) δ 1.00 (t, $J = 7.4$ Hz, 3H), 1.74

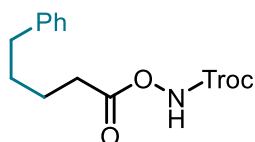
(sextet, $J = 7.4$ Hz, 2H), 2.47 (t, $J = 7.4$ Hz, 2H), 4.80 (s, 2H), 8.26–8.50 (br, 1H). ^{13}C NMR (75 MHz, CDCl_3) δ 13.6, 18.3, 33.5, 75.3, 94.6, 154.7, 172.4. HRMS calcd for $[\text{C}_7\text{H}_{10}\text{Cl}_3\text{NO}_4\text{Na}]^+$ $[(\text{M} + \text{Na})^+]$: 299.9568; found: 299.9573.

2,2,2-Trichloroethyl (octanoyloxy)carbamate (**1h**)



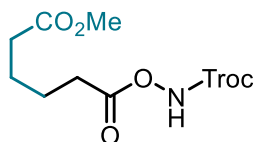
DCC coupling of octanoic acid with TrocNHOH gave 2,2,2-trichloroethyl (octanoyloxy)carbamate (**1h**) as a colorless oil (chromatography on silica gel, eluent: EtOAc/*n*-hexane = 1/15): IR (film) ν_{max} : 3281, 2927, 1751, 1231, 1120, 1089, 718 cm^{-1} . ^1H NMR (300 MHz, CDCl_3) δ 0.75–0.96 (m, 3H), 1.14–1.42 (m, 8H), 1.61–1.80 (m, 2H), 2.48 (t, $J = 7.6$ Hz, 2H), 4.80 (s, 2H), 8.18–8.47 (br, 1H). ^{13}C NMR (75 MHz, CDCl_3) δ 14.2, 22.7, 24.7, 28.9, 29.0, 31.68, 31.71, 75.3, 94.6, 154.7, 172.6. HRMS calcd for $[\text{C}_{11}\text{H}_{18}\text{Cl}_3\text{NO}_4\text{Na}]^+$ $[(\text{M} + \text{Na})^+]$: 356.0194; found: 356.0194.

2,2,2-Trichloroethyl ((5-phenylpentanoyl)oxy)carbamate (**1i**)



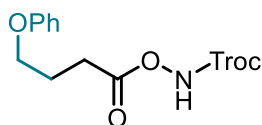
DCC coupling of 5-phenylpentanoic acid with TrocNHOH gave 2,2,2-trichloroethyl ((5-phenylpentanoyl)oxy)carbamate (**1i**) as a colorless oil (chromatography on silica gel, eluent: EtOAc/*n*-hexane = 1/10): IR (film) ν_{max} : 3282, 2936, 1753, 1112, 746, 721, 708 cm^{-1} . ^1H NMR (300 MHz, CDCl_3) δ 1.61–1.86 (m, 4H), 2.41–2.58 (m, 2H), 2.58–2.75 (m, 2H), 4.80 (s, 2H), 7.09–7.24 (m, 3H), 7.24–7.36 (m, 2H), 8.28–8.46 (br, 1H). ^{13}C NMR (75 MHz, CDCl_3) δ 24.3, 30.7, 31.5, 35.5, 75.2, 94.6, 126.0, 128.49, 128.51, 141.8, 154.7, 172.3. HRMS calcd for $[\text{C}_{14}\text{H}_{16}\text{Cl}_3\text{NO}_4\text{Na}]^+$ $[(\text{M} + \text{Na})^+]$: 390.0037; found: 390.0042.

Methyl 6-oxo-6-(((2,2,2-trichloroethoxy)carbonyl)amino)oxy)hexanoate (**1j**)



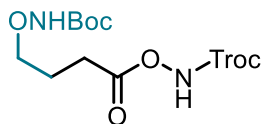
DCC coupling of 6-methoxy-6-oxohexanoic acid with TrocNHOH gave methyl 6-oxo-6-(((2,2,2-trichloroethoxy)carbonyl)amino)oxy)hexanoate (**1j**) as a colorless oil (chromatography on silica gel, eluent: EtOAc/*n*-hexane = 1/5): **IR** (film) ν_{\max} : 3258, 2954, 1730, 1227, 1110, 718 cm^{-1} . **¹H NMR** (300 MHz, CDCl_3) δ 1.65–1.80 (m, 4H), 2.28–2.40 (m, 2H), 2.42–2.59 (m, 2H), 3.66 (s, 3H), 4.79 (s, 2H), 8.43–8.60 (br, 1H). **¹³C NMR** (75 MHz, CDCl_3) δ 24.1, 24.2, 31.3, 33.6, 51.8, 75.2, 94.6, 154.7, 172.0, 173.7. **HRMS** calcd for $[\text{C}_{10}\text{H}_{14}\text{Cl}_3\text{NO}_6\text{Na}]^+$ $[(\text{M} + \text{Na})^+]$: 371.9779; found: 371.9780.

2,2,2-Trichloroethyl ((4-phenoxybutanoyl)oxy)carbamate (**1k**)



DCC coupling of 4-phenoxybutanoic acid with TrocNHOH gave 2,2,2-trichloroethyl ((4-phenoxybutanoyl)oxy)carbamate (**1k**) as a colorless oil (chromatography on silica gel, eluent: EtOAc/*n*-hexane = 1/5): **IR** (film) ν_{\max} : 3285, 2956, 1754, 1237, 1115, 1047, 750, 718 cm^{-1} . **¹H NMR** (300 MHz, CDCl_3) δ 2.20 (tt, $J = 7.3, 6.0$ Hz, 2H), 2.73 (t, $J = 7.3$ Hz, 2H), 4.04 (t, $J = 6.0$ Hz, 2H), 4.80 (s, 2H), 6.82–6.92 (m, 2H), 6.92–7.01 (m, 1H), 7.18–7.36 (m, 2H), 8.19–8.55 (br, 1H). **¹³C NMR** (75 MHz, CDCl_3) δ 24.5, 28.5, 66.1, 75.3, 94.5, 114.6, 121.1, 129.6, 154.7, 158.7, 172.1; **HRMS** calcd for $[\text{C}_{13}\text{H}_{14}\text{Cl}_3\text{NO}_5\text{Na}]^+$ $[(\text{M} + \text{Na})^+]$: 391.9830; found: 391.9835.

2,2,2-Trichloroethyl ((4-((*tert*-butoxycarbonyl)amino)butanoyl)oxy)carbamate (**1l**)

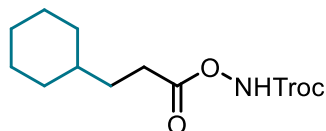


EDCI coupling of 4-((*tert*-butoxycarbonyl)amino)butanoic acid with TrocNHOH gave 2,2,2-trichloroethyl ((4-((*tert*-butoxycarbonyl)amino)-butanoyl)oxy)carbamate (**1l**) as a white solid (chromatography on silica gel, eluent: EtOAc/*n*-hexane = 1/2): **IR** (film) ν_{\max} : 3384, 3120, 2940, 1747, 1679, 1528, 1258, 1155, 1121, 719 cm^{-1} . **¹H NMR** (300 MHz, CDCl_3) δ 1.43 (s, 9H), 1.81–1.96 (m, 2H), 2.52 (t, $J = 7.3$ Hz, 2H), 3.19 (q, $J = 6.5$ Hz, 2H), 4.74 (t, $J = 6.5$ Hz, 1H), 4.79 (s, 2H), 8.67–8.89

(br, 1H). ^{13}C NMR (75 MHz, CDCl_3) δ 25.2, 28.5, 29.0, 39.6, 75.2, 79.7, 94.6, 154.8, 156.2, 172.1.

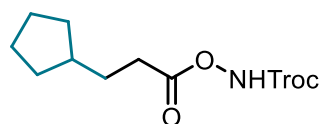
HRMS calcd for $[\text{C}_{12}\text{H}_{19}\text{Cl}_3\text{N}_2\text{O}_6\text{Na}]^+ [(M + \text{Na})^+]$: 415.0201; found: 415.0202.

2,2,2-Trichloroethyl ((3-cyclohexylpropanoyl)oxy)carbamate (**1m**)



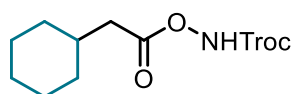
DCC coupling of 3-cyclohexylpropanoic acid with TrocNHOH gave 2,2,2-trichloroethyl ((3-cyclohexylpropanoyl)oxy)carbamate (**1m**) as a colorless oil (chromatography on silica gel, eluent: EtOAc/*n*-hexane = 1/15): IR (film) ν_{max} : 3277, 2924, 2852, 1755, 1450, 1233, 1115, 720 cm^{-1} . ^1H NMR (300 MHz, CDCl_3) δ 0.80–1.00 (m, 2H), 1.06–1.39 (m, 4H), 1.55–1.66 (m, 3H), 1.66–1.77 (m, 4H), 2.40–2.56 (m, 2H), 4.80 (s, 2H), 8.22–8.45 (br, 1H). ^{13}C NMR (75 MHz, CDCl_3) δ 26.2, 26.6, 29.3, 32.0, 33.0, 37.2, 75.3, 94.6, 154.7, 172.9. HRMS calcd for $[\text{C}_{12}\text{H}_{18}\text{Cl}_3\text{NO}_4\text{Na}]^+ [(M + \text{Na})^+]$: 368.0194; found: 368.0195.

2,2,2-Trichloroethyl ((3-cyclopentylpropanoyl)oxy)carbamate (**1n**)



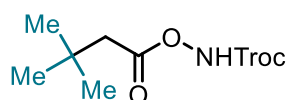
DCC coupling of 3-cyclopentylpropanoic acid with TrocNHOH gave 2,2,2-trichloroethyl ((3-cyclopentylpropanoyl)oxy)carbamate (**1n**) as a colorless oil (chromatography on silica gel, eluent: EtOAc/*n*-hexane = 1/15): IR (film) ν_{max} : 3278, 2949, 2866, 1754, 1227, 1117, 720 cm^{-1} . ^1H NMR (300 MHz, CDCl_3) δ 0.96–1.19 (m, 2H), 1.43–1.65 (m, 4H), 1.65–1.87 (m, 5H), 2.38–2.58 (m, 2H), 4.80 (s, 2H), 8.29–8.46 (br, 1H). ^{13}C NMR (75 MHz, CDCl_3) δ 25.2, 30.9, 31.0, 32.4, 39.6, 75.3, 94.6, 154.7, 172.6. HRMS calcd for $[\text{C}_{11}\text{H}_{16}\text{Cl}_3\text{NO}_4\text{Na}]^+ [(M + \text{Na})^+]$: 354.0037; found: 354.0039.

2,2,2-Trichloroethyl (2-cyclohexylacetoxy)carbamate (**1o**)



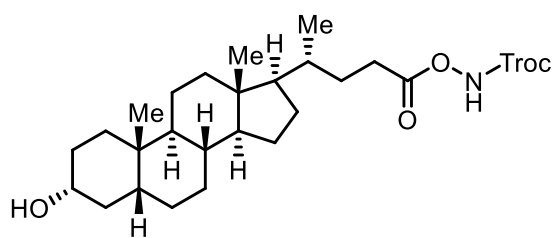
DCC coupling of 2-cyclohexylacetic acid with TrocNHOH gave 2,2,2-trichloroethyl (2-cyclohexylacetoxycarbamate (**1o**) as a colorless oil (chromatography on silica gel, eluent: EtOAc/*n*-hexane = 1/15): **IR** (film) ν_{\max} : 3275, 2926, 2852, 1749, 1214, 1113, 717 cm^{-1} . **¹H NMR** (300 MHz, CDCl_3) δ 0.92–1.10 (m, 2H), 1.10–1.36 (m, 3H), 1.61–1.93 (m, 6H), 2.36 (d, $J = 7.0$ Hz, 2H), 4.80 (s, 2H), 8.24–8.42 (br, 1H). **¹³C NMR** (75 MHz, CDCl_3) δ 26.0, 26.1, 33.0, 34.9, 39.3, 75.3, 94.6, 154.7, 171.8. **HRMS** calcd for $[\text{C}_{11}\text{H}_{16}\text{Cl}_3\text{NO}_4\text{Na}]^+$ $[(M + \text{Na})^+]$: 354.0037; found: 354.0040.

2,2,2-Trichloroethyl ((3,3-dimethylbutanoyl)oxy)carbamate (**1p**)



DCC coupling of 3,3-dimethylbutanoic acid with TrocNHOH gave 2,2,2-trichloroethyl ((3,3-dimethylbutanoyl)oxy)carbamate (**1p**) as a white solid (chromatography on silica gel, eluent: EtOAc/*n*-hexane = 1/20): **IR** (film) ν_{\max} : 3286, 2961, 1791, 1741, 1473, 1253, 1123, 731 cm^{-1} . **¹H NMR** (300 MHz, CDCl_3) δ 1.08 (s, 9H), 2.37 (s, 2H), 4.80 (s, 2H), 8.24–8.48 (br, 1H). **¹³C NMR** (75 MHz, CDCl_3) δ 29.6, 31.3, 45.2, 75.3, 94.6, 154.7, 170.9. **HRMS** calcd for $[\text{C}_9\text{H}_{14}\text{Cl}_3\text{NO}_4\text{Na}]^+$ $[(M + \text{Na})^+]$: 327.9881; found: 327.9889.

(((*R*)-4-(((3*R*,5*R*,8*R*,9*S*,10*S*,13*R*,14*S*,17*R*)-3-Hydroxy-10,13-dimethylhexadecahydro-1*H*-cyclopent a[*a*]phenanthren-17-yl)pentanoyl)oxy)carbamate (**1q**)



EDCI coupling of lithocholic acid with TrocNHOH gave (((*R*)-4-(((3*R*,5*R*,8*R*,9*S*,10*S*,13*R*,14*S*,17*R*)-3-hydroxy-10,13-dimethylhexadecahydro-1*H*-cyclopenta[*a*]phenanthren-17-yl)pentanoyl)oxy)carbamate (**1q**) as a white solid (chromatography on silica gel, eluent: EtOAc/*n*-hexane = 1/2): **IR** (film) ν_{\max} : 3484, 3167, 2928, 2858, 1744, 1116, 1066, 1029, 764 cm^{-1} . **¹H NMR** (300 MHz, CDCl_3) δ 0.64 (s, 3H), 0.85–0.95 (m, 6H), 1.00–1.99 (m, 27H), 2.32–2.45 (m, 1H), 2.45–2.60 (m, 1H), 3.54–3.71 (m, 1H), 4.79 (s, 2H), 8.48–8.68 (br, 1H). **¹³C NMR** (75 MHz, CDCl_3) δ 12.1, 18.3, 21.0, 23.5, 24.3, 26.5, 27.3, 28.3, 28.7, 30.6, 30.8, 34.7, 35.4, 35.5, 36.0, 36.5,

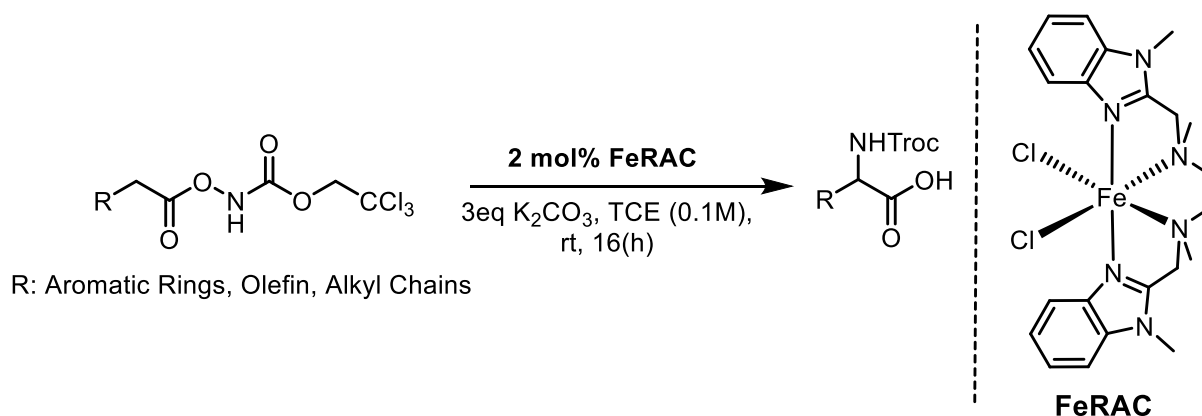
40.3, 40.6, 42.2, 42.9, 56.0, 56.6, 72.0, 75.2, 94.6, 154.7, 173.0. **HRMS** calcd for $[\text{C}_{27}\text{H}_{42}\text{Cl}_3\text{NO}_5\text{Na}]^+$ $[(\text{M} + \text{Na})^+]$: 588.2021; found: 588.2026.

4.3.2 Asymmetric Amination of Secondary CH Bonds Catalyzed by Chiral N4 Iron Catalysts

A pre-dried 10 mL Schlenk tube was charged with substrate (0.2 mmol), K_2CO_3 (0.6 mmol) and (*R,R*)-**FeBIP** (4.0–15.0 mol%). The tube was evacuated and backfilled with N_2 for three times. 1,1,2,2-tetrachloroethane (TCE, 0.1 M) was added, and the mixture was degassed via freeze-pump-thaw for two times. The tube was sealed, and the reaction mixture was stirred at 0 °C for 40 hours or room temperature for 16 hours. To quench the reaction, water (2 mL) and hydrochloric acid (4N) (2.5 mL/mmol substrate) was added. The mixture was extracted with EtOAc for three times and the combined organic layer was dried over anhydrous sodium sulfate. After filtration, the solvent was evaporated under reduced pressure, and the residue was purified by column chromatography on silica gel using indicated solvent as the eluent. Enantiomeric ratios were determined by HPLC analysis on chiral stationary phase. The absolute configuration of product **2b** was confirmed by HPLC analysis as *S*-configuration.

Additional experimental information:

a) Racemic catalytic reactions



b) Control of reaction temperature. The catalytic reactions were set up in a cooling ethanol bath at 0 °C.

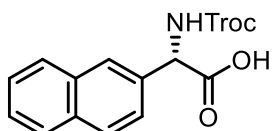


c) **Execution of the reactions.** All catalytic reactions were carried out in 10 mL Schlenk tubes from “Synthware” under N₂ atmosphere (see image below).

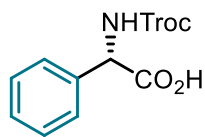


4.3.3 Experimental and Characterization Data of New Products

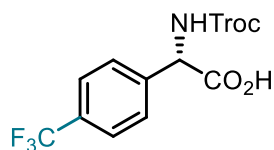
(*S*)-2-(Naphthalen-2-yl)-2-(((2,2,2-trichloroethoxy)carbonyl)amino)acetic acid (**2a**)



Catalyzed by 8 mol% (*R,R*)-**FeBIP**, the 1,3-nitrogen shift of **1a** (75.0 mg, 0.2 mmol) gave **2a** as a white solid (chromatography on silica gel, eluent: EtOAc/*n*-hexane = 1/4 with 0.1% TFA, 72.0 mg, 96% yield) with 90% ee [DAICEL CHIRALPAK IB column, Agilent HPLC 1260, CH₃CN/H₂O (0.1% TFA) = 30:70, 1.0 mL/min, 25 °C, 210 nm; t₁ = 31.0 min, t₂ = 36.0 min]: [α]_D²⁵ = -10.6 (c 1.0, MeOH). **IR** (film) ν_{max}: 1724, 1693, 1504, 1182, 1039, 815, 736 cm⁻¹. **¹H NMR** (300 MHz, CD₃OD) δ 4.79 (d, *J* = 12.3 Hz, 1H), 4.80 (d, *J* = 12.3 Hz, 1H), 5.49 (s, 1H), 7.43–7.51 (m, 2H), 7.51–7.59 (m, 1H), 7.79–7.89 (m, 3H), 7.89–7.95 (m, 1H). **¹³C NMR** (75 MHz, CD₃OD) δ 59.9, 75.6, 97.0, 126.2, 127.4 (2C), 127.8, 128.7, 129.0, 129.5, 134.6, 134.7, 135.4, 156.2, 173.5. **HRMS** calcd for [C₁₅H₁₂Cl₃NO₄Na]⁺ [(M + Na)⁺]: 397.9724; found: 397.9724.

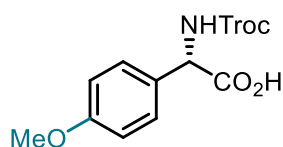
(S)-2-Phenyl-2-(((2,2,2-trichloroethoxy)carbonyl)amino)acetic acid (2b)

Catalyzed by 8 mol% (*R,R*)-**FeBIP**, the 1,3-nitrogen shift of **1b** (65.0 mg, 0.2 mmol) gave **2b** as a white solid (chromatography on silica gel, eluent: EtOAc/*n*-hexane = 1/5 with 0.1% TFA, 61.7 mg, 95% yield) with 91% ee [DAICEL CHIRALPAK ODR column, Agilent HPLC 1260, CH₃CN/H₂O (0.1% TFA) = 40:60, 1.0 mL/min, 25 °C, 210 nm; *t*₁ = 11.0 min, *t*₂ = 12.8 min]: [α]_D²⁵ = -30.4 (*c* 1.0, MeOH). IR (film) ν_{max} : 1692, 1425, 1042, 717 cm⁻¹. ¹H NMR (300 MHz, CD₃OD) δ 4.77 (d, *J* = 12.2 Hz, 1H), 4.80 (d, *J* = 12.2 Hz, 1H), 5.29 (s, 1H), 7.30–7.40 (m, 3H), 7.40–7.49 (m, 2H); ¹³C NMR (75 MHz, CD₃OD) δ 59.8, 75.6, 97.0, 128.6, 129.4, 129.7, 138.1, 156.2, 173.5; HRMS calcd for [C₁₁H₁₀Cl₃NO₄Na]⁺ [(M + Na)⁺]: 347.9568; found: 347.9576.

(S)-2-(((2,2,2-Trichloroethoxy)carbonyl)amino)-2-(4-(trifluoromethyl)phenyl)acetic acid (2c)

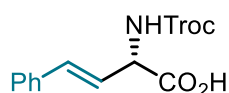
Catalyzed by 8 mol% (*R,R*)-**FeBIP**, the 1,3-nitrogen shift of **1c** (78.6 mg, 0.2 mmol) gave **2c** as a white solid (chromatography on silica gel, eluent: EtOAc/*n*-hexane = 1/4 with 0.1% TFA, 56.6 mg, 72% yield) with 92% ee [DAICEL CHIRALPAK ODR column, Agilent HPLC 1260, CH₃CN/H₂O (0.1% TFA) = 40:60, 1.0 mL/min, 25 °C, 210 nm; *t*₁ = 16.1 min, *t*₂ = 17.2 min]: [α]_D²⁵ = -88.3 (*c* 1.0, MeOH). IR (film) ν_{max} : 1726, 1696, 1541, 1324, 1161, 1121, 814 cm⁻¹. ¹H NMR (300 MHz, CD₃OD) δ 4.79 (d, *J* = 12.2 Hz, 1H), 4.81 (d, *J* = 12.2 Hz, 1H), 5.42 (s, 1H), 7.60–7.65 (m, 2H), 7.65–7.71 (m, 2H). ¹³C NMR (75 MHz, CD₃OD) δ 59.3, 75.7, 96.9, 125.5 (q, *J* = 271.1 Hz), 126.6 (q, *J* = 3.8 Hz), 129.4, 131.4 (q, *J* = 32.4 Hz), 142.7, 156.2, 172.6. ¹⁹F NMR (282 MHz, CD₃OD) δ -62.5. HRMS calcd for [C₁₂H₉Cl₃F₃NO₄Na]⁺ [(M + Na)⁺]: 415.9441; found: 415.9446.

(S)-2-(4-Methoxyphenyl)-2-(((2,2,2-trichloroethoxy)carbonyl)amino)acetic acid (2d)



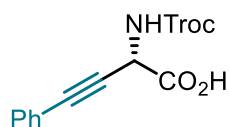
Catalyzed by 8 mol% (*R,R*)-**FeBIP**, the 1,3-nitrogen shift of **1d** (71.0 mg, 0.2 mmol) gave **2d** as a white solid (chromatography on silica gel, eluent: EtOAc/*n*-hexane = 1/3 with 0.1% TFA, 67.5 mg, 95% yield) with 90% ee [DAICEL CHIRALPAK IB column, Agilent HPLC 1260, CH₃CN/H₂O (0.1% TFA) = 30:70, 1.0 mL/min, 35 °C, 220 nm; $t_1 = 33.7$ min, $t_2 = 34.7$ min]: $[\alpha]_D^{25} = -112.9$ (c 1.0, MeOH). **IR** (film) ν_{\max} : 1721, 1506, 1246, 810 cm⁻¹. **¹H NMR** (300 MHz, CD₃OD) δ 3.78 (s, 3H), 4.77 (d, $J = 12.2$ Hz, 1H), 4.79 (d, $J = 12.2$ Hz, 1H), 5.21 (s, 1H), 6.87–6.95 (m, 2H), 7.30–7.38 (m, 2H). **¹³C NMR** (75 MHz, CD₃OD) δ 55.8, 59.2, 75.6, 97.0, 115.1, 129.9 (2C), 156.2, 161.2, 173.9; **HRMS** calcd for [C₁₂H₁₂Cl₃NO₅Na]⁺ [(M + Na)⁺]: 377.9673; found: 377.9683.

(*S,E*)-4-Phenyl-2-(((2,2,2-trichloroethoxy)carbonyl)amino)but-3-enoic acid [(*E*)-2e]



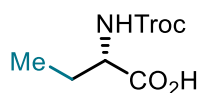
Catalyzed by 8 mol% (*R,R*)-**FeBIP**, the 1,3-nitrogen shift of (*E*)-**1e** (70.2 mg, 0.2 mmol) gave (*E*)-**2e** as a yellow solid (chromatography on silica gel, eluent: EtOAc/*n*-hexane = 1/4 with 0.1% TFA, 30.9 mg, 44% yield) with 86% ee [DAICEL CHIRALPAK ODR column, Agilent HPLC 1260, CH₃CN/H₂O (0.1% TFA) = 50:50, 1.0 mL/min, 25 °C, 210 nm; $t_1 = 23.4$ min, $t_2 = 25.2$ min]: $[\alpha]_D^{25} = -22.3$ (c 1.0, MeOH). **IR** (film) ν_{\max} : 1695, 1427, 1350, 1041, 720 cm⁻¹. **¹H NMR** (300 MHz, CD₃OD) δ 4.78 (d, $J = 12.2$ Hz, 1H), 4.85 (d, $J = 12.2$ Hz, 1H), 4.94 (dd, $J = 6.7, 0.8$ Hz, 1H), 6.34 (dd, $J = 16.0, 6.7$ Hz, 1H), 6.73 (dd, $J = 16.0, 0.8$ Hz, 1H), 7.18–7.36 (m, 3H), 7.36–7.49 (m, 2H). **¹³C NMR** (75 MHz, CD₃OD) δ 57.7, 75.6, 97.0, 124.5, 127.6, 129.1, 129.7, 134.2, 137.6, 156.4, 173.6. **HRMS** calcd for [C₁₃H₁₂Cl₃NO₄Na]⁺ [(M + Na)⁺]: 373.9724; found: 373.9726.

(*S*)-4-Phenyl-2-(((2,2,2-trichloroethoxy)carbonyl)amino)but-3-ynoic acid (2f**)**



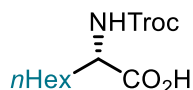
Catalyzed by 8 mol% (*R,R*)-**FeBIP**, the 1,3-nitrogen shift of **1f** (69.8 mg, 0.2 mmol) gave **2f** as a yellow oil (chromatography on silica gel, eluent: EtOAc/*n*-hexane = 1/4 with 0.1% TFA, 9.1 mg, 13% yield) with 44% ee [DAICEL CHIRALPAK IG column, Agilent HPLC 1260, CH₃CN/H₂O (0.1% TFA) = 50:50, 1.0 mL/min, 25 °C, 210 nm; $t_1 = 7.4$ min, $t_2 = 9.0$ min]: $[\alpha]_D^{25} = -11.5$ (c 1.0, MeOH). **IR** (film) ν_{\max} : 1722, 1512, 1213, 1040, 719 cm⁻¹. **¹H NMR** (300 MHz, CD₃OD) δ 4.79 (d, $J = 12.3$ Hz, 1H), 4.85 (d, $J = 12.3$ Hz, 1H), 5.26 (s, 1H), 7.26–7.39 (m, 3H), 7.40–7.52 (m, 2H). **¹³C NMR** (75 MHz, CD₃OD) δ 47.8, 75.7, 83.6, 85.0, 96.9, 123.4, 129.5, 129.9, 132.8, 156.2, 170.5. **HRMS** calcd for [C₁₃H₁₀Cl₃NO₄Na]⁺ [(M + Na)⁺]: 371.9568; found: 371.9570.

(S)-2-(((2,2,2-Trichloroethoxy)carbonyl)amino)butanoic acid (2g)



Catalyzed by 8 mol% (*R,R*)-**FeBIP**, the 1,3-nitrogen shift of **1g** (55.7 mg, 0.2 mmol) gave **2g** as a colorless oil (chromatography on silica gel, eluent: EtOAc/*n*-hexane = 1/5 with 0.1% TFA, 34.3 mg, 62% yield) with 91% ee [DAICEL CHIRALPAK IG column, Agilent HPLC 1260, *i*PrOH/*n*-hexane = 10/90 (v/v) with 0.1% TFA, 1.0 mL/min, 25 °C, 210 nm; $t_1 = 9.0$ min, $t_2 = 14.0$ min]: $[\alpha]_D^{25} = -40.0$ (c 1.0, MeOH). **IR** (film) ν_{\max} : 1723, 1686, 1460, 1393, 1105, 813, 722 cm⁻¹. **¹H NMR** (300 MHz, CD₃OD) δ 1.00 (t, $J = 7.4$ Hz, 3H), 1.62–1.82 (m, 1H), 1.82–2.02 (m, 1H), 4.10 (dd, $J = 8.6, 5.1$ Hz, 1H), 4.74 (d, $J = 12.2$ Hz, 1H), 4.83 (d, $J = 12.2$ Hz, 1H). **¹³C NMR** (75 MHz, CD₃OD) δ 10.6, 26.0, 57.0, 75.5, 97.1, 156.7, 175.5. **HRMS** calcd for [C₇H₁₀Cl₃NO₄Na]⁺ [(M + Na)⁺]: 299.9568; found: 299.9567.

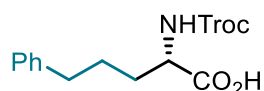
(S)-2-(((2,2,2-Trichloroethoxy)carbonyl)amino)octanoic acid (2h)



Catalyzed by 8 mol% (*R,R*)-**FeBIP**, the 1,3-nitrogen shift of **1h** (66.9 mg, 0.2 mmol) gave **2h** as a colorless oil (chromatography on silica gel, eluent: EtOAc/*n*-hexane = 1/6 with 0.1% TFA, 50.5 mg, 75% yield) with 92% ee [DAICEL CHIRALPAK IG column, Agilent HPLC 1260, *i*PrOH/*n*-hexane = 5/95 (v/v) with 0.1% TFA, 1.0 mL/min, 25 °C, 210 nm; $t_1 = 13.4$ min, $t_2 = 20.8$ min]: $[\alpha]_D^{25} = +9.5$ (c 1.0, MeOH). **IR** (film) ν_{\max} : 2957, 2926, 1719, 1688, 1395, 1117, 810, 720 cm⁻¹. **¹H NMR** (300 MHz,

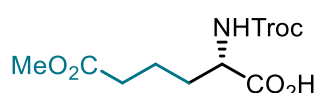
CD₃OD) δ 0.71–1.04 (m, 3H), 1.16–1.56 (m, 8H), 1.60–1.78 (m, 1H), 1.78–1.96 (m, 1H), 4.15 (dd, J = 9.1, 4.8 Hz, 1H), 4.73 (d, J = 12.2 Hz, 1H), 4.84 (d, J = 12.2 Hz, 1H). ¹³C NMR (75 MHz, CD₃OD) δ 14.4, 23.6, 26.8, 29.8, 32.7, 32.8, 55.5, 75.5, 97.1, 156.7, 175.7. HRMS calcd for [C₁₁H₁₈Cl₃NO₄Na]⁺ [(M + Na)⁺]: 356.0194; found: 356.0194.

(S)-5-Phenyl-2-(((2,2,2-trichloroethoxy)carbonyl)amino)pentanoic acid (2i)

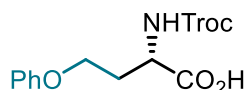


Catalyzed by 8 mol% (*R,R*)-**FeBIP**, the 1,3-nitrogen shift of **1i** (73.7 mg, 0.2 mmol) gave **2i** as a colorless oil (chromatography on silica gel, eluent: EtOAc/*n*-hexane = 1/5 with 0.1% TFA, 43.9 mg, 60% yield) with 91% ee [DAICEL CHIRALPAK IG column, Agilent HPLC 1260, *i*PrOH/*n*-hexane = 10/90 (v/v) with 0.1% TFA, 1.0 mL/min, 25 °C, 210 nm; t_1 = 10.7 min, t_2 = 14.0 min]: $[\alpha]_D^{25}$ = –26.3 (*c* 1.0, MeOH). IR (film) ν_{\max} : 1710, 1416, 1336, 1097, 1050, 724, 699 cm⁻¹. ¹H NMR (300 MHz, CD₃OD) δ 1.62–1.80 (m, 3H), 1.80–1.99 (m, 1H), 2.54–2.73 (m, 2H), 4.21 (dd, J = 8.3, 4.6 Hz, 1H), 4.72 (d, J = 12.2 Hz, 1H), 4.84 (d, J = 12.2 Hz, 1H), 7.09–7.20 (m, 3H), 7.20–7.31 (m, 2H). ¹³C NMR (75 MHz, CD₃OD) δ 28.8, 32.3, 36.2, 55.3, 75.5, 97.1, 126.8, 129.3, 129.4, 143.2, 156.7, 175.6. HRMS calcd for [C₁₄H₁₆Cl₃NO₄Na]⁺ [(M + Na)⁺]: 390.0037; found: 390.0037.

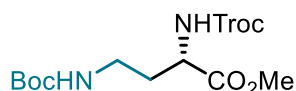
(S)-6-Methoxy-6-oxo-2-(((2,2,2-trichloroethoxy)carbonyl)amino)hexanoic acid (2j)



Catalyzed by 8 mol% (*R,R*)-**FeBIP**, the 1,3-nitrogen shift of **1j** (70.1 mg, 0.2 mmol) gave **2j** as a colorless oil (chromatography on silica gel, eluent: EtOAc/*n*-hexane = 1/2 with 0.1% TFA, 49.2 mg, 70% yield) with 90% ee [DAICEL CHIRALCEL OD-H column, Agilent HPLC 1260, *i*PrOH/*n*-hexane = 10/90 (v/v) with 0.1% TFA, 1.0 mL/min, 25 °C, 210 nm; t_1 = 7.7 min, t_2 = 9.0 min]: $[\alpha]_D^{25}$ = –33.2 (*c* 1.0, MeOH). IR (film) ν_{\max} : 1709, 1430, 1204, 724 cm⁻¹. ¹H NMR (300 MHz, CD₃OD) δ 1.59–1.82 (m, 3H), 1.82–1.99 (m, 1H), 2.27–2.47 (m, 2H), 3.66 (s, 3H), 4.17 (dd, J = 8.5, 4.6 Hz, 1H), 4.74 (d, J = 12.2 Hz, 1H), 4.84 (d, J = 12.2 Hz, 1H). ¹³C NMR (75 MHz, CD₃OD) δ 22.4, 31.9, 34.1, 52.1, 55.2, 75.5, 97.1, 156.7, 175.3, 175.4. HRMS calcd for [C₁₀H₁₄Cl₃NO₆Na]⁺ [(M + Na)⁺]: 371.9779; found: 371.9778.

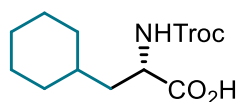
***O*-Phenyl-*N*-((2,2,2-trichloroethoxy)carbonyl)-*L*-homoserine (2k)**

Catalyzed by 15 mol% (*R,R*)-**FeBIP**, the 1,3-nitrogen shift of **1k** (55.6 mg, 0.15 mmol) gave **2k** as a colorless oil (chromatography on silica gel, eluent: EtOAc/*n*-hexane = 1/4 with 0.1% TFA, 29.7 mg, 53% yield) with 90% ee [DAICEL CHIRALPAK IG column, Agilent HPLC 1260, *i*PrOH/*n*-hexane = 20/80 (v/v) with 0.1% TFA, 1.0 mL/min, 25 °C, 210 nm; $t_1 = 6.6$ min, $t_2 = 8.1$ min]: $[\alpha]_D^{25} = +6.8$ (c 1.0, MeOH). **IR** (film) ν_{\max} : 1713, 1497, 1233, 1103, 1048, 751, 723, 691 cm^{-1} . **^1H NMR** (300 MHz, CD_3OD) δ 2.01–2.22 (m, 1H), 2.30–2.48 (m, 1H), 3.96–4.16 (m, 2H), 4.46 (dd, $J = 9.5, 4.6$ Hz, 1H), 4.71 (d, $J = 12.2$ Hz, 1H), 4.81 (d, $J = 12.2$ Hz, 1H), 6.81–6.99 (m, 3H), 7.13–7.31 (m, 2H). **^{13}C NMR** (75 MHz, CD_3OD) δ 32.3, 52.8, 65.2, 75.3, 97.0, 115.7, 121.9, 130.4, 156.7, 160.2, 175.3. **HRMS** calcd for $[\text{C}_{13}\text{H}_{14}\text{Cl}_3\text{NO}_5\text{Na}]^+$ $[(\text{M} + \text{Na})^+]$: 391.9830; found: 391.9832.

Methyl(*S*)-4-((*tert*-butoxycarbonyl)amino)-2-(((2,2,2-trichloroethoxy)carbonyl)amino)-butanoate (2l)

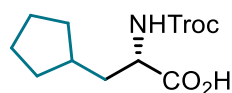
Catalyzed by 8 mol% (*R,R*)-**FeBIP** at room temperature for 16 hours, the 1,3-nitrogen shift of **1l** (78.7 mg, 0.2 mmol) and the successive methylation by trimethylsilyldiazomethane gave **2l** as a colorless oil (chromatography on silica gel, eluent: EtOAc/*n*-hexane = 1/3, 41.5 mg, 51% yield for two steps) with 90% ee [DAICEL CHIRALPAK IC column, Agilent HPLC 1260, *i*PrOH/*n*-hexane = 10/90 (v/v), 1.0 mL/min, 25 °C, 210 nm; $t_1 = 10.0$ min, $t_2 = 14.3$ min]: $[\alpha]_D^{25} = -16.9$ (c 1.0, MeOH). **IR** (film) ν_{\max} : 3346, 2972, 1721, 1692, 1514, 1246, 1165, 1100, 726 cm^{-1} . **^1H NMR** (300 MHz, CDCl_3) δ 1.43 (s, 9H), 1.77–1.92 (m, 1H), 2.02–2.16 (m, 1H), 2.96–3.14 (m, 1H), 3.29–3.47 (m, 1H), 3.76 (s, 3H), 4.44 (dt, $J = 8.5, 4.5$ Hz, 1H), 4.69 (d, $J = 12.1$ Hz, 1H), 4.78 (d, $J = 12.1$ Hz, 1H), 4.83–5.09 (br, 1H), 5.87 (d, $J = 8.5$ Hz, 1H). **^{13}C NMR** (75 MHz, CDCl_3) δ 28.5, 33.2, 36.7, 51.9, 52.9, 74.8, 79.7, 95.5, 154.7, 156.1, 172.4. **HRMS** calcd for $[\text{C}_{13}\text{H}_{21}\text{Cl}_3\text{N}_2\text{O}_6\text{Na}]^+$ $[(\text{M} + \text{Na})^+]$: 429.0357; found: 429.0363.

(*S*)-3-Cyclohexyl-2-(((2,2,2-trichloroethoxy)carbonyl)amino)propanoic acid (2m)



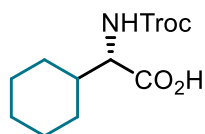
Catalyzed by 8 mol% (*R,R*)-**FeBIP**, the 1,3-nitrogen shift of **1m** (69.3 mg, 0.2 mmol) gave **2m** as a colorless oil (chromatography on silica gel, eluent: EtOAc/*n*-hexane = 1/6 with 0.1% TFA, 39.8 mg, 57% yield) with 91% ee [DAICEL CHIRALPAK IG column, Agilent HPLC 1260, *i*PrOH/*n*-hexane = 10/90 (v/v) with 0.1% TFA, 1.0 mL/min, 25 °C, 210 nm; $t_1 = 9.4$ min, $t_2 = 12.7$ min]: $[\alpha]_D^{25} = -28.3$ (c 1.0, MeOH). **IR** (film) ν_{\max} : 2925, 2851, 1709, 1417, 1336, 1043, 723 cm^{-1} . **¹H NMR** (300 MHz, CD₃OD) δ 0.85–1.06 (m, 2H), 1.15–1.34 (m, 3H), 1.36–1.53 (m, 1H), 1.53–1.77 (m, 6H), 1.77–1.92 (m, 1H), 4.24 (dd, $J = 10.1, 5.0$ Hz, 1H), 4.72 (d, $J = 12.2$ Hz, 1H), 4.86 (d, $J = 12.2$ Hz, 1H). **¹³C NMR** (75 MHz, CD₃OD) δ 27.2, 27.4, 27.6, 33.1, 34.8, 35.4, 40.2, 53.3, 75.5, 97.2, 156.7, 176.3. **HRMS** calcd for [C₁₂H₁₈Cl₃NO₄Na]⁺ [(M + Na)⁺]: 368.0194; found: 368.0190.

(S)-3-Cyclopentyl-2-(((2,2,2-trichloroethoxy)carbonyl)amino)propanoic acid (2n)



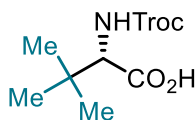
Catalyzed by 8 mol% (*R,R*)-**FeBIP**, the 1,3-nitrogen shift of **1n** (66.5 mg, 0.2 mmol) gave **2n** as a colorless oil (chromatography on silica gel, eluent: EtOAc/*n*-hexane = 1/6 with 0.1% TFA, 43.5 mg, 65% yield) with 92% ee [DAICEL CHIRALPAK IG column, Agilent HPLC 1260, *i*PrOH/*n*-hexane = 10/90 (v/v) with 0.1% TFA, 1.0 mL/min, 25 °C, 210 nm; $t_1 = 9.3$ min, $t_2 = 13.3$ min]: $[\alpha]_D^{25} = -11.6$ (c 1.0, MeOH). **IR** (film) ν_{\max} : 2951, 1710, 1411, 1335, 1107, 1045, 722 cm^{-1} . **¹H NMR** (300 MHz, CD₃OD) δ 1.04–1.26 (m, 2H), 1.46–1.72 (m, 4H), 1.72–1.89 (m, 4H), 1.89–2.05 (m, 1H), 4.17 (dd, $J = 8.4, 6.3$ Hz, 1H), 4.73 (d, $J = 12.2$ Hz, 1H), 4.84 (d, $J = 12.2$ Hz, 1H). **¹³C NMR** (75 MHz, CD₃OD) δ 25.9, 26.1, 33.0, 33.8, 38.1, 38.8, 55.2, 75.5, 97.1, 156.7, 176.0. **HRMS** calcd for [C₁₁H₁₆Cl₃NO₄Na]⁺ [(M + Na)⁺]: 354.0037; found: 354.0037.

(S)-2-Cyclohexyl-2-(((2,2,2-trichloroethoxy)carbonyl)amino)acetic acid (2o)



Catalyzed by 8 mol% (*R,R*)-**FeBIP**, the 1,3-nitrogen shift of **1o** (66.5 mg, 0.2 mmol) gave **2o** as a colorless oil (chromatography on silica gel, eluent: EtOAc/*n*-hexane = 1/6 with 0.1% TFA, 32.0 mg, 48% yield) with 89% ee [DAICEL CHIRALCEL OD-H column, Agilent HPLC 1260, *i*PrOH/*n*-hexane = 5/95 (v/v) with 0.1% TFA, 1.0 mL/min, 25 °C, 210 nm; $t_1 = 6.5$ min, $t_2 = 9.2$ min]: $[\alpha]_D^{25} = +4.4$ (c 1.0, MeOH). **IR** (film) ν_{\max} : 2929, 2856, 1708, 1420, 1336, 1100, 722 cm^{-1} . **$^1\text{H NMR}$** (300 MHz, CD_3OD) δ 1.00–1.43 (m, 5H), 1.44–1.96 (m, 6H), 4.08 (d, $J = 6.1$ Hz, 1H), 4.74 (d, $J = 12.2$ Hz, 1H), 4.84 (d, $J = 12.2$ Hz, 1H). **$^{13}\text{C NMR}$** (75 MHz, CD_3OD) δ 27.09, 27.14 (2C), 29.4, 30.8, 41.4, 60.8, 75.6, 97.1, 156.9, 174.8. **HRMS** calcd for $[\text{C}_{11}\text{H}_{16}\text{Cl}_3\text{NO}_4\text{Na}]^+$ $[(\text{M} + \text{Na})^+]$: 354.0037; found: 354.0038.

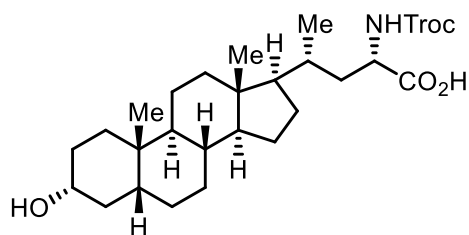
(S)-3,3-Dimethyl-2-(((2,2,2-trichloroethoxy)carbonyl)amino)butanoic acid (2p)



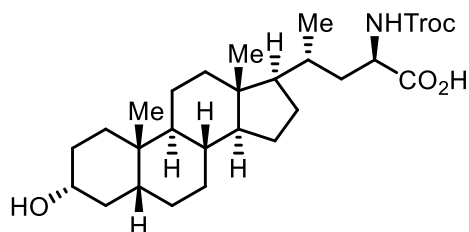
Catalyzed by 15 mol% (*R,R*)-**FeBIP**, the 1,3-nitrogen shift of **1p** (76.6 mg, 0.25 mmol) gave **2p** as a colorless oil (chromatography on silica gel, eluent: EtOAc/*n*-hexane = 1/7 with 0.1% TFA, 15.6 mg, 56% yield) with 85% ee [DAICEL CHIRALCEL OD-H column, Agilent HPLC 1260, *i*PrOH/*n*-hexane = 5/95 (v/v) with 0.1% TFA, 1.0 mL/min, 25 °C, 210 nm; $t_1 = 6.0$ min, $t_2 = 8.5$ min]: $[\alpha]_D^{25} = -10.4$ (c 1.0, MeOH). **IR** (film) ν_{\max} : 2967, 1690, 1453, 1167, 812 cm^{-1} . **$^1\text{H NMR}$** (300 MHz, CD_3OD) δ 1.04 (s, 9H), 4.05 (s, 1H), 4.74 (d, $J = 12.2$ Hz, 1H), 4.86 (d, $J = 12.2$ Hz, 1H). **$^{13}\text{C NMR}$** (75 MHz, CD_3OD) δ 27.1, 35.1, 64.4, 75.6, 97.1, 156.8, 174.2. **HRMS** calcd for $[\text{C}_9\text{H}_{14}\text{Cl}_3\text{NO}_4\text{Na}]^+$ $[(\text{M} + \text{Na})^+]$: 327.9881; found: 327.9883.

(2S,4R)-4-(((3R,5R,8R,9S,10S,13R,14S,17R)-3-Hydroxy-10,13-dimethylhexadecahydro-1H-cyclopenta[*a*]phenanthren-17-yl)-2-(((2,2,2-trichloroethoxy)carbonyl)amino)-pentanoic acid (2q)

Catalyzed by 8 mol% (*R,R*)-**FeBIP** at room temperature for 16 hours, the 1,3-nitrogen shift of **1q** (85.0 mg, 0.15 mmol) gave **2q** and its epimer (*2-epi-2q*) in 77% combined yield (chromatography on silica gel, eluent: EtOAc/*n*-hexane = 1/3 with 0.1% TFA, 65.6 mg) with 23:1 d.r. [determined by HPLC analysis: DAICEL CHIRALCEL OD-H column, Agilent HPLC 1260, *i*PrOH/*n*-hexane = 20/80 (v/v) with 0.1% TFA, 1.0 mL/min, 25 °C, 210 nm; t_1 (**2q**) = 9.7 min, t_2 (*2-epi-2q*) = 13.4 min].



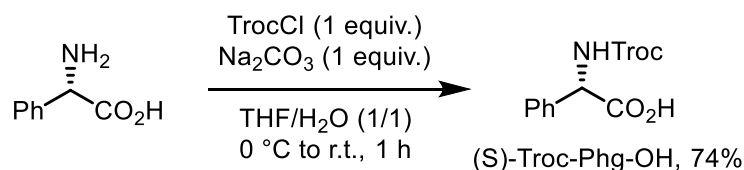
2q (less polar, major diastereomer): $[\alpha]_D^{25} = -4.9$ (*c* 1.0, MeOH); **IR** (film) ν_{\max} : 2931, 2861, 1702, 1214, 1158, 1041, 724 cm^{-1} . **¹H NMR** (300 MHz, CD₃OD) δ 0.69 (s, 3H), 0.94 (s, 3H), 1.05 (d, *J* = 6.4 Hz, 3H), 1.08–2.09 (m, 26H), 3.42–3.64 (m, 1H), 4.20 (dd, *J* = 8.2, 6.3 Hz, 1H), 4.71 (d, *J* = 12.2 Hz, 1H), 4.84 (d, *J* = 12.2 Hz, 1H). **¹³C NMR** (75 MHz, CD₃OD) δ 12.4, 19.6, 21.9, 24.0, 25.3, 27.6, 28.4, 29.3, 31.2, 35.1, 35.7, 36.5, 37.17, 37.22, 39.8, 41.5, 41.9, 43.6, 44.0, 54.3, 57.9 (2C), 72.4, 75.5, 97.1, 156.3, 176.0. **HRMS** calcd for [C₂₇H₄₂Cl₃NO₅Na]⁺ [(M + Na)⁺]: 588.2021; found: 588.2019.



2-*epi*-2q (more polar, minor diastereomer): $[\alpha]_D^{25} = +24.0$ (*c* 1.0, MeOH). **IR** (film) ν_{\max} : 2932, 2862, 1718, 1211, 1157, 725 cm^{-1} . **¹H NMR** (300 MHz, CD₃OD) δ 0.68 (s, 3H), 0.95 (s, 3H), 0.97–1.01 (m, 3H), 1.08–2.09 (m, 26H), 3.42–3.64 (m, 1H), 4.28 (dd, *J* = 12.0, 2.5 Hz, 1H), 4.71 (d, *J* = 12.2 Hz, 1H), 4.87 (d, *J* = 12.2 Hz, 1H). **¹³C NMR** (75 MHz, CD₃OD) δ 12.6, 18.3, 22.0, 24.0, 25.3, 27.6, 28.4, 29.2, 31.2, 34.0, 35.7, 36.5, 37.17, 37.24, 39.1, 41.6, 41.9, 43.5, 44.1, 53.1, 57.9 (2C), 72.4, 75.5, 97.2, 156.9, 176.4. **HRMS** calcd for [C₂₇H₄₂Cl₃NO₅Na]⁺ [(M + Na)⁺]: 588.2021; found: 588.2016.

4.3.4 Determining the Absolute Configuration of the α -Amino Acids

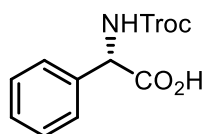
For determining the absolute configuration of the α -amino acids, enantiopure (*S*)-Troc-Phg-OH was synthesized from (*S*)-phenylglycine.



General procedure for *N*-Troc protection of α -amino acids: to a solution of α -amino acid (1.0 mmol, 1.0 equiv.) and Na₂CO₃ (106 mg, 1.0 mmol, 1.0 equiv.) in tetrahydrofuran/water (*v/v* = 1/1, 5 mL) at 0

°C was added 2,2,2-trichloroethyl carbonochloridate (0.14 mL, 1.0 mmol, 1.0 equiv.) dropwise. The reaction mixture was stirred at room temperature for 1 hour. To quench the reaction, the mixture was acidified with hydrochloric acid (aqueous solution, 10%) and was extracted with EtOAc for three times. The combined organic layer was dried over anhydrous sodium sulfate. After filtration, the solvent was evaporated under reduced pressure, and the residue was purified by column chromatography on silica gel eluted with indicated solvent.

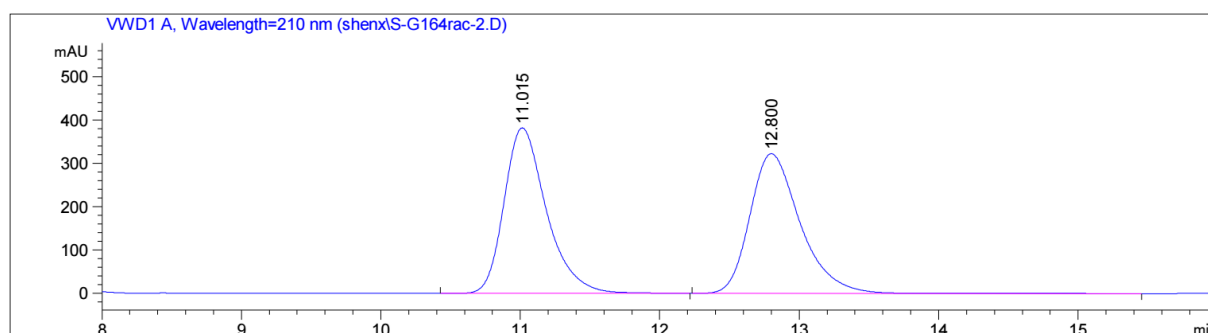
(*S*)-Troc-Phg-OH



Following the general procedure, (*S*)-Troc-Phg-OH was obtained as a white solid (eluent: EtOAc/*n*-hexane = 1/5 with 0.1% TFA, 243 mg, 74% yield): $[\alpha]_{\text{D}}^{25} = +96.4$ (*c* 1.0, MeOH, 99% ee). $^1\text{H NMR}$ (300 MHz, CD_3OD) δ 4.77 (d, $J = 12.2$ Hz, 1H), 4.80 (d, $J = 12.2$ Hz, 1H), 5.29 (s, 1H), 7.28–7.40 (m, 3H), 7.40–7.49 (m, 2H). $^{13}\text{C NMR}$ (75 MHz, CD_3OD) δ 59.7, 75.6, 96.9, 128.6, 129.4, 129.7, 138.1, 156.2, 173.5. The $^1\text{H NMR}$ and $^{13}\text{C NMR}$ data of (*S*)-Troc-Phg-OH are identical with those of **2b**.

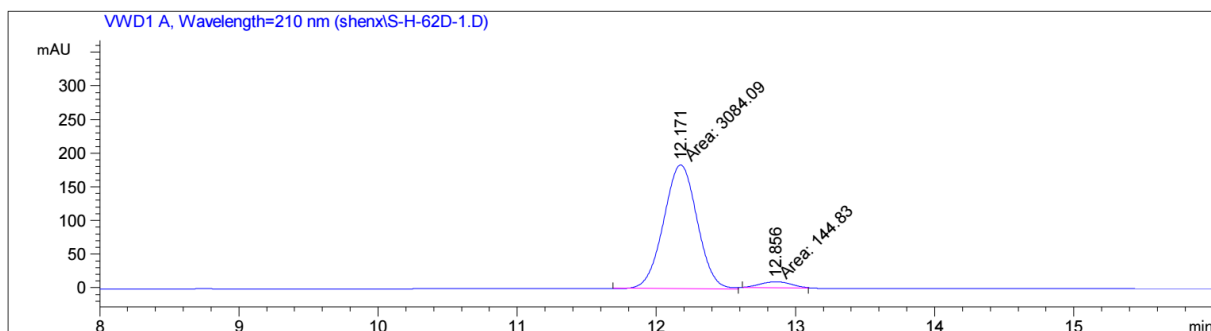
The absolute configuration of α -amino acids **2b** was assigned by comparison of the HPLC retention time with that of (*S*)-Troc-Phg-OH.

For α -amino acid **2b**:



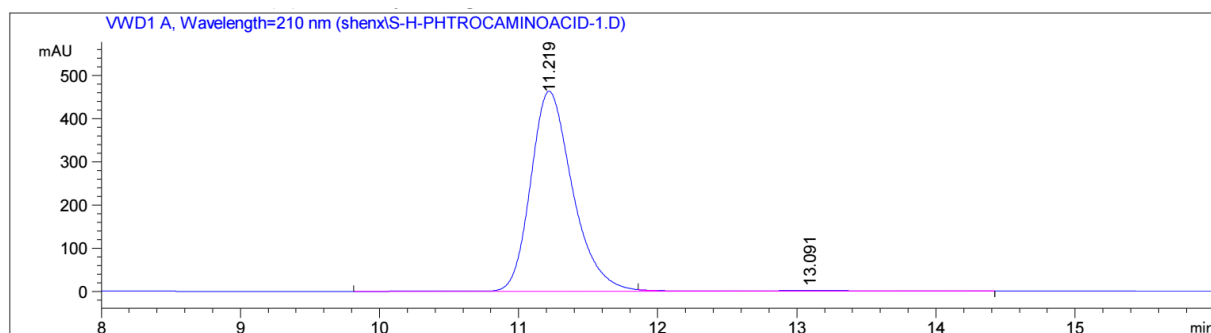
HPLC of racemic **2b** (CHIRALPAK ODR, 25 °C, $\text{CH}_3\text{CN}/\text{H}_2\text{O}$ (0.1% TFA) = 40:60, 1.0 mL/min, 210 nm).

Chapter 4. Experimental Part



Peak #	RetTime [min]	Type	Width [min]	Area mAU *s	Height [mAU]	Area %
1	12.171	MM	0.2781	3084.08789	184.84370	95.5146
2	12.856	MM	0.2641	144.82953	9.14128	4.4854

HPLC of enantioenriched **2b** derived from (*R,R*)-**FeBIP** catalyzed 1,3-nitrogen shift.

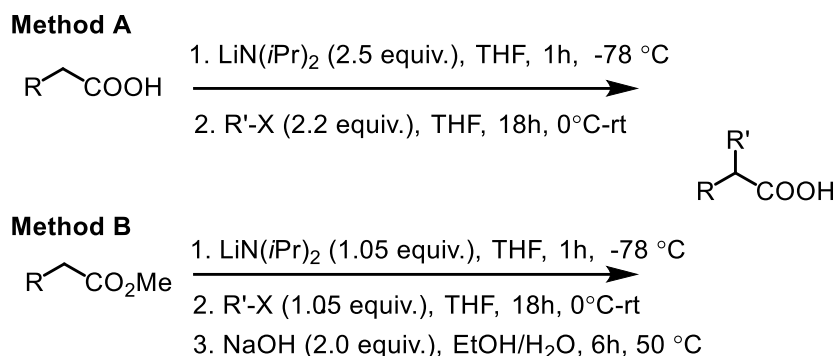


Peak #	RetTime [min]	Type	Width [min]	Area mAU *s	Height [mAU]	Area %
1	11.219	BV R	0.3149	9647.70508	459.39618	99.2650
2	13.091	VB E	0.6225	71.43502	1.57456	0.7350

HPLC of (*S*)-Troc-Phg-OH.

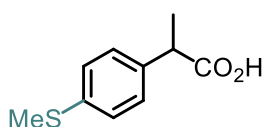
4.4 Enantioconvergent Tertiary CH Bonds Amination Catalyzed by Chiral N4 Iron Catalysts

4.4.1 Synthesis of Carboxylic Acids



Method A: To a solution of acid (3.0 mmol, 1.0 equiv.) which dissolved in THF (6 mL) added a solution of the lithium diisopropylamide (7.5 mmol, 2.5 equiv.) in THF (6 mL) at -78 °C. The mixture was allowed to stir at -78 °C for 1 h. Then, the halogenated alkanes were added and stirred at room temperature for 18h. After that, the reaction mixture was acidified with HCl (4N) until pH to 2-3. The two phases were separated and the aqueous phase was extracted twice with EtOAc. The combined organic layers were dried over MgSO₄, filtered, and evaporated under reduced pressure. The resulting mixture was purified by flash chromatography (EtOAc/*n*-hexane) to provide the acid for the next step.

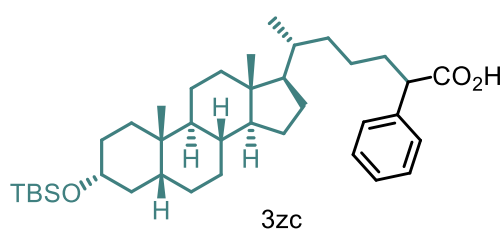
Method B: To a solution of ester (1.0 mmol, 1.0 equiv.) dissolved in THF (5 mL) was added a solution of lithium diisopropylamide (1.05 mmol, 1.05 equiv.) in THF (2 mL) at -78 °C. The mixture was allowed to stir at -78 °C for 1 h. Then, the halogenated alkanes were added and stirred at room temperature for 18 h. After that, the reaction mixture was acidified with HCl (4N) until pH 7. Then, the mixture was extracted with ethyl acetate (3 x 20 mL). Then combined organic layers were dried over MgSO₄, filtered, and evaporated under reduced pressure. The resulting mixture was purified by flash chromatography (EtOAc/*n*-hexane) to provide the ester (0.9 mmol). The ester was dissolved in 1.8 mL EtOH/H₂O (3/1) acidified with HCl (4N) until pH 5. The mixture was extracted with ethyl acetate (5 x 9 mL). After evaporation, the product was obtained.



Synthesis of 3i: According to method A, to a solution of acid (546.7 mg, 3.0 mmol, 1.0 equiv.) dissolved in THF (6 mL) was added a solution of the lithium diisopropylamide (3.75 mL, 7.5 mmol, 2.5 equiv.) in THF (6 mL) at $-78\text{ }^{\circ}\text{C}$. The mixture was allowed to stir at $-78\text{ }^{\circ}\text{C}$ for 1 h. Then, iodomethane (937.2 mg, 6.6 mmol, 2.2 equiv.) was added and stirred at room temperature for 18 h. After that, the reaction mixture was acidified with HCl (4 N) until pH 2-3. The two phases were separated and the aqueous phase was extracted twice with EtOAc. The combined organic layers were dried over MgSO_4 , filtered, and evaporated under reduced pressure. The resulting mixture was purified by flash chromatography (EtOAc/*n*-hexane) to provide **3i** as a white solid (410.0 mg, 2.09 mmol, 70% yield).

3i: $^1\text{H NMR}$ (300 MHz, CDCl_3) δ 7.24 (m, 4H), 3.70 (q, $J = 7.2$ Hz, 1H), 2.47 (s, 3H), 1.50 (d, $J = 7.2$ Hz, 3H). $^{13}\text{C NMR}$ (75 MHz, CDCl_3) δ 180.77, 137.75, 136.72, 128.22, 127.10, 44.95, 18.14, 16.05.

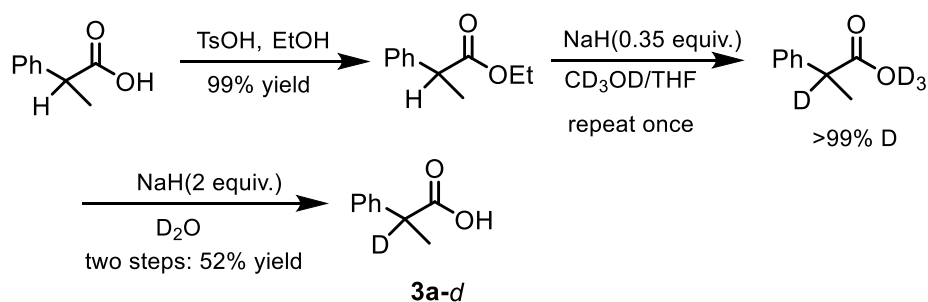
IR (film): ν (cm^{-1}) 3146, 1719, 1674, 1492, 1204, 1170, 854, 653, 627, 530, 412. **HRMS (ESI, m/z)** calcd. for $[\text{C}_{10}\text{H}_{12}\text{O}_2\text{SNa}]^+ [(M + \text{Na})^+]$: 219.0450, found: 219.0450.



Synthesis of 3zc: According to method B, to a solution of methyl 2-phenylacetate (138.2 mg, 0.92 mmol, 1.0 equiv.) dissolved in THF (4.6 mL) was added a solution of lithium diisopropylamide (0.46 mL, 0.966 mmol, 1.05 equiv.) in THF (1.5 mL) at $-78\text{ }^{\circ}\text{C}$. The mixture was allowed to stir at $-78\text{ }^{\circ}\text{C}$ for 1 h. Then, (3 α ,5 β)-3-[[[1,1-dimethylethyl]dimethylsilyl]oxy]-24-iodocholane¹ (566.0mg, 0.966 mmol, 1.05 eq) was added and stirred at room temperature for 18 h. After that, the reaction mixture was acidified with HCl (4N) until pH 7. Then, the mixture was extracted with ethyl acetate (3 x 10 mL). The combined organic layers were dried over MgSO_4 , filtered, and evaporated under reduced pressure. The resulting mixture was purified by flash chromatography (EtOAc/*n*-hexane) to provide the ester (522.0, 0.8 mmol). The ester was dissolved in 1.6 mL EtOH/ H_2O (3/1) NaOH solution (1M) at room temperature. The mixture was further stirred at $50\text{ }^{\circ}\text{C}$ for 4 h and afterwards acidified with

HCl (4N) until pH 5. The mixture was extracted with ethyl acetate (5 x 8 mL). After evaporation, **3zc** was obtained as a white solid (339.0 mg, 0.57 mmol, 62% yield).

3zc: $^1\text{H NMR}$ (300 MHz, CDCl_3) δ 7.42 – 7.21 (m, 5H), 3.66 – 3.49 (m, 2H), 2.18 – 0.94 (m, 30H), 0.93 – 0.79 (m, 15H), 0.61 (d, $J = 3.3$ Hz, 3H), 0.06 (s, 6H). $^{13}\text{C NMR}$ (75 MHz, CDCl_3) δ 179.21, 138.73, 138.59, 128.63, 128.10, 128.03, 127.38, 72.52, 56.42, 56.36, 51.55, 42.71, 42.35, 40.26, 40.18, 36.95, 35.89, 35.62, 35.58, 34.61, 33.60, 33.43, 31.04, 28.32, 27.34, 26.44, 26.00, 24.24, 24.10, 23.41, 20.83, 18.54, 18.34, 12.02, -4.57. **IR (film):** ν (cm^{-1}) 2928, 2857, 1706, 1252, 1173, 1123, 1093, 835, 774, 729, 697, 667. **HRMS (ESI, m/z)** calcd. for $[\text{C}_{38}\text{H}_{62}\text{O}_3\text{SiNa}]^+ [(M + \text{Na})^+]$: 617.4360, found: 617.4360.



3a-d: Toluene-*p*-sulphonic acid (0.21 g, 1.2 mmol, 0.1 equiv.) was added to a stirred solution of 2-phenylpropionic acid (1.8 g, 12.0 mmol, 1.0 equiv.) in ethanol (anhydrous, 30 ml) at room temperature. The solution was then heated to 85 °C and left to reflux for 12 h. The resulting solution was cooled down to room temperature and the solvent was removed under reduced pressure. The residue was dissolved in dichloromethane and washed with aqueous potassium hydroxide (20 mL). The organic phases were dried over MgSO_4 and evaporated under reduced pressure to give ethyl 2-phenylpropionate (2.11 g, 99% yield) as a colourless oil. In a separate reaction, sodium hydride (100.3 mg, 60% dispersion in oil, 4.18 mmol) was slowly added to a stirred solution of methanol-*d*₄ (7.26 ml, 179.0 mmol) in THF (28 ml) at 0 °C. The resulting solution was stirred for 15 min at 0 °C. Then, ethyl 2-phenylpropionate (2.11 g, 11.87 mmol) was slowly added dropwise and the solution was allowed to warm up to room temperature over 12 h. The reaction was quenched with D_2O (5 mL) and extracted with dichloromethane (3 x 10 ml). The combined organic layers were dried over MgSO_4 and evaporated under reduced pressure to give trideuteriomethyl 2-deuterio-2-phenylpropionate. The second step was repeated to obtain over 99% D/H trideuteriomethyl 2-deuterio-2-phenylpropionate.

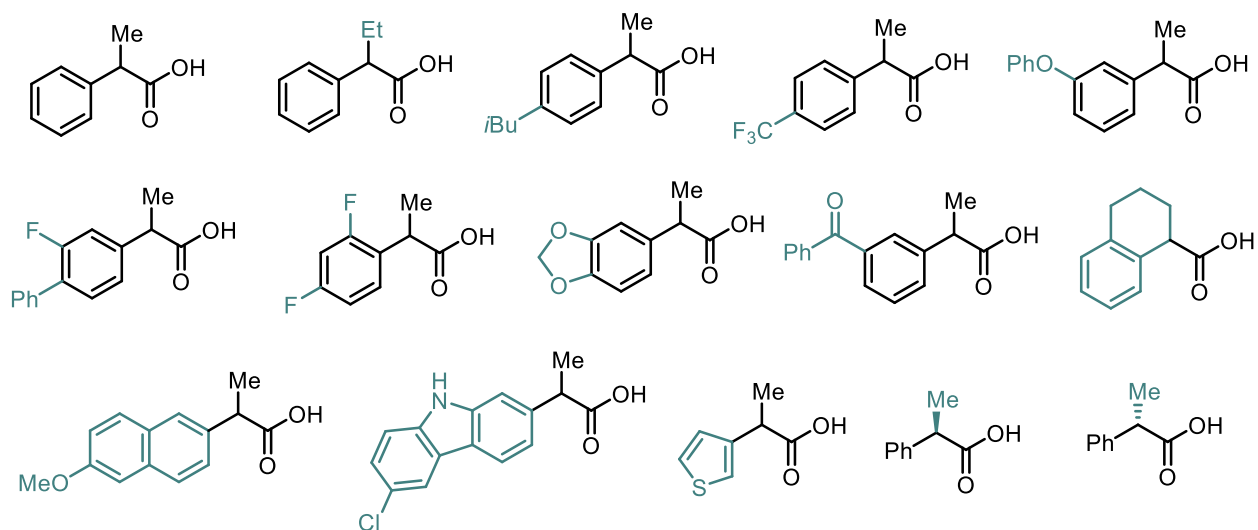
Sodium hydride (0.49 g, 12.31 mmol) was slowly added to a stirred solution of trideuteriomethyl 2-deuterio-2-phenylpropionate (1.0 g, 6.16 mmol) in THF/D₂O (30 ml, 3:1) at room temperature. The resulting solution was stirred for 12 h. The reaction was quenched with D₂O (10 ml), acidified with HCl (4N) and extracted with dichloromethane (3 x 10 ml). The combined organic layers were dried over MgSO₄ and evaporated under reduced pressure to give **3a-d** as a colorless liquid (0.94 g, yield over three steps: 52%).

3a-d: ¹H NMR (300 MHz, CDCl₃) δ 7.45 – 7.24 (m, 5H), 1.53 (s, 3H). ¹³C NMR (75 MHz, CDCl₃) δ 181.05, 139.84, 128.82, 127.73, 127.54, 45.15(t, *J* = 19.5 Hz), 18.12. **IR (film)**: ν (cm⁻¹) 2923, 1700, 1449, 1406, 1286, 1230, 1140, 938, 723, 695, 570, 500. **HRMS (ESI, *m/z*)** calcd. for [C₉H₉DO₂Na]⁺ [(M + Na)⁺]: 174.0636, found: 174.0636.

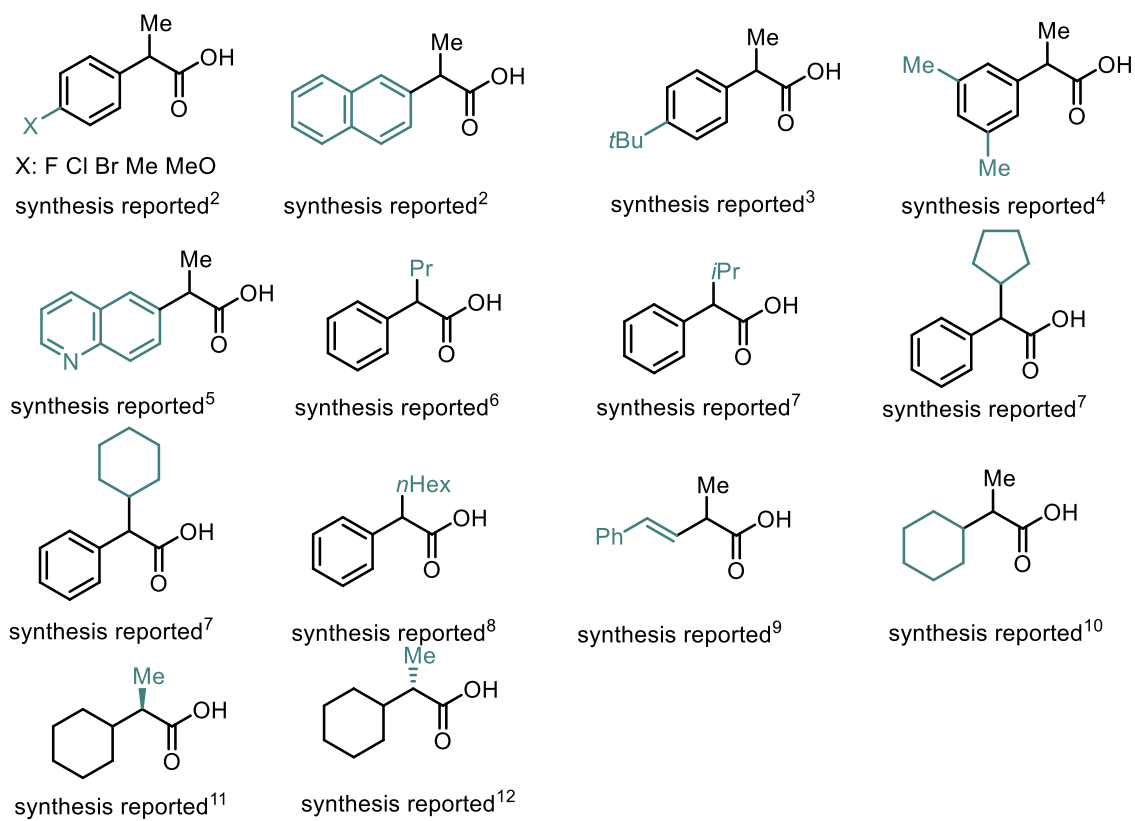
All other acids have been reported or are commercialized.

Chapter 4. Experimental Part

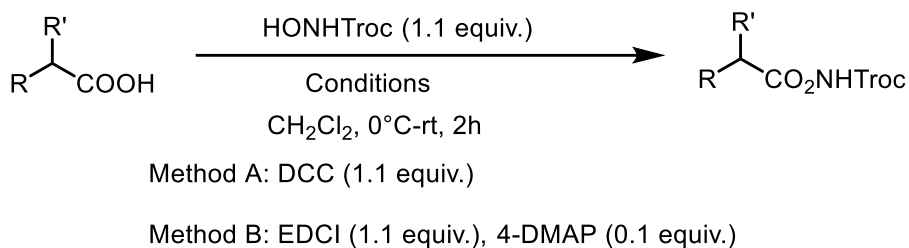
commercial sources:



reported sources:

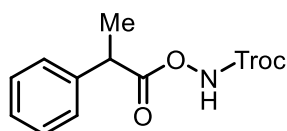


4.4.2 Synthesis of Substrates



Method A: To a solution of carboxylic acid (1.0 equiv.) and *N*-protected hydroxylamine (1.1 equiv.) in dichloromethane (0.2 M) at 0 °C was added DCC (1.1 equiv.) in one portion. The reaction mixture was warmed to room temperature and was stirred for 2 hours. After completion, the reaction mixture was filtered and washed with dichloromethane. After being concentrated under reduced pressure, the residue was purified by chromatography on silica gel using indicated solvent as the eluent.

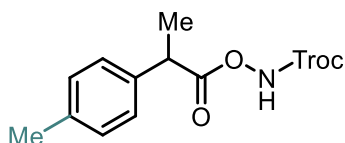
Method B: To a solution of carboxylic acid (1.0 equiv.), 4-DMAP (0.1 equiv.) and *N*-protected hydroxylamine (1.1 equiv.) in dichloromethane (0.2 M) at 0 °C was added EDCI (1.1 equiv.) in one portion. The reaction mixture was warmed to room temperature and was stirred for 1 hour. After completion, water was added, and the mixture was extracted with EtOAc for three times. The combined organic layer was washed with brine and was dried over anhydrous sodium sulfate. After filtration, the solvent was evaporated under reduced pressure, and the residue was purified by chromatography on silica gel using indicated solvent as the eluent.

2,2,2-Trichloroethyl ((2-phenylpropanoyl)oxy)carbamate (**4a**)

DCC coupling of 2-phenylpropanoic acid with TrocNHOH gave the product **4a** as a white solid (chromatography on silica gel, eluent: EtOAc/*n*-hexane = 1/10): **¹H NMR** (300 MHz, CDCl₃) δ 8.16 (s, 1H), 7.40 – 7.28 (m, 5H), 4.76 (d, *J* = 12.0 Hz, 1H), 4.71 (d, *J* = 12.0 Hz, 1H), 3.93 (q, *J* = 7.2 Hz, 1H), 1.61 (d, *J* = 7.2 Hz, 3H). **¹³C NMR** (75 MHz, CDCl₃) δ 173.42, 154.60, 138.55, 129.03, 127.94, 127.71, 94.49, 75.29, 43.41, 18.56. **IR (film):** ν (cm⁻¹) 3263, 1740, 1383, 1316, 1131, 1095, 1039, 809,

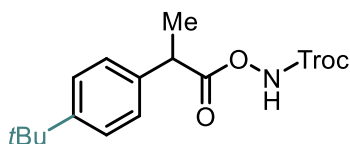
717, 599 cm^{-1} . **HRMS (ESI, m/z)** calcd for $[\text{C}_{12}\text{H}_{12}\text{Cl}_3\text{NO}_4\text{Na}]^+ [(M + \text{Na})^+]$: 361.9724, found: 361.9724.

2,2,2-Trichloroethyl ((2-(*p*-tolyl)propanoyl)oxy)carbamate (4b)



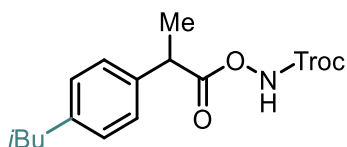
DCC coupling of 2-(*p*-tolyl)propanoic acid with TrocNHOH gave the product **4b** as a white solid (chromatography on silica gel, eluent: EtOAc/*n*-hexane = 1/10): **$^1\text{H NMR}$** (300 MHz, CDCl_3) δ 8.21 (s, 1H), 7.25 – 7.12 (m, 4H), 4.81 (d, $J = 12.0$ Hz, 1H), 4.79 (d, $J = 12.0$ Hz, 1H), 3.89 (q, $J = 7.2$ Hz, 1H), 2.34 (s, 3H), 1.59 (d, $J = 7.2$ Hz, 3H). **$^{13}\text{C NMR}$** (75 MHz, CDCl_3) δ 173.56, 154.62, 137.66, 135.57, 129.69, 127.56, 94.51, 75.28, 43.00, 21.18, 18.56. **IR (film)**: ν (cm^{-1}) 3239, 1790, 1729, 1480, 1243, 1102, 759, 564 cm^{-1} . **HRMS (ESI, m/z)** calcd for $[\text{C}_{13}\text{H}_{14}\text{Cl}_3\text{NO}_4\text{Na}]^+ [(M + \text{Na})^+]$: 375.9881, found: 375.9881.

2,2,2-Trichloroethyl((2-(4-(*tert*-butyl)phenyl)propanoyl)oxy)carbamate (4c)



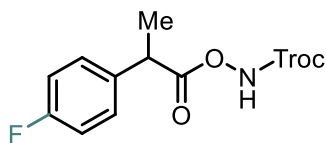
DCC coupling of 2-(4-(*tert*-butyl)phenyl)propanoic acid with TrocNHOH gave the product **4c** as a colorless oil (chromatography on silica gel, eluent: EtOAc/*n*-hexane = 1/10): **$^1\text{H NMR}$** (300 MHz, CDCl_3) δ 8.23 (s, 1H), 7.41 – 7.22 (m, 4H), 4.80 (d, $J = 12.0$ Hz, 1H), 4.75 (d, $J = 12.0$ Hz, 1H), 3.90 (q, $J = 7.2$ Hz, 1H), 1.60 (d, $J = 7.2$ Hz, 3H), 1.31 (s, 9H). **$^{13}\text{C NMR}$** (75 MHz, CDCl_3) δ 173.56, 154.64, 150.84, 135.46, 127.35, 125.93, 94.50, 75.28, 42.90, 34.64, 31.44, 18.52. **IR (film)**: ν (cm^{-1}) 3296, 2962, 1750, 1454, 1321, 1226, 1110, 716, 565 cm^{-1} . **HRMS (ESI, m/z)** calcd for $[\text{C}_{16}\text{H}_{20}\text{Cl}_3\text{NO}_4\text{Na}]^+ [(M + \text{Na})^+]$: 418.0350, found: 418.0350.

2,2,2-Trichloroethyl ((2-(4-isobutylphenyl)propanoyl)oxy)carbamate (4d)



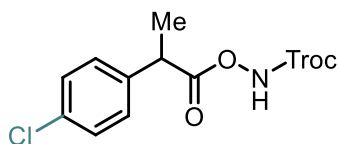
DCC coupling of 2-(4-isobutylphenyl)propanoic acid with TrocNHOH gave the product as a white solid (chromatography on silica gel, eluent: EtOAc/*n*-hexane = 1/10): **¹H NMR** (300 MHz, CDCl₃) δ 8.24 (s, 1H), 7.34 – 7.26 (m, 2H), 7.21 – 7.12 (m, 2H), 4.85 (d, *J* = 12.0 Hz, 1H), 4.80 (d, *J* = 12.0 Hz, 1H), 3.94 (q, *J* = 7.2 Hz, 1H), 2.50 (d, *J* = 7.2 Hz, 2H), 1.83-1.96 (m, 1H), 1.64 (d, *J* = 7.2 Hz, 3H), 0.95 (d, *J* = 6.6 Hz, 6H). **¹³C NMR** (75 MHz, CDCl₃) δ 173.46, 154.48, 141.32, 135.62, 129.59, 127.26, 94.38, 75.16, 45.03, 42.89, 30.15, 22.38, 18.42. **IR (film)**: *ν* (cm⁻¹) 3258, 2952, 1741, 1384, 1098, 892, 810, 563, 464 cm⁻¹. **HRMS (ESI, *m/z*)** calcd for [C₁₆H₂₀Cl₃NO₄Na]⁺ [(M + Na)⁺]: 418.0350, found: 418.0350.

2,2,2-Trichloroethyl ((2-(4-fluorophenyl)propanoyl)oxy)carbamate (4e)



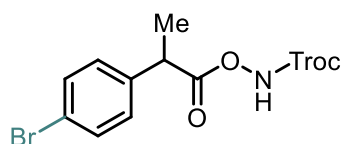
DCC coupling of 2-(4-fluorophenyl)propanoic acid with TrocNHOH gave the product **4e** as a colorless oil (chromatography on silica gel, eluent: EtOAc/*n*-hexane = 1/10): **¹H NMR** (300 MHz, CDCl₃) δ 8.22 (s, 1H), 7.36 – 7.22 (m, 2H), 7.09 – 6.92 (m, 2H), 4.76 (s, 2H), 3.89 (q, *J* = 7.2 Hz, 1H), 1.57 (d, *J* = 7.2 Hz, 3H). **¹³C NMR** (75 MHz, CDCl₃) δ 173.15, δ 162.31 (d, *J*_{C-F} = 246.5 Hz), 154.52, 134.13 (d, *J* = 3.0 Hz), 129.23 (d, *J*_{C-F} = 8.2 Hz), 115.77 (d, *J*_{C-F} = 21 Hz), 94.34, 75.18, 42.53, 18.55. **¹⁹F NMR** (282 MHz, CDCl₃) δ -114.47. **IR (film)**: *ν* (cm⁻¹) 3180, 2983, 1725, 1511, 1259, 1130, 1097, 854, 776, 587, 403 cm⁻¹. **HRMS (ESI, *m/z*)** calcd for [C₁₂H₁₁Cl₃FNO₄Na]⁺ [(M + Na)⁺]: 379.9630, found: 379.9630.

2,2,2-Trichloroethyl ((2-(4-chlorophenyl)propanoyl)oxy)carbamate (4f)



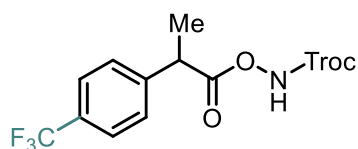
DCC coupling of 2-(4-chlorophenyl)propanoic acid with TrocNHOH gave the product **4f** as a white solid (chromatography on silica gel, eluent: EtOAc/*n*-hexane = 1/10): **¹H NMR** (300 MHz, CDCl₃) δ 8.25 (s, 1H), 7.37-7.23 (m, 4H), 4.80 (d, *J* = 12.0 Hz, 1H), 4.75 (d, *J* = 12.0 Hz, 1H), 3.90 (q, *J* = 7.2 Hz, 1H), 1.59 (d, *J* = 7.0 Hz, 3H). **¹³C NMR** (75 MHz, CDCl₃) δ 173.06, 154.57, 136.96, 133.91, 129.19, 129.11, 94.45, 75.32, 42.82, 18.55. **IR (film)**: ν (cm⁻¹) 3238, 1788, 1731, 1484, 1243, 1088, 1051, 719, 516 cm⁻¹. **HRMS (ESI, *m/z*)** calcd for [C₁₂H₁₁Cl₄NO₄Na]⁺ [(M + Na)⁺]: 395.9334, found: 395.9334.

2,2,2-Trichloroethyl ((2-(4-bromophenyl)propanoyl)oxy)carbamate (**4g**)



DCC coupling of 2-(4-bromophenyl)propanoic acid with TrocNHOH gave the product **4g** as a white solid (chromatography on silica gel, eluent: EtOAc/*n*-hexane = 1/10): **¹H NMR** (300 MHz, CDCl₃) δ 8.22 (s, 1H), 7.50 – 7.41 (m, 2H), 7.27 – 7.14 (m, 2H), 4.75 (s, 2H), 3.93 – 3.78 (m, 1H), 1.57 (d, *J* = 6.0 Hz, 3H). **¹³C NMR** (75 MHz, CDCl₃) δ 172.97, 154.56, 137.49, 132.16, 129.46, 122.00, 94.45, 75.33, 42.90, 18.50. **IR (film)**: ν (cm⁻¹) 3210, 1793, 1732, 1487, 1266, 1117, 1024, 981, 719, 522 cm⁻¹. **HRMS (ESI, *m/z*)** calcd for [C₁₂H₁₁BrCl₃NO₄Na]⁺ [(M + Na)⁺]: 439.8829, found: 439.8829.

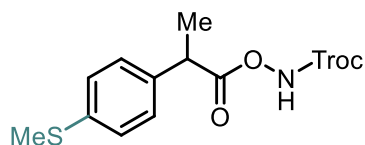
2,2,2-Trichloroethyl((2-(4-(trifluoromethyl)phenyl)propanoyl)oxy)carbamate (**4h**)



DCC coupling of 2-(4-(trifluoromethyl)phenyl)propanoic acid with TrocNHOH gave the product **4h** as a white solid (chromatography on silica gel, eluent: EtOAc/*n*-hexane = 1/10): **¹H NMR** (300 MHz, CDCl₃) δ 8.24 (s, 1H), 7.62 (d, *J* = 8.2 Hz, 2H), 7.47 (d, *J* = 8.1 Hz, 2H), 4.80 (d, *J* = 12.0 Hz, 1H), 4.75 (d, *J* = 12.0 Hz, 1H), 3.99 (q, *J* = 7.2 Hz, 1H), 1.63 (d, *J* = 7.2 Hz, 3H). **¹³C NMR** (75 MHz, CDCl₃) δ 172.76, 154.55, 142.42 (d, *J*_{C-F} = 1.5 Hz), 130.33 (d, *J*_{C-F} = 32.5 Hz), 128.22, 126.02 (q, *J*_{C-F} = 3.8 Hz), 122.30, 94.43, 75.36, 43.30 18.57. **¹⁹F NMR** (282 MHz, CDCl₃) δ -62.65. **IR (film)**: ν

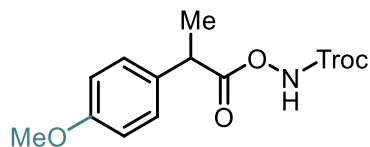
(cm^{-1}) 3222, 1794, 1735, 1322, 1265, 1113, 1067, 842, 722, 605, 451 cm^{-1} . **HRMS (ESI, m/z)** calcd for $[\text{C}_{13}\text{H}_{11}\text{Cl}_3\text{F}_3\text{NO}_4\text{Na}]^+ [(M + \text{Na})^+]$: 429.9598, found: 429.9598.

2,2,2-Trichloroethyl((2-(4-(methylthio)phenyl)propanoyl)oxy)carbamate (4i)



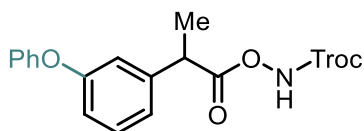
DCC coupling of 2-(4-(methylthio)phenyl)propanoic acid with TrocNHOH gave the product as a white solid (chromatography on silica gel, eluent: EtOAc/*n*-hexane = 1/10): **^1H NMR** (300 MHz, CDCl_3) δ 8.31 (s, 1H), 7.35 – 7.23 (m, 4H), 4.82 (d, $J = 2.3$ Hz, 2H), 3.93 (q, $J = 7.2$ Hz, 1H), 2.52 (s, 3H), 1.63 (d, $J = 7.2$ Hz, 3H). **^{13}C NMR** (75 MHz, CDCl_3) δ 173.19, 154.48, 138.22, 135.15, 128.05, 126.97, 94.36, 75.17, 42.76, 18.38, 15.79. **IR (film)**: ν (cm^{-1}) 3245, 1737, 1476, 1237, 1127, 809, 717, 566 cm^{-1} . **HRMS (ESI, m/z)** calcd for $[\text{C}_{13}\text{H}_{14}\text{Cl}_3\text{NO}_4\text{SNa}]^+ [(M + \text{Na})^+]$: 407.9601, found: 407.9601.

2,2,2-Trichloroethyl((2-(4-methoxyphenyl)propanoyl)oxy)carbamate (4j)



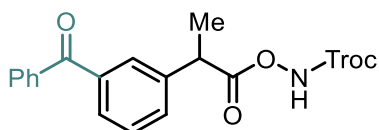
DCC coupling of 2-(4-methoxyphenyl)propanoic acid with TrocNHOH gave the product **4j** as a white solid (chromatography on silica gel, eluent: EtOAc/*n*-hexane = 1/10): **^1H NMR** (300 MHz, CDCl_3) δ 8.26 (s, 1H), 7.27 (d, $J = 8.8$ Hz, 2H), 6.89 (d, $J = 8.7$ Hz, 2H), 4.85 (d, $J = 12.0$ Hz, 1H), 4.80 (d, $J = 12.0$ Hz, 1H), 3.88 (q, $J = 7.2$ Hz, 1H), 3.81 (s, 3H), 1.59 (d, $J = 7.2$ Hz, 3H). **^{13}C NMR** (75 MHz, CDCl_3) δ 173.65, 159.29, 154.63, 130.60, 128.77, 114.41, 94.51, 75.28, 55.43, 42.56, 18.60. **IR (film)**: ν (cm^{-1}) 3247, 1737, 1507, 1472, 1274, 1099, 812, 731, 535 cm^{-1} . **HRMS (ESI, m/z)** calcd for $[\text{C}_{13}\text{H}_{14}\text{Cl}_3\text{NO}_5\text{Na}]^+ [(M + \text{Na})^+]$: 391.9830, found: 391.9830.

2,2,2-Trichloroethyl((2-(3-phenoxyphenyl)propanoyl)oxy)carbamate (4k)



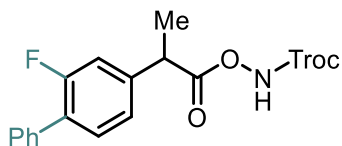
DCC coupling of 2-(3-phenoxyphenyl)propanoic acid with TrocNHOH gave the product **4k** as a colorless oil (chromatography on silica gel, eluent: EtOAc/*n*-hexane = 1/10): **¹H NMR** (300 MHz, CDCl₃) δ 8.27 (s, 1H), 7.40 – 7.25 (m, 3H), 7.17 – 6.98 (m, 5H), 6.95 – 6.86 (m, 1H), 4.79 (d, *J* = 12.0 Hz, 1H), 4.74(d, *J* = 12.0 Hz, 1H), 3.89 (q, *J* = 7.2 Hz, 1H), 1.59 (d, *J* = 7.2 Hz, 3H). **¹³C NMR** (75 MHz, CDCl₃) δ 173.12, 157.81, 156.95, 154.58, 140.43, 130.24, 129.95, 123.65, 122.42, 119.18, 118.25, 117.98, 94.49, 75.28, 43.24, 18.50. **IR (film)**: ν (cm⁻¹) 3294, 1750, 1583, 1485, 1229, 1113, 691, 568 cm⁻¹. **HRMS (ESI, *m/z*)** calcd for [C₁₈H₁₆Cl₃NO₅Na]⁺ [(M + Na)⁺]: 453.9986, found: 453.9986.

2,2,2-Trichloroethyl((2-(3-benzoylphenyl)propanoyl)oxy)carbamate (**4l**)



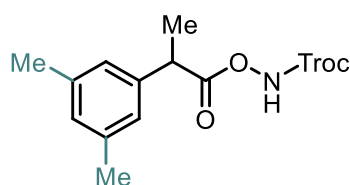
DCC coupling of 2-(3-benzoylphenyl)propanoic acid with TrocNHOH gave the product **4l** as a colorless oil (chromatography on silica gel, eluent: EtOAc/*n*-hexane = 1/10): **¹H NMR** (300 MHz, CDCl₃) δ 8.33 (s, 1H), 7.84 – 7.75 (m, 3H), 7.75 – 7.66 (m, 1H), 7.66 – 7.55 (m, 2H), 7.54 – 7.41 (m, 3H), 4.79 (d, *J* = 12.0 Hz, 1H), 4.74(d, *J* = 12.0 Hz, 1H), 4.00 (q, *J* = 7.2 Hz, 1H), 1.64 (d, *J* = 7.2 Hz, 3H). **¹³C NMR** (75 MHz, CDCl₃) δ 196.27, 172.88, 154.44, 138.82, 138.20, 137.33, 132.63, 131.55, 130.11, 129.61, 129.19, 128.82, 128.38, 94.35, 75.16, 43.17, 18.46. **IR (film)**: ν (cm⁻¹) 3271, 1763, 1653, 1448, 1282, 1114, 709, 568 cm⁻¹. **HRMS (ESI, *m/z*)** calcd for [C₁₉H₁₆Cl₃NO₅Na]⁺ [(M + Na)⁺]: 465.9986, found: 465.9986.

2,2,2-Trichloroethyl((2-(2-fluoro-[1,1'-biphenyl]-4-yl)propanoyl)oxy)carbamate (**4m**)



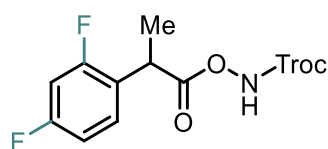
DCC coupling of 2-(2-fluoro-[1,1'-biphenyl]-4-yl)propanoic acid with TrocNHOH gave the product **4m** as a white solid (chromatography on silica gel, eluent: EtOAc/*n*-hexane = 1/10): **¹H NMR** (300 MHz, CDCl₃) δ 8.22 (s, 1H), 7.47 – 7.20 (m, 6H), 7.12 – 7.00 (m, 2H), 4.70 (d, *J* = 12.0 Hz, 1H), 4.66(d, *J* = 12.0 Hz, 1H), 3.85 (q, *J* = 7.2 Hz, 1H), 1.53 (d, *J* = 7.2 Hz, 3H). **¹³C NMR** (75 MHz, CDCl₃) δ 172.91, 159.9 (d, *J*_{C-F} = 246.7 Hz), 154.62, 139.68 (d, *J*_{C-F} = 7.7 Hz), 135.36 (d, *J*_{C-F} = 1.7 Hz), 131.22 (d, *J*_{C-F} = 3.9 Hz), 129.07 (d, *J*_{C-F} = 2.8 Hz), 128.60 (d, *J*_{C-F} = 1.9 Hz), 127.96, 123.77 (d, *J*_{C-F} = 3.6 Hz), 115.53 (d, *J*_{C-F} = 23.9 Hz), 94.46, 75.32, 42.88 (d, *J*_{C-F} = 1.7 Hz), 18.47. **¹⁹F NMR** (282 MHz, CDCl₃) δ -116.88. **IR (film)**: ν (cm⁻¹) 3294, 1753, 1451, 1224, 1111, 696, 569 cm⁻¹. **HRMS (ESI, *m/z*)** calcd for [C₁₈H₁₅Cl₃FNO₄ Na]⁺ [(M + Na)⁺]: 455.9943, found: 455.9943.

2,2,2-Trichloroethyl ((2-(3,5-dimethylphenyl)propanoyl)oxy)carbamate (**4n**)



DCC coupling of 2-(3,5-dimethylphenyl)propanoic acid with TrocNHOH gave the product **4n** as a white solid (chromatography on silica gel, eluent: EtOAc/*n*-hexane = 1/10): **¹H NMR** (300 MHz, CDCl₃) δ 8.29 (s, 1H), 7.00 (s, 3H), 4.87 (d, *J* = 12.0 Hz, 1H), 4.82(d, *J* = 12.0 Hz, 1H), 3.91 (q, *J* = 7.1 Hz, 1H), 2.38 (s, 6H), 1.64 (d, *J* = 7.2 Hz, 3H). **¹³C NMR** (75 MHz, CDCl₃) δ 173.56, 154.62, 138.59, 138.45, 129.58, 125.45, 94.52, 75.28, 43.25, 21.40, 18.56. **IR (film)**: ν (cm⁻¹) 3230, 2961, 1736, 1486, 1239, 1084, 753, 618, 564 cm⁻¹. **HRMS (ESI, *m/z*)** calcd for [C₁₄H₁₆Cl₃NO₄Na]⁺ [(M + Na)⁺]: 390.0037, found: 390.0037.

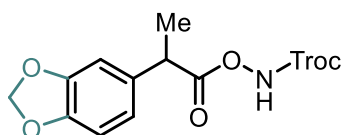
2,2,2-Trichloroethyl ((2-(2,4-difluorophenyl)propanoyl)oxy)carbamate (**4o**)



DCC coupling of 2-(2,4-difluorophenyl)propanoic acid with TrocNHOH gave the product **4o** as a colorless oil (chromatography on silica gel, eluent: EtOAc/*n*-hexane = 1/10): **¹H NMR** (300 MHz,

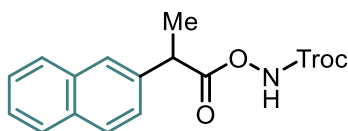
CDCl₃) δ 8.27 (s, 1H), 7.40 – 7.26 (m, 1H), 7.02 – 6.76 (m, 2H), 4.81 (d, *J* = 12.0 Hz, 1H), 4.76 (d, *J* = 12.0 Hz, 1H), 4.18 (q, *J* = 7.2 Hz, 1H), 1.59 (d, *J* = 7.3 Hz, 3H). ¹³C NMR (75 MHz, CDCl₃) δ 172.68, 162.56 (dd, *J*_{C-F} = 247.5, 12.0 Hz), 160.47 (dd, *J*_{C-F} = 247.5, 12.0 Hz), 154.58, 129.74 (dd, *J*_{C-F} = 9.6, 5.2 Hz), 121.86 (dd, *J*_{C-F} = 15.0, 4.0 Hz), 111.89 (dd, *J*_{C-F} = 21.3, 3.7 Hz), 104.27 (t, *J*_{C-F} = 25.7 Hz), 94.46, 75.34, 36.13 (d, *J*_{C-F} = 2.8 Hz), 17.59. ¹⁹F NMR (282 MHz, CDCl₃) δ -110.47, -113.44. IR (film): ν (cm⁻¹) 3292, 1750, 1504, 1278, 1115, 716, 568 cm⁻¹. HRMS (ESI, *m/z*) calcd for [C₁₂H₁₀Cl₃F₂NO₄Na]⁺ [(M + Na)⁺]: 397.9536, found: 397.9536.

2,2,2-Trichloroethyl((2-(benzo[d][1,3]dioxol-5-yl)propanoyl)oxy)carbamate (4p)



DCC coupling of 2-(benzo[d][1,3]dioxol-5-yl)propanoic acid with TrocNHOH gave the product **4p** as a white solid (chromatography on silica gel, eluent: EtOAc/*n*-hexane = 1/10): ¹H NMR (300 MHz, CDCl₃) (300 MHz, CDCl₃) δ 8.25 (s, 1H), 6.83 (s, 1H), 6.80 – 6.71 (m, 2H), 5.94 (s, 2H), 4.83 – 4.70 (m, 2H), 3.83 (q, *J* = 6.4 Hz, 1H), 1.55 (d, *J* = 6.0 Hz, 3H). ¹³C NMR (75 MHz, CDCl₃) δ 173.42, 154.61, 148.16, 147.33, 132.22, 121.12, 108.61, 108.08, 101.34, 94.49, 75.30, 43.03, 18.67. IR (film): ν (cm⁻¹) 3232, 1735, 1481, 1233, 1103, 1037, 716, 566 cm⁻¹. HRMS (ESI, *m/z*) calcd for [C₁₃H₁₂Cl₃NO₆Na]⁺ [(M + Na)⁺]: 405.9622, found: 405.9622.

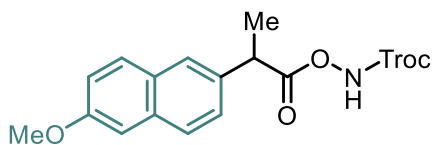
2,2,2-Trichloroethyl ((2-(naphthalen-2-yl)propanoyl)oxy)carbamate (4q)



DCC coupling of 2-(naphthalen-2-yl)propanoic acid with TrocNHOH gave the product **4q** as a white solid (chromatography on silica gel, eluent: EtOAc/*n*-hexane = 1/10): ¹H NMR (300 MHz, CDCl₃) δ 8.24 (s, 1H), 7.88 – 7.76 (m, 4H), 7.56 – 7.41 (m, 3H), 4.79 (d, *J* = 12.0 Hz, 1H), 4.74 (d, *J* = 12.0 Hz, 1H), 4.09 (q, *J* = 7.2 Hz, 1H), 1.70 (d, *J* = 7.2 Hz, 3H). ¹³C NMR (75 MHz, CDCl₃) δ 173.40, 154.61, 135.91, 133.56, 132.96, 128.83, 127.99, 127.81, 126.66, 126.55, 126.33, 125.52, 94.48, 75.28, 43.55,

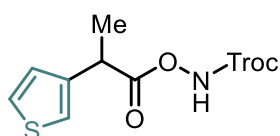
18.56. **IR (film)**: ν (cm⁻¹) 3202, 1793, 1448, 1137, 858, 712, 535, 475 cm⁻¹. **HRMS (ESI, *m/z*)** calcd for [C₁₆H₁₄Cl₃NO₄Na]⁺ [(M + Na)⁺]: 411.9881, found: 411.9881.

2,2,2-Trichloroethyl((2-(6-methoxynaphthalen-2-yl)propanoyl)oxy)carbamate (4r)



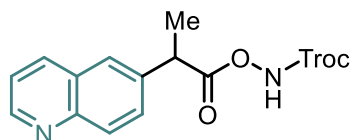
DCC coupling of 2-(6-methoxynaphthalen-2-yl)propanoic acid with TrocNHOH gave the product **4r** as a white solid (chromatography on silica gel, eluent: EtOAc/*n*-hexane = 1/10): **¹H NMR** (300 MHz, CDCl₃) δ 8.29 (s, 1H), 7.76 – 7.65 (m, 3H), 7.42 (dd, *J* = 8.5, 2.0 Hz, 1H), 7.20 – 7.08 (m, 2H), 4.79 (d, *J* = 12.0 Hz, 1H), 4.79 (d, *J* = 12.0 Hz, 1H), 4.74 (d, *J* = 12.0 Hz, 1H), 4.05 (q, *J* = 7.2 Hz, 1H), 3.91 (s, 3H), 1.68 (d, *J* = 7.2 Hz, 3H). **¹³C NMR** (75 MHz, CDCl₃) δ 173.53, 158.02, 154.63, 134.12, 133.60, 129.46, 129.02, 127.61, 126.44, 126.03, 119.36, 105.78, 94.49, 75.26, 55.45, 43.34, 18.54. **IR (film)**: ν (cm⁻¹) 3267, 1764, 1605, 1503, 1448, 1196, 1095, 760, 566 cm⁻¹. **HRMS (ESI, *m/z*)** calcd for [C₁₇H₁₆Cl₃NO₅Na]⁺ [(M + Na)⁺]: 441.9986, found: 441.9986.

2,2,2-Trichloroethyl ((2-(thiophen-3-yl)propanoyl)oxy)carbamate (4s)



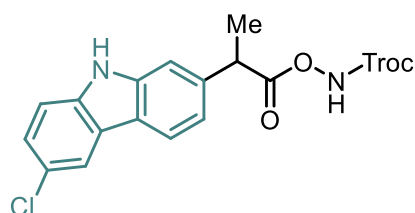
DCC coupling of 2-(thiophen-3-yl)propanoic acid with TrocNHOH gave the product **4s** as a white solid (chromatography on silica gel, eluent: EtOAc/*n*-hexane = 1/10): **¹H NMR** (300 MHz, CDCl₃) δ 8.33 (s, 1H), 7.35 – 7.26 (m, 1H), 7.25 – 7.18 (m, 1H), 7.09 (dd, *J* = 5.0, 1.4 Hz, 1H), 4.81 (d, *J* = 12.0 Hz, 1H), 4.76 (d, *J* = 12.0 Hz, 1H), 4.04 (q, *J* = 7.2 Hz, 1H), 1.61 (d, *J* = 7.2 Hz, 3H). **¹³C NMR** (75 MHz, CDCl₃) δ 173.00, 154.64, 138.48, 126.99, 126.37, 122.25, 94.48, 75.29, 38.87, 18.25. **IR (film)**: ν (cm⁻¹) 3259, 1762, 1380, 1313, 1093, 891, 754, 693, 563 cm⁻¹. **HRMS (ESI, *m/z*)** calcd for [C₁₀H₁₀Cl₃NO₄SNa]⁺ [(M + Na)⁺]: 367.9288, found: 367.9288.

2,2,2-Trichloroethyl ((2-(quinolin-6-yl)propanoyl)oxy)carbamate (4t)



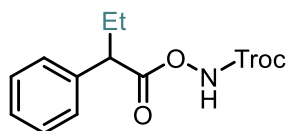
EDCI coupling of 2-(quinolin-6-yl)propanoic acid with TrocNHOH gave the product **4t** as a white solid (chromatography on silica gel, eluent: CH₂Cl₂/MeOH = 1/15): **¹H NMR** (300 MHz, CDCl₃) δ 8.88 (d, *J* = 4.5 Hz, 1H), 8.09 (d, *J* = 8.2 Hz, 1H), 7.85 (d, *J* = 8.9 Hz, 1H), 7.72 (s, 1H), 7.51 (d, *J* = 8.5 Hz, 1H), 7.38 (dd, *J* = 8.3, 4.2 Hz, 1H), 4.81 (s, 2H), 4.12 (q, *J* = 7.1 Hz, 1H), 1.67 (d, *J* = 7.0 Hz, 3H). **¹³C NMR** (75 MHz, CDCl₃) δ 173.00, 155.01, 150.47, 147.08, 137.33, 136.68, 129.55, 129.34, 128.33, 126.49, 121.65, 94.75, 75.20, 43.41, 18.39. **IR (film)**: ν (cm⁻¹) 3248, 1751, 1507, 1234, 1069, 758, 709, 560 cm⁻¹. **HRMS (ESI, *m/z*)** calcd for [C₁₅H₁₄Cl₃N₂O₄]⁺ [(M + H)⁺]: 391.0014, found: 391.0014.

2,2,2-Trichloroethyl((2-(6-chloro-9H-carbazol-2-yl)propanoyl)oxy)carbamate (**4u**)



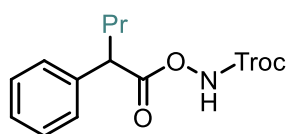
DCC coupling of 2-(6-chloro-9H-carbazol-2-yl)propanoic acid with TrocNHOH gave the product as a white solid (chromatography on silica gel, eluent: EtOAc/*n*-hexane = 1/2): **¹H NMR** (300 MHz, CDCl₃) δ 8.31 (s, 1H), 8.10 (s, 1H), 7.96 – 7.86 (m, 2H), 7.38 – 7.22 (m, 3H), 7.16 (dd, *J* = 8.1, 1.6 Hz, 1H), 4.78 (d, *J* = 12.0 Hz, 1H), 4.74 (d, *J* = 12.0 Hz, 1H), 4.04 (q, *J* = 7.2 Hz, 1H), 1.66 (d, *J* = 7.2 Hz, 3H). **¹³C NMR** (75 MHz, CDCl₃) δ 173.61, 154.71, 140.39, 138.21, 137.01, 126.20, 125.20, 124.21, 122.19, 120.94, 120.16, 119.54, 111.79, 109.94, 94.47, 75.30, 43.78, 18.89. **IR (film)**: ν (cm⁻¹) 3429, 3314, 1759, 1449, 1193, 997, 804, 732, 581 cm⁻¹. **HRMS (ESI, *m/z*)** calcd for [C₁₈H₁₄Cl₄N₂O₄Na]⁺ [(M + Na)⁺]: 484.9600, found: 484.9611.

2,2,2-Trichloroethyl ((2-phenylbutanoyl)oxy)carbamate (**4v**)



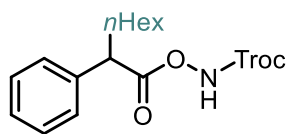
DCC coupling of 2-phenylbutanoic acid with TrocNHOH gave the product **4v** as a white solid (chromatography on silica gel, eluent: EtOAc/*n*-hexane = 1/10): **¹H NMR** (300 MHz, CDCl₃) δ 8.21 (s, 1H), 7.39 – 7.26 (m, 5H), 4.80 (d, *J* = 12.0 Hz, 1H), 4.78(d, *J* = 12.0 Hz, 1H), 3.65 (t, *J* = 7.7 Hz, 1H), 2.27 – 2.09 (m, 1H), 2.01 – 1.80 (m, 1H), 0.95 (t, *J* = 7.4 Hz, 3H). **¹³C NMR** (75 MHz, CDCl₃) δ 172.99, 154.61, 137.16, 128.97, 128.19, 127.97, 94.51, 75.28, 51.10, 26.89, 12.09. **IR (film)**: ν (cm⁻¹) 3344, 1746, 1381, 1094, 1046, 939, 841, 718, 569 cm⁻¹. **HRMS (ESI, *m/z*)** calcd for [C₁₃H₁₄Cl₃NO₄Na]⁺ [(M + Na)⁺]: 375.9881, found: 375.9881.

2,2,2-Trichloroethyl ((2-phenylpentanoyl)oxy)carbamate (**4w**)



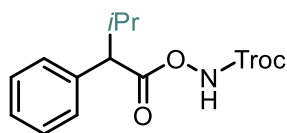
DCC coupling of 2-phenylpentanoic acid with TrocNHOH gave the product **4w** as a white solid (chromatography on silica gel, eluent: EtOAc/*n*-hexane = 1/15): **¹H NMR** (300 MHz, CDCl₃) δ 8.24 (s, 1H), 7.37–7.28 (m, 5H), 4.79 (d, *J* = 12.0 Hz, 1H), 4.75(d, *J* = 12.0 Hz, 1H), 3.75 (t, *J* = 7.7 Hz, 1H), 2.22 – 2.04 (m, 1H), 1.92–1.79 (m, 1H), 1.40–1.27 (m, 2H), 0.93 (t, *J* = 7.3 Hz, 3H). **¹³C NMR** (75 MHz, CDCl₃) δ 173.06, 154.61, 137.33, 128.96, 128.17, 127.93, 94.50, 75.27, 49.13, 35.61, 20.65, 13.81. **IR (film)**: ν (cm⁻¹) 3351, 1751, 1319, 1183, 1104, 753, 695, 512 cm⁻¹. **HRMS (ESI, *m/z*)** calcd for [C₁₄H₁₆Cl₃NO₄Na]⁺ [(M + Na)⁺]: 390.0037, found: 390.0037.

2,2,2-Trichloroethyl ((2-phenyloctanoyl)oxy)carbamate (**4x**)



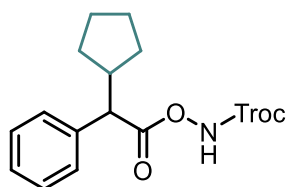
DCC coupling of 2-phenyloctanoic acid with TrocNHOH gave the product **4x** as a colorless oil (chromatography on silica gel, eluent: EtOAc/*n*-hexane = 1/15): **¹H NMR** (300 MHz, CDCl₃) δ 8.17 (s, 1H), 7.33 – 7.18 (m, 5H), 4.79 (d, *J* = 12.0 Hz, 1H), 4.75(d, *J* = 12.0 Hz, 1H), 3.66 (t, *J* = 7.7 Hz, 1H), 2.16 – 1.99 (m, 1H), 1.89 – 1.74 (m, 1H), 1.31 – 1.09 (m, 8H), 0.80 (t, *J* = 6.8 Hz, 3H). **¹³C NMR** (75 MHz, CDCl₃) δ 173.07, 154.59, 137.36, 128.96, 128.16, 127.93, 94.51, 75.27, 49.40, 33.54, 31.63, 29.01, 27.37, 22.67, 14.14. **IR (film)**: ν (cm⁻¹) 3296, 2928, 1752, 1453, 1221, 1114, 893, 720, 697, 571 cm⁻¹. **HRMS (ESI, *m/z*)** calcd for [C₁₇H₂₂Cl₃NO₄Na]⁺ [(M + Na)⁺]: 432.0507, found: 432.0511.

2,2,2-Trichloroethyl ((3-methyl-2-phenylbutanoyl)oxy)carbamate (**4y**)



DCC coupling of 3-methyl-2-phenylbutanoic acid with TrocNHOH gave the product **4y** as a white solid (chromatography on silica gel, eluent: EtOAc/*n*-hexane = 1/15): **¹H NMR** (300 MHz, CDCl₃) δ 8.24 (s, 1H), 7.37 – 7.23 (m, 5H), 4.77 (s, 2H), 3.35 (d, *J* = 10.5 Hz, 1H), 2.50 – 2.30 (m, 1H), 1.11 (d, *J* = 6.5 Hz, 3H), 0.76 (d, *J* = 6.7 Hz, 3H). **¹³C NMR** (75 MHz, CDCl₃) δ 172.85, 154.58, 137.30, 128.87, 128.69, 128.00, 94.51, 75.25, 57.45, 32.32, 21.40, 20.27. **IR (film)**: ν (cm⁻¹) 3292, 1746, 1388, 1105, 1047, 892, 698, 610 cm⁻¹. **HRMS (ESI, *m/z*)** calcd for [C₁₄H₁₆Cl₃NO₄Na]⁺ [(M + Na)⁺]: 390.0037, found: 390.0037.

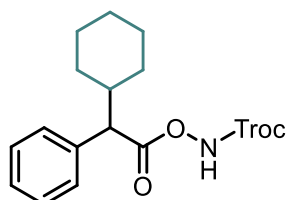
2,2,2-Trichloroethyl (2-cyclopentyl-2-phenylacetoxy)carbamate (**4z**)



DCC coupling of 2-cyclopentyl-2-phenylacetic acid with TrocNHOH gave the product **4z** as a white solid (chromatography on silica gel, eluent: EtOAc/*n*-hexane = 1/15): **¹H NMR** (300 MHz, CDCl₃) δ 8.23 (s, 1H), 7.39 – 7.23 (m, 5H), 4.77 (s, 2H), 3.47 (d, *J* = 11.1 Hz, 1H), 2.72 – 2.52 (m, 1H), 2.04 – 1.92 (m, 1H), 1.76 – 1.20 (m, 6H), 1.12– 0.99 (m, 1H). **¹³C NMR** (75 MHz, CDCl₃) δ 172.82, 154.59,

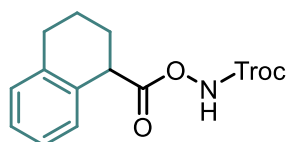
137.19, 128.88, 128.46, 127.94, 94.52, 75.26, 55.32, 43.60, 31.51, 30.91, 25.29, 24.88. **IR (film):** ν (cm^{-1}) 3347, 1753, 1324, 1162, 1105, 890, 696, 576 cm^{-1} . **HRMS (ESI, m/z)** calcd for $[\text{C}_{16}\text{H}_{18}\text{Cl}_3\text{NO}_4\text{Na}]^+ [(M + \text{Na})^+]$: 416.0194, found: 416.0194.

2,2,2-Trichloroethyl (2-cyclohexyl-2-phenylacetoxy)carbamate (**4za**)



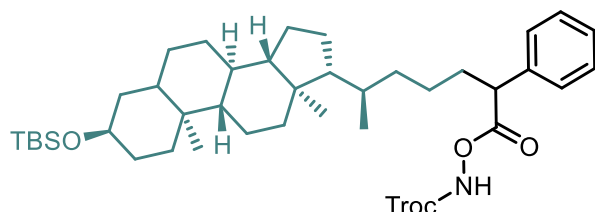
DCC coupling of 2-cyclohexyl-2-phenylacetic acid with TrocNHOH gave the product **4za** as a white solid (chromatography on silica gel, eluent: EtOAc/*n*-hexane = 1/15): **^1H NMR** (300 MHz, CDCl_3) δ 8.24 (s, 1H), 7.36 – 7.23 (m, 5H), 4.76 (s, 2H), 3.42 (d, $J = 10.5$ Hz, 1H), 2.17 – 1.99 (m, 1H), 1.96 – 1.86 (m, 1H), 1.81 – 1.72 (m, 1H), 1.68 – 1.60 (m, 2H), 1.41 – 1.04 (m, 5H), 0.88 – 0.70 (m, 1H). **^{13}C NMR** (75 MHz, CDCl_3) δ 172.80, 154.57, 136.10, 128.85, 128.78, 127.94, 94.51, 75.27, 56.29, 41.34, 31.90, 30.47, 26.28, 26.00, 25.98. **IR (film):** ν (cm^{-1}) 3347, 1765, 1311, 1077, 992, 721, 698 cm^{-1} . **HRMS (ESI, m/z)** calcd for $[\text{C}_{17}\text{H}_{20}\text{Cl}_3\text{NO}_4\text{Na}]^+ [(M + \text{Na})^+]$: 430.0350, found: 430.0352.

2,2,2-Trichloroethyl((1,2,3,4-tetrahydronaphthalene-1-carbonyl)oxy)carbamate (**4zb**)



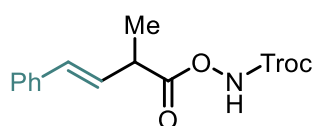
DCC coupling of 1,2,3,4-tetrahydronaphthalene-1-carboxylic acid with TrocNHOH gave the product **4zb** as a colorless oil (chromatography on silica gel, eluent: EtOAc/*n*-hexane = 1/10): **^1H NMR** (300 MHz, CDCl_3) δ 8.33 (s, 1H), 7.29 – 7.09 (m, 4H), 4.81 (s, 2H), 4.04 (t, $J = 5.8$ Hz, 1H), 2.95 – 2.70 (m, 2H), 2.32 – 1.93 (m, 3H), 1.90 – 1.73 (m, 1H). **^{13}C NMR** (75 MHz, CDCl_3) δ 173.86, 154.75, 137.51, 131.39, 129.78, 129.53, 127.61, 126.23, 94.53, 75.33, 42.71, 29.00, 26.70, 20.47. **IR (film):** ν (cm^{-1}) 3292, 2941, 1749, 1450, 1225, 1113, 740, 570 cm^{-1} . **HRMS (ESI, m/z)** calcd for $[\text{C}_{14}\text{H}_{14}\text{Cl}_3\text{NO}_4\text{Na}]^+ [(M + \text{Na})^+]$: 387.9881, found: 387.9881.

2,2,2-Trichloroethyl(((6*R*)-6-((3*R*,8*R*,9*S*,10*S*,13*R*,14*S*,17*R*)-3-((*tert*-butyldimethylsilyl)oxy)-10,13-dimethylhexadecahydro-1*H*-cyclopenta[*a*]phenanthren-17-yl)-2-phenylheptanoyl)oxy)carbamate (4zc)

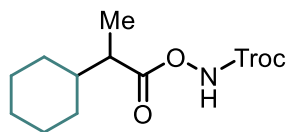


DCC coupling of **3zc** with TrocNHOH gave product **4zc** (dr:1/1) as a white solid (chromatography on silica gel, eluent: EtOAc/*n*-hexane = 1/10): $^1\text{H NMR}$ (300 MHz, CDCl_3) δ 8.16 (s, 1H), 7.29 – 7.18 (m, 5H), 4.70 (s, 2H), 3.71 – 3.61 (m, 1H), 3.58 – 3.44 (m, 1H), 2.15 – 1.63 (m, 7H), 1.55 – 0.89 (m, 23H), 0.85 – 0.72 (m, 15H), 0.54 (d, $J = 3.3$ Hz, 3H), -0.01 (s, 6H). $^{13}\text{C NMR}$ (75 MHz, CDCl_3) δ 173.13, 173.08, 154.56, 137.43, 137.30, 128.97, 128.21, 128.14, 127.94, 94.53, 75.28, 73.00, 56.57, 56.43, 56.39, 49.44, 42.85, 42.47, 40.40, 40.31, 37.09, 36.03, 35.75, 35.73, 35.68, 35.62, 34.75, 34.02, 33.92, 31.19, 28.47, 27.47, 26.57, 26.14, 24.38, 24.13, 24.03, 23.55, 20.97, 18.68, 18.65, 18.48, 12.17, -4.43. **IR (film)**: ν (cm^{-1}) 2929, 2857, 1768, 1450, 1376, 1253, 1077, 869, 725, 576 cm^{-1} . **HRMS (ESI, m/z)** calcd for $[\text{C}_{41}\text{H}_{64}\text{Cl}_3\text{NO}_5\text{SiNa}]^+ [(M + \text{Na})^+]$: 806.3512, found: 806.3512.

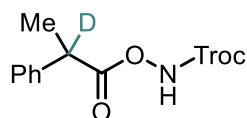
2,2,2-Trichloroethyl (*E*)-((2-methyl-4-phenylbut-3-enoyl)oxy)carbamate (4zd)



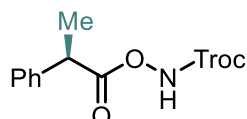
DCC coupling of 2-methyl-4-phenylbut-3-enoic acid with TrocNHOH gave the product **4zd** (*Z/E*:1/8.5) as a white solid (chromatography on silica gel, eluent: EtOAc/*n*-hexane = 1/10): $^1\text{H NMR}$ (300 MHz, CDCl_3) δ 8.35 (s, 1H), 7.44 – 7.16 (m, 5H), 6.59 (d, $J = 15.9$ Hz, 1H), 6.28 (dd, $J = 15.9, 7.9$ Hz, 1H), 4.83 (s, 2H), 3.85 – 3.43 (m, 1H), 1.59 – 1.38 (m, 3H). $^{13}\text{C NMR}$ (75 MHz, CDCl_3) δ 173.37, 154.67, 136.46, 132.85, 128.75, 128.07, 126.59, 126.45, 94.50, 75.32, 41.16, 17.47. **IR (film)**: ν (cm^{-1}) 3241, 1790, 1729, 1488, 1259, 1097, 970, 719, 560 cm^{-1} . **HRMS (ESI, m/z)** calcd for $[\text{C}_{14}\text{H}_{14}\text{Cl}_3\text{NO}_4\text{Na}]^+ [(M + \text{Na})^+]$: 387.9881, found: 387.9881.

2,2,2-Trichloroethyl ((2-cyclohexylpropanoyl)oxy)carbamate (4ze)

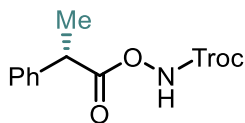
DCC coupling of 2-cyclohexylpropanoic acid with TrocnHOH gave the product **4ze** as a colorless oil (chromatography on silica gel, eluent: EtOAc/*n*-hexane = 1/20): **¹H NMR** (300 MHz, CDCl₃) δ 7.56 (s, 1H), 4.06 (s, 2H), 1.71 (p, *J* = 7.0 Hz, 1H), 1.06 – 0.80 (m, 6H), 0.59 – 0.15 (m, 8H). **¹³C NMR** (75 MHz, CDCl₃) δ 175.25, 154.74, 94.60, 75.29, 43.46, 40.75, 31.06, 29.68, 26.31, 14.01. **IR (film)**: ν (cm⁻¹) 3285, 2926, 1749, 1449, 1224, 1114, 717, 568 cm⁻¹. **HRMS (ESI, *m/z*)** calcd for [C₁₂H₁₈Cl₃NO₄Na]⁺ [(*M* + Na)⁺]: 368.0194, found: 368.0194.

2,2,2-Trichloroethyl ((2-phenylpropanoyl-2-d)oxy)carbamate (4a-d)

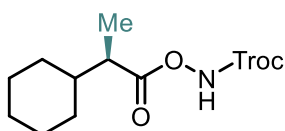
DCC coupling of 2-phenylpropanoic-2-*d* acid with TrocnHOH gave the product **4a-d** as a white solid (chromatography on silica gel, eluent: EtOAc/*n*-hexane = 1/10): **¹H NMR** (300 MHz, CDCl₃) δ 8.28 (s, 1H), 7.40 – 7.27 (m, 5H), 4.82 – 4.72 (m, 2H), 1.60 (s, 3H). **¹³C NMR** (75 MHz, CDCl₃) δ 173.30, 154.65, 138.47, 128.90, 127.80, 127.61, 94.46, 75.13, 43.18, 42.91(t, *J* = 20.25 Hz), 42.64, 17.64. **IR (film)**: ν (cm⁻¹) 3262, 1739, 1450, 1382, 1091, 882, 565 cm⁻¹. **HRMS (ESI, *m/z*)** calcd for [C₁₂H₁₁DCl₃NO₄Na]⁺ [(*M* + Na)⁺]: 362.9787, found: 362.9787.

2,2,2-Trichloroethyl (*R*)-((2-phenylpropanoyl)oxy)carbamate (*R*)-4a

DCC coupling of (*R*)-2-phenylpropanoic acid with TrocnHOH gave the product as a white solid (chromatography on silica gel, eluent: EtOAc/*n*-hexane = 1/10): [**α**]_D²² = -85.5° (*c* = 1.0, MeOH); The **¹H NMR** and **¹³C NMR** data of (*R*)-**4a** are identical with those of (±)-**4a**.

2,2,2-Trichloroethyl (*S*)-((2-phenylpropanoyl)oxy)carbamate (*S*)-4a

DCC coupling of (*S*)-2-phenylpropanoic acid with TrocNHOH gave the product as a white solid (chromatography on silica gel, eluent: EtOAc/*n*-hexane = 1/10): $[\alpha]_D^{22} = 65.3^\circ$ ($c = 1.0$, MeOH); The ^1H NMR and ^{13}C NMR data of (*S*)-**4a** are identical with those of (\pm)-**4a**.

2,2,2-Trichloroethyl (*R*)-((2-cyclohexylpropanoyl)oxy)carbamate (*R*)-4ze

DCC coupling of (*R*)-2-cyclohexylpropanoic acid with TrocNHOH gave the product as a colorless oil (chromatography on silica gel, eluent: EtOAc/*n*-hexane = 1/20): $[\alpha]_D^{22} = 41.6^\circ$ ($c = 1.0$, MeOH).; The ^1H NMR and ^{13}C NMR data of (*R*)-**4ze** are identical with those of (\pm)-**4ze**.

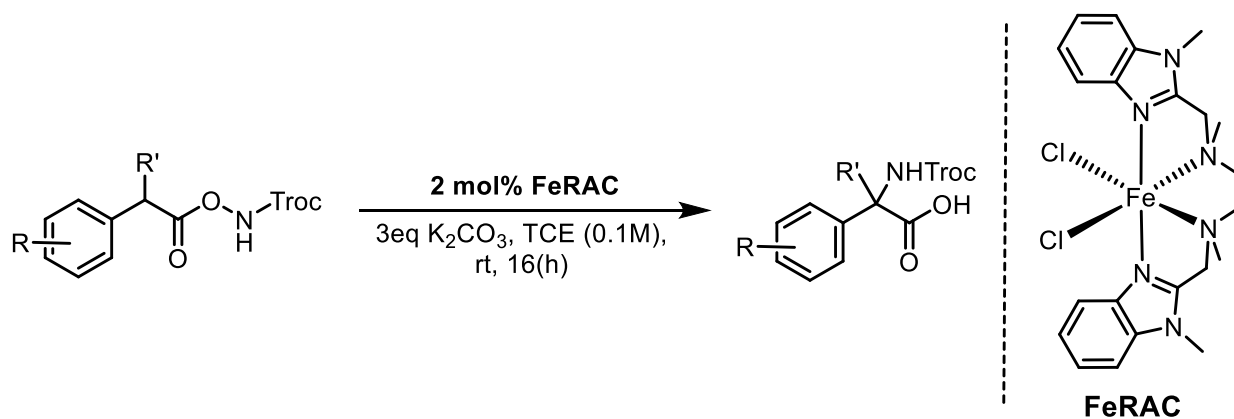
Synthetic note: All data of (*S*)-**4ze** are consistent with the literature ¹².

4.4.3 Catalytic Enantioconvergent C(sp³)-H Aminations

A pre-dried 10 mL Schlenk tube was charged with substrate (0.2 mmol), K_2CO_3 (0.6 mmol) and (*R,R*)-**FeBIP** (4.0–8.0 mol%). The tube was evacuated and backfilled with N_2 for three times. 1,1,2,2-tetrachloroethane (TCE, 0.1 M) was added, and the mixture was degassed via freeze-pump-thaw for two times. The tube was sealed, and the reaction mixture was stirred at 0 °C for 40 hours. To quench the reaction, water (2 mL) and hydrochloric acid (4N) (2.5 mL/mmol substrate) was added. The mixture was extracted with EtOAc for three times and the combined organic layer was dried over anhydrous sodium sulfate. After filtration, the solvent was evaporated under reduced pressure, and the residue was purified by column chromatography on silica gel using indicated solvent as the eluent. Enantiomeric ratios were determined by HPLC analysis on chiral stationary phase. The absolute configuration of the product **5q** was confirmed by single crystallography and X-ray structure analysis as *S*-configuration.

Additional experimental information:

a) Racemic catalytic reactions



Control of reaction temperature. The catalytic reactions were set up in a cooling ethanol bath at 0 °C.

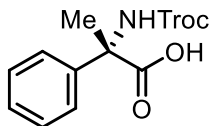


b) Execution of the reactions. All catalytic reactions were carried out in 10 mL Schlenk tubes from “Synthware” under N₂ atmosphere (see image below).

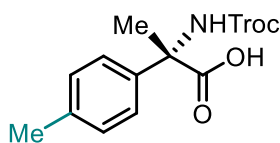


c) Catalyst activity test. We tested the standard catalyst (*R,R*)-FeBIP which was placed on the bench under air for 30 days. The catalysis results were unchanged.

4.3.4 Experimental and Characterization Data of the Products

(S)-2-Phenyl-2-(((2,2,2-trichloroethoxy)carbonyl)amino)propanoic acid (5a)

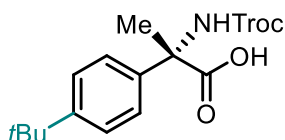
Starting from 2,2,2-trichloroethyl ((2-phenylpropanoyl)oxy)carbamate (68.0 mg, 0.20 mmol) according to the general procedure to provide **5a** as a white solid (chromatography on silica gel, eluent: EtOAc/*n*-hexane = 1/5 with 0.1% TFA, 59.0 mg, 87% yield) and with 83% ee as determined by HPLC analysis (column: Daicel Chiralpak ODR 250 x 4.6 mm, Particle size: 10 μ m, absorption: λ = 210 nm, mobile phase: CH₃CN/H₂O (0.1% TFA) = 40:60, flow rate: 1.0 mL/min, column temperature: 25 °C, retention times: t_r (major) = 18.3 min, t_r (minor) = 16.1 min). $[\alpha]_D^{22}$ = 15.9° (c = 1.0, MeOH). **¹H NMR** (300 MHz, MeOD) δ 7.57 – 7.48 (m, 2H), 7.40 – 7.23 (m, 3H), 4.80 – 4.65 (m, 2H), 1.98 (s, 3H). **¹³C NMR** (75 MHz, MeOD) δ 172.71, 151.92, 138.97, 126.44, 125.89, 124.33, 94.18, 72.29, 60.27, 20.60. **IR (film)**: ν (cm⁻¹) 3398, 2953, 1713, 1494, 1450, 1245, 1102, 765, 696, 569 cm⁻¹. **HRMS (ESI, m/z)** calcd. for [C₁₂H₁₂Cl₃NO₄H]⁺ [(M + H)⁺]: 339.9905, found: 339.9905.

(S)-2-(*p*-Tolyl)-2-(((2,2,2-trichloroethoxy)carbonyl)amino)propanoic acid (5b)

Starting from 2,2,2-trichloroethyl ((2-(*p*-tolyl)propanoyl)oxy)carbamate (70.6 mg, 0.20 mmol) according to the general procedure to provide **5b** as a colorless oil (chromatography on silica gel, eluent: EtOAc/*n*-hexane = 1/5 with 0.1% TFA, 66.0 mg, 93% yield) and with 87% ee as determined by HPLC analysis (column: Daicel Chiralpak IG 250 x 4.6 mm, Particle size: 5 μ m, absorption: λ = 210 nm, mobile phase: CH₃CN/H₂O (0.1% TFA) = 50:50, flow rate: 1.0 mL/min, column temperature: 25 °C, retention times: t_r (major) = 11.3 min, t_r (minor) = 13.0 min). $[\alpha]_D^{22}$ = 23.1° (c = 1.0, MeOH). **¹H NMR** (300 MHz, MeOD) δ 7.21 – 7.12 (m, 2H), 6.92 (d, J = 8.3 Hz, 2H), 4.56 – 4.40 (m, 2H), 2.08 (s, 3H), 1.72 (s, 3H). **¹³C NMR** (75 MHz, MeOD) δ 173.97, 152.98, 137.04, 136.89, 128.17,

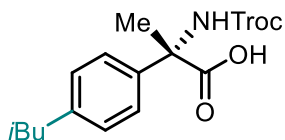
125.31, 95.30, 73.38, 61.15, 21.61, 19.23. **IR (film)**: ν (cm^{-1}) 3400, 2951, 1700, 1406, 1245, 1099, 1053, 815, 719, 569 cm^{-1} . **HRMS (ESI, m/z)** calcd. for $[\text{C}_{13}\text{H}_{14}\text{Cl}_3\text{NO}_4\text{Na}]^+ [(M + \text{Na})^+]$: 375.9881, found: 375.9881.

(S)-2-(4-(*tert*-Butyl)phenyl)-2-(((2,2,2-trichloroethoxy)carbonyl)amino)propanoic acid (5c)



Starting from 2,2,2-trichloroethyl ((2-(4-(*tert*-butyl)phenyl)propanoyl)oxy)carbamate (79.0 mg, 0.20 mmol) according to the general procedure to provide **5c** as a white solid (chromatography on silica gel, eluent: EtOAc/*n*-hexane = 1/5 with 0.1% TFA, 49.0 mg, 62% yield) and with 84% ee as determined by HPLC analysis (column: Daicel Chiralpak IG 250 x 4.6 mm, Particle size: 5 μm , absorption: λ = 210 nm, mobile phase: $\text{CH}_3\text{CN}/\text{H}_2\text{O}$ (0.1% TFA) = 50:50, flow rate: 1.0 mL/min, column temperature: 25 $^\circ\text{C}$, retention times: t_r (major) = 13.7 min, t_r (minor) = 15.9 min). $[\alpha]_D^{22}$ = 12.9 $^\circ$ (c = 1.0, MeOH). **^1H NMR** (300 MHz, MeOD) δ 7.49 – 7.34 (m, 4H), 4.73 (s, 2H), 1.97 (s, 3H), 1.31 (s, 9H). **^{13}C NMR** (75 MHz, MeOD) δ 174.90, 153.97, 151.00, 137.96, 126.07, 125.42, 96.24, 74.35, 62.08, 34.42, 30.86, 22.60. **IR (film)**: ν (cm^{-1}) 3331, 2958, 1703, 1495, 1234, 1097, 819, 712, 564 cm^{-1} . **HRMS (ESI, m/z)** calcd. for $[\text{C}_{16}\text{H}_{20}\text{Cl}_3\text{NO}_4\text{Na}]^+ [(M + \text{Na})^+]$: 418.0350, found: 418.0350.

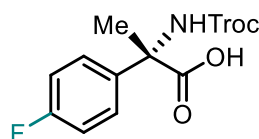
(S)-2-(4-Isobutylphenyl)-2-(((2,2,2-trichloroethoxy)carbonyl)amino)propanoic acid (5d)



Starting from 2,2,2-trichloroethyl ((2-(4-isobutylphenyl)propanoyl)oxy)carbamate (79.0 mg, 0.20 mmol) according to the general procedure to provide **5d** as a white solid (chromatography on silica gel, eluent: EtOAc/*n*-hexane = 1/5 with 0.1% TFA, 55.0 mg, 70% yield) and with 85% ee as determined by HPLC analysis (column: Daicel Chiralpak ODR 250 x 4.6 mm, Particle size: 10 μm , absorption: λ = 210 nm, mobile phase: $\text{CH}_3\text{CN}/\text{H}_2\text{O}$ (0.1% TFA) = 50:50, flow rate: 1.0 mL/min, column temperature: 25 $^\circ\text{C}$, retention times: t_r (major) = 17.9 min, t_r (minor) = 16.1 min). $[\alpha]_D^{22}$ = 24.2 $^\circ$ (c =

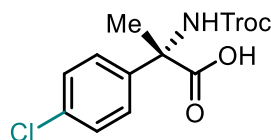
127.4, MeOH, 99% ee). $^1\text{H NMR}$ (300 MHz, MeOD) δ 7.50 – 7.37 (m, 2H), 7.23 – 7.05 (m, 2H), 4.80 – 4.65 (m, 2H), 2.47 (d, J = 7.2 Hz, 2H), 1.96 (s, 3H), 1.92–1.77 (m, 1H), 0.90 (d, J = 6.6 Hz, 6H). $^{13}\text{C NMR}$ (75 MHz, MeOD) δ 174.41, 153.48, 141.14, 137.82, 128.72, 125.64, 95.75, 73.82, 61.64, 44.56, 29.98, 22.11, 21.36. **IR (film)**: ν (cm^{-1}) 3277, 2954, 1711, 1493, 1246, 1100, 815, 722, 537 cm^{-1} . **HRMS (ESI, m/z)** calcd. for $[\text{C}_{16}\text{H}_{20}\text{Cl}_3\text{NO}_4\text{Na}]^+ [(M + \text{Na})^+]$: 418.0350, found: 418.0350.

(S)-2-(4-Fluorophenyl)-2-(((2,2,2-trichloroethoxy)carbonyl)amino)propanoic acid (5e)



Starting from 2,2,2-trichloroethyl ((2-(4-fluorophenyl)propanoyl)oxy)carbamate (71.4 mg, 0.20 mmol) according to the general procedure to provide **5e** as a colorless oil (chromatography on silica gel, eluent: EtOAc/*n*-hexane = 1/5 with 0.1% TFA, 62.0 mg, 86% yield) and with 83% ee as determined by HPLC analysis (column: Daicel Chiralpak ODR 250 x 4.6 mm, Particle size: 10 μm , absorption: λ = 210 nm, mobile phase: $\text{CH}_3\text{CN}/\text{H}_2\text{O}$ (0.1% TFA) = 45:55, flow rate: 1.0 mL/min, column temperature: 25 $^\circ\text{C}$, retention times: t_r (major) = 12.1 min, t_r (minor) = 10.3 min). $[\alpha]_D^{22}$ = 13.4 $^\circ$ (c = 1.0, MeOH). $^1\text{H NMR}$ (300 MHz, MeOD) δ 7.61 – 7.48 (m, 2H), 7.13 – 6.97 (m, 2H), 4.78 – 4.67 (m, 2H), 1.96 (s, 3H). $^{13}\text{C NMR}$ (75 MHz, MeOD) δ 174.57, 162.81 (d, $J_{\text{C-F}}$ = 245.1 Hz), 153.00, 137.10, 128.55 (d, $J_{\text{C-F}}$ = 8.3 Hz), 115.03 (d, $J_{\text{C-F}}$ = 21.7 Hz), 96.22, 74.35, 61.85, 22.84. $^{19}\text{F NMR}$ (282 MHz, MeOD) δ -117.17. **IR (film)**: ν (cm^{-1}) 3398, 2999, 1709, 1509, 1406, 1232, 1105, 808, 720, 568 cm^{-1} . **HRMS (ESI, m/z)** calcd. for $[\text{C}_{12}\text{H}_{11}\text{Cl}_3\text{FNO}_4\text{Na}]^+ [(M + \text{Na})^+]$: 379.9630, found: 379.9630.

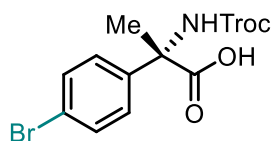
(S)-2-(4-Chlorophenyl)-2-(((2,2,2-trichloroethoxy)carbonyl)amino)propanoic acid (5f)



Starting from 2,2,2-trichloroethyl ((2-(4-chlorophenyl)propanoyl)oxy)carbamate (74.6 mg, 0.20 mmol) according to the general procedure to provide **5f** as a colorless oil (chromatography on silica gel, eluent: EtOAc/*n*-hexane = 1/5 with 0.1% TFA, 72.0 mg, 96% yield) and with 83% ee as determined by HPLC analysis (column: Daicel Chiralpak IG 250 x 4.6 mm, Particle size: 5 μm , absorption: λ =

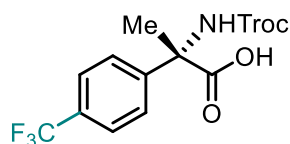
210 nm, mobile phase: CH₃CN/H₂O (0.1% TFA) = 50:50, flow rate: 1.0 mL/min, column temperature: 25 °C, retention times: t_r (major) = 10.2 min, t_r (minor) = 11.7 min). $[\alpha]_D^{22} = 12.6^\circ$ ($c = 1.0$, MeOH). **¹H NMR** (300 MHz, MeOD) δ 7.56 – 7.46 (m, 2H), 7.39 – 7.30 (m, 2H), 4.73 (s, 2H), 1.95 (s, 3H). **¹³C NMR** (75 MHz, MeOD) δ 174.31, 153.95, 139.94, 133.79, 128.47, 128.22, 96.19, 74.37, 61.91, 22.85. **IR (film)**: ν (cm⁻¹) 3400, 2953, 1707, 1491, 1263, 1094, 818, 719, 569 cm⁻¹. **HRMS (ESI, m/z)** calcd. for [C₁₂H₁₁Cl₄NO₄Na]⁺ [(M + Na)⁺]: 395.9334, found: 395.9334.

(S)-2-(4-Bromophenyl)-2-(((2,2,2-trichloroethoxy)carbonyl)amino)propanoic acid (5g)



Starting from 2,2,2-trichloroethyl ((2-(4-bromophenyl)propanoyl)oxy)carbamate (83.4 mg, 0.20 mmol) according to the general procedure to provide **5g** as a white solid (chromatography on silica gel, eluent: EtOAc/*n*-hexane = 1/5 with 0.1% TFA, 51.0 mg, 61% yield) and with 82% ee as determined by HPLC analysis (column: Daicel Chiralpak IG 250 x 4.6 mm, Particle size: 5 μ m, absorption: $\lambda = 210$ nm, mobile phase: CH₃CN/H₂O (0.1% TFA) = 50:50, flow rate: 1.0 mL/min, column temperature: 25 °C, retention times: t_r (major) = 11.6 min, t_r (minor) = 13.0 min). $[\alpha]_D^{22} = 3.3^\circ$ ($c = 1.0$, MeOH). **¹H NMR** (300 MHz, MeOD) δ 7.54 – 7.40 (m, 4H), 4.73 (s, 2H), 1.94 (s, 3H). **¹³C NMR** (75 MHz, MeOD) δ 174.24, 153.97, 140.48, 131.50, 128.56, 121.82, 96.22, 74.38, 61.99, 22.82. **IR (film)**: ν (cm⁻¹) 3307, 2954, 1708, 1487, 1183, 1008, 809, 717, 568 cm⁻¹. **HRMS (ESI, m/z)** calcd. for [C₁₂H₁₁BrCl₃NO₄Na]⁺ [(M + Na)⁺]: 439.8829, found: 439.8829.

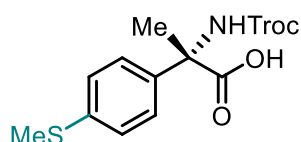
(S)-2-(((2,2,2-Trichloroethoxy)carbonyl)amino)-2-(4-(trifluoromethyl)phenyl)propanoic acid (5h)



Starting from 2,2,2-trichloroethyl ((2-(4-(trifluoromethyl)phenyl)propanoyl)oxy)carbamate (81.4 mg, 0.20 mmol) according to the general procedure to provide **5h** as a white solid (chromatography on silica gel, eluent: EtOAc/*n*-hexane = 1/5 with 0.1% TFA, 53.0 mg, 65% yield) and with 80% ee as

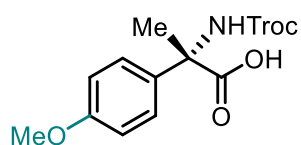
determined by HPLC analysis (column: Daicel Chiralpak ODR 250 x 4.6 mm, Particle size: 10 μm , absorption: $\lambda = 210$ nm, mobile phase: $\text{CH}_3\text{CN}/\text{H}_2\text{O}$ (0.1% TFA) = 40:60, flow rate: 1.0 mL/min, column temperature: 25 $^\circ\text{C}$, retention times: t_r (major) = 29.8 min, t_r (minor) = 25.7 min). $[\alpha]_{\text{D}}^{22} = 22.4^\circ$ ($c = 1.0$, MeOH). $^1\text{H NMR}$ (300 MHz, MeOD) δ 7.77 – 7.60 (m, 4H), 4.74 (s, 2H), 1.99 (s, 3H). $^{13}\text{C NMR}$ (75 MHz, MeOD) δ 173.99, 154.01, 145.62, 129.95 (q, $J_{\text{C-F}} = 32.3$ Hz), 127.33, 125.27 (q, $J_{\text{C-F}} = 3.8$ Hz), 124.75 (q, $J_{\text{C-F}} = 269.3$ Hz), 96.16, 74.41, 62.22, 23.08. $^{19}\text{F NMR}$ (282 MHz, MeOD) δ -64.06. **IR (film)**: ν (cm^{-1}) 3332, 1713, 1497, 1323, 1058, 838, 731, 568 cm^{-1} . **HRMS (ESI, m/z)** calcd. for $[\text{C}_{13}\text{H}_{11}\text{Cl}_3\text{F}_3\text{NO}_4\text{Na}]^+ [(M + \text{Na})^+]$: 429.9598, found: 429.9598.

(S)-2-(4-(Methylthio)phenyl)-2-(((2,2,2-trichloroethoxy)carbonyl)amino)propanoic acid (5i)



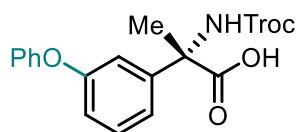
Starting from 2,2,2-trichloroethyl ((2-(4-(methylthio)phenyl)propanoyl)oxy)carbamate (77.0 mg, 0.20 mmol) according to the general procedure to provide **5i** as a white solid (chromatography on silica gel, eluent: EtOAc/*n*-hexane = 1/5 with 0.1% TFA, 68.0 mg, 88% yield) and with 80% ee as determined by HPLC analysis (column: Daicel Chiralpak ODR 250 x 4.6 mm, Particle size: 10 μm , absorption: $\lambda = 210$ nm, mobile phase: $\text{CH}_3\text{CN}/\text{H}_2\text{O}$ (0.1% TFA) = 40:60, flow rate: 1.0 mL/min, column temperature: 25 $^\circ\text{C}$, retention times: t_r (major) = 35.3 min, t_r (minor) = 27.9 min). $[\alpha]_{\text{D}}^{22} = 4.8^\circ$ ($c = 1.0$, MeOH). $^1\text{H NMR}$ (300 MHz, MeOD) δ 7.49 – 7.40 (m, 2H), 7.27 – 7.19 (m, 2H), 4.73 (s, 2H), 2.45 (s, 3H), 1.95 (s, 3H). $^{13}\text{C NMR}$ (75 MHz, MeOD) δ 174.65, 153.93, 138.96, 137.67, 126.94, 126.38, 96.21, 74.34, 61.97, 22.57, 14.70. **IR (film)**: ν (cm^{-1}) 3397, 1700, 1490, 1451, 1143, 1100, 820, 701, 560 cm^{-1} . **HRMS (ESI, m/z)** calcd. for $[\text{C}_{13}\text{H}_{14}\text{Cl}_3\text{NO}_4\text{SNa}]^+ [(M + \text{Na})^+]$: 407.9601, found: 407.9601.

(S)-2-(4-Methoxyphenyl)-2-(((2,2,2-trichloroethoxy)carbonyl)amino)propanoic acid (5j)



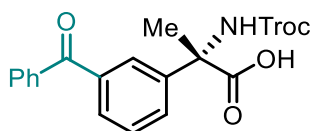
Starting from 2,2,2-trichloroethyl ((2-(4-methoxyphenyl)propanoyl)oxy)carbamate (73.6 mg, 0.20 mmol) according to the general procedure to provide **5j** as a white solid (chromatography on silica gel, eluent: EtOAc/*n*-hexane = 1/5 with 0.1% TFA, 71.4 mg, 97% yield) and with 56% ee as determined by HPLC analysis (column: Daicel Chiralpak ODR 250 x 4.6 mm, Particle size: 10 μ m, absorption: λ = 210 nm, mobile phase: CH₃CN/H₂O (0.1% TFA) = 40:60, flow rate: 1.0 mL/min, column temperature: 25 °C, retention times: t_r (major) = 22.8 min, t_r (minor) = 16.8 min). $[\alpha]_D^{22}$ = 17.4° (c = 1.0, MeOH). **¹H NMR** (300 MHz, MeOD) δ 7.49 – 7.39 (m, 2H), 6.94 – 6.84 (m, 2H), 4.78 – 4.65 (m, 2H), 3.77 (s, 3H), 1.95 (s, 3H). **¹³C NMR** (75 MHz, MeOD) δ 174.99, 159.85, 153.94, 132.85, 127.61, 113.82, 96.25, 74.32, 61.82, 54.87, 22.50. **IR (film)**: ν (cm⁻¹) 2954, 1709, 1510, 1249, 1180, 1097, 817, 721, 568 cm⁻¹. **HRMS (ESI, m/z)** calcd. for [C₁₃H₁₄Cl₃NO₅Na]⁺ [(M + Na)⁺]: 391.9830, found: 391.9830.

(S)-2-(3-Phenoxyphenyl)-2-(((2,2,2-trichloroethoxy)carbonyl)amino)propanoic acid (5k)



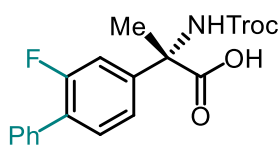
Starting from 2,2,2-trichloroethyl ((2-(3-phenoxyphenyl)propanoyl)oxy)carbamate (86.2 mg, 0.20 mmol) according to the general procedure to provide **5k** as a white solid (chromatography on silica gel, eluent: EtOAc/*n*-hexane = 1/5 with 0.1% TFA, 71.0 mg, 82% yield) and with 77% ee as determined by HPLC analysis (column: Daicel Chiralpak IG 250 x 4.6 mm, Particle size: 5 μ m, absorption: λ = 210 nm, mobile phase: CH₃CN/H₂O (0.1% TFA) = 40:60, flow rate: 1.0 mL/min, column temperature: 25 °C, retention times: t_r (major) = 78.9 min, t_r (minor) = 73.6 min). $[\alpha]_D^{22}$ = 36.6° (c = 1.0, MeOH). **¹H NMR** (300 MHz, MeOD) δ 7.38 – 7.24 (m, 4H), 7.21 – 7.15 (m, 1H), 7.09 (t, J = 7.4 Hz, 1H), 6.97 (d, J = 8.1 Hz, 2H), 6.93 – 6.84 (m, 1H), 4.80 – 4.63 (m, 2H), 1.94 (s, 3H). **¹³C NMR** (75 MHz, MeOD) δ 174.44, 157.71, 157.68, 153.87, 143.24, 130.46, 129.81, 123.55, 121.45, 118.92, 118.13, 117.26, 96.17, 74.31, 62.15, 22.86. **IR (film)**: ν (cm⁻¹) 3333, 2953, 1709, 1485, 1243, 1101, 810, 690, 569 cm⁻¹. **HRMS (ESI, m/z)** calcd. for [C₁₈H₁₆Cl₃NO₅Na]⁺ [(M + Na)⁺]: 453.9986, found: 453.9986.

(S)-2-(3-Benzoylphenyl)-2-(((2,2,2-trichloroethoxy)carbonyl)amino)propanoic acid (5l)



Starting from 2,2,2-trichloroethyl ((2-(3-benzoylphenyl)propanoyl)oxy)carbamate (88.6 mg, 0.20 mmol) according to the general procedure to provide **5l** as a white solid (chromatography on silica gel, eluent: EtOAc/*n*-hexane = 1/5 with 0.1% TFA, 75.3 mg, 85% yield) and with 82% ee as determined by HPLC analysis (column: Daicel Chiralpak IG 250 x 4.6 mm, Particle size: 5 μ m, absorption: λ = 210 nm, mobile phase: CH₃CN/H₂O (0.1% TFA) = 40:60, flow rate: 1.0 mL/min, column temperature: 25 °C, retention times: t_r (major) = 48.7 min, t_r (minor) = 44.8 min). $[\alpha]_D^{22}$ = 16.8° (c = 1.0, MeOH). **¹H NMR** (300 MHz, MeOD) δ 7.98 (s, 1H), 7.89 – 7.61 (m, 6H), 7.59 – 7.48 (m, 3H), 4.74 (s, 2H), 2.01 (s, 3H). **¹³C NMR** (75 MHz, MeOD) δ 197.34, 173.97, 154.00, 141.64, 137.78, 133.00, 130.98, 130.19, 129.46, 128.64, 128.16, 96.13, 74.33, 62.19, 23.24. **IR (film)**: ν (cm⁻¹) 3397, 2953, 1718, 1656, 1498, 1280, 1103, 818, 716, 569 cm⁻¹. **HRMS (ESI, m/z)** calcd. for [C₁₉H₁₆Cl₃NO₅Na]⁺ [(M + Na)⁺]: 465.9986, found: 465.9986.

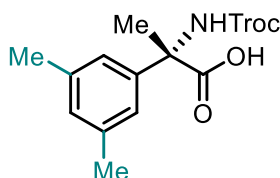
(S)-2-(2-Fluoro-[1,1'-biphenyl]-4-yl)-2-(((2,2,2-trichloroethoxy)carbonyl)amino)propanoic acid (5m)



Starting from 2,2,2-trichloroethyl ((2-(2-fluoro-[1,1'-biphenyl]-4-yl)propanoyl)oxy)carbamate (86.6 mg, 0.20 mmol) according to the general procedure to provide **5m** as a white solid (chromatography on silica gel, eluent: EtOAc/*n*-hexane = 1/5 with 0.1% TFA, 70.0 mg, 81% yield) and with 80% ee as determined by HPLC analysis (column: Daicel Chiralpak ODR 250 x 4.6 mm, Particle size: 10 μ m, absorption: λ = 210 nm, mobile phase: CH₃CN/H₂O (0.1% TFA) = 50:50, flow rate: 1.0 mL/min, column temperature: 25 °C, retention times: t_r (major) = 19.7 min, t_r (minor) = 17.7 min). $[\alpha]_D^{22}$ = 94.3° (c = 1.0, MeOH). **¹H NMR** (300 MHz, MeOD) δ 7.69 – 7.27 (m, 8H), 4.76 (s, 2H), 1.99 (s, 3H). **¹³C NMR** (75 MHz, MeOD) δ 174.25, 159.89 (d, J_{C-F} = 244.5 Hz), 153.93, 142.87 (d, J_{C-F} = 7.2 Hz), 135.75 (d, J_{C-F} = 1.4 Hz), 130.69 (d, J_{C-F} = 3.9 Hz), 129.08 (d, J_{C-F} = 3.0 Hz), 128.61, 127.95, 122.66

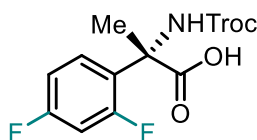
(d, $J_{C-F} = 3.6$ Hz), 114.49 (d, $J_{C-F} = 25.3$ Hz), 96.18, 74.36, 61.92, 22.91. ^{19}F NMR (282 MHz, MeOD) δ -119.76. **IR (film)**: ν (cm^{-1}) 3325, 2955, 1723, 1560, 1409, 1275, 1109, 720, 569 cm^{-1} . **HRMS (ESI, m/z)** calcd. for $[\text{C}_{18}\text{H}_{15}\text{Cl}_3\text{FNO}_4\text{Na}]^+ [(M + \text{Na})^+]$: 455.9943, found: 455.9943.

(S)-2-(3,5-Dimethylphenyl)-2-(((2,2,2-trichloroethoxy)carbonyl)amino)propanoic acid (5n)



Starting from 2,2,2-trichloroethyl ((2-(3,5-dimethylphenyl)propanoyl)oxy)carbamate (73.4 mg, 0.20 mmol) according to the general procedure to provide **5n** as a white solid (chromatography on silica gel, eluent: EtOAc/*n*-hexane = 1/5 with 0.1% TFA, 46.3 mg, 63% yield) and with 75% ee as determined by HPLC analysis (column: Daicel Chiralpak IG 250 x 4.6 mm, Particle size: 5 μm , absorption: $\lambda = 210$ nm, mobile phase: $\text{CH}_3\text{CN}/\text{H}_2\text{O}$ (0.1% TFA) = 50:50, flow rate: 1.0 mL/min, column temperature: 25 $^\circ\text{C}$, retention times: t_r (major) = 12.7 min, t_r (minor) = 9.6 min). $[\alpha]_{\text{D}}^{22} = 32.5^\circ$ ($c = 1.0$, MeOH, 99% ee). ^1H NMR (300 MHz, MeOD) δ 7.12 (s, 2H), 6.93 (s, 1H), 4.81 – 4.62 (m, 2H), 2.29 (s, 6H), 1.95 (s, 3H). ^{13}C NMR (75 MHz, MeOD) δ 174.89, 153.91, 140.82, 138.10, 129.42, 124.07, 96.29, 74.28, 62.19, 22.56, 20.65. **IR (film)**: ν (cm^{-1}) 3398, 2854, 1707, 1494, 1233, 1098, 809, 710, 568 cm^{-1} . **HRMS (ESI, m/z)** calcd. for $[\text{C}_{14}\text{H}_{16}\text{Cl}_3\text{NO}_4\text{Na}]^+ [(M + \text{Na})^+]$: 390.0037, found: 390.0037.

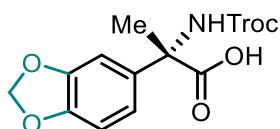
(S)-2-(2,4-Difluorophenyl)-2-(((2,2,2-trichloroethoxy)carbonyl)amino)propanoic acid (5o)



Starting from 2,2,2-trichloroethyl ((2-(2,4-difluorophenyl)propanoyl)oxy)carbamate (75.0 mg, 0.20 mmol) according to the general procedure to provide **5o** as a white solid (chromatography on silica gel, eluent: EtOAc/*n*-hexane = 1/5 with 0.1% TFA, 52.0 mg, 69% yield) and with 83% ee as determined by HPLC analysis (column: Daicel Chiralpak ODR 250 x 4.6 mm, Particle size: 10 μm , absorption: $\lambda = 210$ nm, mobile phase: $\text{CH}_3\text{CN}/\text{H}_2\text{O}$ (0.1% TFA) = 40:60, flow rate: 1.0 mL/min, column

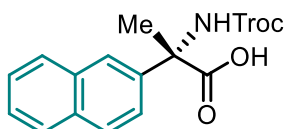
temperature: 25 °C, retention times: t_r (major) = 19.6 min, t_r (minor) = 16.9 min). $[\alpha]_D^{22} = 13.9^\circ$ ($c = 1.0$, MeOH). $^1\text{H NMR}$ (300 MHz, MeOD) δ 7.68 – 7.54 (m, 1H), 7.03 – 6.86 (m, 2H), 4.79 – 4.63 (m, 2H), 2.03 (s, 3H). $^{13}\text{C NMR}$ (126 MHz, MeOD) δ 173.70, 162.66 (dd, $J_{\text{C-F}} = 248.2, 12.6$ Hz), 161.67 (dd, $J_{\text{C-F}} = 252.0, 12.6$ Hz), 152.69, 129.96 (dd, $J_{\text{C-F}} = 10.1, 5.0$ Hz), 124.24 (dd, $J_{\text{C-F}} = 12.6, 3.8$ Hz), 110.02 (d, $J_{\text{C-F}} = 22.9$ Hz), 103.48 (t, $J_{\text{C-F}} = 26.2$ Hz), 95.68, 73.64, 58.78, 21.78. $^{19}\text{F NMR}$ (282 MHz, MeOD) δ -109.53 (d, $J = 8.7$ Hz), -113.06 (d, $J = 8.2$ Hz). **IR (film)**: ν (cm^{-1}) 3400, 3086, 1716, 1501, 1274, 1099, 972, 814, 721, 568 cm^{-1} . **HRMS (ESI, m/z)** calcd. for $[\text{C}_{12}\text{H}_{10}\text{Cl}_3\text{F}_2\text{NO}_4\text{Na}]^+ [(M + \text{Na})^+]$: 397.9536, found: 397.9536.

(S)-2-(Benzo[d][1,3]dioxol-5-yl)-2-(((2,2,2-trichloroethoxy)carbonyl)amino)propanoic acid (5p)



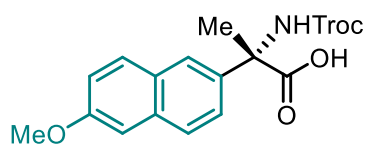
Starting from 2,2,2-trichloroethyl ((2-(benzo[d][1,3]dioxol-5-yl)propanoyl)oxy)carbamate (76.4 mg, 0.20 mmol) according to the general procedure to provide **5p** as a white solid (chromatography on silica gel, eluent: EtOAc/*n*-hexane = 1/5 with 0.1% TFA, 58.0 mg, 76% yield) and with 68% ee as determined by HPLC analysis (column: Daicel Chiralpak ODR 250 x 4.6 mm, Particle size: 10 μm , absorption: $\lambda = 210$ nm, mobile phase: $\text{CH}_3\text{CN}/\text{H}_2\text{O}$ (0.1% TFA) = 40:60, flow rate: 1.0 mL/min, column temperature: 25 °C, retention times: t_r (major) = 22.9 min, t_r (minor) = 18.6 min). $[\alpha]_D^{22} = 10.7^\circ$ ($c = 1.0$, MeOH). $^1\text{H NMR}$ (300 MHz, MeOD) δ 7.04 – 6.95 (m, 2H), 6.81 – 6.72 (m, 1H), 5.93 (s, 2H), 4.80 – 4.65 (m, 2H), 1.94 (s, 3H). $^{13}\text{C NMR}$ (75 MHz, MeOD) δ 174.40, 153.39, 147.82, 147.26, 134.34, 119.43, 107.36, 106.65, 101.19, 95.73, 73.82, 61.52, 22.09. **IR (film)**: ν (cm^{-1}) 3372, 2955, 1713, 1502, 1270, 1094, 1037, 819, 711, 563 cm^{-1} . **HRMS (ESI, m/z)** calcd. for $[\text{C}_{13}\text{H}_{12}\text{Cl}_3\text{NO}_6\text{Na}]^+ [(M + \text{Na})^+]$: 405.9622, found: 405.9622.

(S)-2-(Naphthalen-2-yl)-2-(((2,2,2-trichloroethoxy)carbonyl)amino)propanoic acid (5q)



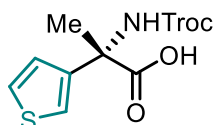
Starting from 2,2,2-trichloroethyl ((2-(naphthalen-2-yl)propanoyl)oxy)carbamate (78.0 mg, 0.20 mmol) according to the general procedure to provide **5q** as a white solid (chromatography on silica gel, eluent: EtOAc/*n*-hexane = 1/5 with 0.1% TFA, 70.0 mg, 90% yield) and with 84% ee as determined by HPLC analysis (column: Daicel Chiralpak ODR 250 x 4.6 mm, Particle size: 10 μ m, absorption: λ = 210 nm, mobile phase: CH₃CN/H₂O (0.1% TFA) = 50:50, flow rate: 1.0 mL/min, column temperature: 25 °C, retention times: t_r (major) = 14.2 min, t_r (minor) = 12.6 min). $[\alpha]_D^{22}$ = 34.7° (c = 1.0, MeOH, 99% ee). **¹H NMR** (300 MHz, MeOD) δ 8.00 (d, J = 2.1 Hz, 1H), 7.88 – 7.76 (m, 3H), 7.64 (dd, J = 8.8, 2.1 Hz, 1H), 7.51 – 7.42 (m, 2H), 4.82 – 4.66 (m, 2H), 2.09 (s, 3H). **¹³C NMR** (75 MHz, MeOD) δ 174.73, 154.01, 138.33, 133.64, 133.36, 128.39, 128.16, 127.57, 126.47, 126.41, 125.49, 124.33, 96.26, 74.34, 62.45, 22.72. **IR (film)**: ν (cm⁻¹) 3335, 3023, 1730, 1502, 1289, 1106, 860, 737, 569, 473 cm⁻¹. **HRMS (ESI, m/z)** calcd. for [C₁₆H₁₄Cl₃NO₄Na]⁺ [(M + Na)⁺]: 411.9881, found: 411.9881.

(S)-2-(6-Methoxynaphthalen-2-yl)-2-(((2,2,2-trichloroethoxy)carbonyl)amino)propanoic acid (5r)



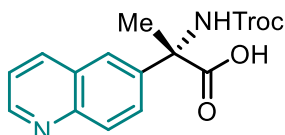
Starting from 2,2,2-trichloroethyl ((2-(6-methoxynaphthalen-2-yl)propanoyl)oxy)carbamate (83.8 mg, 0.20 mmol) according to the general procedure to provide **5r** as a white solid (chromatography on silica gel, eluent: EtOAc/*n*-hexane = 1/5 with 0.1% TFA, 82.9 mg, 99% yield) and with 64% ee as determined by HPLC analysis (column: Daicel Chiralpak IG 250 x 4.6 mm, Particle size: 5 μ m, absorption: λ = 210 nm, mobile phase: CH₃CN/H₂O (0.1% TFA) = 50:50, flow rate: 1.0 mL/min, column temperature: 25 °C, retention times: t_r (major) = 21.3 min, t_r (minor) = 15.4 min). $[\alpha]_D^{22}$ = 49.4° (c = 1.0, MeOH). **¹H NMR** (300 MHz, MeOD) δ 7.91 (d, J = 2.2 Hz, 1H), 7.73 (dd, J = 9.0, 2.1 Hz, 2H), 7.58 (dd, J = 8.8, 2.1 Hz, 1H), 7.18 (d, J = 2.6 Hz, 1H), 7.11 (dd, J = 8.9, 2.5 Hz, 1H), 4.81 – 4.66 (m, 2H), 3.87 (s, 3H), 2.07 (s, 3H). **¹³C NMR** (75 MHz, MeOD) δ 174.87, 158.68, 154.00, 135.92, 134.64, 129.83, 129.05, 127.16, 125.27, 124.73, 119.19, 105.60, 96.28, 74.34, 62.34, 54.89, 22.61. **IR (film)**: ν (cm⁻¹) 3333, 2951, 1700, 1452, 1264, 1051, 812, 733, 567 cm⁻¹. **HRMS (ESI, m/z)** calcd. for [C₁₇H₁₆Cl₃NO₅Na]⁺ [(M + Na)⁺]: 441.9986, found: 441.9986.

(S)-2-(Thiophen-3-yl)-2-(((2,2,2-trichloroethoxy)carbonyl)amino)propanoic acid (5s)



Starting from 2,2,2-trichloroethyl ((2-(thiophen-3-yl)propanoyl)oxy)carbamate (69.0 mg, 0.20 mmol) according to the general procedure to provide **5s** as a oil (chromatography on silica gel, eluent: EtOAc/*n*-hexane = 1/5 with 0.1% TFA, 65.0 mg, 94% yield) and with 83% ee as determined by HPLC analysis (column: Daicel Chiralpak IG 250 x 4.6 mm, Particle size: 5 μ m, absorption: λ = 210 nm, mobile phase: CH₃CN/H₂O (0.1% TFA) = 40:60, flow rate: 1.0 mL/min, column temperature: 25 °C, retention times: t_r (major) = 20.6 min, t_r (minor) = 19.2 min). $[\alpha]_D^{22}$ = 13.8° (c = 1.0, MeOH). **¹H NMR** (300 MHz, MeOD) δ 7.47 – 7.40 (m, 1H), 7.40 – 7.31 (m, 1H), 7.20 (dd, J = 5.1, 1.4 Hz, 1H), 4.83 – 4.66 (m, 2H), 1.94 (s, 3H). **¹³C NMR** (75 MHz, MeOD) δ 174.43, 154.14, 142.15, 126.61, 125.74, 122.42, 96.19, 74.38, 60.30, 23.57. **IR (film)**: ν (cm⁻¹) 3394, 2953, 1701, 1452, 1195, 1125, 1102, 796, 722, 568 cm⁻¹. **HRMS (ESI, m/z)** calcd. for [C₁₀H₁₀Cl₃NO₄SNa]⁺ [(M + Na)⁺]: 367.9288, found: 367.9288.

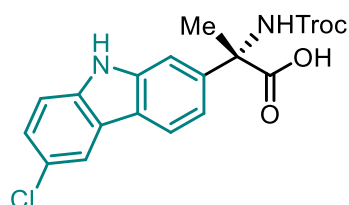
(S)-2-(Quinolin-6-yl)-2-(((2,2,2-trichloroethoxy)carbonyl)amino)propanoic acid (5t)



Starting from 2,2,2-trichloroethyl ((2-(quinolin-6-yl)propanoyl)oxy)carbamate (78.0 mg, 0.20 mmol) according to the general procedure to provide **5t** as a white solid (chromatography on silica gel, eluent: EtOAc/*n*-hexane = 1/5 with 0.1% TFA, 67.0 mg, 86% yield) and with 70% ee as determined by HPLC analysis (column: Daicel Chiralpak ODR 250 x 4.6 mm, Particle size: 10 μ m, absorption: λ = 210 nm, mobile phase: CH₃CN/H₂O (0.1% TFA) = 20:80, flow rate: 1.0 mL/min, column temperature: 25 °C, retention times: t_r (major) = 8.4 min, t_r (minor) = 7.5 min). $[\alpha]_D^{22}$ = 14.1° (c = 1.0, MeOH). **¹H NMR** (300 MHz, MeOD) δ 9.20 – 9.07 (m, 2H), 8.47 (s, 1H), 8.37 – 8.19 (m, 2H), 8.03 (dd, J = 8.4, 5.4 Hz, 1H), 4.74 (s, 2H), 2.10 (s, 3H). **¹³C NMR** (75 MHz, MeOD) δ 173.61, 154.14, 146.88, 145.65, 143.75, 138.67, 133.99, 129.36, 126.97, 122.37, 121.35, 96.12, 74.42, 62.36, 23.52. **IR (film)**: ν (cm⁻¹) 3367,

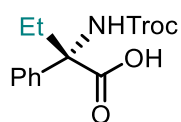
2953, 1669, 1385, 1183, 1100, 799, 718, 568 cm^{-1} . **HRMS (ESI, m/z)** calcd. for $[\text{C}_{15}\text{H}_{13}\text{Cl}_3\text{N}_2\text{O}_4\text{H}]^+$ $[(\text{M} + \text{H})^+]$: 391.0014, found: 391.0014.

(S)-2-(6-Chloro-9H-carbazol-2-yl)-2-(((2,2,2-trichloroethoxy)carbonyl)amino)propanoic acid (5u)



Starting from 2,2,2-trichloroethyl ((2-(6-chloro-9H-carbazol-2-yl)propanoyl)oxy)carbamate (92.4 mg, 0.20 mmol) according to the general procedure to provide **5u** as a white solid (chromatography on silica gel, eluent: EtOAc/*n*-hexane = 1/5 with 0.1% TFA, 24.1 mg, 26% yield) and with 72% ee as determined by HPLC analysis (column: Daicel Chiralpak IG 250 x 4.6 mm, Particle size: 5 μm , absorption: $\lambda = 210 \text{ nm}$, mobile phase: $\text{CH}_3\text{CN}/\text{H}_2\text{O}$ (0.1% TFA) = 50:50, flow rate: 1.0 mL/min, column temperature: 25 $^\circ\text{C}$, retention times: t_r (major) = 40.1 min, t_r (minor) = 29.2 min). $[\alpha]_{\text{D}}^{22} = 10.8^\circ$ ($c = 1.0$, MeOH). **$^1\text{H NMR}$** (300 MHz, MeOD) δ 8.04 – 7.96 (m, 2H), 7.65 (d, $J = 1.8 \text{ Hz}$, 1H), 7.44 – 7.27 (m, 3H), 4.81 – 4.68 (m, 2H), 2.09 (s, 3H). **$^{13}\text{C NMR}$** (126 MHz, MeOD) δ 174.52, 153.47, 140.64, 138.94, 138.75, 125.24, 123.88, 123.72, 121.58, 119.71, 119.32, 116.95, 111.56, 108.69, 95.74, 73.84, 62.20, 22.23. **IR (film)**: ν (cm^{-1}) 3416, 2923, 2532, 1699, 1468, 1270, 1097, 809, 692, 563 cm^{-1} . **HRMS (ESI, m/z)** calcd. for $[\text{C}_{18}\text{H}_{14}\text{Cl}_4\text{N}_2\text{O}_4\text{Na}]^+$ $[(\text{M} + \text{Na})^+]$: 484.9600, found: 484.9600.

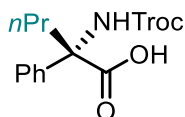
(S)-2-Phenyl-2-(((2,2,2-trichloroethoxy)carbonyl)amino)butanoic acid (5v)



Starting from 2,2,2-trichloroethyl ((2-phenylbutanoyl)oxy)carbamate (70.6 mg, 0.20 mmol) according to the general procedure to provide **5v** as a colorless oil (chromatography on silica gel, eluent: EtOAc/*n*-hexane = 1/5 with 0.1% TFA, 60.0 mg, 85% yield) and with 83% ee as determined by HPLC analysis (column: Daicel Chiralpak ODR 250 x 4.6 mm, Particle size: 10 μm , absorption: $\lambda = 210 \text{ nm}$,

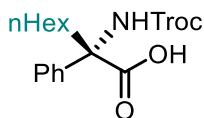
mobile phase: CH₃CN/H₂O(0.1% TFA) = 50:50, flow rate: 1.0 mL/min, column temperature: 25 °C, retention times: t_r (major) = 12.4 min, t_r (minor) = 9.9 min). $[\alpha]_D^{22} = 66.5^\circ$ ($c = 1.0$, MeOH). **¹H NMR** (300 MHz, MeOD) δ 7.55 – 7.47 (m, 2H), 7.38 – 7.20 (m, 3H), 4.81 – 4.64 (m, 2H), 2.70 – 2.47 (m, 2H), 0.92 (t, $J = 7.2$ Hz, 3H). **¹³C NMR** (75 MHz, MeOD) δ 174.06, 153.12, 140.61, 128.42, 127.78, 126.46, 96.31, 74.14, 66.23, 26.58, 7.88. **IR (film)**: ν (cm⁻¹) 3398, 2960, 1712, 1493, 1406, 1232, 1105, 725, 696, 568 cm⁻¹. **HRMS (ESI, m/z)** calcd. for [C₁₃H₁₄Cl₃NO₄Na]⁺ [(M + Na)⁺]: 375.9881, found: 375.9881.

(S)-2-Phenyl-2-(((2,2,2-trichloroethoxy)carbonyl)amino)pentanoic acid (5w)



Starting from 2,2,2-trichloroethyl ((2-phenylpentanoyl)oxy)carbamate (73.4 mg, 0.20 mmol) according to the general procedure to provide **5w** as a white solid (chromatography on silica gel, eluent: EtOAc/*n*-hexane = 1/5 with 0.1% TFA, 67.0 mg, 91% yield) and with 82% ee as determined by HPLC analysis (column: Daicel Chiralpak IG 250 x 4.6 mm, Particle size: 5 μ m, absorption: $\lambda = 210$ nm, mobile phase: CH₃CN/H₂O (0.1% TFA) = 40:60, flow rate: 1.0 mL/min, column temperature: 25 °C, retention times: t_r (major) = 26.7 min, t_r (minor) = 30.2 min). $[\alpha]_D^{22} = 9.83^\circ$ ($c = 1.0$, MeOH). **¹H NMR** (300 MHz, MeOD) δ 7.55 – 7.47 (m, 2H), 7.39 – 7.21 (m, 3H), 4.81 – 4.65 (m, 2H), 2.66 – 2.42 (m, 2H), 1.54 – 1.36 (m, 1H), 1.34 – 1.16 (m, 1H), 0.99 (t, $J = 7.4$ Hz, 3H). **¹³C NMR** (75 MHz, MeOD) δ 174.18, 153.14, 140.80, 128.42, 127.77, 126.39, 96.34, 74.15, 65.65, 35.88, 17.74, 13.54. **IR (film)**: ν (cm⁻¹) 3397, 2961, 1710, 1493, 1403, 1227, 1107, 1054, 720, 695, 568 cm⁻¹. **HRMS (ESI, m/z)** calcd. for [C₁₄H₁₆Cl₃NO₄Na]⁺ [(M + Na)⁺]: 390.0037, found: 390.0037.

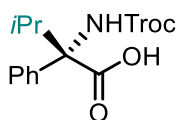
(S)-2-Phenyl-2-(((2,2,2-trichloroethoxy)carbonyl)amino)octanoic acid (5x)



Starting from 2,2,2-trichloroethyl ((2-phenyloctanoyl)oxy)carbamate (81.8 mg, 0.20 mmol) according to the general procedure to provide **5x** as a white solid (chromatography on silica gel, eluent:

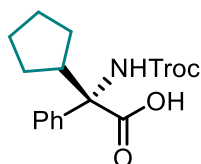
EtOAc/*n*-hexane = 1/5 with 0.1% TFA, 74.0 mg, 90% yield) and with 82% ee as determined by HPLC analysis (column: Daicel Chiralpak IG 250 x 4.6 mm, Particle size: 5 μ m, absorption: λ = 210 nm, mobile phase: CH₃CN/H₂O (0.1% TFA) = 50:50, flow rate: 1.0 mL/min, column temperature: 25 °C, retention times: t_r (major) = 24.2 min, t_r (minor) = 21.3 min). $[\alpha]_D^{22}$ = 23.8° (c = 1.0, MeOH). **¹H NMR** (300 MHz, MeOD) δ 7.55 – 7.47 (m, 2H), 7.38 – 7.20 (m, 3H), 4.83 – 4.63 (m, 2H), 2.71 – 2.44 (m, 2H), 1.48 – 1.15 (m, 8H), 0.95 – 0.85 (m, 3H). **¹³C NMR** (75 MHz, MeOD) δ 174.16, 153.05, 140.76, 128.42, 127.77, 126.37, 96.36, 74.10, 65.63, 33.52, 31.94, 29.40, 24.30, 22.67, 13.53. **IR (film)**: ν (cm⁻¹) 3428, 2930, 1752, 1690, 1484, 1146, 922, 906, 723, 691, 571, 464 cm⁻¹. **HRMS (ESI, *m/z*)** calcd. for [C₁₇H₂₂Cl₃NO₄Na]⁺ [(M + Na)⁺]: 432.0507, found: 432.0507.

(S)-3-Methyl-2-phenyl-2-(((2,2,2-trichloroethoxy)carbonyl)amino)butanoic acid (5y)



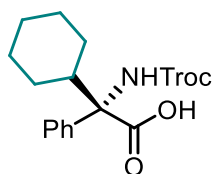
Starting from 2,2,2-trichloroethyl ((3-methyl-2-phenylbutanoyl)oxy)carbamate (73.4 mg, 0.20 mmol) according to the general procedure to provide **5y** as a white solid (chromatography on silica gel, eluent: EtOAc/*n*-hexane = 1/5 with 0.1% TFA, 65.0 mg, 88% yield) and with 88% ee as determined by HPLC analysis (column: Daicel Chiralpak IG 250 x 4.6 mm, Particle size: 5 μ m, absorption: λ = 210 nm, mobile phase: CH₃CN/H₂O(0.1% TFA) = 40:60, flow rate: 1.0 mL/min, column temperature: 25 °C, retention times: t_r (major) = 21.7 min, t_r (minor) = 30.6 min). $[\alpha]_D^{22}$ = 5.9° (c = 1.0, MeOH). **¹H NMR** (300 MHz, MeOD) δ 7.57 (d, J = 7.4 Hz, 2H), 7.36 – 7.19 (m, 3H), 4.77 (d, J = 12.0 Hz, 1H), 4.69 (d, J = 12.0 Hz, 1H), 2.86 – 2.67 (m, 1H), 0.96 (d, J = 6.0 Hz, 3H), 0.92 (d, J = 6.0 Hz, 3H). **¹³C NMR** (75 MHz, MeOD) δ 173.79, 154.45, 138.84, 127.82, 127.69, 127.31, 96.35, 74.37, 69.56, 35.50, 17.51. **IR (film)**: ν (cm⁻¹) 3285, 2972, 1704, 1400, 1321, 1121, 773, 704, 570 cm⁻¹. **HRMS (ESI, *m/z*)** calcd. for [C₁₄H₁₆Cl₃NO₄Na]⁺ [(M + Na)⁺]: 390.0037, found: 390.0037.

(S)-2-Cyclopentyl-2-phenyl-2-(((2,2,2-trichloroethoxy)carbonyl)amino)acetic acid (5z)



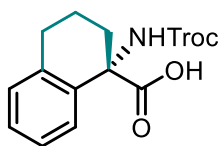
Starting from 2,2,2-trichloroethyl (2-cyclopentyl-2-phenylacetoxycarbamate (78.6 mg, 0.20 mmol) according to the general procedure to provide **5z** as a white solid (chromatography on silica gel, eluent: EtOAc/*n*-hexane = 1/5 with 0.1% TFA, 34.6 mg, 44% yield) and with 82% ee as determined by HPLC analysis (column: Daicel Chiralpak IG 250 x 4.6 mm, Particle size: 5 μ m, absorption: λ = 210 nm, mobile phase: CH₃CN/H₂O (0.1% TFA) = 45:55, flow rate: 1.0 mL/min, column temperature: 25 °C, retention times: t_r (major) = 21.3 min, t_r (minor) = 27.3 min). $[\alpha]_D^{22} = 2.3^\circ$ (c = 1.0, MeOH). **¹H NMR** (300 MHz, MeOD) δ 7.61 – 7.53 (m, 2H), 7.35 – 7.18 (m, 3H), 4.76 (d, J = 12.0 Hz, 1H), 4.68 (d, J = 12.0 Hz, 1H), 3.14 – 2.82 (m, 1H), 1.82 – 1.42 (m, 8H). **¹³C NMR** (75 MHz, MeOD) δ 174.01, 154.28, 139.95, 127.95, 127.46, 127.34, 96.34, 74.34, 68.04, 27.99, 27.84, 25.38, 25.28. **IR (film)**: ν (cm⁻¹) 3286, 2953, 1709, 1494, 1399, 1200, 1106, 766, 699, 569 cm⁻¹. **HRMS (ESI, m/z)** calcd. for [C₁₆H₁₈Cl₃NO₄Na]⁺ [(M + Na)⁺]: 416.0194, found: 416.0194.

(S)-2-Cyclohexyl-2-phenyl-2-(((2,2,2-trichloroethoxy)carbonyl)amino)acetic acid (5za)



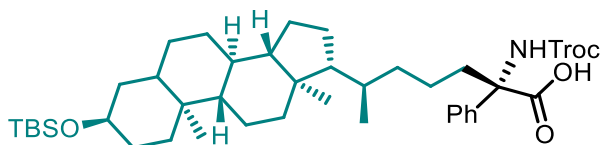
Starting from 2,2,2-trichloroethyl (2-cyclohexyl-2-phenylacetoxycarbamate (81.4 mg, 0.20 mmol) according to the general procedure to provide **5za** as a white solid (chromatography on silica gel, eluent: EtOAc/*n*-hexane = 1/5 with 0.1% TFA, 49.6 mg, 61% yield) and with 82% ee as determined by HPLC analysis (column: Daicel Chiralpak IB 250 x 4.6 mm, Particle size: 5 μ m, absorption: λ = 210 nm, mobile phase: CH₃CN/H₂O (0.1% TFA) = 50:50, flow rate: 1.0 mL/min, column temperature: 25 °C, retention times: t_r (major) = 16.8 min, t_r (minor) = 18.3 min). $[\alpha]_D^{22} = 6.2^\circ$ (c = 1.0, MeOH). **¹H NMR** (300 MHz, MeOD) δ 7.59 – 7.51 (m, 2H), 7.35 – 7.18 (m, 3H), 4.77 (d, J = 12.0 Hz, 1H), 4.69 (d, J = 12.0 Hz, 1H), 2.43 – 2.30 (m, 1H), 1.85 – 1.60 (m, 5H), 1.38 – 1.19 (m, 2H), 1.07 – 1.05 (m, 3H). **¹³C NMR** (75 MHz, MeOD) δ 173.56, 154.44, 138.66, 127.79, 127.67, 127.25, 96.37, 74.35, 69.44, 46.01, 28.45, 26.90, 26.82, 26.54. **IR (film)**: ν (cm⁻¹) 3280, 2925, 1712, 1399, 1243, 1057, 887, 765, 651, 463 cm⁻¹. **HRMS (ESI, m/z)** calcd. for [C₁₇H₂₀Cl₃NO₄Na]⁺ [(M + Na)⁺]: 430.0350, found: 430.0350.

(S)-1-(((2,2,2-Trichloroethoxy)carbonyl)amino)-1,2,3,4-tetrahydronaphthalene-1-carboxylic acid (5zb)



Starting from 2,2,2-trichloroethyl ((1,2,3,4-tetrahydronaphthalene-1-carbonyl)oxy)carbamate (73.0 mg, 0.20 mmol) according to the general procedure to provide **5zb** as a white solid (chromatography on silica gel, eluent: EtOAc/*n*-hexane = 1/5 with 0.1% TFA, 41.0 mg, 56% yield) and with 68% ee as determined by HPLC analysis (column: Daicel Chiralpak ODR 250 x 4.6 mm, Particle size: 10 μ m, absorption: λ = 210 nm, mobile phase: CH₃CN/H₂O (0.1% TFA) = 40:60, flow rate: 1.0 mL/min, column temperature: 25 °C, retention times: t_r (major) = 30.9 min, t_r (minor) = 27.6 min). $[\alpha]_D^{22}$ = 11.2° (c = 1.0, MeOH). ¹H NMR (300 MHz, MeOD) δ 7.46 (d, J = 7.7 Hz, 1H), 7.25 – 7.09 (m, 3H), 4.77 (d, J = 12.0 Hz, 1H), 4.69 (d, J = 12.0 Hz, 1H), 2.93 – 2.73 (m, 2H), 2.63 – 2.51 (m, 1H), 2.44 – 2.32 (m, 1H), 2.22 – 1.97 (m, 1H), 1.95 – 1.80 (m, 1H). ¹³C NMR (75 MHz, MeOD) δ 175.21, 153.76, 138.73, 134.95, 129.60, 128.23, 127.53, 126.46, 96.31, 74.30, 61.36, 31.56, 29.53, 19.70. IR (film): ν (cm⁻¹) 3421, 2923, 1703, 1454, 1213, 1058, 721, 569 cm⁻¹. HRMS (ESI, m/z) calcd. for [C₁₄H₁₄Cl₃NO₄Na]⁺ [(M + Na)⁺]: 387.9881, found: 387.9881.

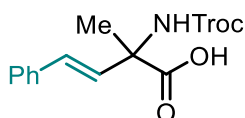
(2S,6R)-6-((3R,8R,9S,10S,13R,14S,17R)-3-((*tert*-Butyldimethylsilyl)oxy)-10,13-dimethylhexadecahydro-1H-cyclopenta[*a*]phenanthren-17-yl)-2-phenyl-2-(((2,2,2-trichloroethoxy)carbonyl)amino)heptanoic acid (5zc)



Starting from **4zc** (153.4 mg, 0.20 mmol) according to the general procedure to provide **5zc** (dr: 90/10) as a white solid (chromatography on silica gel, eluent: EtOAc/*n*-hexane = 1/5 with 0.1% TFA, 63.0 mg, 41% yield) and with 90:10 dr as determined by HPLC analysis (column: Daicel Chiralpak ODR 250 x 4.6 mm, Particle size: 10 μ m, absorption: λ = 210 nm, mobile phase: CH₃CN/H₂O (0.1% TFA) =

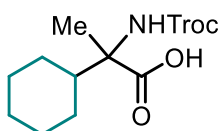
80:20, flow rate: 1.0 mL/min, column temperature: 25 °C, retention times: t_r (major) = 19.9 min, t_r (minor) = 16.1 min). $[\alpha]_D^{22} = 25.6^\circ$ ($c = 1.0$, MeOH). $^1\text{H NMR}$ (300 MHz, MeOD) δ 7.89 – 7.80 (m, 2H), 7.73 – 7.55 (m, 3H), 5.19 – 4.95 (m, 2H), 4.05 – 3.83 (m, 1H), 2.96 – 2.76 (m, 2H), 2.44 – 2.08 (m, 5H), 1.96 – 1.42 (m, 24H), 1.32 – 1.23 (m, 14H), 1.04 (s, 3H), 0.42 (s, 6H). $^{13}\text{C NMR}$ (75 MHz, MeOD) δ 173.98, 152.87, 140.66, 128.27, 127.61, 126.21, 96.25, 73.97, 73.08, 71.39, 65.53, 56.89, 56.40, 42.86, 42.55, 40.86, 40.55, 37.08, 36.22, 36.02, 35.88, 35.55, 34.63, 33.77, 31.10, 30.17, 28.35, 27.38, 26.67, 25.45, 25.32, 24.27, 22.98, 20.95, 20.54, 18.24, 18.00, 11.57, -5.35, -6.75. **IR (film)**: ν (cm^{-1}) 3398, 2929, 1716, 1491, 1250, 1107, 1010, 800, 696, 568 cm^{-1} . **HRMS (ESI, m/z)** calcd. for $[\text{C}_{14}\text{H}_{14}\text{Cl}_3\text{NO}_4\text{Na}]^+ [(M + \text{Na})^+]$: 387.9881, found: 387.9881.

(*E*)-2-Methyl-4-phenyl-2-(((2,2,2-trichloroethoxy)carbonyl)amino)but-3-enoic acid (5zd)



Starting from 2,2,2-trichloroethyl (*E*)-((2-methyl-4-phenylbut-3-enoyl)oxy)carbamate (73.0 mg, 0.20 mmol) according to the general procedure to provide **5zd** as a white solid (chromatography on silica gel, eluent: EtOAc/*n*-hexane = 1/5 with 0.1% TFA, 38.3 mg, 52% yield) and with 5% ee as determined by HPLC analysis (column: Daicel Chiralpak IG 250 x 4.6 mm, Particle size: 5 μm , absorption: $\lambda = 210$ nm, mobile phase: $\text{CH}_3\text{CN}/\text{H}_2\text{O}$ (0.1% TFA) = 45:55, flow rate: 1.0 mL/min, column temperature: 25 °C, retention times: t_r (major) = 15.7 min, t_r (minor) = 17.6 min). $^1\text{H NMR}$ (300 MHz, MeOD) δ 7.43 – 7.17 (m, 5H), 6.62 (s, 2H), 4.82 – 4.72 (m, 2H), 1.68 (s, 3H). $^{13}\text{C NMR}$ (75 MHz, MeOD) δ 175.14, 154.46, 137.12, 129.87, 128.77, 128.61, 127.96, 126.73, 96.34, 74.48, 60.61, 23.70. **IR (film)**: ν (cm^{-1}) 3397, 2961, 1710, 1493, 1267, 1107, 802, 720, 568 cm^{-1} . **HRMS (ESI, m/z)** calcd. for $[\text{C}_{14}\text{H}_{14}\text{Cl}_3\text{NO}_4\text{Na}]^+ [(M + \text{Na})^+]$: 387.9881, found: 387.9881.

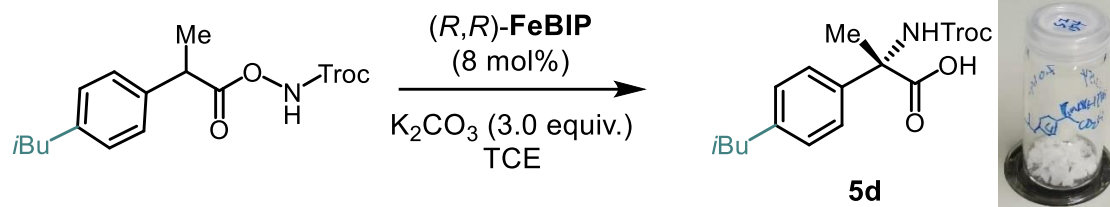
2-Cyclohexyl-2-(((2,2,2-trichloroethoxy)carbonyl)amino)propanoic acid (5ze)



Starting from 2,2,2-trichloroethyl ((2-cyclohexylpropanoyl)oxy)carbamate (69.0 mg, 0.20 mmol) according to the general procedure to provide **5ze** as a white solid (chromatography on silica gel, eluent: EtOAc/*n*-hexane = 1/5 with 0.1% TFA, 29.0 mg, 42% yield) and with 10% ee as determined by HPLC analysis (column: Daicel Chiralpak IG 250 x 4.6 mm, Particle size: 5 μ m, absorption: λ = 210 nm, mobile phase: CH₃CN/H₂O (0.1% TFA) = 50:50, flow rate: 1.0 mL/min, column temperature: 25 °C, retention times: t_r (major) = 16.2 min, t_r (minor) = 21.7 min). **¹H NMR** (300 MHz, MeOD) δ 4.80 (d, J = 12.0 Hz, 1H), 4.72 (d, J = 12.0 Hz, 1H), 1.90 – 1.60 (m, 6H), 1.49 (s, 3H), 1.39 – 1.03 (m, 5H). **¹³C NMR** (75 MHz, MeOD) δ 175.92, 154.65, 96.32, 74.36, 63.27, 44.51, 27.95, 27.56, 26.80, 26.77, 26.52, 18.38. **IR (film)**: ν (cm⁻¹) 2929, 1706, 1403, 1275, 1102, 729, 570 cm⁻¹. **HRMS (ESI, *m/z*)** calcd. for [C₁₂H₁₈Cl₃NO₄Na]⁺ [(M + Na)⁺]: 368.0194, found: 368.0194.

4.4.5 Large-Scale Reactions and Mechanistic Study

4.4.5.1 Large-Scale Synthesis of (S)-5d, (S)-5n and (S)-5q



Procedure: To a 100 mL round bottom Schlenk flask was added 2,2,2-trichloroethyl ((2-(4-isobutylphenyl)propanoyl)oxy)carbamate (395.0 mg, 1.0 mmol, 1.0 equiv.), K₂CO₃ (414.0 mg, 3.0 mmol, 3.0 equiv.) and (R,R)-FeBIP (44 mg, 0.08 mmol). The tube was evacuated and backfilled with N₂ for three times. 1,1,2,2-tetrachloroethane (10 mL) was added and the mixture was degassed via freeze-pump-thaw for two times. The tube was sealed, and the reaction mixture was stirred at 0 °C for 40 hours. To quench the reaction, water (10 mL) and hydrochloric acid (4N) (2.5 mL) were added. The mixture was extracted with EtOAc (5 mL) for three times and the combined organic layer was dried over anhydrous sodium sulfate. After filtration, the solvent was evaporated under reduced pressure, and the residue was purified by column chromatography on silica gel using eluent: EtOAc/*n*-hexane = 1/5 with 0.1% TFA and provided **5d** as a white solid (343.0 mg, 87% yield).

Recrystallization: The white solid **5d** was dissolved in 0.15 mL EtOAc at 70 °C. Then, *n*-hexane (3 mL) was added. The temperature was cooled down to room temperature, the 10 ml round flask bottle sealed with a cap and placed in a freezer (-20 °C) overnight. Afterwards, the solvent was removed with a syringe and the left crystals were washed twice with *n*-hexane (2 x 2 mL) to finally obtain white crystals. The recrystallization step was repeated once which provided colorless crystals (209.0 mg, 61% yield). The enantiomeric ratio was determined by HPLC analysis as 99% ee.

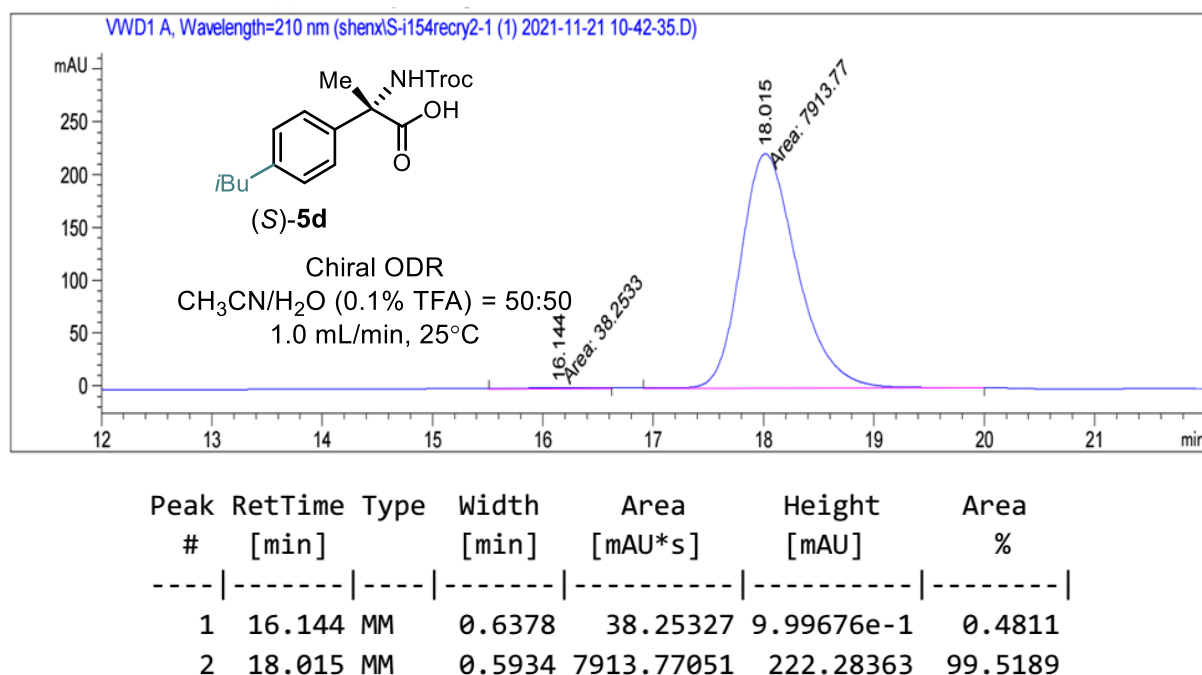
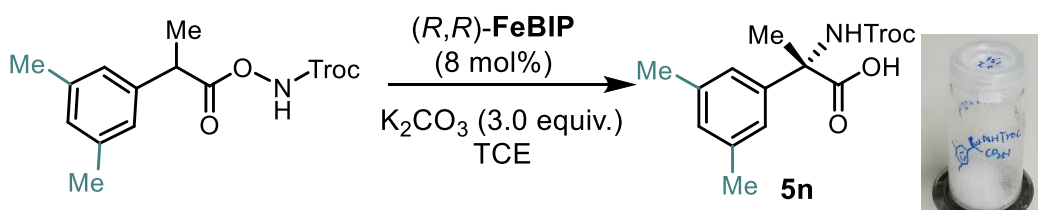


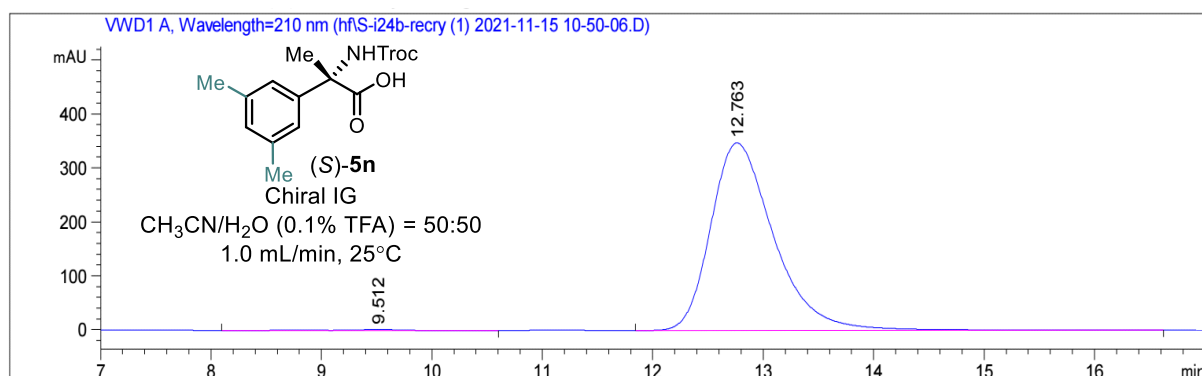
Figure 48. HPLC trace of isolated (*S*)-**5d** from large-scale reaction.



Procedure: To a 100 mL round bottom Schlenk flask was added 2,2,2-trichloroethyl ((2-(3,5-dimethylphenyl)propanoyl)oxy)carbamate (367.0 mg, 1.0 mmol, 1.0 equiv.), K₂CO₃ (414 mg, 0.6 mmol, 3.0 equiv.) and (*R,R*)-**FeBIP** (44.0 mg, 0.08 mmol). The tube was evacuated and backfilled with N₂ for three times. 1,1,2,2-tetrachloroethane (10 mL) was added and the mixture was degassed via freeze-pump-thaw for two times. The tube was sealed and the reaction mixture was stirred at 0 °C for 40 hours. To quench the reaction, water (10 mL) and hydrochloric acid (4N) (2.5 mL) were added.

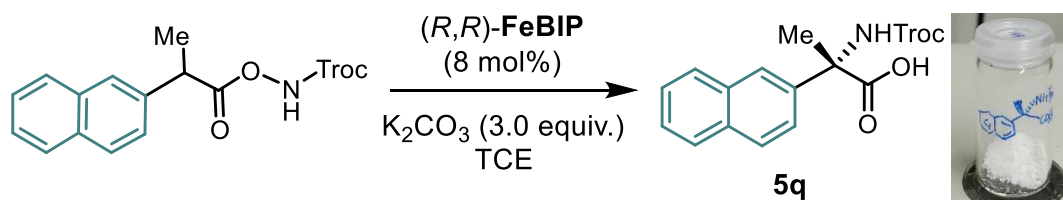
The mixture was extracted with EtOAc (5 mL) for three times and the combined organic layer was dried over anhydrous sodium sulfate. After filtration, the solvent was evaporated under reduced pressure, and the residue was purified by column chromatography on silica gel using eluent: EtOAc/*n*-hexane = 1/5 with 0.1% TFA and provided **5n** as a white solid (345.0 mg, 94% yield).

Recrystallization: The white solid **5n** was dissolved in 0.10 mL EtOAc at 70 °C. Then, *n*-hexane (2.5 mL) was added. The temperature was cooled down to room temperature, the 10 ml round flask bottle sealed with a cap and placed in a freezer (-20 °C). After overnight, to aspirate the solvent with a syringe, and then wash the left crystals twice with *n*-hexane (2 x 1.5 mL), and finally obtained white crystals. The recrystallization step was repeated once which provided colorless crystals (245.0 mg, 67% yield). The enantiomeric ratio was determined by HPLC analysis as 99% ee.



Peak #	RetTime [min]	Type	Width [min]	Area [mAU*s]	Height [mAU]	Area %
1	9.512	VB R	0.3382	47.79940	2.07855	0.3439
2	12.763	BV R	0.6040	1.38505e4	347.30237	99.6561

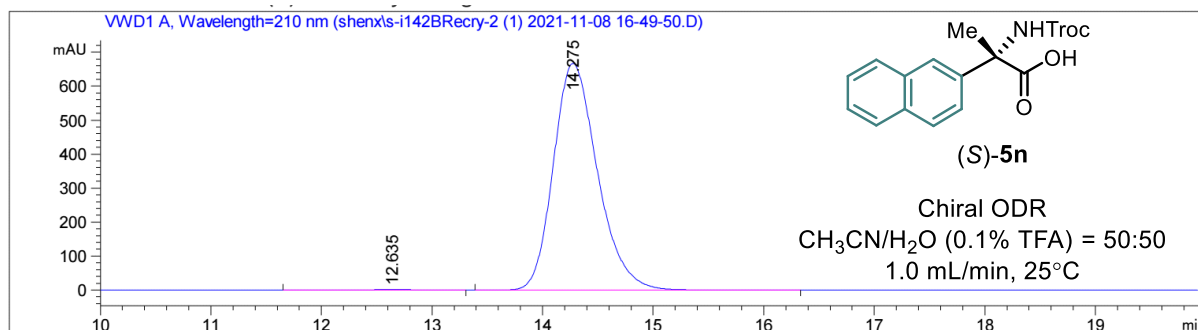
Figure 49. HPLC trace of isolated (*S*)-**5n** from large-scale reaction.



Procedure: To a 100 mL round bottom Schlenk flask was added 2,2,2-trichloroethyl ((2-(naphthalen-2-yl)propanoyl)oxy)carbamate (389.0 mg, 1 mmol, 1.0 equiv.), K₂CO₃(414.0 mg, 0.6

mmol, 3.0 equiv.) and (*R,R*)-**FeBIP** (44 mg, 0.08 mmol). The tube was evacuated and backfilled with N₂ for three times. 1,1,2,2-tetrachloroethane (10 mL) was added and the mixture was degassed via freeze-pump-thaw for two times. The tube was sealed and the reaction mixture was stirred at 0 °C for 40 hours. To quench the reaction, water (10 mL) and hydrochloric acid (4N) (2.5 mL) were added. The mixture was extracted with EtOAc (5 mL) for three times and the combined organic layer was dried over anhydrous sodium sulfate. After filtration, the solvent was evaporated under reduced pressure and the residue was purified by column chromatography on silica gel using eluent: EtOAc/*n*-hexane = 1/5 with 0.1% TFA. Compound **5q** was provided as a white solid (342.3 mg, 88% yield).

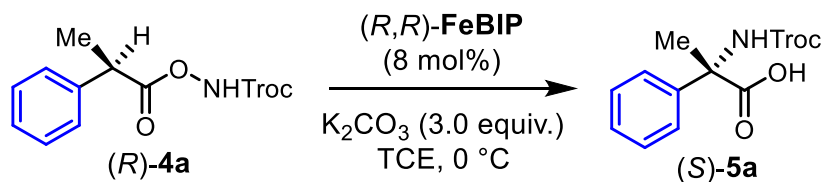
Recrystallization: The white solid **5q** was dissolved in 0.20 mL EtOAc at 70 °C. Then, *n*-hexane (3.0 mL) was added. The temperature was cooled down to room temperature, the 10 ml round flask bottle sealed with a cap and placed in a freezer (-20 °C). After overnight, to aspirate the solvent with a syringe, and then wash the left crystals twice with *n*-hexane (2 x 2.5 mL), and finally obtained white crystals. The recrystallization step was repeated once which provided colorless crystals (250.0 mg, 73% yield). The enantiomeric ratio was determined by HPLC analysis as 99% ee.



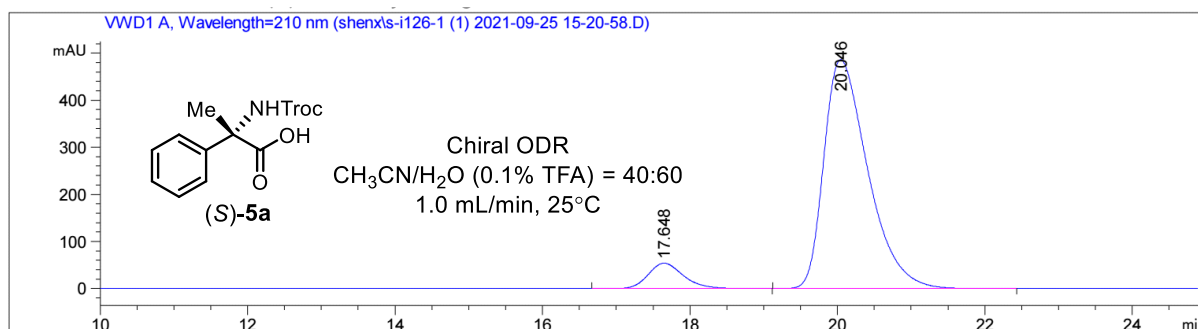
Peak #	RetTime [min]	Type	Width [min]	Area [mAU*s]	Height [mAU]	Area %
1	12.635	BB	0.3619	41.79725	1.73910	0.2255
2	14.275	BB	0.4288	1.84959e4	666.16901	99.7745

Figure 50. HPLC trace of isolated (*S*)-**5q** from large-scale reaction.

4.4.5.2 Catalytic Reactions with Enantiomerically Pure Substrates

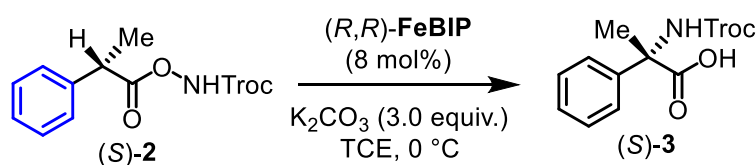


Procedure: To a 10 mL round bottom Schlenk flask was added (*R*)-**4a** (67.8 mg, 0.2 mmol, 1.0 equiv.), K_2CO_3 (82.8 mg, 0.6 mmol, 3.0 equiv.) and (*R,R*)-**FeBIP** (8.8 mg, 0.016 mmol). The tube was evacuated and backfilled with N_2 for three times. 1,1,2,2-tetrachloroethane (2 mL) was added and the mixture was degassed via freeze-pump-thaw for two times. The tube was sealed, and the reaction mixture was stirred at 0 °C for 40 hours. To quench the reaction, water (2 mL) and hydrochloric acid (4N) (0.5 mL) were added. The mixture was extracted with EtOAc (3 mL) for three times and the combined organic layer was dried over anhydrous sodium sulfate. After filtration, the solvent was evaporated under reduced pressure, and the residue was purified by column chromatography on silica gel using eluent: EtOAc/*n*-hexane = 1/5 with 0.1% TFA. Compound **5a** was provided as a white solid (53.0 mg, 78% yield). Enantiomeric ratio was determined by HPLC analysis as 84% ee.



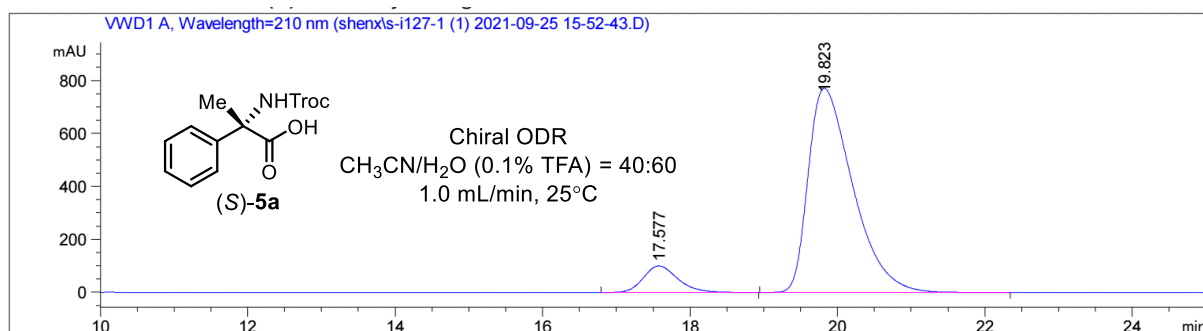
Peak #	RetTime [min]	Type	Width [min]	Area [mAU*s]	Height [mAU]	Area %
1	17.648	BB	0.5159	1788.91699	53.82471	8.1682
2	20.046	BB	0.6345	2.01120e4	485.72891	91.8318

Figure 51. HPLC trace of isolated (*S*)-**5a** from conversion of enantiomerically pure (*R*)-**4a**.



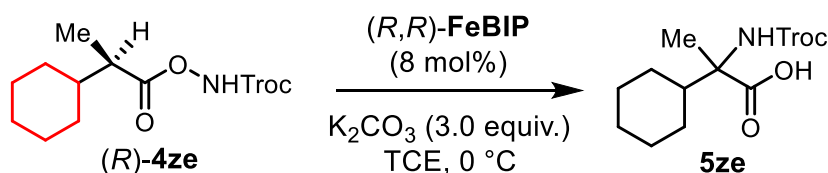
Procedure: To a 10 mL round bottom Schlenk flask was added (*S*)-**4a** (67.8 mg, 0.2 mmol, 1.0 equiv.), K_2CO_3 (82.8 mg, 0.6 mmol, 3.0 equiv.) and (*R,R*)-**FeBIP** (8.8 mg, 0.016 mmol). The tube was evacuated and backfilled with N_2 for three times. 1,1,2,2-tetrachloroethane (2 mL) was added, and the

mixture was degassed via freeze-pump-thaw for two times. The tube was sealed and the reaction mixture was stirred at 0 °C for 40 hours. To quench the reaction, water (2 mL) and hydrochloric acid (4N) (0.5 mL) were added. The mixture was extracted with EtOAc (3 mL) for three times and the combined organic layer was dried over anhydrous sodium sulfate. After filtration, the solvent was evaporated under reduced pressure, and the residue was purified by column chromatography on silica gel using eluent: EtOAc/*n*-hexane = 1/5 with 0.1% TFA. Compound **5a** was provided as a white solid (55.0 mg, 81% yield). Enantiomeric ratio was determined by HPLC analysis as 82% ee.



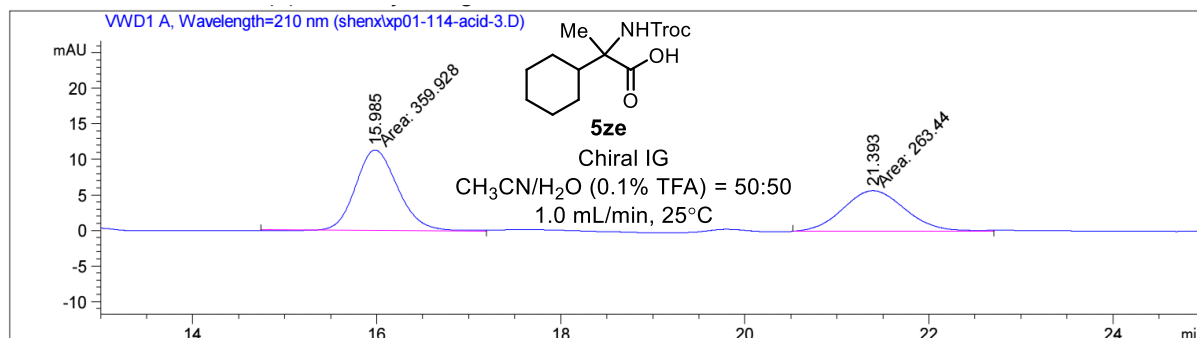
Peak #	RetTime [min]	Type	Width [min]	Area [mAU*s]	Height [mAU]	Area %
1	17.577	BB	0.4950	3244.53174	100.00965	9.0898
2	19.823	BB	0.6542	3.24497e4	770.82819	90.9102

Figure 52. HPLC trace of isolated (*S*)-**4a** from conversion of enantiomerically pure (*S*)-**5a**.



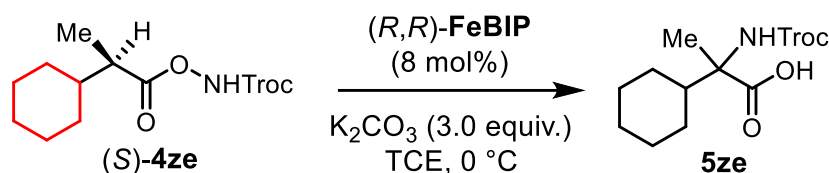
Procedure: To a 10 mL round bottom Schlenk flask was added (*R*)-**4ze** (69 mg, 0.2 mmol, 1.0 equiv.), K_2CO_3 (82.8 mg, 0.6 mmol, 3.0 equiv.) and (*R,R*)-**FeBIP** (8.8 mg, 0.016 mmol). The tube was evacuated and backfilled with N_2 for three times. 1,1,2,2-tetrachloroethane (2 mL) was added, and the mixture was degassed via freeze-pump-thaw for two times. The tube was sealed, and the reaction mixture was stirred at 0 °C for 40 hours. To quench the reaction, water (2 mL) and hydrochloric acid (4N) (0.5 mL) was added. The mixture was extracted with EtOAc (3 mL) for three times and the combined organic layer was dried over anhydrous sodium sulfate. After filtration, the solvent was

evaporated under reduced pressure, and the residue was purified by column chromatography on silica gel using eluent: EtOAc/*n*-hexane = 1/5 with 0.1% TFA. Compound **5ze** was provided as a white solid (34.0 mg, 49% yield). Enantiomeric ratio was determined by HPLC analysis as 16% ee.

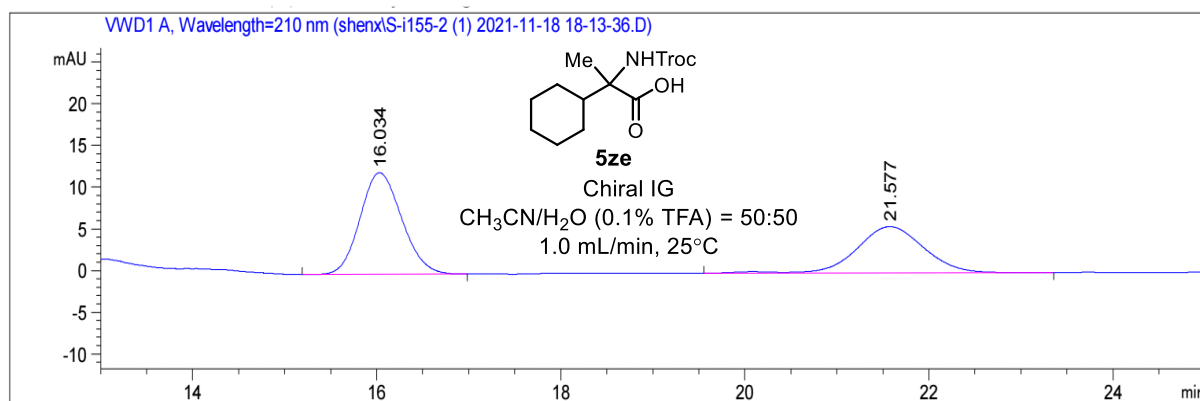


Peak #	RetTime [min]	Type	Width [min]	Area [mAU*s]	Height [mAU]	Area %
1	15.985	MM	0.5297	359.92841	11.32414	57.7393
2	21.393	MM	0.7735	263.44009	5.67658	42.2607

Figure 53. HPLC trace of isolated **5ze** from conversion of enantiomerically pure (*R*)-**4ze**.



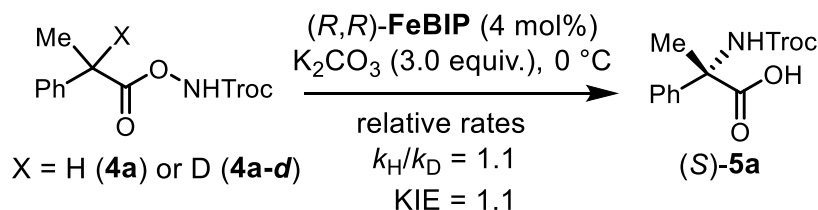
Procedure: To a 10 mL round bottom Schlenk flask was added (*S*)-**4ze** (69 mg, 0.2 mmol, 1.0 equiv.), K_2CO_3 (82.8 mg, 0.6 mmol, 3.0 equiv.) and (*R,R*)-**FeBIP** (8.8 mg, 0.016 mmol). The tube was evacuated and backfilled with N_2 for three times. 1,1,2,2-tetrachloroethane (2 mL) was added and the mixture was degassed via freeze-pump-thaw for two times. The tube was sealed and the reaction mixture was stirred at 0 °C for 40 hours. To quench the reaction, water (2 mL) and hydrochloric acid (4N) (0.5 mL) were added. The mixture was extracted with EtOAc (3 mL) for three times and the combined organic layer was dried over anhydrous sodium sulfate. After filtration, the solvent was evaporated under reduced pressure, and the residue was purified by column chromatography on silica gel using eluent: EtOAc/*n*-hexane = 1/5 with 0.1% TFA. Compound **5ze** was provided as a white solid (33.1 mg, 48% yield). Enantiomeric ratio was determined by HPLC analysis as 15% ee.



Peak #	RetTime [min]	Type	Width [min]	Area [mAU*s]	Height [mAU]	Area %
1	16.034	BB	0.4965	384.22696	12.16755	57.6239
2	21.577	VB R	0.7810	282.55725	5.54399	42.3761

Figure 54. HPLC trace of isolated **5ze** from conversion of enantiomerically pure (*S*)-**4ze**.

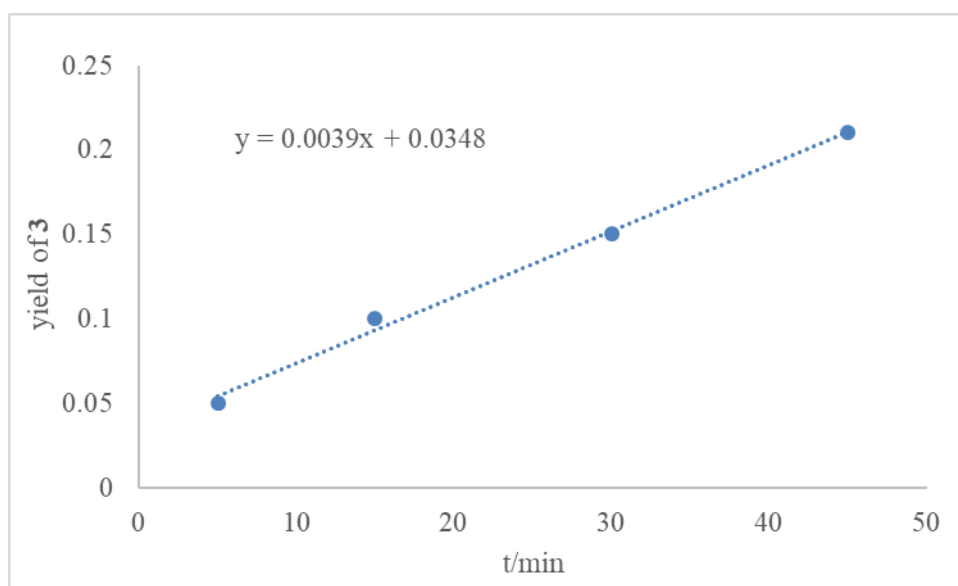
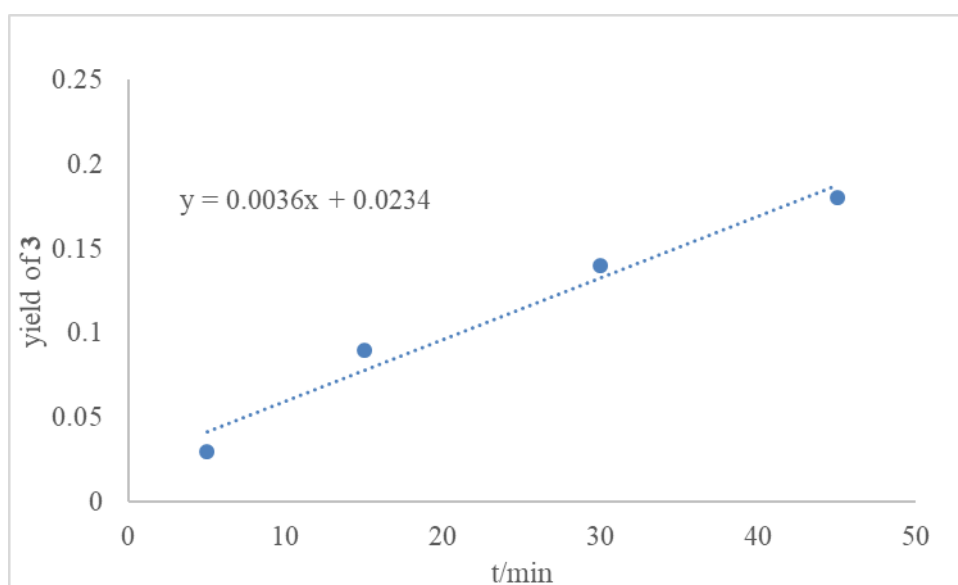
4.4.5.3 Kinetic Isotope Effects



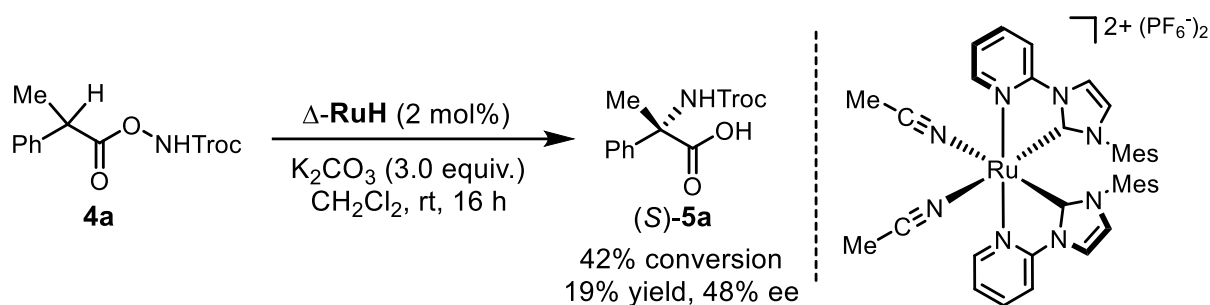
Procedure: Under argon atmosphere, four oven-dried resealable Schlenk tubes equipped with a magnetic stir bar were charged with **4a** (68.0mg, 0.20 mmol, 1.0 equiv.) or **4a-d** (68.0 mg, 0.20 mmol, 1.0 equiv.), (*R,R*)-**FeBIP** (8.8 mg, 0.016mmol, 8 mol%), K_2CO_3 (82.8 mg, 0.60 mmol, 3.0 equiv.) and 1,1,2,2-tetrachloroethane (2 mL). The mixture was degassed via two freeze-pump-thaw cycles. The resulting mixture was stirred at 0 °C. The reaction progress was monitored by ^1H NMR analysis to determine the yields of product **5a**. At specific time intervals (5, 15, 30, 40 min), 2 mL of the reaction mixture was taken out via syringe, acidified with HCl (4N), then extracted with EtOAc for 3 times, and then the solvent was removed. The residue was dissolved in 5 mL EtOAc/TFA (9/1) and filtered through a short pad of silica gel. The filtrate was concentrated under reduced pressure, and the residue was analyzed with ^1H NMR in methanol- d_4 using PhMe as the internal standard. The reaction rate constants were determined by plotting yield of the corresponding product over time (h) and extracting the slope after linear fitting. Finally, the KIE value was determined to be 1.1.

Table 4. Yields of product **5a** monitored at specific time intervals during reaction

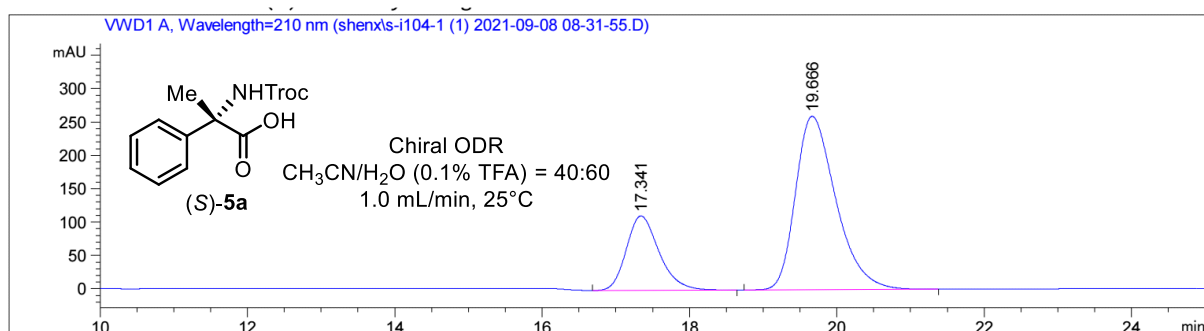
Time (min)	Yield of 5a (reaction of 4a)	Yield of 5a (reaction of 4a-d)
5	5%	3%
15	10%	9%
30	15%	14%
45	21%	18%

**Figure 55.** Plot of yield versus reaction time for substrate **4a**.**Figure 56.** Plot of yield versus reaction time for substrate **4a-d**.

4.4.5.4 Comparison with Ru-Catalyzed 1,3-Nitrogen Migration



Procedure: To a 10 mL round bottom Schlenk flask was added **4a** (67.8 mg, 0.2 mmol, 1.0 equiv.), K_2CO_3 (82.8 mg, 0.6 mmol, 3.0 equiv.) and Δ -**RuH** (3.5 mg, 0.004 mmol). The tube was evacuated and backfilled with N_2 for three times. Dichloromethane (2 mL) was added, and the mixture was degassed via freeze-pump-thaw for two times. The tube was sealed, and the reaction mixture was stirred at room temperature for 16 hours. To quench the reaction, water (2 mL) and hydrochloric acid (4N) (0.5 mL) were added. The mixture was extracted with EtOAc (3 mL) for three times and the combined organic layer was dried over anhydrous sodium sulfate. After filtration, the solvent was evaporated under reduced pressure, and the residue was purified by column chromatography on silica gel using eluent: EtOAc/*n*-hexane = 1/5 with 0.1% TFA. Compound **5a** was provided as a white solid (12.8 mg, 19% yield). Enantiomeric ratio was determined by HPLC analysis as 48% ee.



Peak #	RetTime [min]	Type	Width [min]	Area [mAU*s]	Height [mAU]	Area %
1	17.341	BB	0.4769	3440.06543	111.34277	25.7869
2	19.666	BB	0.5844	9900.28418	259.77374	74.2131

Figure 57. HPLC trace of isolated **5a** from conversion of **4a** with Δ -RuH.

4.4.6 Single Crystal X-Ray Analysis of Compound (*S*)-**5q**

Crystallography of compound (*S*)-5q**:** Single crystals of **5q** were obtained by slow diffusion from the solution in EtOAc layered with hexane at room temperature. Data collection and analysis was performed by Dr. Ivlev (Department of Chemistry). A suitable crystal of $C_{16}H_{14}Cl_3NO_4$ was selected under inert oil and mounted using a MiTeGen loop. Intensity data of the crystal were recorded with a D8 Quest diffractometer (Bruker AXS). The instrument was operated with Mo-K α radiation (0.71073 Å, microfocus source) and equipped with a PHOTON III C14 detector. Evaluation, integration and reduction of the diffraction data was carried out using the Bruker APEX 3 software suite.¹³ Multi-scan and numerical absorption corrections were applied using the SADABS program.^{14,15} The structure was solved using dual-space methods (SHELXT-2018/2) and refined against F^2 (SHELXL-2018/3 using ShelXle interface).¹⁶⁻¹⁸ All non-hydrogen atoms were refined with anisotropic displacement parameters. The hydrogen atoms were refined using the “riding model” approach with isotropic displacement parameters 1.2 times (1.5 times for terminal methyl groups) of that of the preceding carbon atom. CCDC 2126461 contains the supplementary crystallographic data for this paper. These data can be obtained free of charge from The Cambridge Crystallographic Data Centre via www.ccdc.cam.ac.uk/structures.

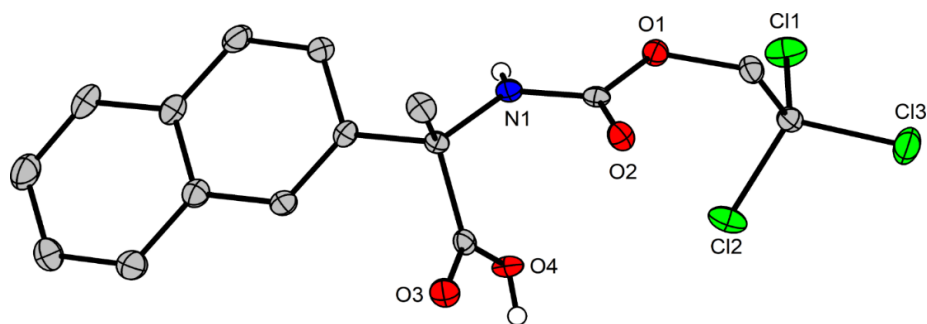


Figure 58. X-ray crystallography. Crystal structure of the deracemized compound (*S*)-**5q**. The disordered fluorine atom is shown on the position with its major probability. Displacement ellipsoids are shown at 50% probability level at 100 K. The hydrogen atoms are shown with arbitrary radii.

Table 5. Selected crystallographic data and details of the structure determination for C₁₆H₁₄Cl₃NO₄.

Identification code	SH134P
Empirical formula	C ₁₆ H ₁₄ Cl ₃ NO ₄
Molar mass / g·mol⁻¹	390.63
Space group (No.)	P2 ₁ 2 ₁ 2 ₁ (19)
<i>a</i> / Å	6.0078(3)
<i>b</i> / Å	9.8875(5)
<i>c</i> / Å	28.3336(17)
<i>V</i> / Å³	1683.08(16)
<i>Z</i>	4
$\rho_{calc.}$ / g·cm⁻³	1.542
μ / mm⁻¹	0.565
Color	colorless
Crystal habitus	needle
Crystal size / mm³	0.354 x 0.058 x 0.053
<i>T</i> / K	100
λ / Å	0.71073 (Mo-K α)
θ range / °	2.182 to 28.312
Range of Miller indices	-8 ≤ <i>h</i> ≤ 8 -13 ≤ <i>k</i> ≤ 13 -37 ≤ <i>l</i> ≤ 37
Absorption correction	multi-scan and numerical
<i>T</i>_{min}, <i>T</i>_{max}	0.8745, 0.9712
<i>R</i>_{int}, <i>R</i>_{σ}	0.0466, 0.0232
Completeness of the data set	0.999
No. of measured reflections	43957
No. of independent reflections	4176
No. of parameters	223
No. of restraints	0
<i>S</i> (all data)	1.093
<i>R</i>(<i>F</i>) (<i>I</i> ≥ 2σ(<i>I</i>), all data)	0.0271, 0.0282
<i>wR</i>(<i>F</i>²) (<i>I</i> ≥ 2σ(<i>I</i>), all data)	0.0616, 0.0620
Extinction coefficient	not refined
Flack parameter <i>x</i>	-0.006(18)
$\Delta\rho_{max}$, $\Delta\rho_{min}$ / e·Å⁻³	0.329, -0.186

Reference

1. M. Das, Y. Du, J. S. Mortensen, H. E. Bae, B. Byrne, C. J. Loland, B. K. Kobilka, P. S. Chae, *Chem. Eur. J.* **2018**, *24*, 9860.
2. Z. Z. Zhang, Y. Q. Han, B. B. Zhan, S. Wang, B. F. Shi, *Angew. Chem. Int. Ed.* **2017**, *56*, 13145.
3. T. Muller, L. Johann, B. Jannack, M. Bruckner, D. A. Lanfranchi, H. Bauer, C. Sanchez, V. Yardley, C. Deregnaucourt, J. Schrevel, M. Lanzer, R. H. Schirmer, E. Davioud-Charvet, *J. Am. Chem. Soc.* **2011**, *133*, 11557.
4. Z. T. He, J. F. Hartwig, *J. Am. Chem. Soc.* **2019**, *141*, 11749.
5. J. J. Cui, H. Shen, M. Tran-Dube, M. Nambu, M. McTigue, N. Grodsky, K. Ryan, S. Yamazaki, S. Aguirre, M. Parker, Q. Li, H. Zou, J. Christensen, *J. Med. Chem.* **2013**, *56*, 6651.
6. F. Wang, Y. Nishimoto, M. Yasuda, *J. Am. Chem. Soc.* **2021**, *143*, 20616.
7. K. Wang, Y. Li, X. Li, D. Li, H. Bao, *Org. Lett.* **2021**, *23*, 8847.
8. J. Charton, S. Girault-Mizzi, M. A. Debreu-Fontaine, F. Foufelle, I. Hainault, J. G. Bizot-Espiard, D. H. Caignard, C. Sergheraert, *Bioorg. Med. Chem.* **2006**, *14*, 4490.
9. H. Trabulsi, G. Rousseau, *Synth. Commun.* **2011**, *41*, 2123.
10. Y. Aihara, N. Chatani, *J. Am. Chem. Soc.* **2014**, *136*, 898.
11. X. Feng, C. Sippel, A. Bracher, F. Hausch, *J. Med. Chem.* **2015**, *58*, 7796.
12. C.-X. Ye, X. Shen, S.-M. Chen, E. Meggers, *Nat. Chem.* **2022** accepted for publication.
13. *APEX3*, Bruker AXS Inc., Madison, Wisconsin, USA, **2018**.
14. *SADABS*, Bruker AXS Inc., Madison, Wisconsin, USA, **2016**.
15. L. Krause, R. Herbst-Irmer, G. M. Sheldrick, D. Stalke, *J. Appl. Crystallogr.* **2015**, *48*, 3.
16. G. M. Sheldrick, *Acta Crystallogr., Sect. A: Found. Adv.* **2015**, *71*, 3.
17. G. M. Sheldrick, *Acta Crystallogr., Sect. C: Struct. Chem.* **2015**, *71*, 3.
18. C. B. Hübschle, G. M. Sheldrick, B. Dittrich, *J. Appl. Crystallogr.* **2011**, *44*, 1281.

Chapter 5: Appendices

5.1 List of Abbreviations

^1H NMR	proton nuclear magnetic resonance spectroscopy
^{13}C NMR	carbon nuclear magnetic resonance spectroscopy
^9F NMR	fluorine nuclear magnetic resonance spectroscopy
δ	chemical shift
J	coupling constant
br	broad
s	singlet
d	doublet
t	triplet
q	quartet
m	multiplet
ppm	parts per million
AcOH	acetic acid
aq	aqueous
Ar	Aryl-group
$\text{CH}_2\text{Cl}_2/\text{DCM}$	dichloromethane
CD_2Cl_2	dideuteromethylenechloride
CHCl_3	chloroform
CDCl_3	deuteriochloroform
MeOD	deuteromethanol
$\text{CH}_3\text{CN}/\text{MeCN}$	acetonitrile
conc	concentrated
DMAP	4-dimethylaminopyridine
DMF	dimethylformamide
DMSO	dimethyl sulfoxide
DCE	1,2-dichloroethane
TCE	1,1,2,2-tetrachloroethane

Statement

dr	diastereomeric ratio
ee	enantiomeric excesses
et al.	et alii (lat.: and others)
EtOH	ethanol
Et ₂ O	diethyl ether
Et ₃ N	triethyl amine
EtOAc	ethyl acetate
EDG	electron donating group
EWG	electron withdrawing group
HAT	hydrogen atom transfer
HAA	hydrogen atom abstraction
h	hour(s)
HPLC	high performance liquid chromatography
HRMS	high resolution mass spectrometry
IR spectra	infrared spectra
Ir	iridium
Rh	rhodium
Ru	ruthenium
Fe	iron
Ag	silver
Mn	manganese
L	liter(s)
M	mol/liter
<i>m</i>	meta-
min	minute(s)
mL	milliliter(s)
mmol	millimole
MS	mass spectroscopy
N ₂	nitrogen
Ph	phenyl

Statement

ppm	parts per million
<i>rac</i>	racemate
rt	room temperature
RR	radical rebound
TFA	trifluoroacetic acid
THF	tetrahydrofuran
TLC	thin layer chromatography
TBAB	Tetrabutylammonium bromide

5.2 List of Figures

Figure 1. Construction of C-N bonds by enantioselective azidation and amination.	2
Figure 2. The development of N4 iron complexes.	2
Figure 3. Prosthetic of cysteinato-heme enzymes and two possible reaction pathways in hydroxylation reactions catalyzed by P450 enzymes.	3
Figure 4. Aliphatic hydroxylation catalyzed by Iron (III) porphyrin.....	4
Figure 5. Aliphatic C–H hydroxylation and the epoxidation of terminal olefins catalyzed by N4 Fe complexes.....	5
Figure 6. Useful aliphatic C–H oxidation reaction catalyzed by N4 Iron complex 4 and 5	6
Figure 7. Asymmetric epoxidation with H ₂ O ₂ by manipulating the electronic properties of non-heme Iron catalysts.	7
Figure 8. The epoxidation of double bonds catalyzed by N4 iron catalysts.	8
Figure 9. The asymmetric epoxidation of cyclic enones and cyclohexene ketones catalyzed by N4 iron catalysts.	9
Figure 10. The synthesis of oxoiron(V) complexes.....	10
Figure 11. Different N4 iron complexes catalysis.	11
Figure 12. <i>cis</i> -dihydroxylation of olefins catalyzed by N4 iron complex 46	12
Figure 13. Highly enantioselective epoxidation of olefins catalyzed by N4 complex 50	13
Figure 14. Alkylation of indoles, pyrroles and N,N-disubstituted anilines catalyzed by N4 Iron complex 53	14
Figure 15. Azidation and amination catalyzed by iron complexes or iron-containing cytochromes P450.	15
Figure 16. A simplified mechanism of transition-metal-mediated C=C aziridination or C-H amination or through nitrene transfer.	16
Figure 17. Enantioselective C-N coupling reaction between β -ketoesters and oxindoles catalyzed by Fe complex.....	17
Figure 18. Iron-catalysed asymmetric carboazidation of styrenes.	18
Figure 19. Iron-catalyzed radical asymmetric aminoazidation and diazidation of styrenes.....	19
Figure 20. Iron-catalyzed enantioselective radical carboazidation and diazidation of α,β -Unsaturated Carbonyl Compounds.....	20

Figure 21. Iron(II)-catalyzed asymmetric intramolecular aminohydroxylation of indoles.	21
Figure 22. Enantioselective intermolecular aminooxygenation and aminofluorination of indene.	22
Figure 23. Iron-heme enzyme-catalyzed asymmetric aziridination.	22
Figure 24. Iron-heme enzyme-catalyzed asymmetric aminohydroxylation.	23
Figure 25. Iron-heme enzyme-catalyzed intermolecular benzylic C–H amidation.	24
Figure 26. Iron-heme enzyme-catalyzed asymmetric amidation of primary, secondary, and tertiary C(sp ³)-H bonds.	25
Figure 27. Iron-heme enzyme-catalyzed asymmetric amination of benzylic and allylic C(sp ³)-H bonds.	26
Figure 28. Biocatalytic, intermolecular C-H bond amination for enantioenriched amides.	26
Figure 29. Iron-catalyzed C-H bond asymmetric amination.	27
Figure 30. New N4 iron complexes design.	28
Figure 31. Proposal for N4 iron nitrene intermediates.	32
Figure 32. The synthesis of N4 iron complexes.	33
Figure 33. Synthesis of N4 iron chloride complexes.	34
Figure 34. Synthesis of (<i>R,R</i>)- FeBIP	35
Figure 35. Crystal structure of (<i>R,R</i>)- FeBIP	35
Figure 36. Previous reports and this design for asymmetric amination by N4 iron catalysis.	38
Figure 37. Reaction conditions: reactions were carried out with (<i>R,R</i>)- FeBIP (8-15 mol%), K ₂ CO ₃ (3 equiv.) and 1,1,2,2-tetrachloroethane (TCE, 0.1 M) at 0 °C for 40 h. Enantiomeric excess (ee) values were determined by HPLC analysis (see Supplementary Information section 5 for full details). ^a Isolated after conversion to the methyl ester. ^b Reaction performed at room temperature (25 °C) for 16 h.	42
Figure 38. Proposed mechanism.	43
Figure 39. Design of catalytic enantioconvergent tertiary C (sp ³)-H functionalization. An Organometallic C–H activation and metal-carbenoid/nitrenoid concerted C–H insertion lead to stereospecific functionalization. B, Coupled HAA and radical rebound for metal-oxo-mediated C–H functionalization and stepwise metal-carbenoid/ nitrenoid C–H insertion tend to result in partial or complete chirality retention due to the commonly fast radical rebound. C, Reported C–H functionalization catalysed by a transition metal is amenable only to kinetic resolution, but not yet to enantioconvergent transformations, due to the chirality retention problem.	46

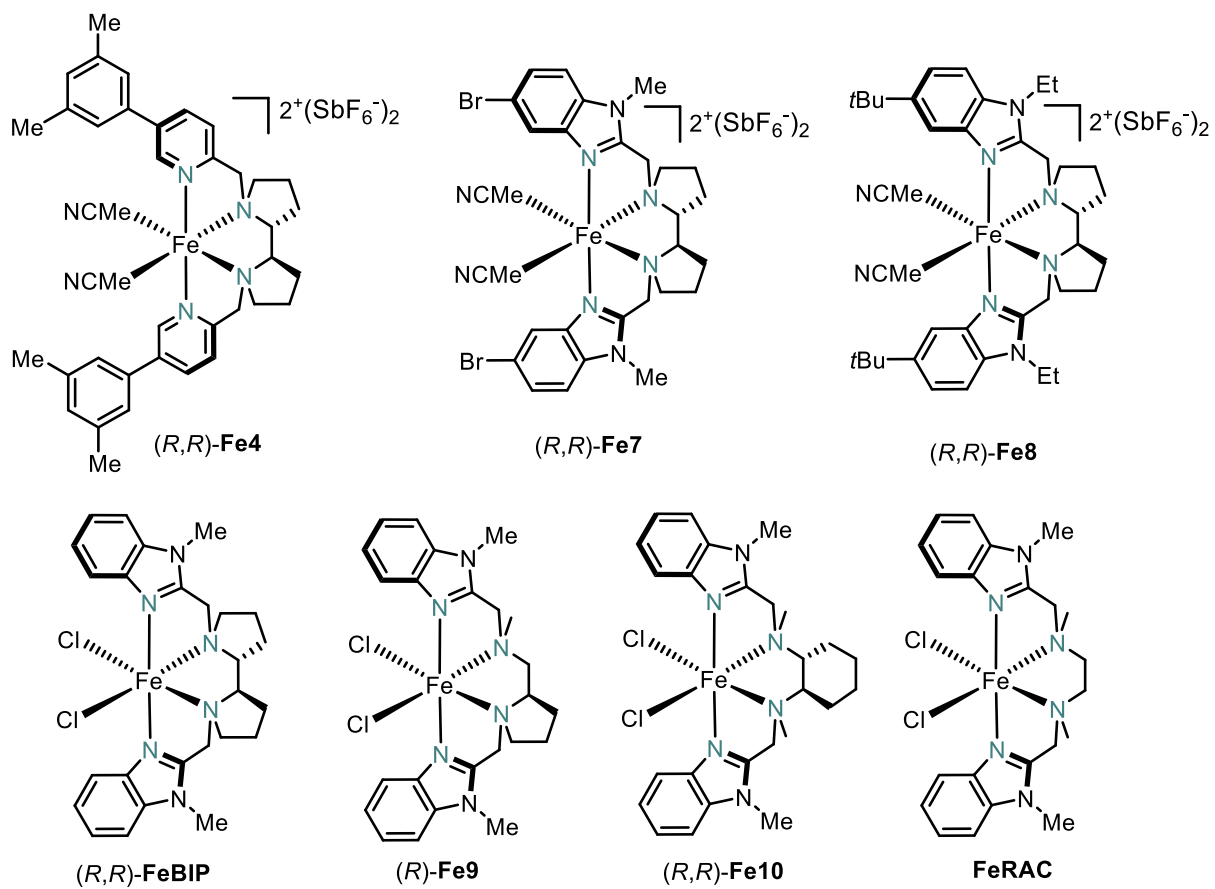
Figure 40. Iron-catalyzed enantioconvergent synthesis of α,α -disubstituted α -amino acids by 1,3-nitrogen migration.....	47
Figure 41. Substrate scope. Standard conditions: Racemic substrates (0.20 mmol), catalyst (8.0 mol%) and K_2CO_3 (0.6 mmol) in 1,1,2,2-tetrachloroethane (2.0 ml) under argon at 0 °C for 40 h. Isolated yields are shown. ^a Increased scale with 1.0 mmol of the substrate.....	51
Figure 42. Additional experiments.	53
Figure 43. Proposed mechanism.....	54
Figure 44. An overview of the key results of this thesis.....	57
Figure 45. Asymmetric amination of secondary C-H bonds catalyzed by chiral N4 iron catalysts.	58
Figure 46. Enantioconvergent tertiary C-H bonds amination catalyzed by chiral N4 iron catalysts.....	59
Figure 47. Crystal structure of (<i>R,R</i>)- FeBIP . Only one symmetry-independent molecule is shown. Only the hydrogen atoms at the stereocenters are shown. Displacement ellipsoids are shown at 50 % probability level at 100 K. The hydrogen atoms are shown with arbitrary radii.....	77
Figure 48. HPLC trace of isolated (<i>S</i>)- 5d from large-scale reaction.	139
Figure 49. HPLC trace of isolated (<i>S</i>)- 5n from large-scale reaction.	140
Figure 50. HPLC trace of isolated (<i>S</i>)- 5q from large-scale reaction.	141
Figure 51. HPLC trace of isolated (<i>S</i>)- 5a from conversion of enantiomerically pure (<i>R</i>)- 4a	142
Figure 52. HPLC trace of isolated (<i>S</i>)- 4a from conversion of enantiomerically pure (<i>S</i>)- 5a	143
Figure 53. HPLC trace of isolated 5ze from conversion of enantiomerically pure (<i>R</i>)- 4ze	144
Figure 54. HPLC trace of isolated 5ze from conversion of enantiomerically pure (<i>S</i>)- 4ze	145
Figure 55. Plot of yield versus reaction time for substrate 4a	146
Figure 56. Plot of yield versus reaction time for substrate 4a-d	146
Figure 57. HPLC trace of isolated 5a from conversion of 4a with Δ - RuH	148
Figure 58. X-ray crystallography. Crystal structure of the deracemized compound (<i>S</i>)- 5q . The disordered fluorine atom is shown on the position with its major probability. Displacement ellipsoids are shown at 50% probability level at 100 K. The hydrogen atoms are shown with arbitrary radii. ..	148
5.3 List of Tables	
Table 1. Initial experiments and optimization. ^a	40
Table 2. Initial experiments and optimization. ^a	49

Table 3. Selected crystallographic data and details of the structure determination for (*R,R*)-**FeBIP**... 78

Table 4. Yields of product **5a** monitored at specific time intervals during reaction 146

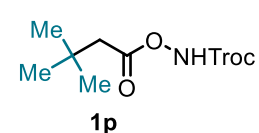
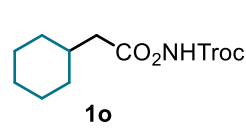
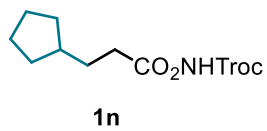
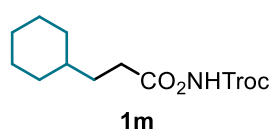
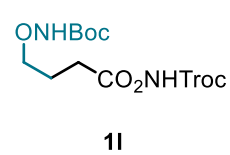
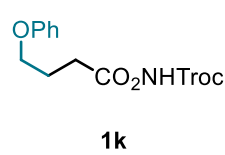
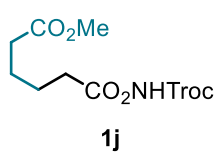
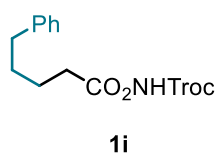
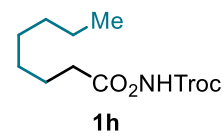
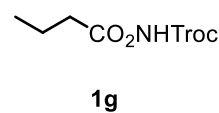
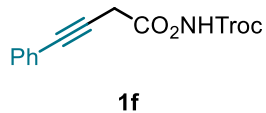
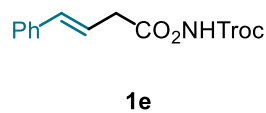
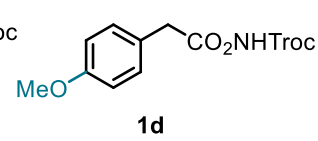
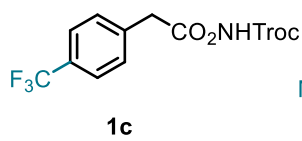
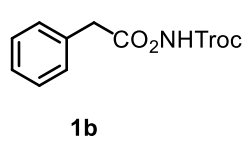
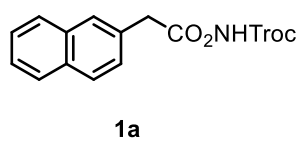
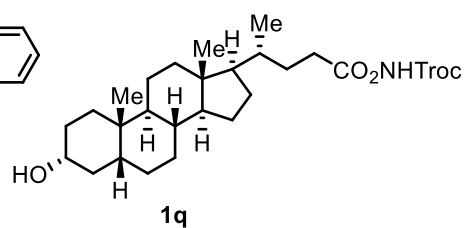
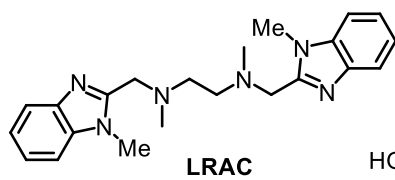
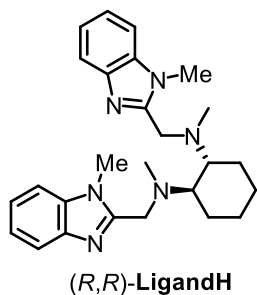
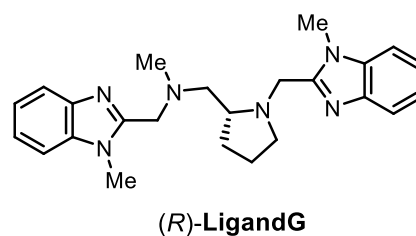
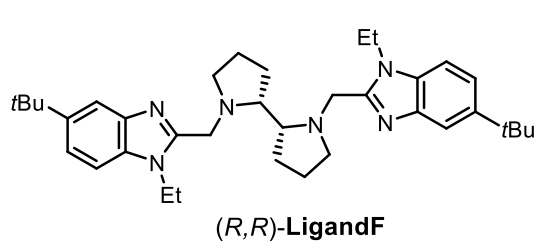
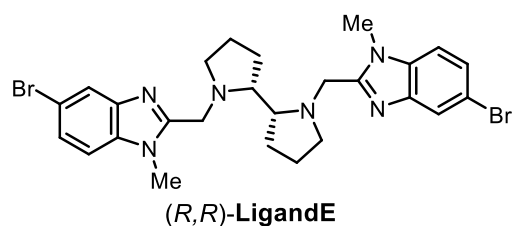
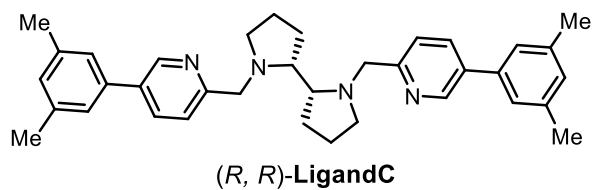
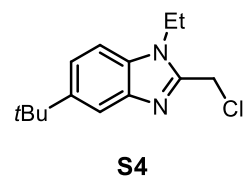
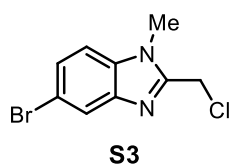
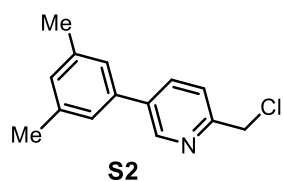
Table 5. Selected crystallographic data and details of the structure determination for C₁₆H₁₄Cl₃NO₄.
..... 149

5.4 List of New N4 Iron Complexes

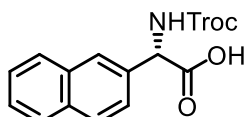


5.5 List of New Organic Compounds

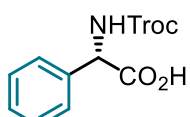
(1) Chapter 2.1 and its Experimental Part



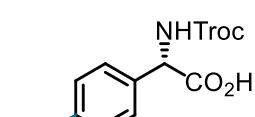
Statement



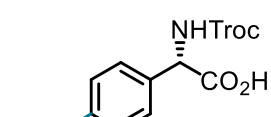
(S) - 2a



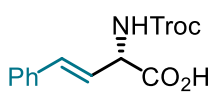
(S) - 2b



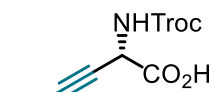
(S) - 2c



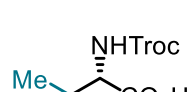
(S) - 2d



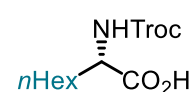
(S) - 2e



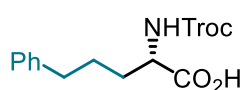
(S) - 2f



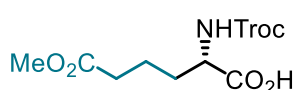
(S) - 2g



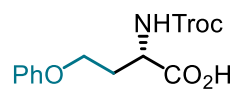
(S) - 2h



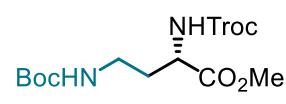
(S) - 2i



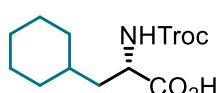
(S) - 2j



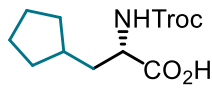
(S) - 2k



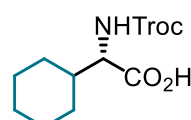
(S) - 2l



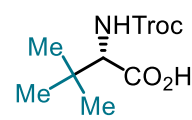
(S) - 2m



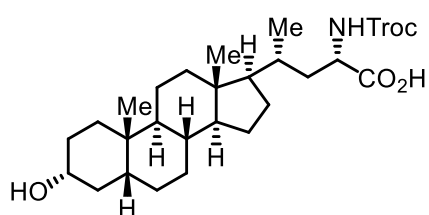
(S) - 2n



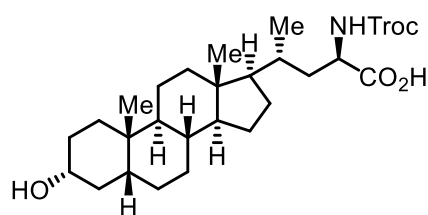
(S) - 2o



(S) - 2p

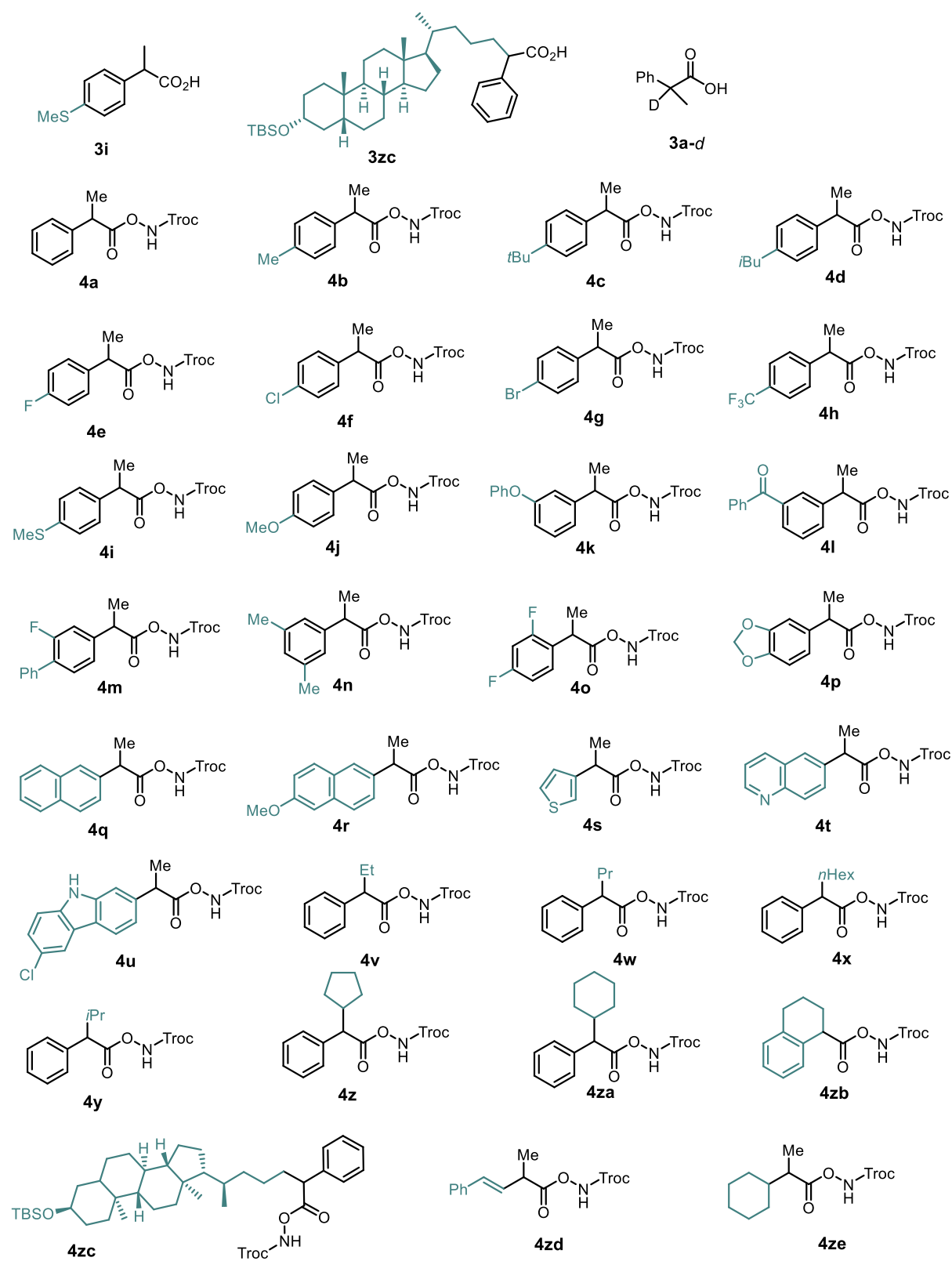


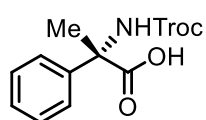
(S) - 2q



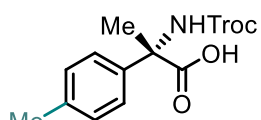
(S) - 2-epi-2q

(2) Chapter 2.2 and its Experimental Part

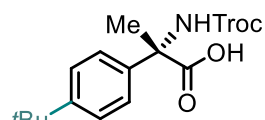




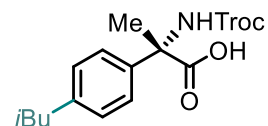
(S) - 5a



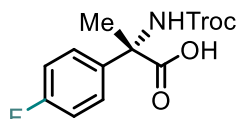
(S) - 5b



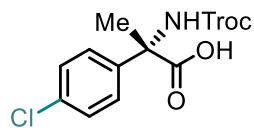
(S) - 5c



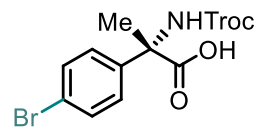
(S) - 5d



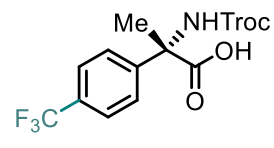
(S) - 5e



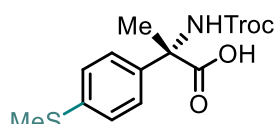
(S) - 5f



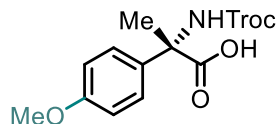
(S) - 5g



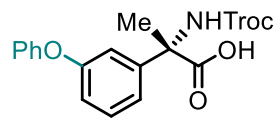
(S) - 5h



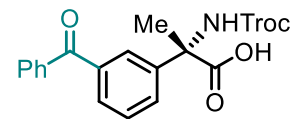
(S) - 5i



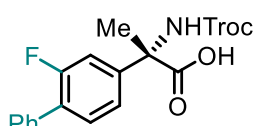
(S) - 5j



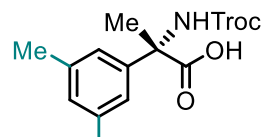
(S) - 5k



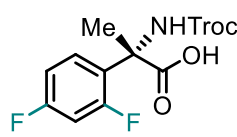
(S) - 5l



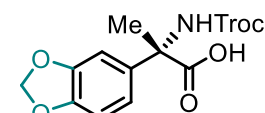
(S) - 5m



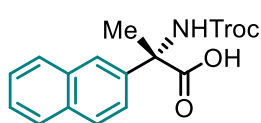
(S) - 5n



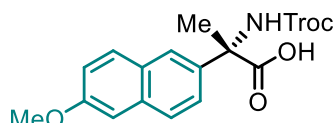
(S) - 5o



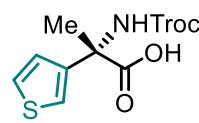
(S) - 5p



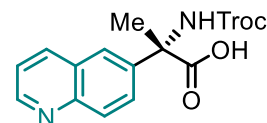
(S) - 5q



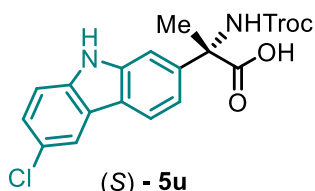
(S) - 5r



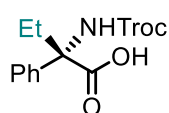
(S) - 5s



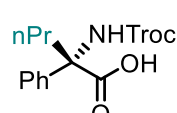
(S) - 5t



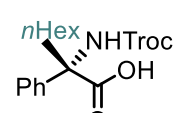
(S) - 5u



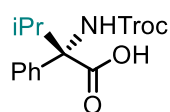
(S) - 5v



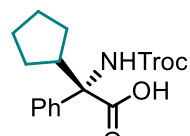
(S) - 5w



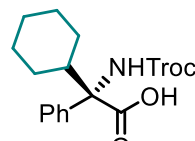
(S) - 5x



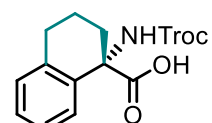
(S) - 5y



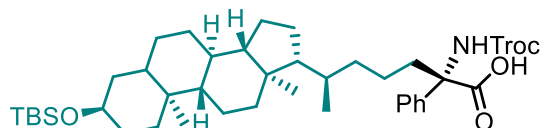
(S) - 5z



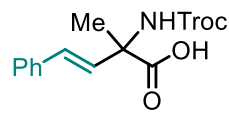
(S) - 5za



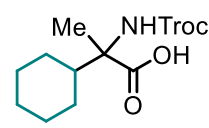
(S) - 5zb



(S) - 5zc

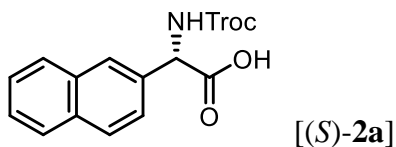


5zd

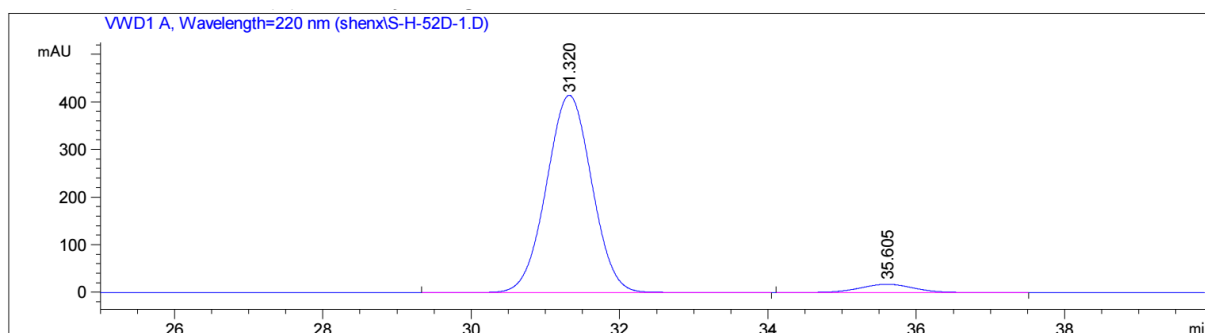
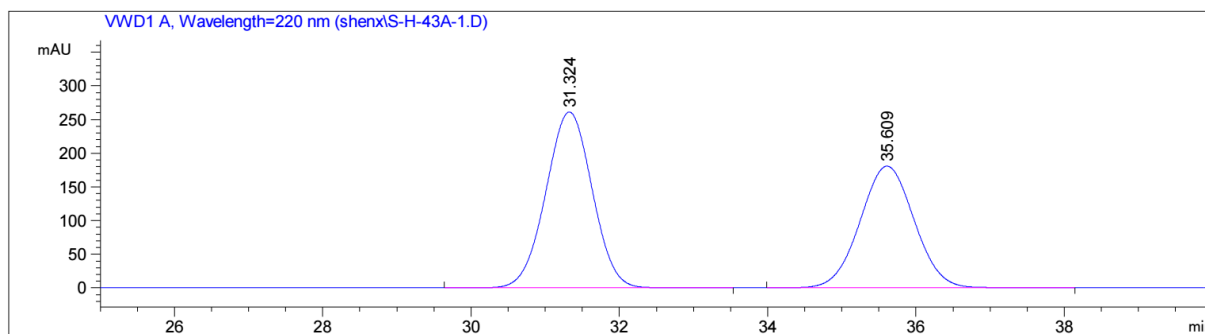


5ze

5.6 Enantiomeric Excess for Catalytic Reactions



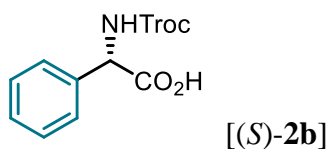
[Chiralpak IB, 25 °C, CH₃CN/H₂O(0.1% TFA) = 40:60, 1.0 mL/min, 220 nm]



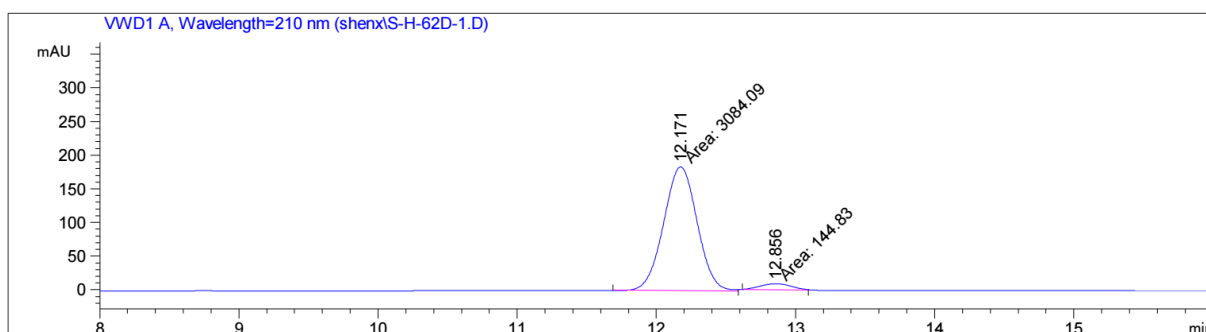
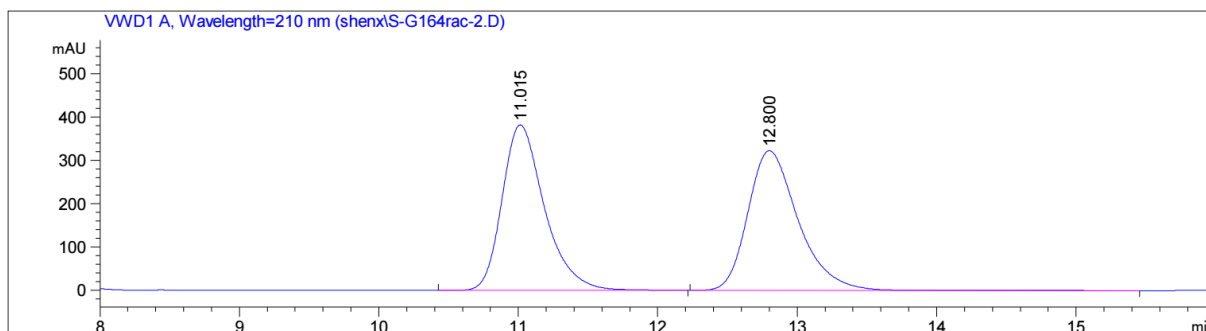
Peak #	RetTime [min]	Type	Width [min]	Area mAU *s	Height [mAU]	Area %
1	31.320	BB	0.6706	1.76072e4	414.27954	95.3460
2	35.605	BB	0.7791	859.43530	17.25377	4.6540

Figure 59. HPLC traces of *rac*-2a and (*S*)-2a (90% ee).

Statement



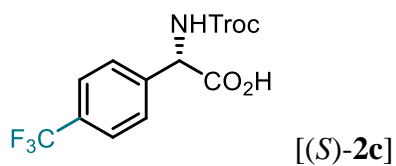
[Chiralpak ODR, 25 °C, CH₃CN/H₂O(0.1% TFA) = 40:60, 1.0 mL/min, 210 nm]



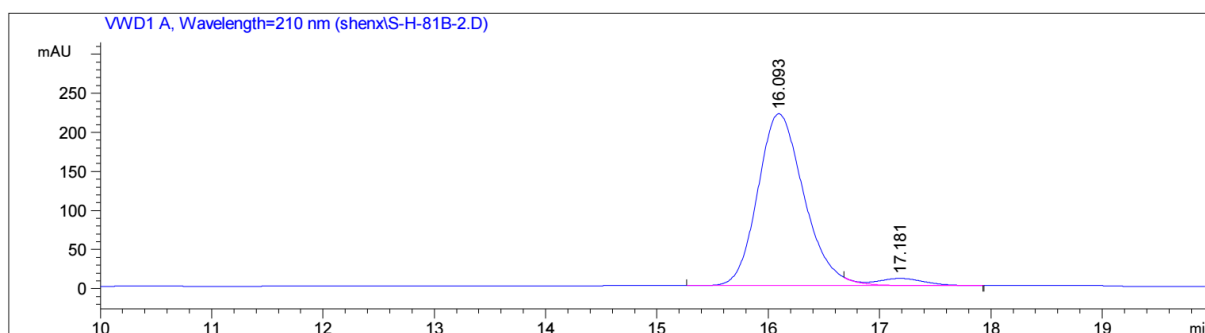
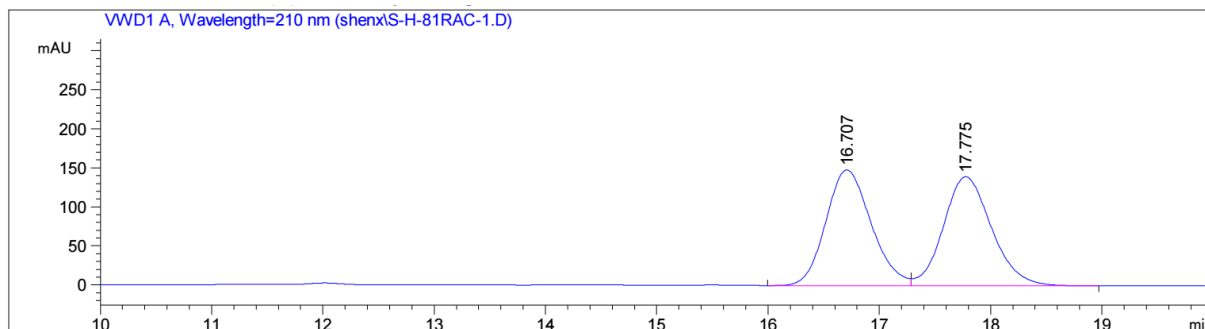
Peak #	RetTime [min]	Type	Width [min]	Area mAU *s	Height [mAU]	Area %
1	12.171	MM	0.2781	3084.08789	184.84370	95.5146
2	12.856	MM	0.2641	144.82953	9.14128	4.4854

Figure 60. HPLC traces of *rac*-2b and (*S*)-2b (91% ee).

Statement



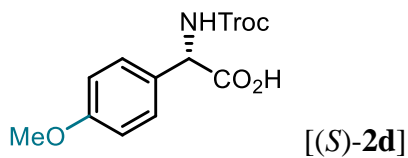
[Chiralpak ODR, 25 °C, CH₃CN/H₂O(0.1% TFA) = 40:60, 1.0 mL/min, 210 nm]



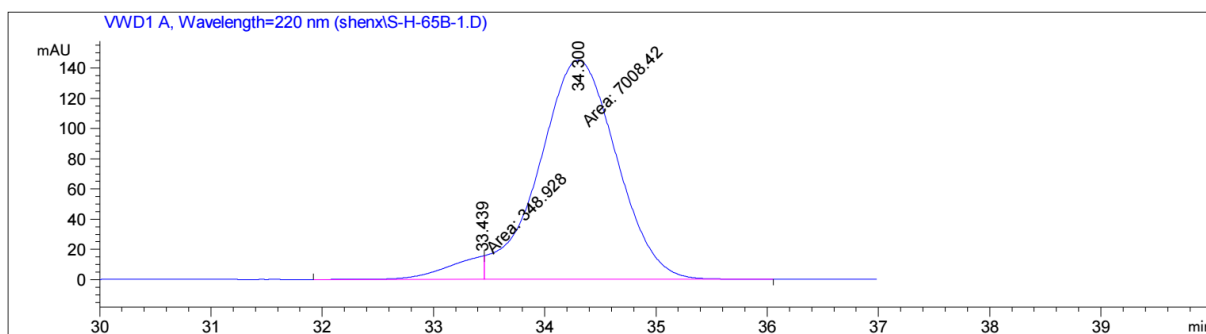
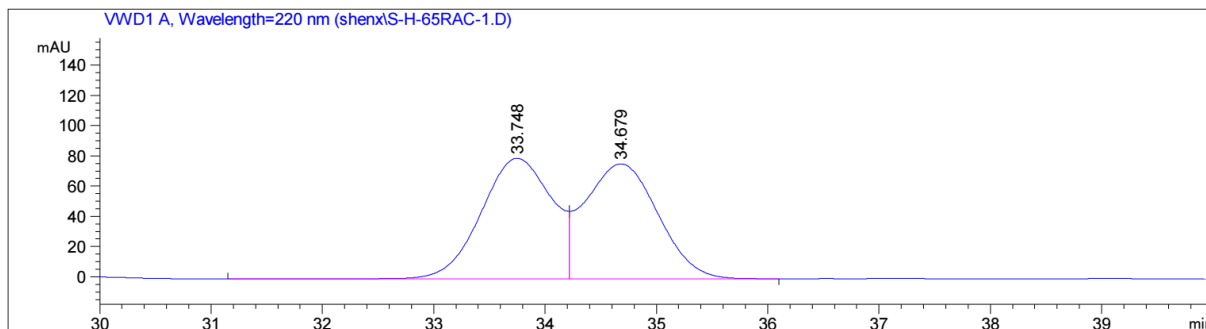
Peak #	RetTime [min]	Type	Width [min]	Area mAU *s	Height [mAU]	Area %
1	16.093	BV R	0.4426	6357.63916	219.57649	96.2188
2	17.181	VB E	0.4445	249.84494	8.88514	3.7812

Figure 61. HPLC traces of *rac*-2c and (*S*)-2c (92% ee).

Statement



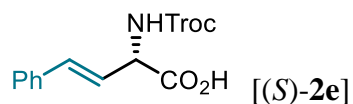
[Chiralpak IB, 25 °C, CH₃CN/H₂O(0.1% TFA) = 30:70, 1.0 mL/min, 210 nm]



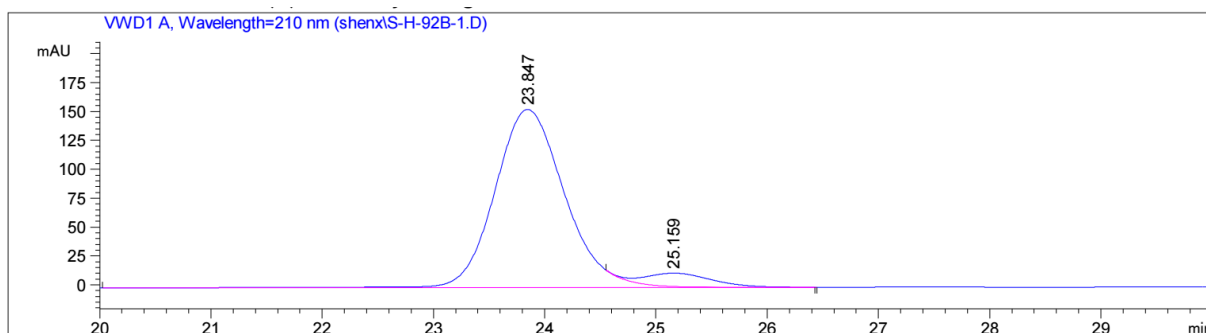
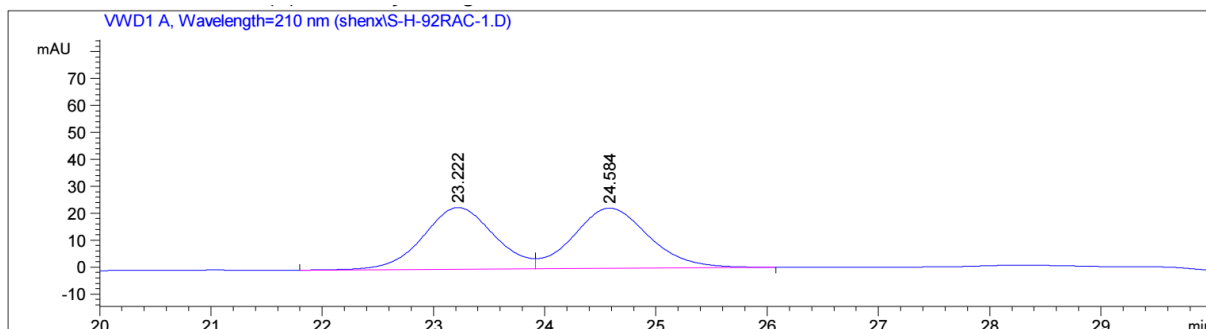
Peak #	RetTime [min]	Type	Width [min]	Area mAU *s	Height [mAU]	Area %
1	33.439	MF	0.3783	348.92822	15.37354	4.7426
2	34.300	FM	0.8048	7008.41895	145.13840	95.2574

Figure 62. HPLC traces of *rac*-2d and (*S*)-2d (90% ee).

Statement



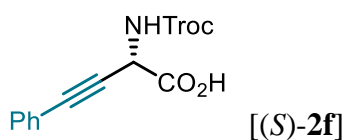
[Chiralpak ODR, 25 °C, CH₃CN/H₂O(0.1% TFA) = 40:60, 1.0 mL/min, 210 nm]



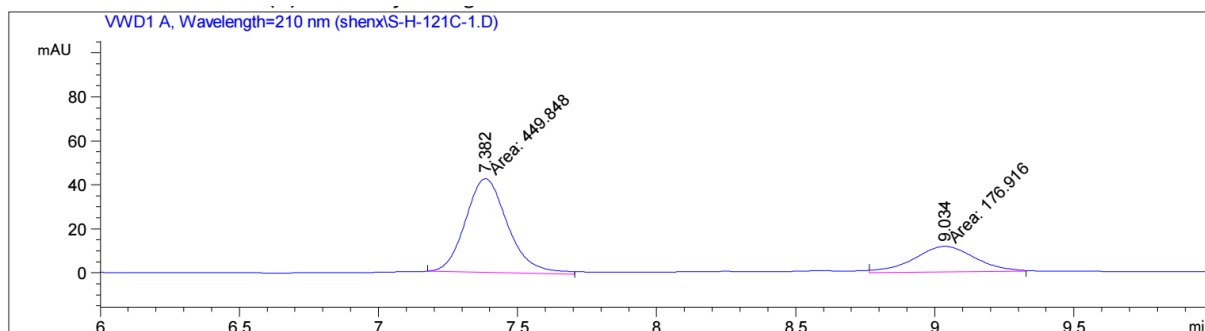
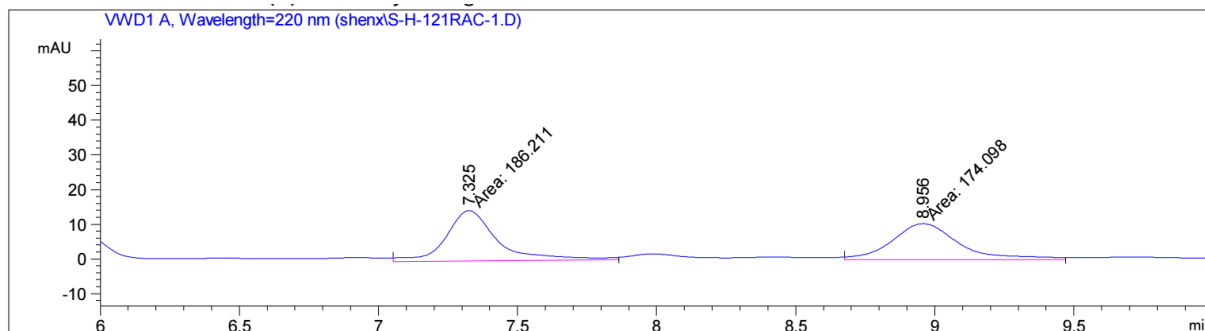
Peak #	RetTime [min]	Type	Width [min]	Area [mAU*s]	Height [mAU]	Area %
1	23.847	BV R	0.6744	6748.53613	153.98459	93.3976
2	25.159	VB E	0.6229	477.06161	11.52077	6.6024

Figure 63. HPLC traces of *rac*-2e and (*S*)-2e (86% ee).

Statement



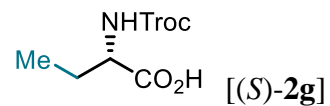
[Chiralpak IG, 25 °C, CH₃CN/H₂O(0.1% TFA) = 50:50, 1.0 mL/min, 210 nm]



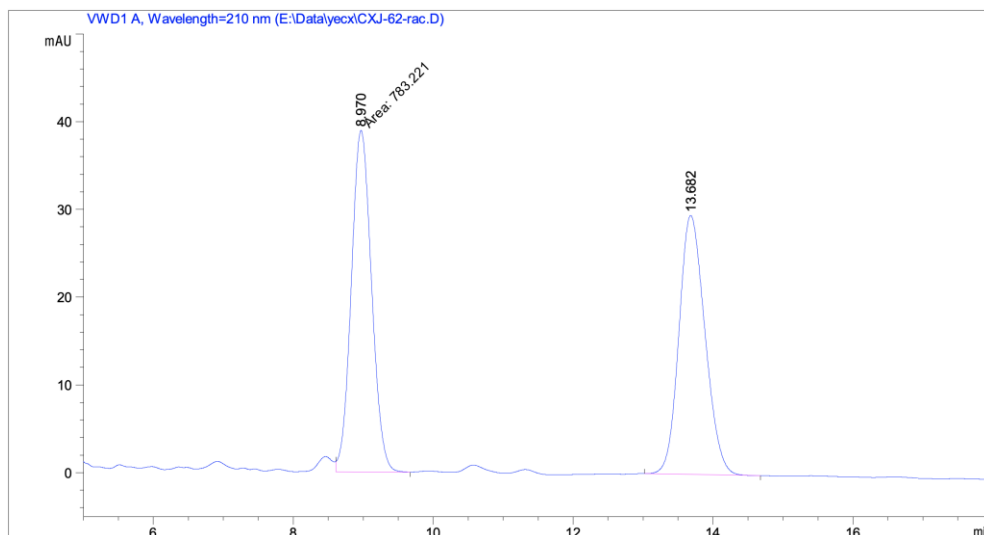
Peak #	RetTime [min]	Type	Width [min]	Area mAU *s	Height [mAU]	Area %
1	7.382	MM	0.1746	449.84848	42.95138	71.7732
2	9.034	MM	0.2528	176.91574	11.66546	28.2268

Figure 64. HPLC traces of *rac*-2f and (S)-2f (44% ee).

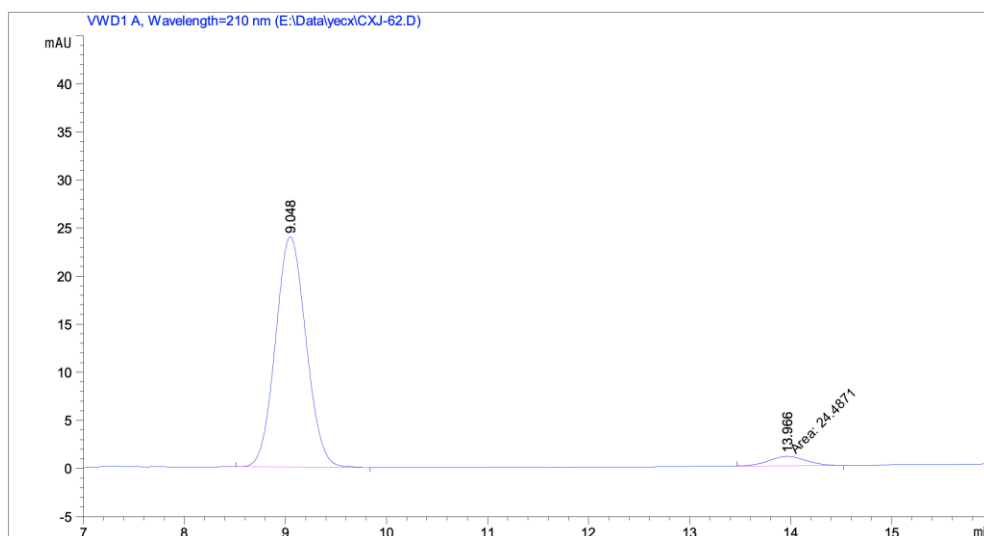
Statement



[CHIRALPAK IG, 25 °C, *i*PrOH/*n*-hexane = 10/90 (v/v) + 0.1% TFA, 1.0 mL/min, 210 nm]



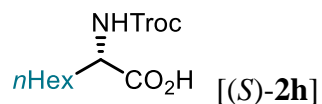
Peak #	RetTime [min]	Type	Width [min]	Area [mAU*s]	Height [mAU]	Area %
1	8.970	FM	0.3355	783.22052	38.91230	50.6177
2	13.682	BB	0.4030	764.10632	29.52205	49.3823



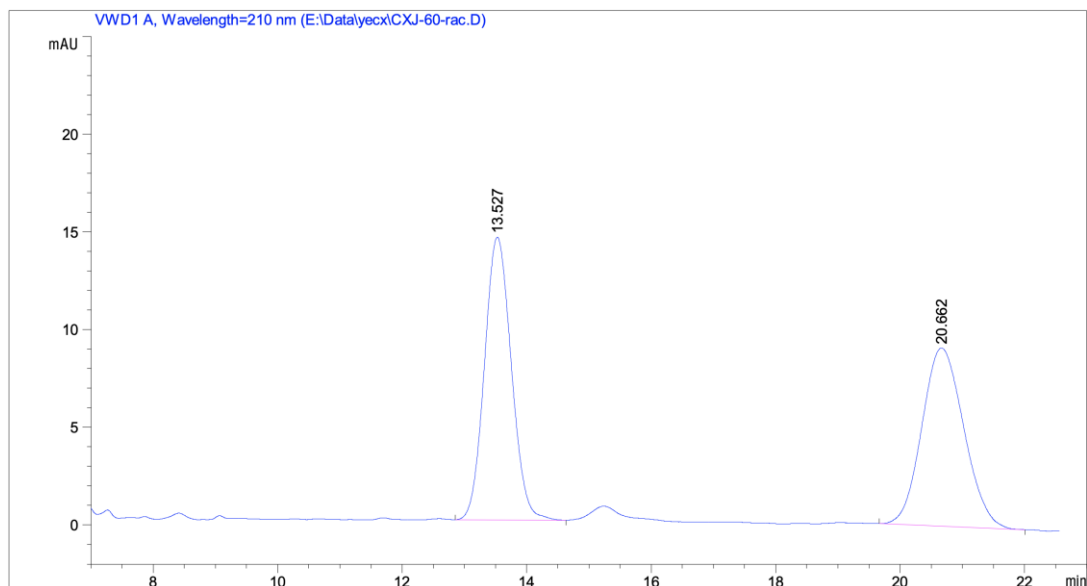
Peak #	RetTime [min]	Type	Width [min]	Area [mAU*s]	Height [mAU]	Area %
1	9.048	BB	0.3268	502.17838	23.93603	95.3505
2	13.966	MM	0.4220	24.48711	9.67133e-1	4.6495

Figure 65. HPLC traces of *rac*-2g and (*S*)-2g (91% ee).

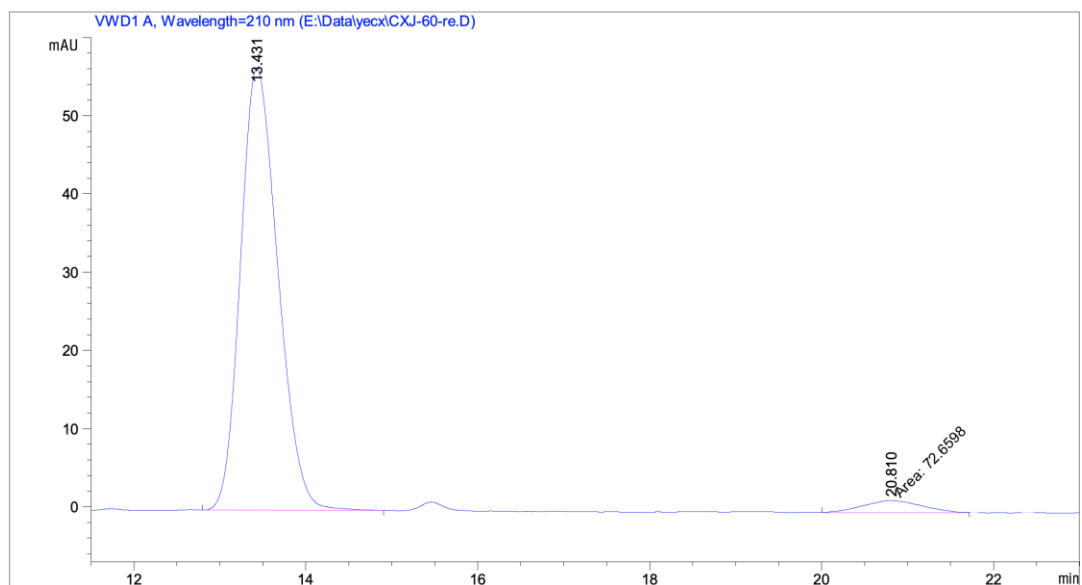
Statement



[CHIRALPAK IG, 25 °C, *i*PrOH/*n*-hexane = 5/95 (v/v) + 0.1% TFA, 1.0 mL/min, 210 nm]



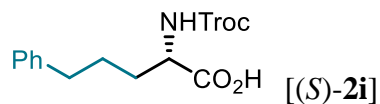
Peak #	RetTime [min]	Type	Width [min]	Area [mAU*s]	Height [mAU]	Area %
1	13.527	BB	0.4657	433.55087	14.46325	50.4008
2	20.662	BB	0.7420	426.65631	9.11614	49.5992



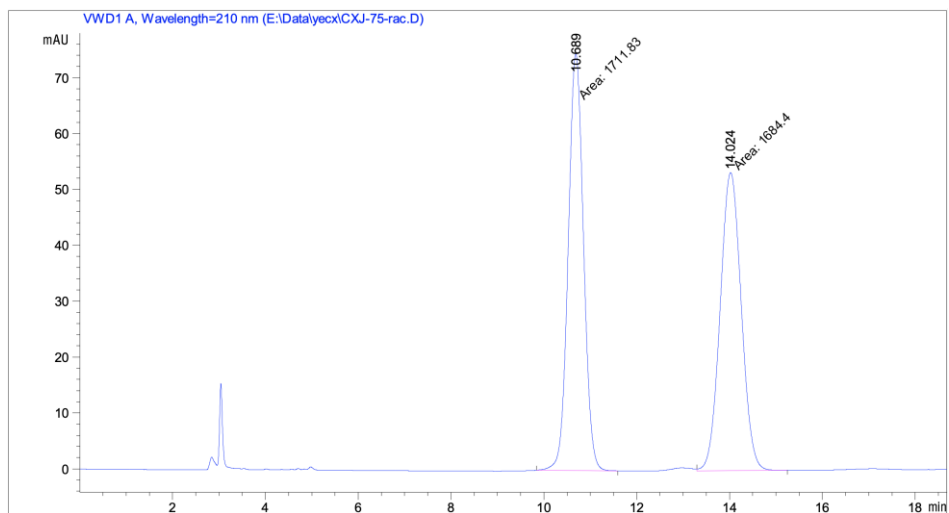
Peak #	RetTime [min]	Type	Width [min]	Area [mAU*s]	Height [mAU]	Area %
1	13.431	BB	0.4686	1707.77881	56.50270	95.9190
2	20.810	MM	0.7834	72.65979	1.54572	4.0810

Figure 66. HPLC traces of *rac*-2h and (*S*)-2h (92% ee).

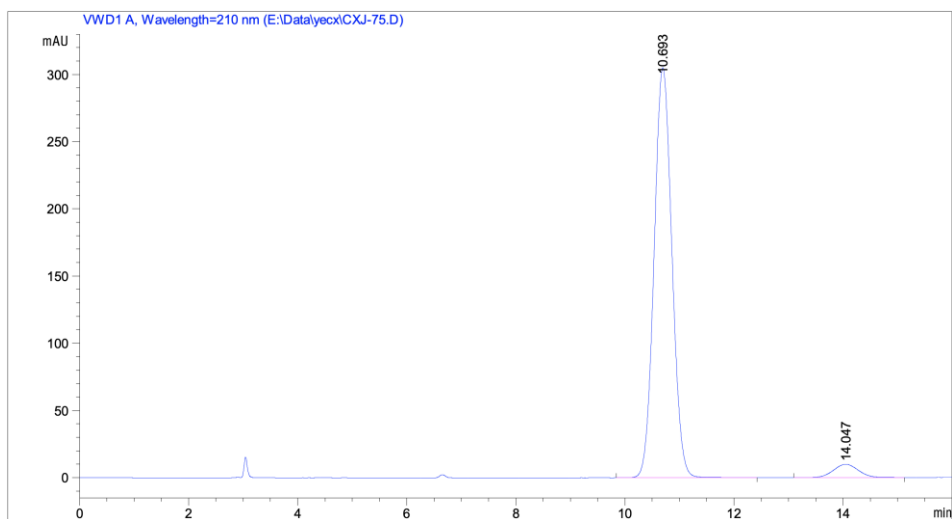
Statement



[CHIRALPAK IG, 25 °C, *i*PrOH/*n*-hexane = 10/90 (v/v) + 0.1% TFA, 1.0 mL/min, 210 nm]



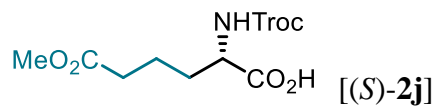
Peak #	RetTime [min]	Type	Width [min]	Area [mAU*s]	Height [mAU]	Area %
1	10.689	MM	0.3824	1711.83459	74.59972	50.4039
2	14.024	FM	0.5264	1684.40125	53.33140	49.5961



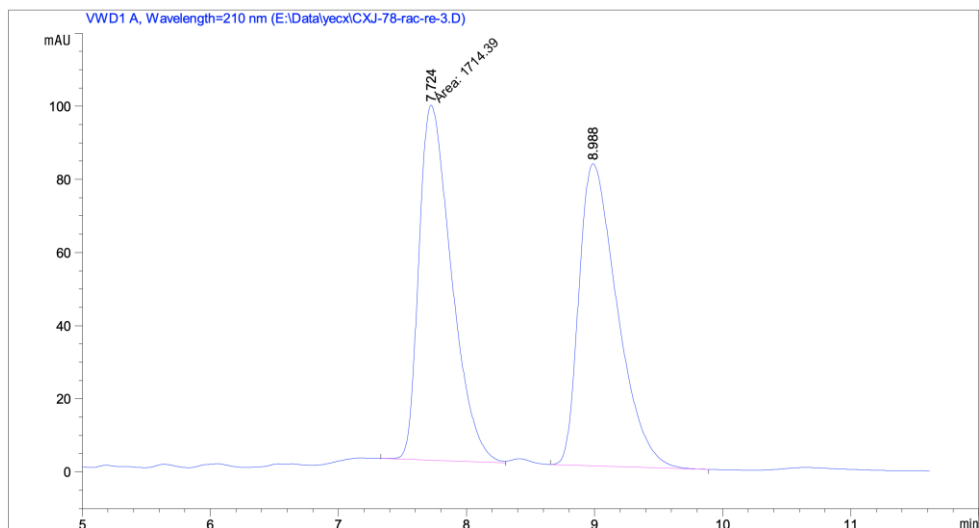
Peak #	RetTime [min]	Type	Width [min]	Area [mAU*s]	Height [mAU]	Area %
1	10.693	BB	0.3531	6905.83643	305.10132	95.6877
2	14.047	BB	0.4928	311.21756	9.84399	4.3123

Figure 67. HPLC traces of *rac*-2i and (*S*)-2i (91% ee).

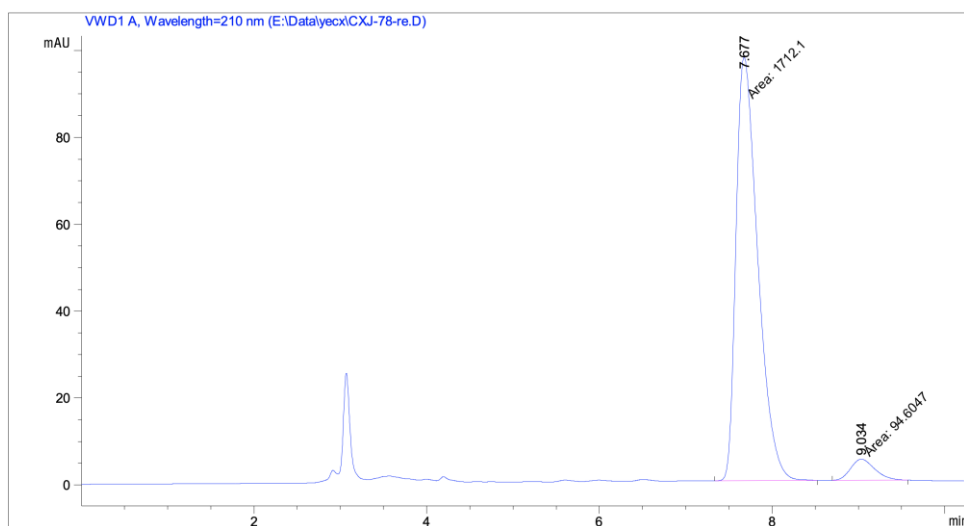
Statement



[CHIRALCEL OD-H, 25 °C, *i*PrOH/*n*-hexane = 10/90 (v/v) + 0.1% TFA, 1.0 mL/min, 210 nm]



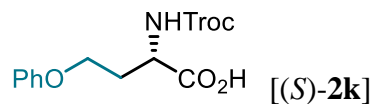
Peak #	RetTime [min]	Type	Width [min]	Area [mAU*s]	Height [mAU]	Area %
1	7.724	MF	0.2942	1714.38965	97.10693	49.9924
2	8.988	BB	0.3192	1714.90845	82.59386	50.0076



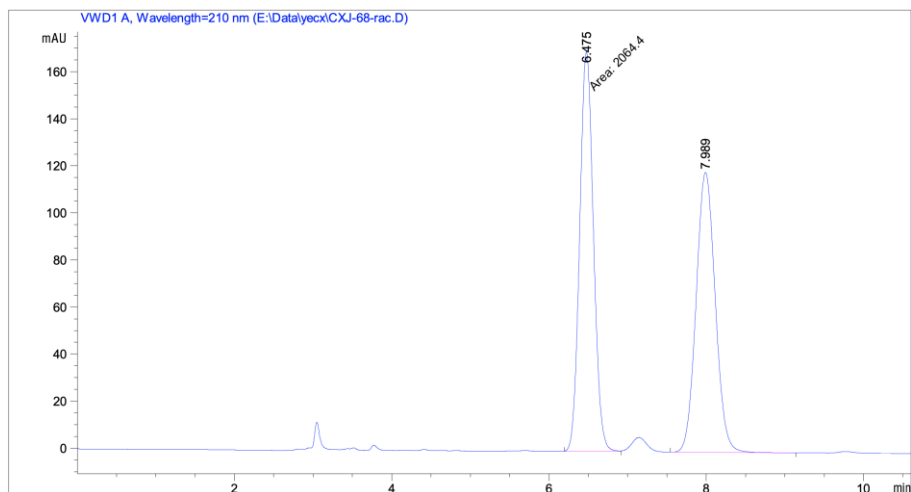
Peak #	RetTime [min]	Type	Width [min]	Area [mAU*s]	Height [mAU]	Area %
1	7.677	MM	0.2926	1712.09814	97.52850	94.7637
2	9.034	MM	0.3250	94.60468	4.85205	5.2363

Figure 68. HPLC traces of *rac*-2j and (*S*)-2j (90% ee).

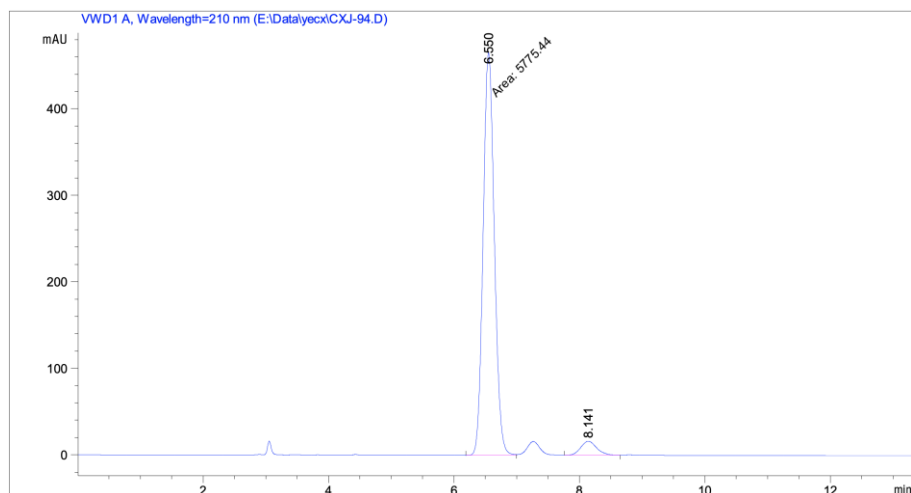
Statement



[CHIRALPAK IG, 25 °C, *i*PrOH/*n*-hexane = 20/80 (v/v) + 0.1% TFA, 1.0 mL/min, 210 nm]



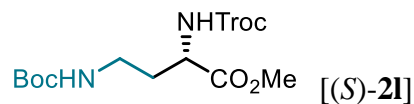
Peak #	RetTime [min]	Type	Width [min]	Area [mAU*s]	Height [mAU]	Area %
1	6.475	MM	0.2026	2064.40381	169.86066	50.6757
2	7.989	BB	0.2631	2009.35510	118.93588	49.3243



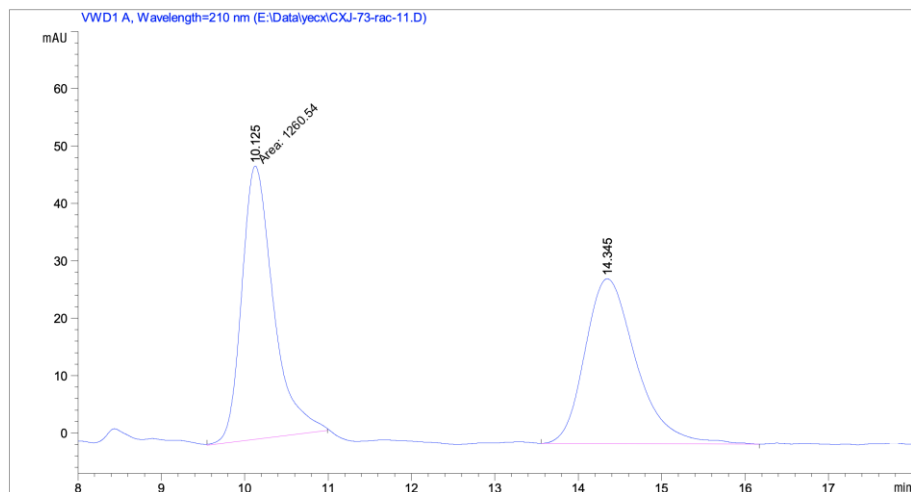
Peak #	RetTime [min]	Type	Width [min]	Area [mAU*s]	Height [mAU]	Area %
1	6.550	MF	0.2068	5775.44092	465.39316	95.2424
2	8.141	BB	0.2736	288.49939	16.21524	4.7576

Figure 69. HPLC traces of *rac*-2k and (*S*)-2k (90% ee).

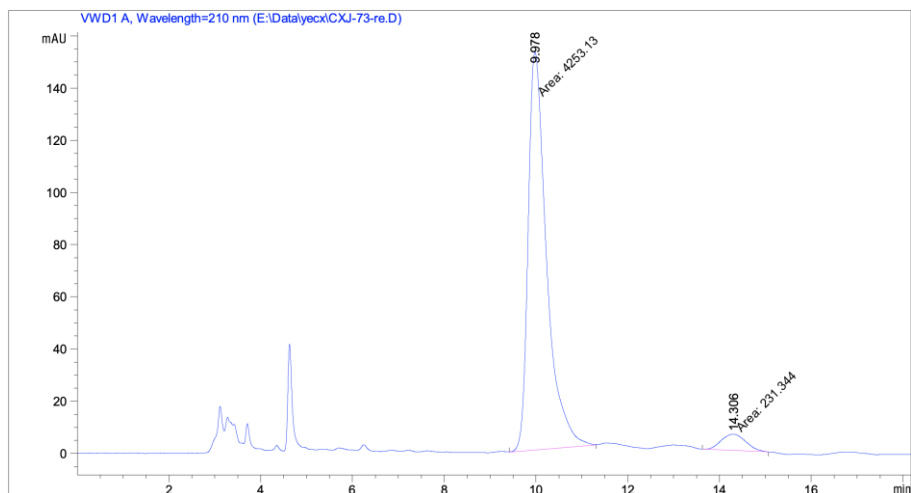
Statement



[CHIRALPAK IC, 25 °C, *i*PrOH/*n*-hexane = 10/90 (v/v), 1.0 mL/min, 210 nm]



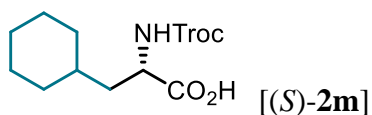
Peak #	RetTime [min]	Type	Width [min]	Area [mAU*s]	Height [mAU]	Area %
1	10.125	MM	0.4410	1260.53625	47.64463	50.7592
2	14.345	BB	0.6529	1222.82703	28.70853	49.2408



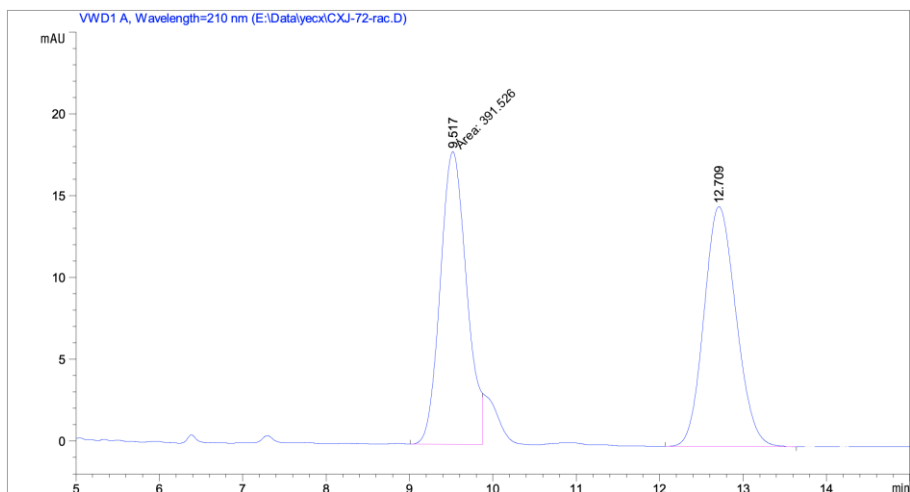
Peak #	RetTime [min]	Type	Width [min]	Area [mAU*s]	Height [mAU]	Area %
1	9.978	MM	0.4650	4253.13086	152.44682	94.8412
2	14.306	MM	0.6176	231.34367	6.24317	5.1588

Figure 70. HPLC traces of *rac*-21 and (*S*)-21 (90% ee).

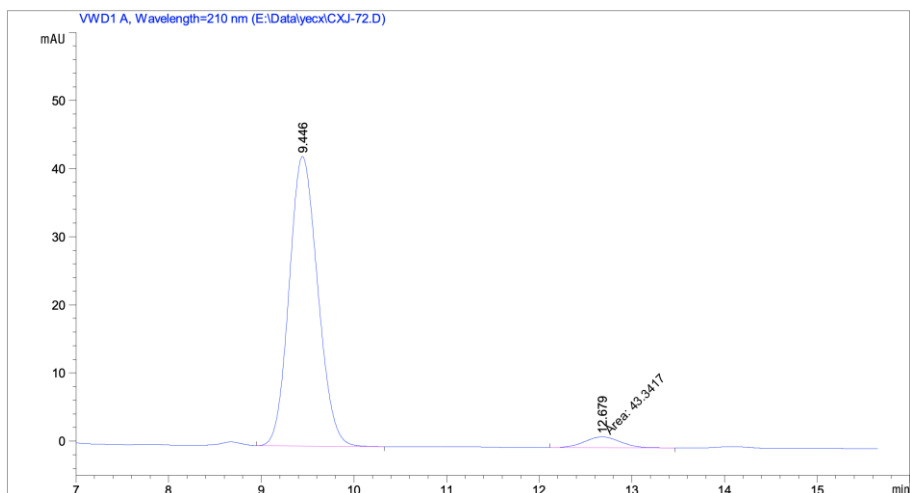
Statement



[CHIRALPAK IG, 25 °C, *i*PrOH/*n*-hexane = 10/90 (v/v) + 0.1% TFA, 1.0 mL/min, 210 nm]



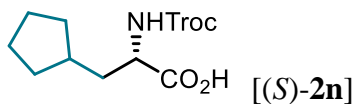
Peak #	RetTime [min]	Type	Width [min]	Area [mAU*s]	Height [mAU]	Area %
1	9.517	MF	0.3649	391.52570	17.88503	49.9479
2	12.709	BB	0.4153	392.34262	14.65629	50.0521



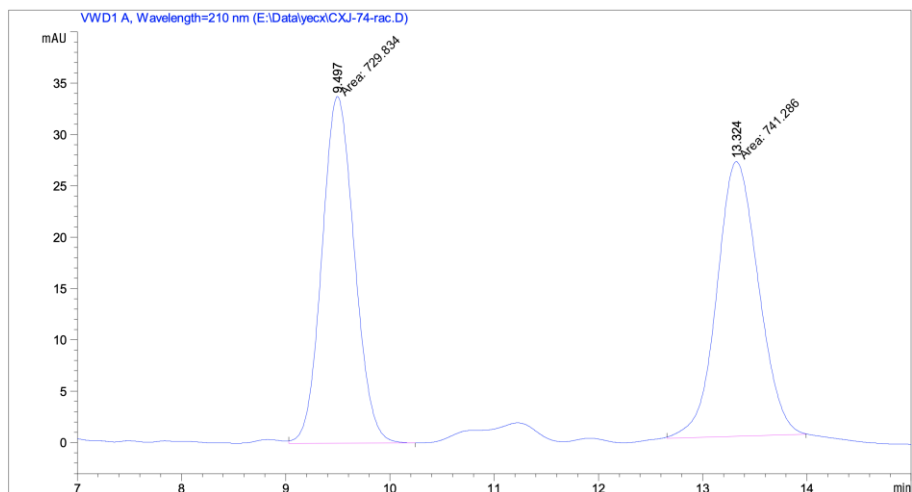
Peak #	RetTime [min]	Type	Width [min]	Area [mAU*s]	Height [mAU]	Area %
1	9.446	BB	0.3337	909.48755	42.49849	95.4513
2	12.679	MM	0.4510	43.34167	1.60182	4.5487

Figure 71. HPLC traces of *rac*-2m and (*S*)-2m (91% ee).

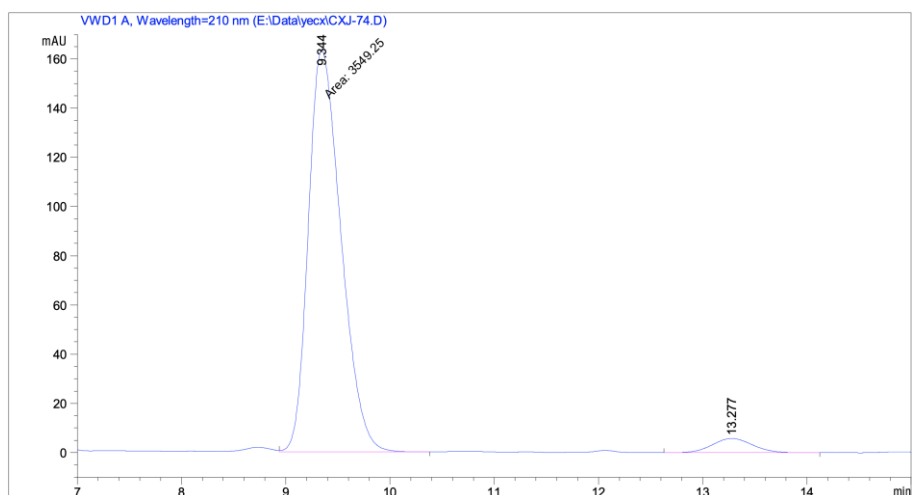
Statement



[CHIRALPAK IG, 25 °C, *i*PrOH/*n*-hexane = 10/90 (v/v) + 0.1% TFA, 1.0 mL/min, 210 nm]



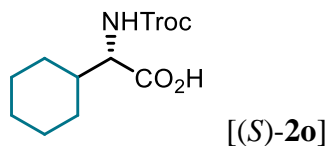
Peak #	RetTime [min]	Type	Width [min]	Area [mAU*s]	Height [mAU]	Area %
1	9.497	FM	0.3607	729.83447	33.72057	49.6108
2	13.324	MM	0.4625	741.28595	26.71083	50.3892



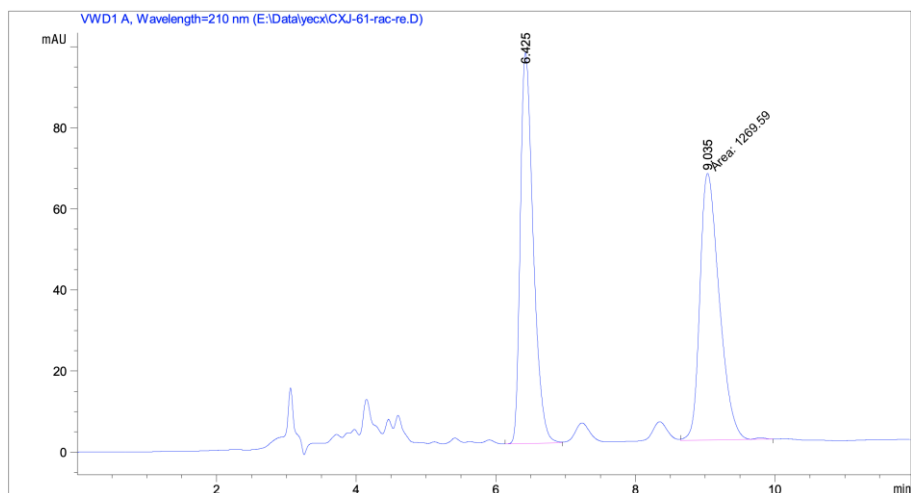
Peak #	RetTime [min]	Type	Width [min]	Area [mAU*s]	Height [mAU]	Area %
1	9.344	FM	0.3625	3549.25171	163.16234	95.8060
2	13.277	BB	0.4183	155.37163	5.78496	4.1940

Figure 72. HPLC traces of *rac*-2n and (S)-2n (92% ee).

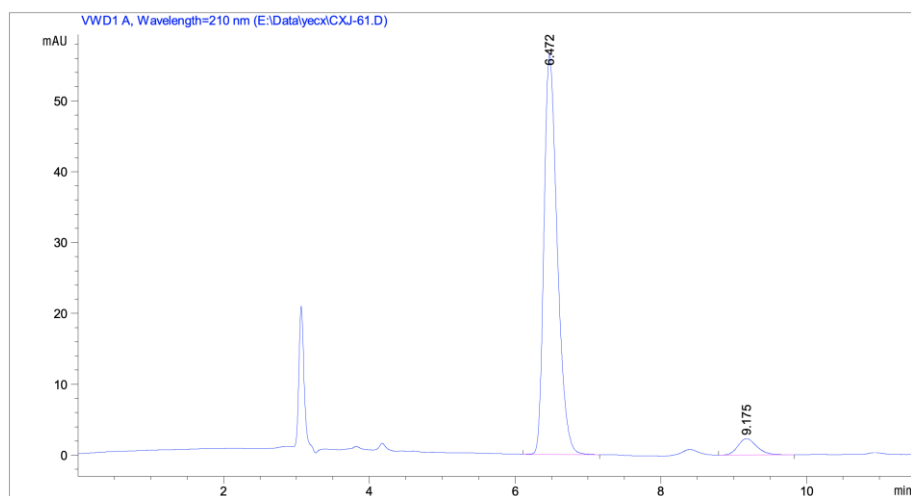
Statement



[CHIRALCEL OD-H, 25 °C, *i*PrOH/*n*-hexane = 5/95 (v/v) + 0.1% TFA, 1.0 mL/min, 210 nm]



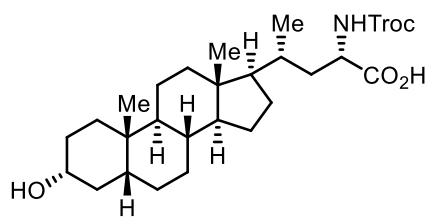
Peak #	RetTime [min]	Type	Width [min]	Area [mAU*s]	Height [mAU]	Area %
1	6.425	BV	0.1962	1240.85315	96.40808	49.4277
2	9.035	FM	0.3215	1269.58875	65.81030	50.5723



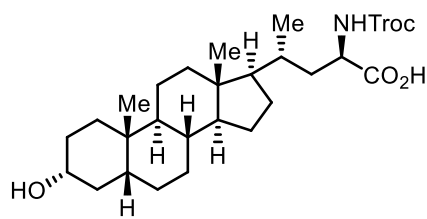
Peak #	RetTime [min]	Type	Width [min]	Area [mAU*s]	Height [mAU]	Area %
1	6.472	BB	0.1938	715.34949	56.45700	94.5799
2	9.175	BB	0.2713	40.99436	2.29575	5.4201

Figure 73. HPLC traces of *rac*-2n and (S)-2o (89% ee).

Statement

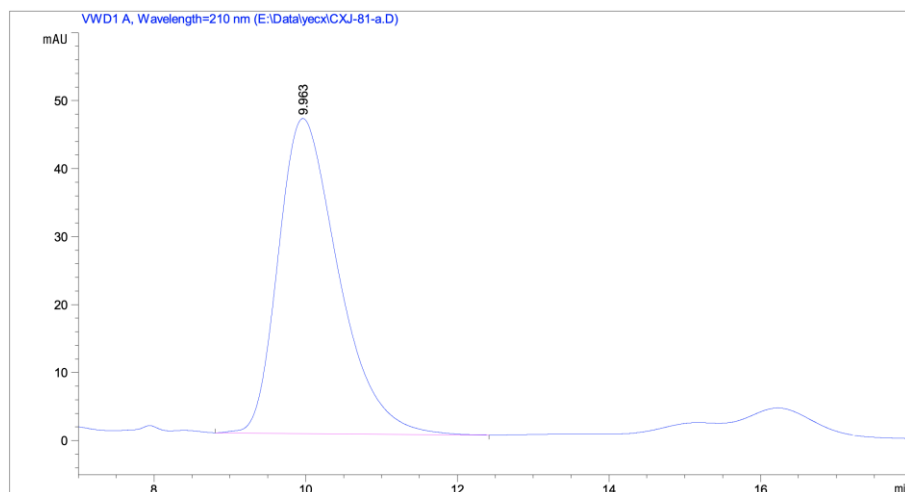


(2q) and



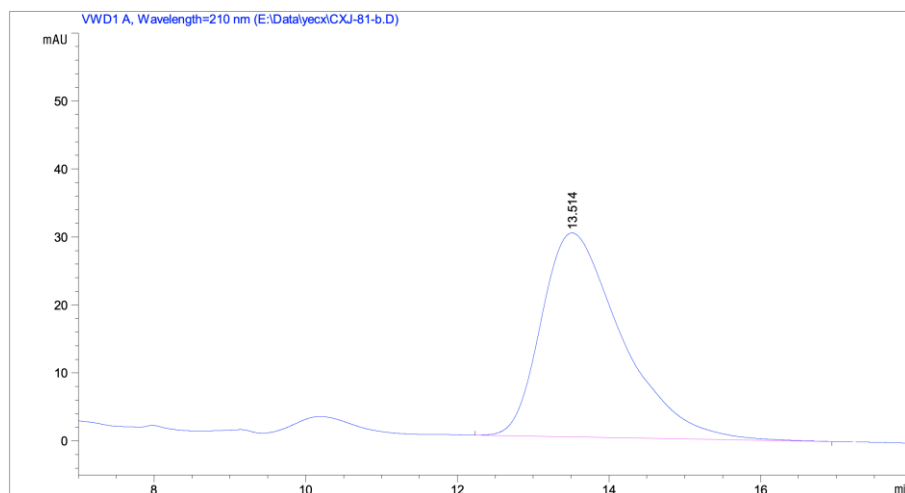
(2-*epi*-2q)

[CHIRALCEL OD-H, 25 °C, *i*PrOH/*n*-hexane = 20/80 (v/v) + 0.1% TFA, 1.0 mL/min, 210 nm]



Peak #	RetTime [min]	Type	Width [min]	Area [mAU*s]	Height [mAU]	Area %
1	9.963	BB	0.8398	2545.03906	46.33273	100.0000

HPLC of 2q.



Peak #	RetTime [min]	Type	Width [min]	Area [mAU*s]	Height [mAU]	Area %
1	13.514	BB	1.0858	2205.16138	29.99280	100.0000

HPLC of 2-*epi*-2q.

Statement

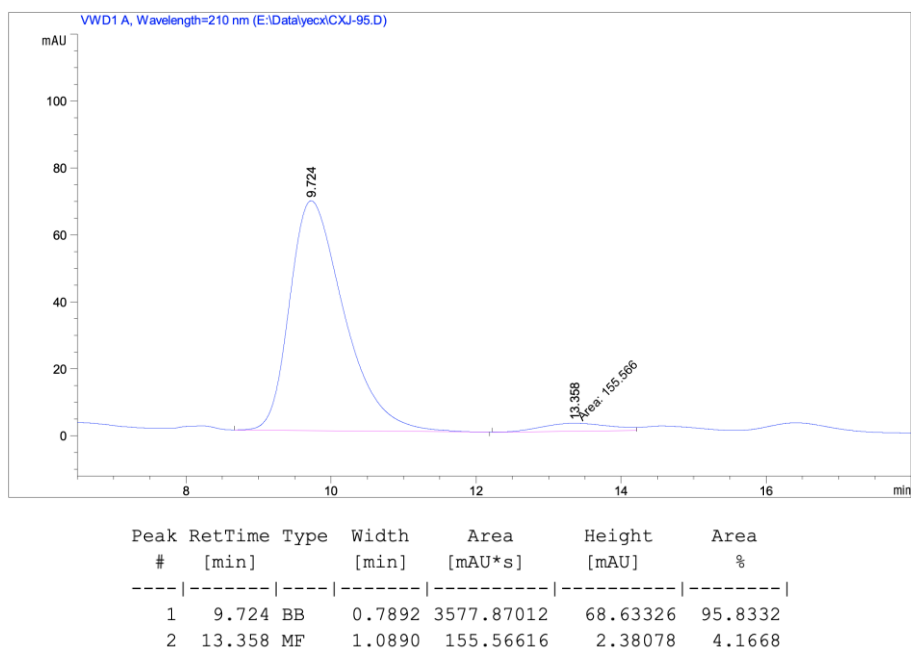
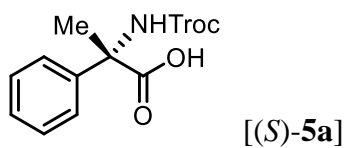
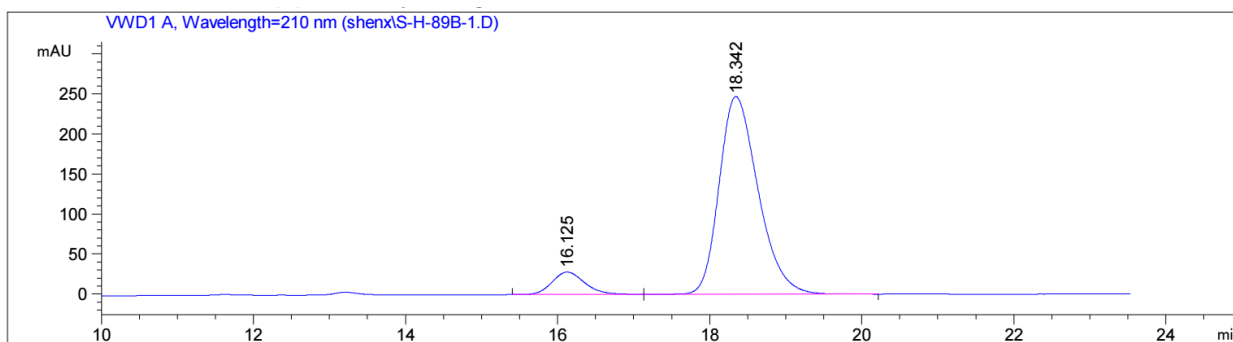
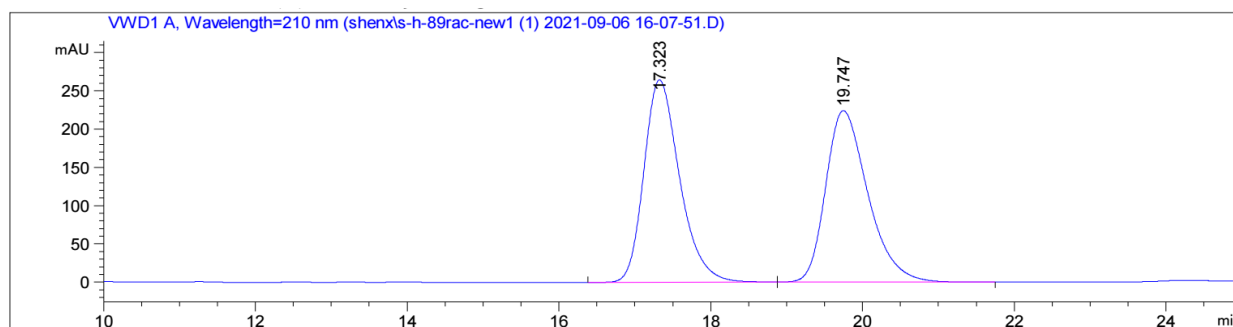


Figure 74.HPLC of the mixture of **2q** and *2-epi-2q* derived from (*R,R*)-**FeBIPCl₂** catalyzed 1,3-nitrogen shift (23:1 d.r.).

Statement



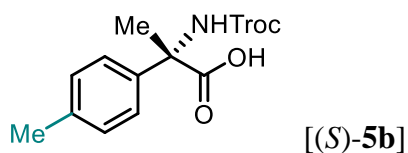
[Chiralpak ODR, 25 °C, CH₃CN/H₂O(0.1% TFA) = 40:60, 1.0 mL/min, 210 nm]



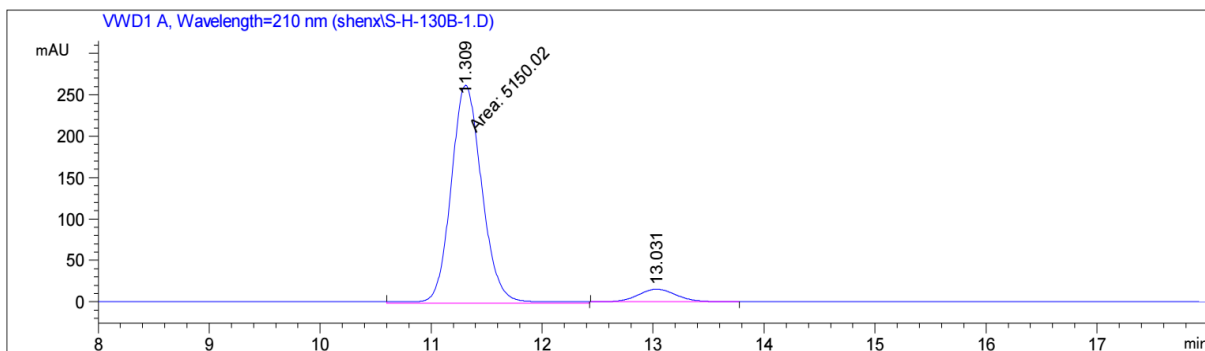
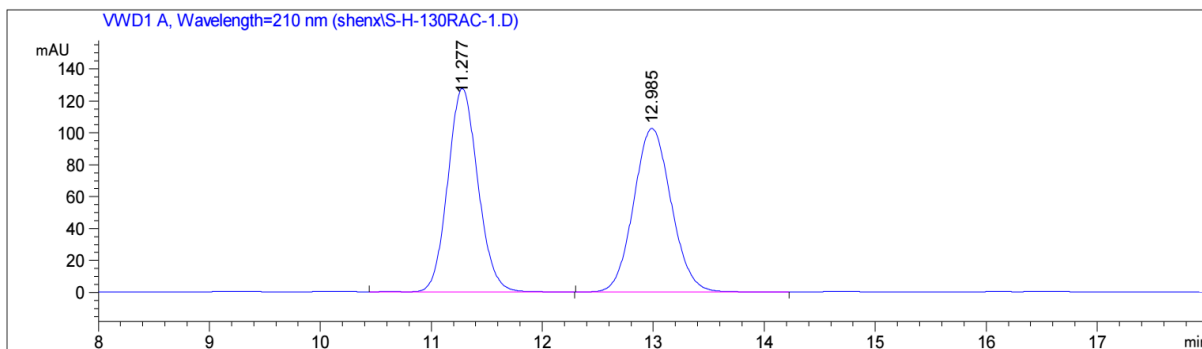
Peak #	RetTime [min]	Type	Width [min]	Area mAU*s	Height [mAU]	Area %
1	16.125	BB	0.4562	828.12207	27.96407	8.6184
2	18.342	BB	0.5475	8780.63770	246.86044	91.3816

Figure 75. HPLC traces of *rac*-5a and (*S*)-5a (83% ee).

Statement



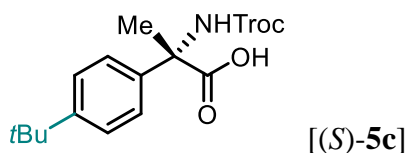
[Chiralpak IG, 25 °C, CH₃CN/H₂O(0.1% TFA) = 50:50, 1.0 mL/min, 210 nm]



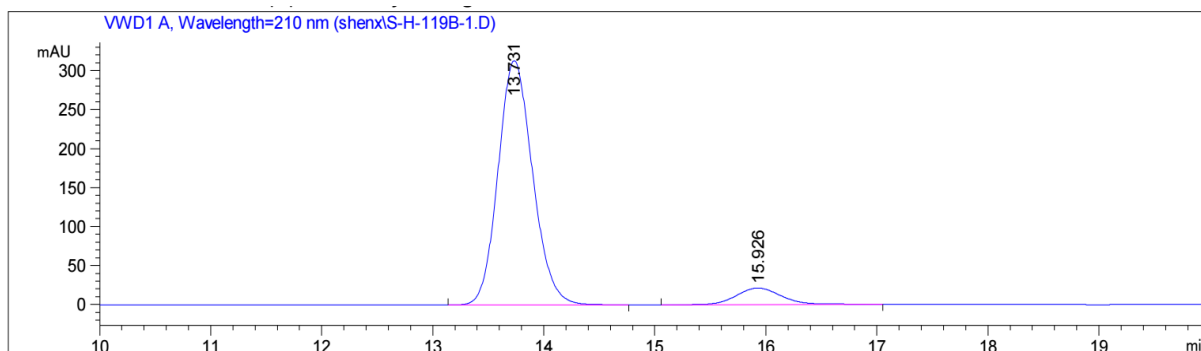
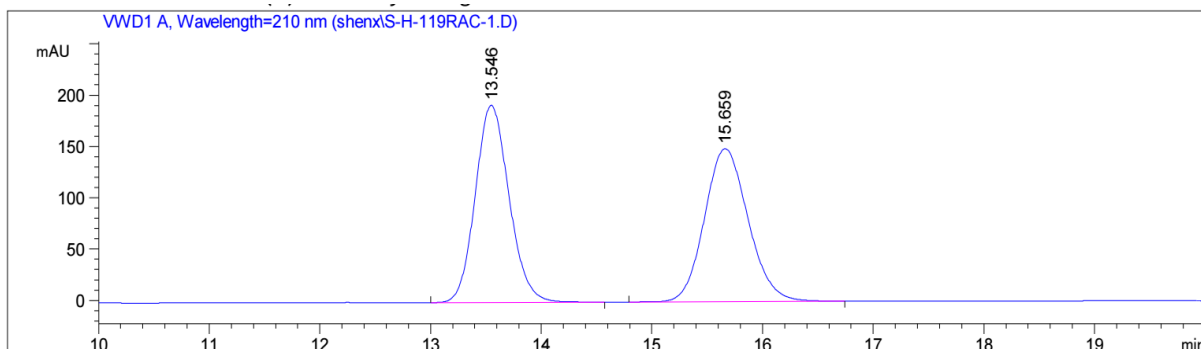
Peak #	RetTime [min]	Type	Width [min]	Area [mAU*s]	Height [mAU]	Area %
1	11.309	MM	0.3257	5150.01660	263.51376	93.5739
2	13.031	BB	0.3621	353.67123	15.09840	6.4261

Figure 76. HPLC traces of *rac*-5b and (*S*)-5b (87% ee).

Statement



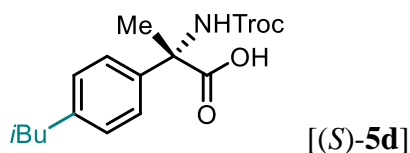
[Chiralpak IG, 25 °C, CH₃CN/H₂O(0.1% TFA) = 50:50, 1.0 mL/min, 210 nm]



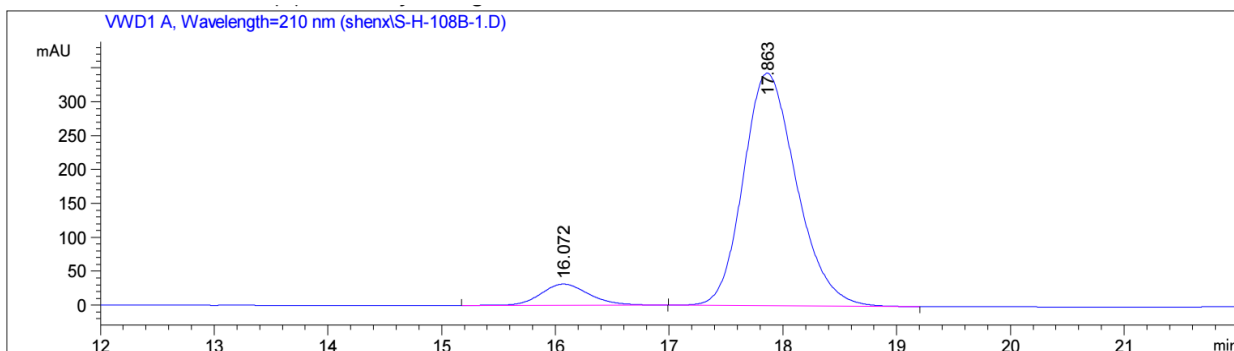
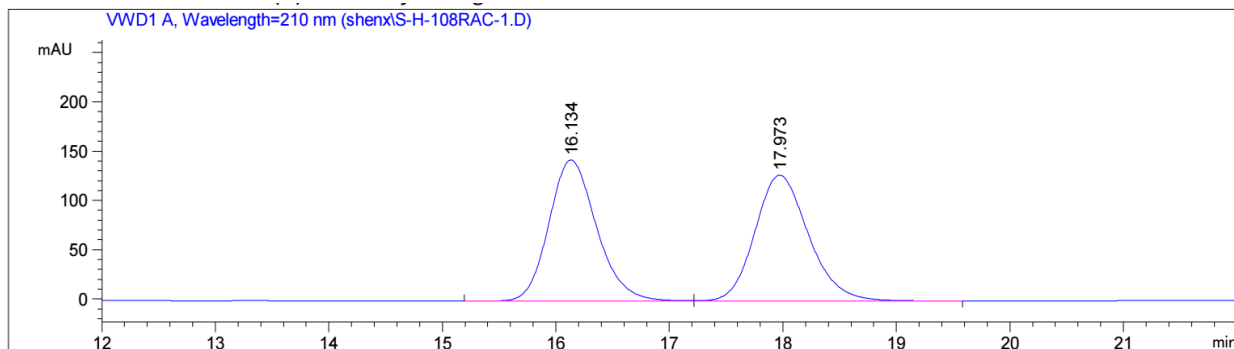
Peak #	RetTime [min]	Type	Width [min]	Area mAU *s	Height [mAU]	Area %
1	13.731	BB	0.3337	6763.45410	312.97281	91.8005
2	15.926	BB	0.4361	604.10345	21.27339	8.1995

Figure 77. HPLC traces of *rac*-5c and (S)-5c (84% ee).

Statement



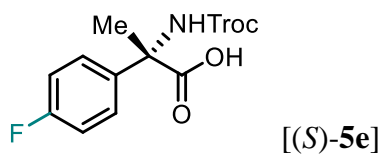
[Chiralpak ODR, 25 °C, CH₃CN/H₂O(0.1% TFA) = 50:50, 1.0 mL/min, 210 nm]



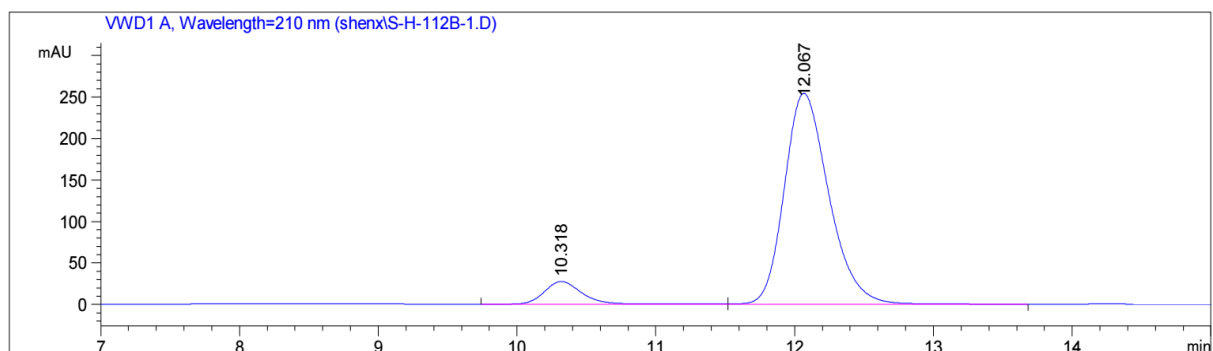
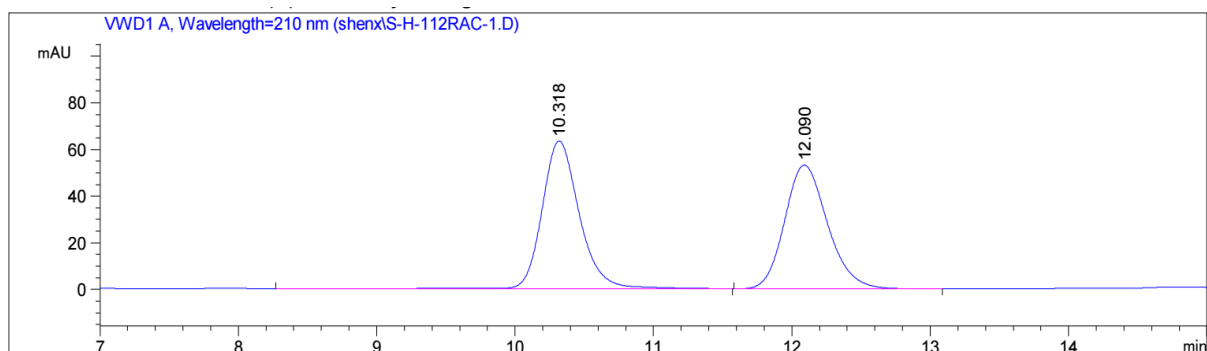
Peak #	RetTime [min]	Type	Width [min]	Area mAU*s	Height [mAU]	Area %
1	16.072	BB	0.4477	906.89819	31.12231	7.5278
2	17.863	BB	0.5026	1.11405e4	343.04327	92.4722

Figure 78. HPLC traces of *rac*-5d and (*S*)-5d (85% ee).

Statement



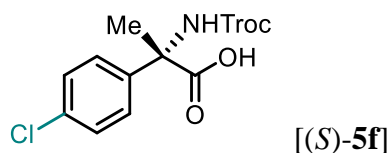
[Chiralpak ODR, 25 °C, CH₃CN/H₂O(0.1% TFA) = 45:55, 1.0 mL/min, 210 nm]



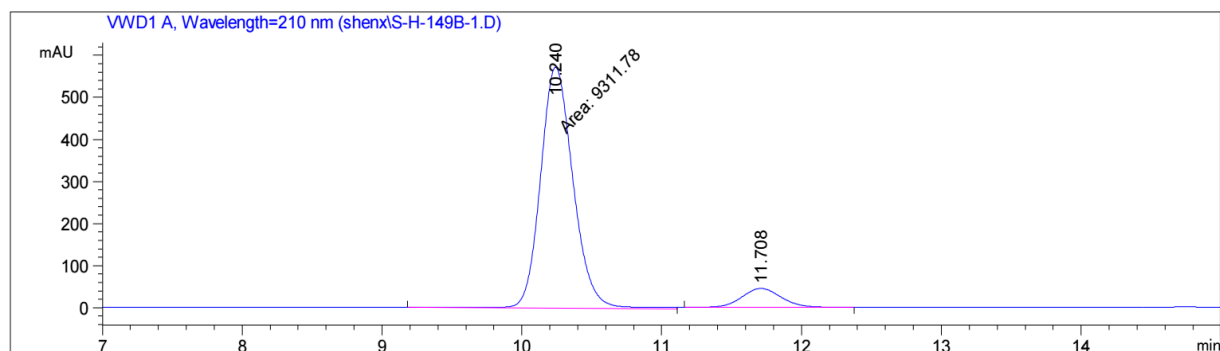
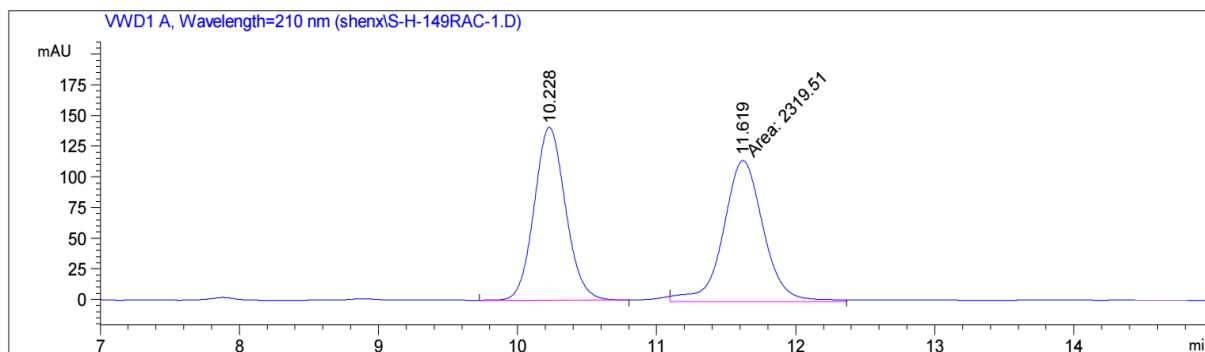
Peak #	RetTime [min]	Type	Width [min]	Area mAU *s	Height [mAU]	Area %
1	10.318	BV R	0.2870	527.83746	27.20548	8.5377
2	12.067	VB	0.3534	5654.60156	253.47838	91.4623

Figure 79. HPLC traces of *rac*-5e and (S)-5e (83% ee).

Statement



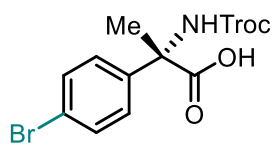
[Chiralpak IG, 25 °C, CH₃CN/H₂O(0.1% TFA) = 50:50, 1.0 mL/min, 210 nm]



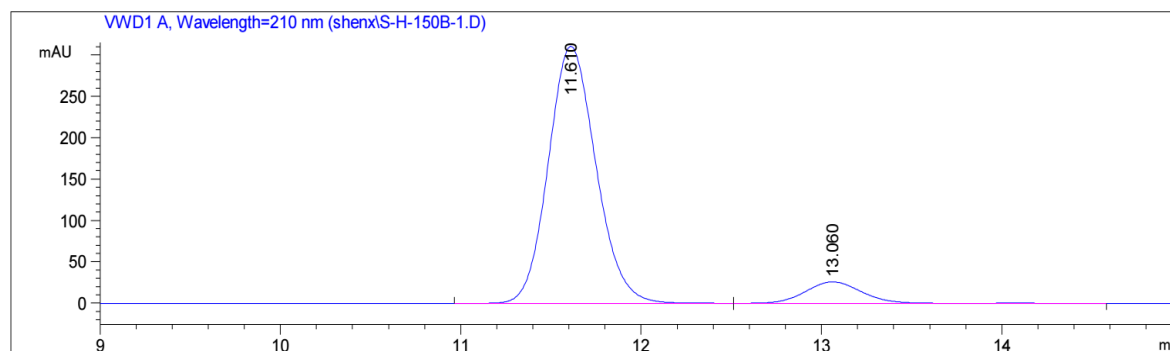
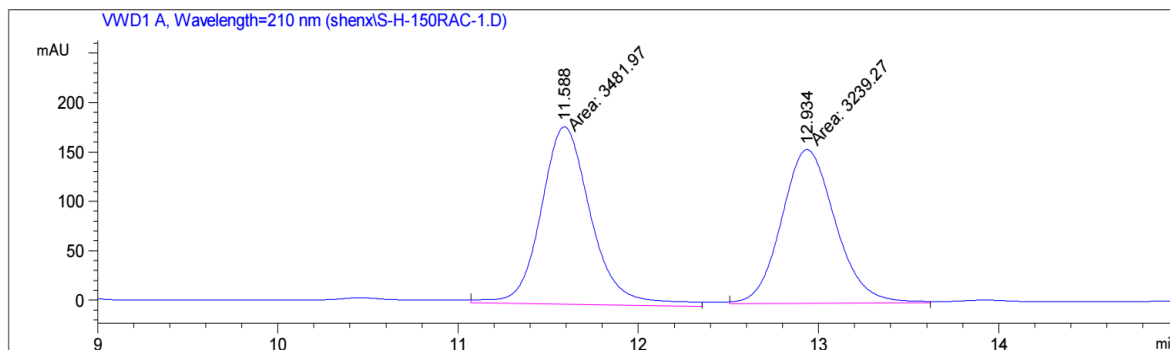
Peak #	RetTime [min]	Type	Width [min]	Area mAU *s	Height [mAU]	Area %
1	10.240	MM	0.2694	9311.78223	576.09467	91.4729
2	11.708	VB	0.3089	868.04834	44.54729	8.5271

Figure 80. HPLC traces of *rac*-5f and (*S*)-5f (83% ee).

Statement



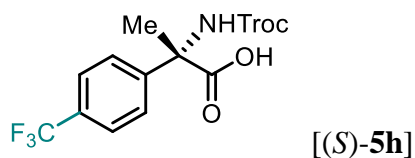
[Chiralpak IG, 25 °C, CH₃CN/H₂O(0.1% TFA) = 50:50, 1.0 mL/min, 210 nm]



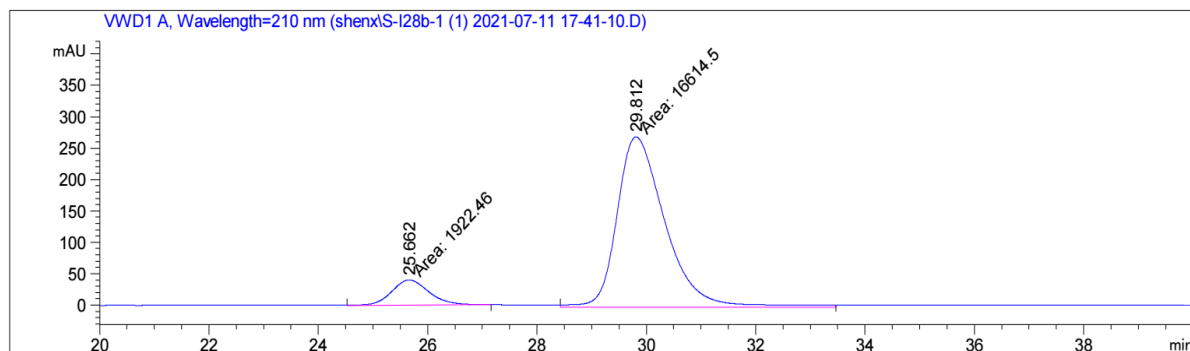
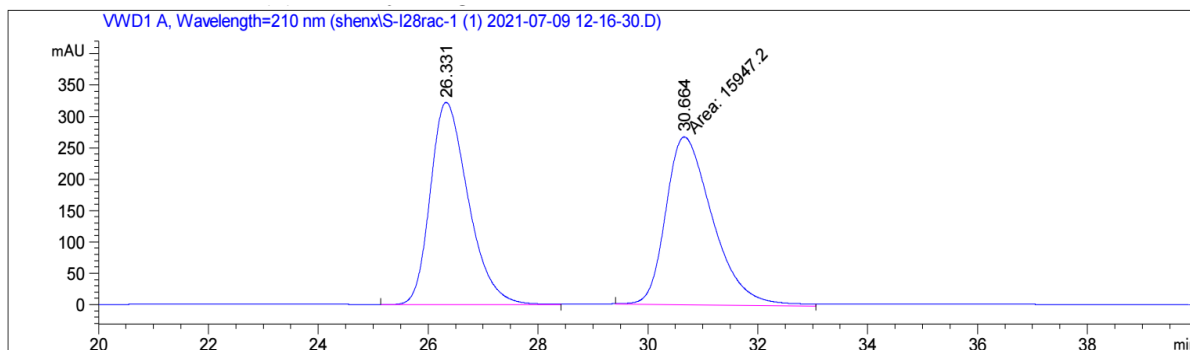
Peak #	RetTime [min]	Type	Width [min]	Area [mAU*s]	Height [mAU]	Area %
1	11.610	BV	0.2857	5709.69141	308.71704	90.9908
2	13.060	VV R	0.3365	565.32635	25.86737	9.0092

Figure 81. HPLC traces of *rac*-5g and (*S*)-5g (82% ee).

Statement



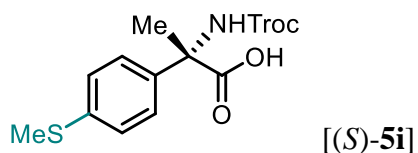
[Chiralpak ODR 25 °C, CH₃CN/H₂O(0.1% TFA) = 40:60, 1.0 mL/min, 210 nm]



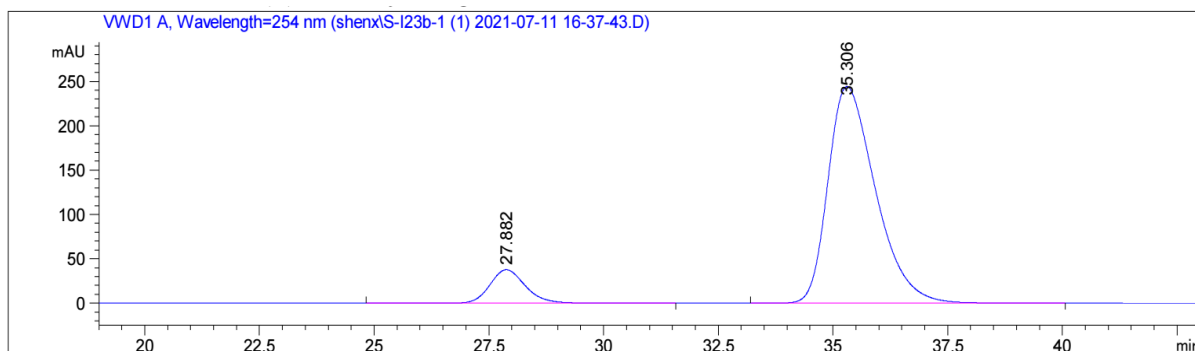
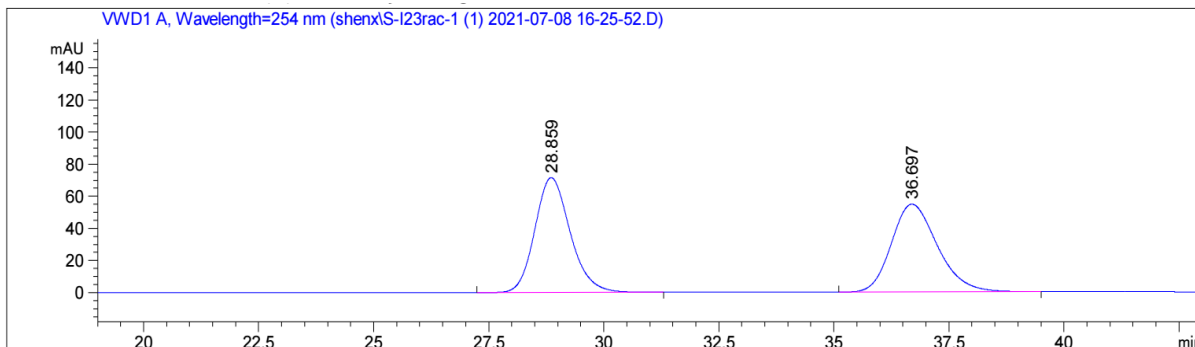
Peak #	RetTime [min]	Type	Width [min]	Area [mAU*s]	Height [mAU]	Area %
1	25.662	MM	0.7963	1922.46326	40.23888	10.3710
2	29.812	MM	1.0218	1.66145e4	270.98953	89.6290

Figure 82. HPLC traces of *rac*-5h and (*S*)-5h (80% ee).

Statement



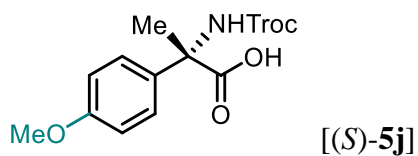
[Chiralpak ODR 25 °C, CH₃CN/H₂O(0.1% TFA) = 40:60, 1.0 mL/min, 210 nm]



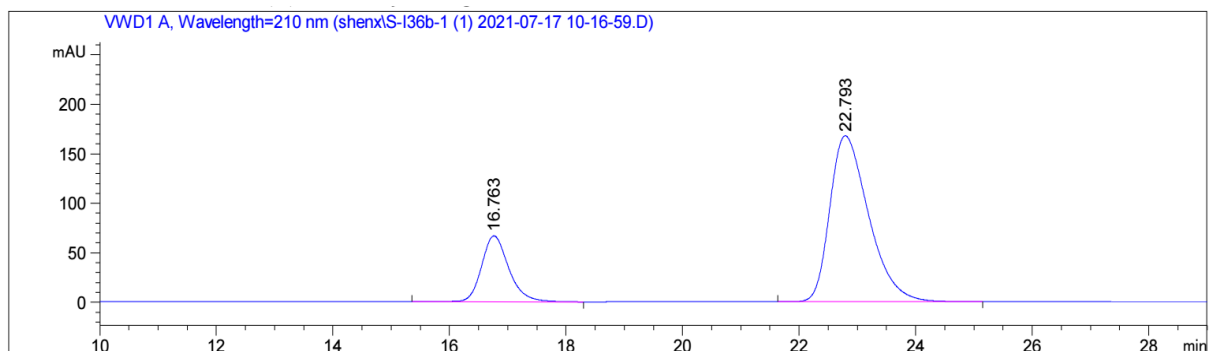
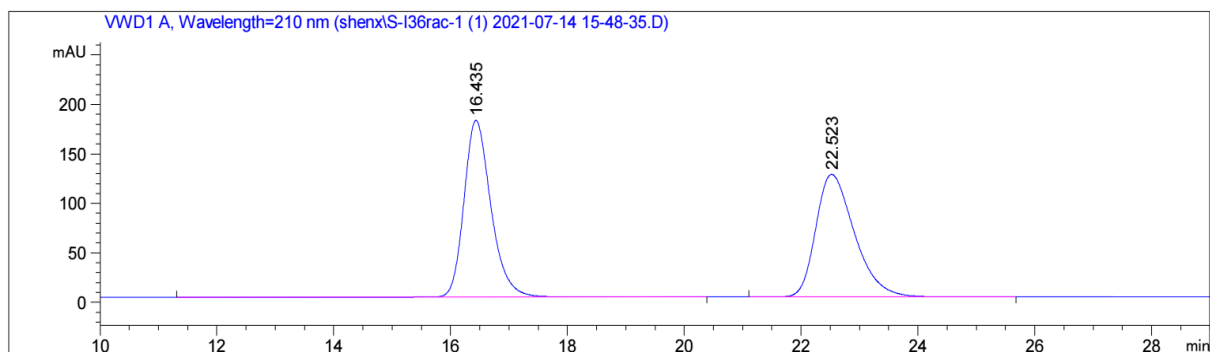
Peak #	RetTime [min]	Type	Width [min]	Area [mAU*s]	Height [mAU]	Area %
1	27.882	BB	0.8222	2013.38916	37.63523	10.2884
2	35.306	BB	1.1077	1.75561e4	243.89500	89.7116

Figure 83. HPLC traces of *rac*-5i and (S)-5i (80% ee).

Statement



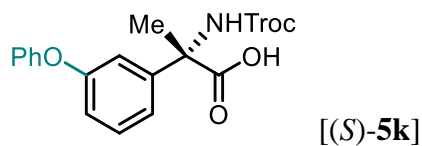
[Chiralpak ODR 25 °C, CH₃CN/H₂O(0.1% TFA) = 40:60, 1.0 mL/min, 210 nm]



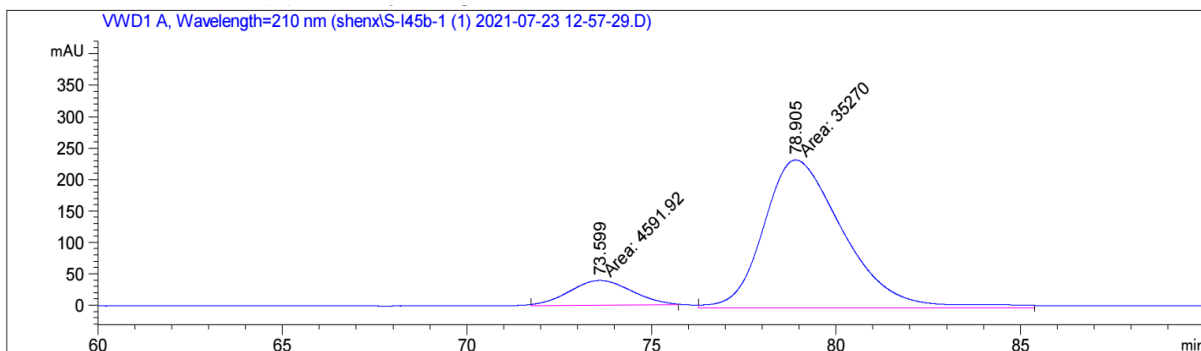
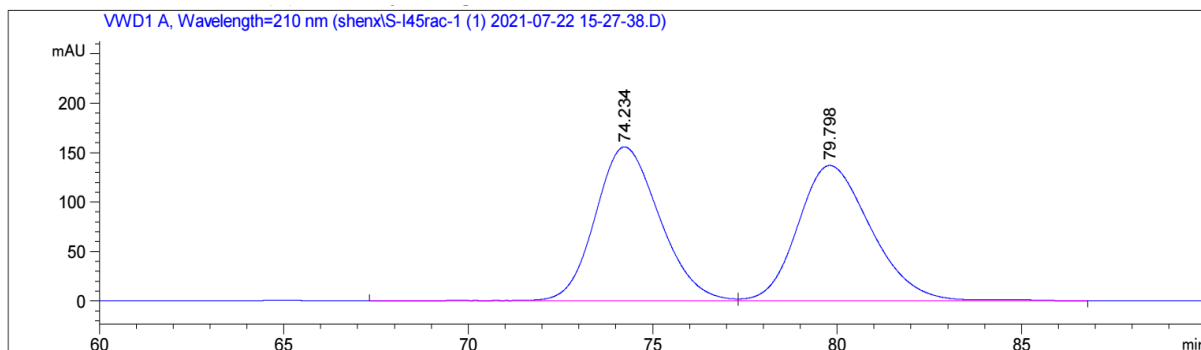
Peak #	RetTime [min]	Type	Width [min]	Area [mAU*s]	Height [mAU]	Area %
1	16.763	BB	0.4946	2148.94800	66.30953	21.7003
2	22.793	BB	0.7153	7753.88623	167.35568	78.2997

Figure 84. HPLC traces of *rac*-5j and (*S*)-5j (56% ee).

Statement



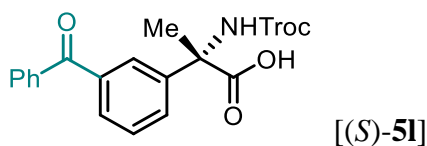
[Chiralpak IG 25 °C, CH₃CN/H₂O(0.1% TFA) = 40:60, 1.0 mL/min, 210 nm]



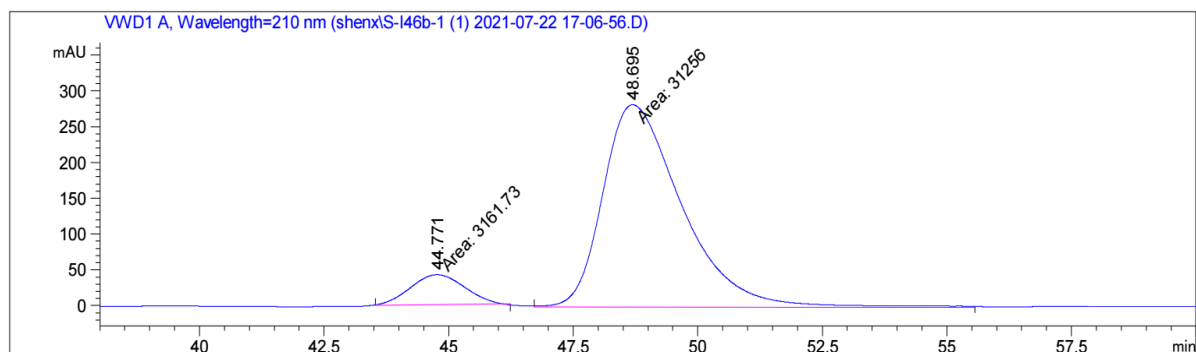
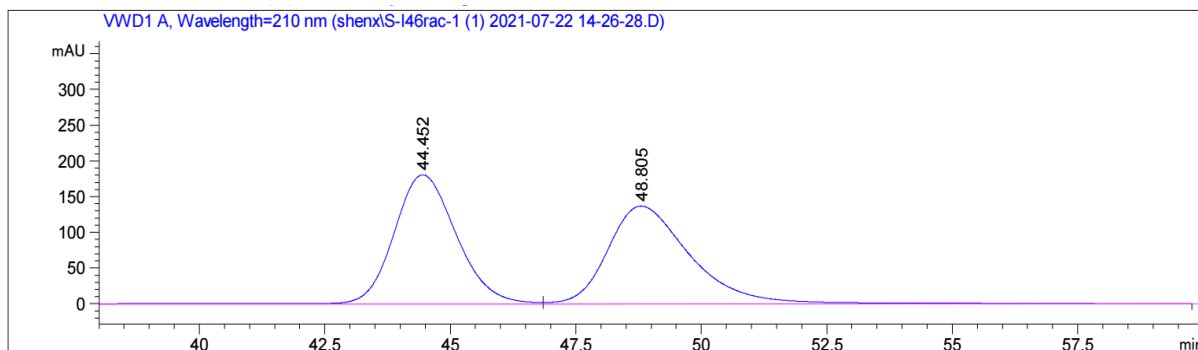
Peak #	RetTime [min]	Type	Width [min]	Area [mAU*s]	Height [mAU]	Area %
1	73.599	MM	1.9525	4591.91797	39.19769	11.5196
2	78.905	MM	2.5013	3.52700e4	235.00708	88.4804

Figure 85. HPLC traces of *rac*-5k and (*S*)-5k (77% ee).

Statement



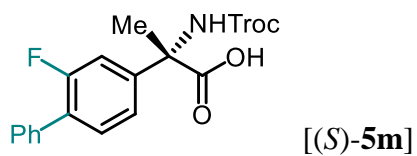
[Chiralpak IG 25 °C, CH₃CN/H₂O(0.1% TFA) = 40:60, 1.0 mL/min, 210 nm]



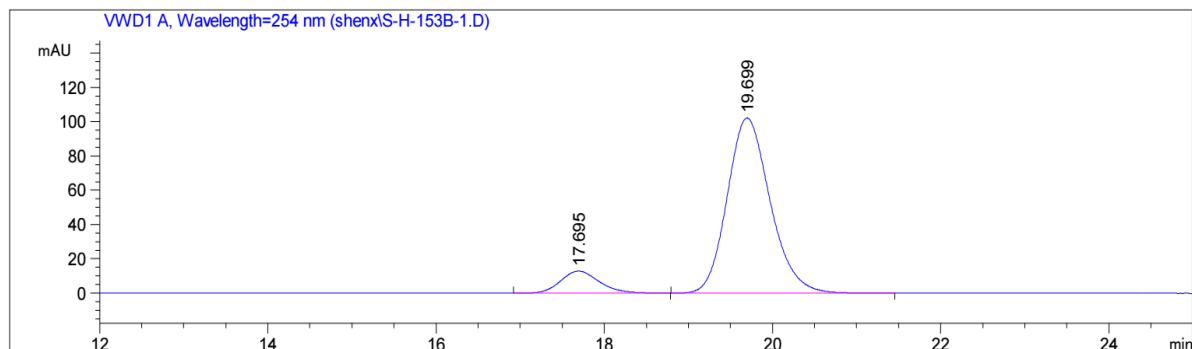
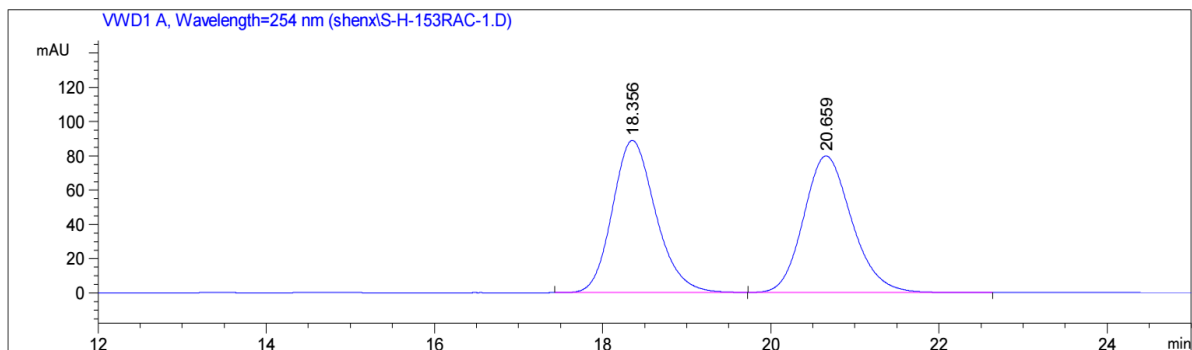
Peak #	RetTime [min]	Type	Width [min]	Area [mAU*s]	Height [mAU]	Area %
1	44.771	MM	1.2567	3161.73096	41.93106	9.1863
2	48.695	MM	1.8439	3.12560e4	282.51120	90.8137

Figure 86. HPLC traces of *rac*-5I and (*S*)-5I (82% ee).

Statement



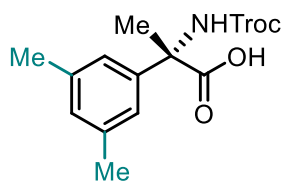
[Chiralpak ODR 25 °C, CH₃CN/H₂O(0.1% TFA) = 50:50, 1.0 mL/min, 210 nm]



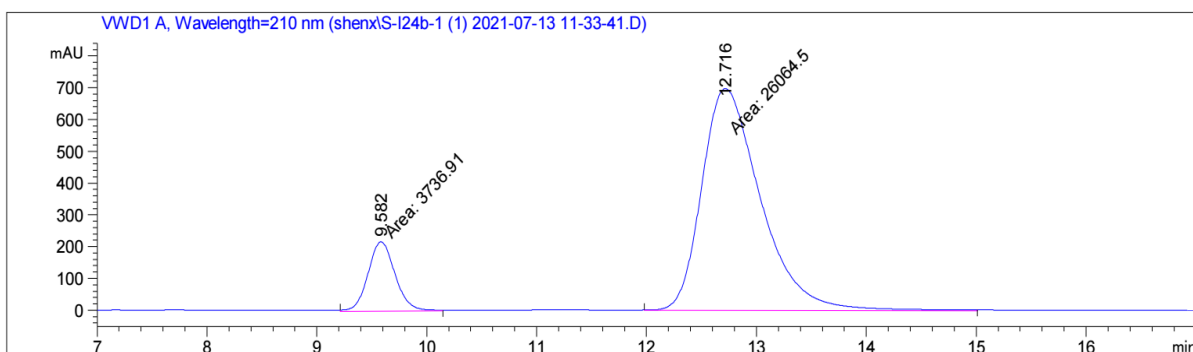
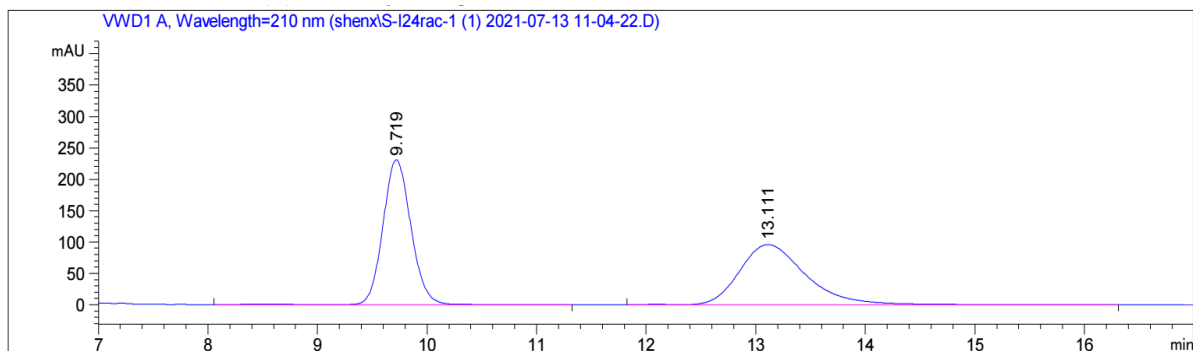
Peak #	RetTime [min]	Type	Width [min]	Area mAU*s	Height [mAU]	Area %
1	17.695	BB	0.4916	409.80869	12.84697	10.1520
2	19.699	BB	0.5435	3626.90430	102.22581	89.8480

Figure 87. HPLC traces of *rac*-5m and (*S*)-5m (80% ee).

Statement



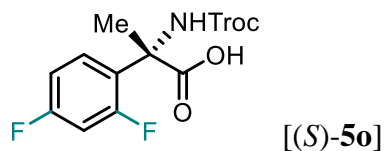
[Chiralpak IG 25 °C, CH₃CN/H₂O(0.1% TFA) = 50:50, 1.0 mL/min, 210 nm]



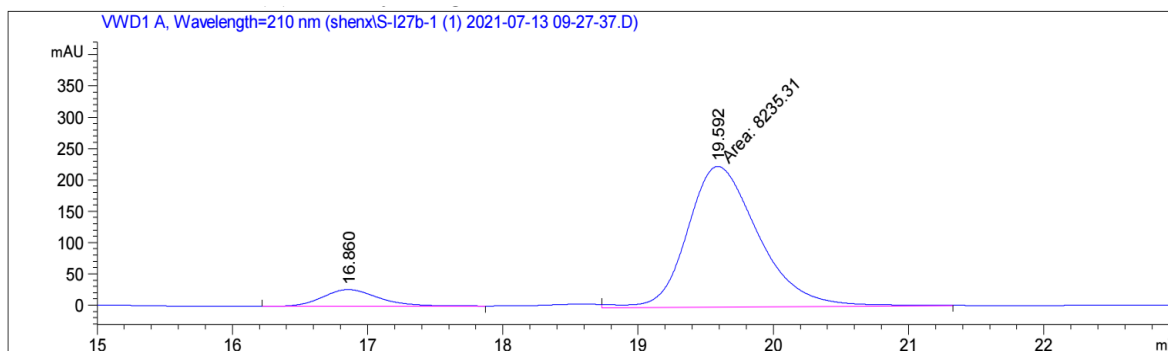
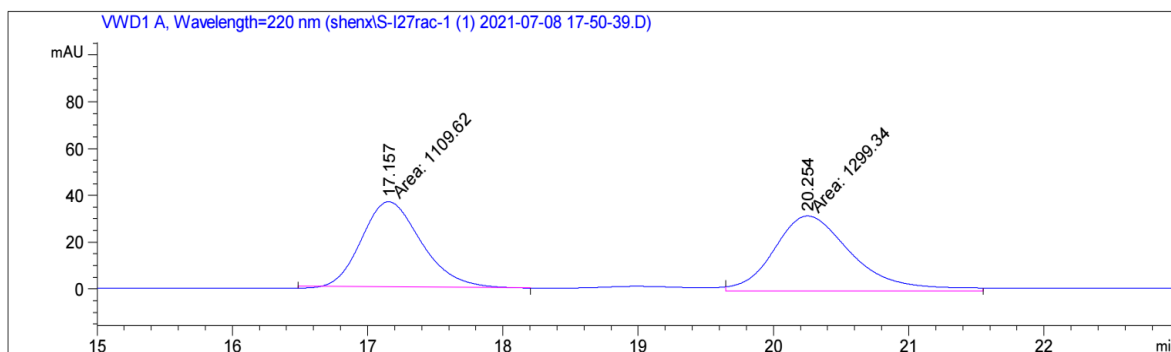
Peak #	RetTime [min]	Type	Width [min]	Area [mAU*s]	Height [mAU]	Area %
1	9.582	MM	0.2842	3736.90503	219.18018	12.5394
2	12.716	MM	0.6215	2.60645e4	699.01160	87.4606

Figure 88. HPLC traces of *rac*-5n and (*S*)-5n (75% ee).

Statement



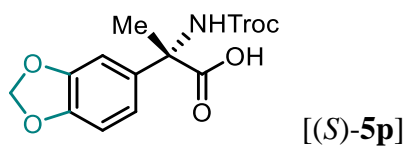
[Chiralpak ODR 25 °C, CH₃CN/H₂O(0.1% TFA) = 40:60, 1.0 mL/min, 210 nm]



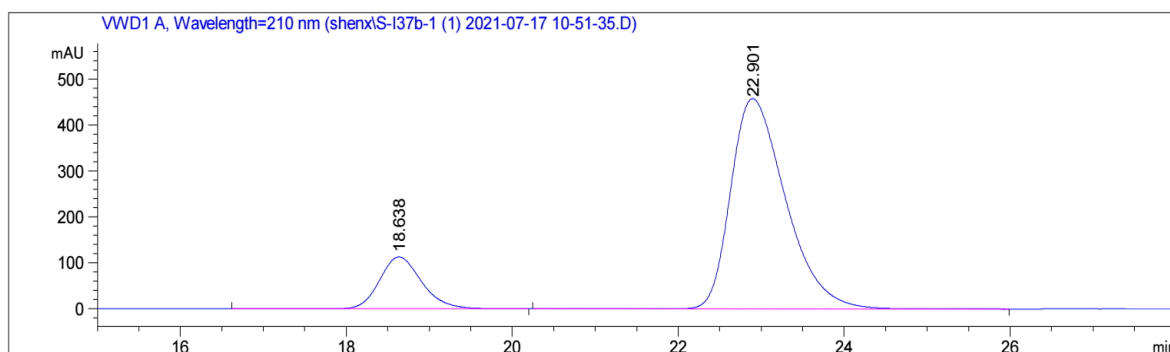
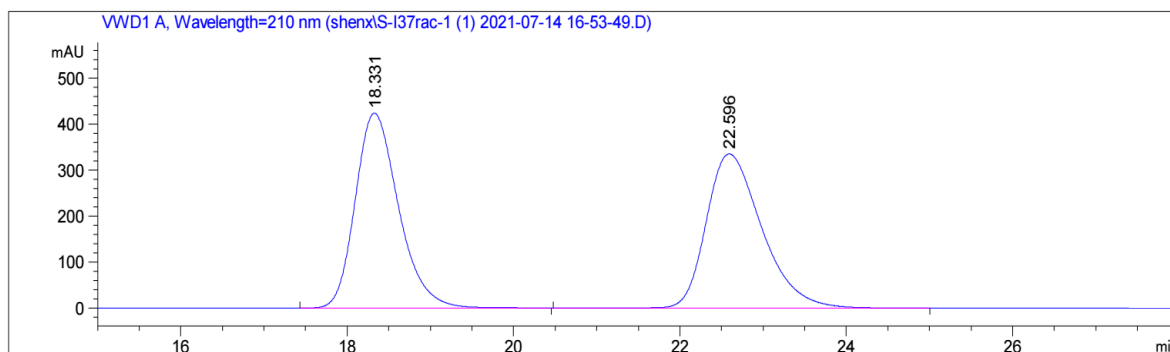
Peak #	RetTime [min]	Type	Width [min]	Area [mAU*s]	Height [mAU]	Area %
1	16.860	BB	0.4400	763.33478	26.56698	8.4828
2	19.592	MM	0.6105	8235.31348	224.83655	91.5172

Figure 89. HPLC traces of *rac*-5o and (*S*)-5o (83% ee).

Statement



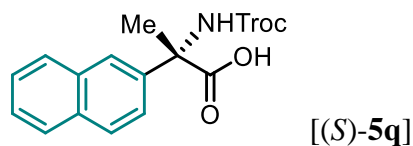
[Chiralpak ODR 25 °C, CH₃CN/H₂O(0.1% TFA) = 40:60, 1.0 mL/min, 210 nm]



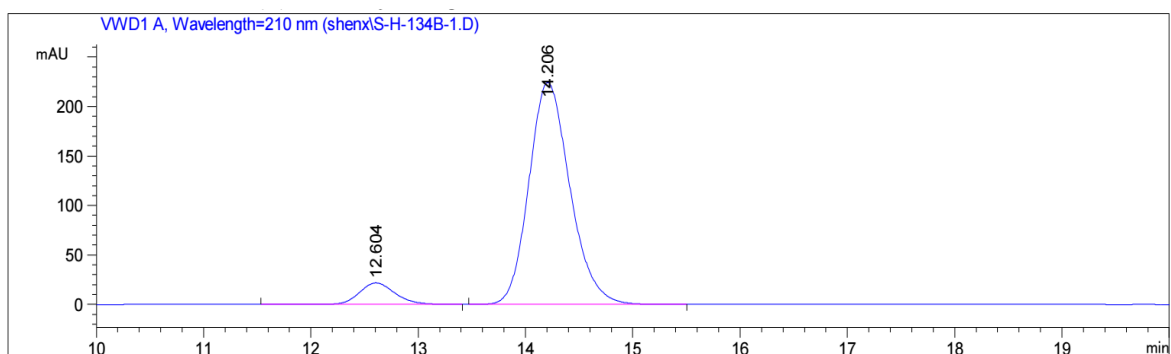
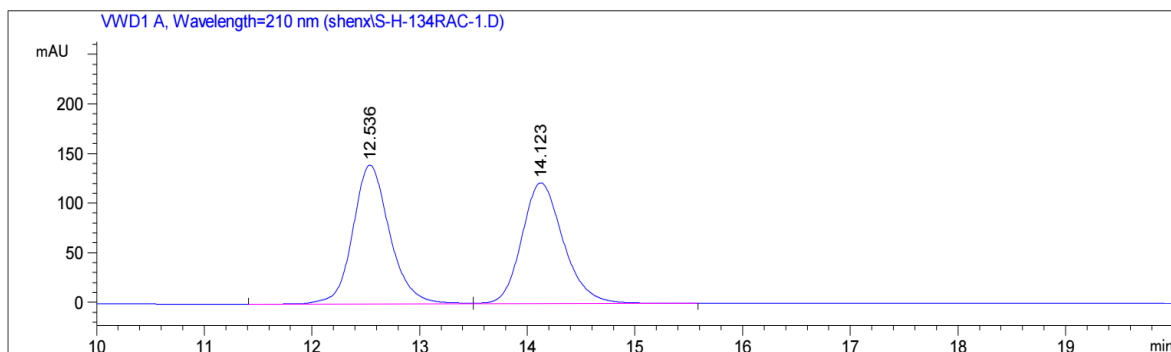
Peak #	RetTime [min]	Type	Width [min]	Area [mAU*s]	Height [mAU]	Area %
1	18.638	BB	0.5517	3983.67383	112.81755	15.9387
2	22.901	BB	0.7106	2.10100e4	457.44217	84.0613

Figure 90. HPLC traces of *rac*-5p and (*S*)-5p (68% ee).

Statement



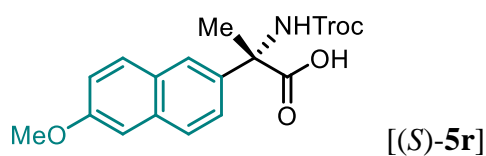
[Chiralpak ODR 25 °C, CH₃CN/H₂O(0.1% TFA) = 50:50, 1.0 mL/min, 210 nm]



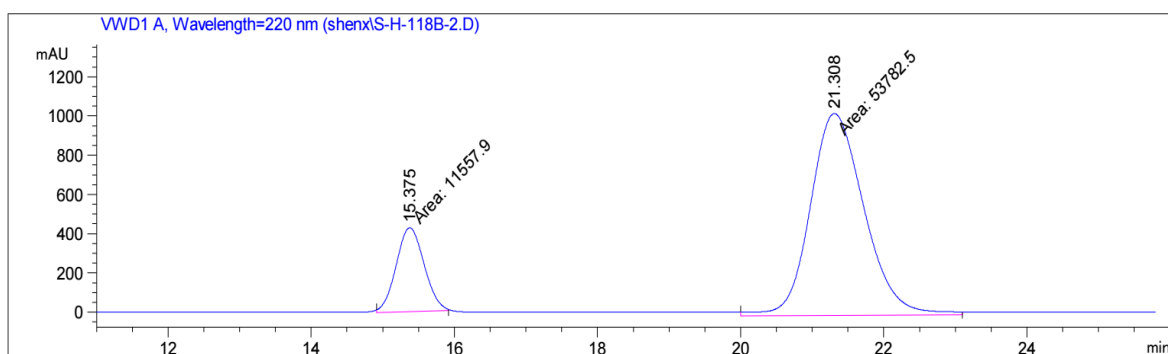
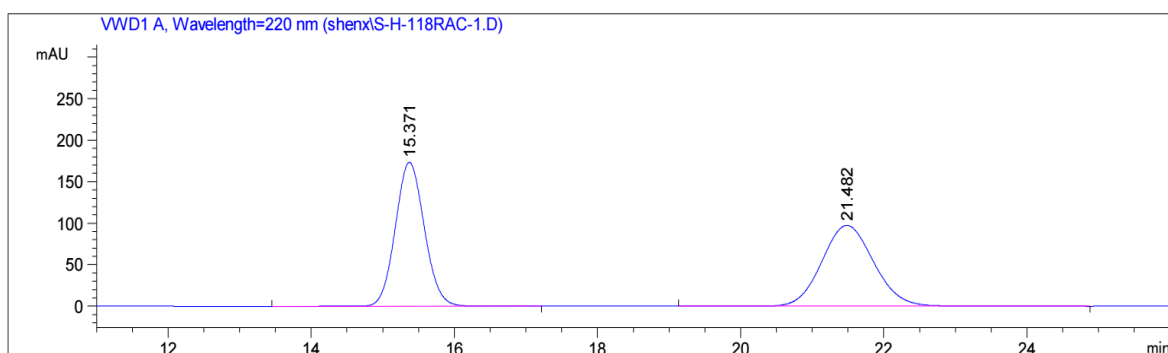
Peak #	RetTime [min]	Type	Width [min]	Area mAU *s	Height [mAU]	Area %
1	12.604	BB	0.3545	504.67804	21.79936	7.8089
2	14.206	BB	0.4089	5958.14404	224.31985	92.1911

Figure 91. HPLC traces of *rac*-5q and (*S*)-5q (84% ee).

Statement



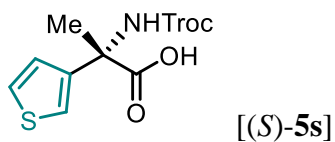
[Chiralpak IG 25 °C, CH₃CN/H₂O(0.1% TFA) = 50:50, 1.0 mL/min, 210 nm]



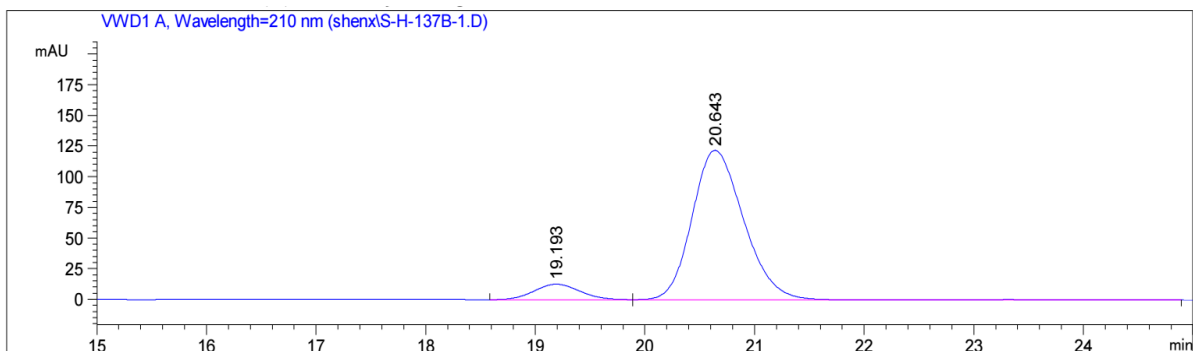
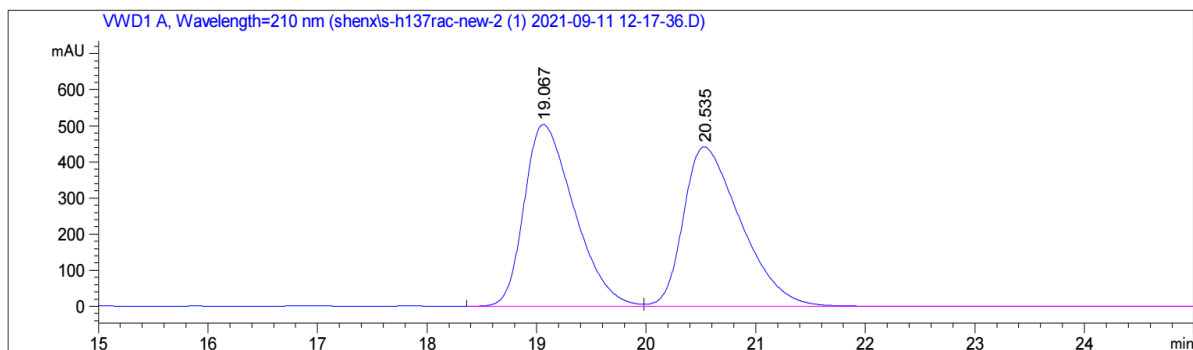
Peak #	RetTime [min]	Type	Width [min]	Area mAU *s	Height [mAU]	Area %
1	15.375	MM	0.4501	1.15579e4	427.99649	17.6888
2	21.308	MM	0.8713	5.37825e4	1028.72754	82.3112

Figure 92. HPLC traces of *rac*-5r and (*S*)-5r (64% ee).

Statement



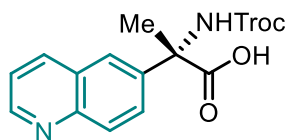
[Chiralpak IG 25 °C, CH₃CN/H₂O(0.1% TFA) = 40:60, 1.0 mL/min, 210 nm]



Peak #	RetTime [min]	Type	Width [min]	Area mAU *s	Height [mAU]	Area %
1	19.193	BV	0.4557	365.28436	12.56194	8.3787
2	20.643	VV R	0.5091	3994.40845	121.70975	91.6213

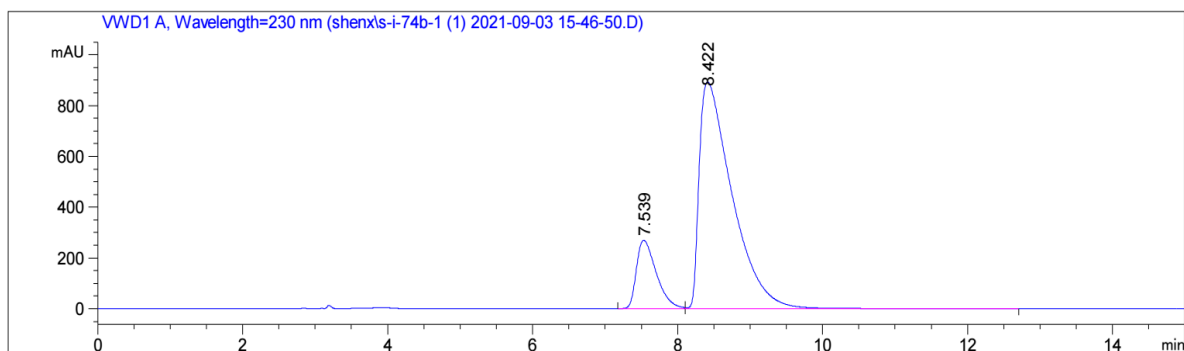
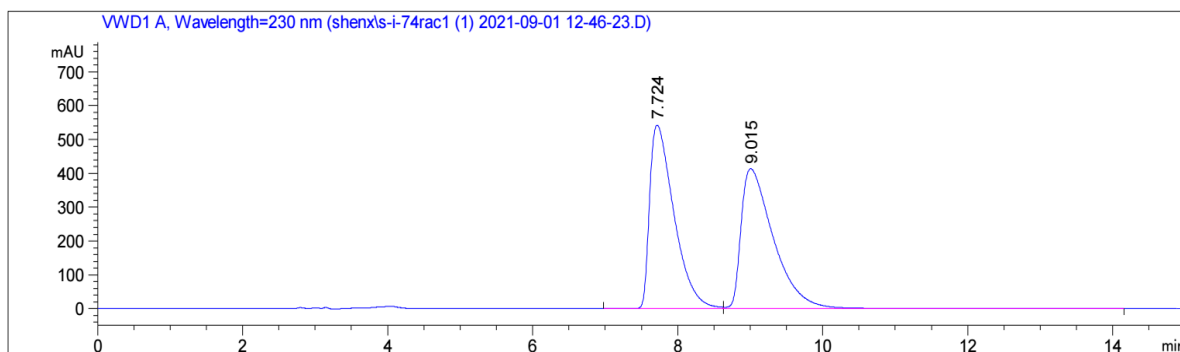
Figure 93. HPLC traces of *rac*-5s and (*S*)-5s (83% ee).

Statement



[(*S*)-5t]

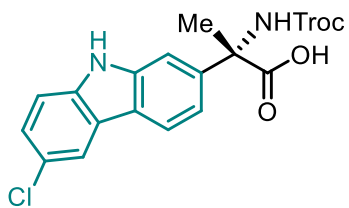
[Chiralpak ODR 25 °C, CH₃CN/H₂O(0.1% TFA) = 20:80, 1.0 mL/min, 210 nm]



Peak #	RetTime [min]	Type	Width [min]	Area [mAU*s]	Height [mAU]	Area %
1	7.539	BV	0.3057	5118.42969	266.41144	15.4386
2	8.422	VB	0.4700	2.80350e4	895.77081	84.5614

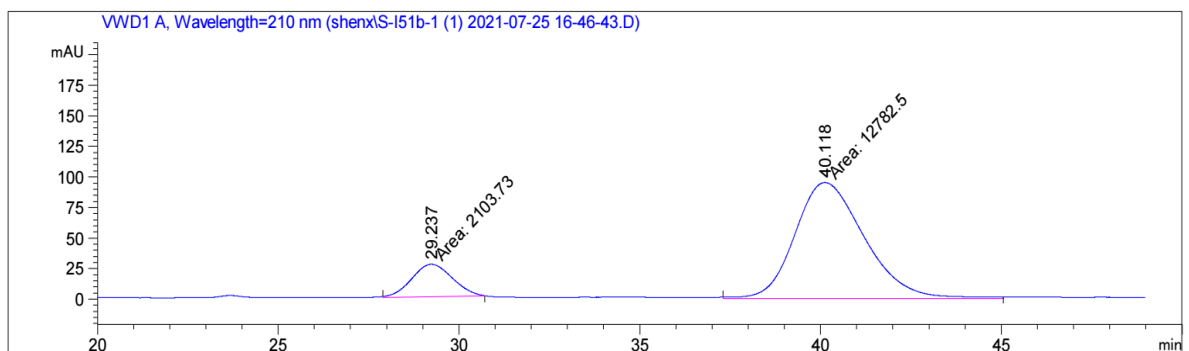
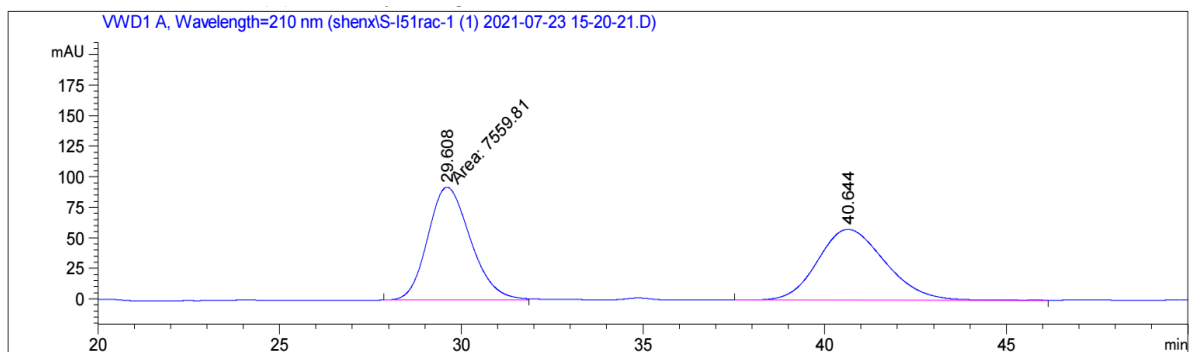
Figure 94. HPLC traces of *rac*-5t and (*S*)-5t (70% ee).

Statement



[(S)-5u]

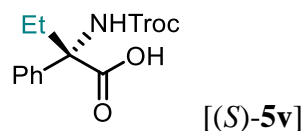
[Chiralpak IG 25 °C, CH₃CN/H₂O(0.1% TFA) = 50:50, 1.0 mL/min, 210 nm]



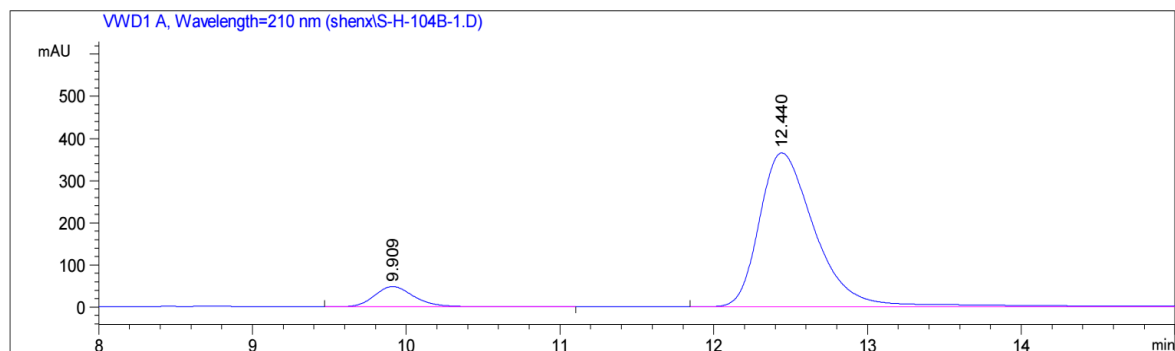
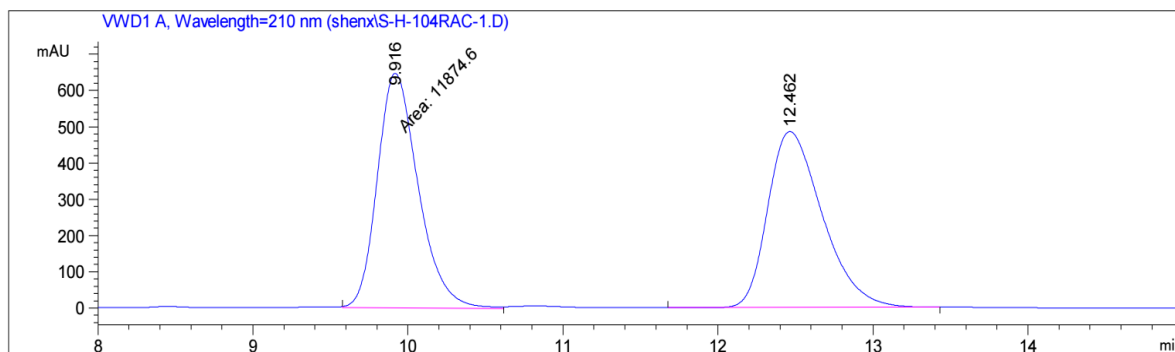
Peak #	RetTime [min]	Type	Width [min]	Area [mAU*s]	Height [mAU]	Area %
1	29.237	MM	1.3120	2103.73096	26.72359	14.1321
2	40.118	MM	2.2407	1.27825e4	95.07812	85.8679

Figure 95. HPLC traces of *rac*-5u and (S)-5u (72% ee).

Statement



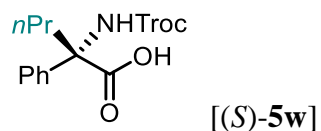
[Chiralpak ODR 25 °C, CH₃CN/H₂O(0.1% TFA) = 50:50, 1.0 mL/min, 210 nm]



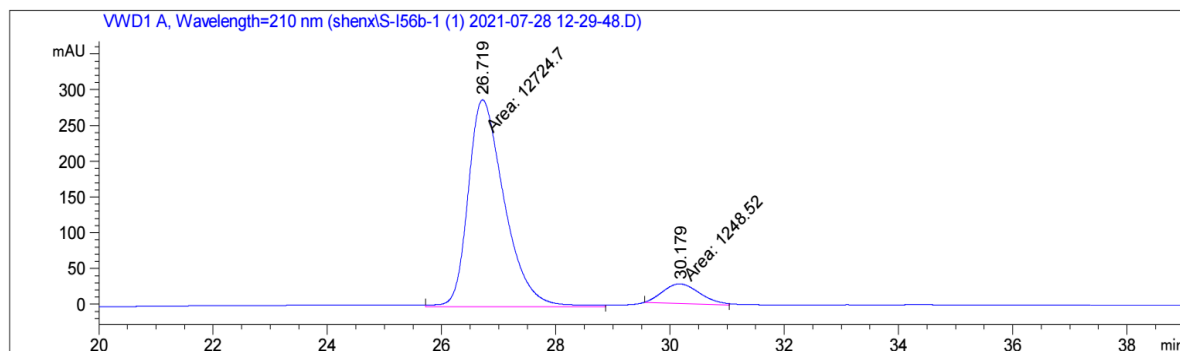
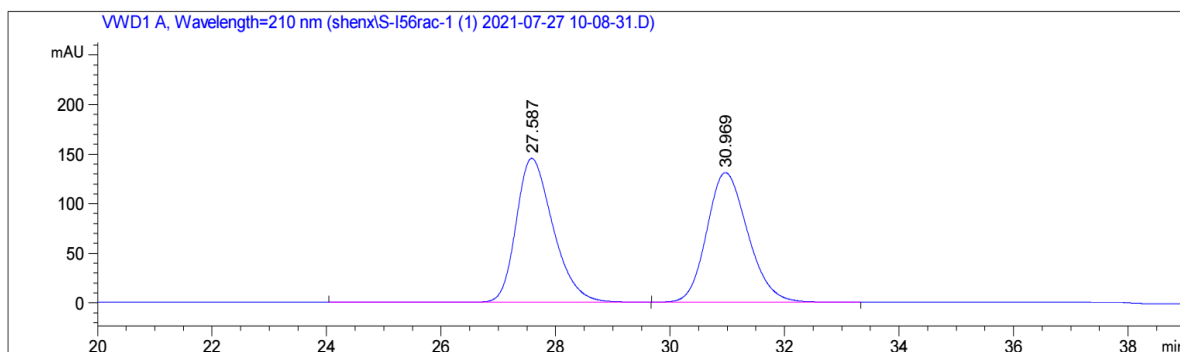
Peak #	RetTime [min]	Type	Width [min]	Area mAU *s	Height [mAU]	Area %
1	9.909	BB	0.2740	868.55566	48.27034	8.5077
2	12.440	BB	0.3888	9340.53027	364.99005	91.4923

Figure 96. HPLC traces of *rac*-5v and (*S*)-5v (83% ee).

Statement



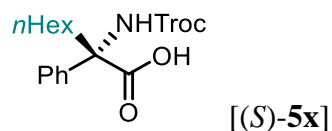
[Chiralpak IG 25 °C, CH₃CN/H₂O(0.1% TFA) = 40:60, 1.0 mL/min, 210 nm]



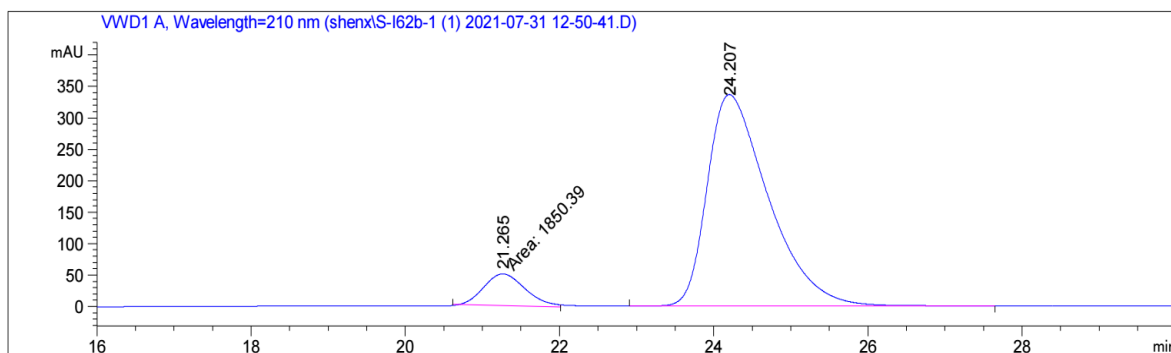
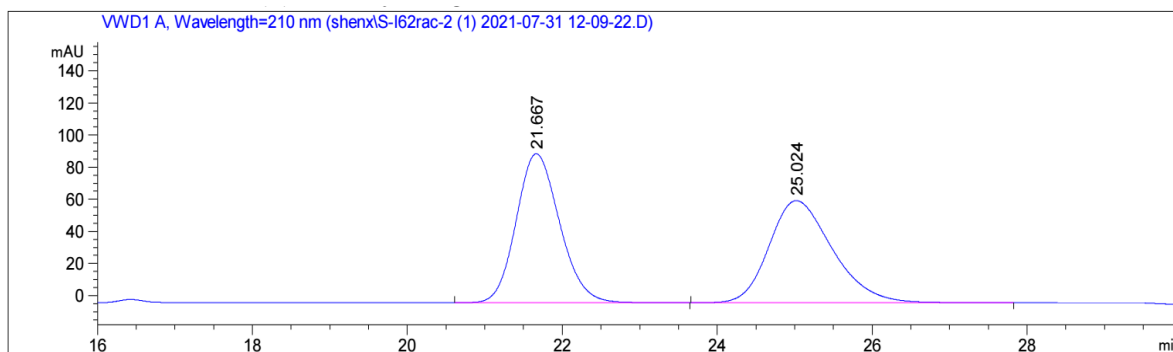
Peak #	RetTime [min]	Type	Width [min]	Area [mAU*s]	Height [mAU]	Area %
1	26.719	MM	0.7333	1.27247e4	289.19965	91.0649
2	30.179	MM	0.7556	1248.51733	27.53798	8.9351

Figure 97. HPLC traces of *rac*-5w and (*S*)-5w (82% ee).

Statement



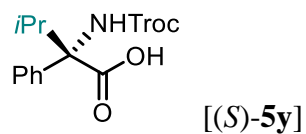
[Chiralpak IG 25 °C, CH₃CN/H₂O(0.1% TFA) = 50:50, 1.0 mL/min, 210 nm]



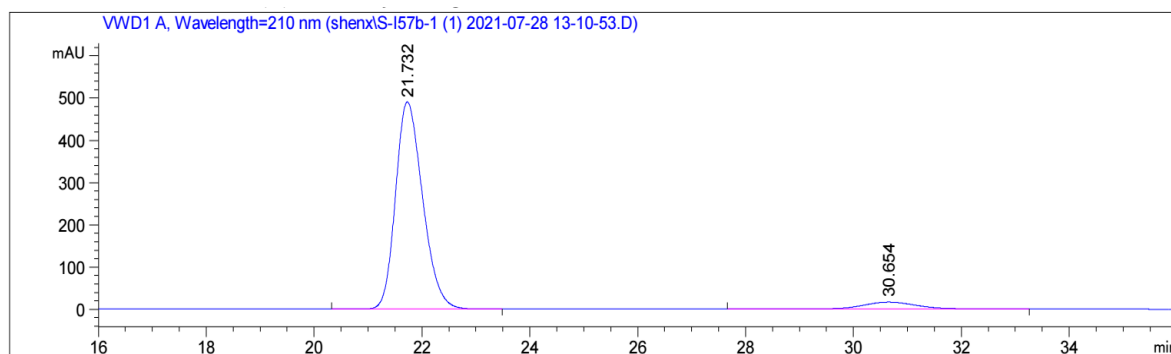
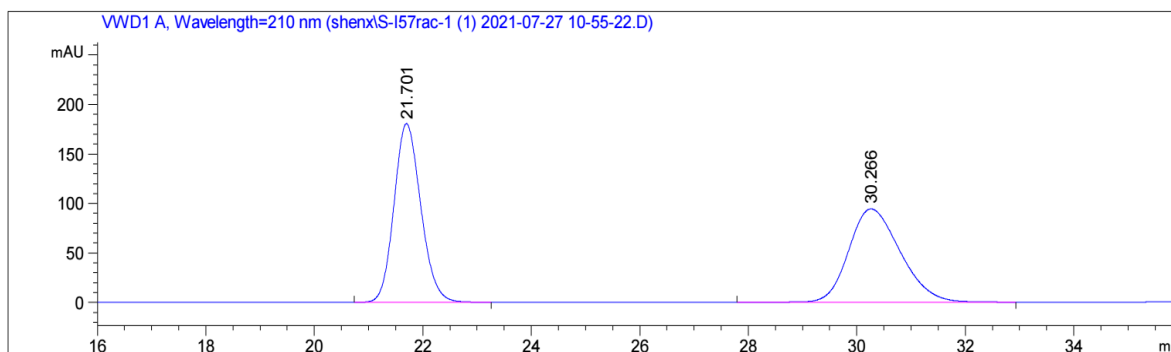
Peak #	RetTime [min]	Type	Width [min]	Area [mAU*s]	Height [mAU]	Area %
1	21.265	MM	0.6167	1850.38843	50.00418	9.0832
2	24.207	BB	0.8294	1.85211e4	336.01141	90.9168

Figure 98. HPLC traces of *rac*-5x and (S)-5x (82% ee).

Statement



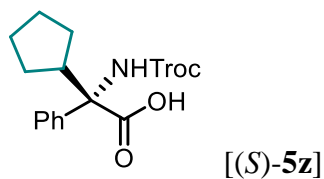
[Chiralpak IG 25 °C, CH₃CN/H₂O(0.1% TFA) = 40:60, 1.0 mL/min, 210 nm]



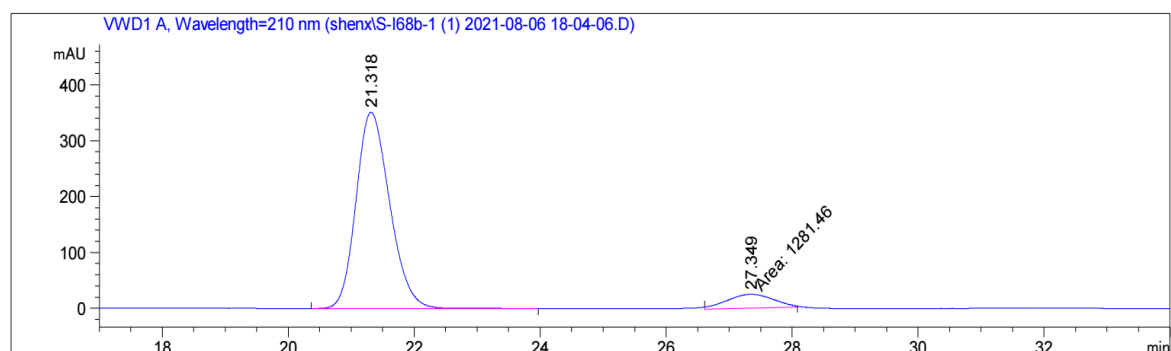
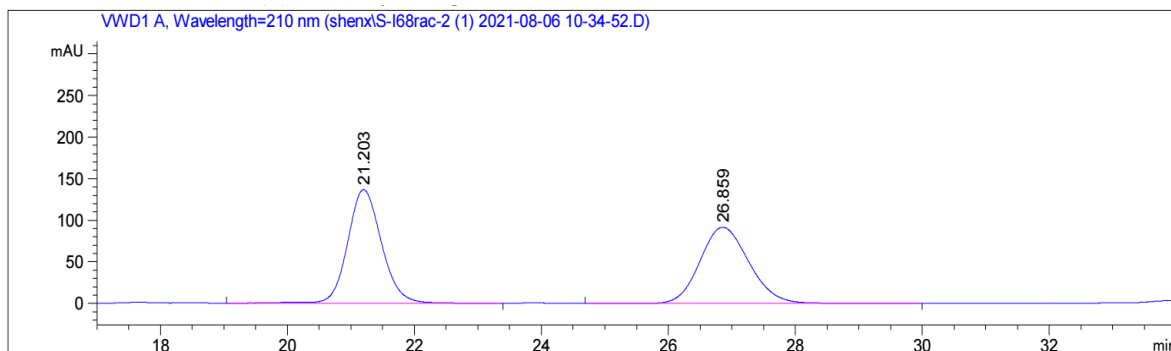
Peak #	RetTime [min]	Type	Width [min]	Area [mAU*s]	Height [mAU]	Area %
1	21.732	BB	0.5470	1.70991e4	489.87143	93.9678
2	30.654	BB	1.0575	1097.67285	16.21961	6.0322

Figure 99. HPLC traces of *rac*-5y and (*S*)-5y (88% ee).

Statement



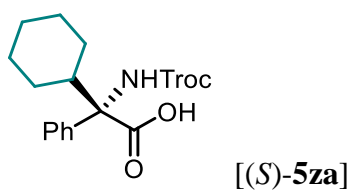
[Chiralpak IG 25 °C, CH₃CN/H₂O(0.1% TFA) = 45:55, 1.0 mL/min, 210 nm]



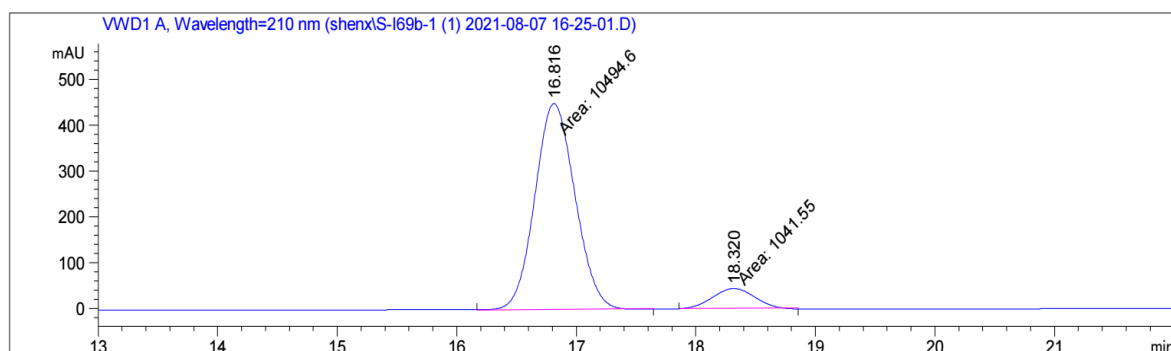
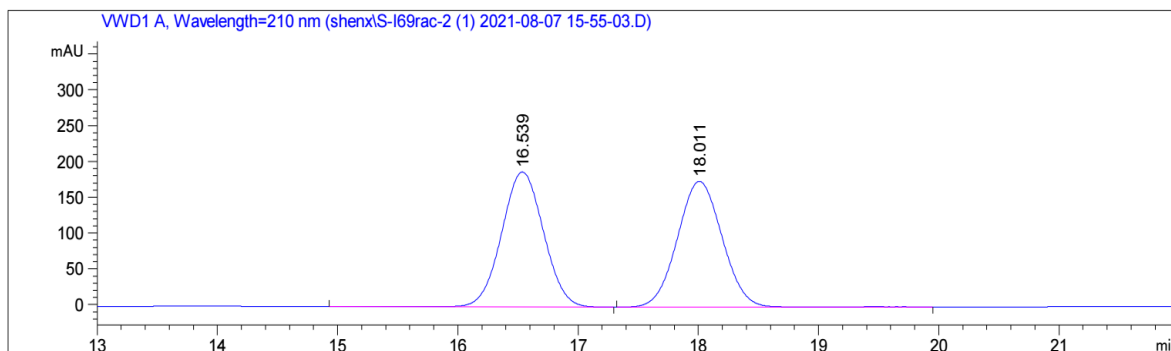
Peak #	RetTime [min]	Type	Width [min]	Area [mAU*s]	Height [mAU]	Area %
1	21.318	BB	0.5734	1.30402e4	350.85791	91.0523
2	27.349	MM	0.8554	1281.45679	24.96921	8.9477

Figure 100. HPLC traces of *rac*-5z and (S)-5z (82% ee).

Statement



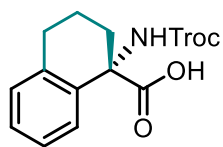
[Chiralpak IB 25 °C, CH₃CN/H₂O(0.1% TFA) = 50:50, 1.0 mL/min, 210 nm]



Peak #	RetTime [min]	Type	Width [min]	Area [mAU*s]	Height [mAU]	Area %
1	16.816	MM	0.3887	1.04946e4	450.03207	90.9714
2	18.320	MM	0.3995	1041.55359	43.44965	9.0286

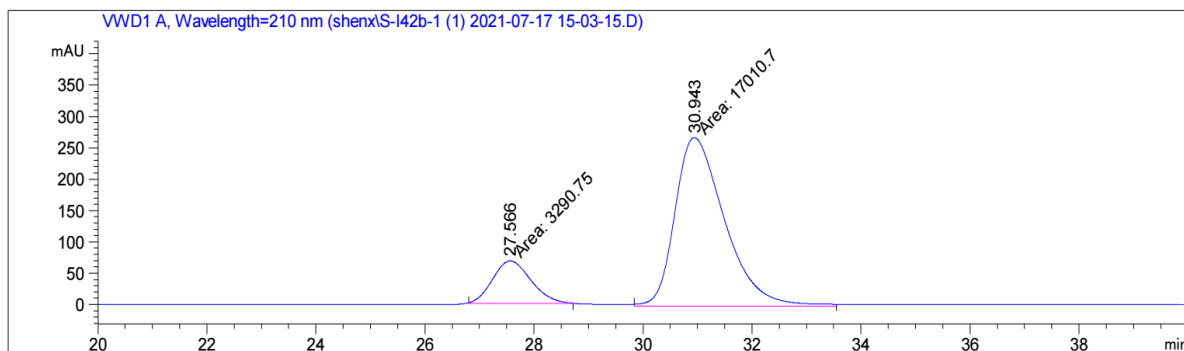
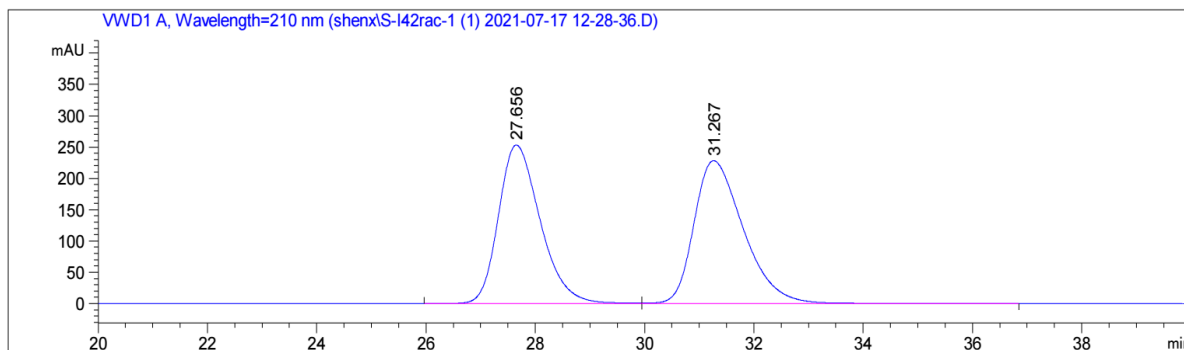
Figure 101. HPLC traces of *rac*-5za and (*S*)-5za (82% ee).

Statement



[(S)-5zb]

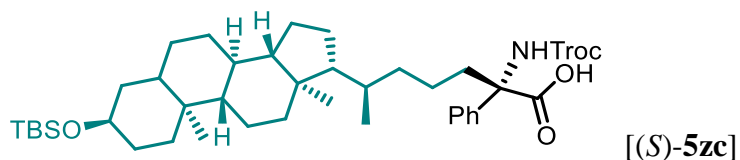
[Chiralpak ODR 25 °C, CH₃CN/H₂O(0.1% TFA) = 40:60, 1.0 mL/min, 210 nm]



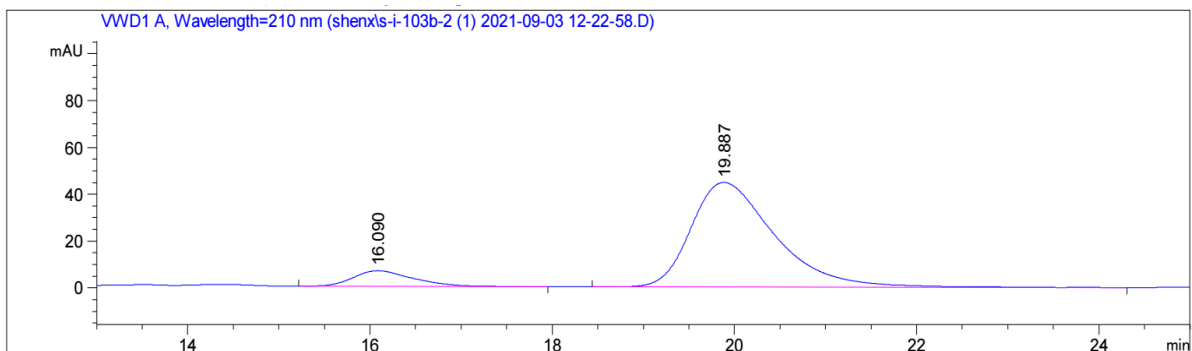
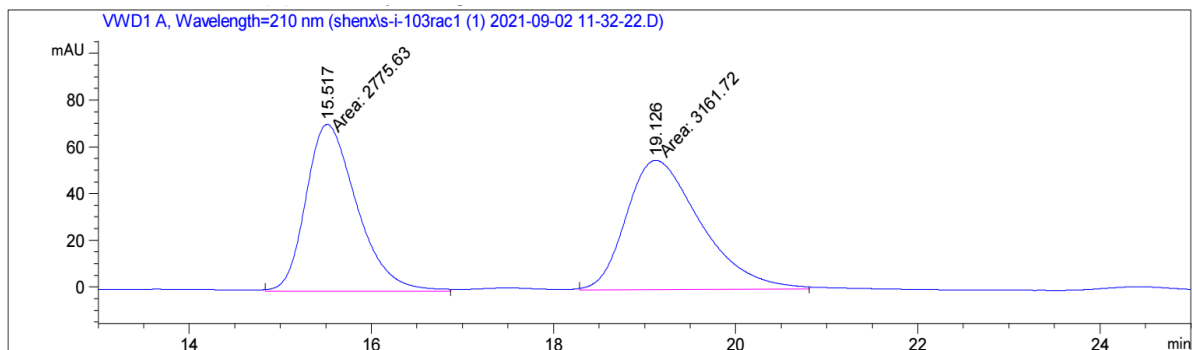
Peak #	RetTime [min]	Type	Width [min]	Area [mAU*s]	Height [mAU]	Area %
1	27.566	MM	0.8118	3290.74731	67.56148	16.2094
2	30.943	MM	1.0546	1.70107e4	268.83868	83.7906

Figure 102. HPLC traces of *rac*-5zb and (*S*)-5zb (68% ee).

Statement



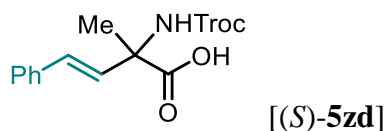
[Chiralpak ODR 25 °C, CH₃CN/H₂O(0.1% TFA) = 80:20, 1.0 mL/min, 210 nm]



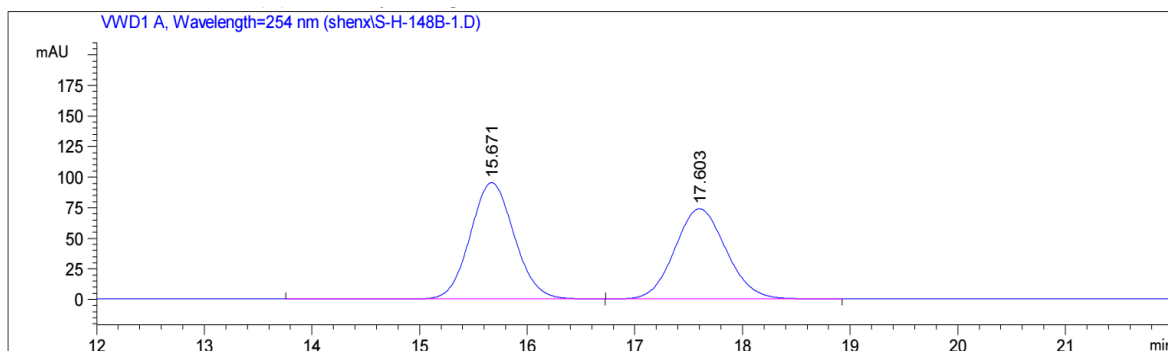
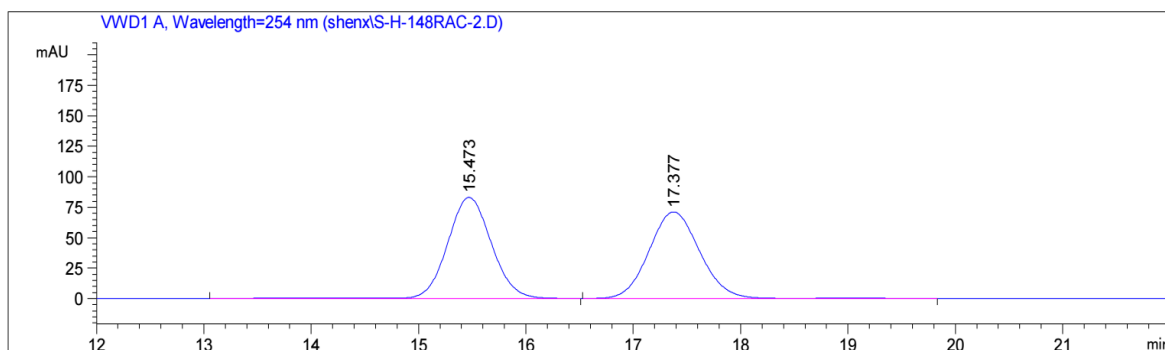
Peak #	RetTime [min]	Type	Width [min]	Area [mAU*s]	Height [mAU]	Area %
1	16.090	BB	0.6800	310.76590	6.71174	9.7943
2	19.887	BV R	0.9691	2862.15869	44.65594	90.2057

Figure 103. HPLC traces of *rac*-5zc and (*S*)-5zc (90:10 dr).

Statement



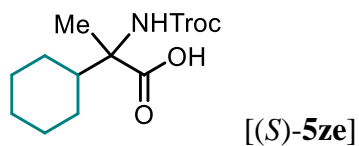
[Chiralpak IG 25 °C, CH₃CN/H₂O(0.1% TFA) = 45:55, 1.0 mL/min, 210 nm]



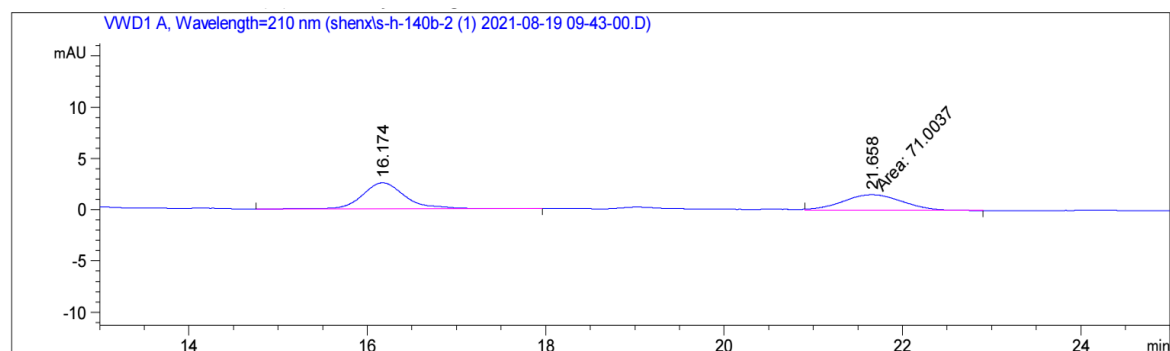
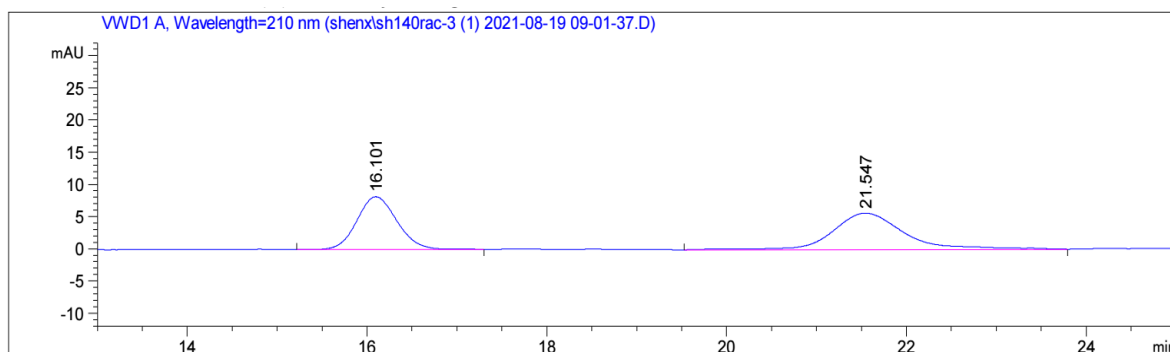
Peak #	RetTime [min]	Type	Width [min]	Area mAU *s	Height [mAU]	Area %
1	15.671	VB R	0.4380	2712.53589	94.99095	52.5770
2	17.603	BB	0.5156	2446.63550	73.66966	47.4230

Figure 104. HPLC traces of *rac*-5zd and (*S*)-5zd (5% ee).

Statement



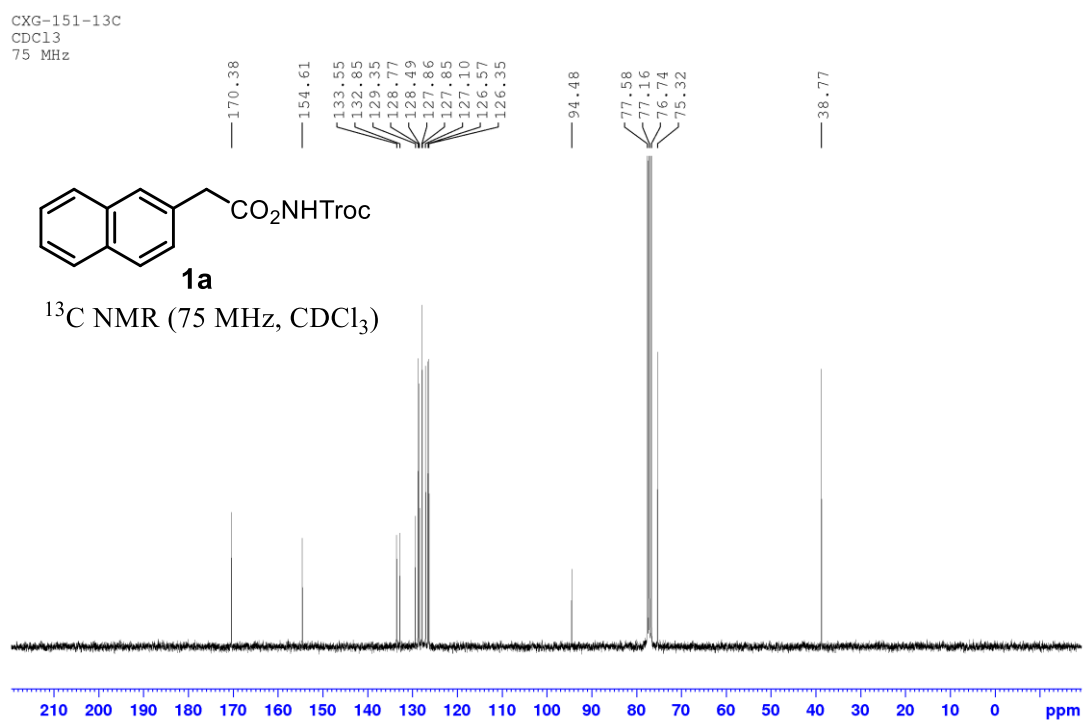
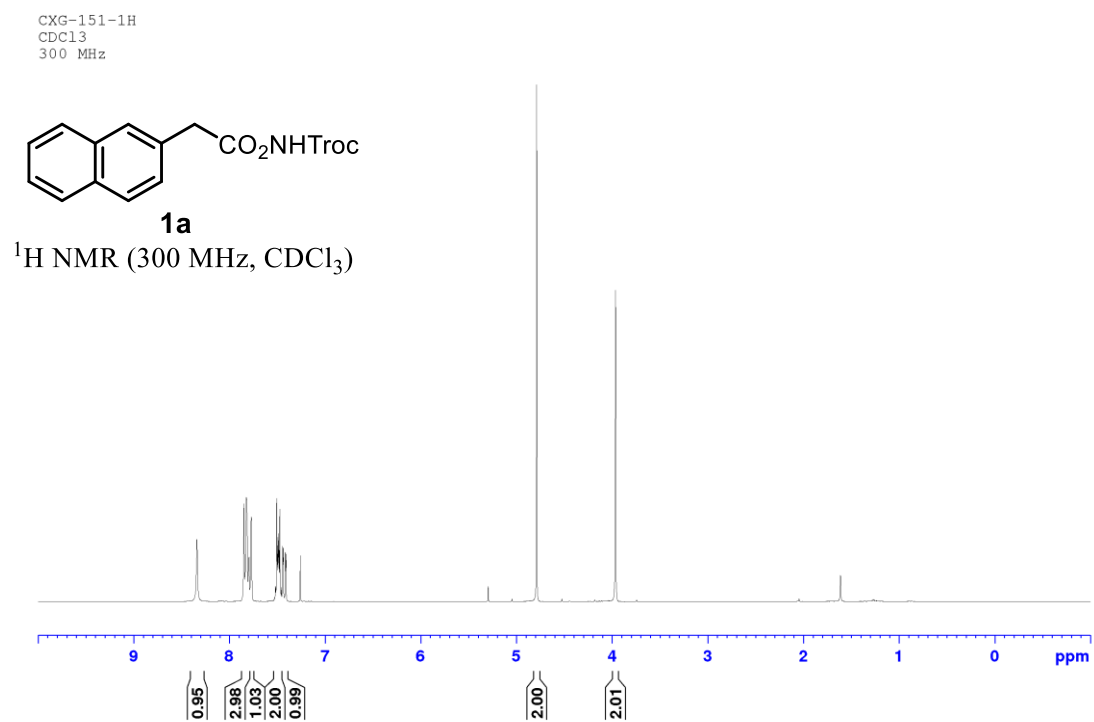
[Chiralpak IG 25 °C, CH₃CN/H₂O(0.1% TFA) = 50:50, 1.0 mL/min, 210 nm]



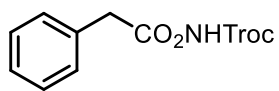
Peak #	RetTime [min]	Type	Width [min]	Area [mAU*s]	Height [mAU]	Area %
1	16.174	BB	0.5264	86.92315	2.54599	55.0401
2	21.658	MM	0.7761	71.00368	1.52486	44.9599

Figure 105. HPLC traces of *rac*-5ze and (*S*)-5ze (10% ee).

5.7 List of NMR Spectra of New Compounds

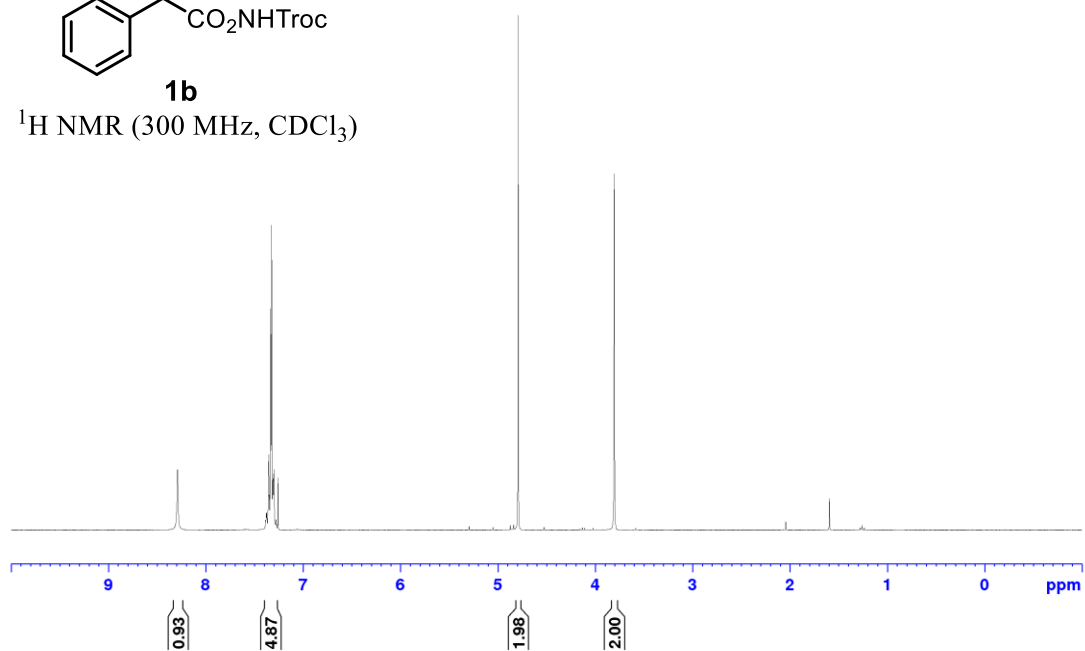


CXF-25-1H
CDCl₃
300 MHz

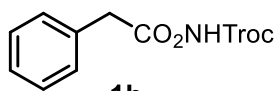


1b

¹H NMR (300 MHz, CDCl₃)

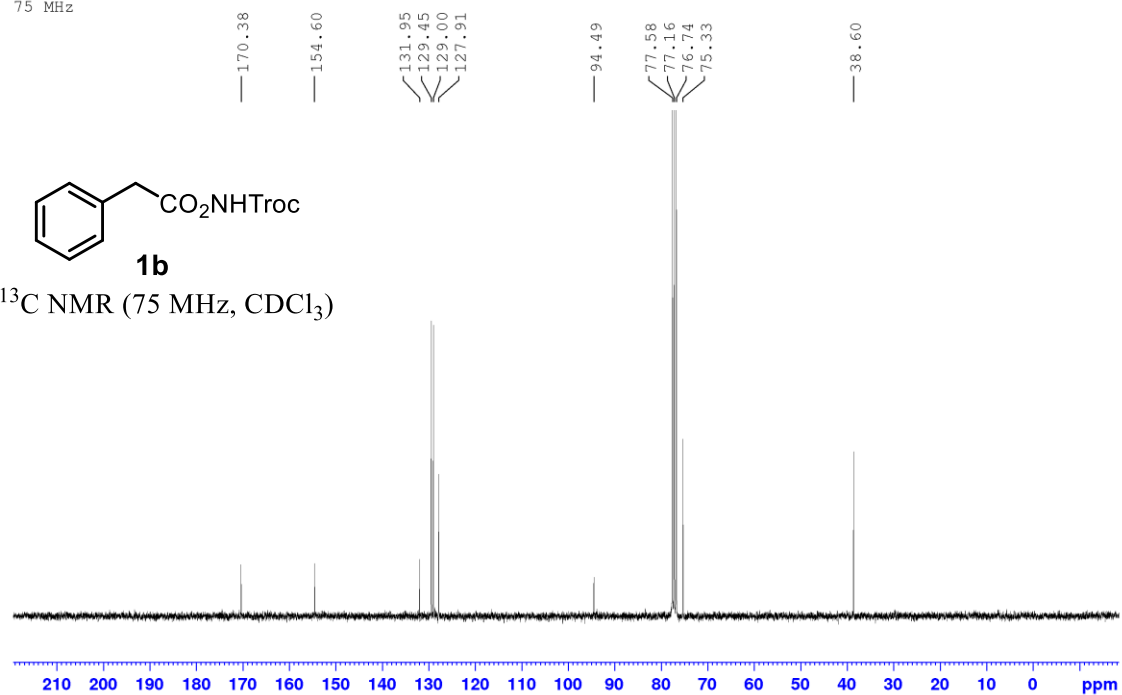


CXF-25-13C
CDCl₃
75 MHz



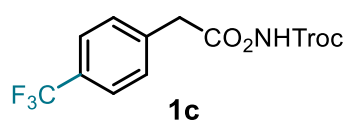
1b

¹³C NMR (75 MHz, CDCl₃)

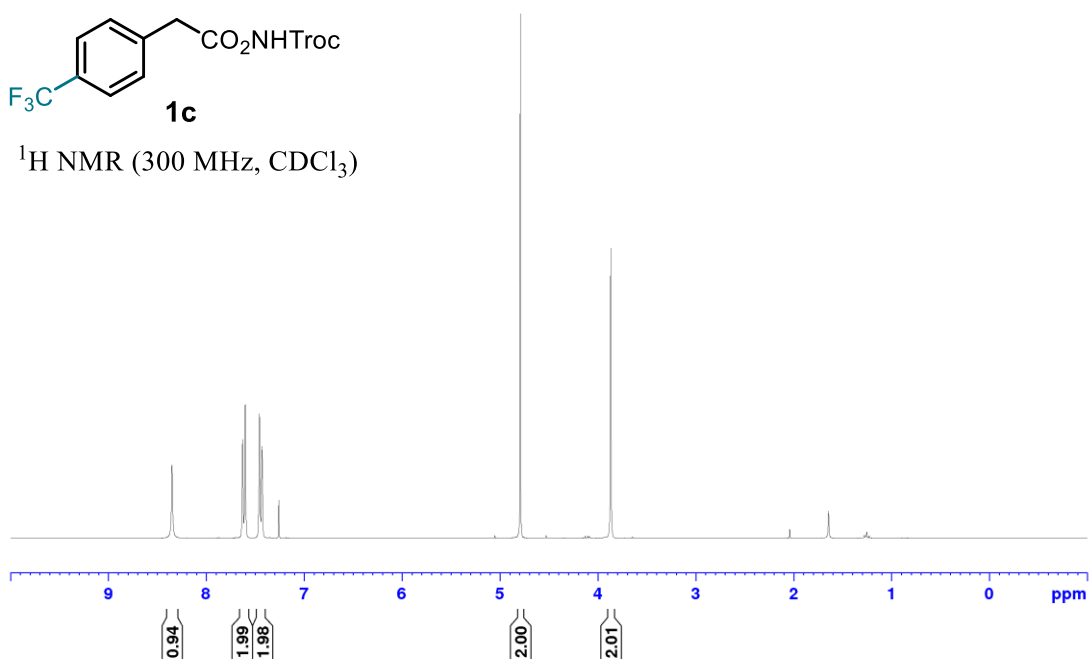


Statement

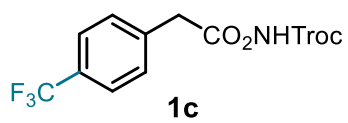
CXG-163-1H
CDCl₃
300 MHz



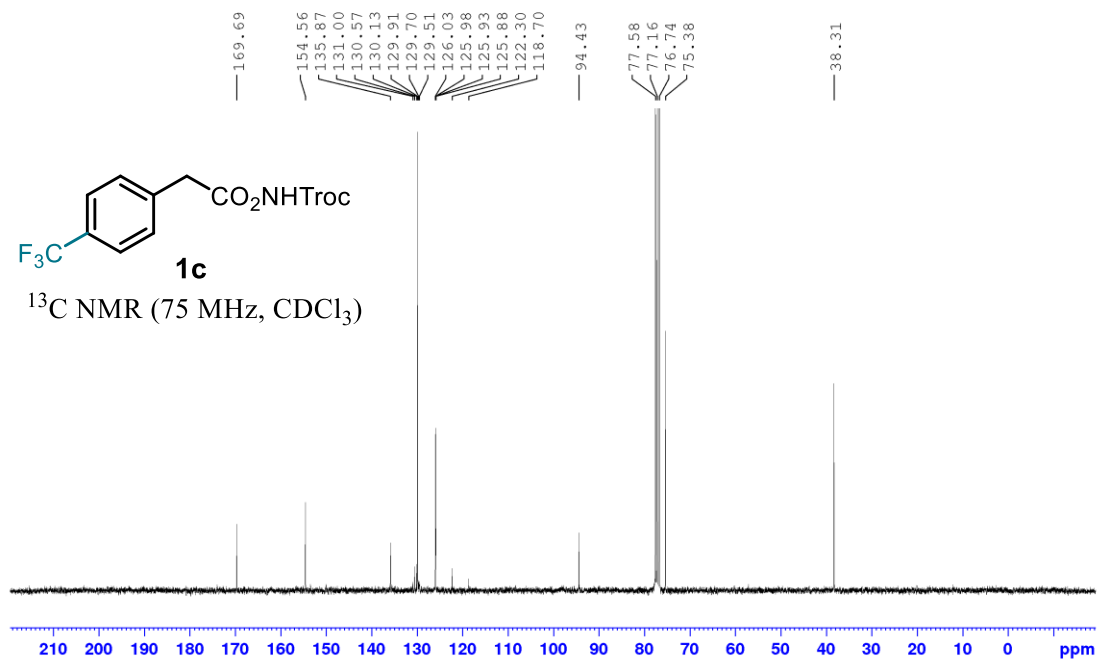
¹H NMR (300 MHz, CDCl₃)



CXG-163-13C
CDCl₃
75 MHz

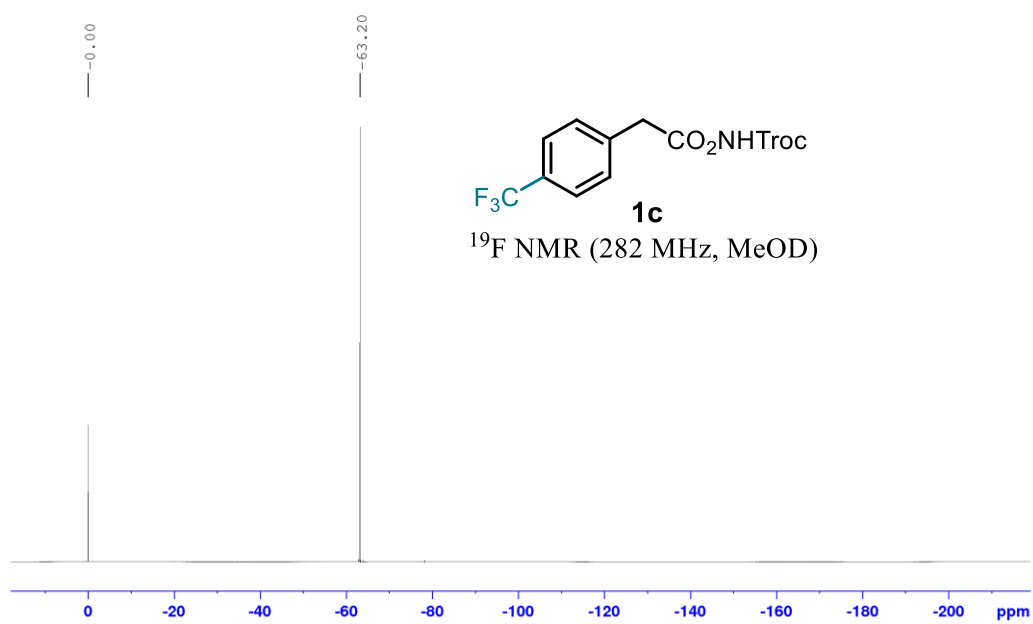


¹³C NMR (75 MHz, CDCl₃)



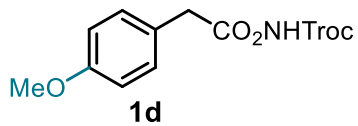
Statement

CXG-163-19F
CDCl3
282 MHz

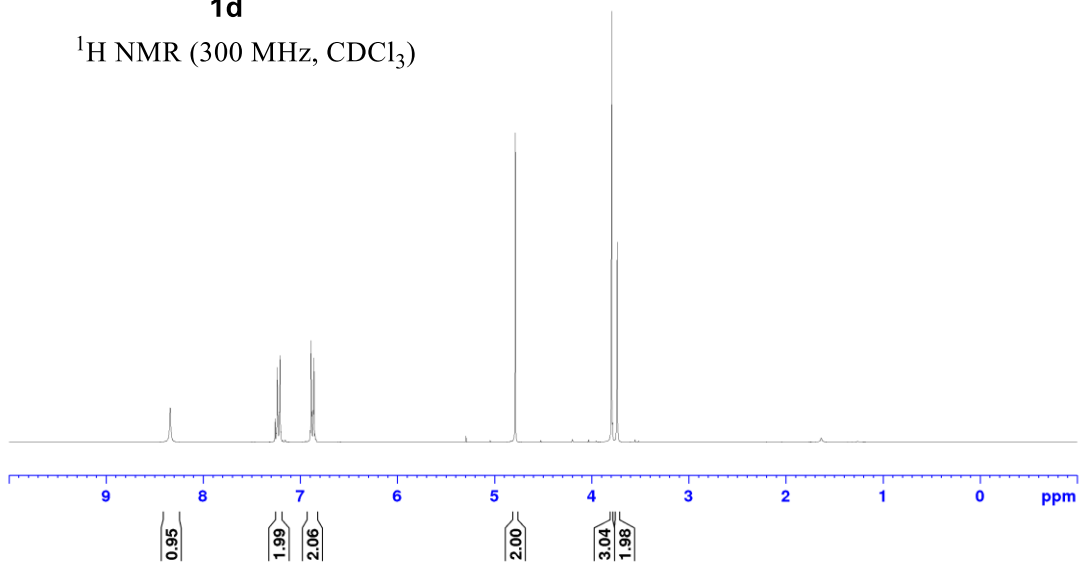


Statement

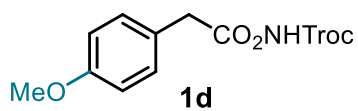
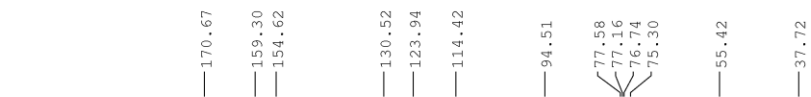
CXG-86-1H
CDCl₃
300 MHz



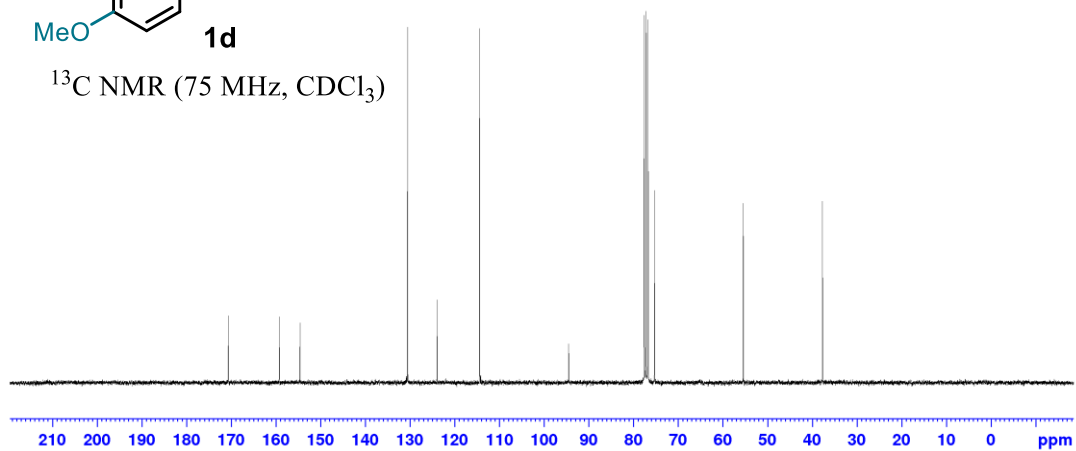
¹H NMR (300 MHz, CDCl₃)

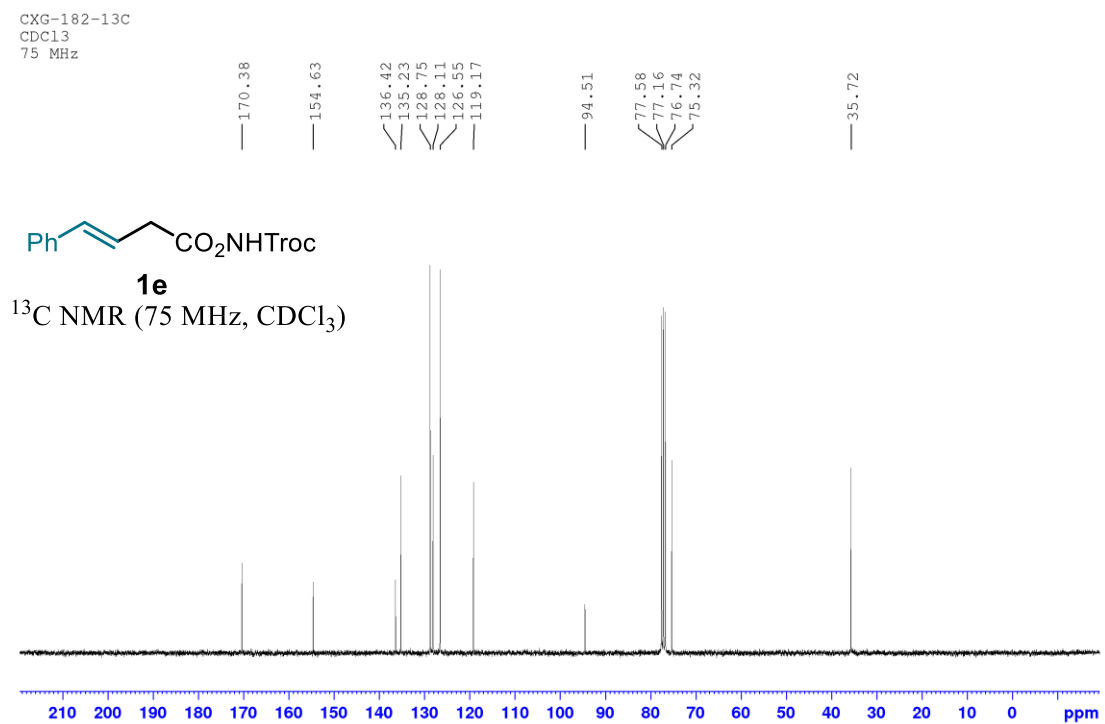
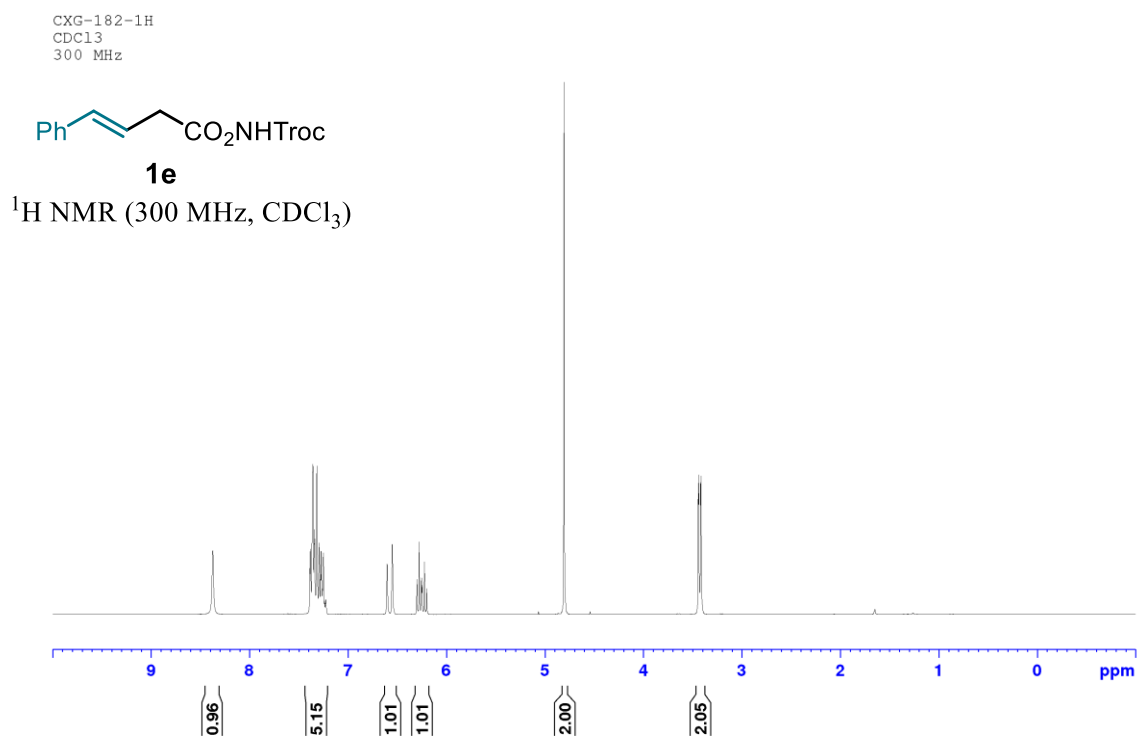


CXG-86-13C
CDCl₃
75 MHz



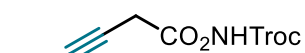
¹³C NMR (75 MHz, CDCl₃)





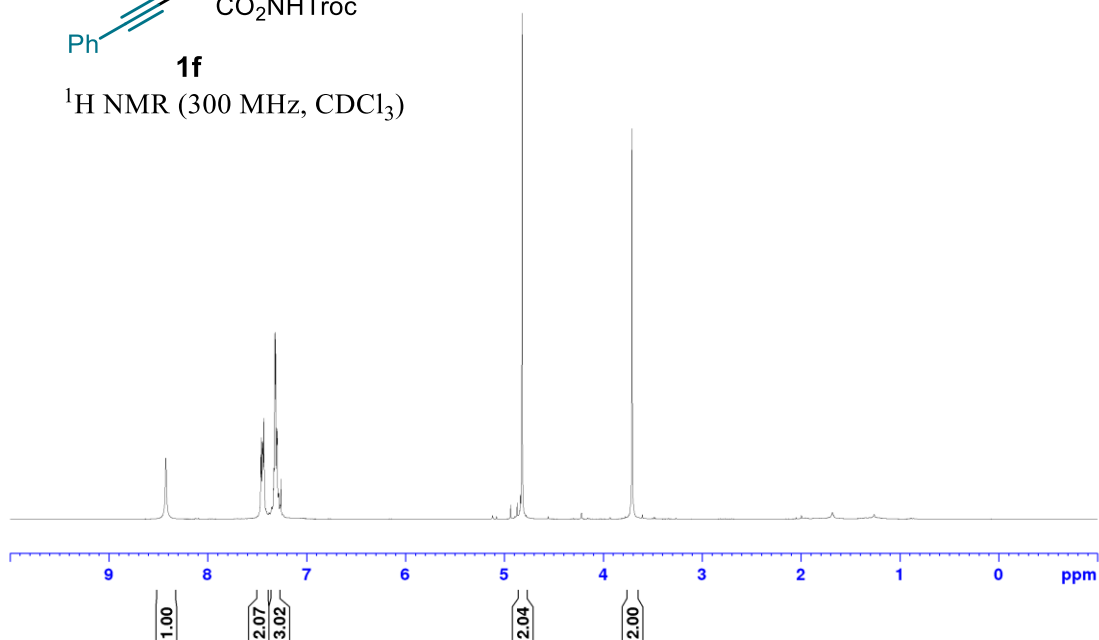
Statement

CXH-161-1H
CDCl₃
300 MHz

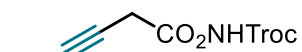


1f

¹H NMR (300 MHz, CDCl₃)

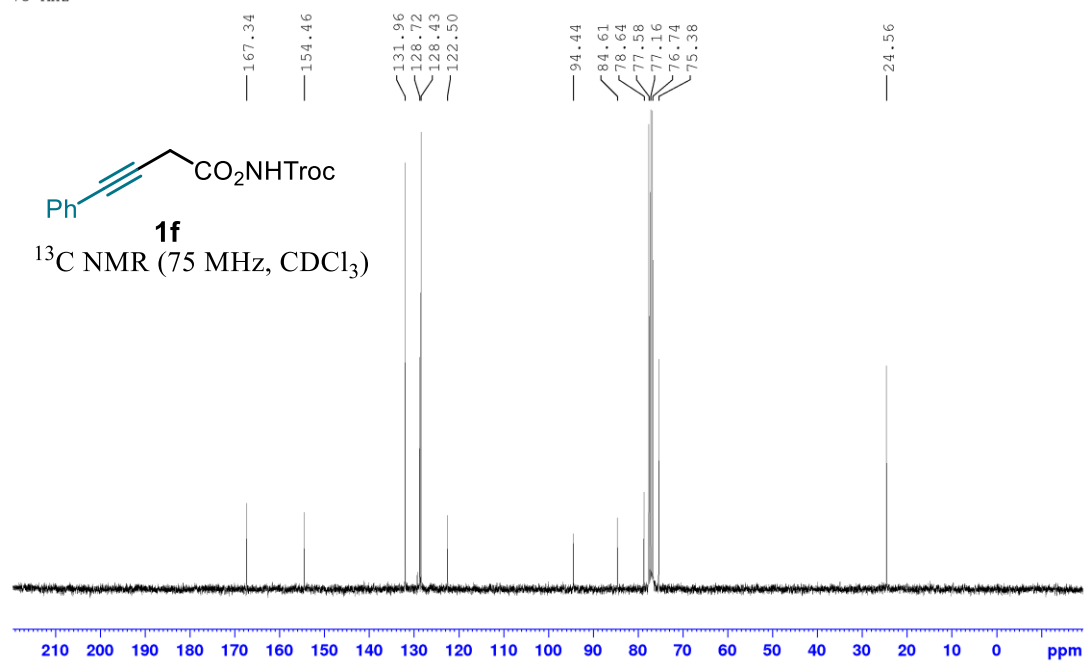


CXH-161-13C
CDCl₃
75 MHz

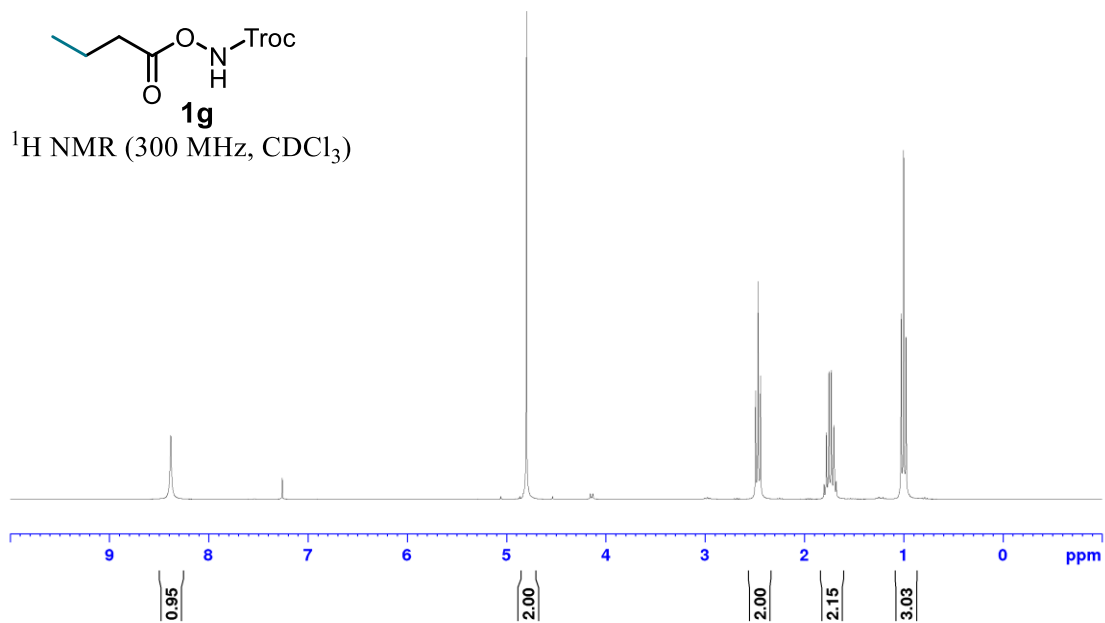


1f

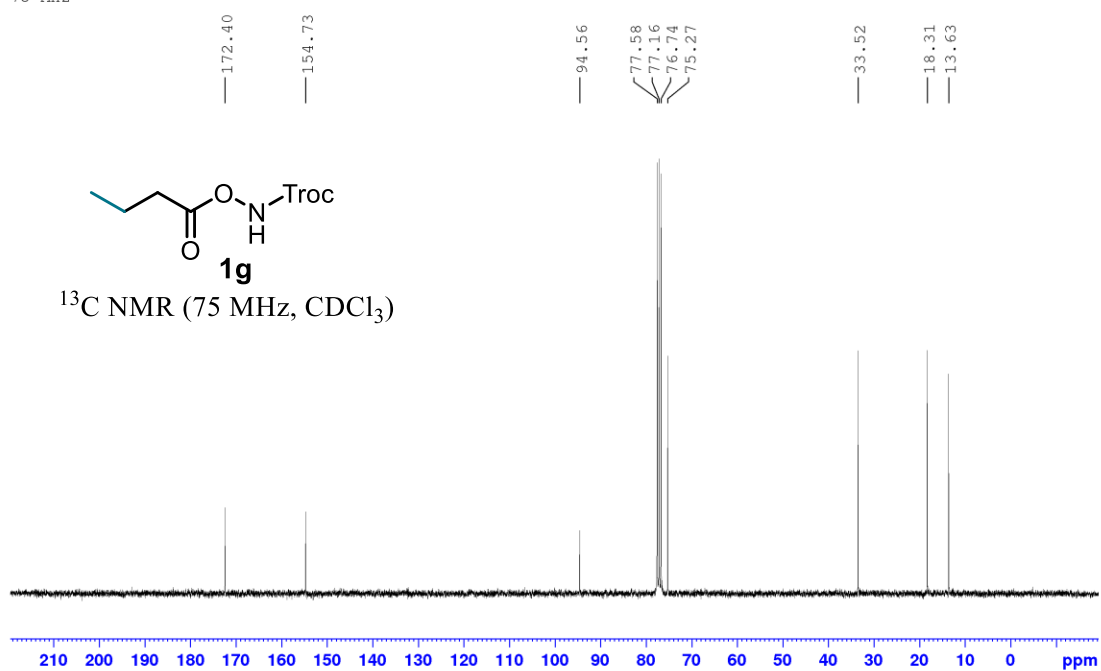
¹³C NMR (75 MHz, CDCl₃)



CXJ-62-SM-1H
CDCl₃
300 MHz

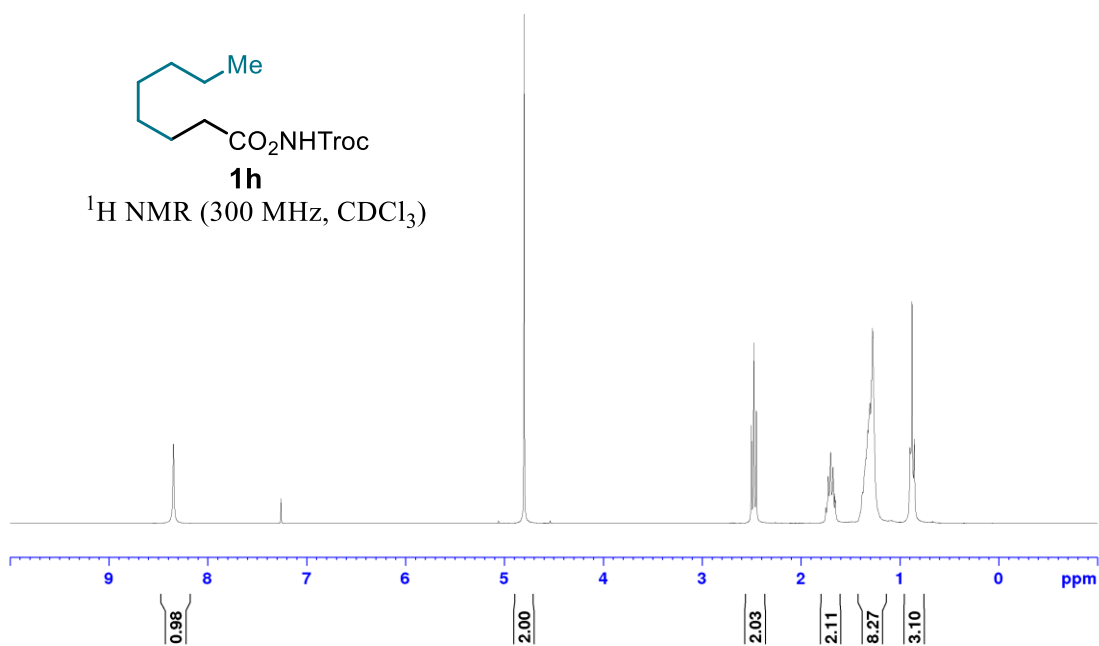


CXJ-62-SM-13C
CDCl₃
75 MHz

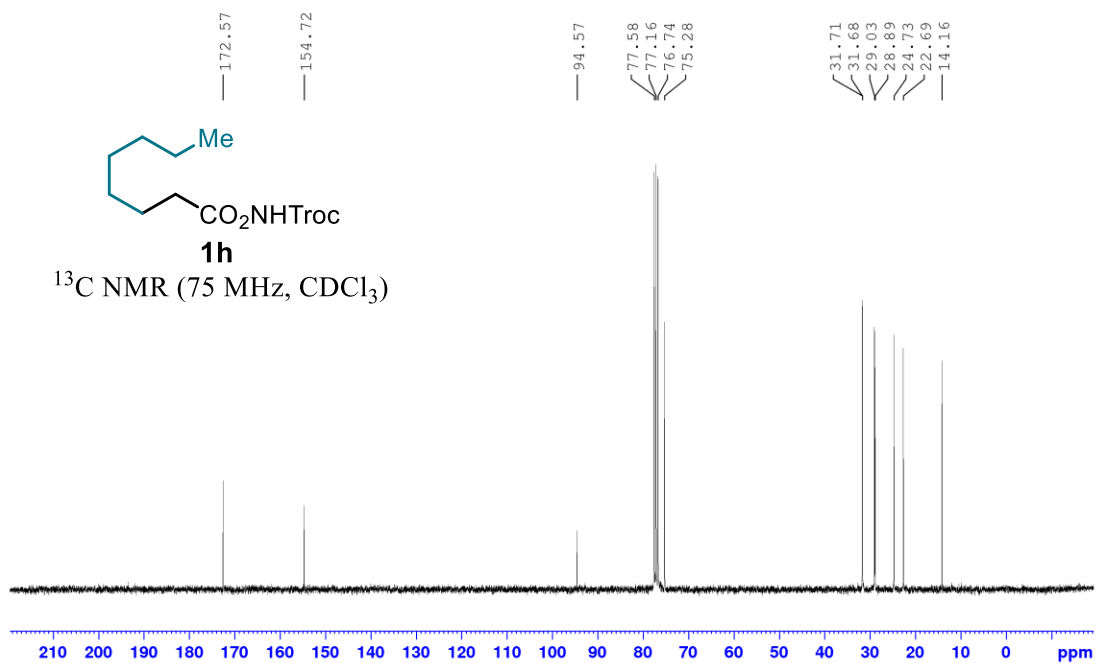


Statement

CXH-183-1H
CDCl₃
300 MHz

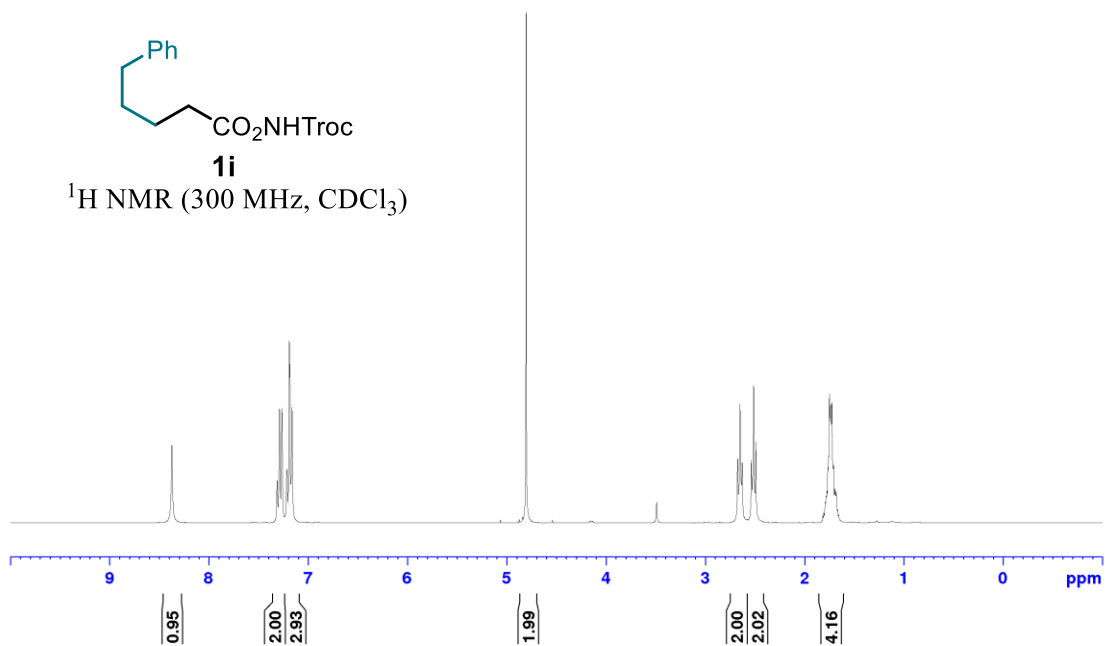
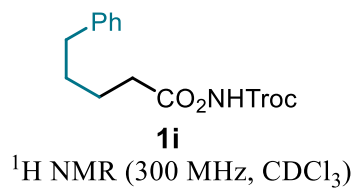


CXH-183-13C
CDCl₃
75 MHz

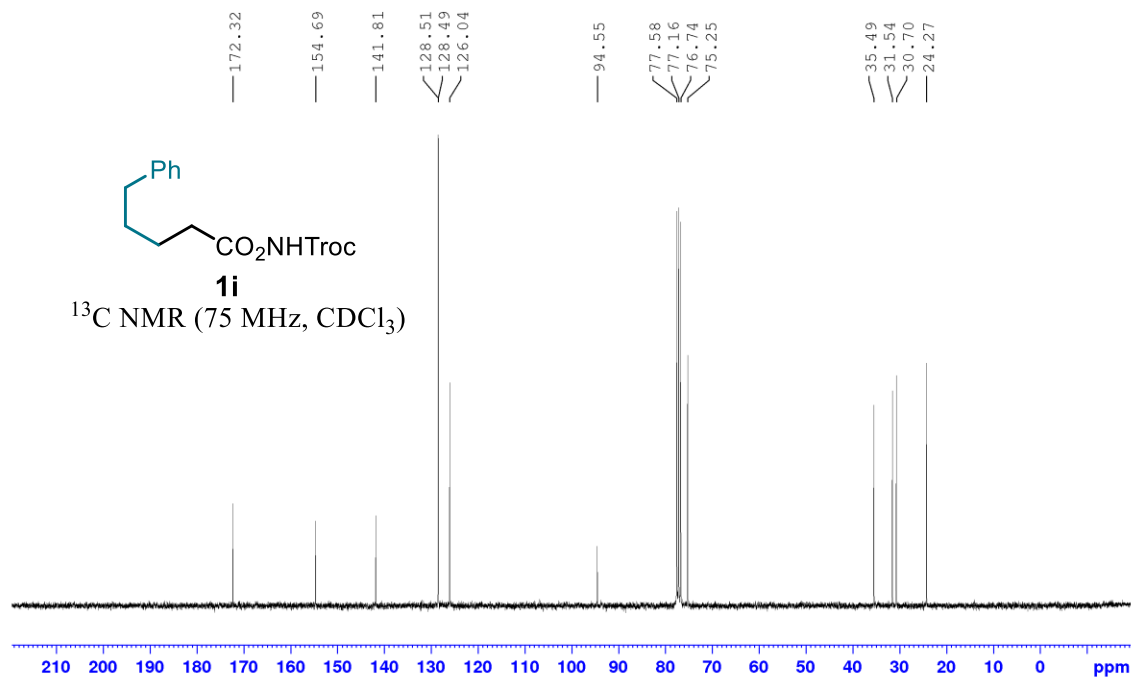
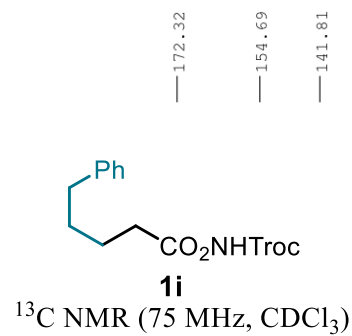


Statement

CXJ-75-SM-1H
CDCl₃
300 MHz

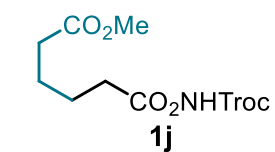


CXJ-75-SM-13C
CDCl₃
75 MHz

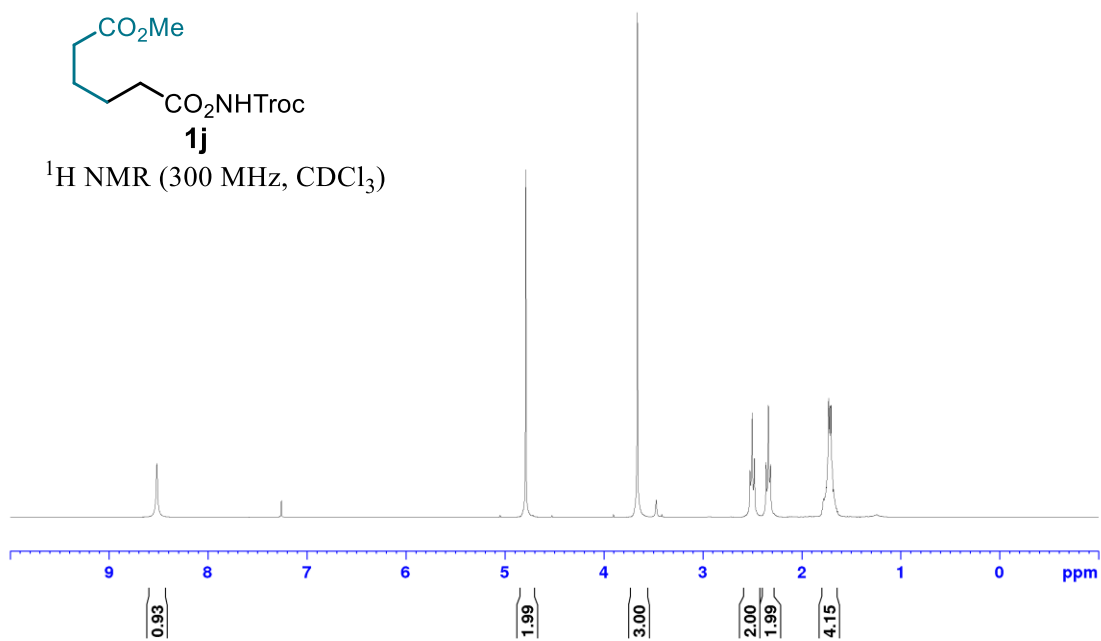


Statement

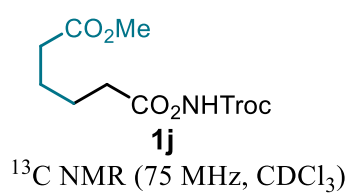
CXJ-78-SM-1H
CDCl₃
300 MHz



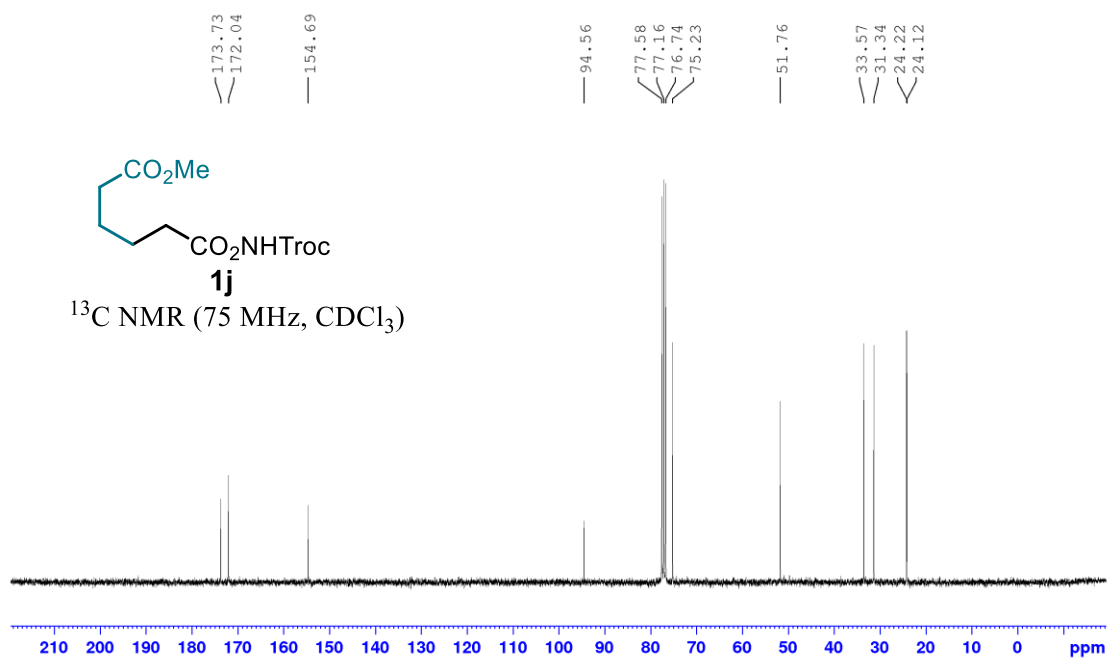
¹H NMR (300 MHz, CDCl₃)



CXJ-78-SM-13C
CDCl₃
75 MHz

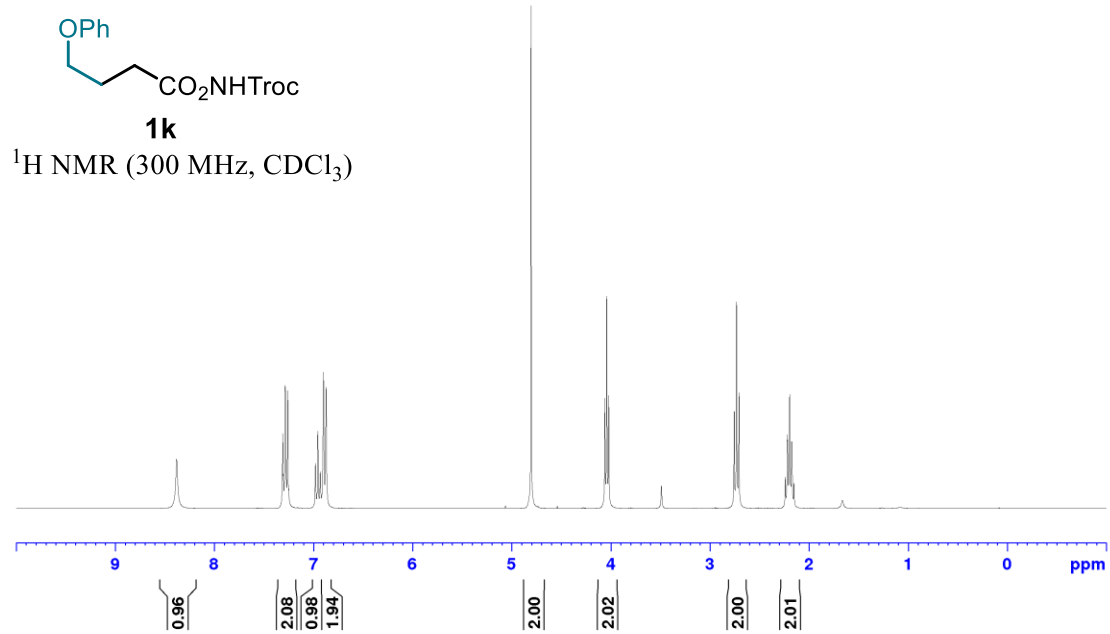


¹³C NMR (75 MHz, CDCl₃)

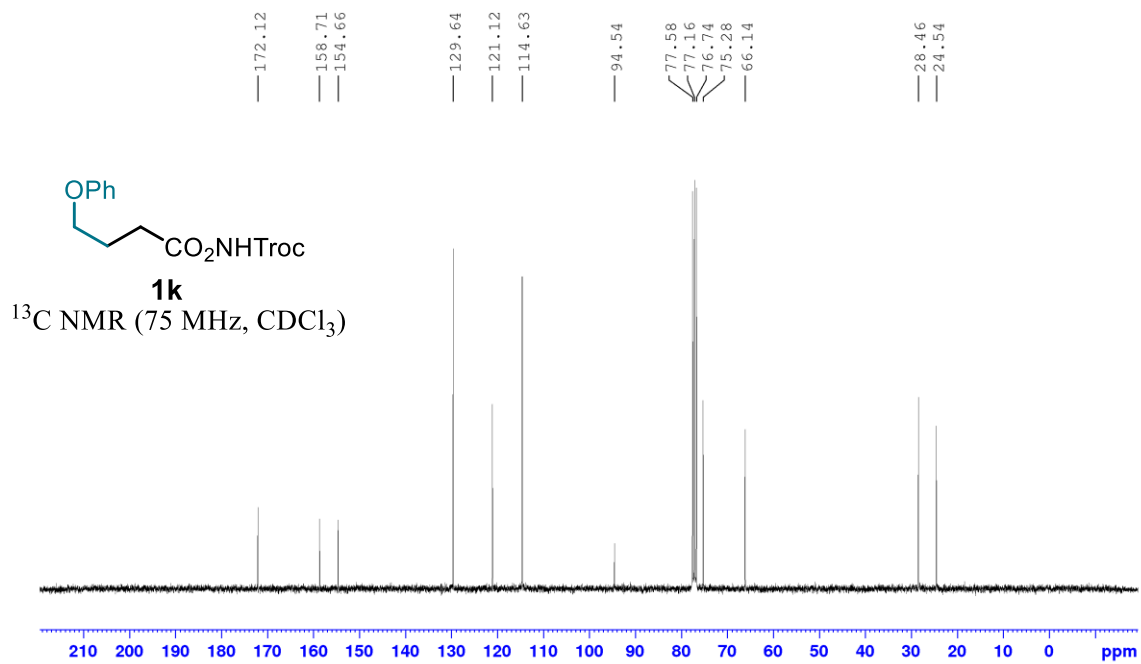


Statement

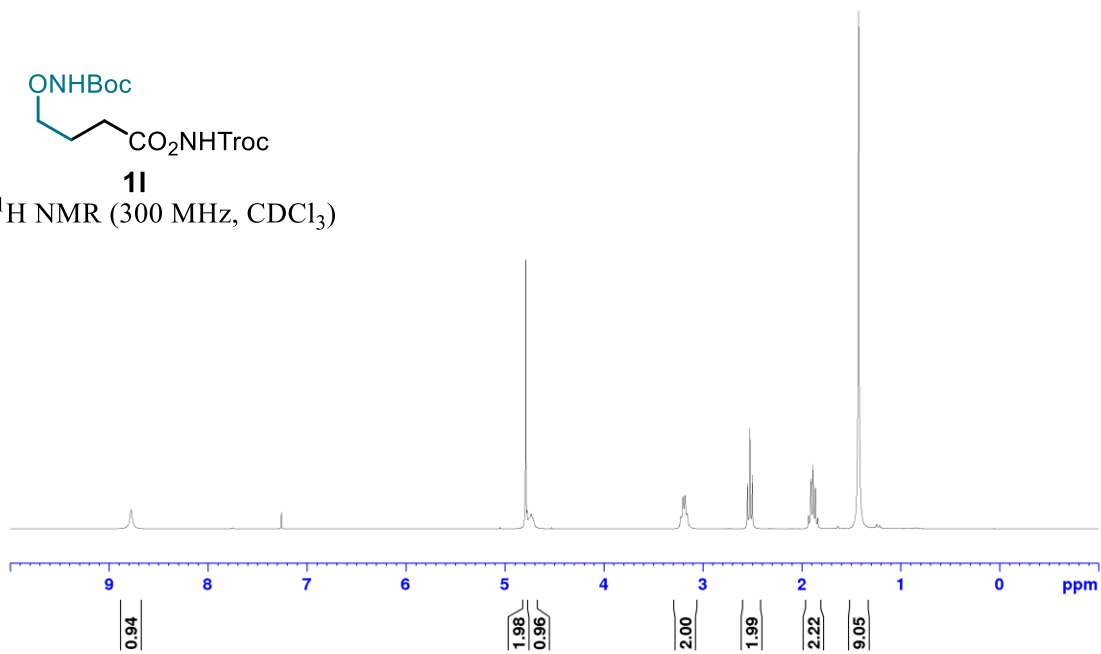
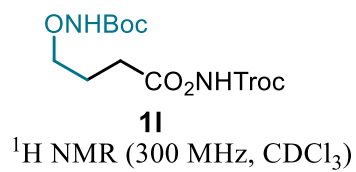
CXJ-68-SM-1H
CDCl₃
300 MHz



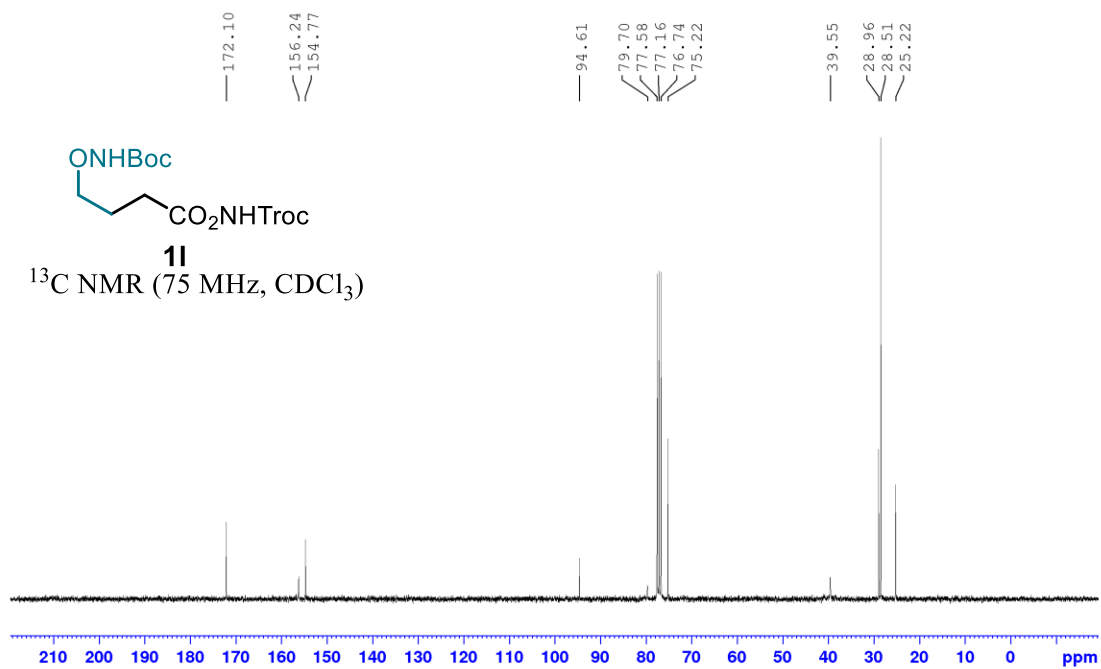
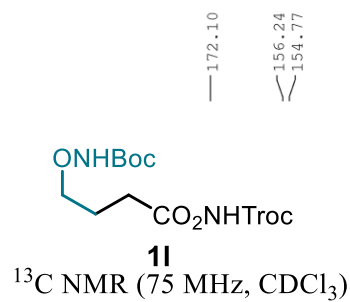
CXJ-68-SM-13C
CDCl₃
75 MHz



CXJ-73-SM-1H
CDCl₃
300 MHz

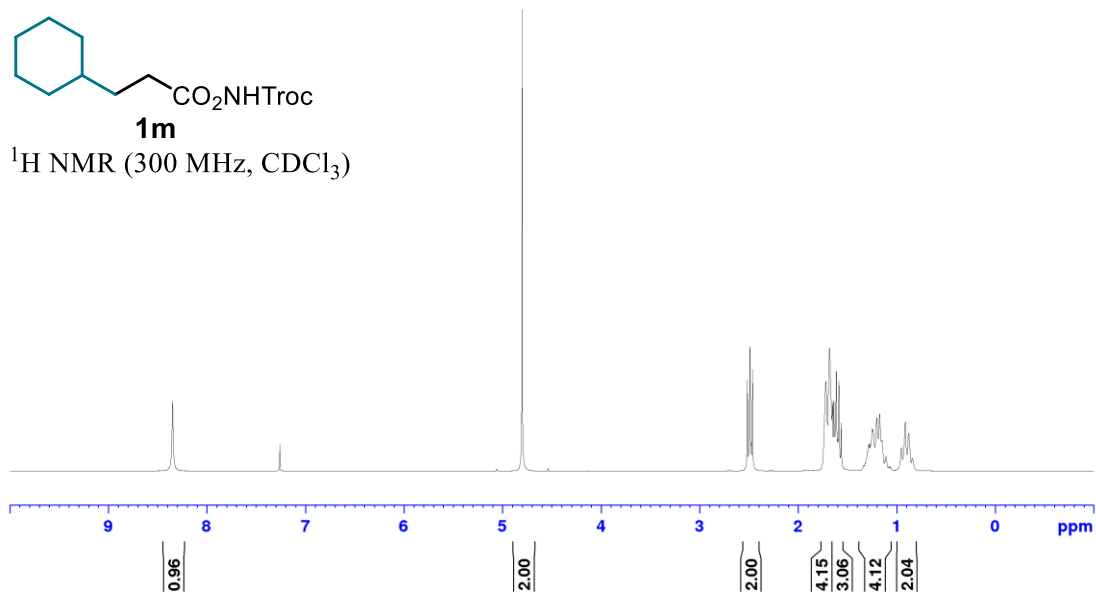


CXJ-73-SM-13C
CDCl₃
75 MHz

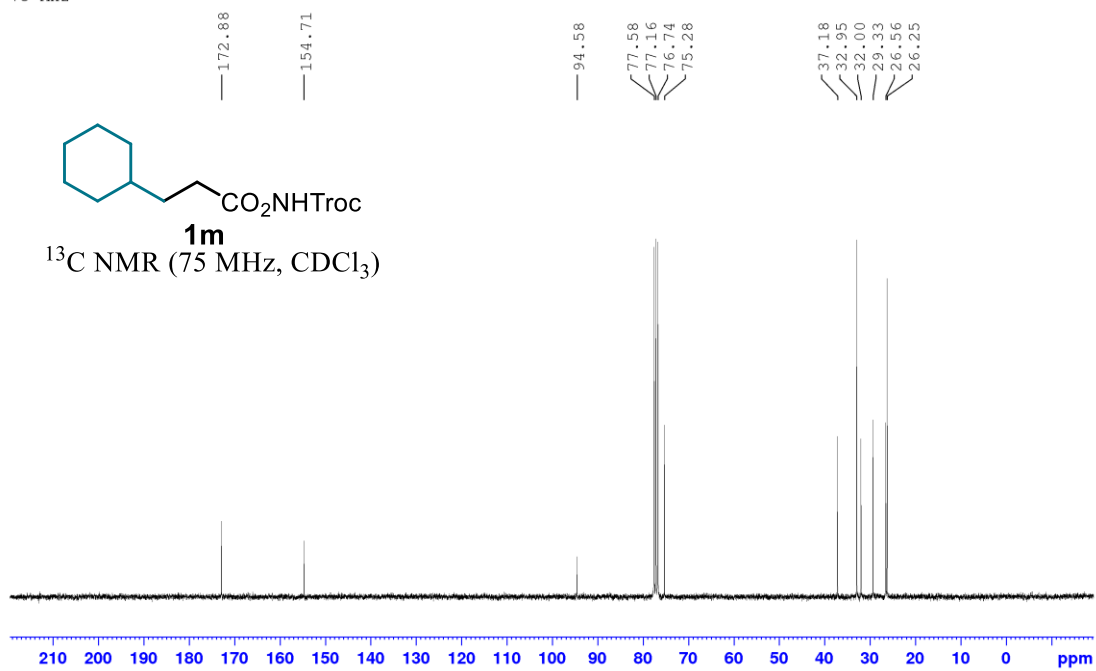


Statement

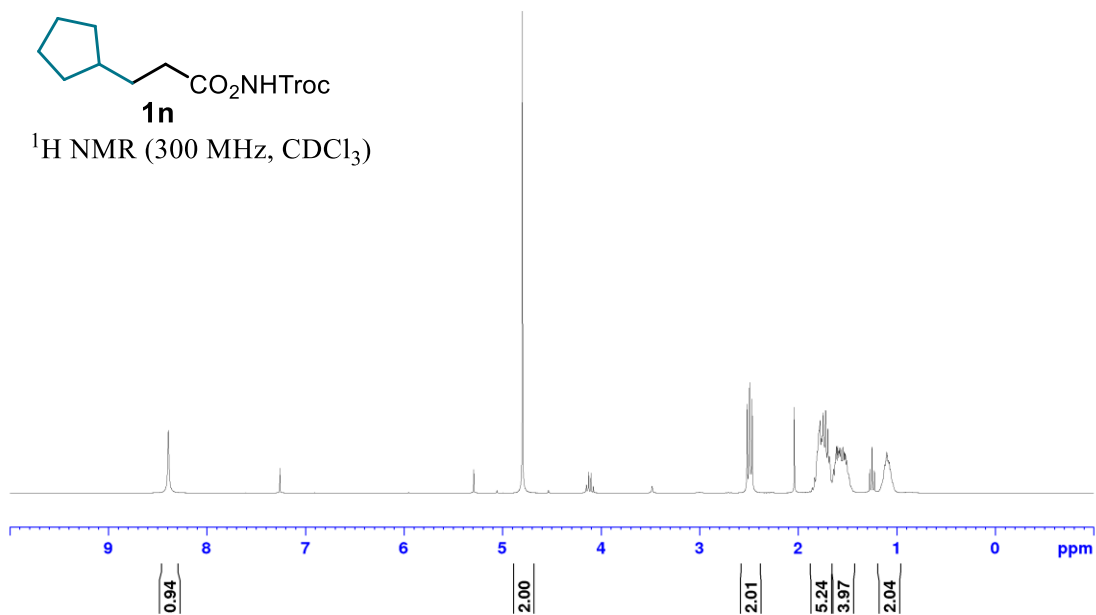
CXJ-72-SM-1H
CDCl₃
300 MHz



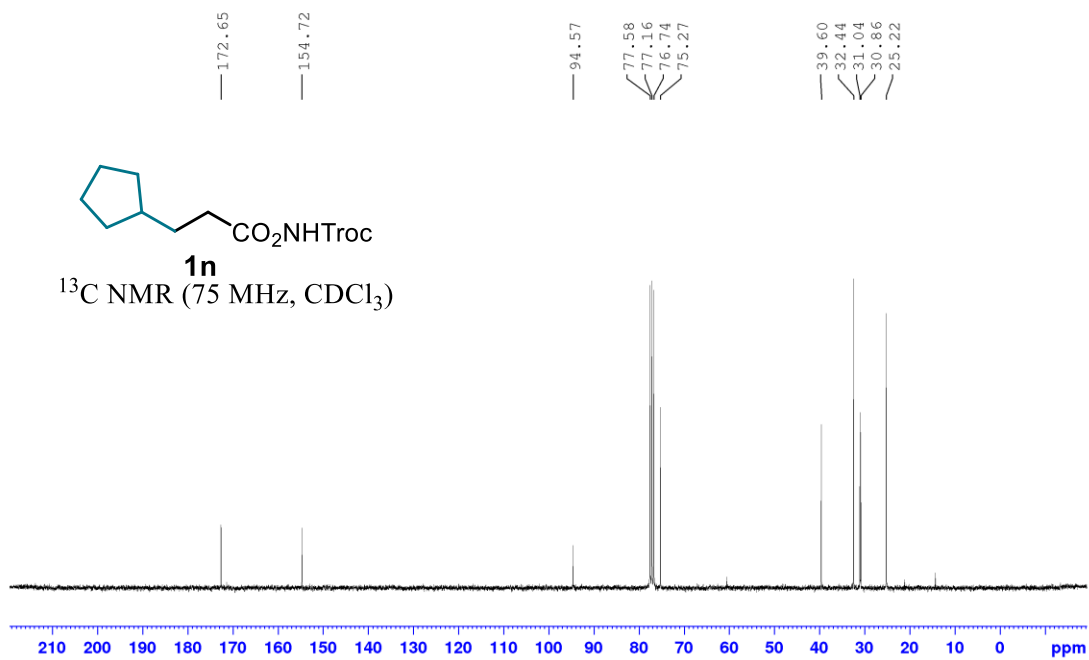
CXJ-72-SM-13C
CDCl₃
75 MHz



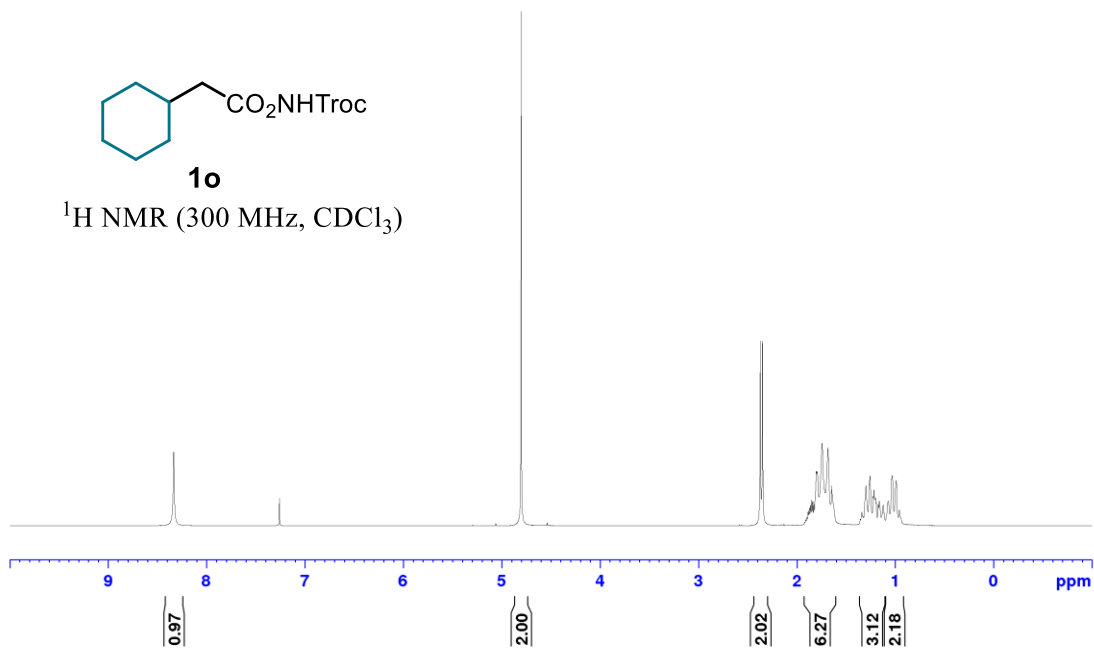
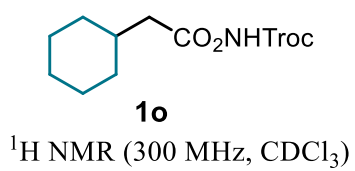
CXJ-74-SM-1H
CDCl₃
300 MHz



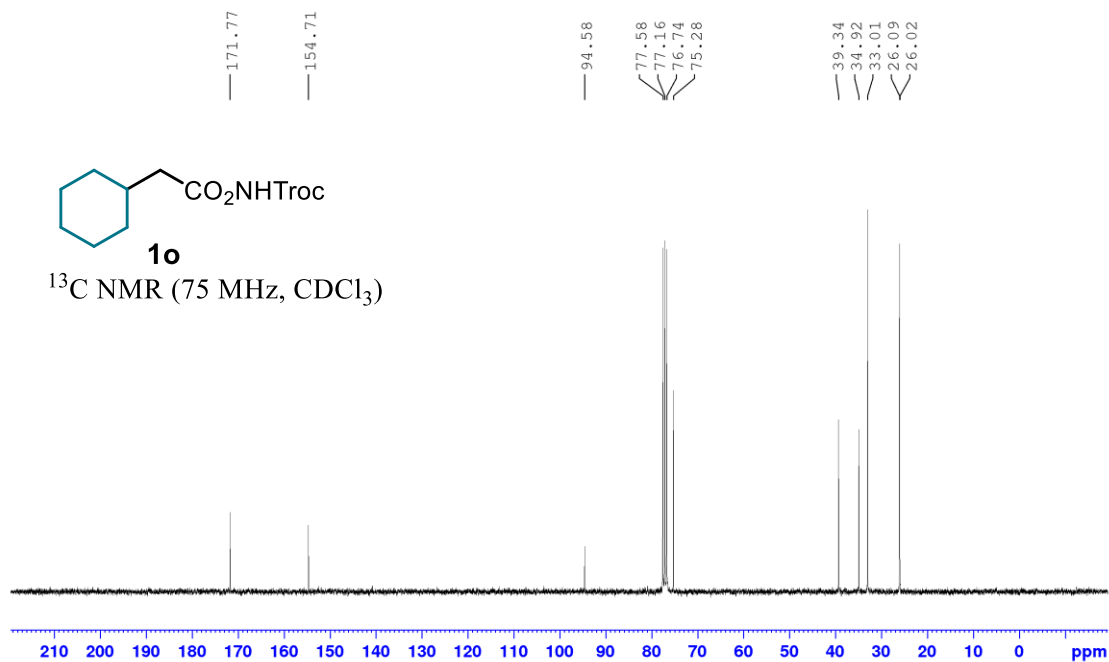
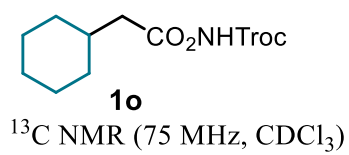
CXJ-74-SM-13C
CDCl₃
75 MHz



CXH-172-1H
CDCl₃
300 MHz

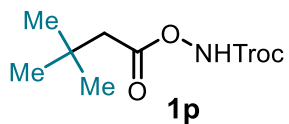


CXH-172-13C
CDCl₃
75 MHz

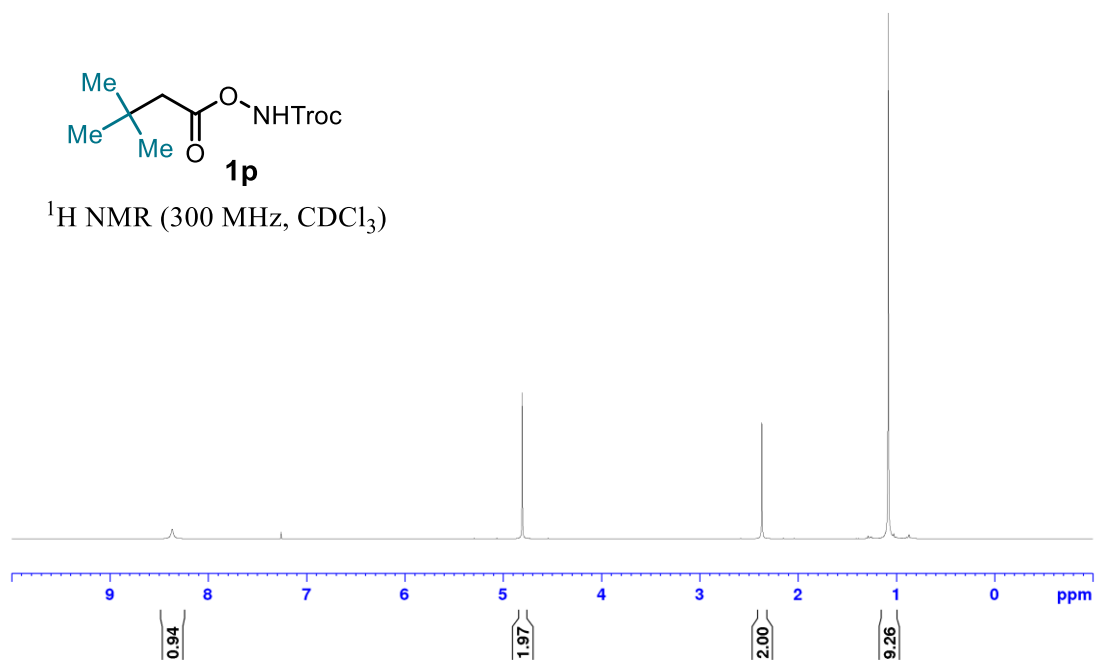


Statement

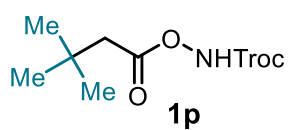
CXI-22-1H
CDCl₃
300 MHz



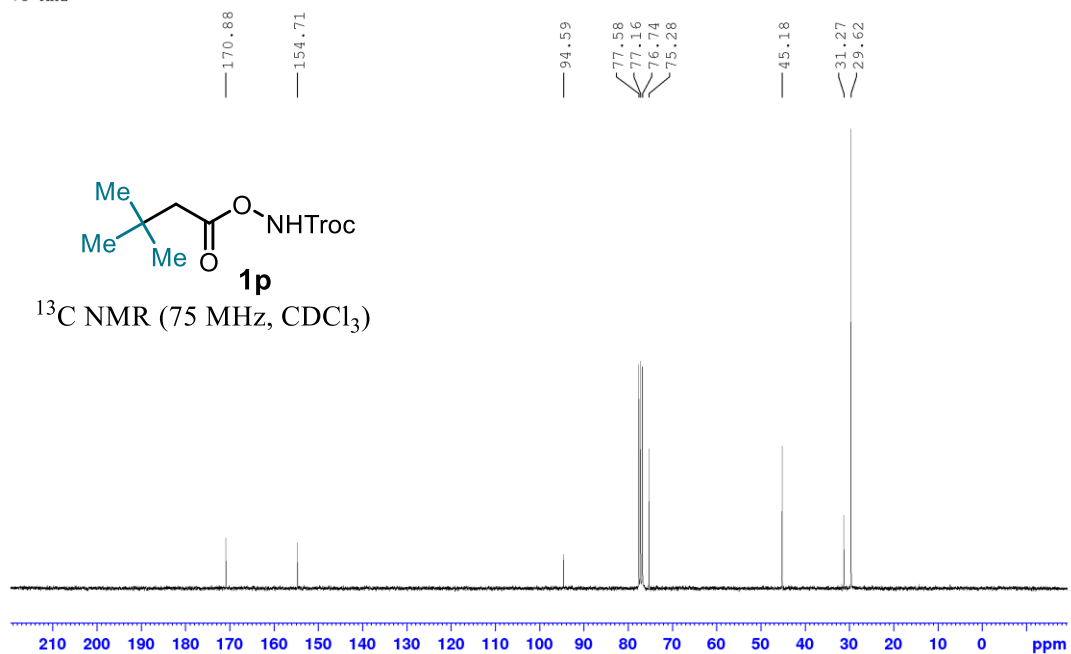
¹H NMR (300 MHz, CDCl₃)



CXI-22-13C
CDCl₃
75 MHz

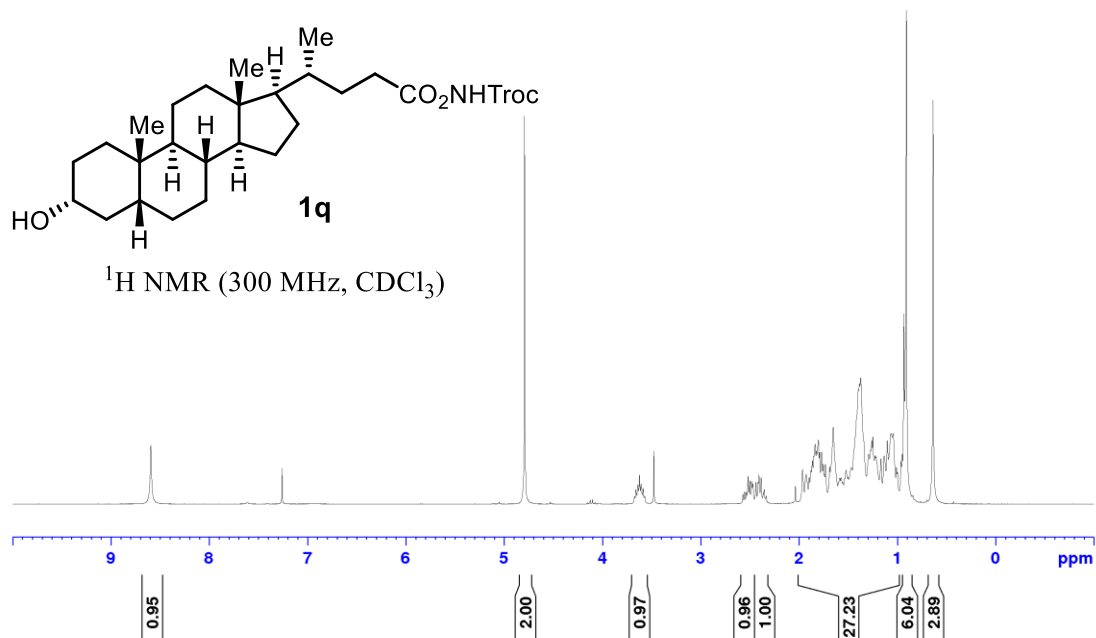


¹³C NMR (75 MHz, CDCl₃)

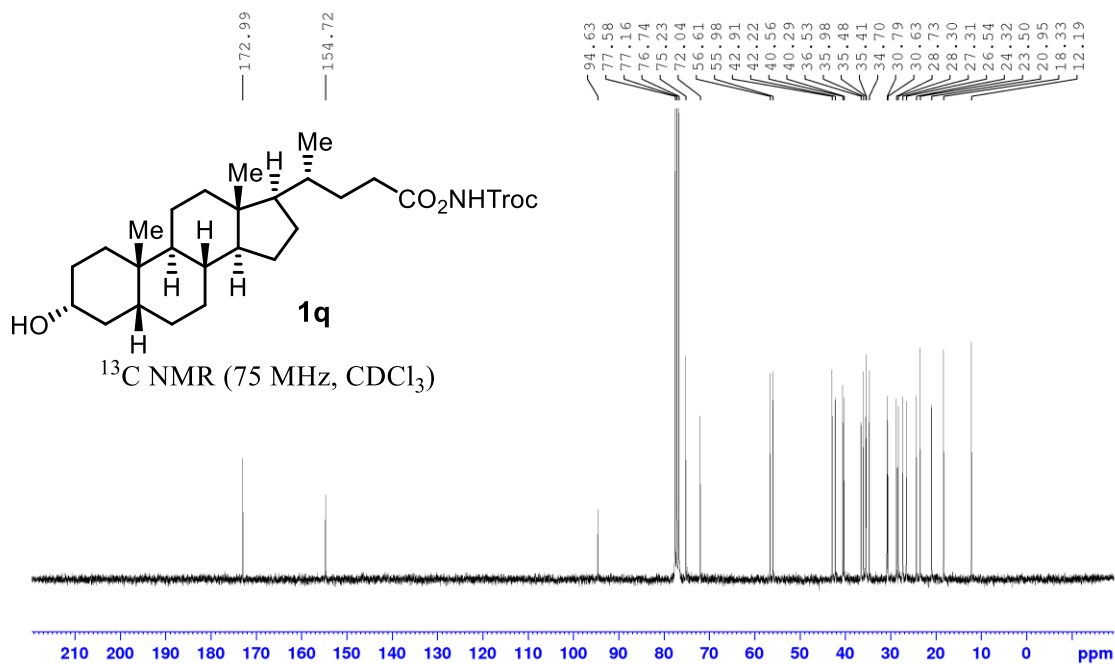


Statement

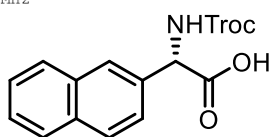
CXJ-81-SM-1H
CDCl₃
300 MHz



CXJ-81-SM-13C
CDCl₃
75 MHz

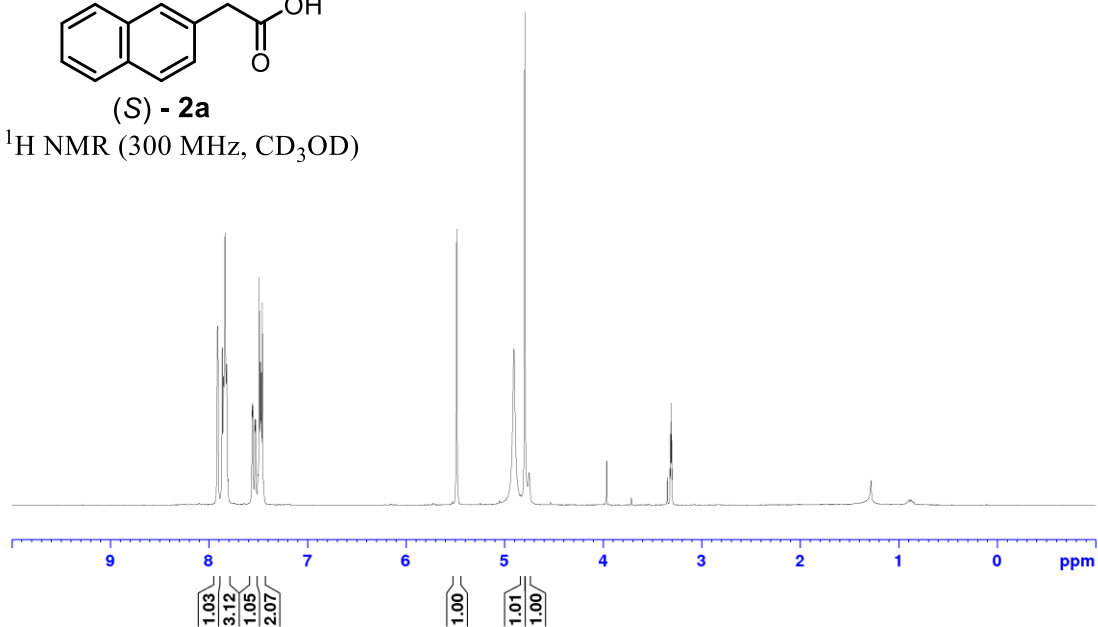


CXG-153-1H
CD3OD
300 MHz

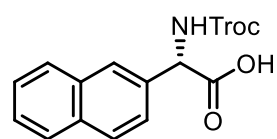


(S) - 2a

^1H NMR (300 MHz, CD_3OD)

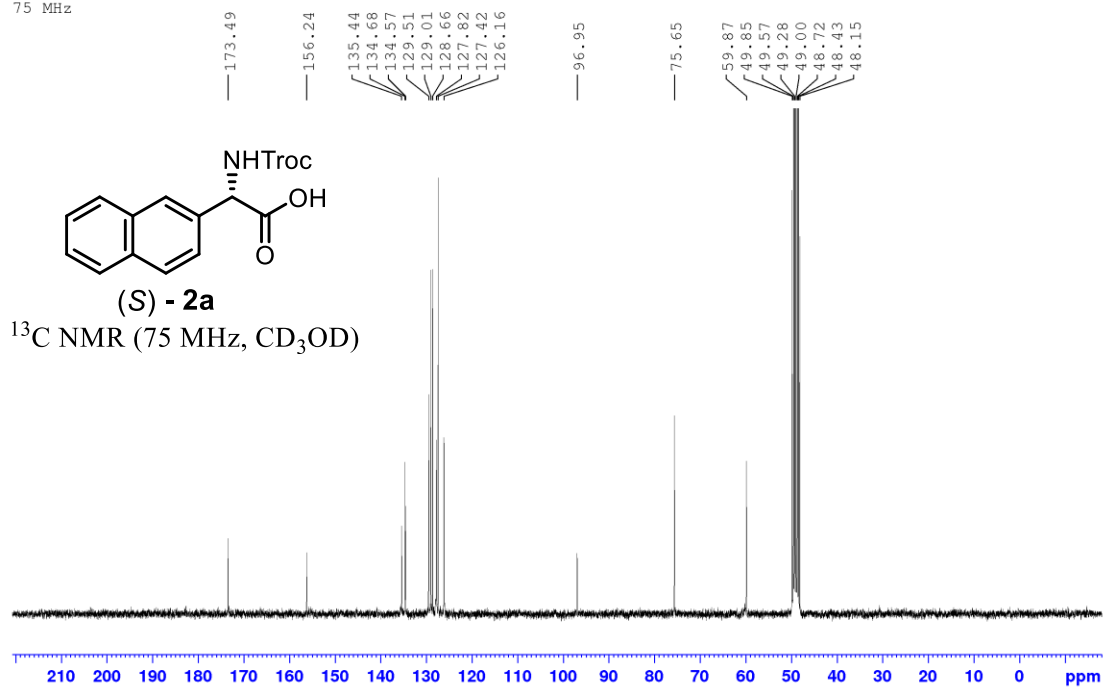


CXG-153-13C
CD3OD
75 MHz

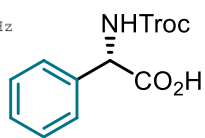


(S) - 2a

^{13}C NMR (75 MHz, CD_3OD)

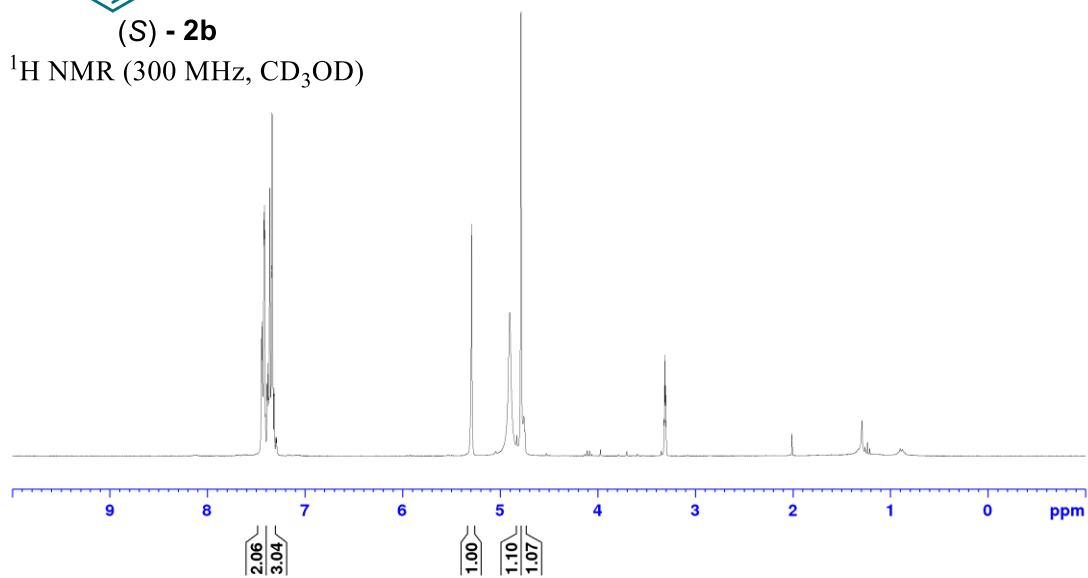


CXG-80-1H
CD3OD
300 MHz

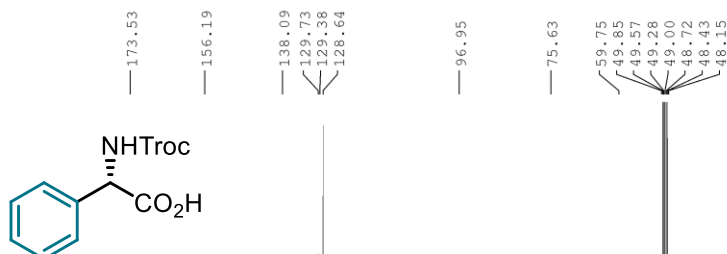


(S) - 2b

¹H NMR (300 MHz, CD₃OD)

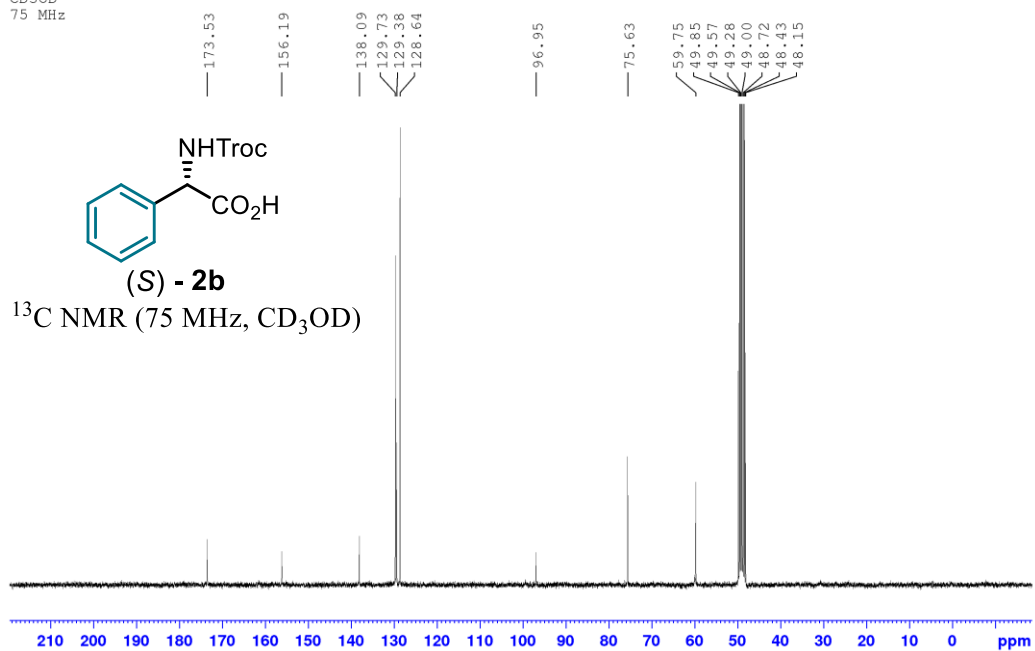


CXG-80-13C
CD3OD
75 MHz



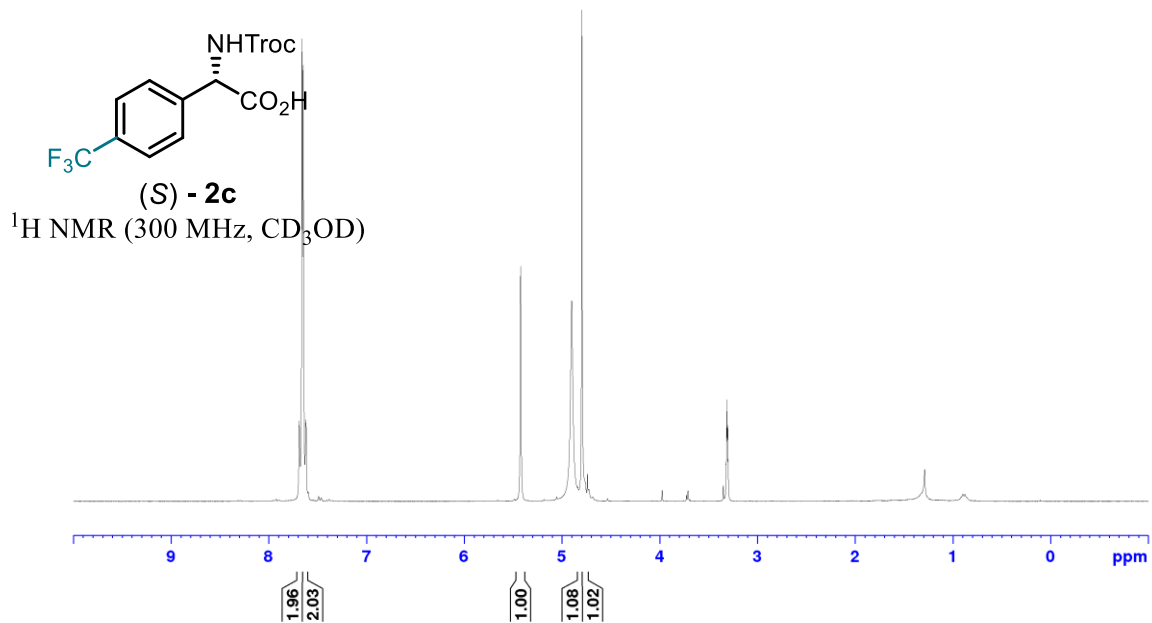
(S) - 2b

¹³C NMR (75 MHz, CD₃OD)

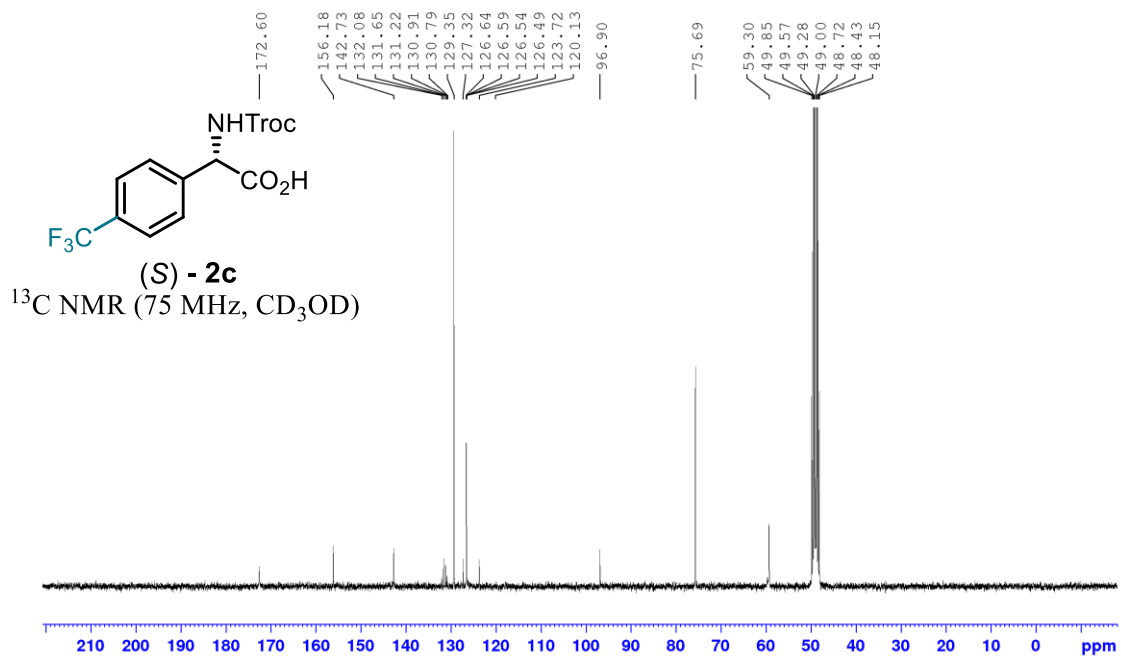


Statement

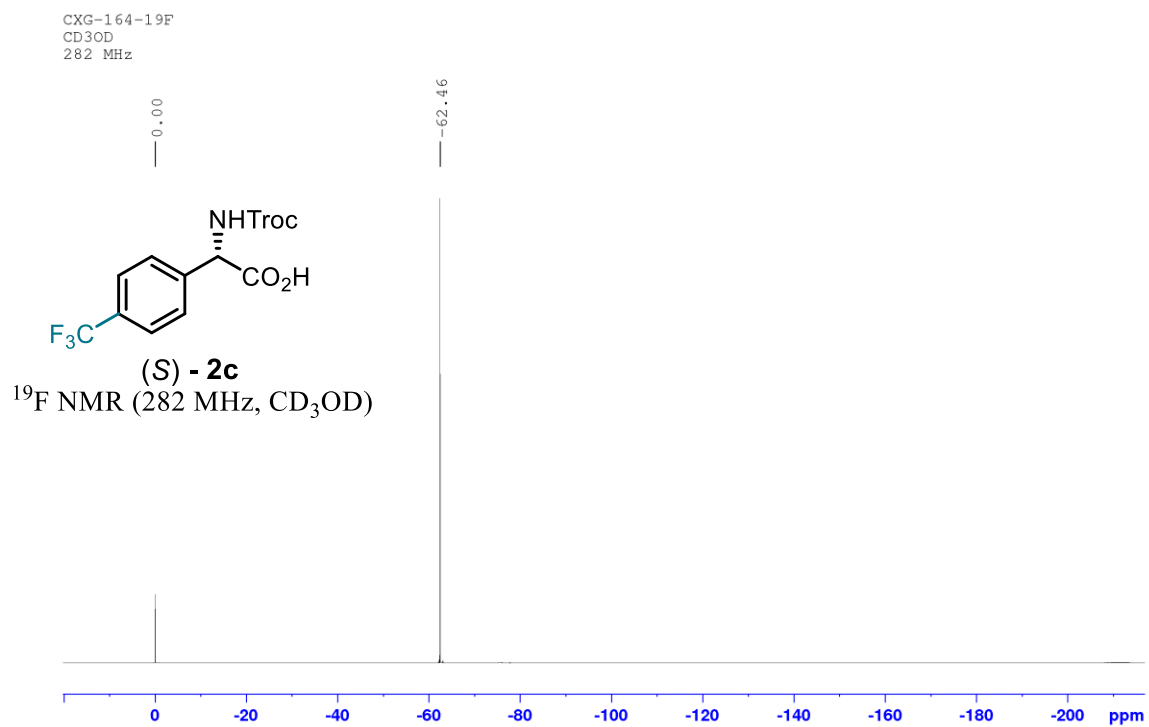
CXG-164-1H
CD3OD
300 MHz



CXG-164-13C
CD3OD
75 MHz

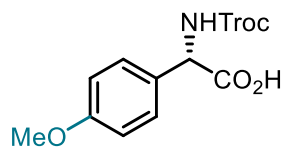


Statement



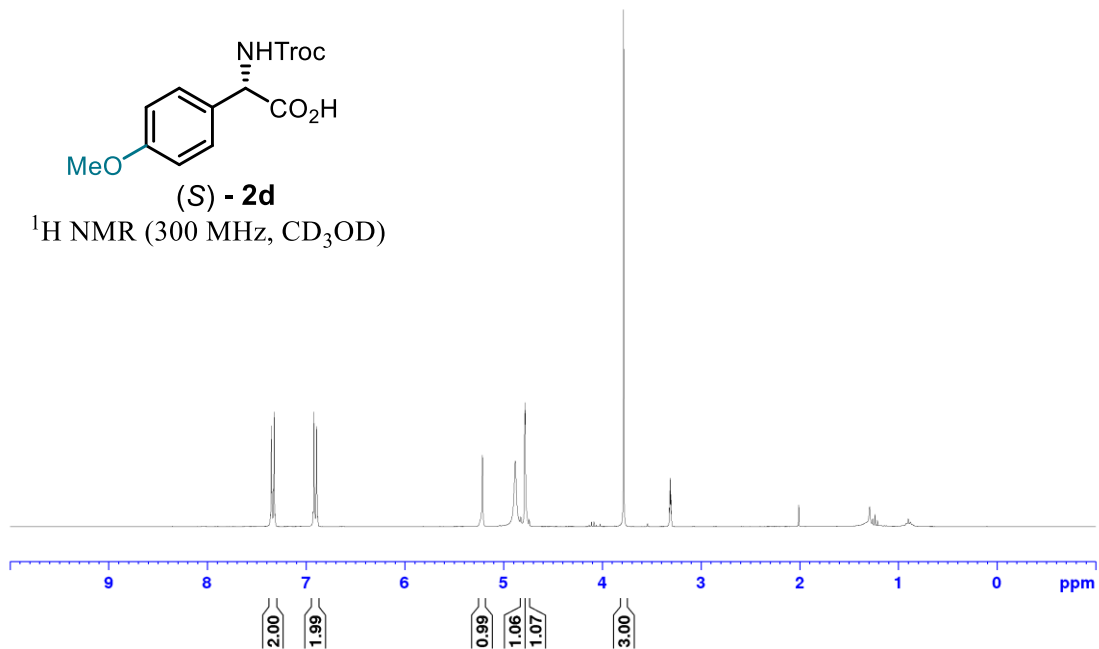
Statement

CXG-77-1H
CD3OD
300 MHz

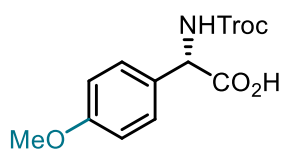


(S) - 2d

¹H NMR (300 MHz, CD₃OD)

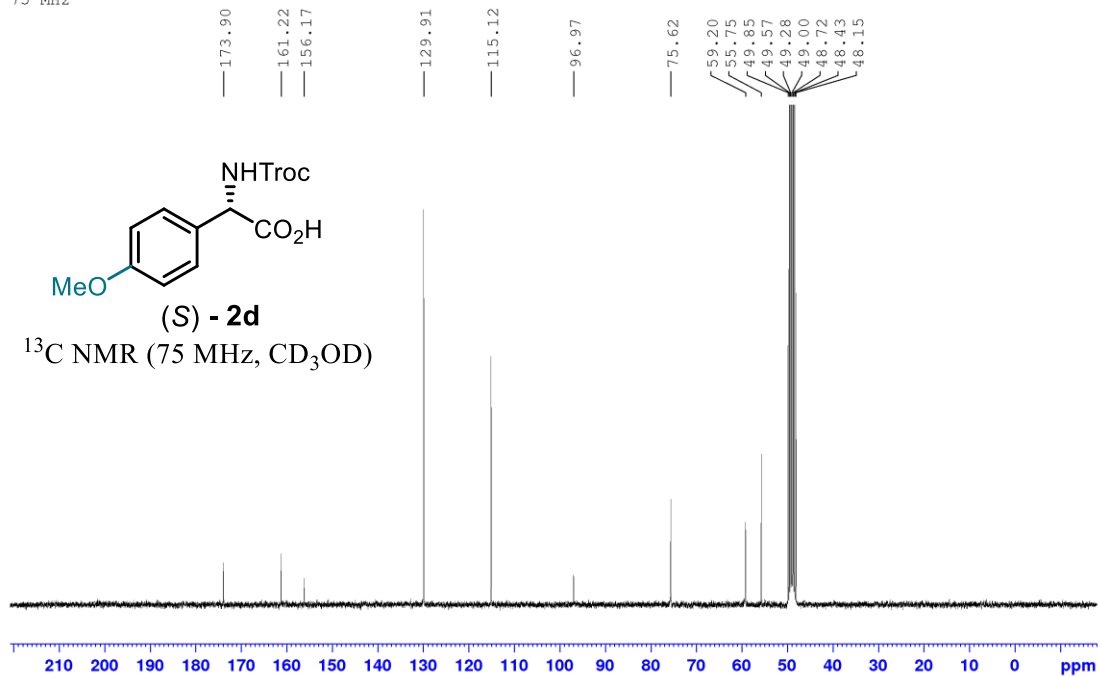


CXG-77-13C
CD3OD
75 MHz

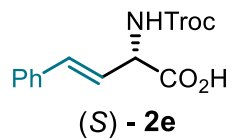


(S) - 2d

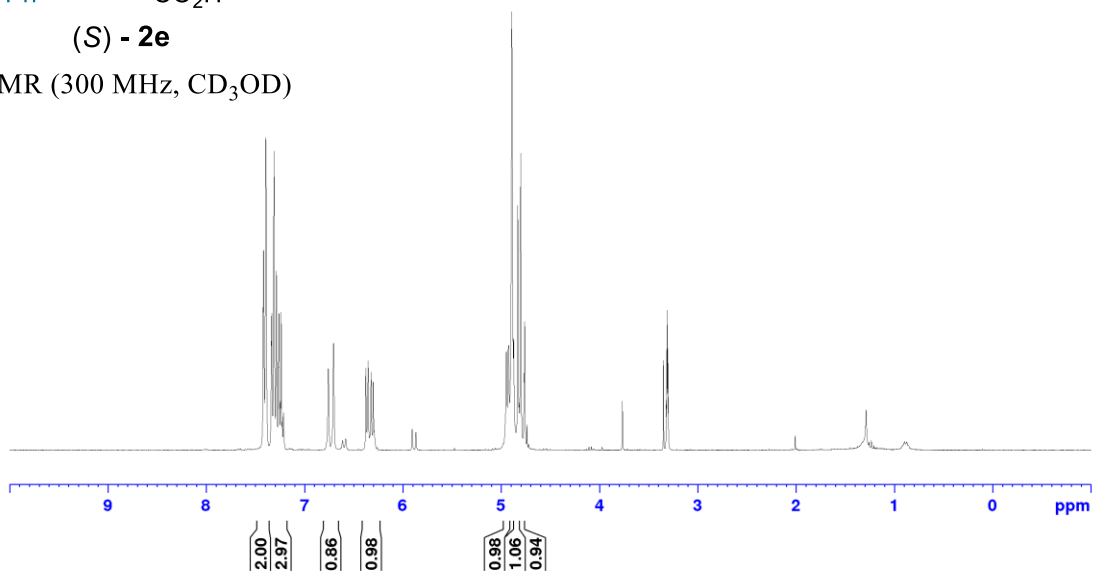
¹³C NMR (75 MHz, CD₃OD)



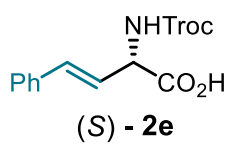
CXG-187-1H
CD3OD
300 MHz



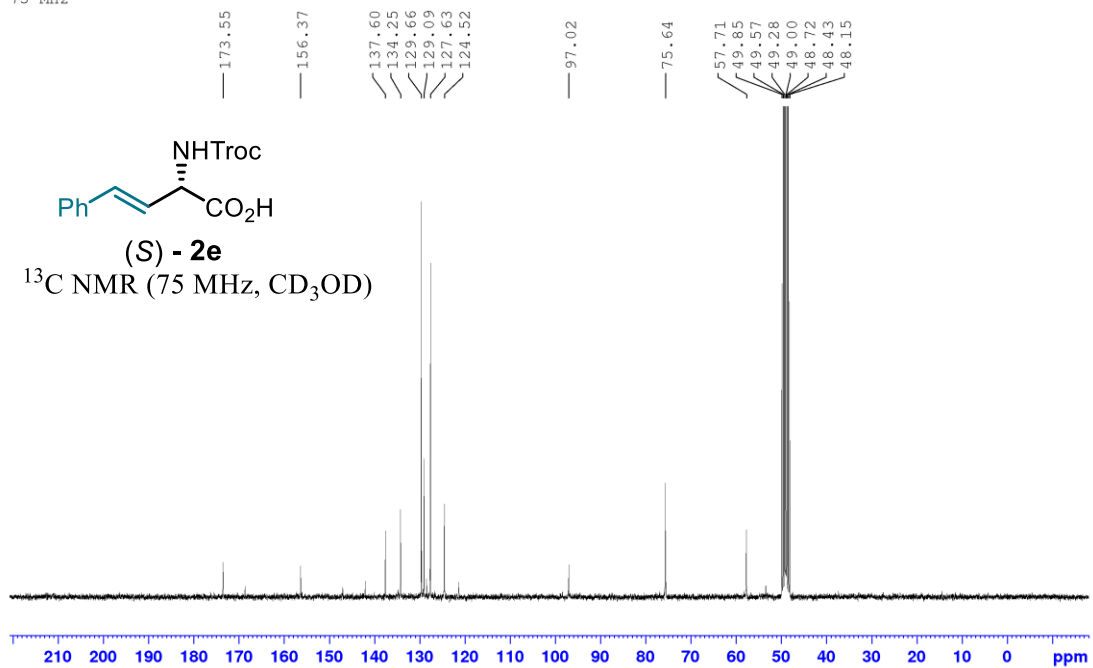
¹H NMR (300 MHz, CD₃OD)



CXG-187-13C
CD3OD
75 MHz

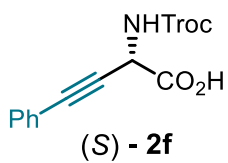


¹³C NMR (75 MHz, CD₃OD)

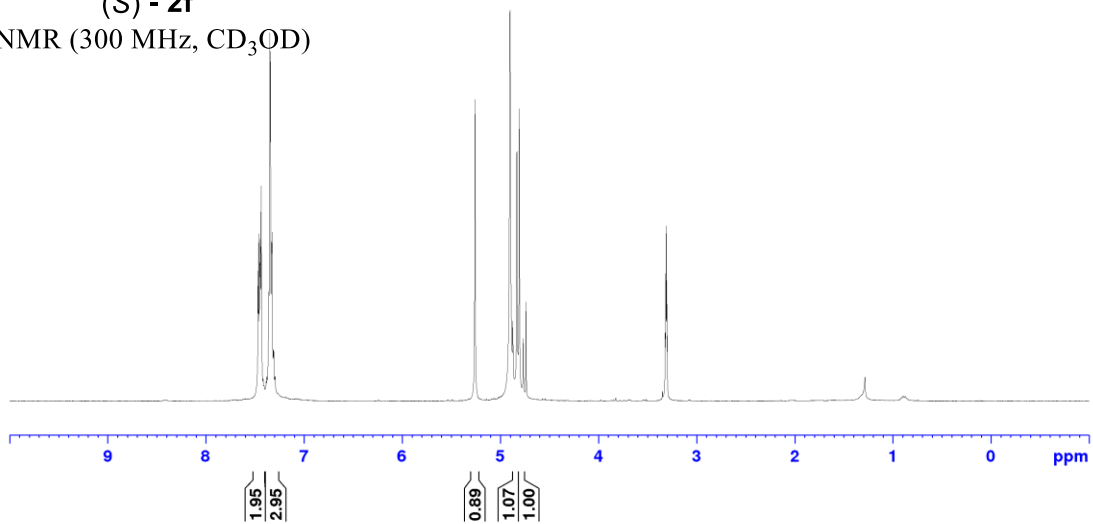


Statement

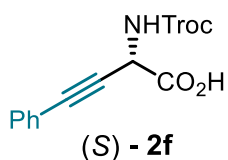
CXH-163-1H
CD3OD
300 MHz



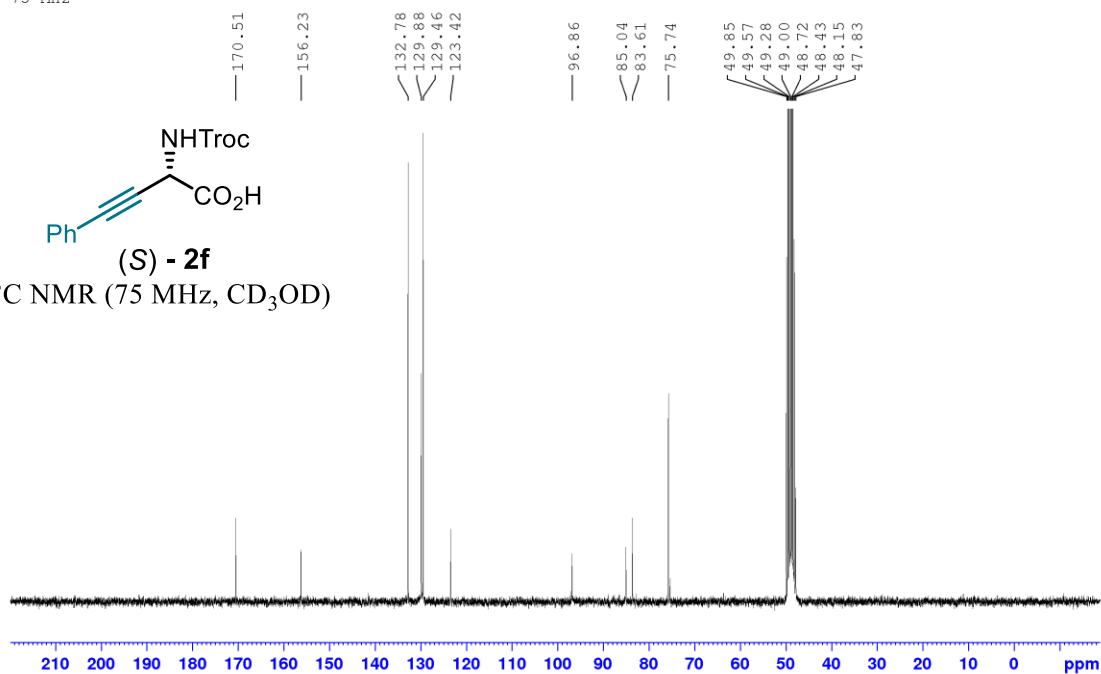
(S) - 2f
¹H NMR (300 MHz, CD₃OD)



CXH-163-13C
CD3OD
75 MHz

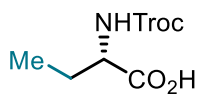


(S) - 2f
¹³C NMR (75 MHz, CD₃OD)



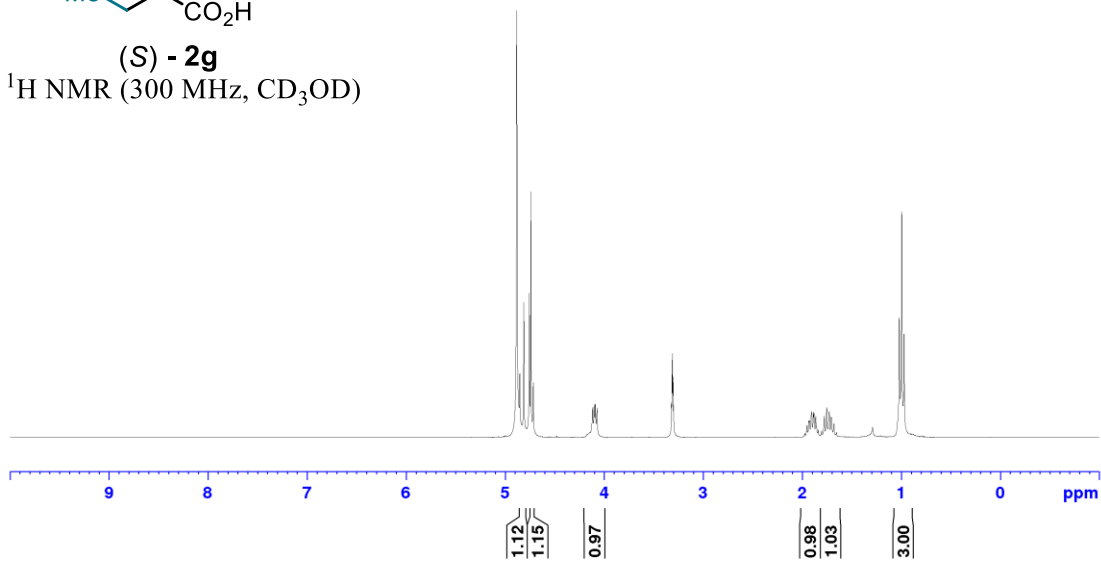
Statement

CXJ-62-1H
CD3OD
300 MHz

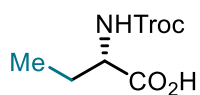


(S) - 2g

^1H NMR (300 MHz, CD_3OD)

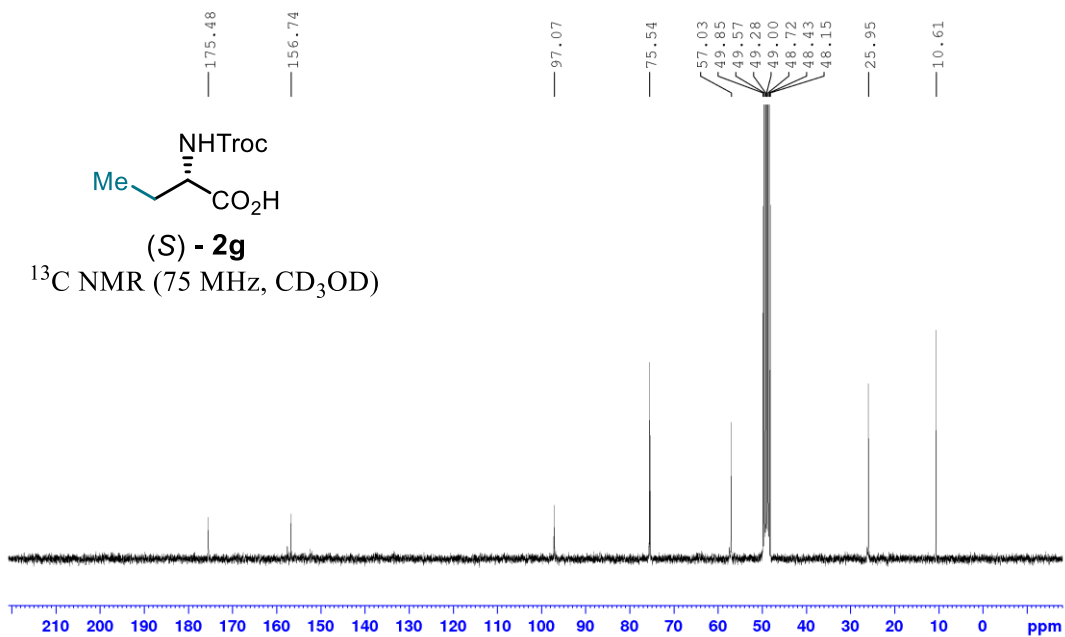


CXJ-62-13C
CD3OD
75 MHz



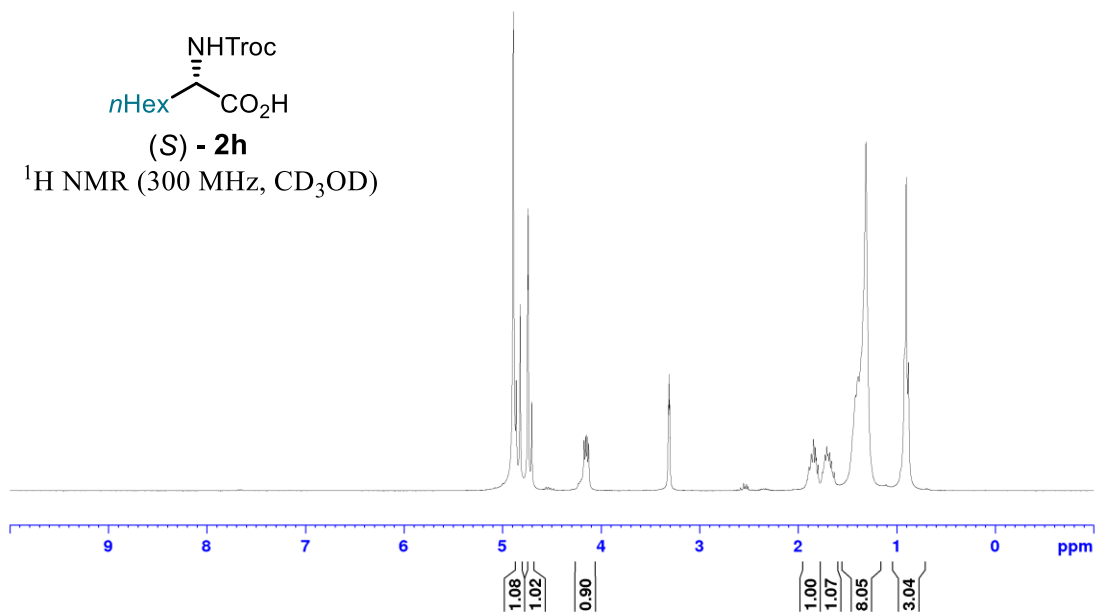
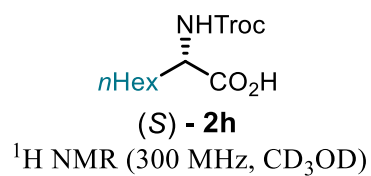
(S) - 2g

^{13}C NMR (75 MHz, CD_3OD)

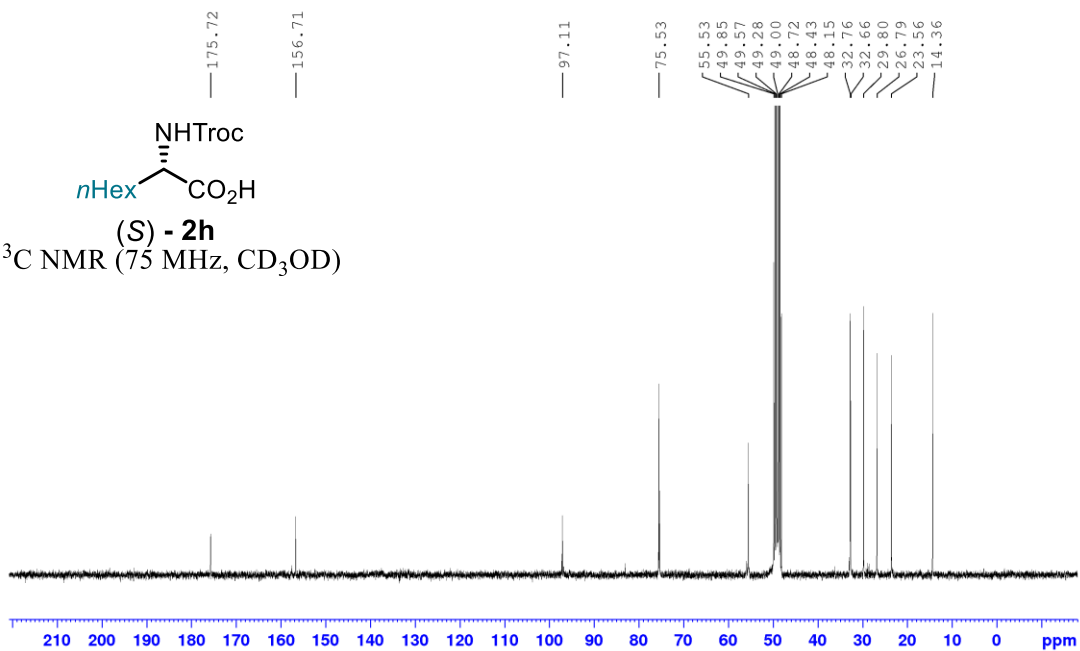
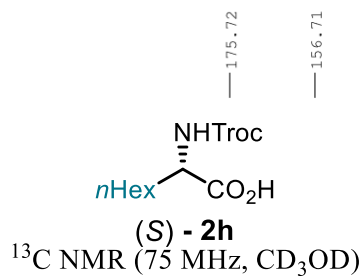


Statement

CXJ-60-1H
CD3OD
300 MHz

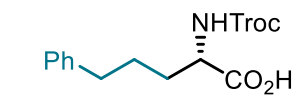


CXJ-60-13C
CD3OD
75 MHz



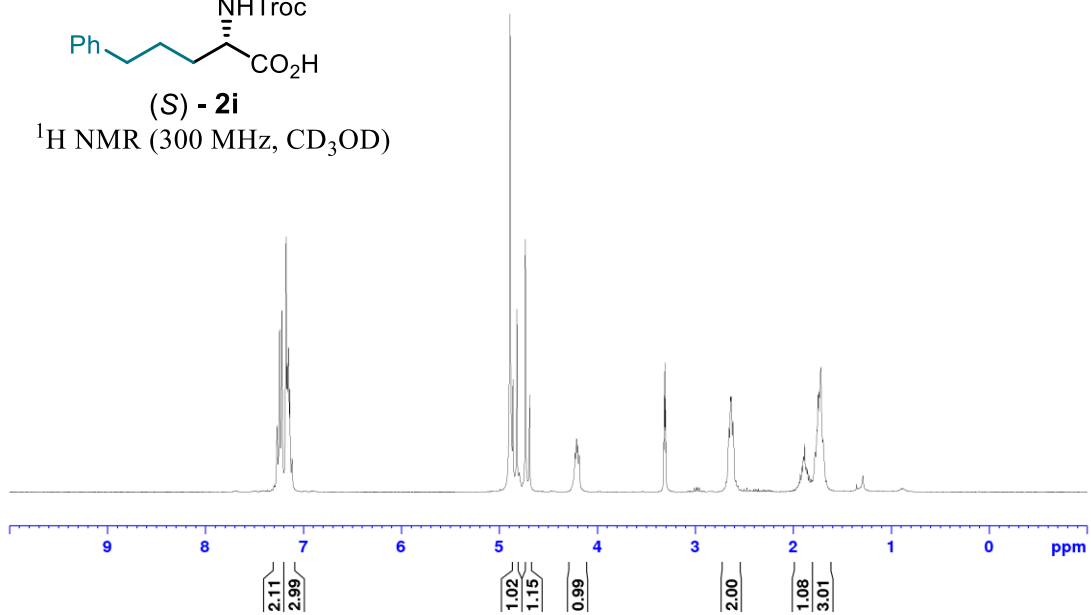
Statement

CXJ-75-1H
CD3OD
300 MHz

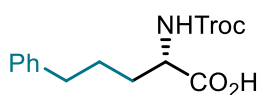


(S) - 2i

¹H NMR (300 MHz, CD₃OD)

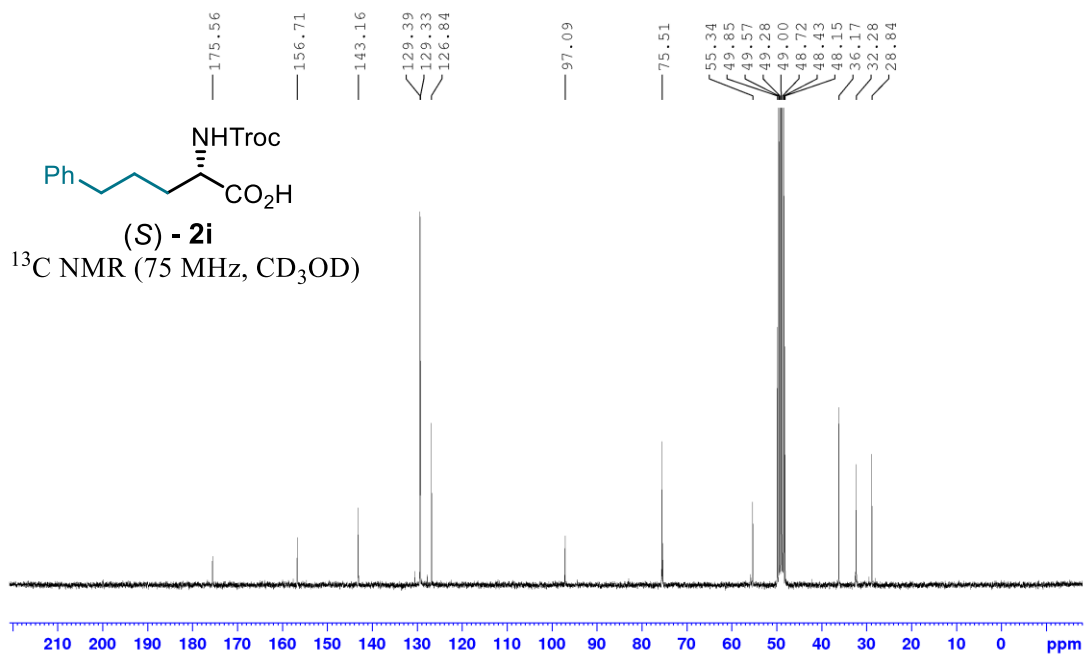


CXJ-75-13C
CD3OD
75 MHz



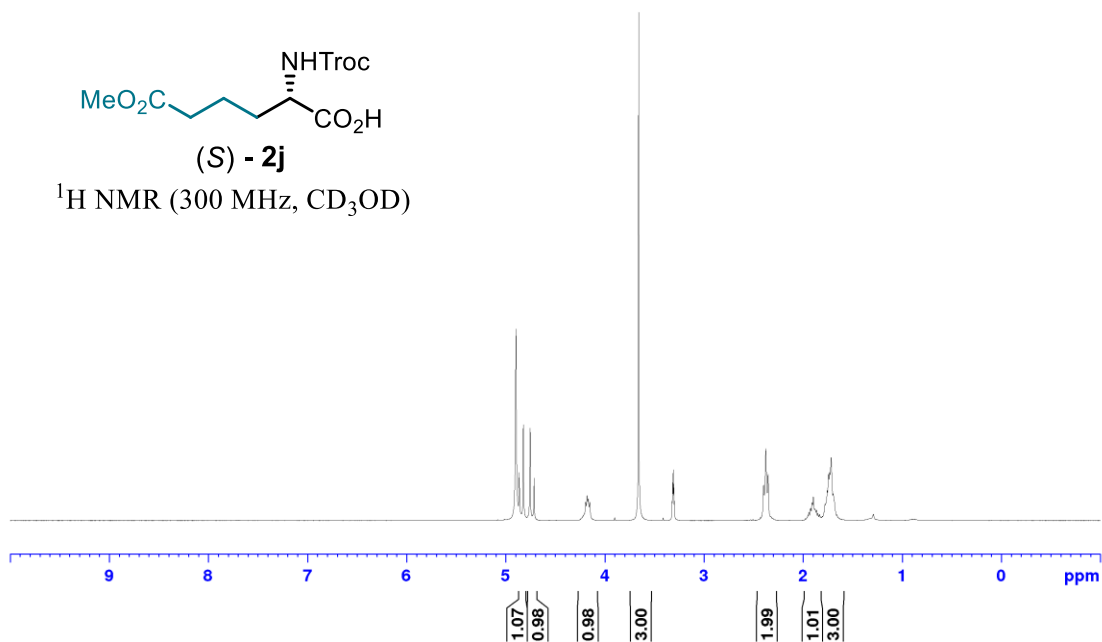
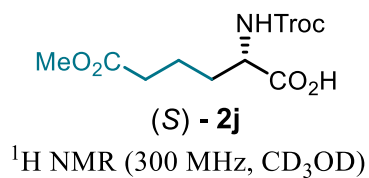
(S) - 2i

¹³C NMR (75 MHz, CD₃OD)

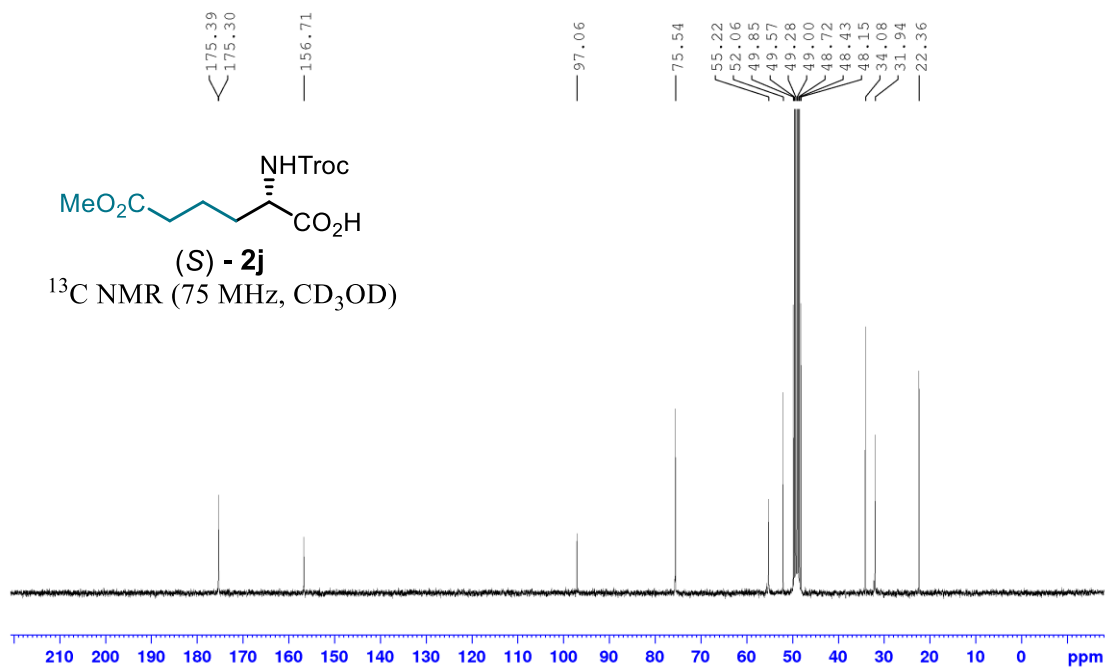
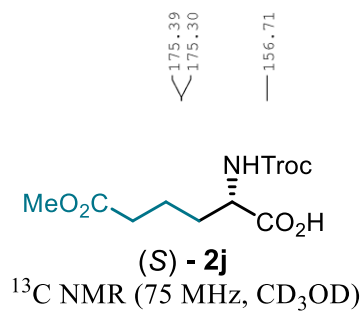


Statement

CXJ-78-1H
CD3OD
300 MHz

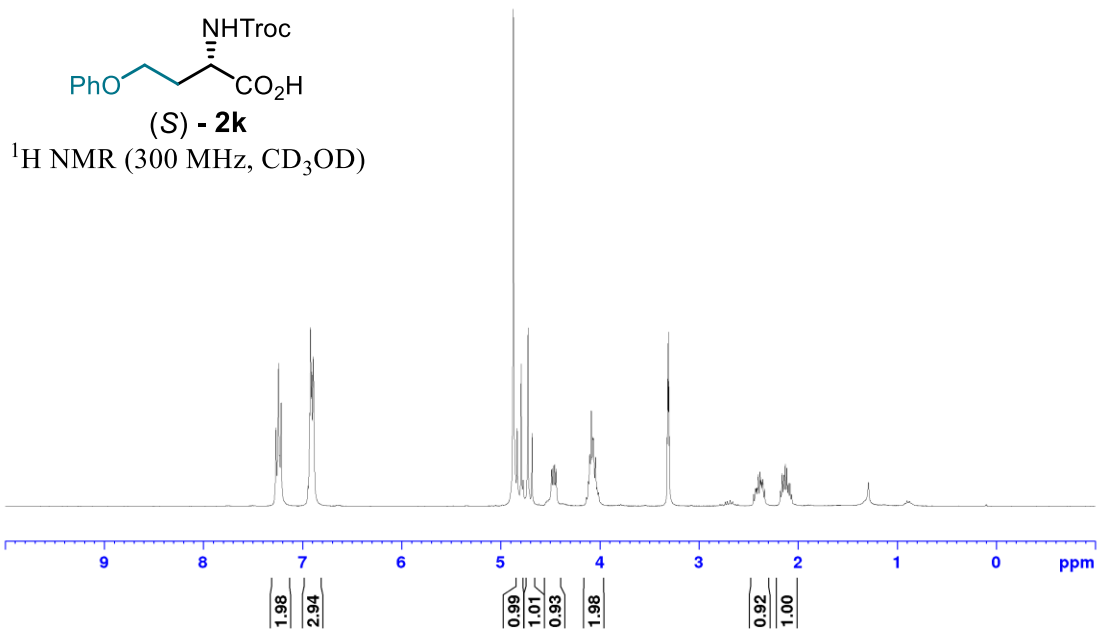


CXJ-78-13C
CD3OD
75 MHz

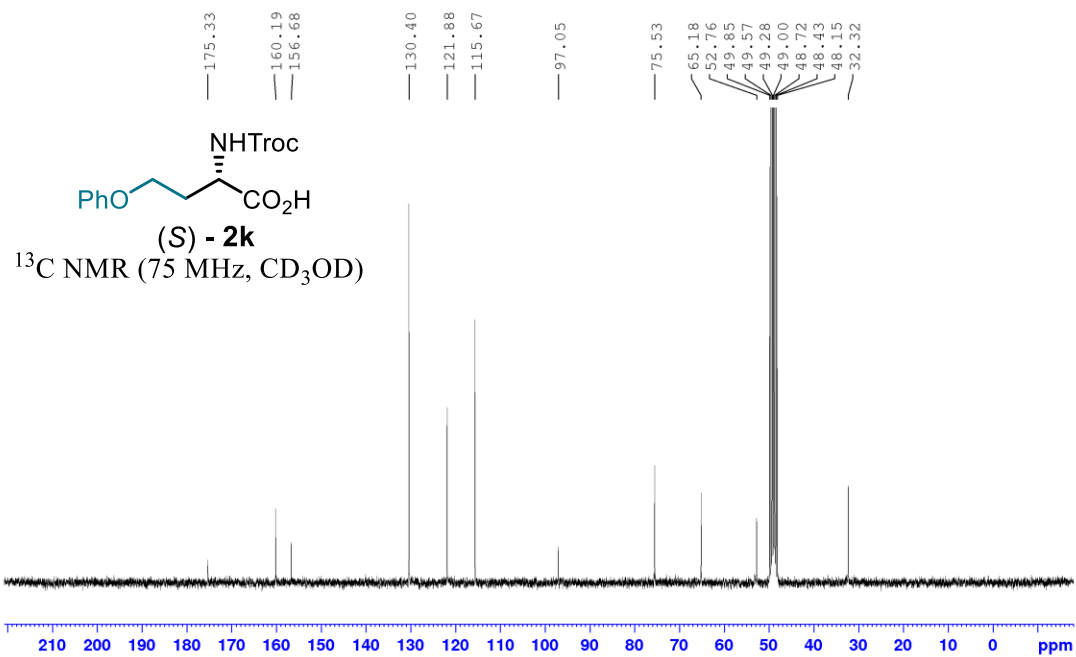


Statement

CXJ-68-1H
CD3OD
300 MHz

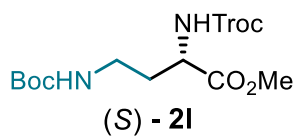


CXJ-68-13C
CD3OD
75 MHz

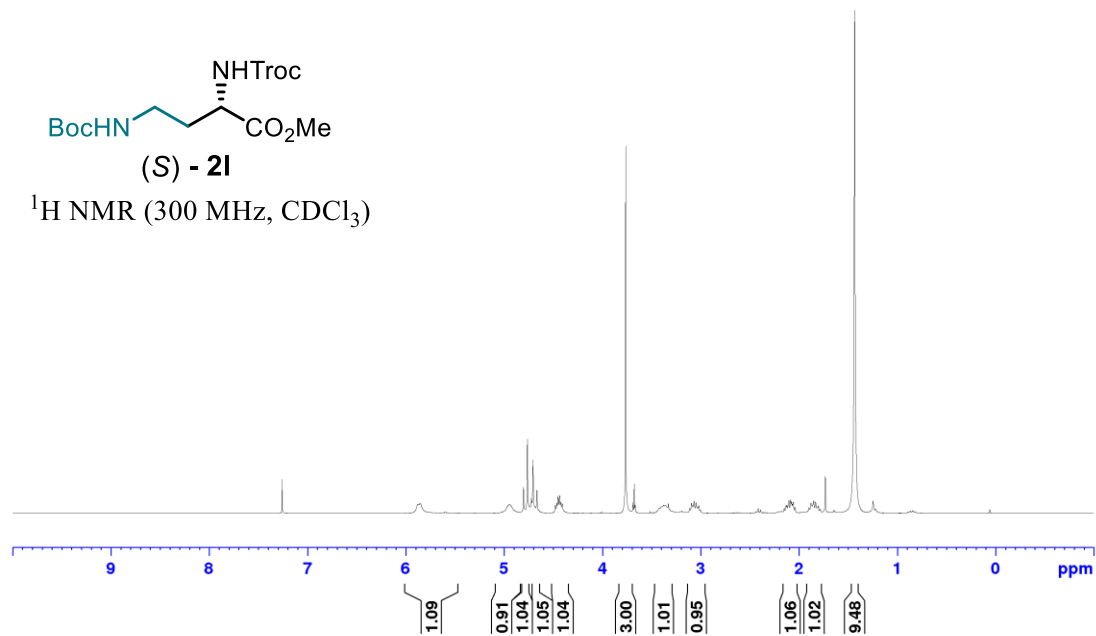


Statement

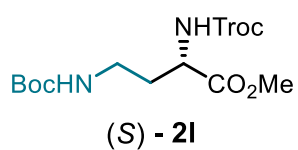
CXJ-73-1H
CDCl₃
300 MHz



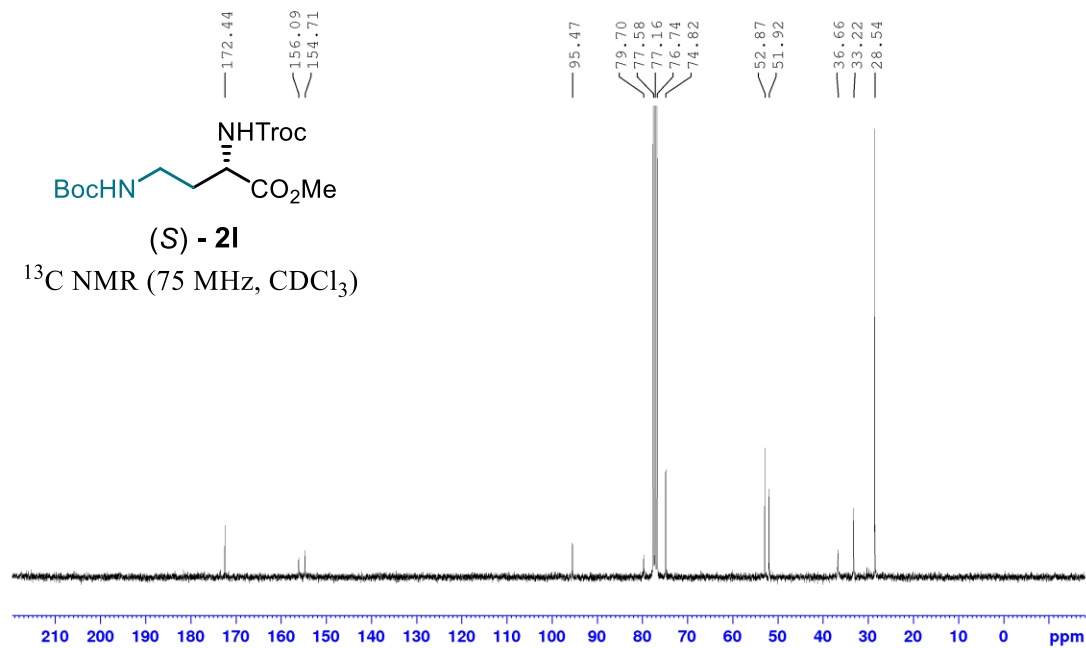
¹H NMR (300 MHz, CDCl₃)



CXJ-73-13C
CDCl₃
75 MHz

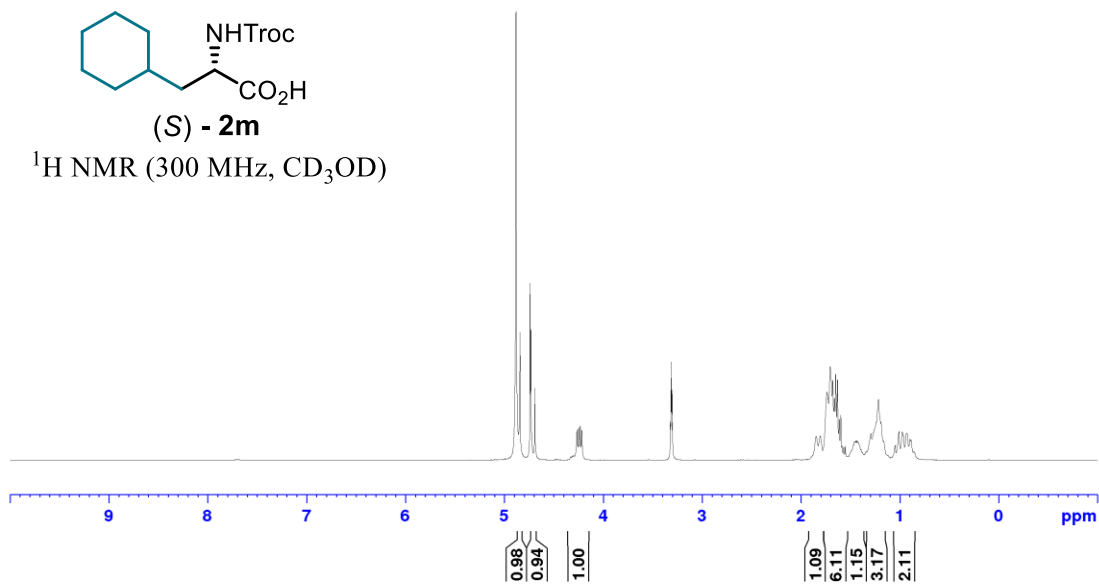
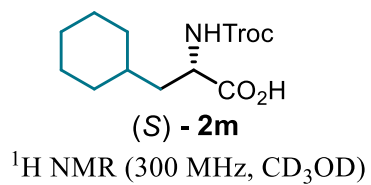


¹³C NMR (75 MHz, CDCl₃)

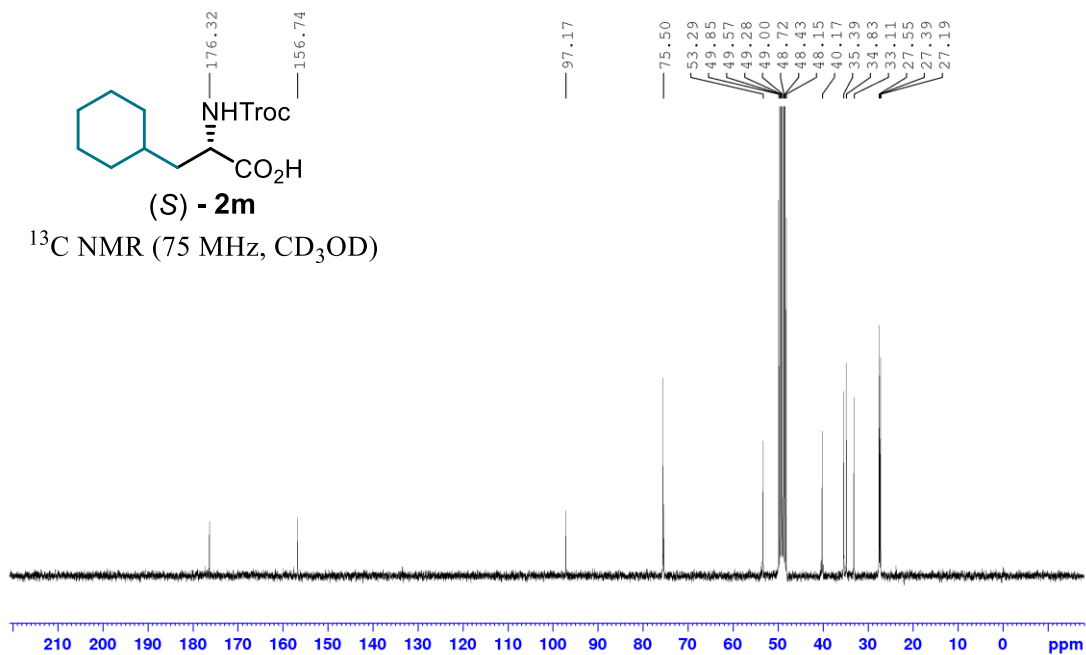
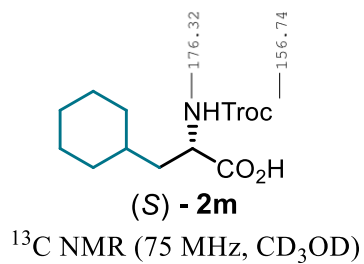


Statement

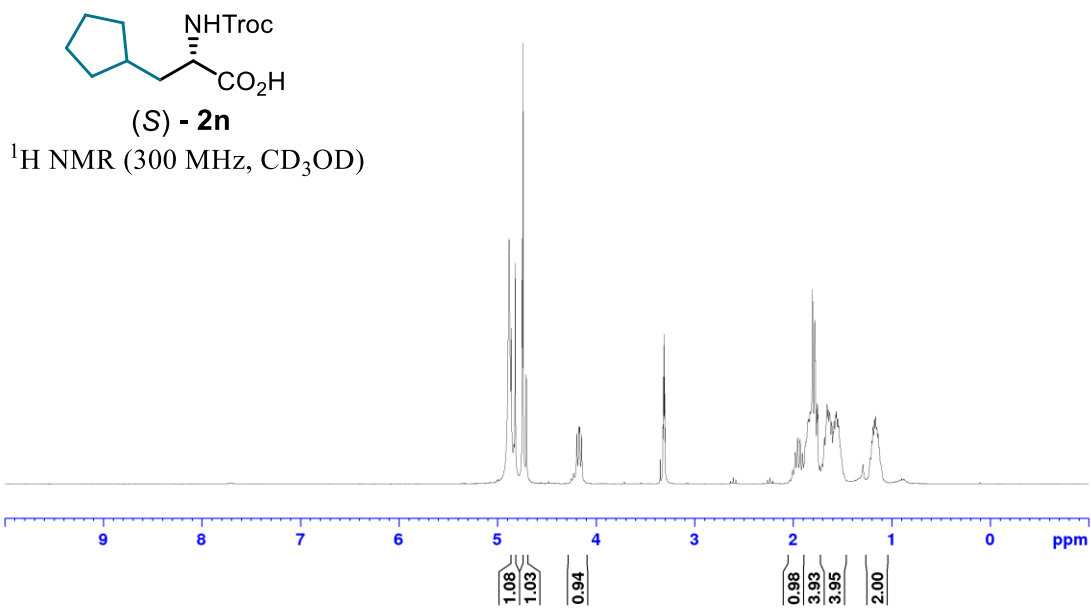
CXJ-72-1H
CD3OD
300 MHz



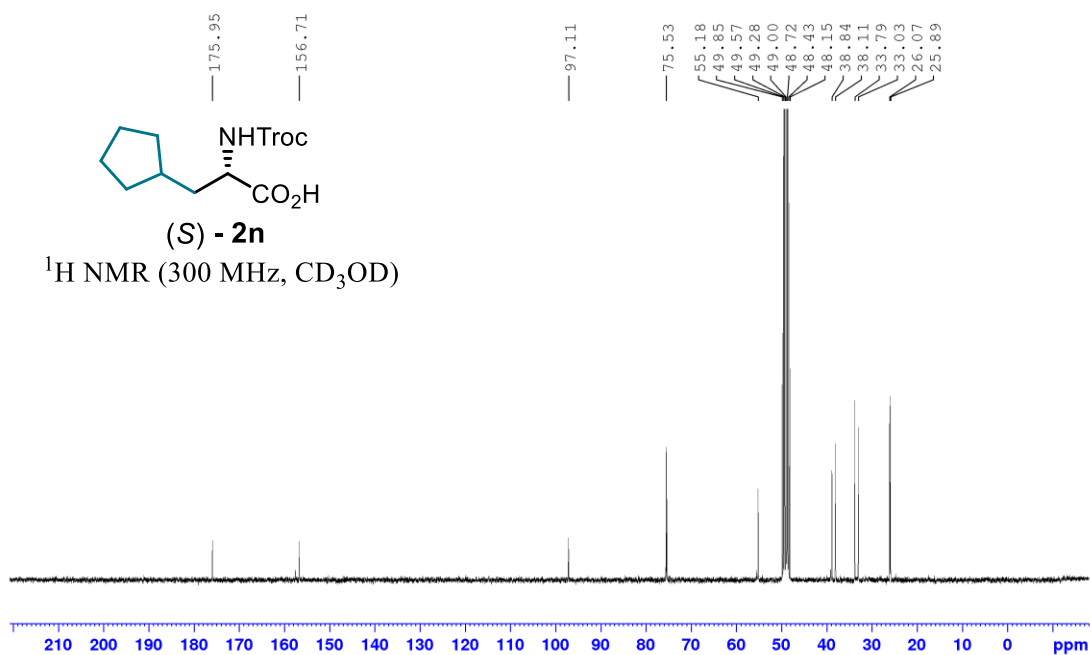
CXJ-72-13C
CD3OD
75 MHz



CXJ-74-1H
CD3OD
300 MHz

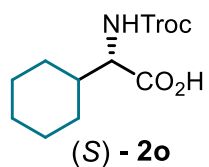


CXJ-74-13C
CD3OD
75 MHz

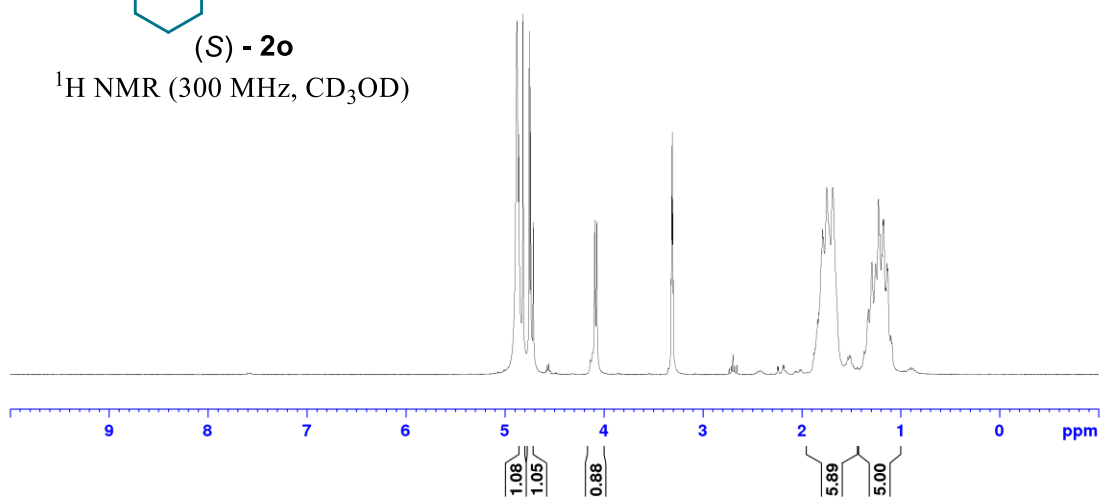


Statement

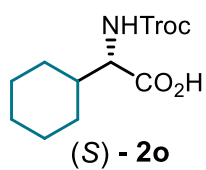
CXJ-61-1H
CD3OD
300 MHz



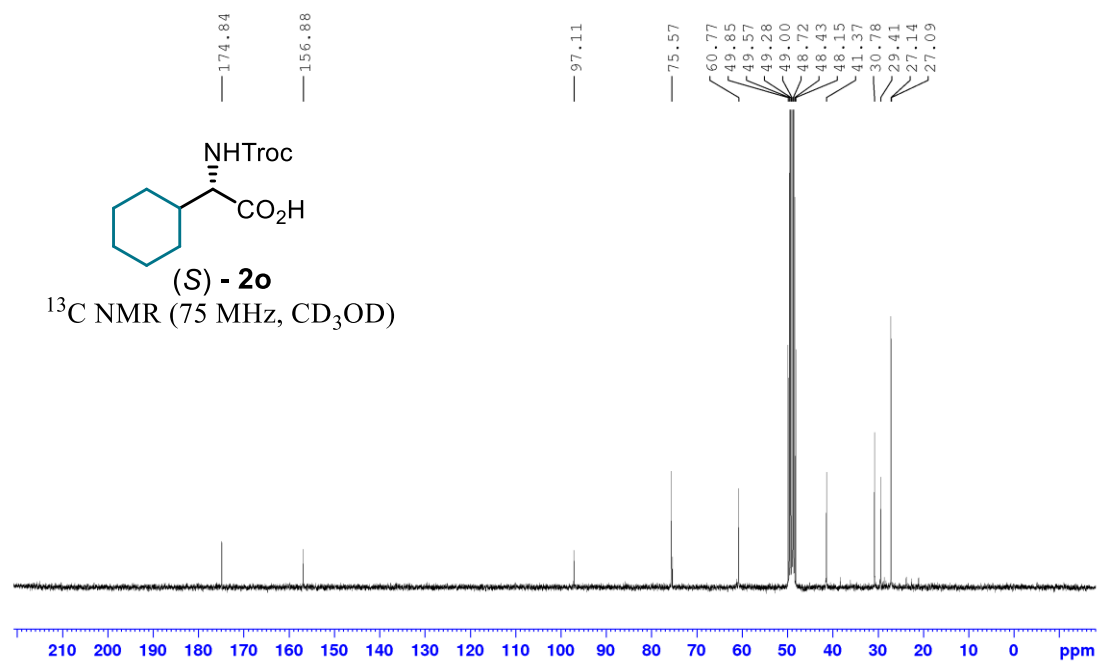
^1H NMR (300 MHz, CD_3OD)



CXJ-61-13C
CD3OD
75 MHz

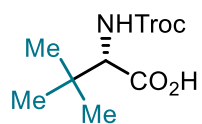


^{13}C NMR (75 MHz, CD_3OD)



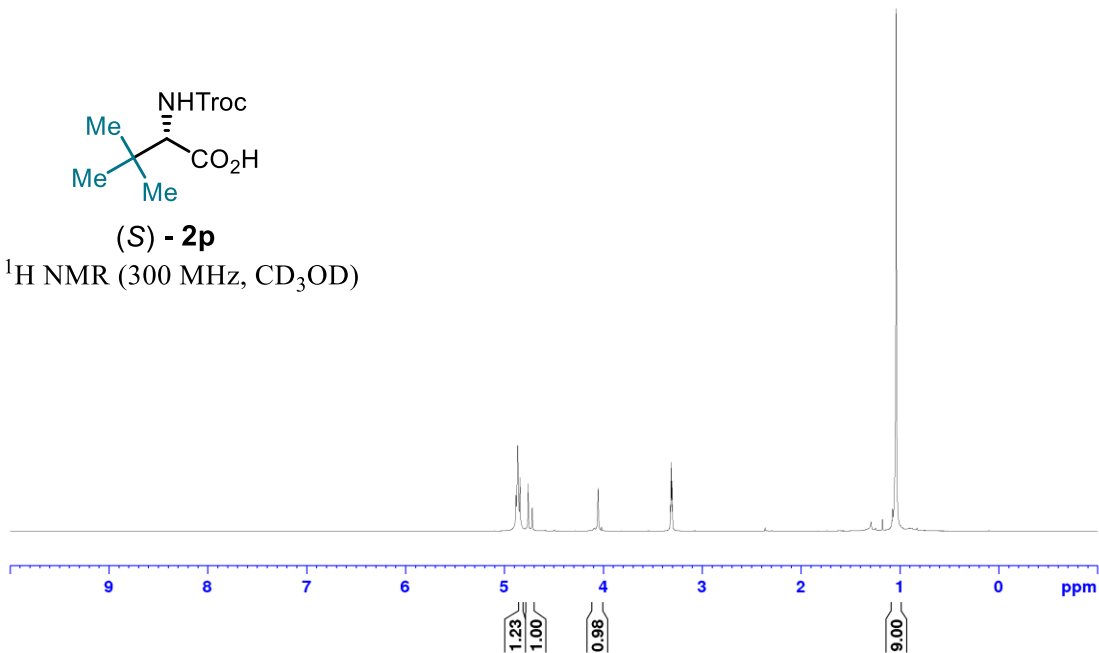
Statement

CXI-33-1H
CD3OD
300 MHz

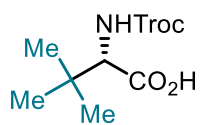


(S) - 2p

¹H NMR (300 MHz, CD₃OD)

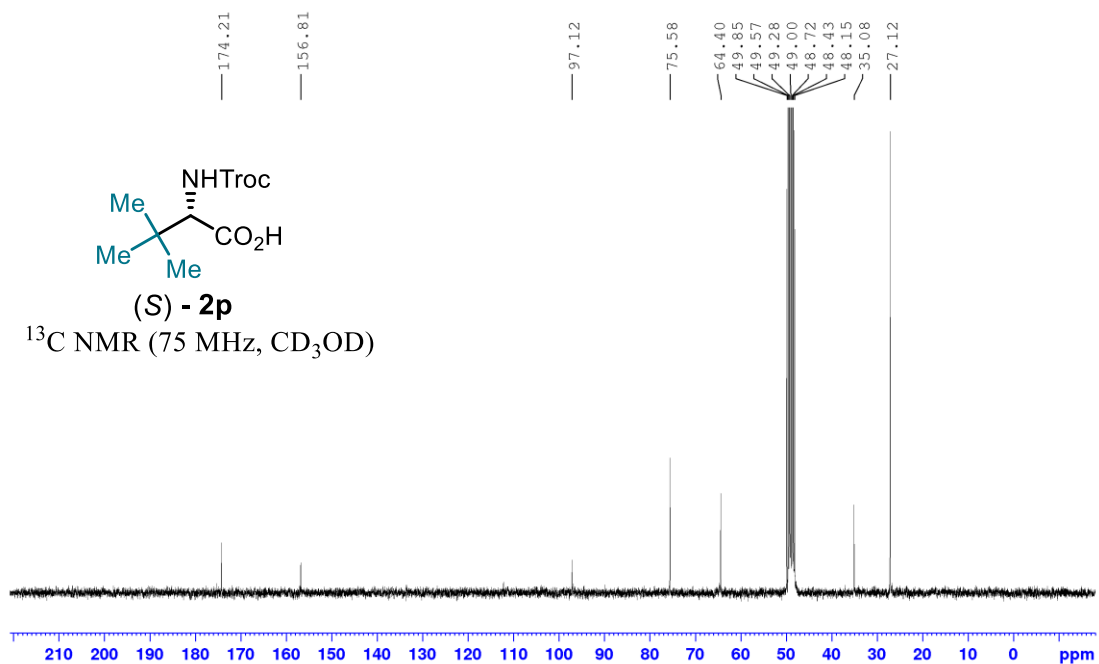


CXI-33-13C
CD3OD
75 MHz



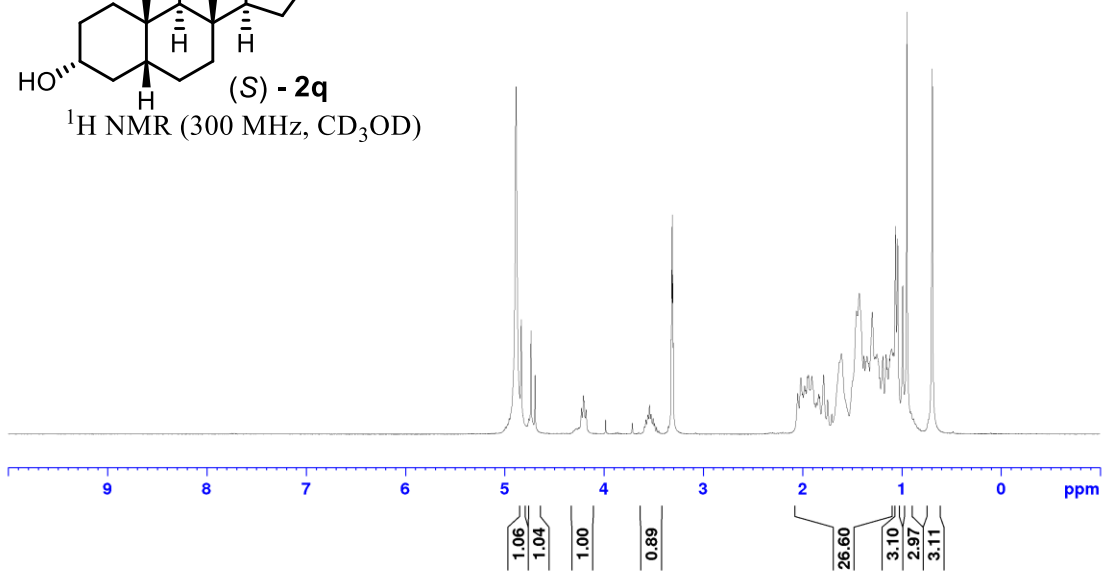
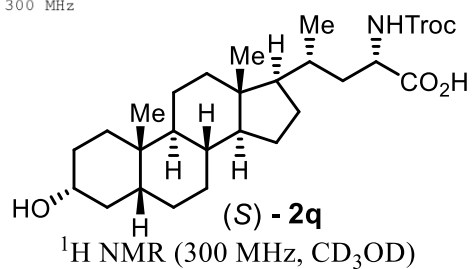
(S) - 2p

¹³C NMR (75 MHz, CD₃OD)

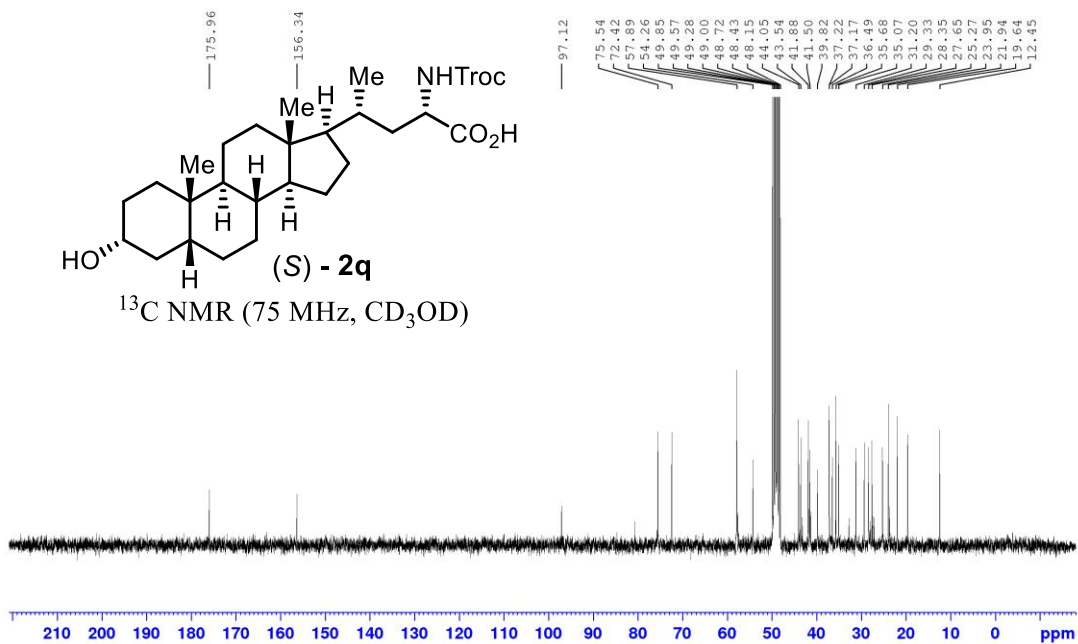
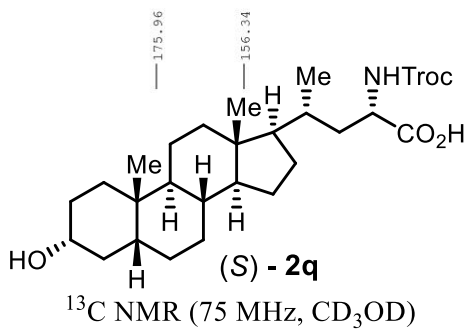


Statement

CXJ-81-a-1H
CD3OD
300 MHz

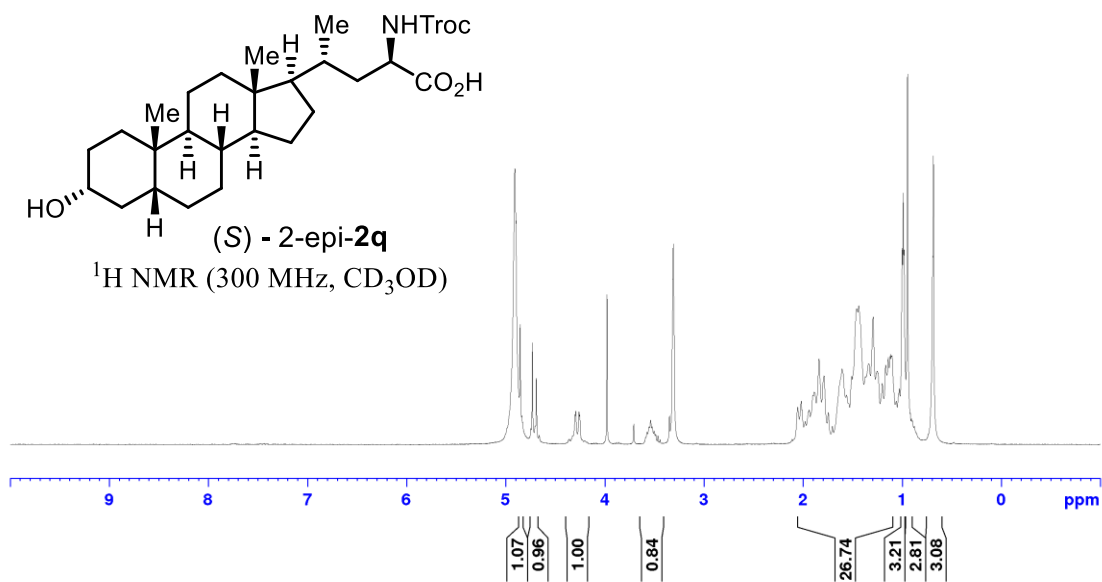


CXJ-81-a-13C
CD3OD
75 MHz

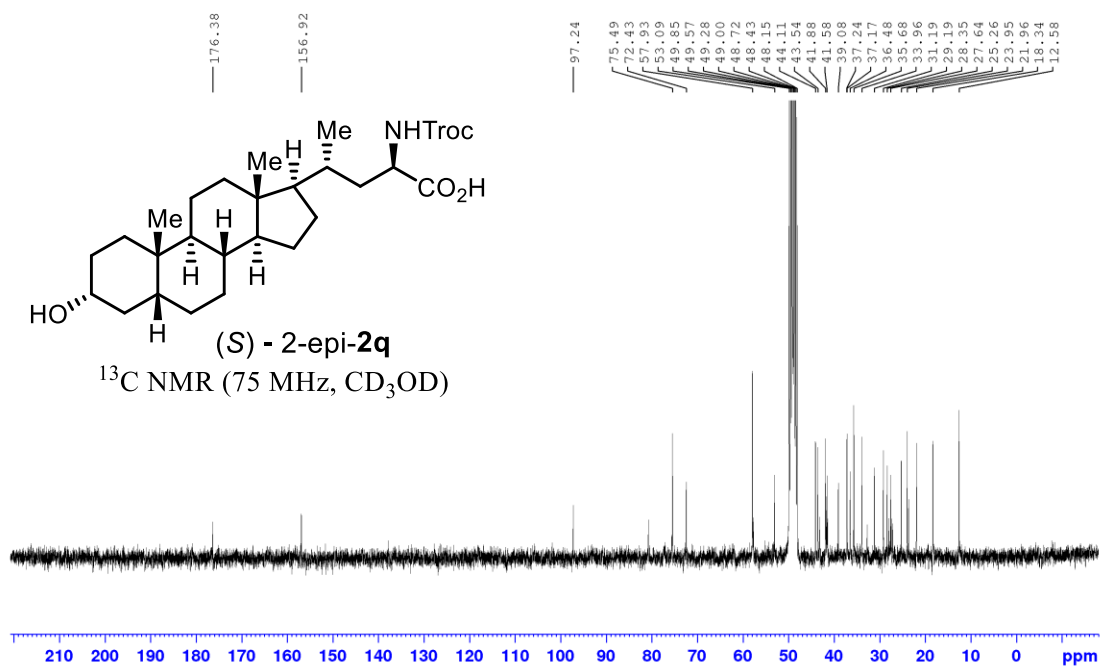


Statement

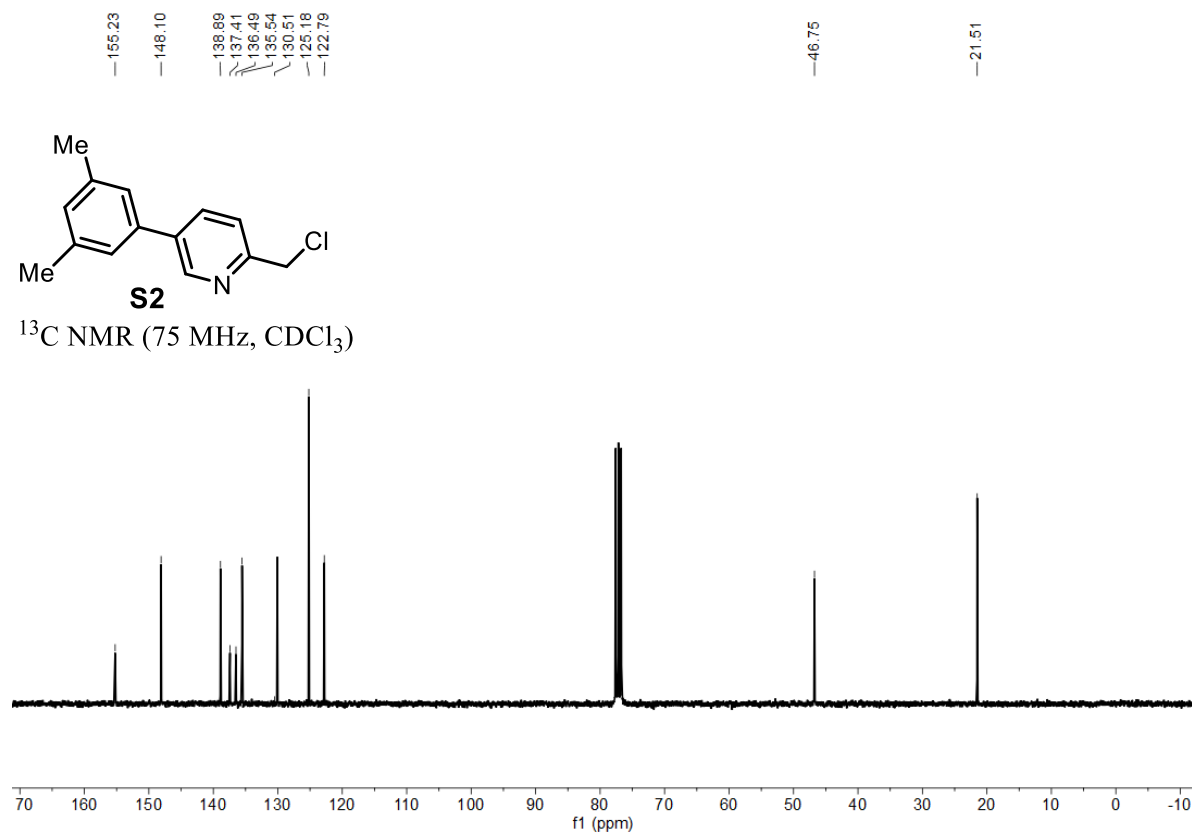
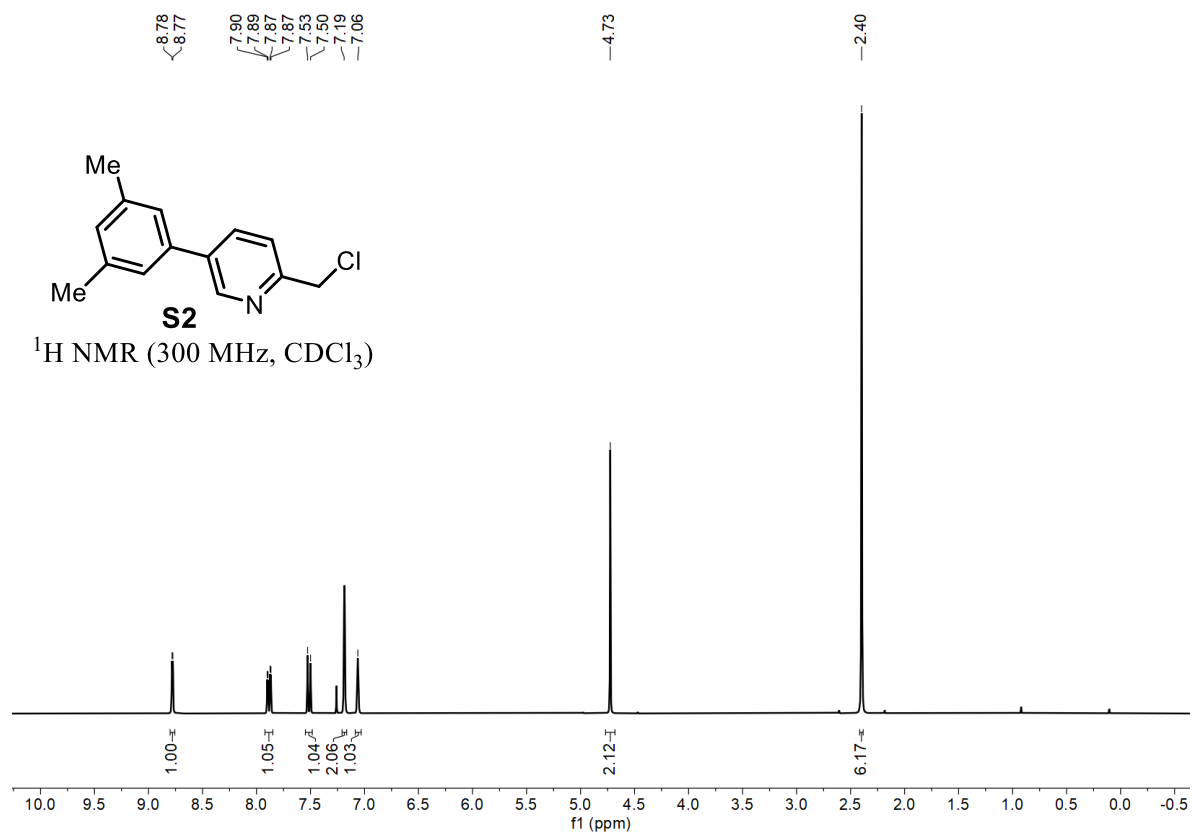
CXJ-81-b-1H
CD3OD
300 MHz



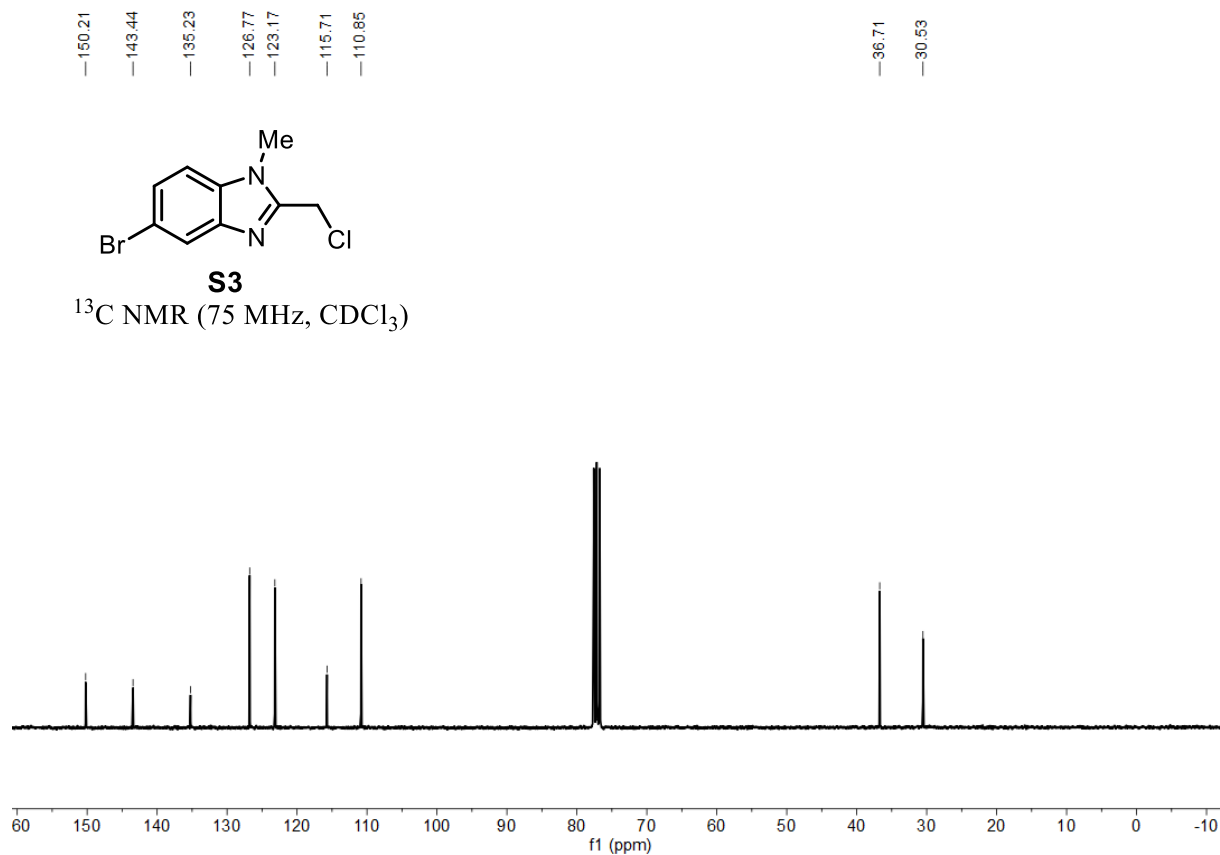
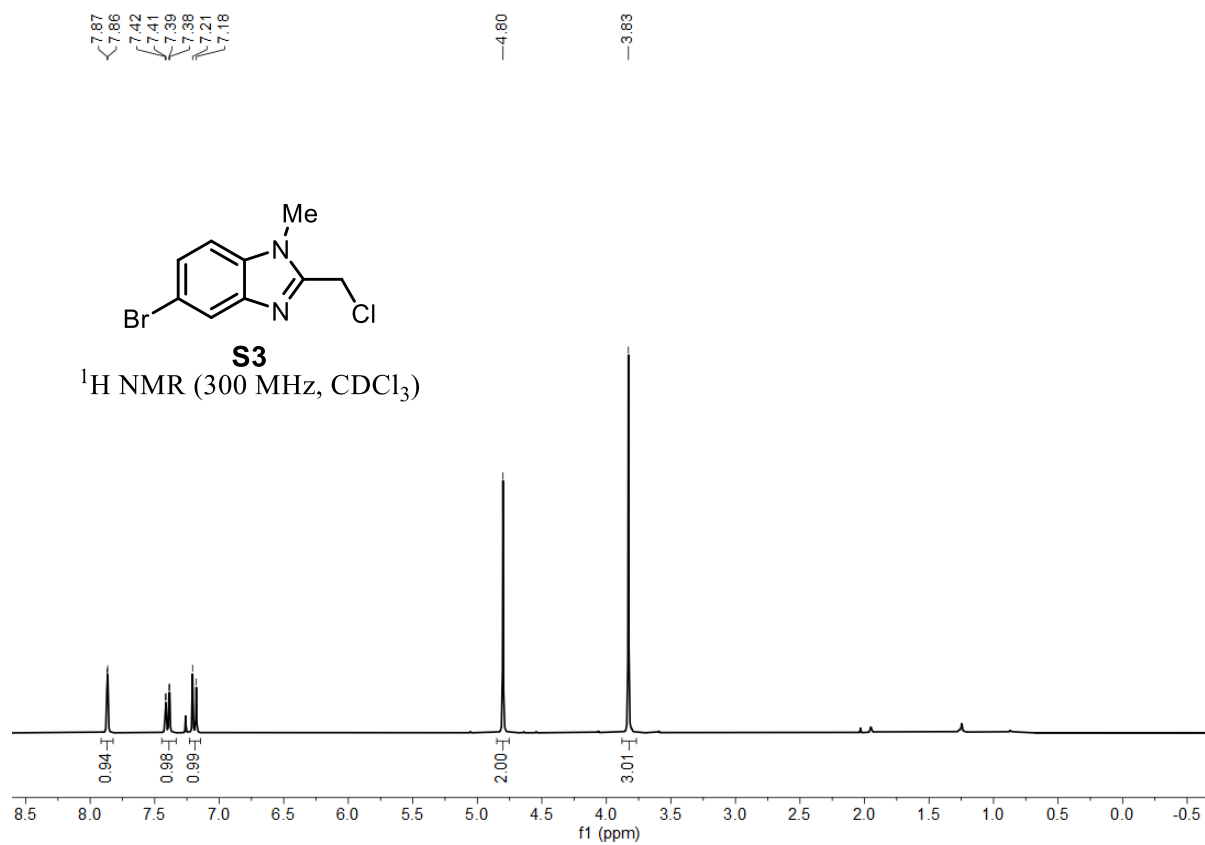
CXJ-81-b-13C
CD3OD
75 MHz



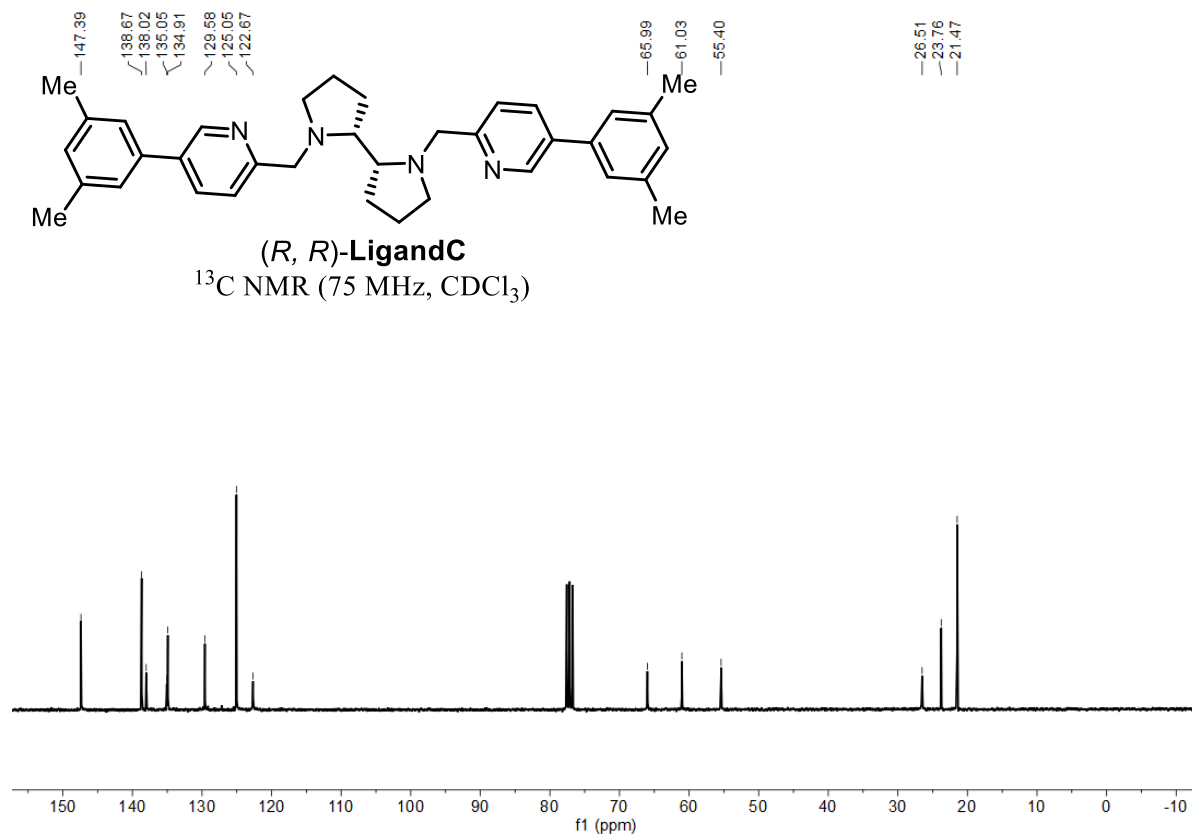
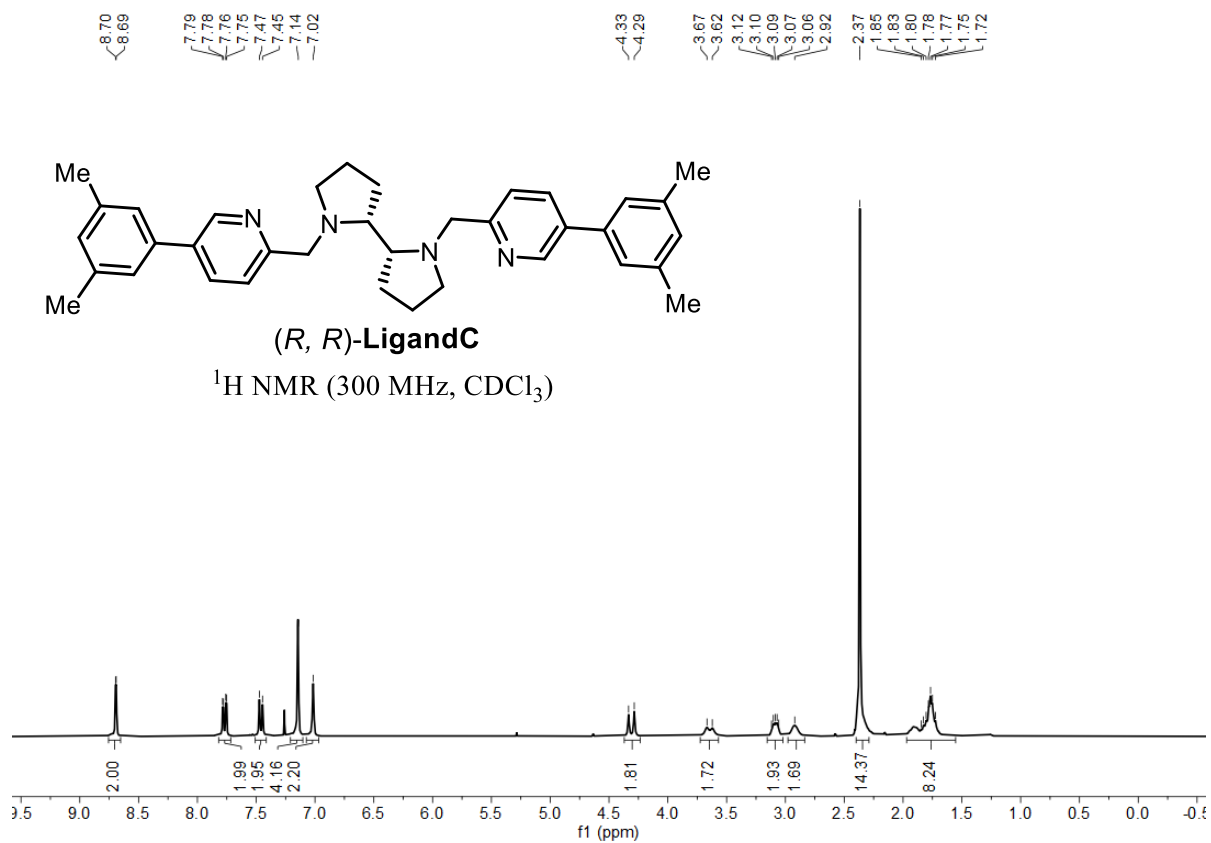
Statement



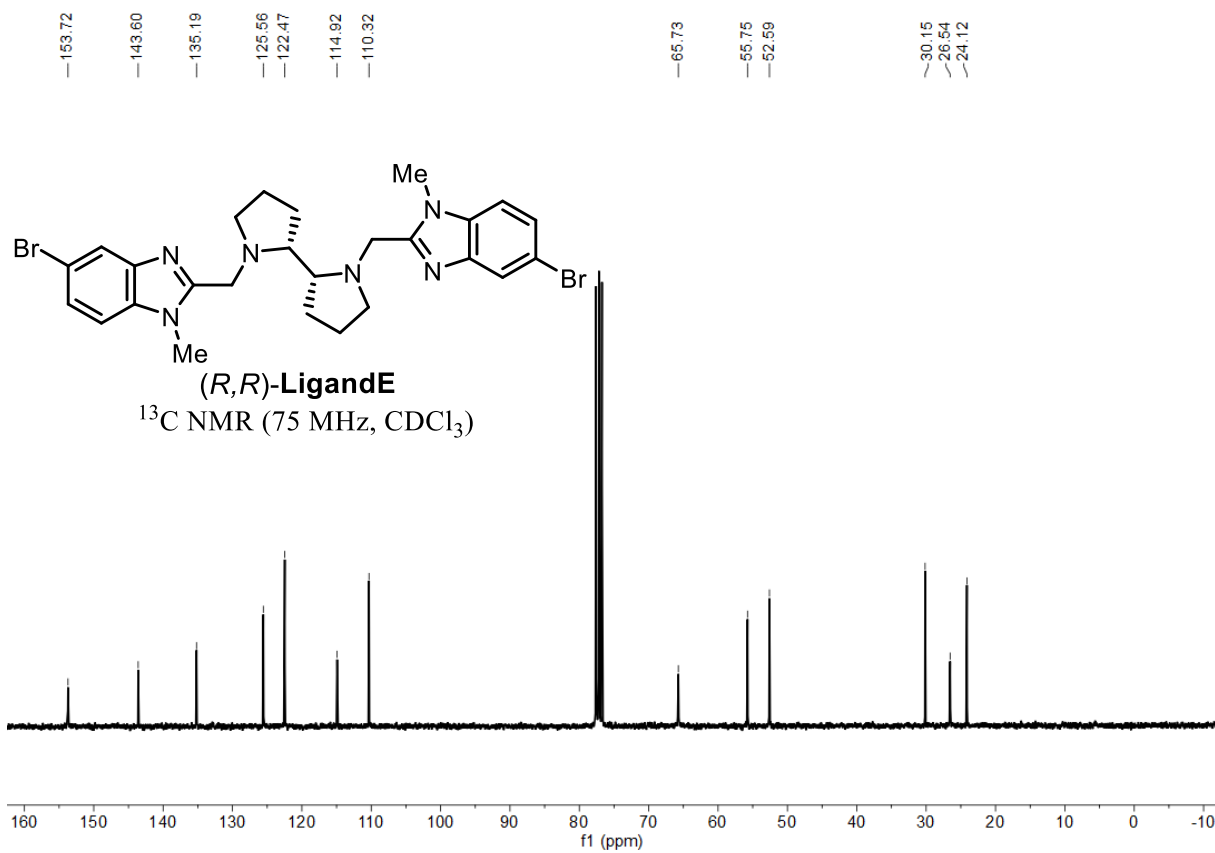
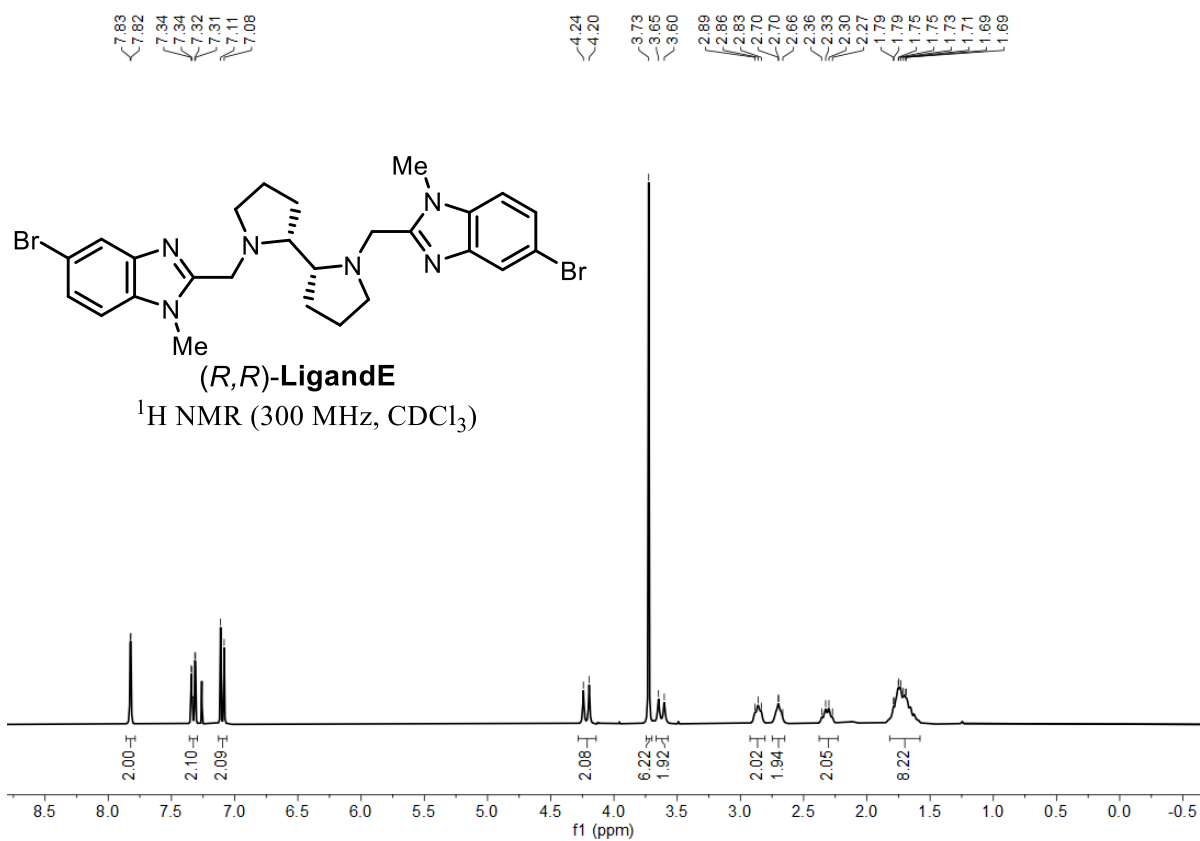
Statement



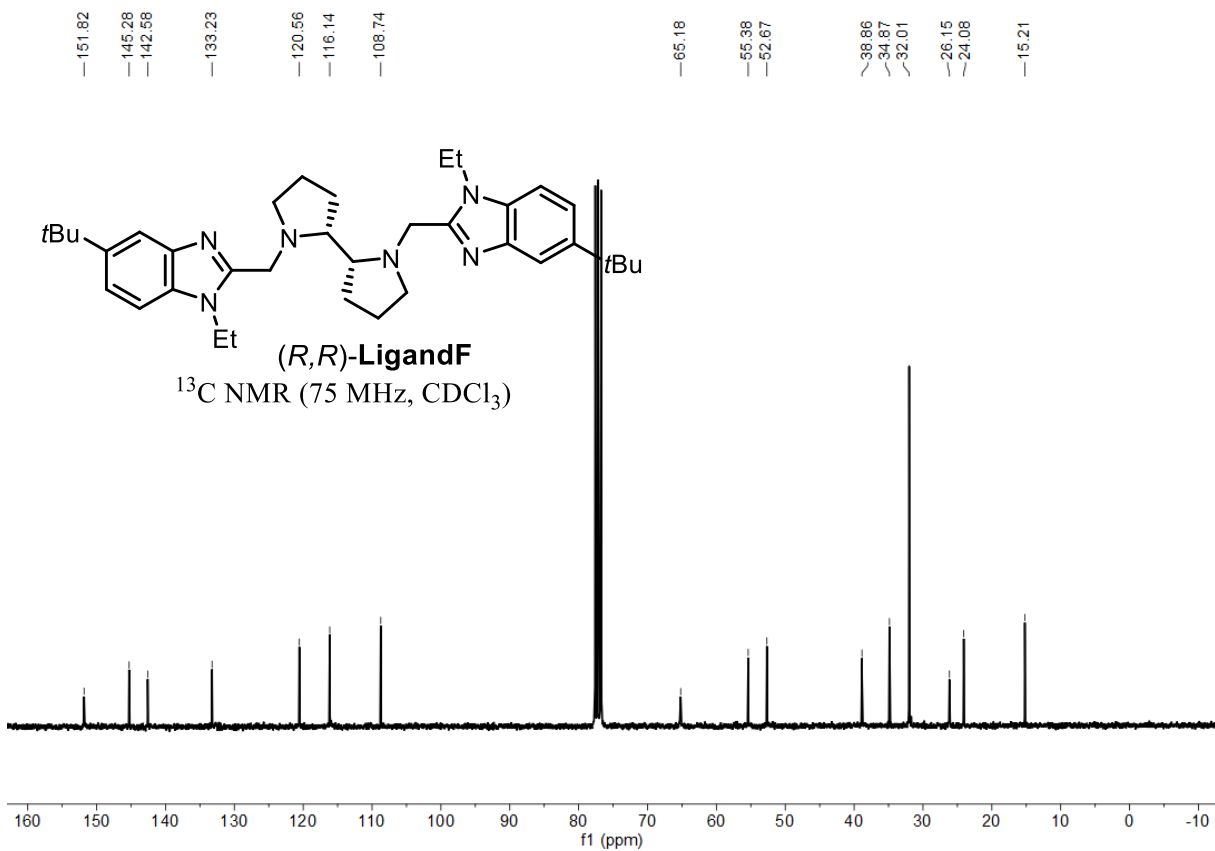
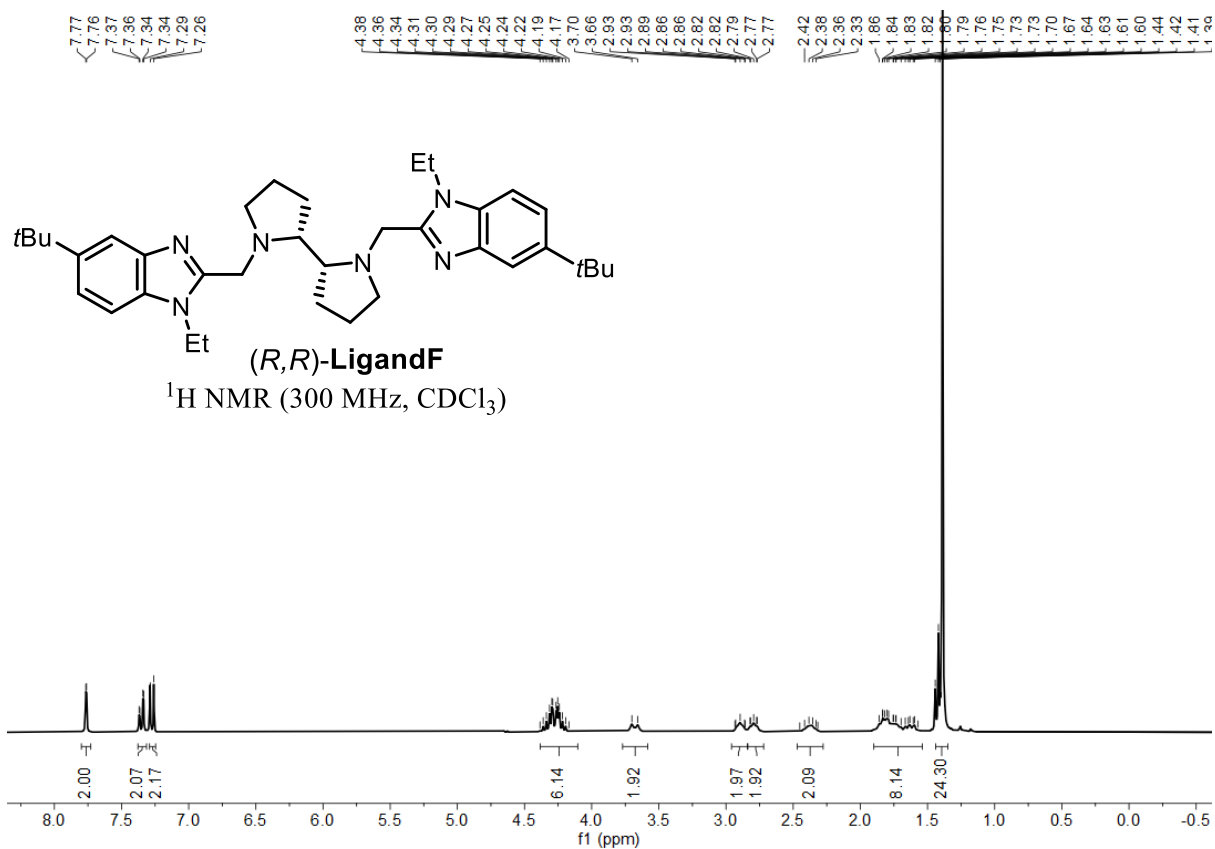
Statement



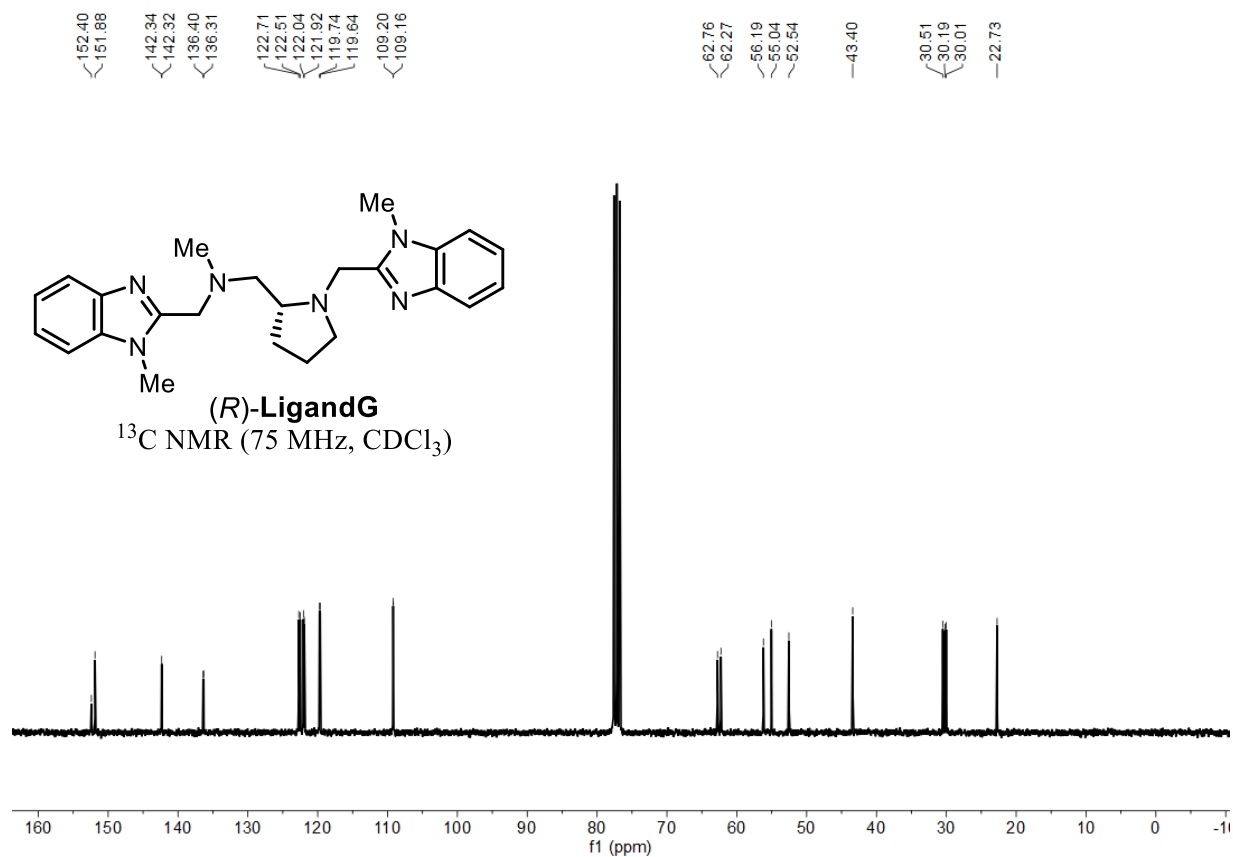
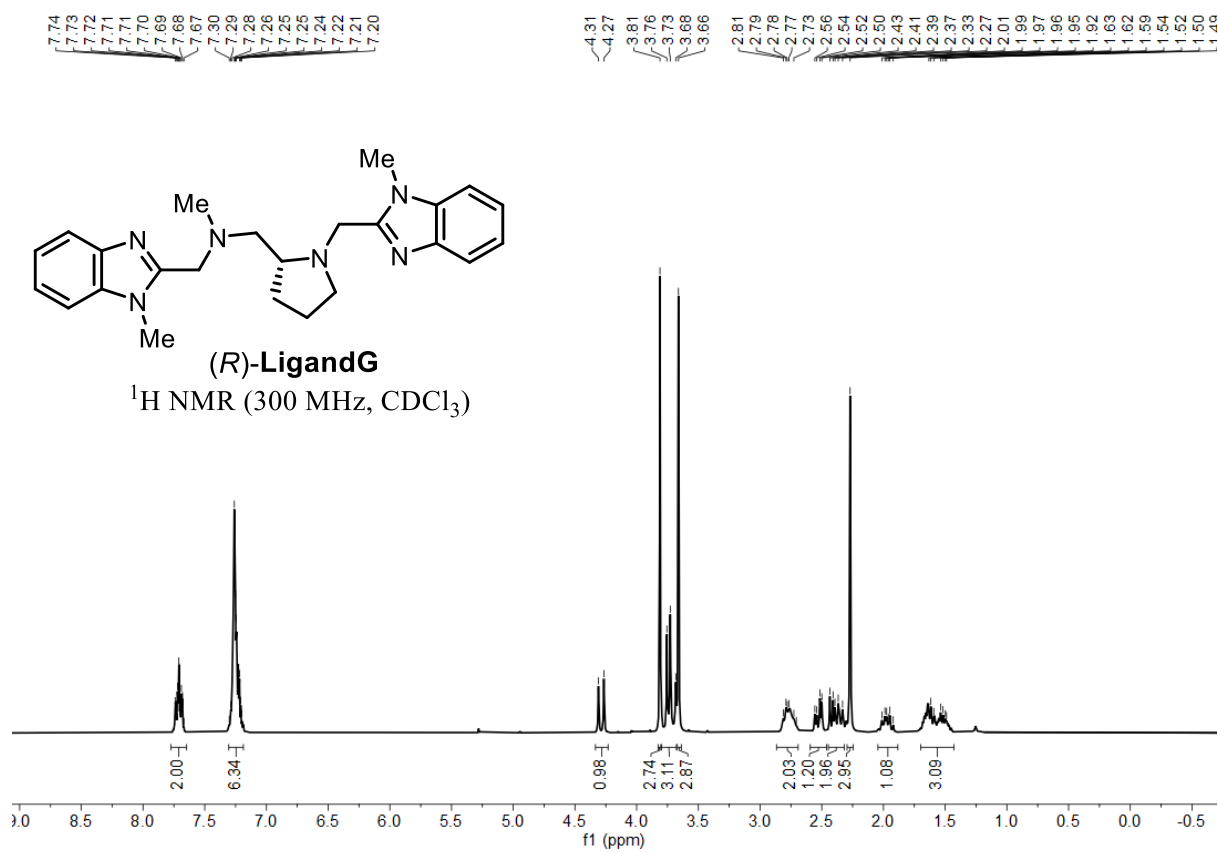
Statement



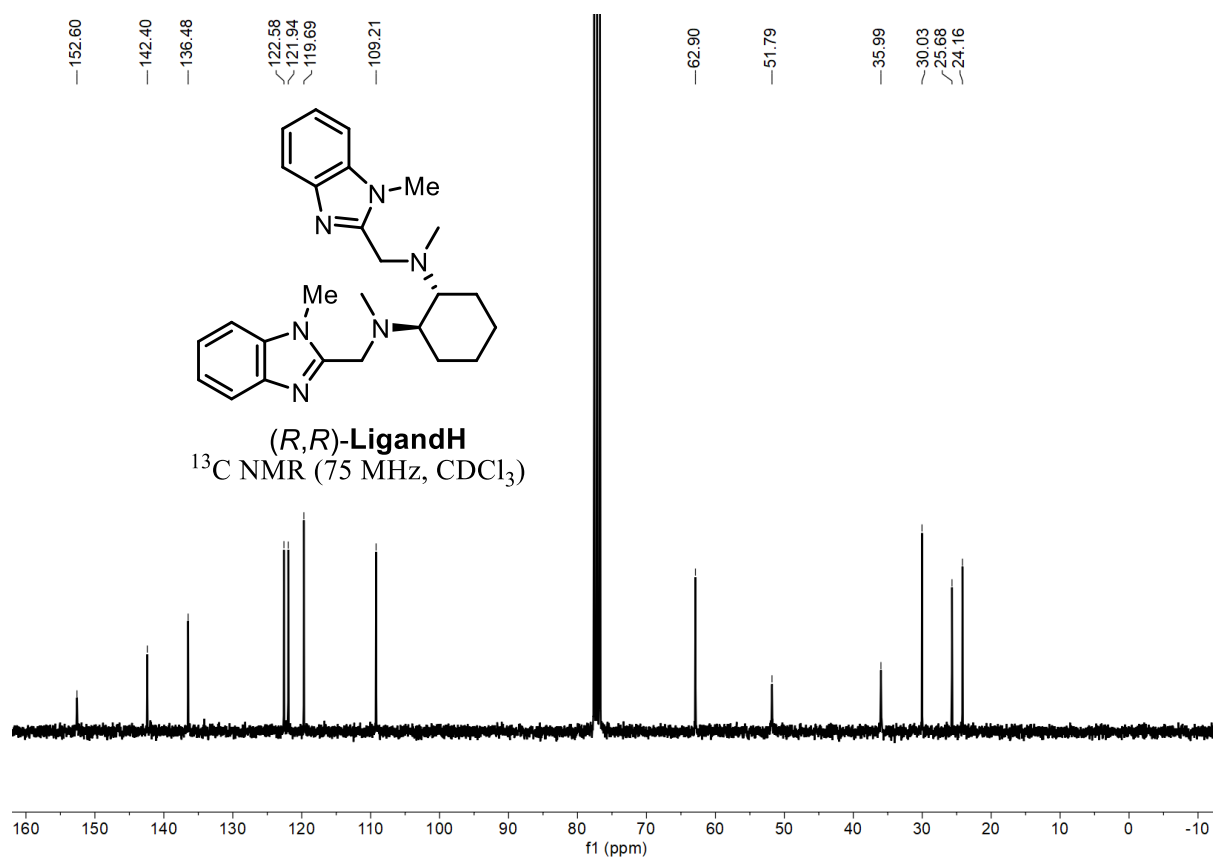
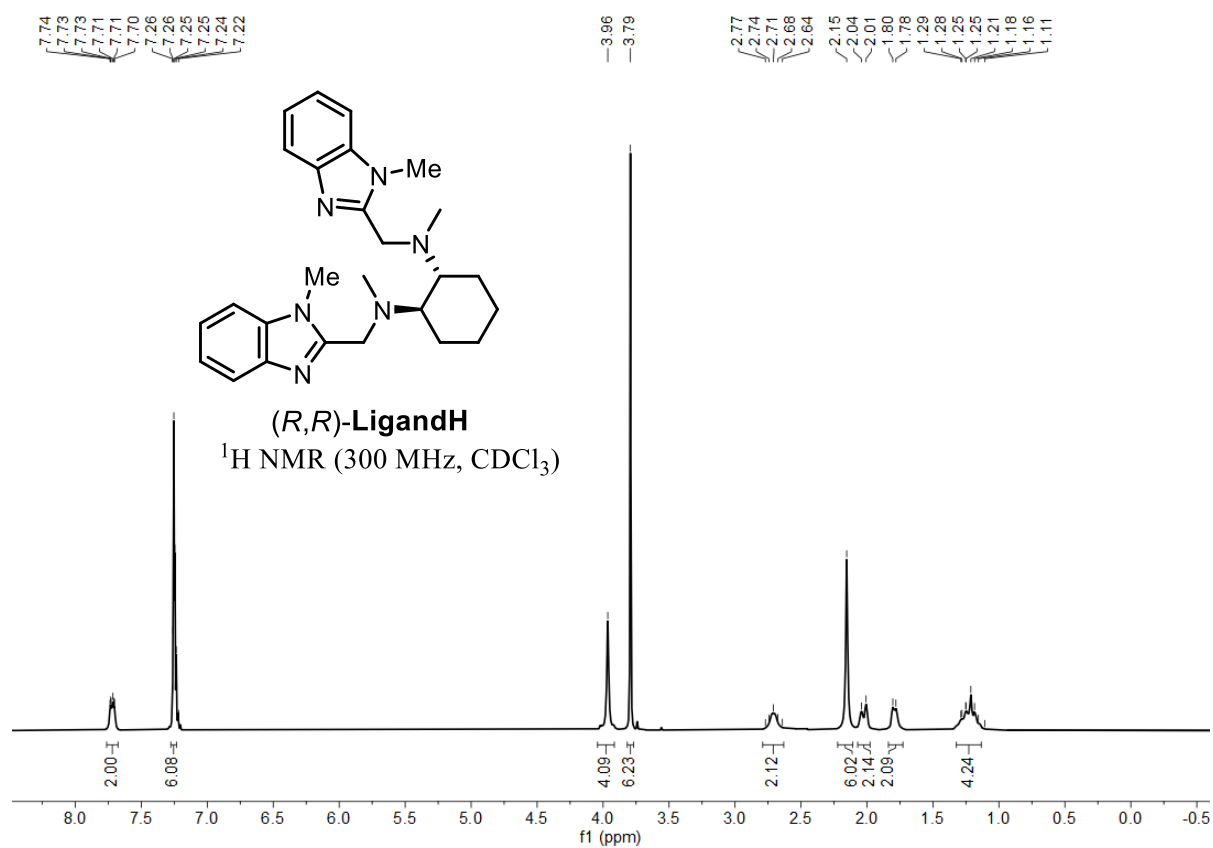
Statement



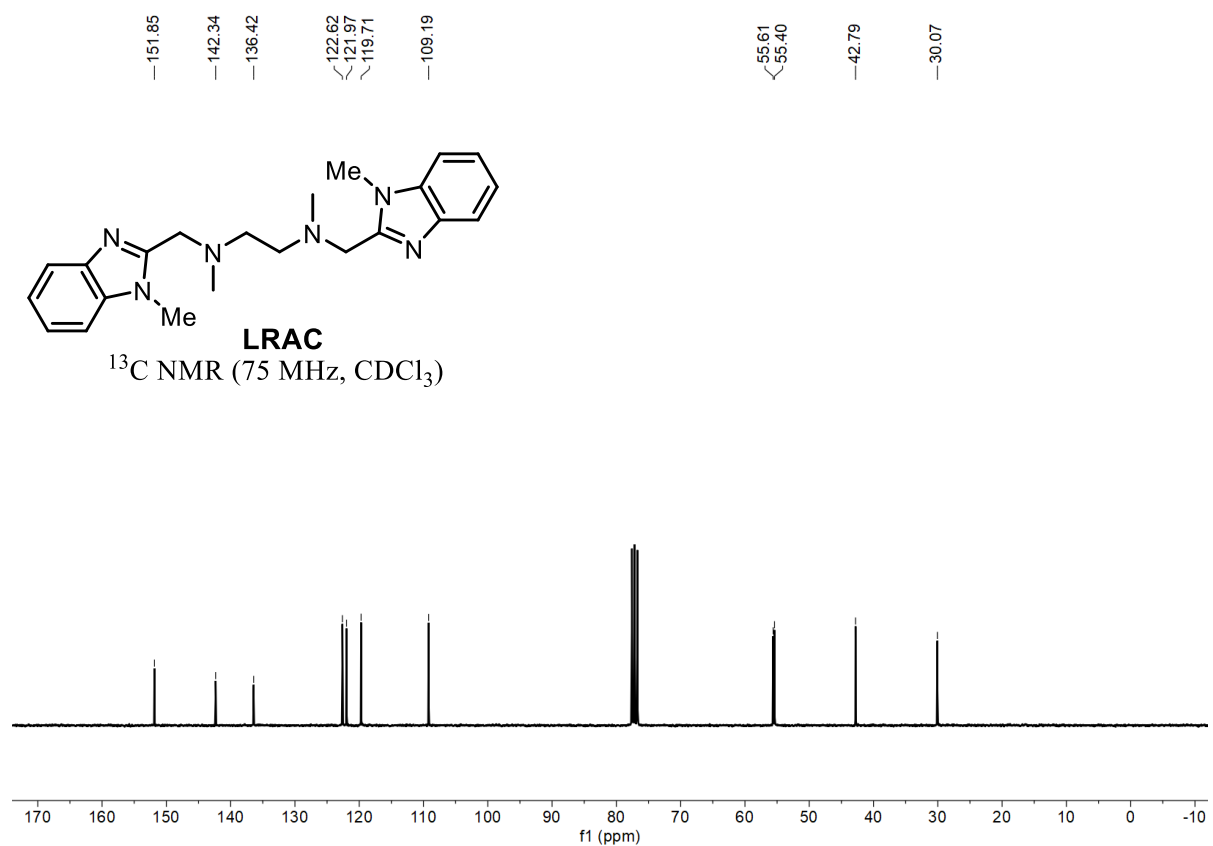
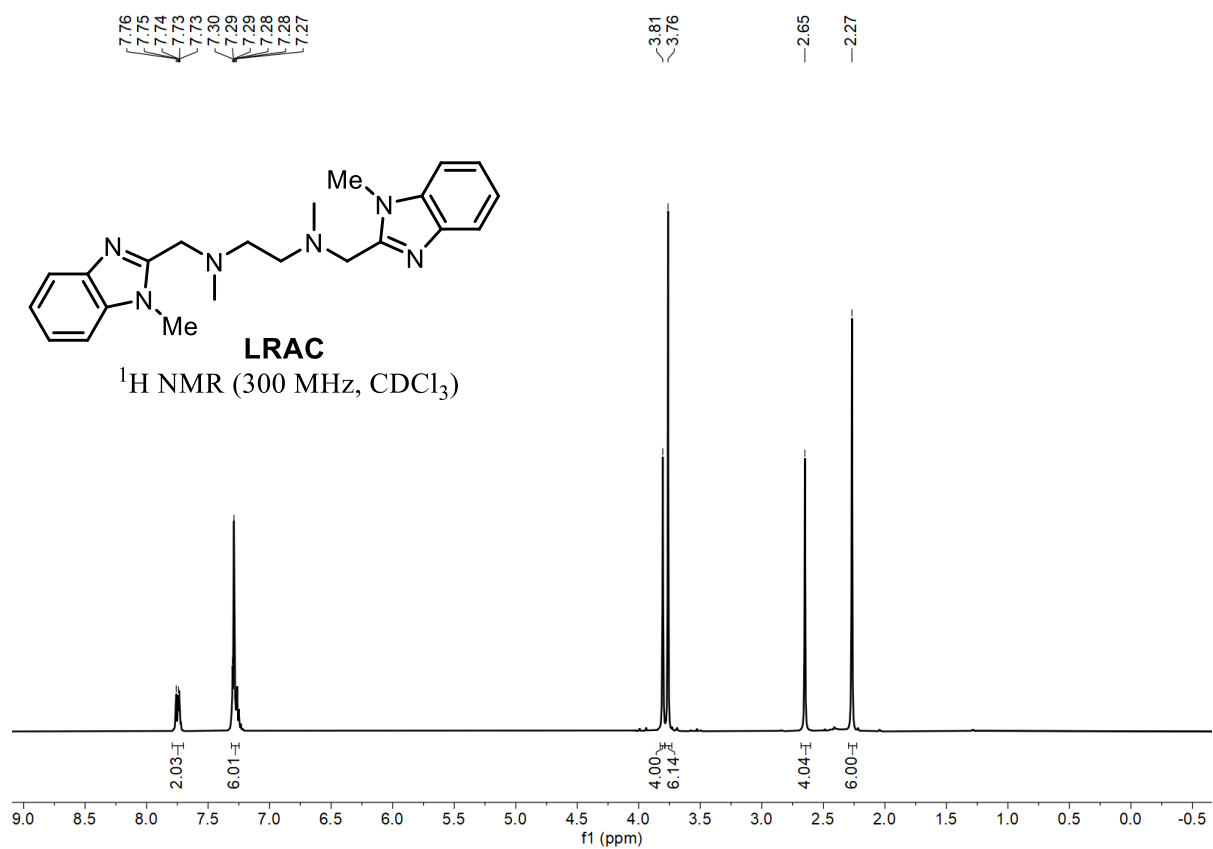
Statement



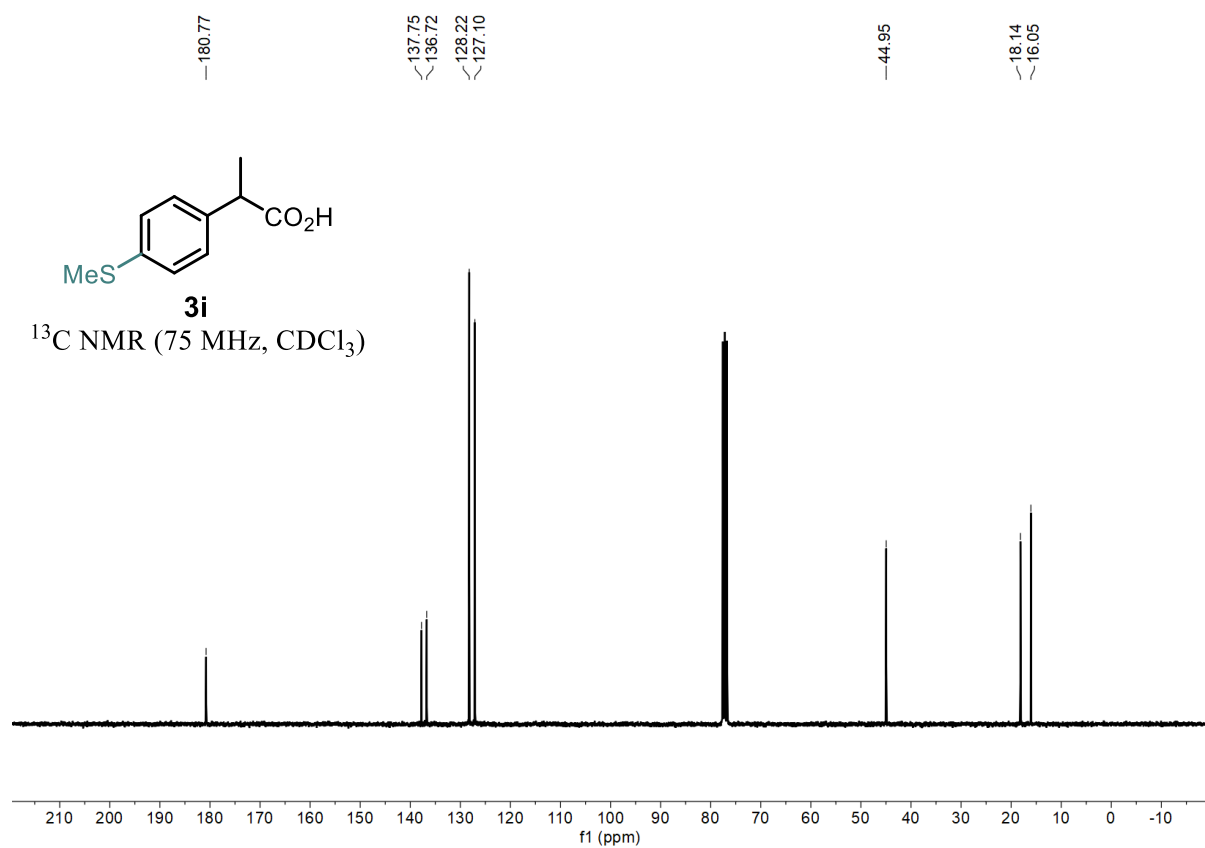
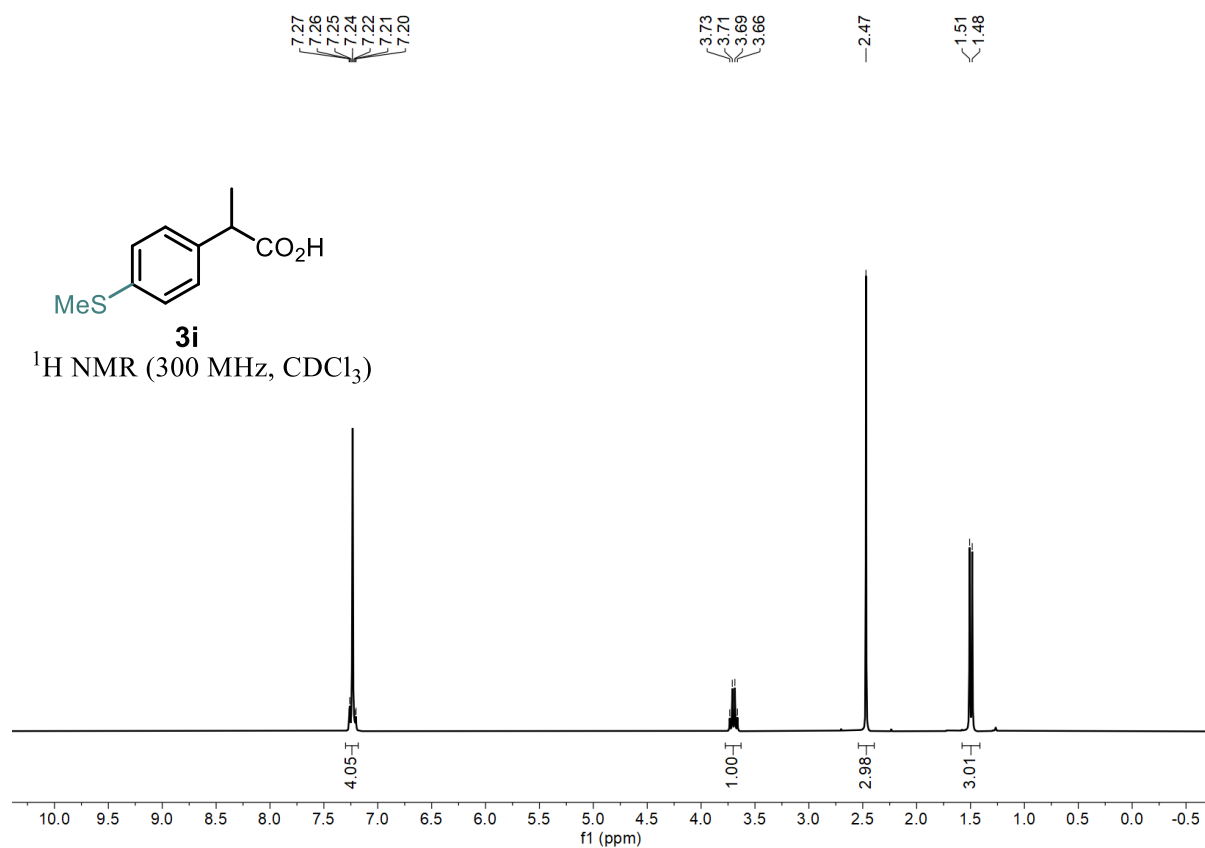
Statement



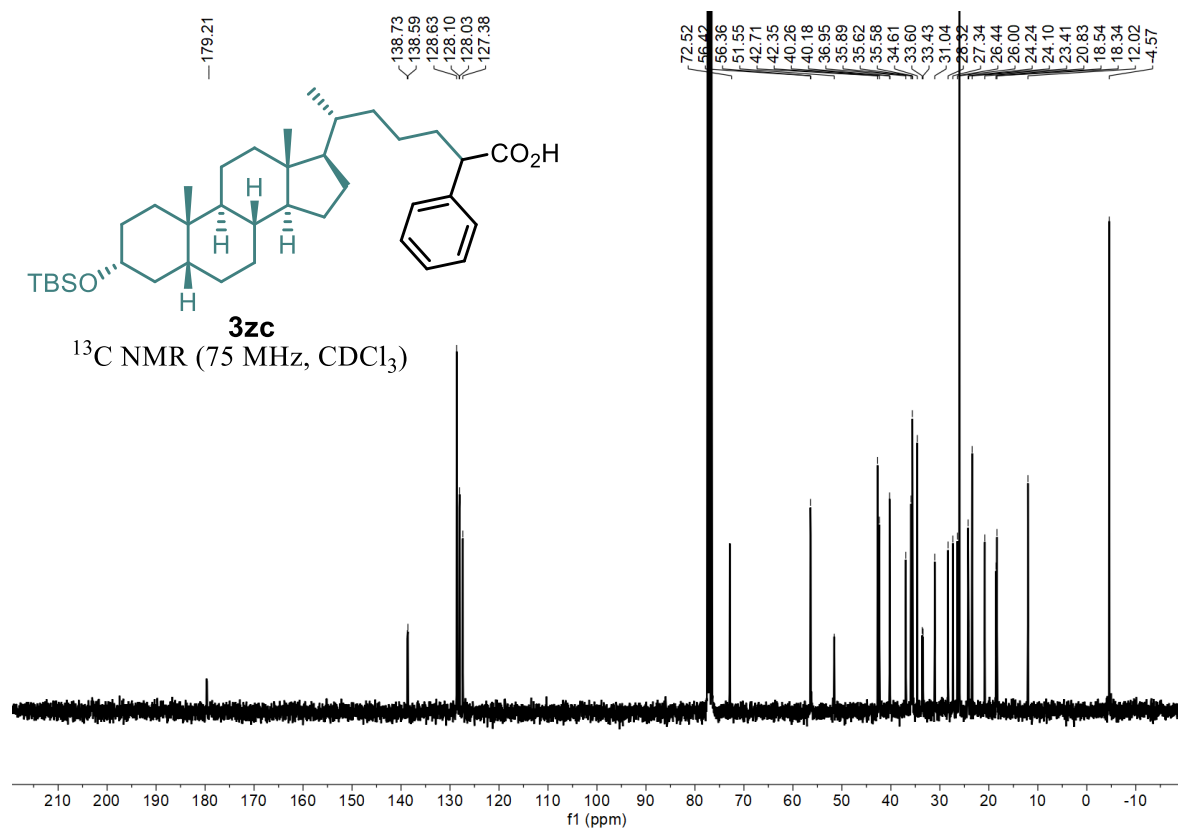
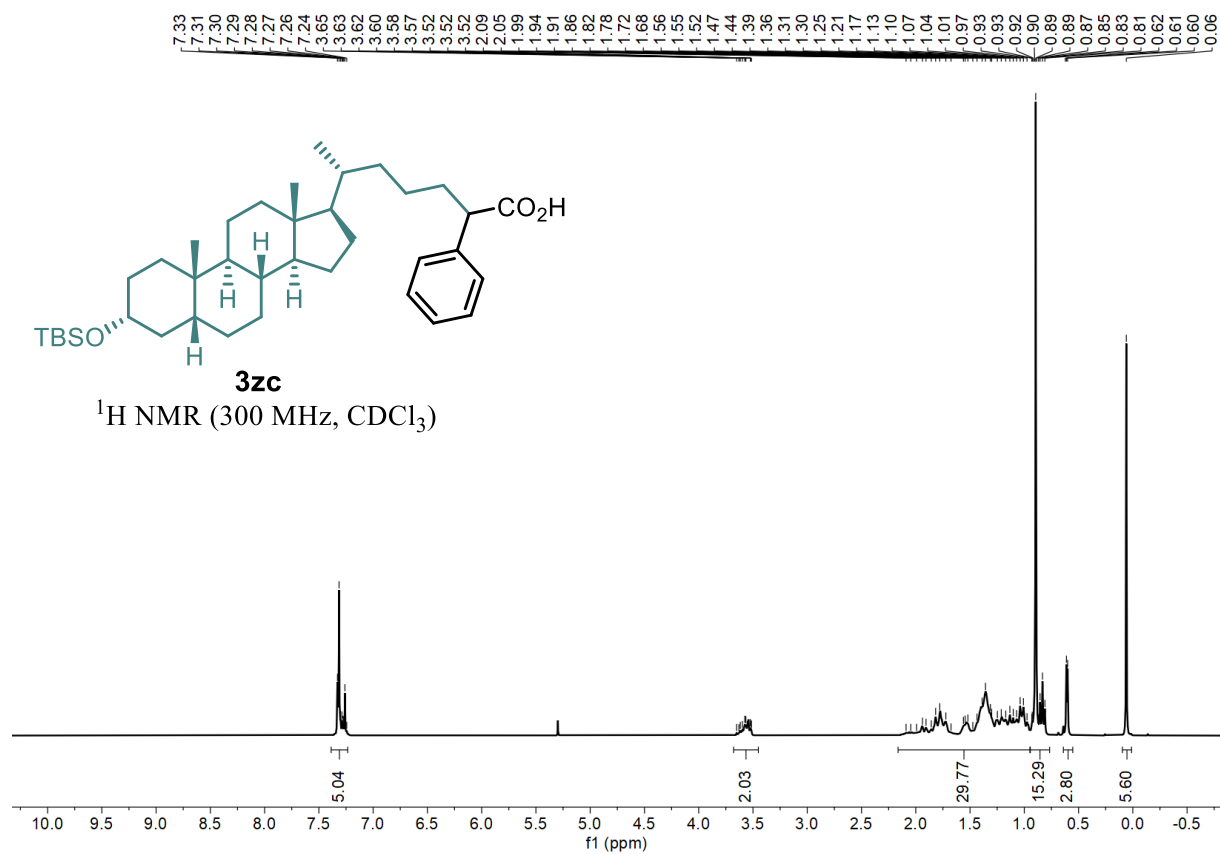
Statement



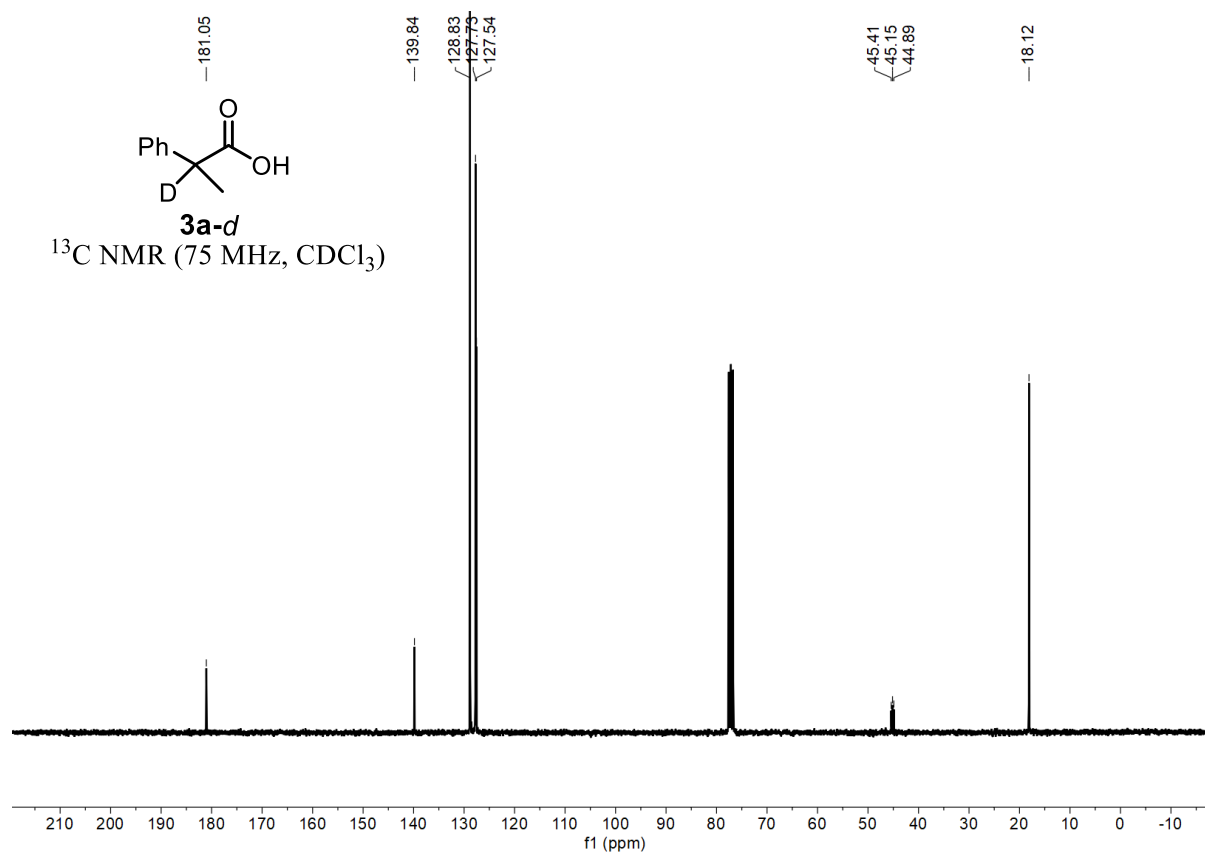
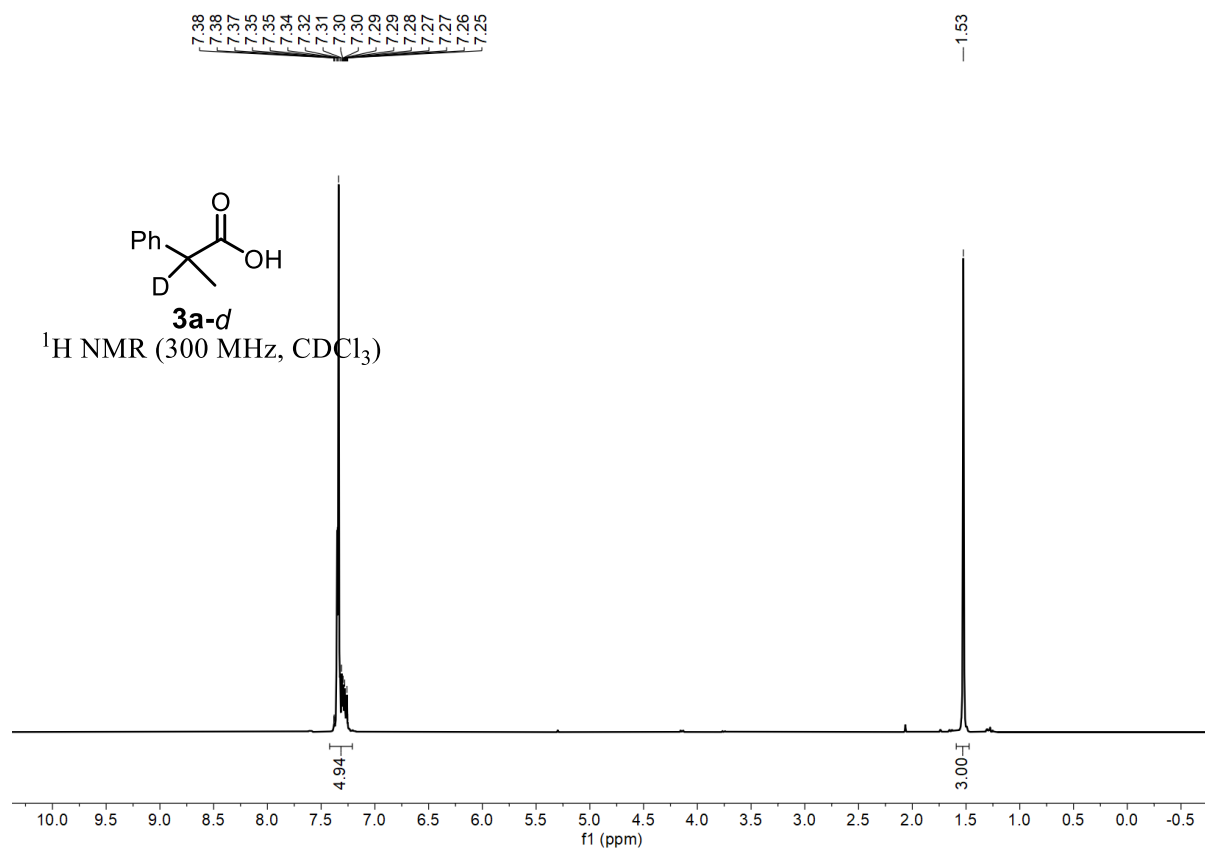
Statement



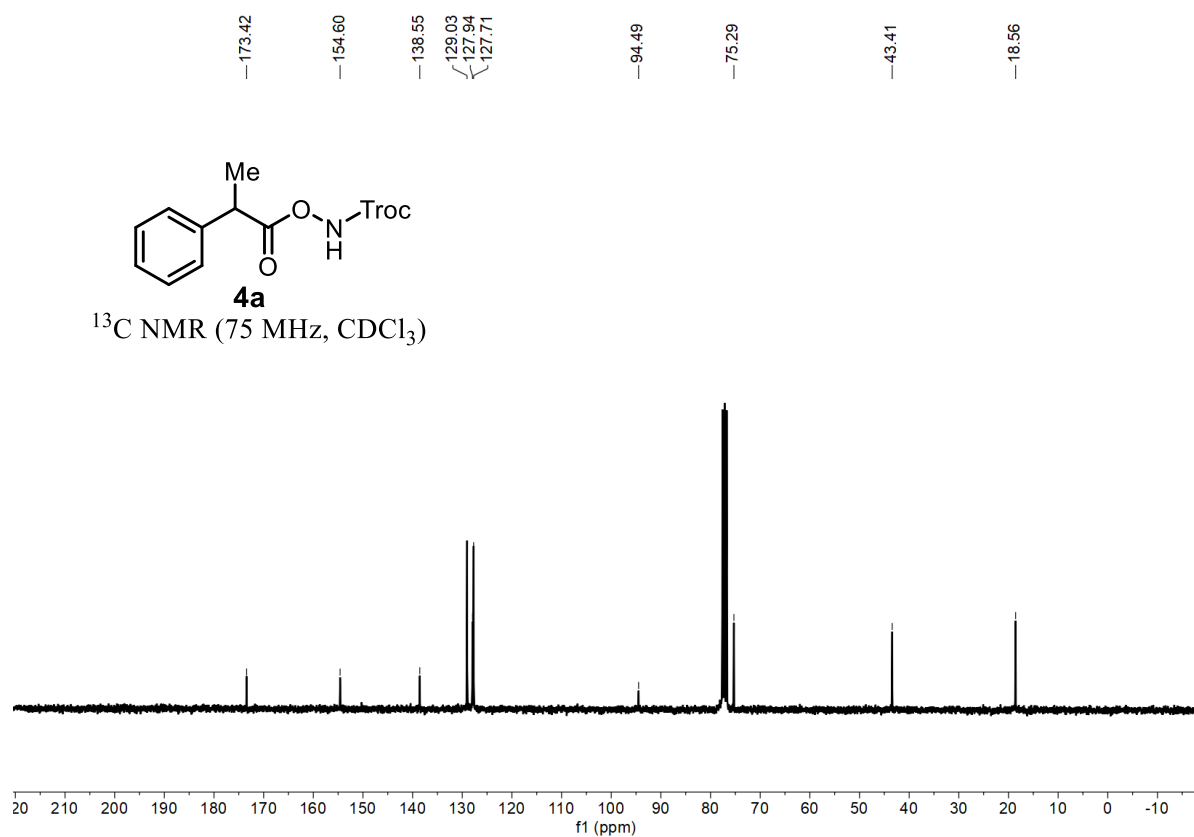
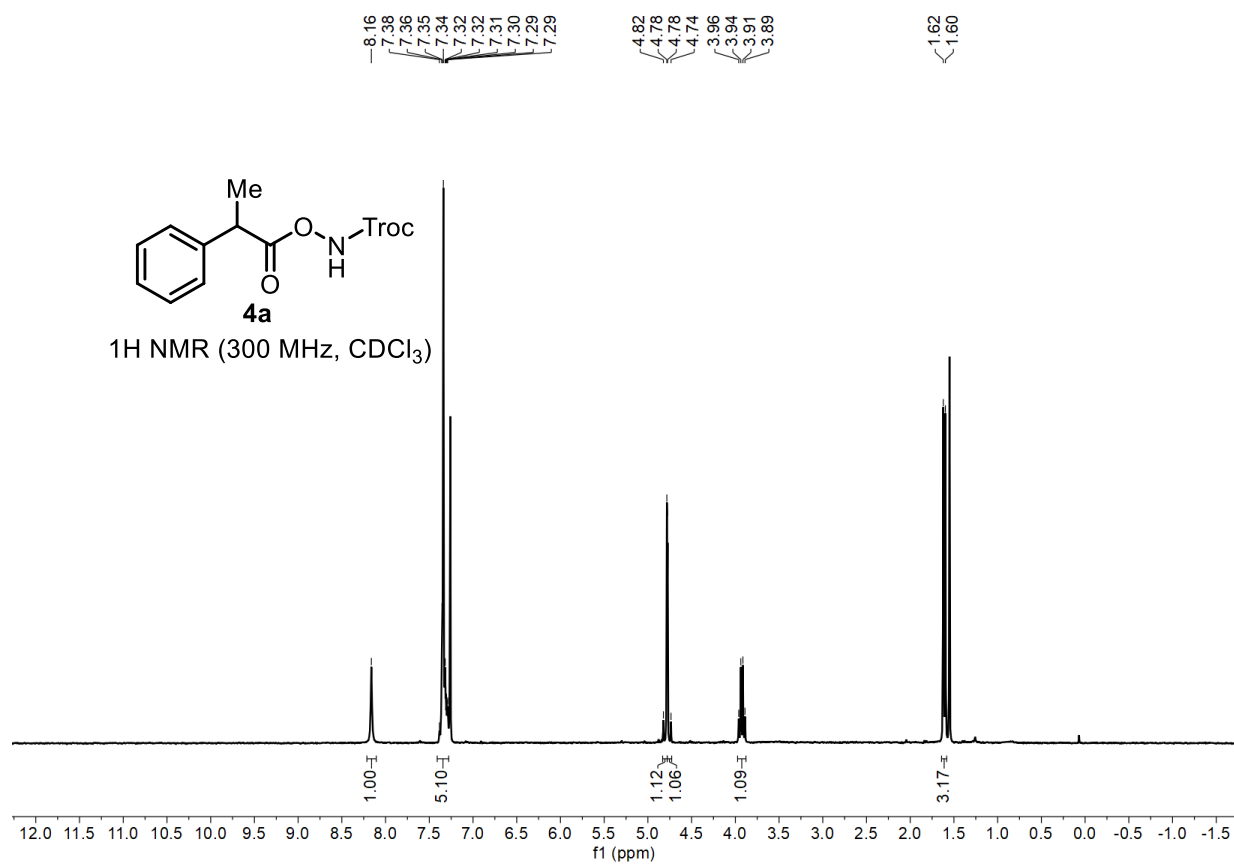
Statement



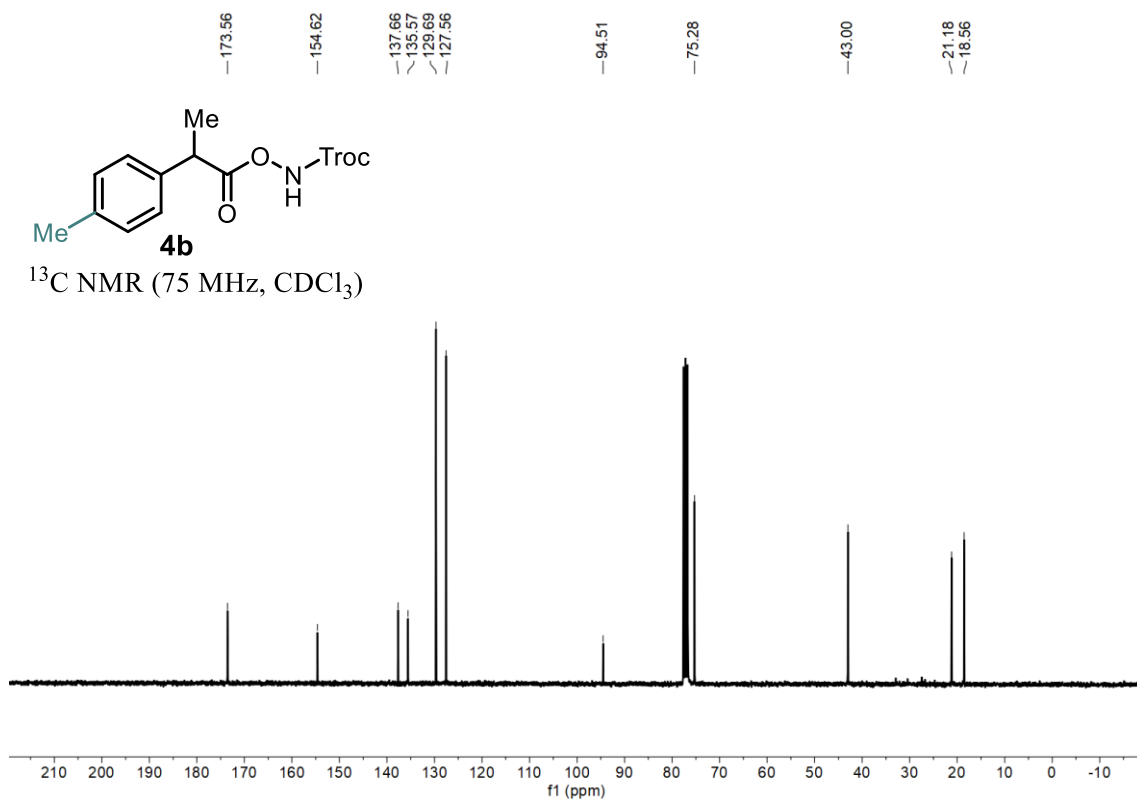
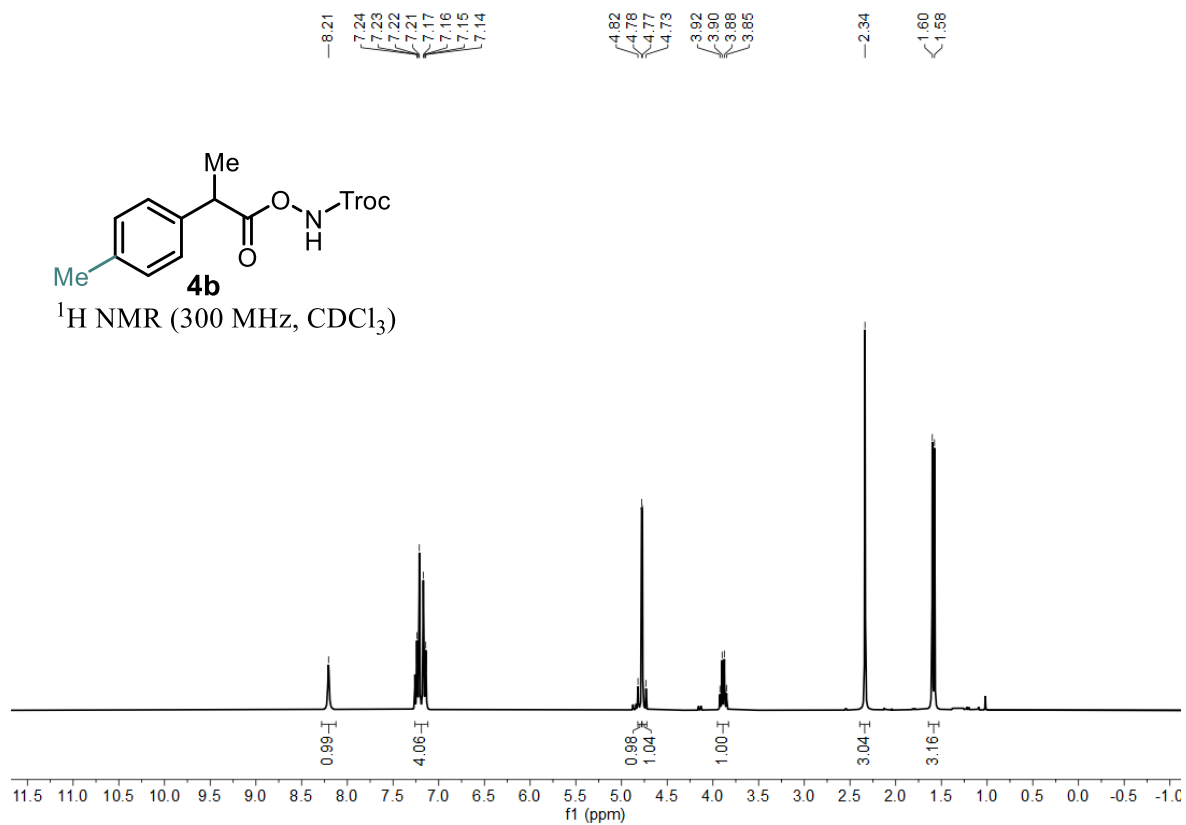
Statement



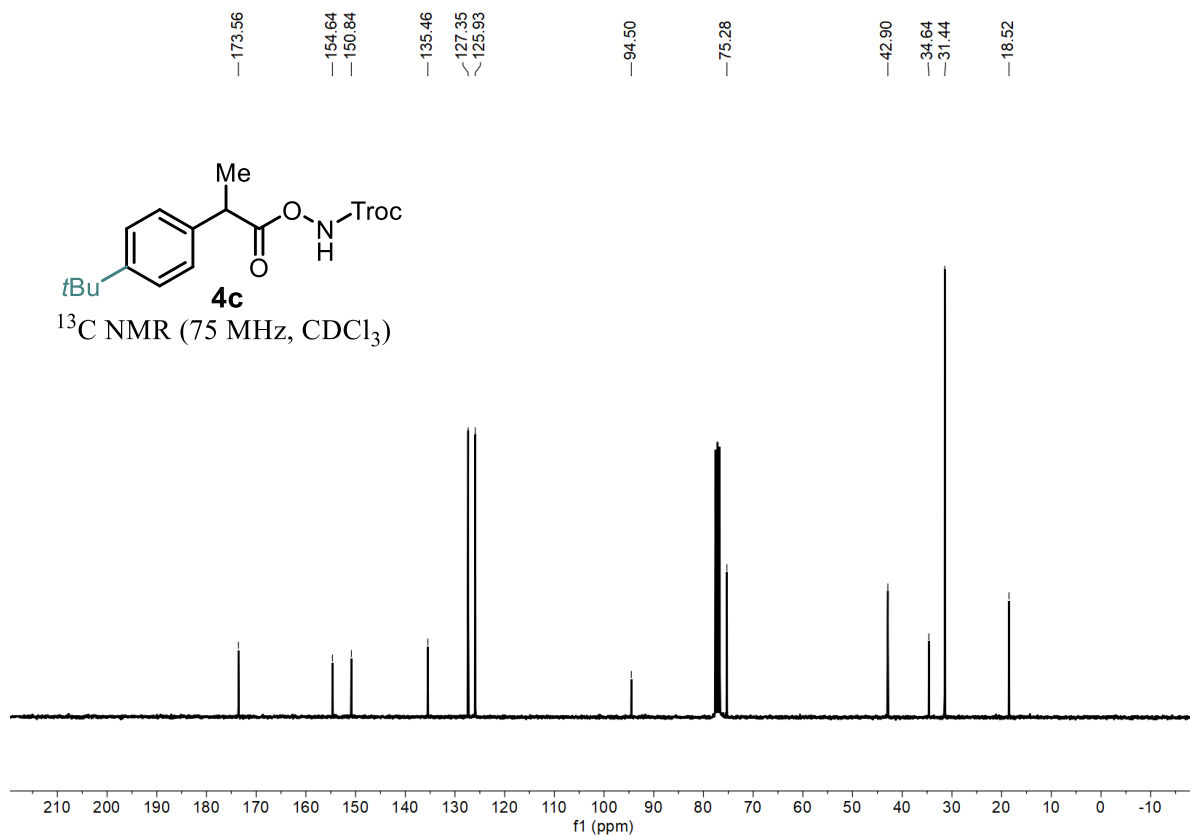
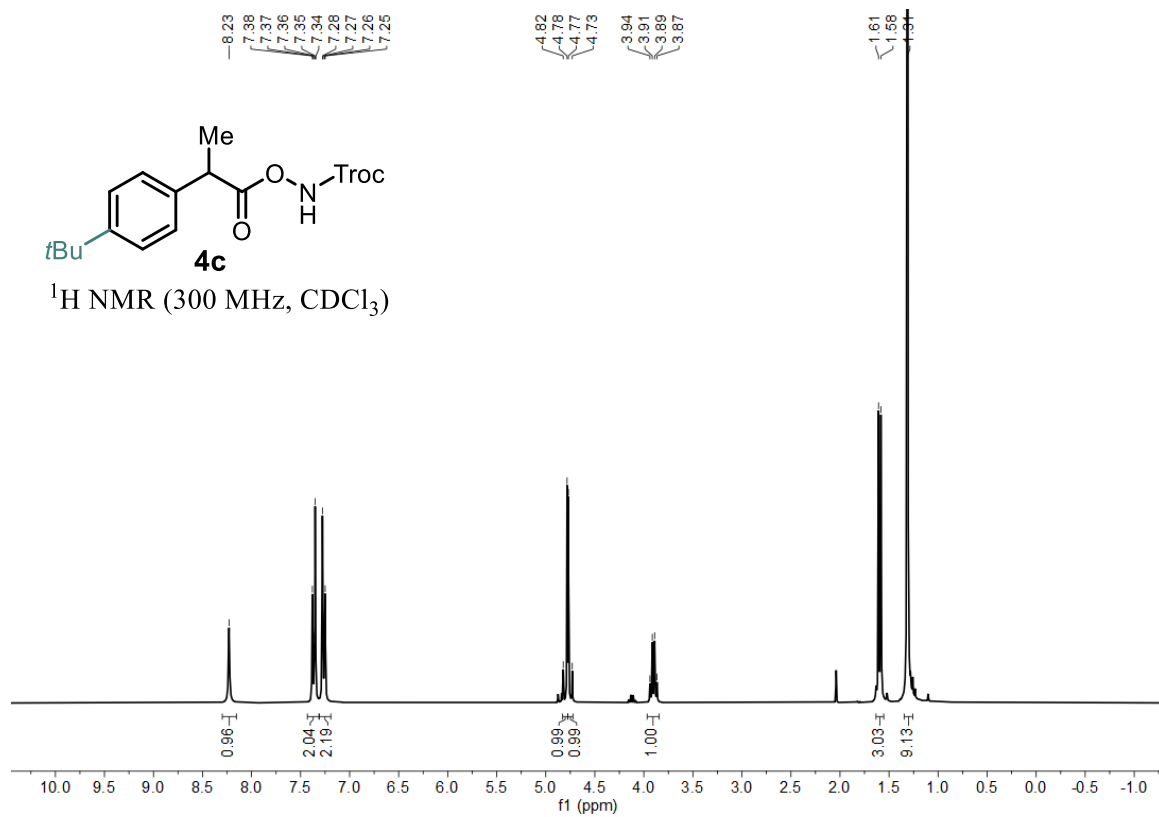
Statement



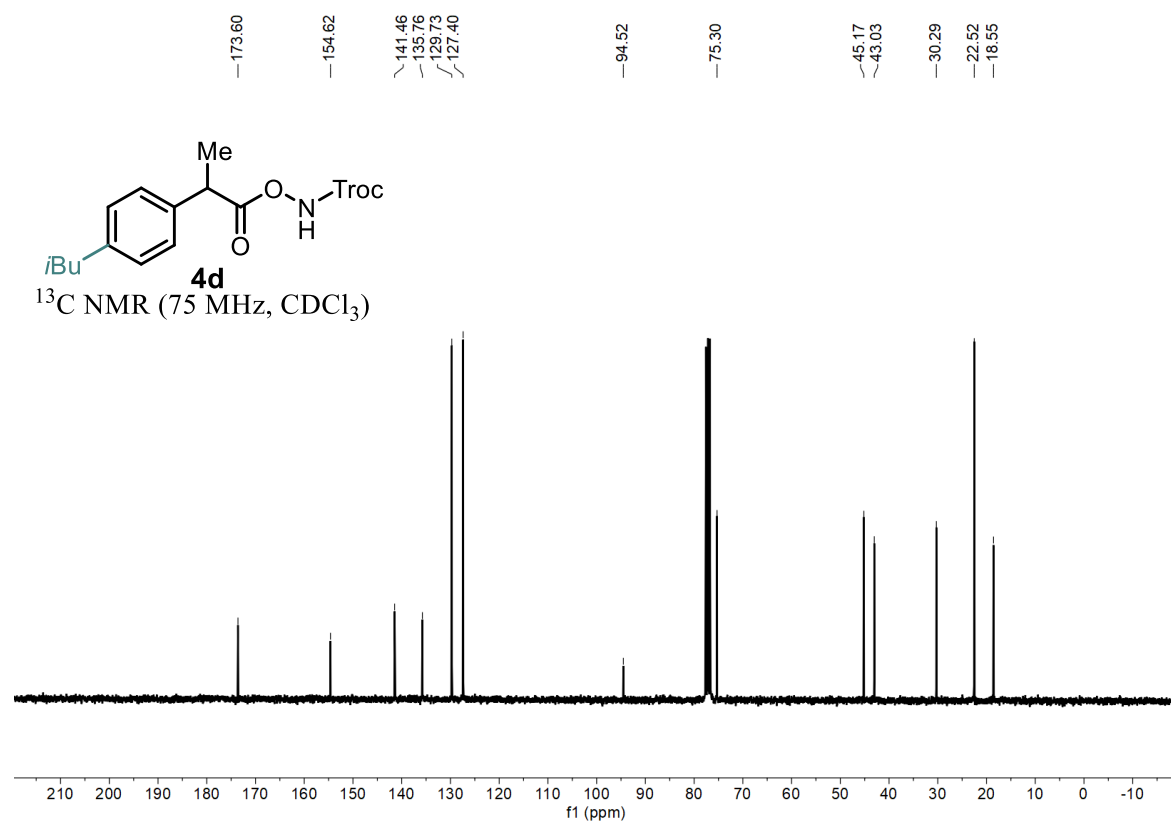
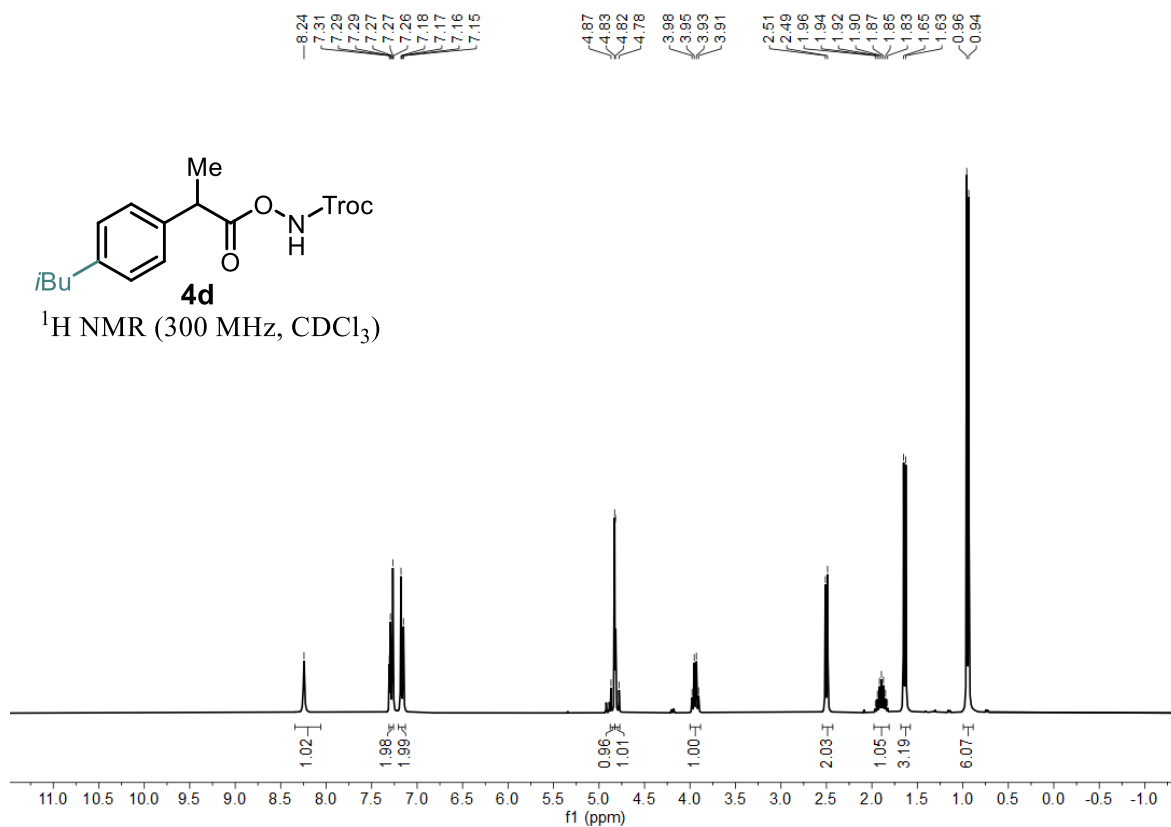
Statement



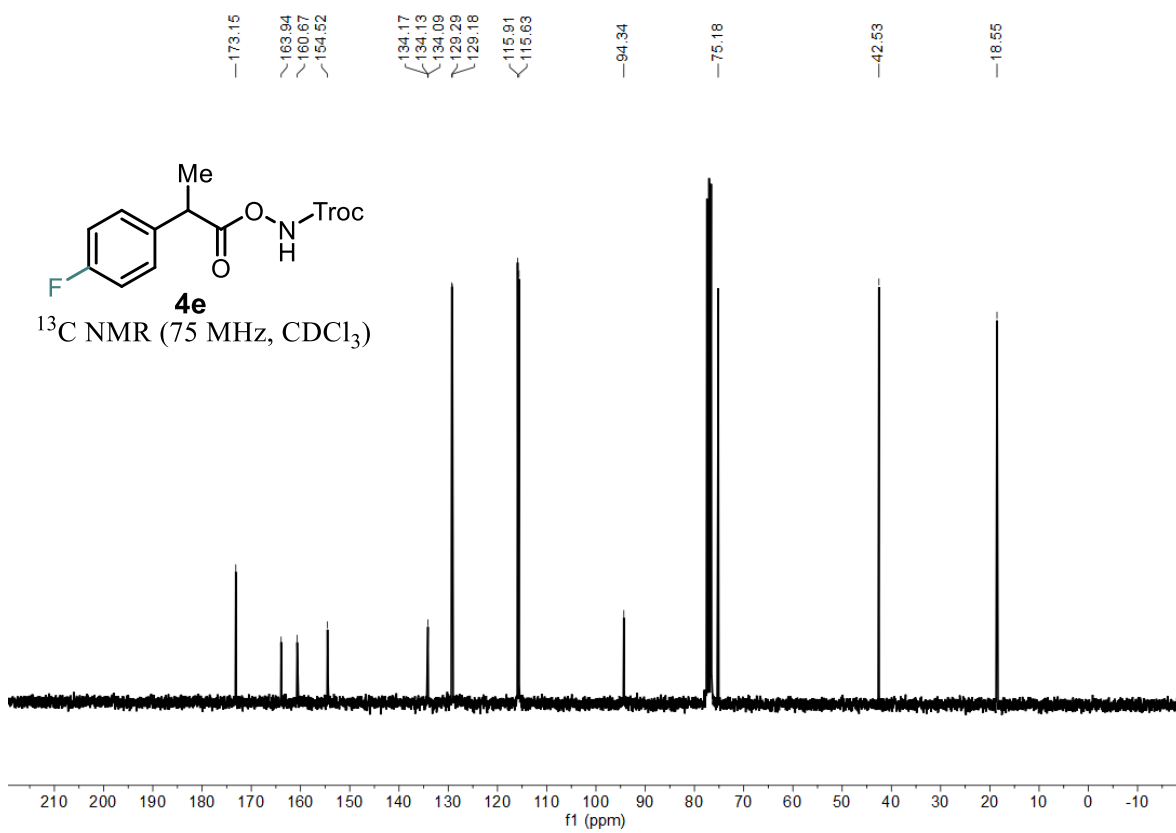
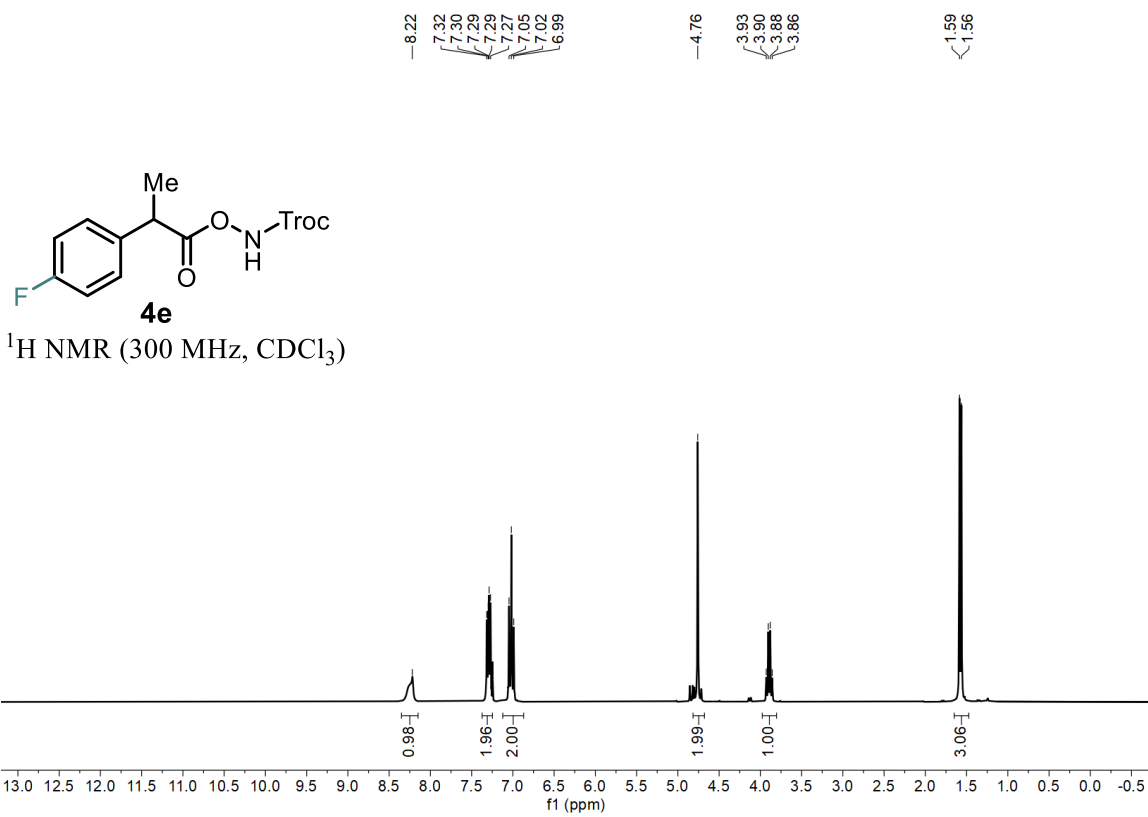
Statement



Statement

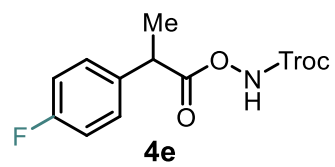


Statement

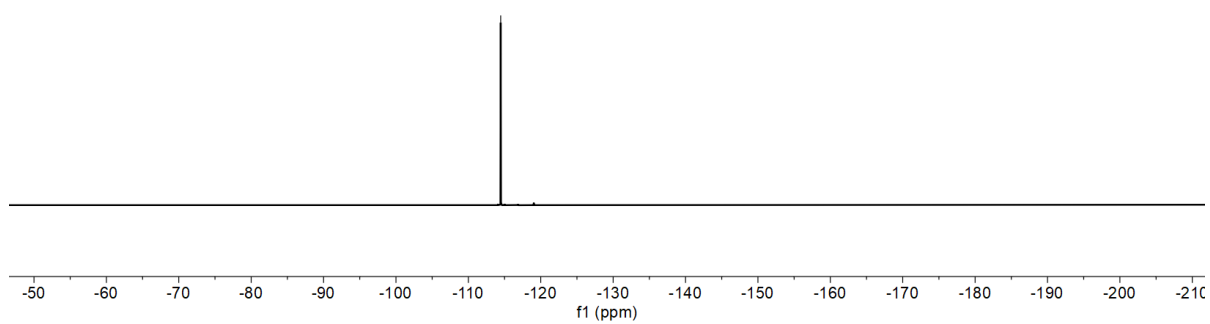


Statement

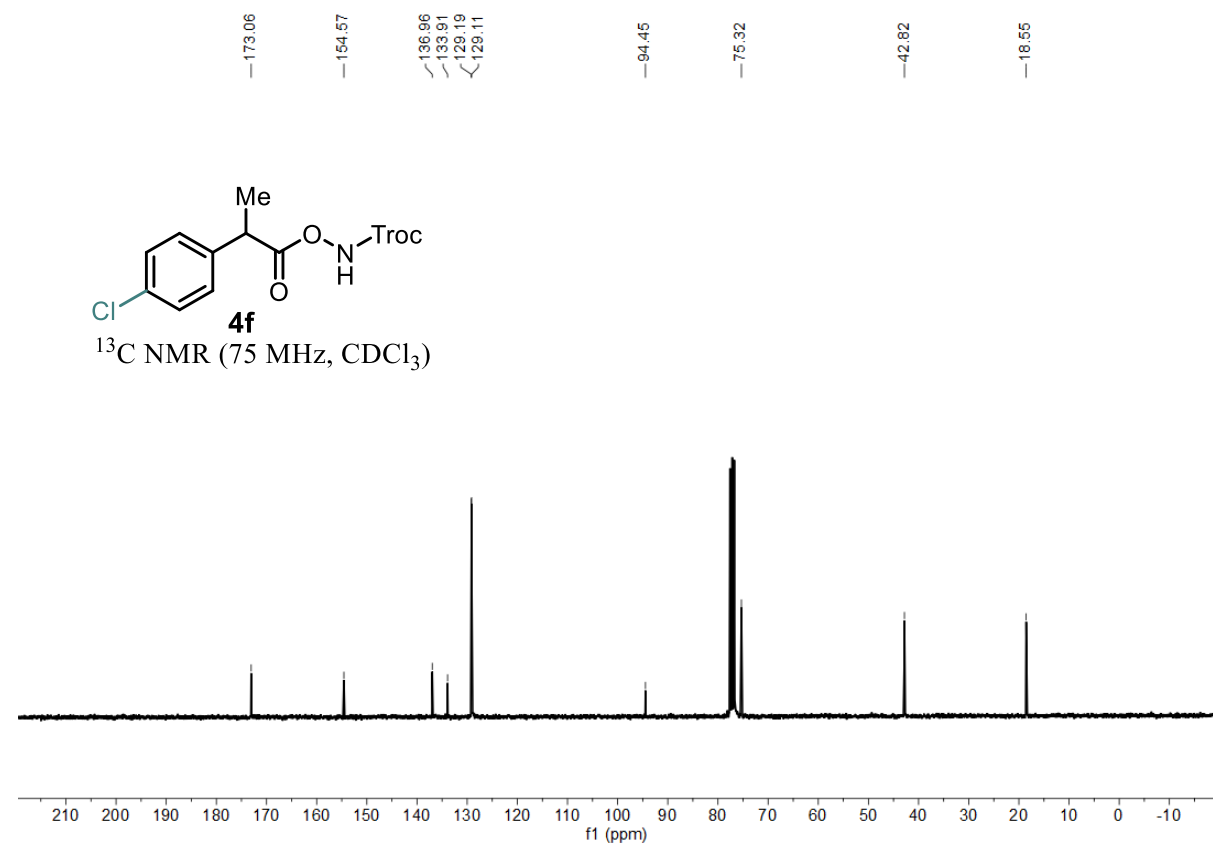
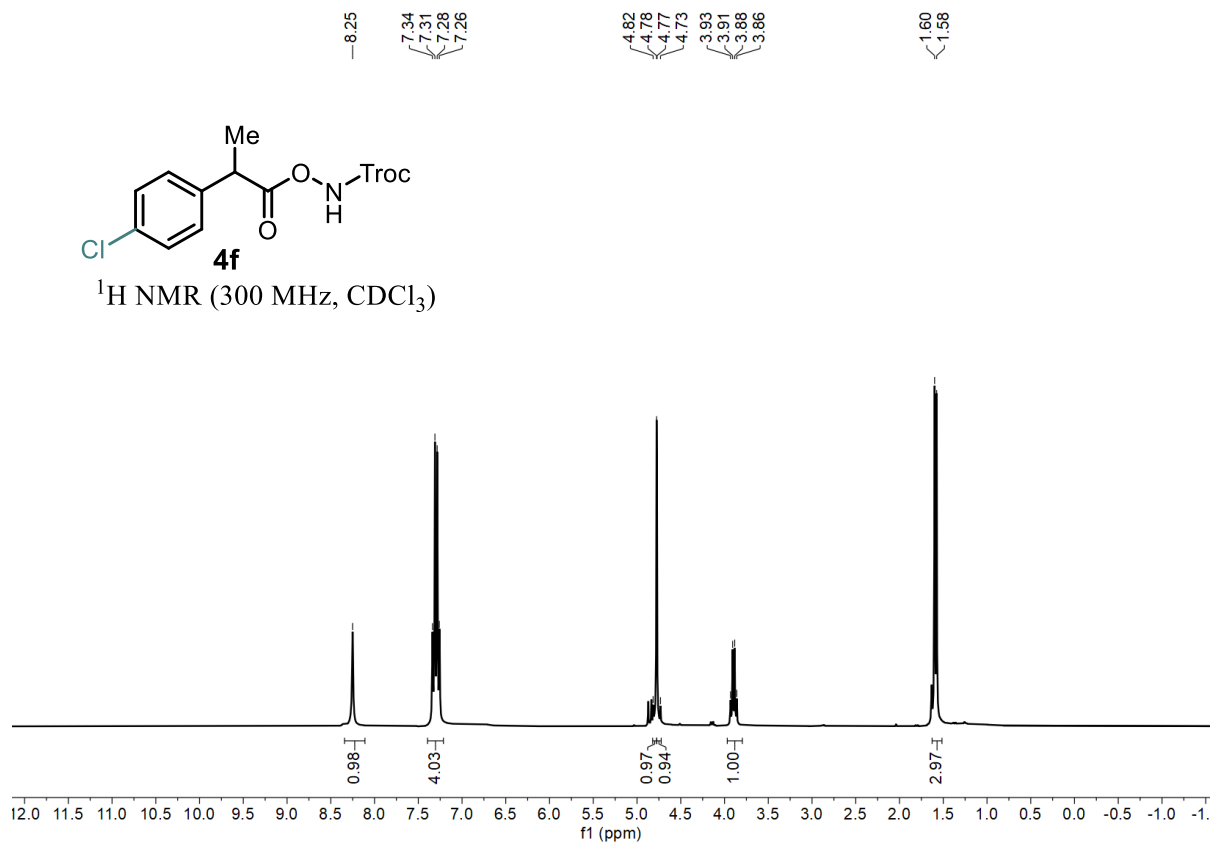
-114.47



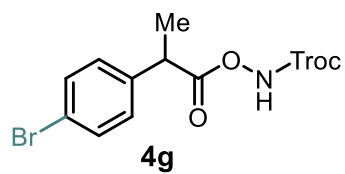
¹⁹F NMR (282 MHz, CDCl₃)



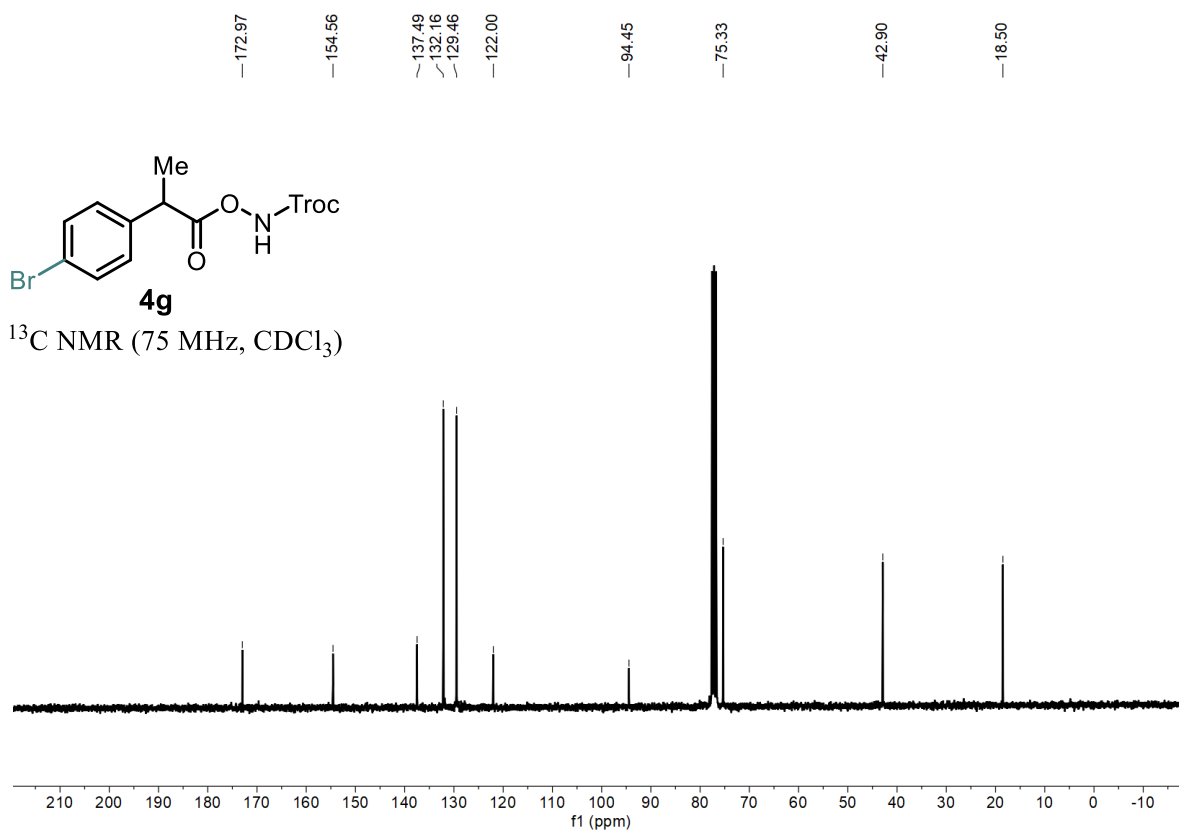
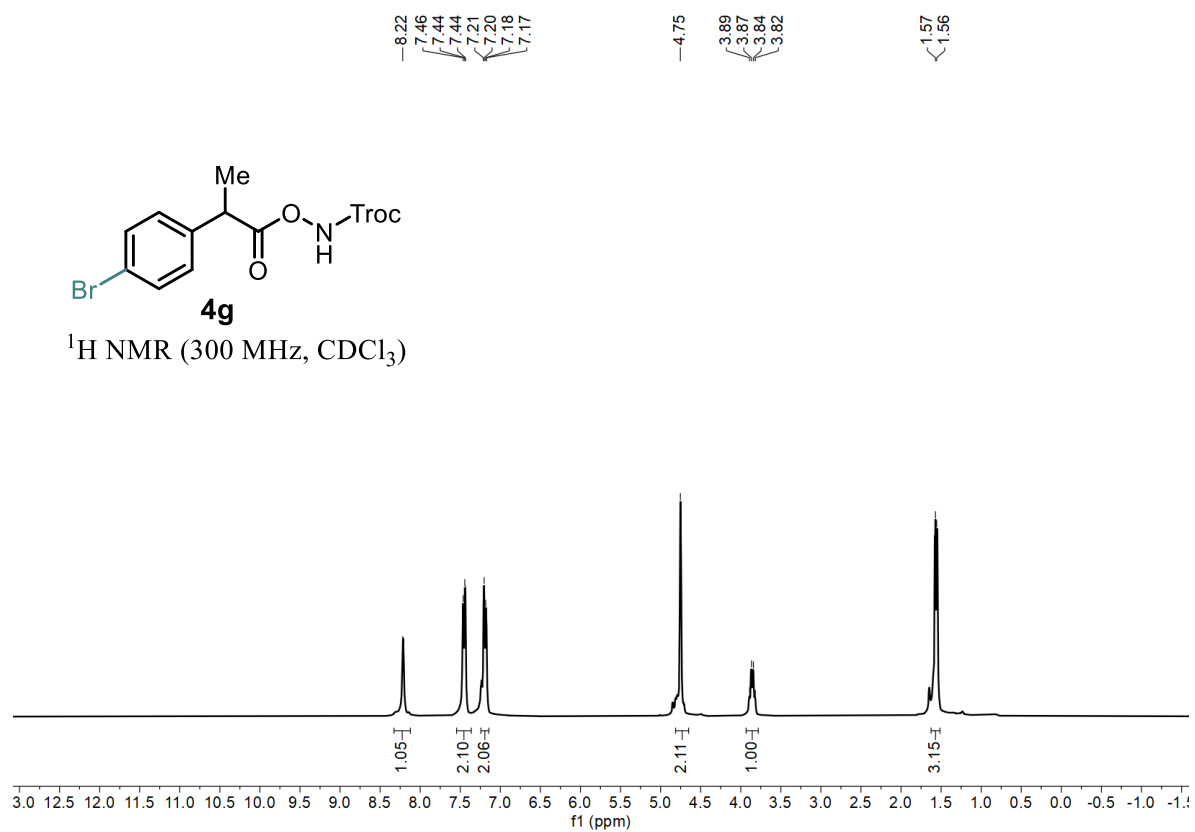
Statement



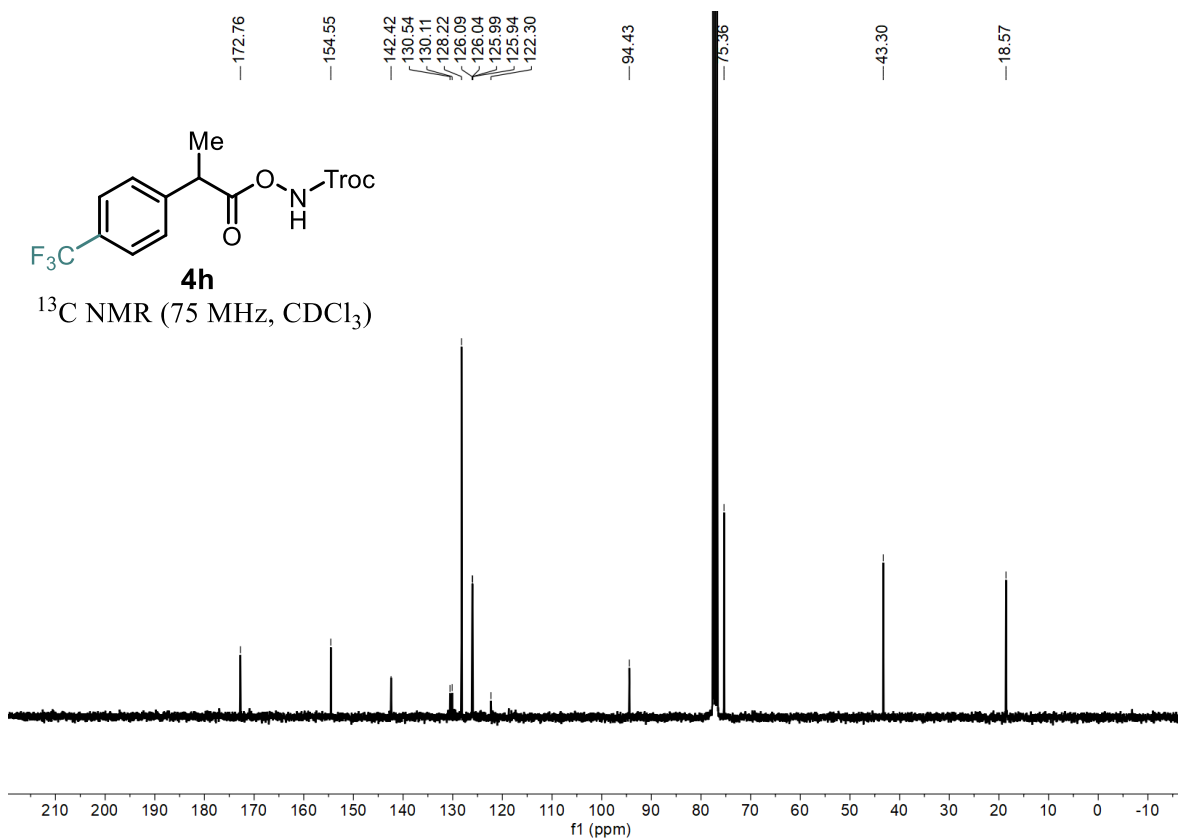
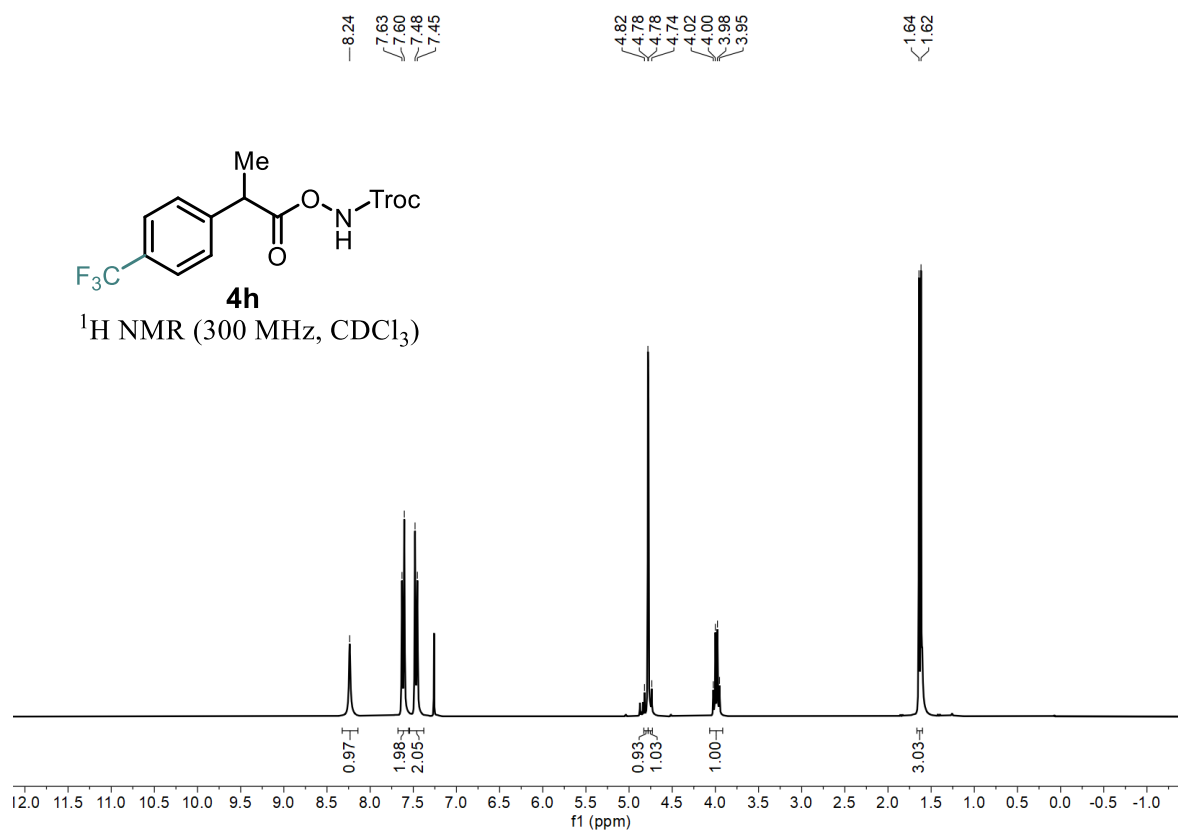
Statement



$^1\text{H NMR}$ (300 MHz, CDCl_3)

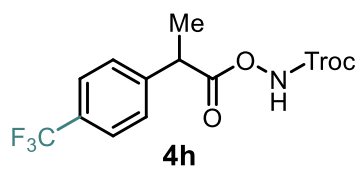


Statement

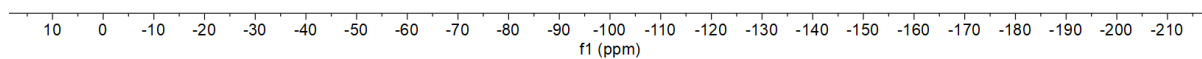


Statement

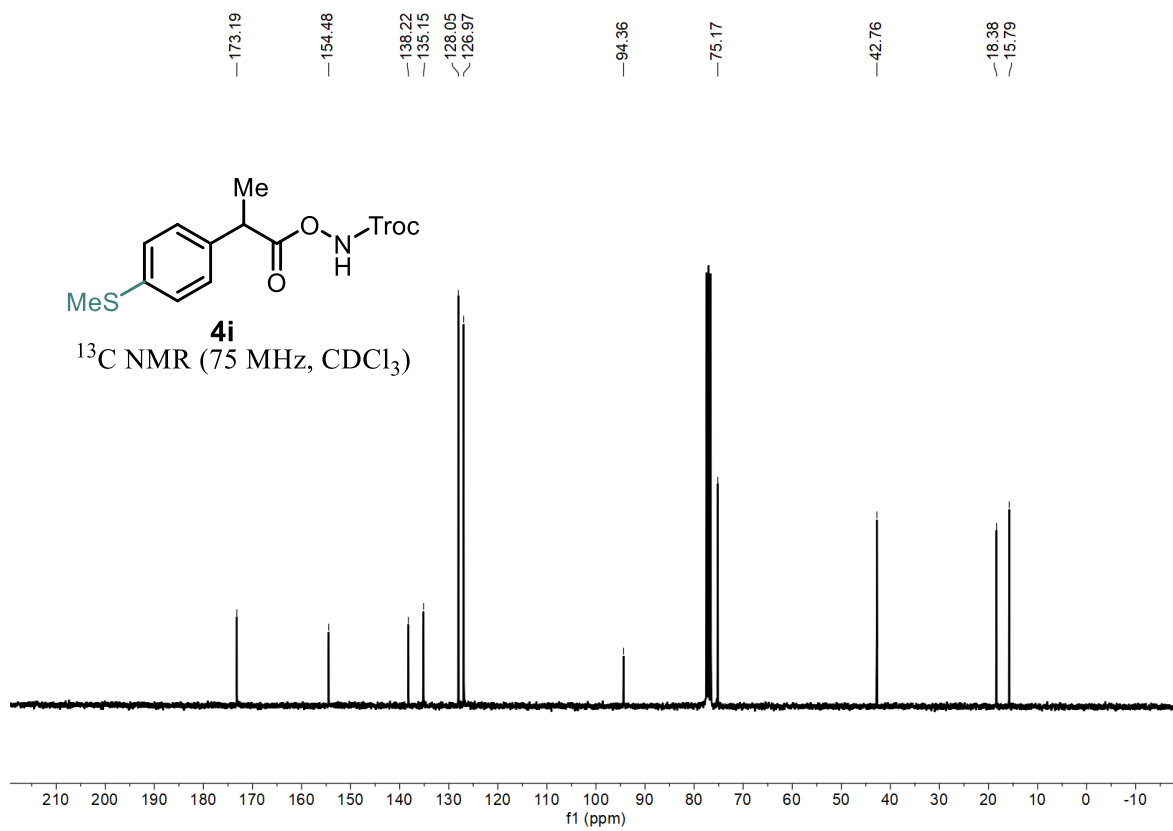
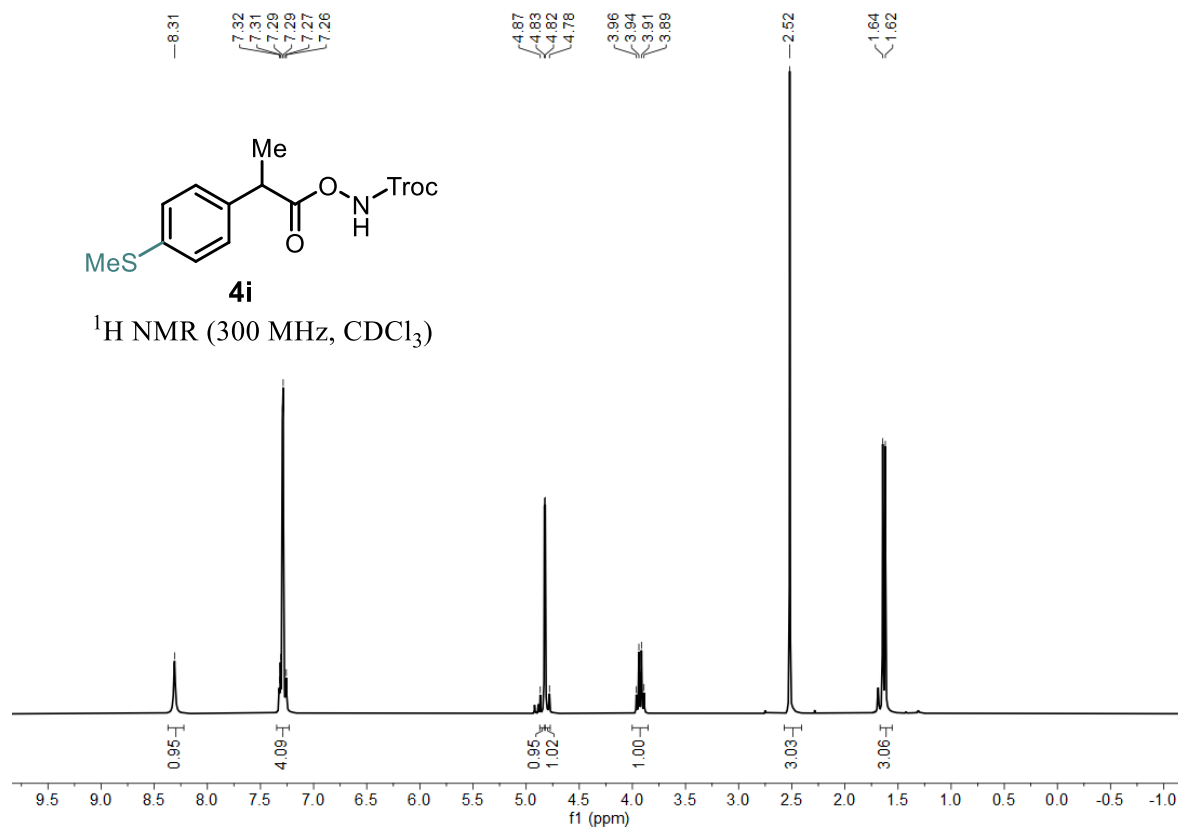
—62.65



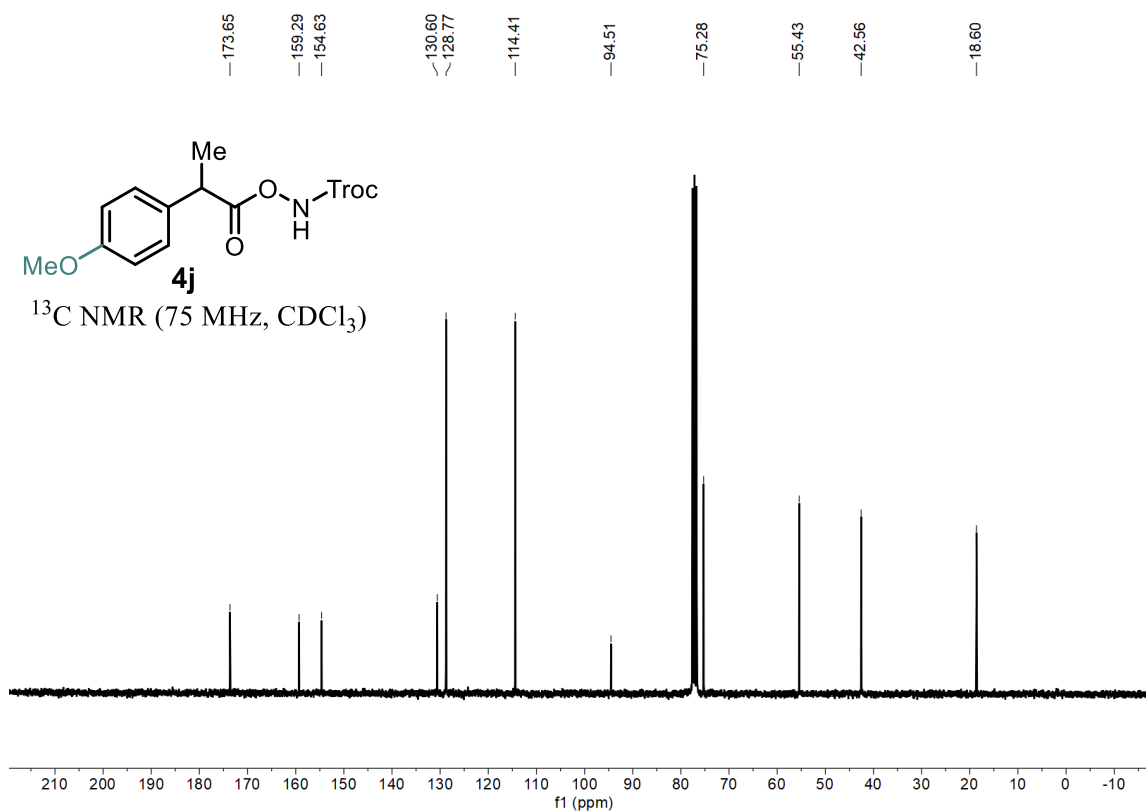
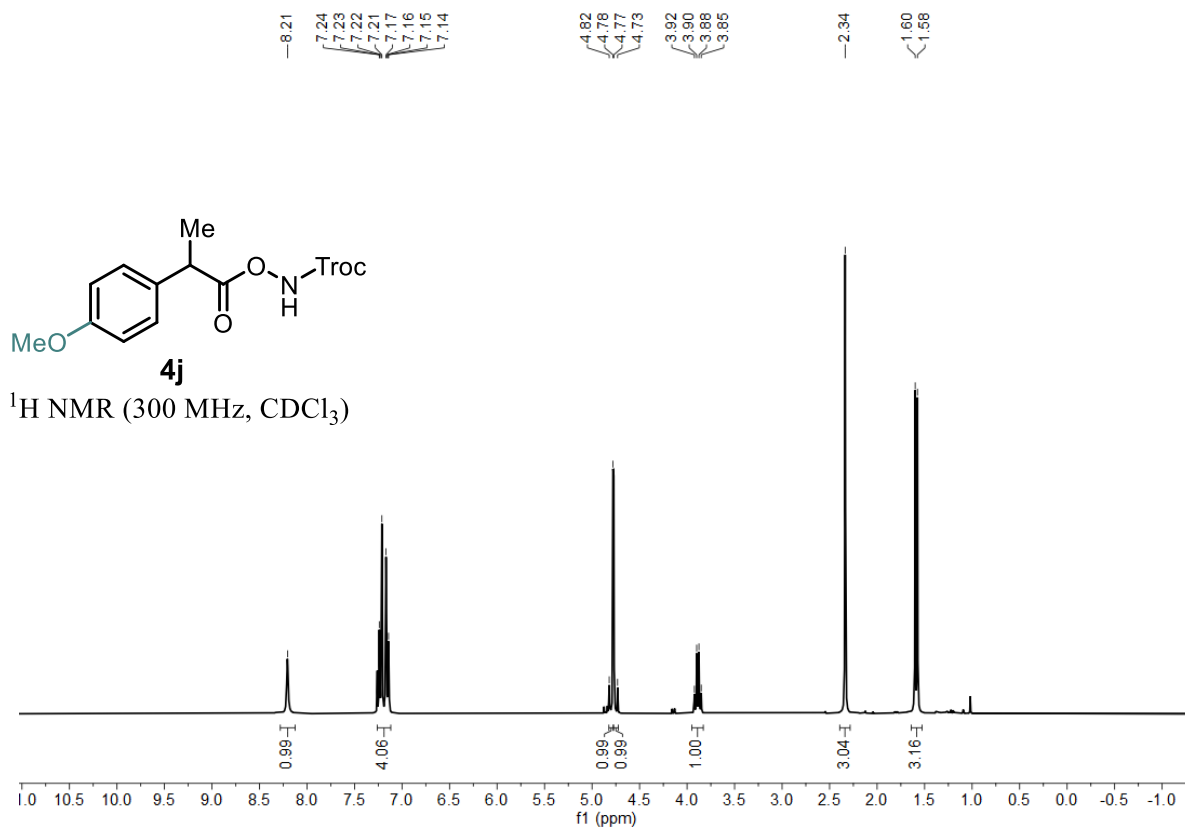
^{19}F NMR (282 MHz, $CDCl_3$)



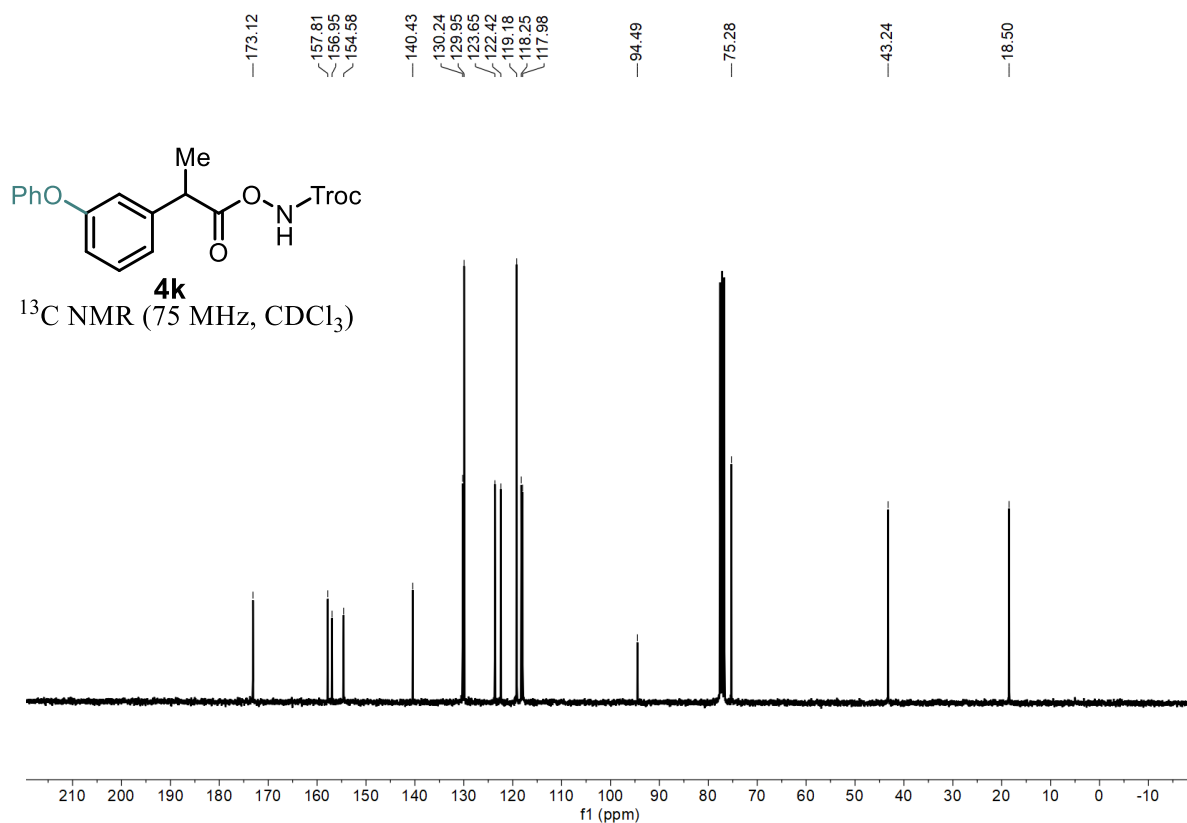
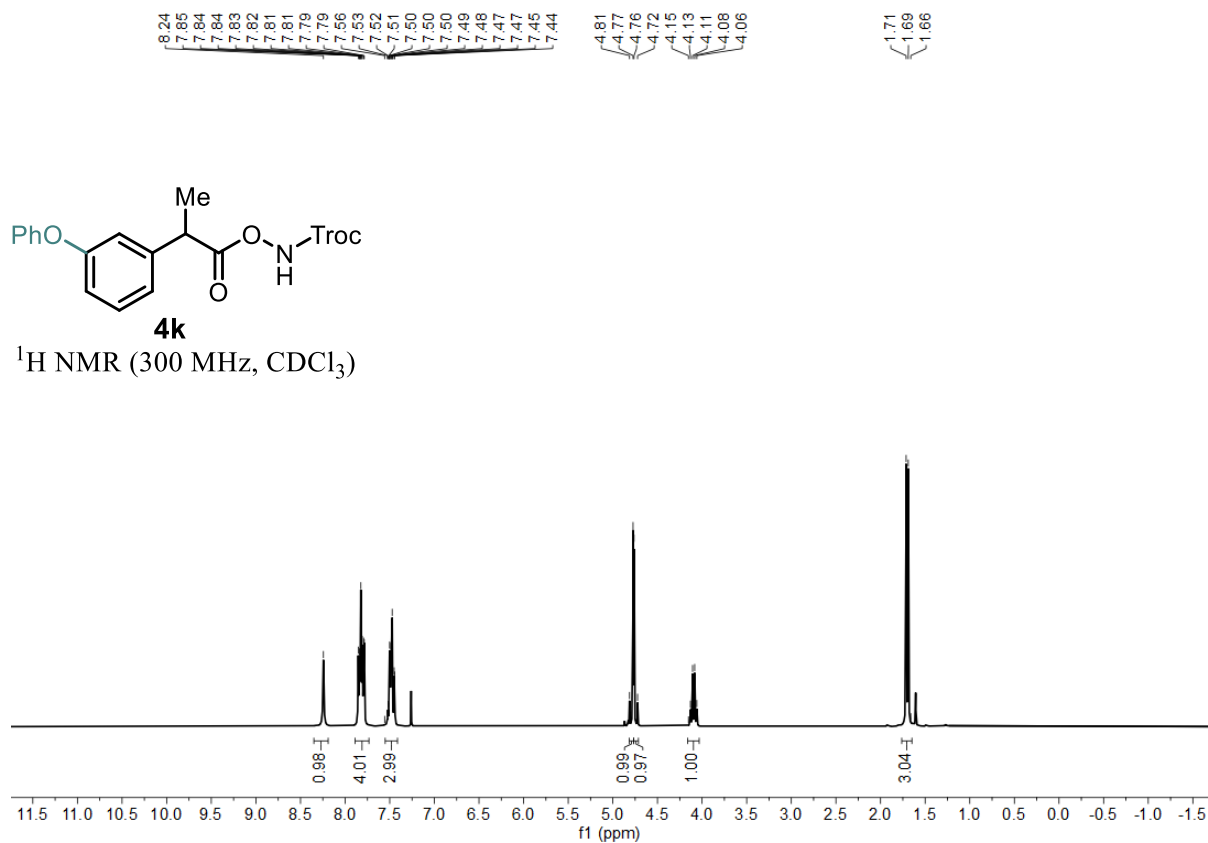
Statement



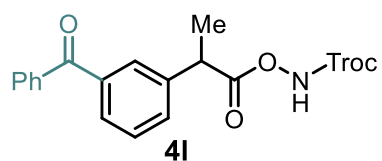
Statement



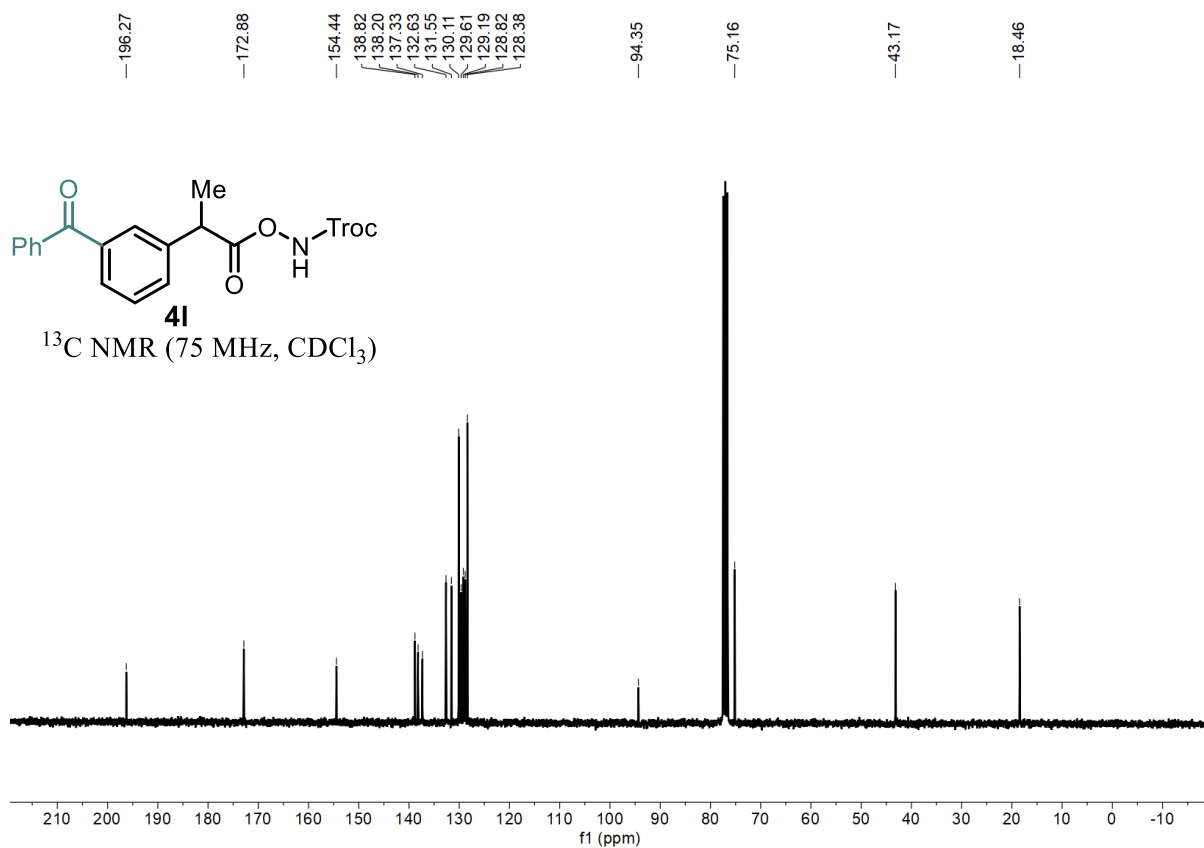
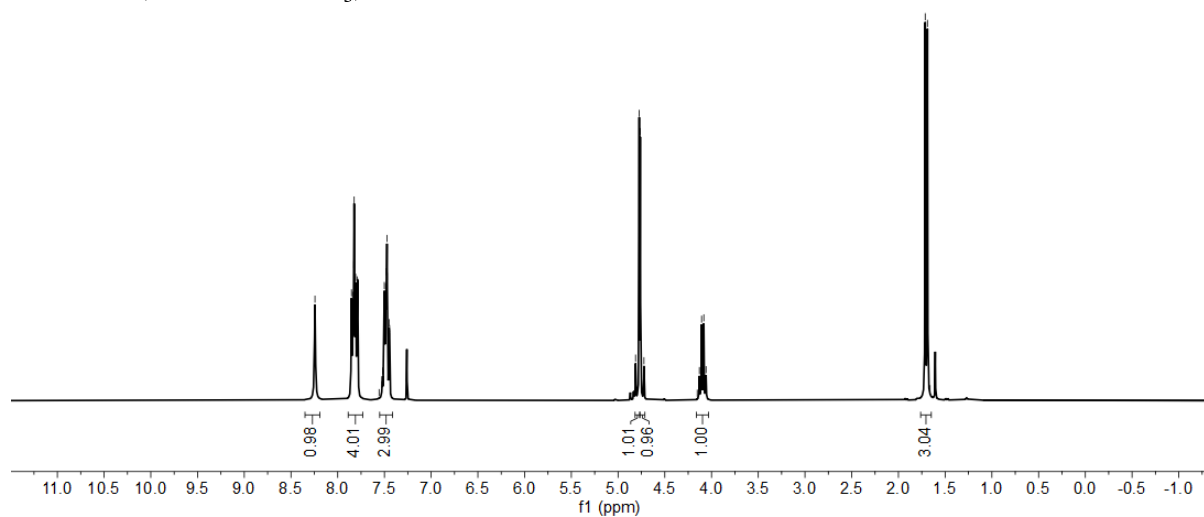
Statement



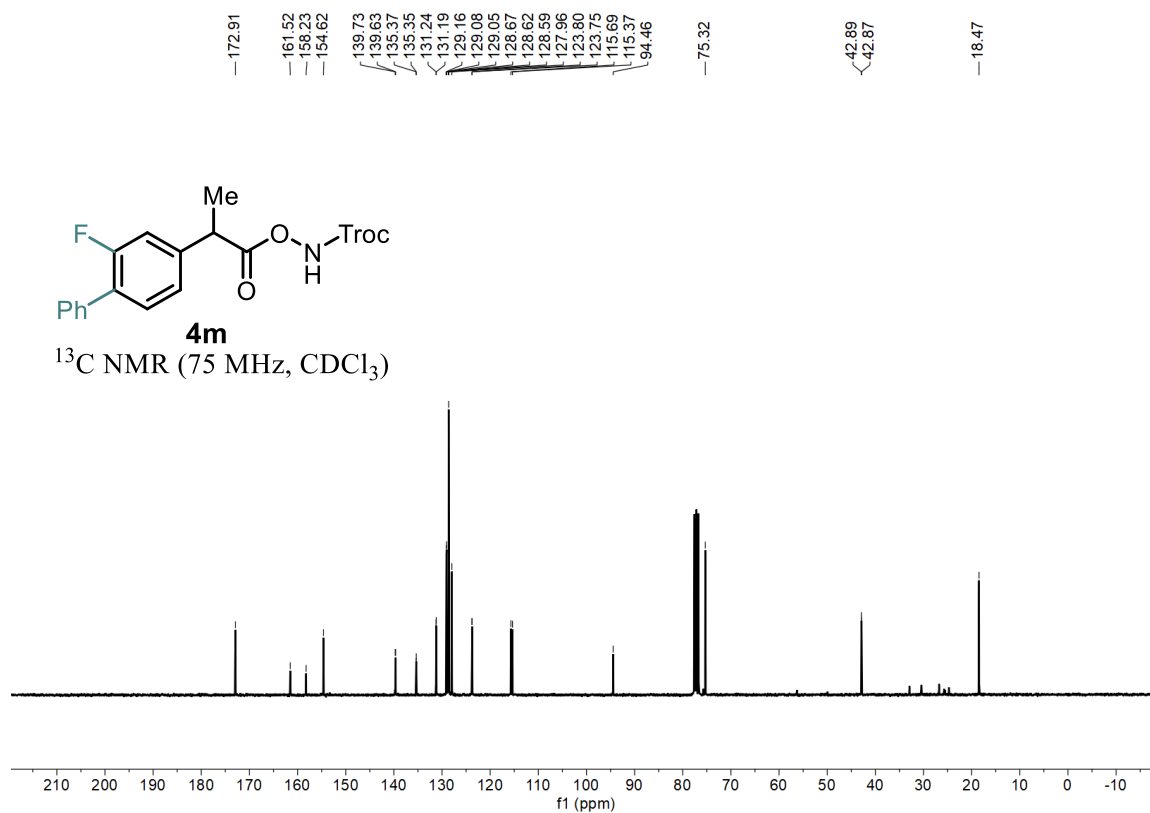
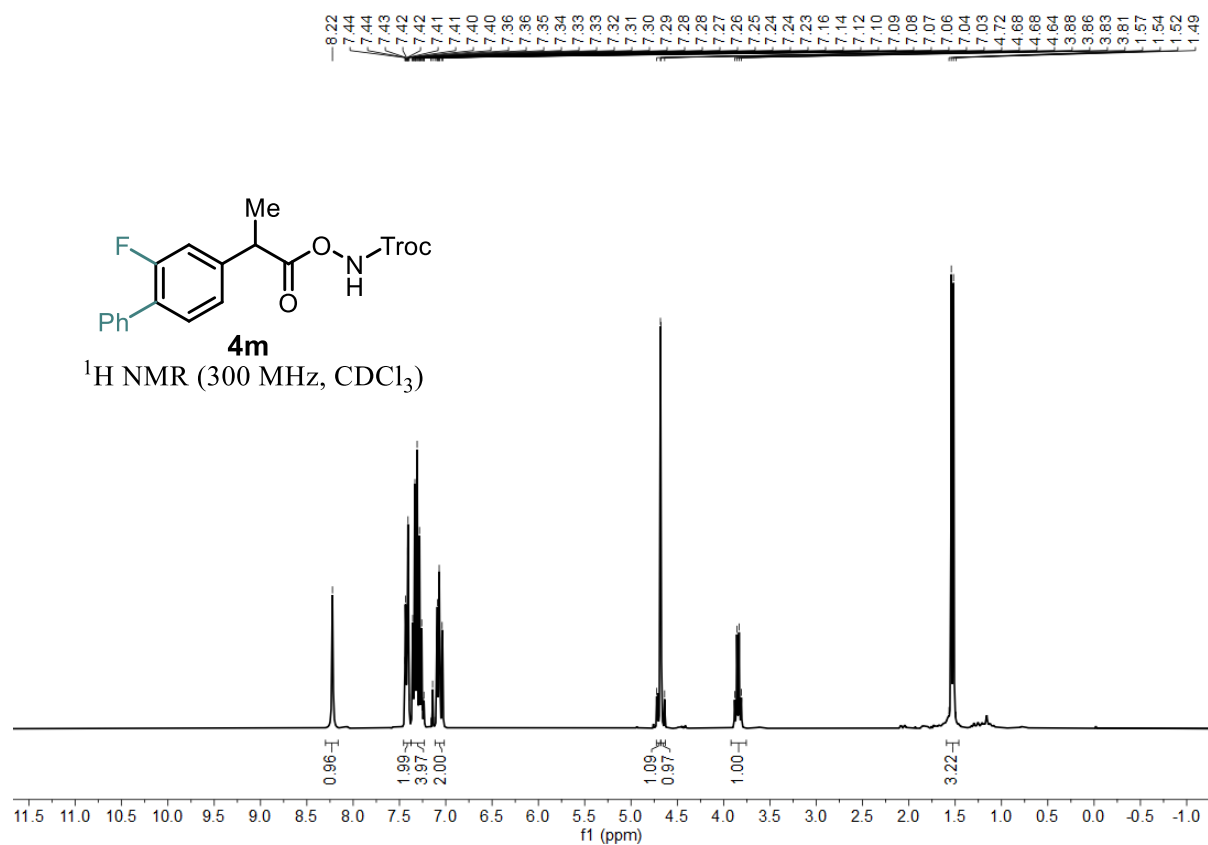
Statement



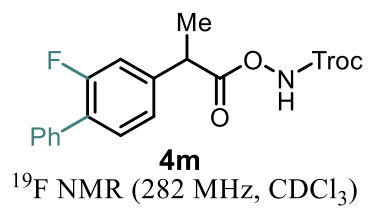
$^1\text{H NMR}$ (300 MHz, CDCl_3)



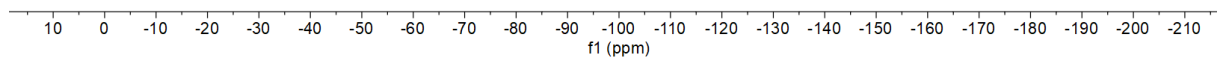
Statement



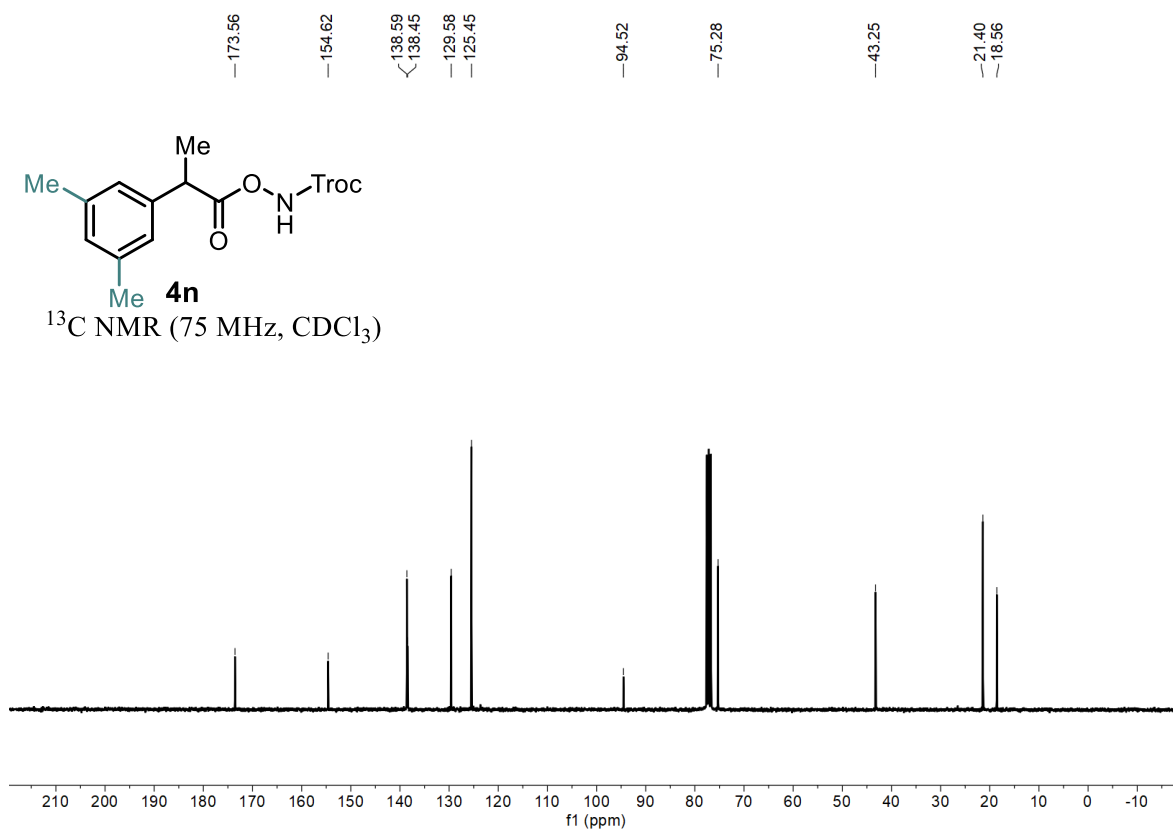
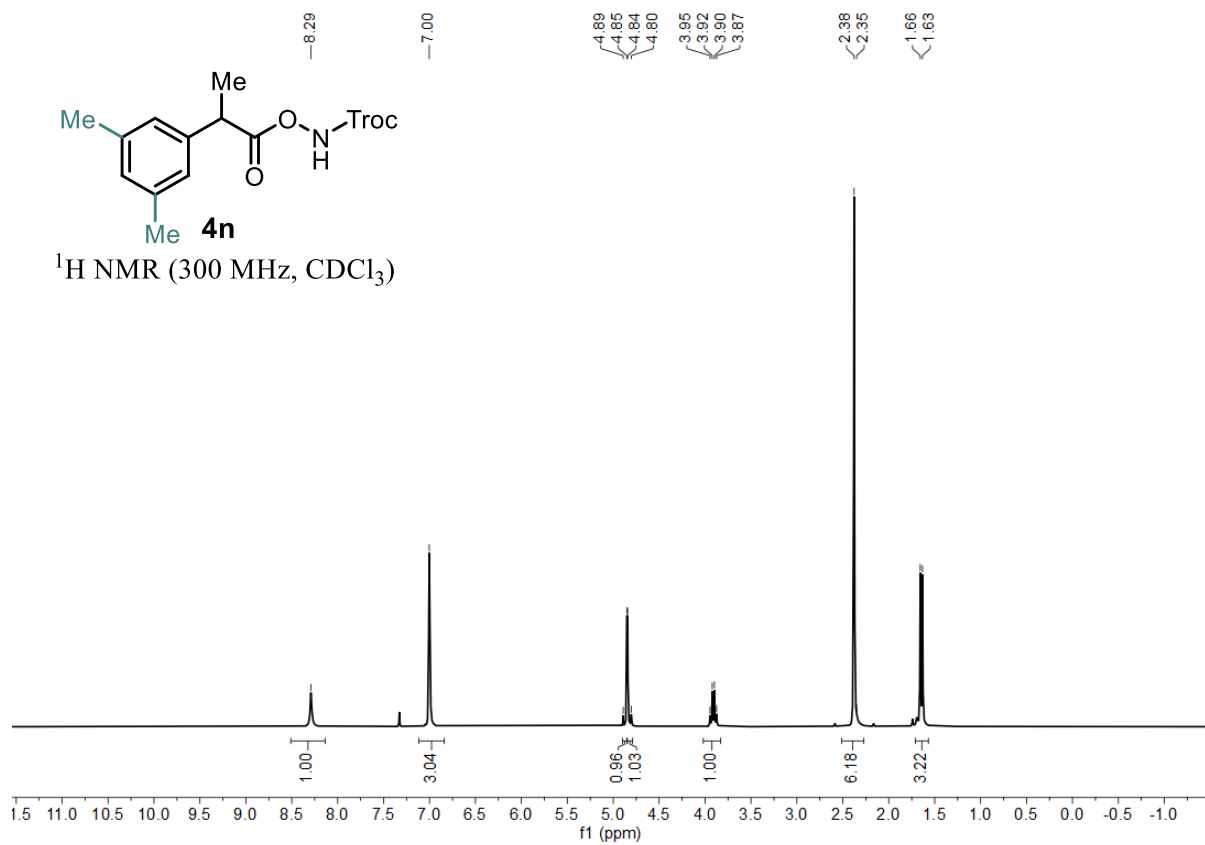
Statement



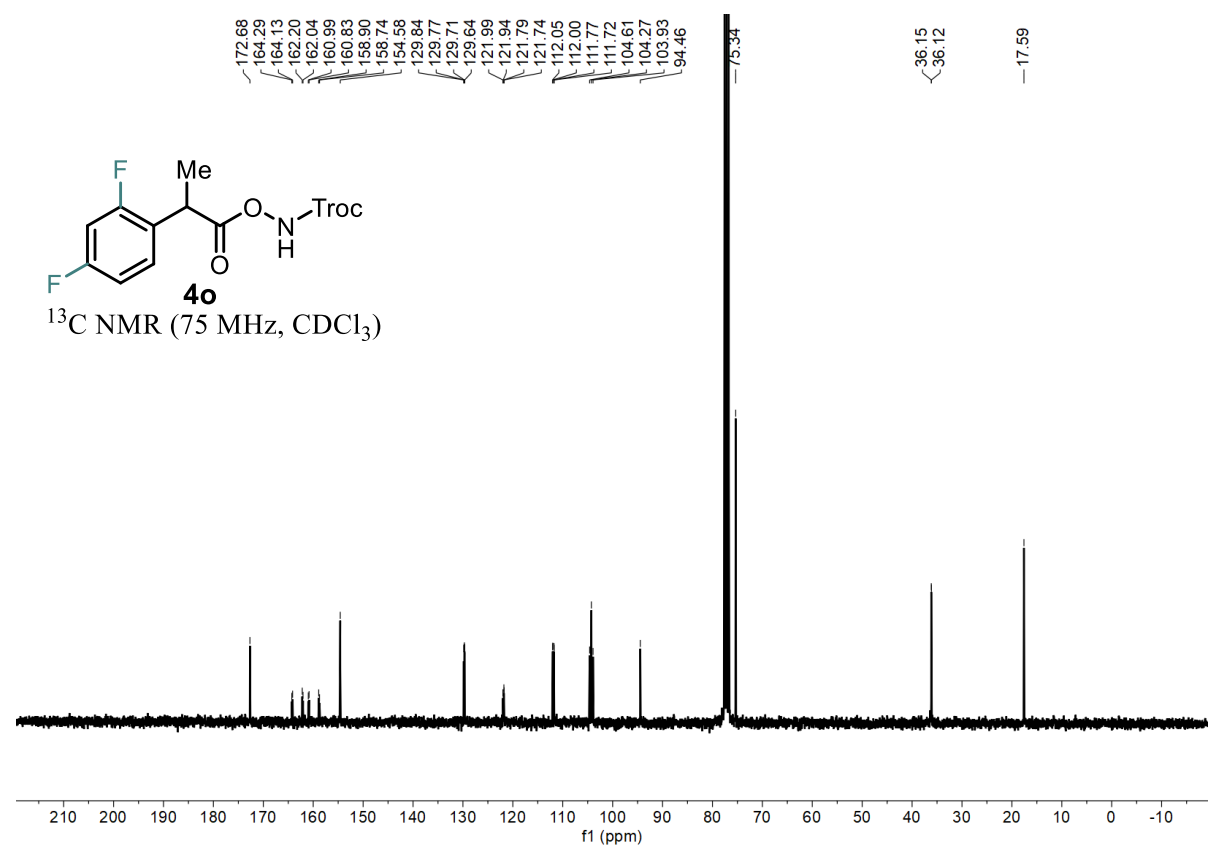
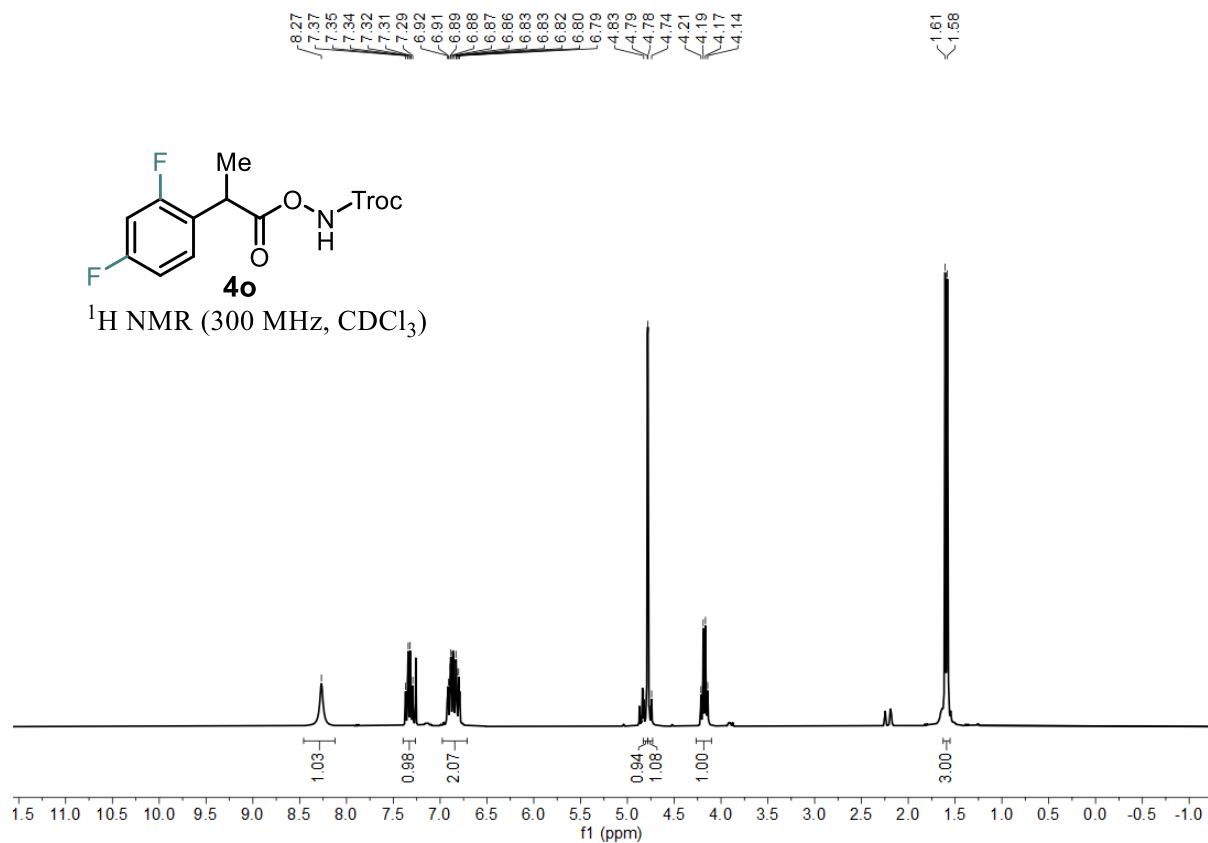
---116.88



Statement

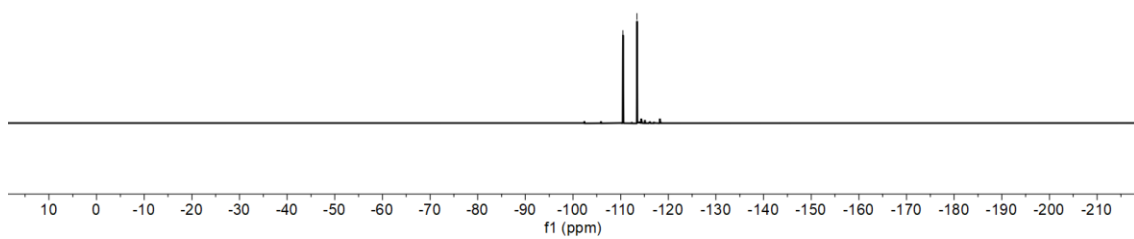
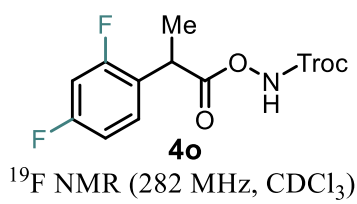


Statement

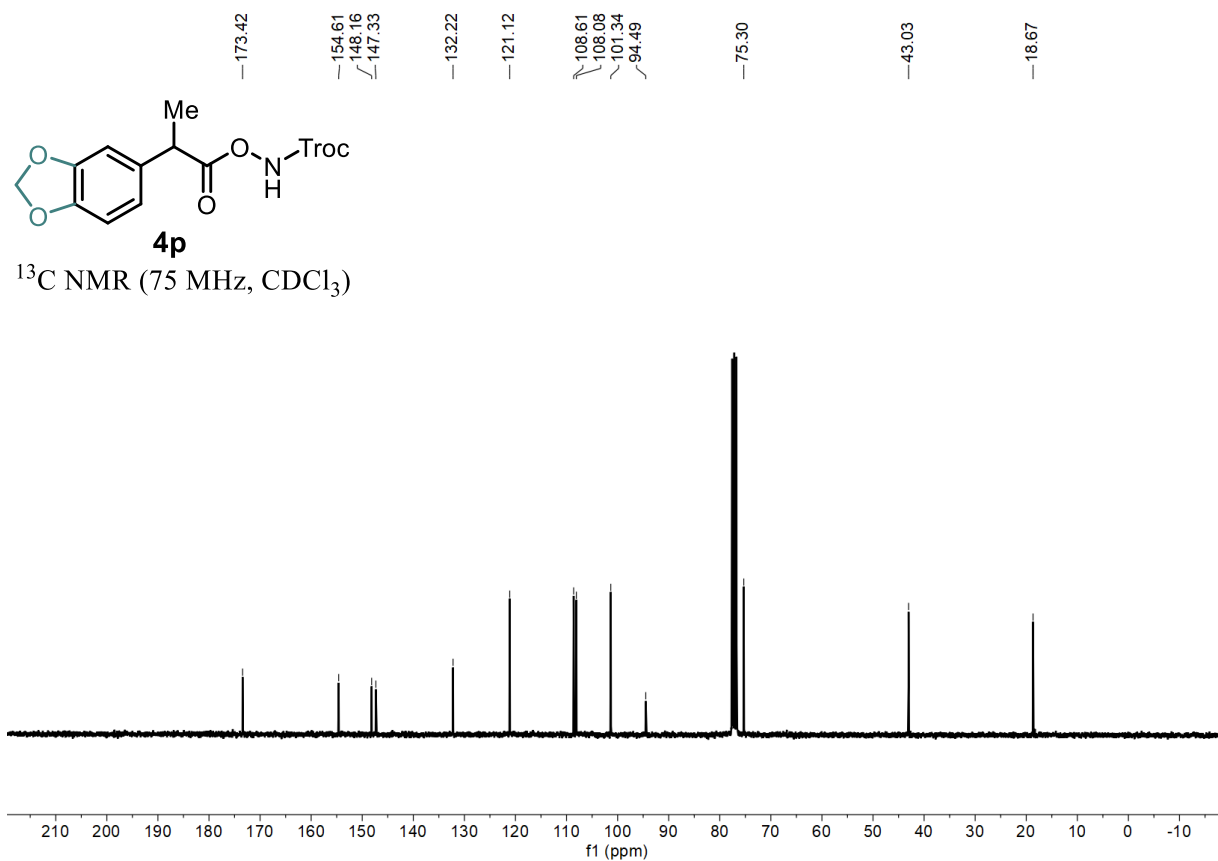
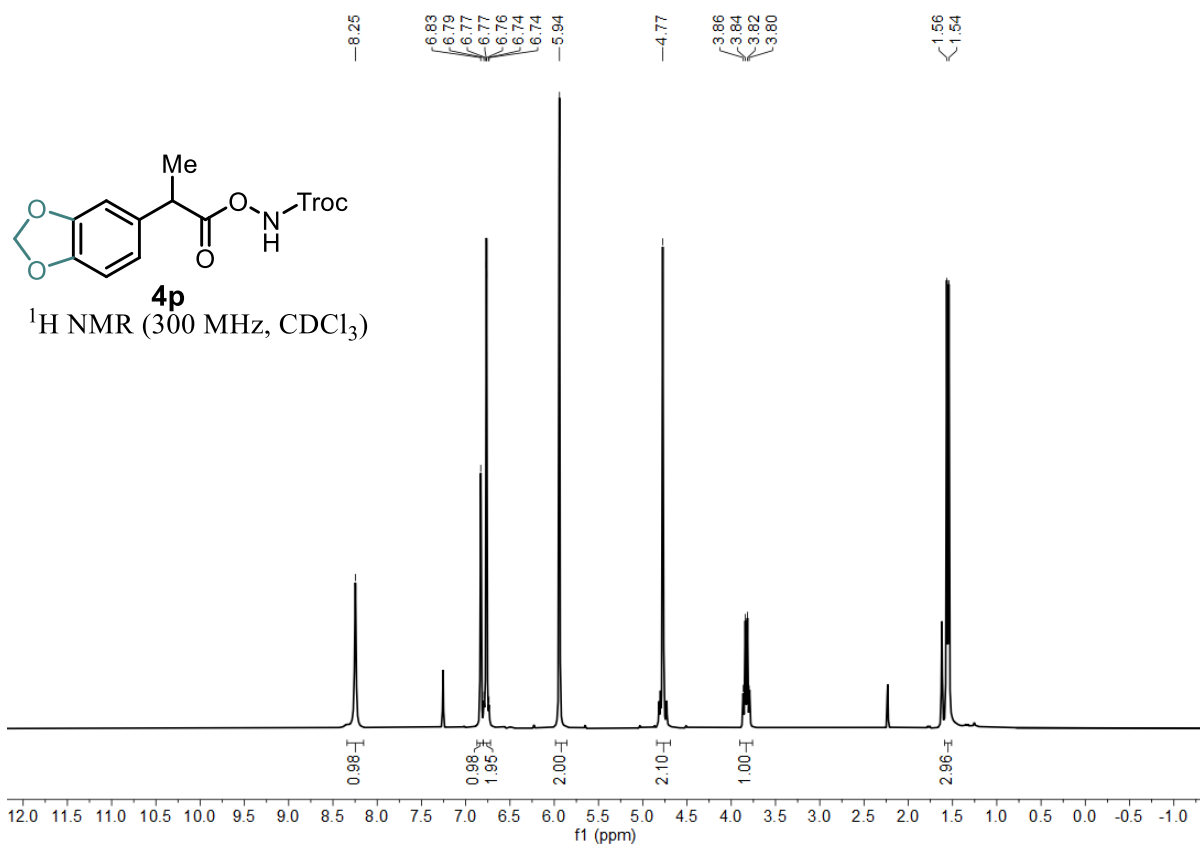


Statement

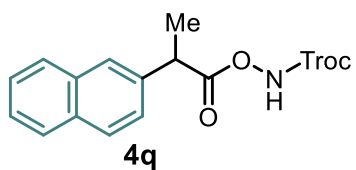
110.47
113.44



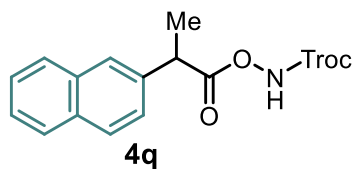
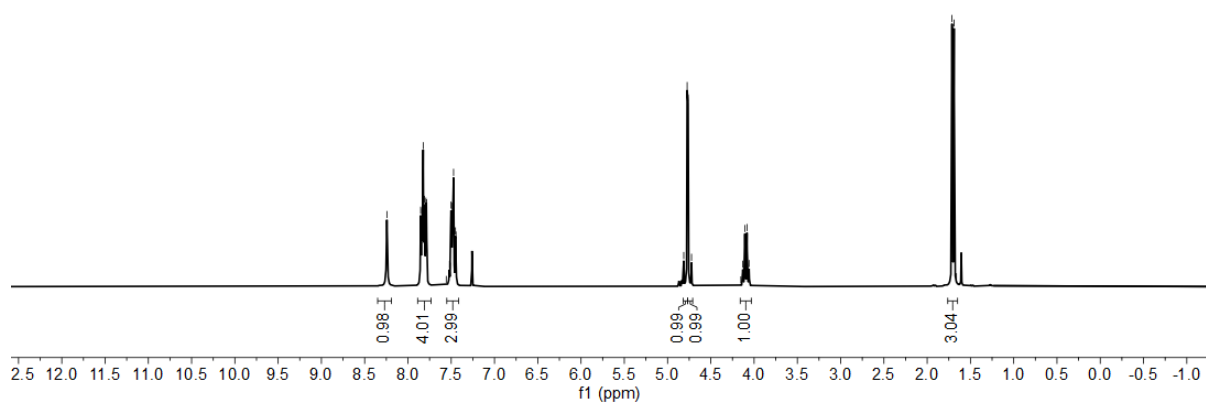
Statement



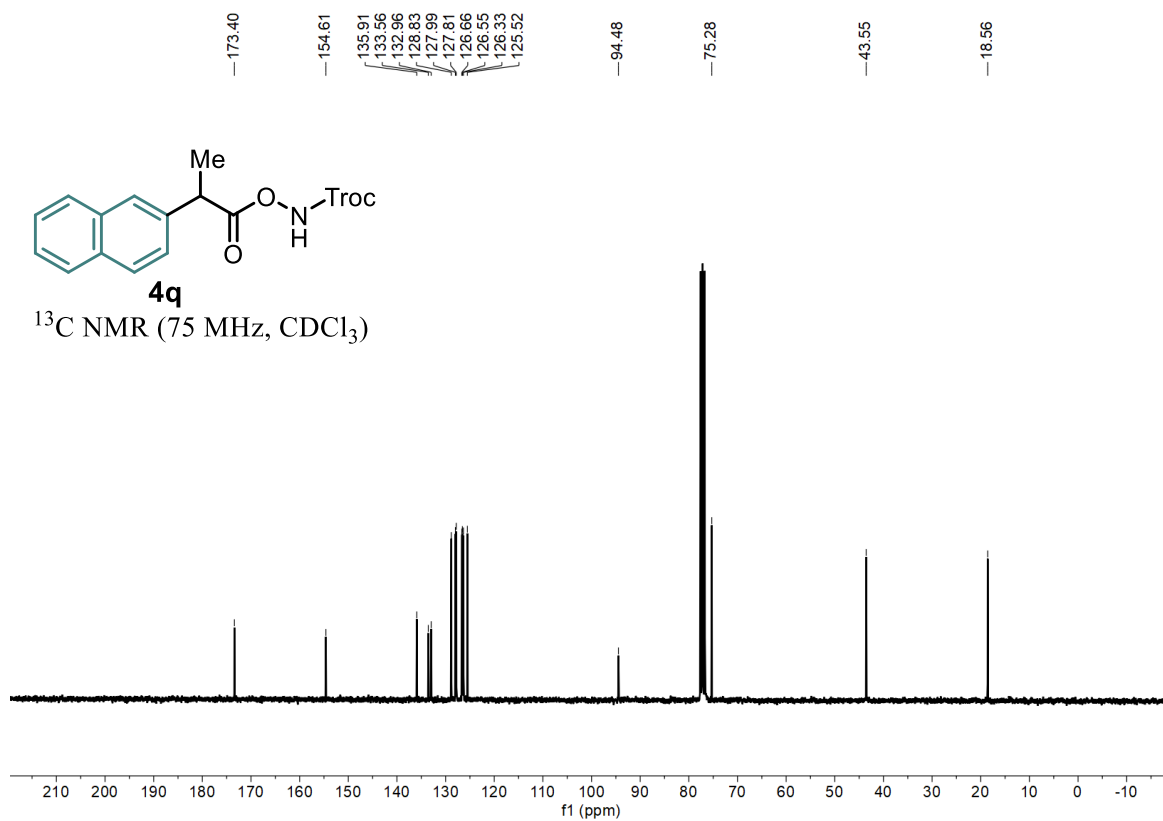
Statement



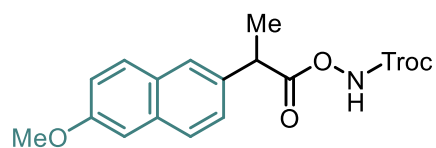
$^1\text{H NMR}$ (300 MHz, CDCl_3)



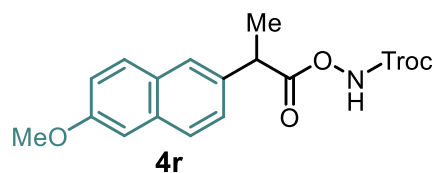
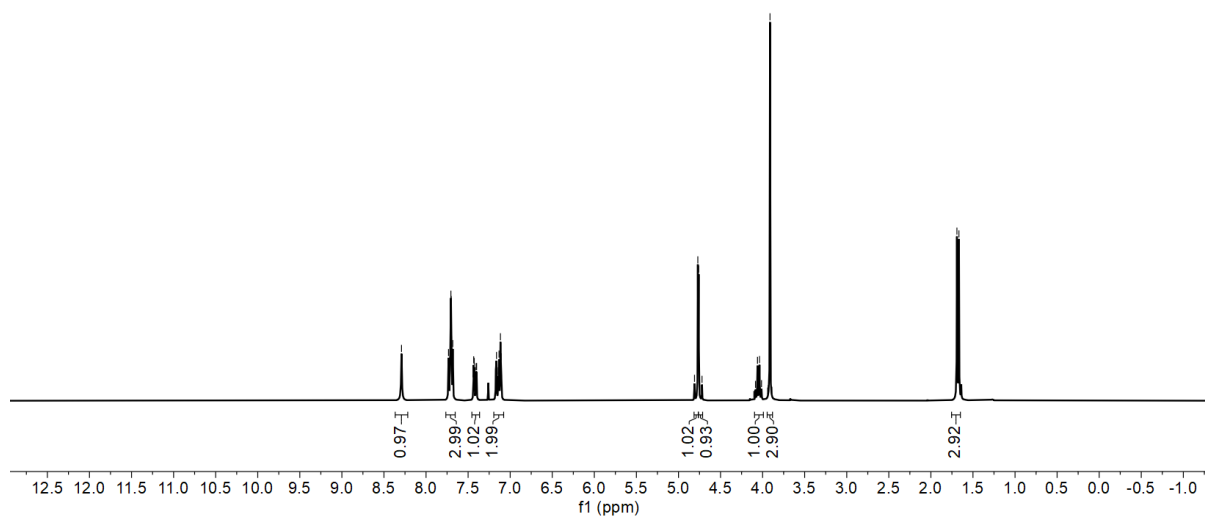
$^{13}\text{C NMR}$ (75 MHz, CDCl_3)



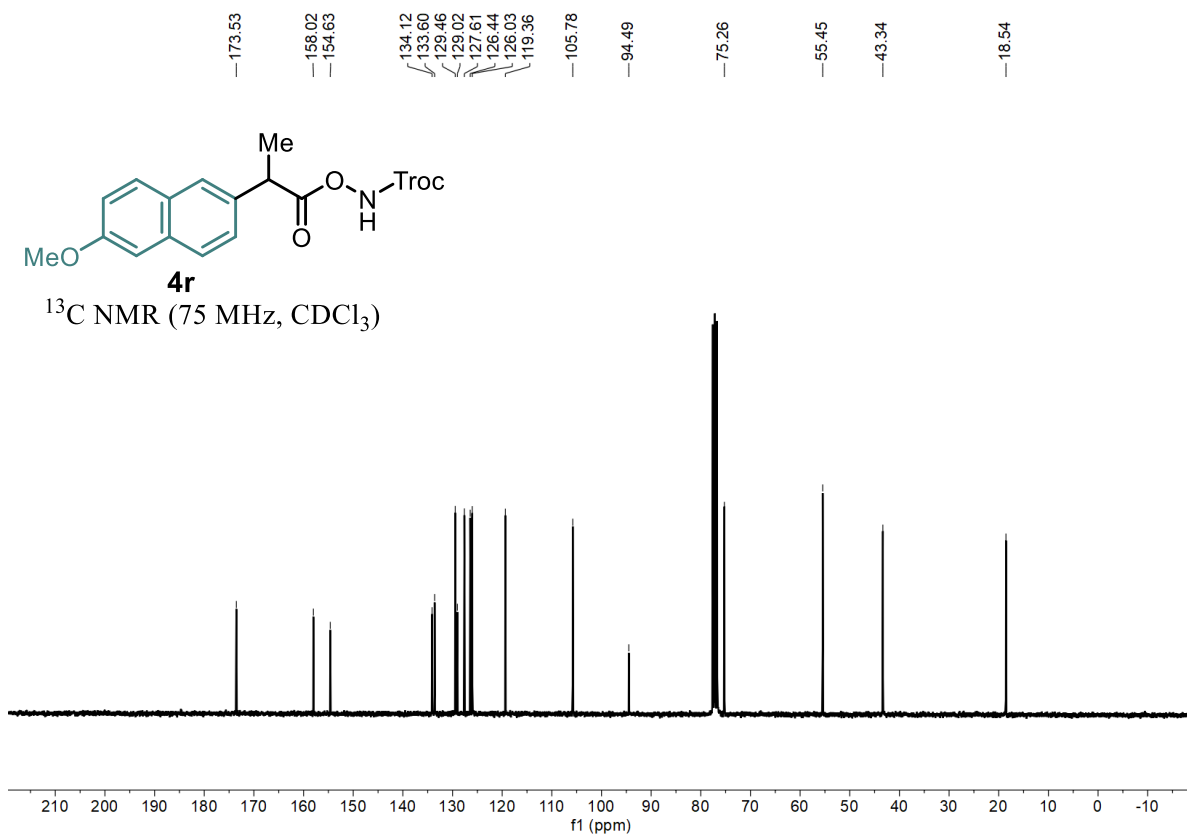
Statement



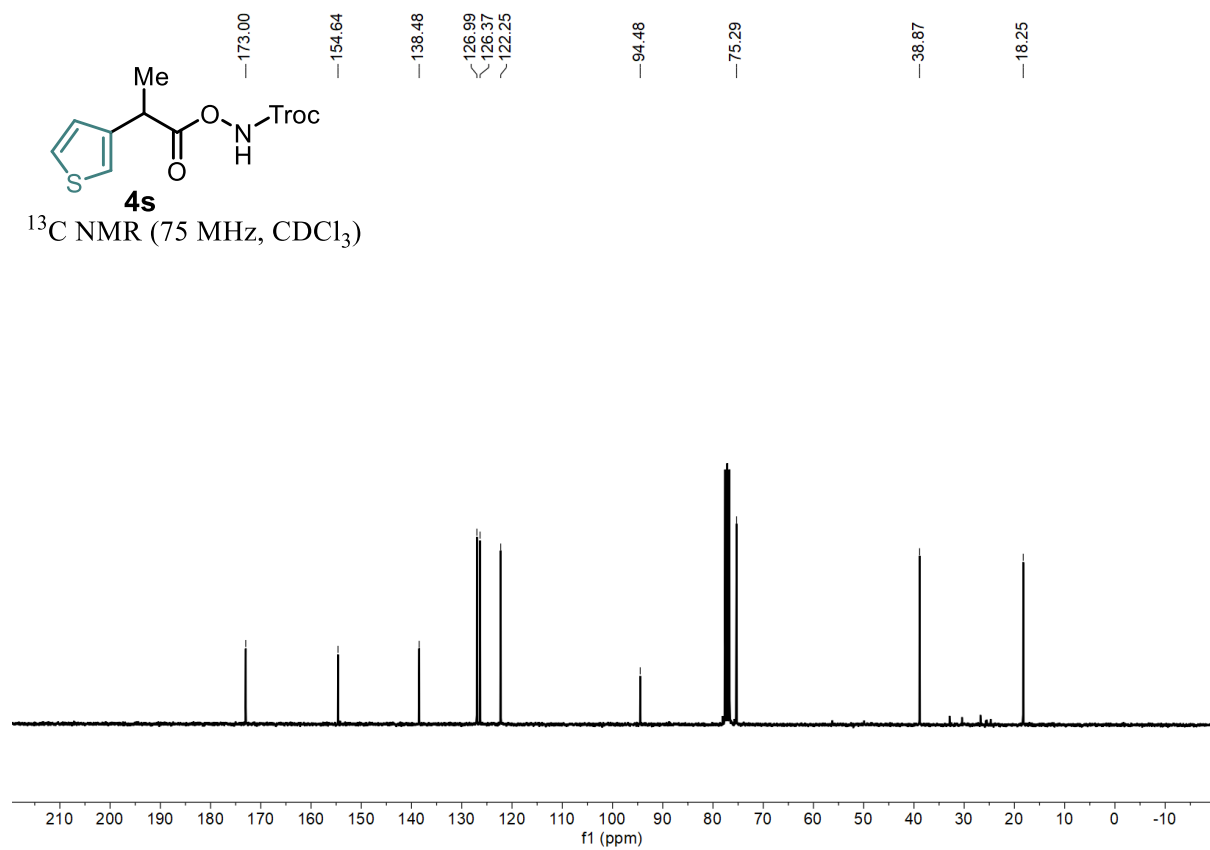
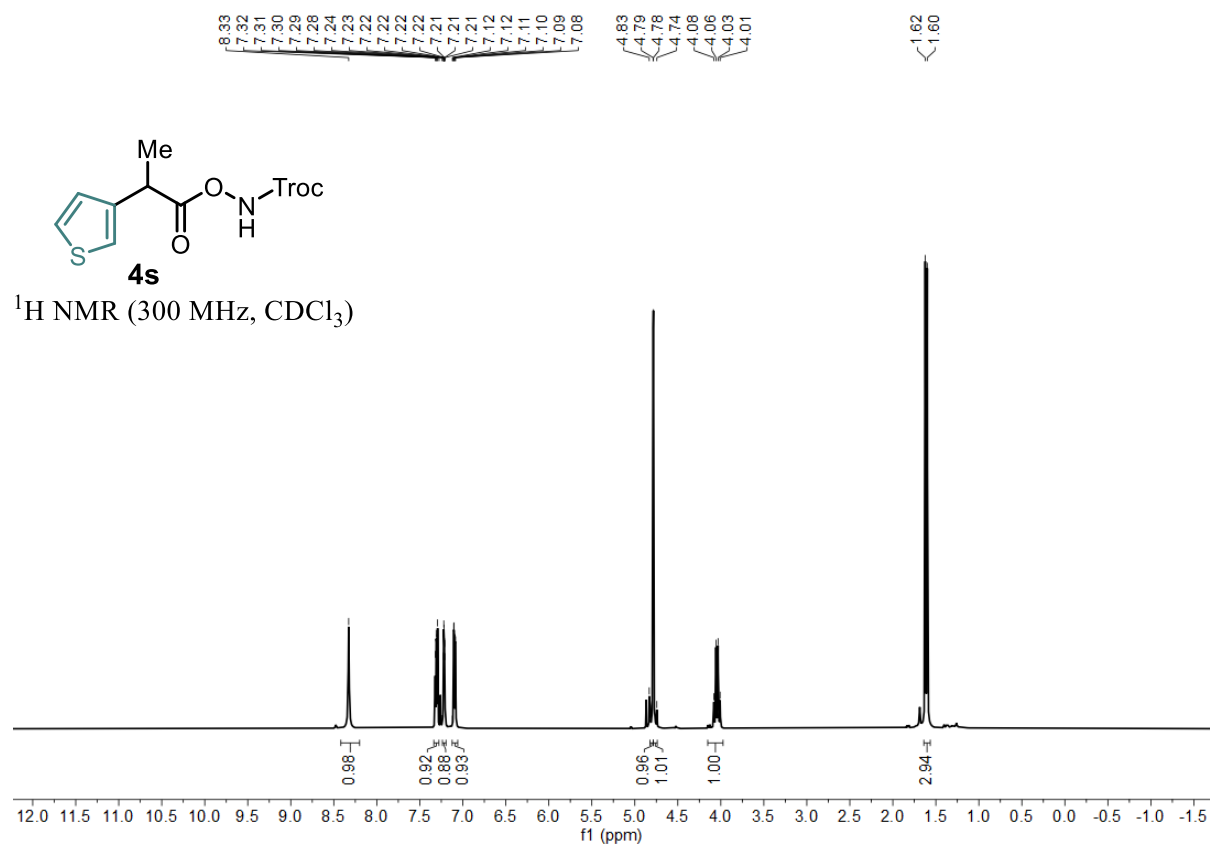
$^1\text{H NMR}$ (300 MHz, CDCl_3)



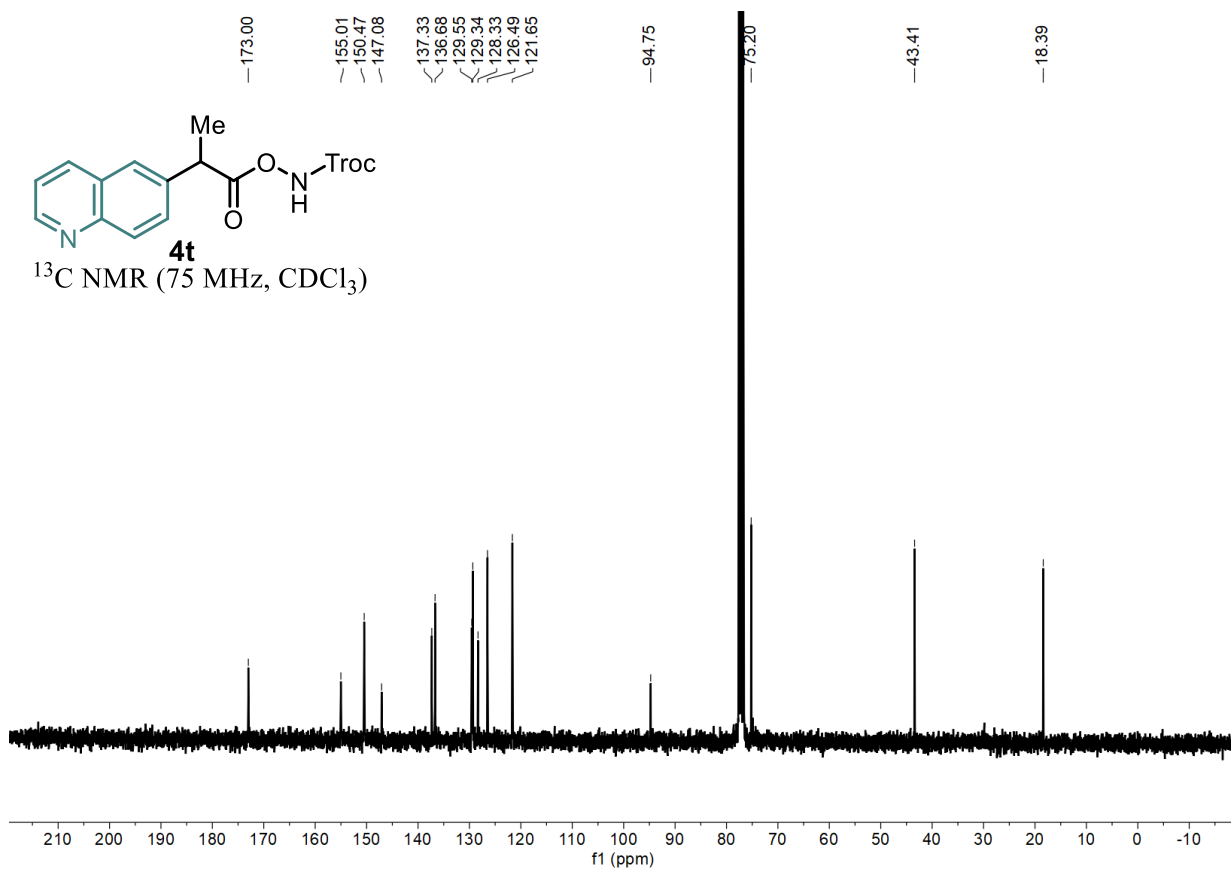
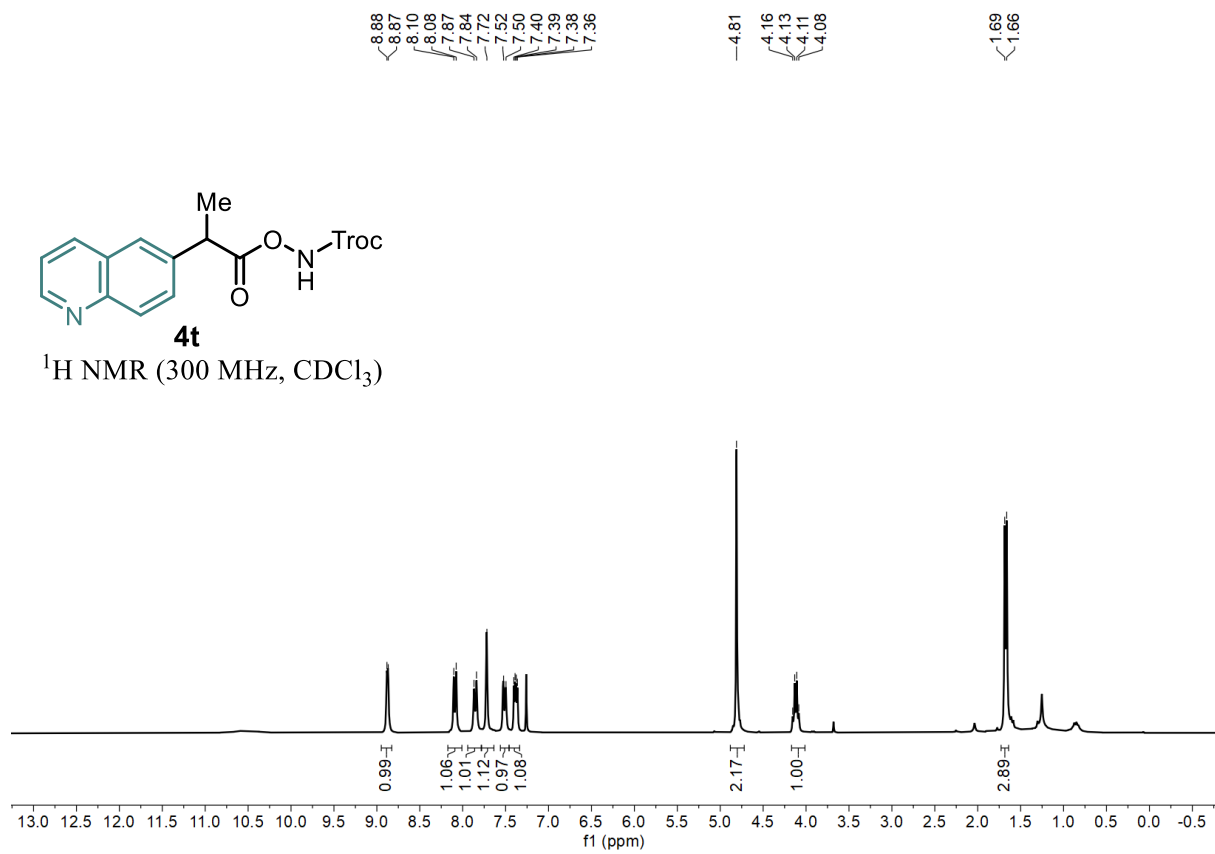
$^{13}\text{C NMR}$ (75 MHz, CDCl_3)



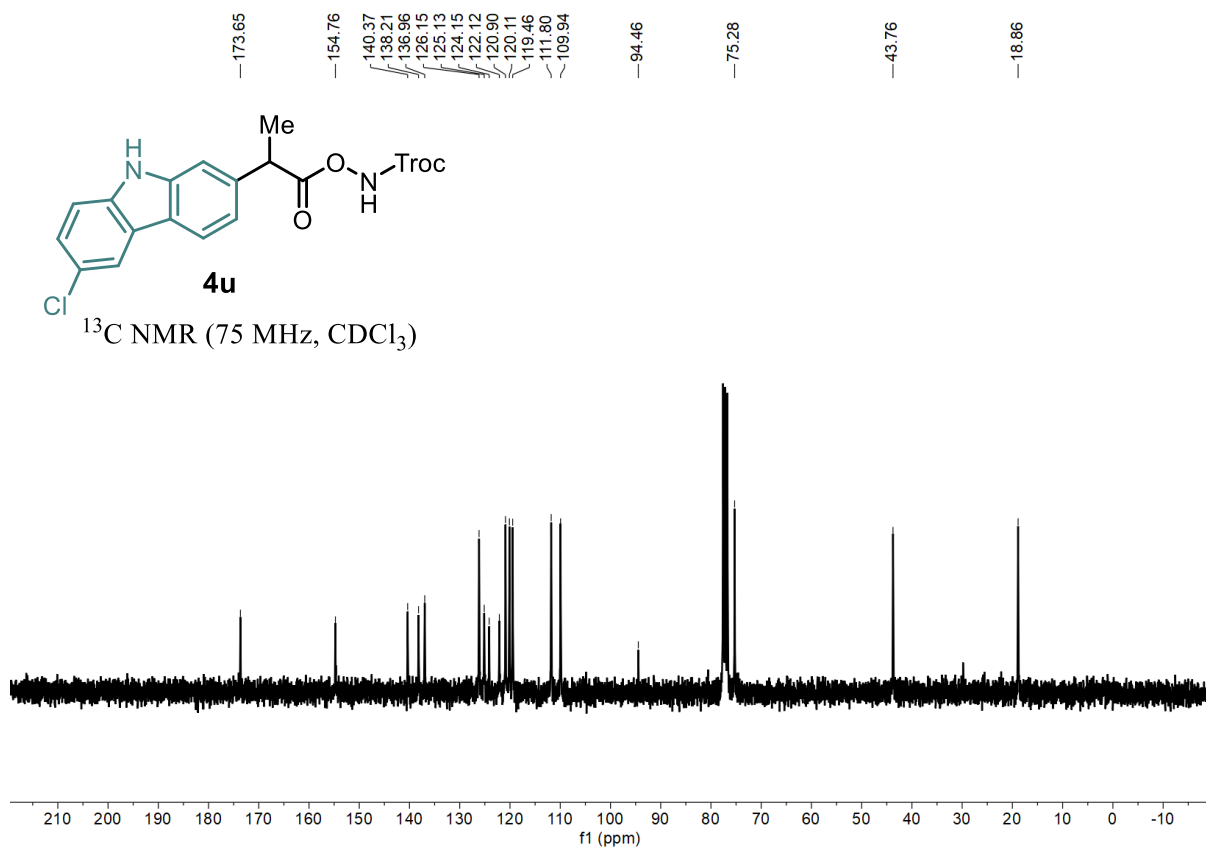
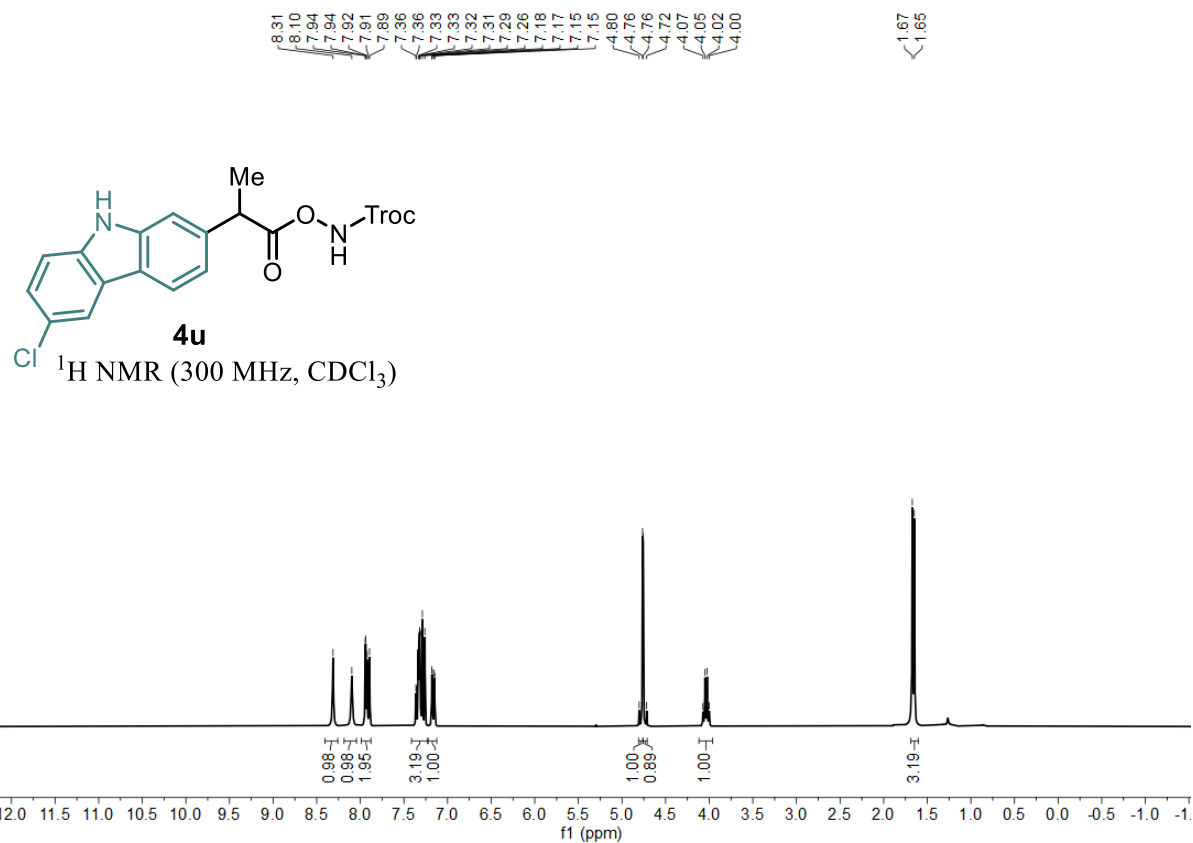
Statement



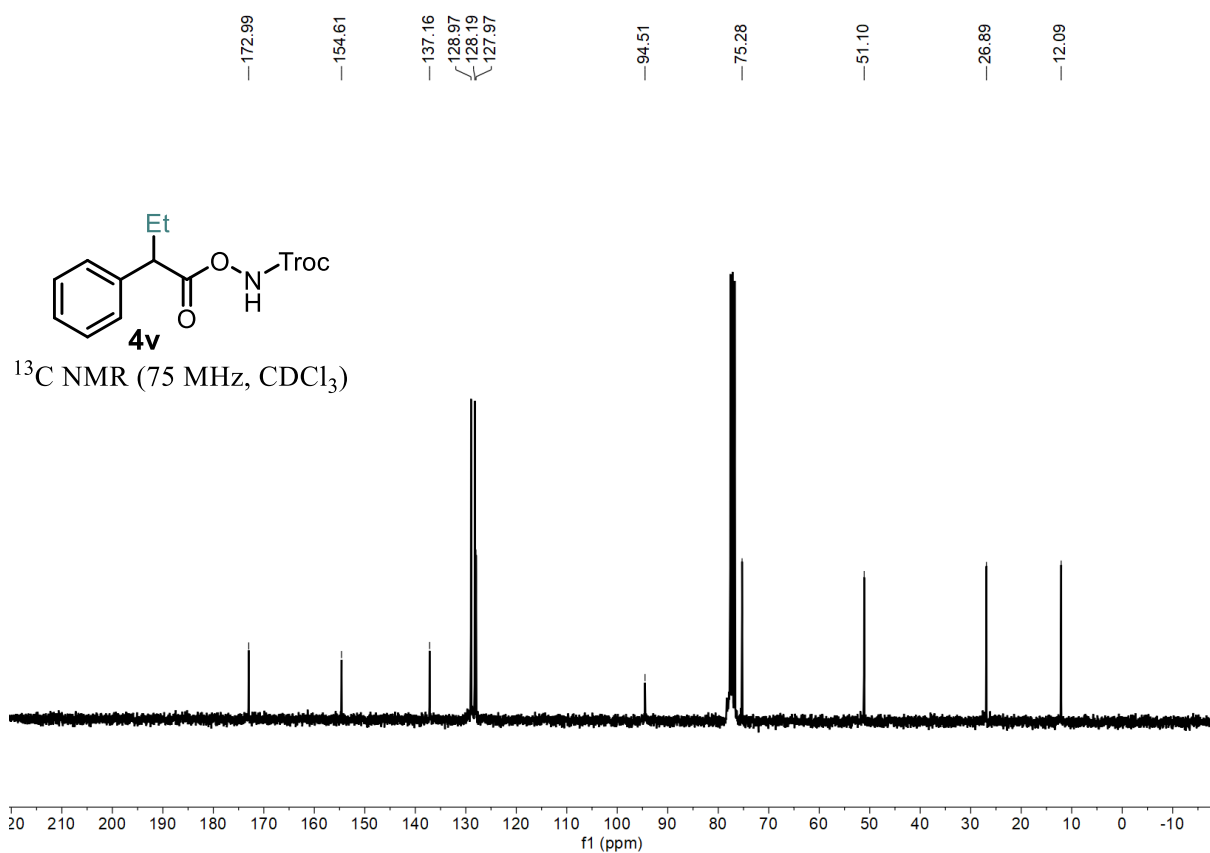
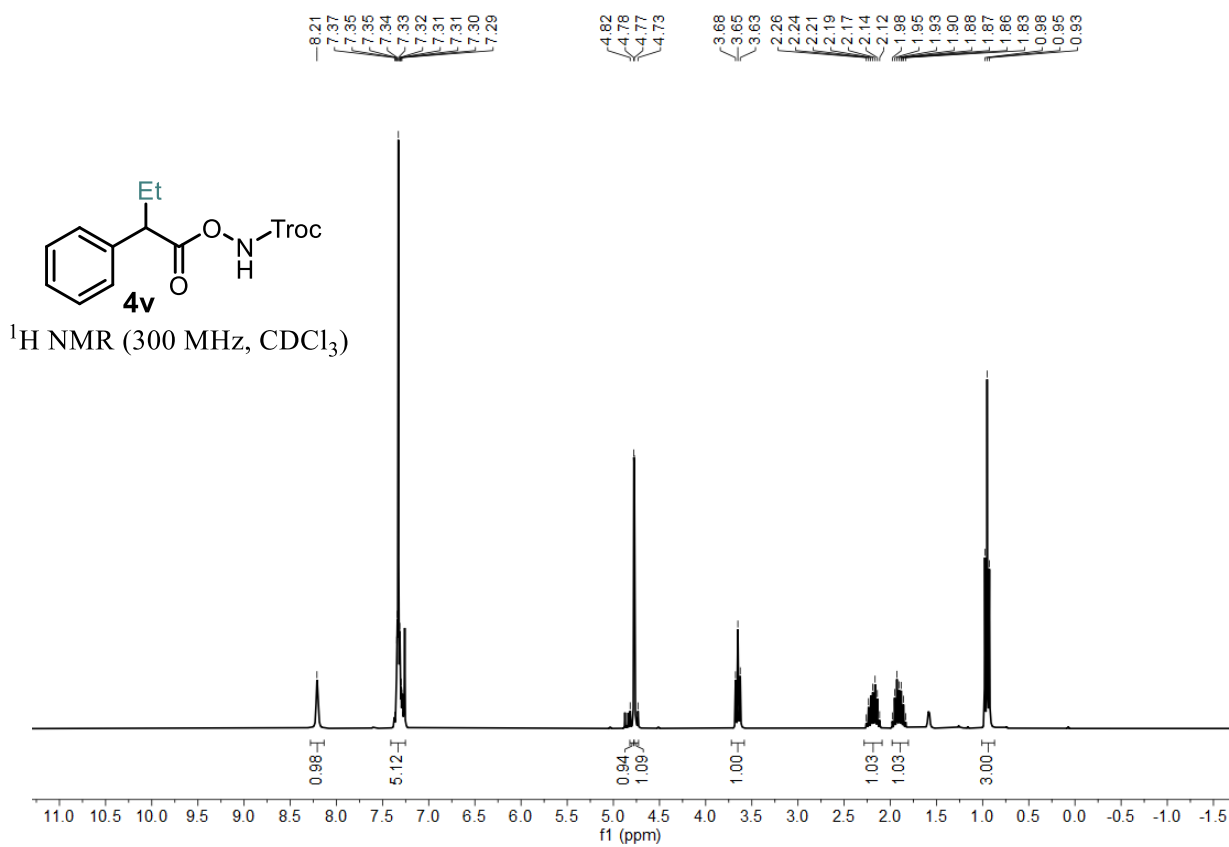
Statement



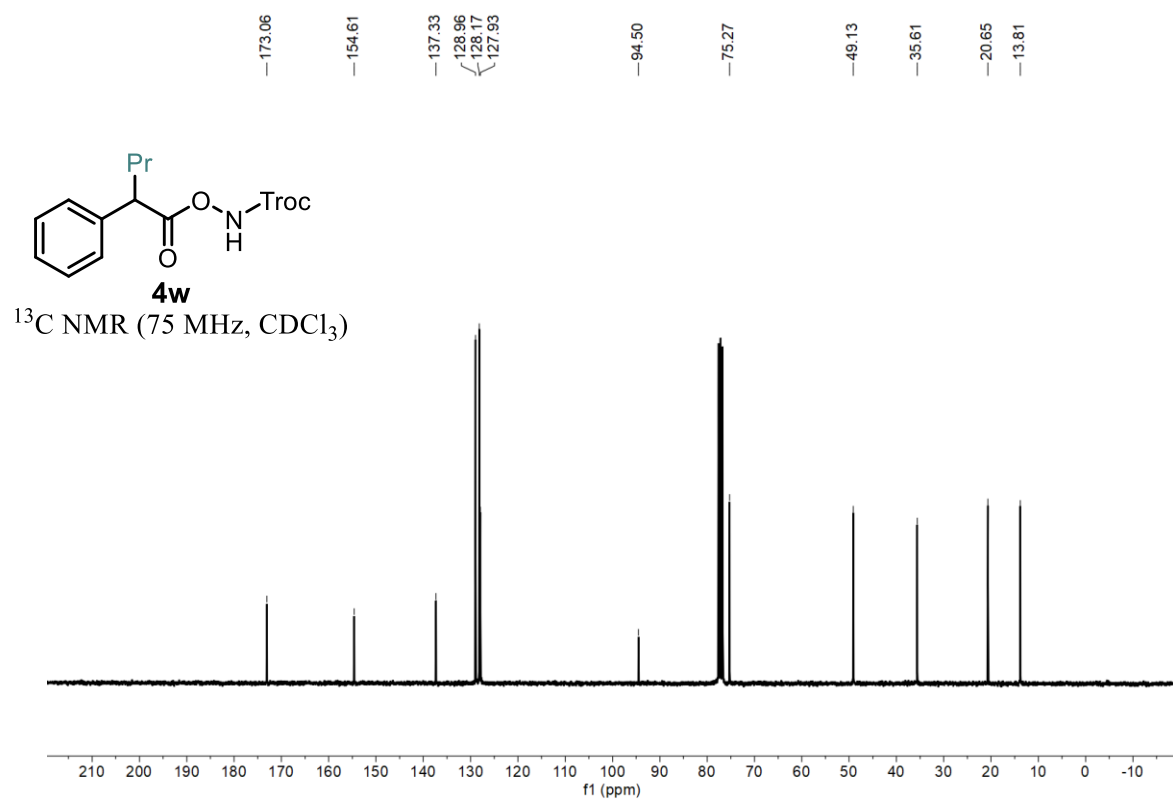
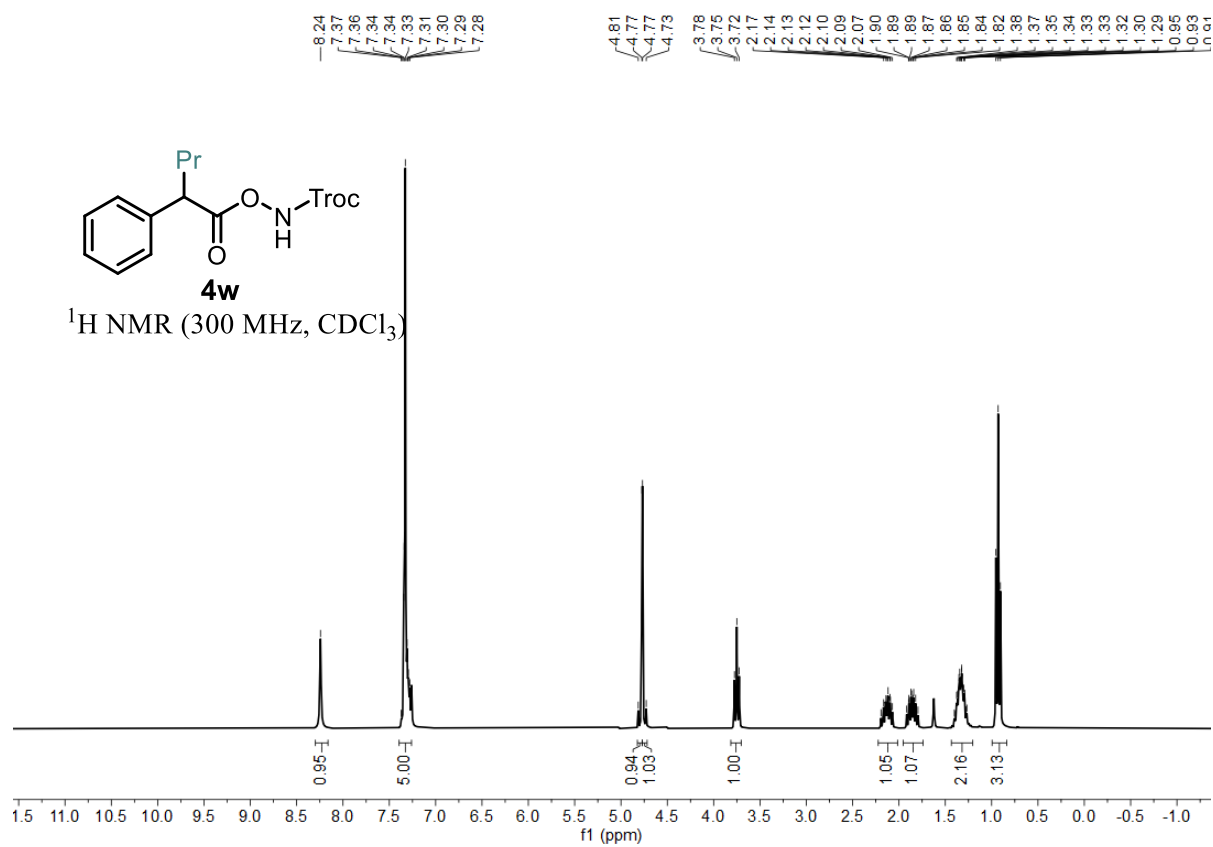
Statement



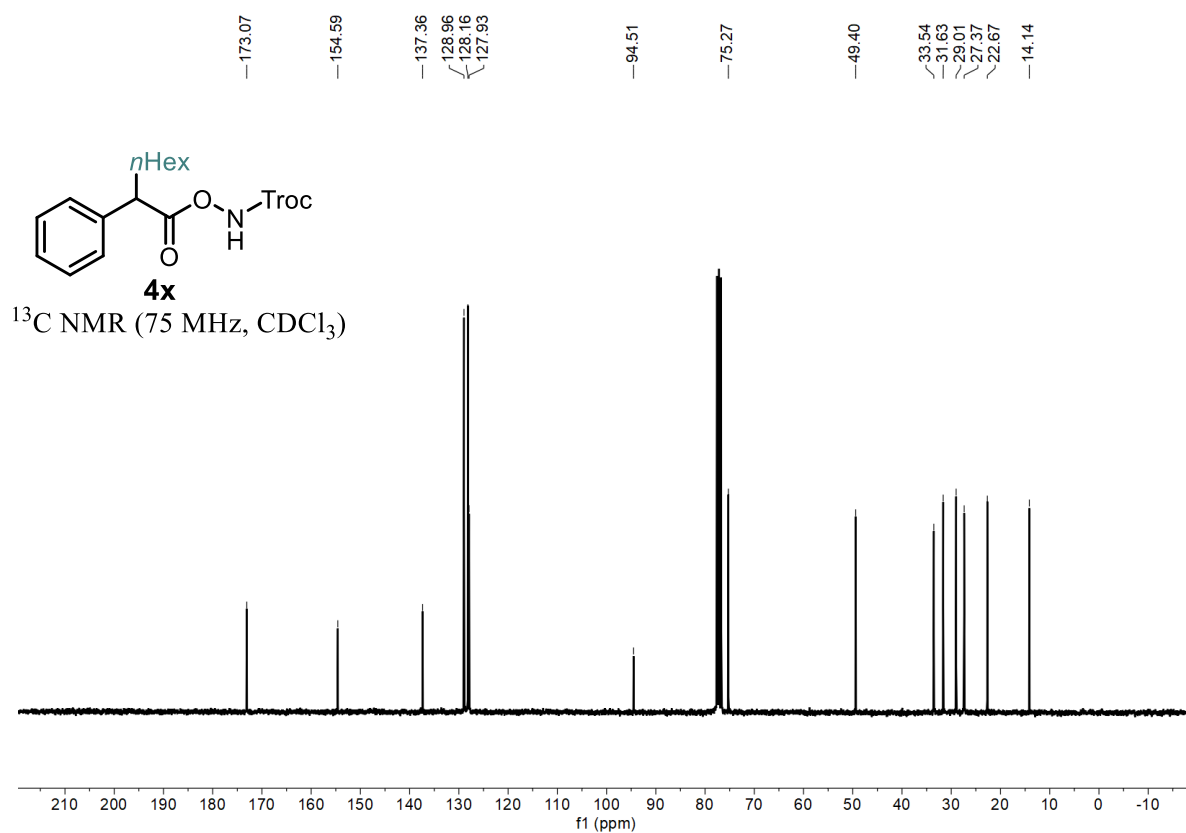
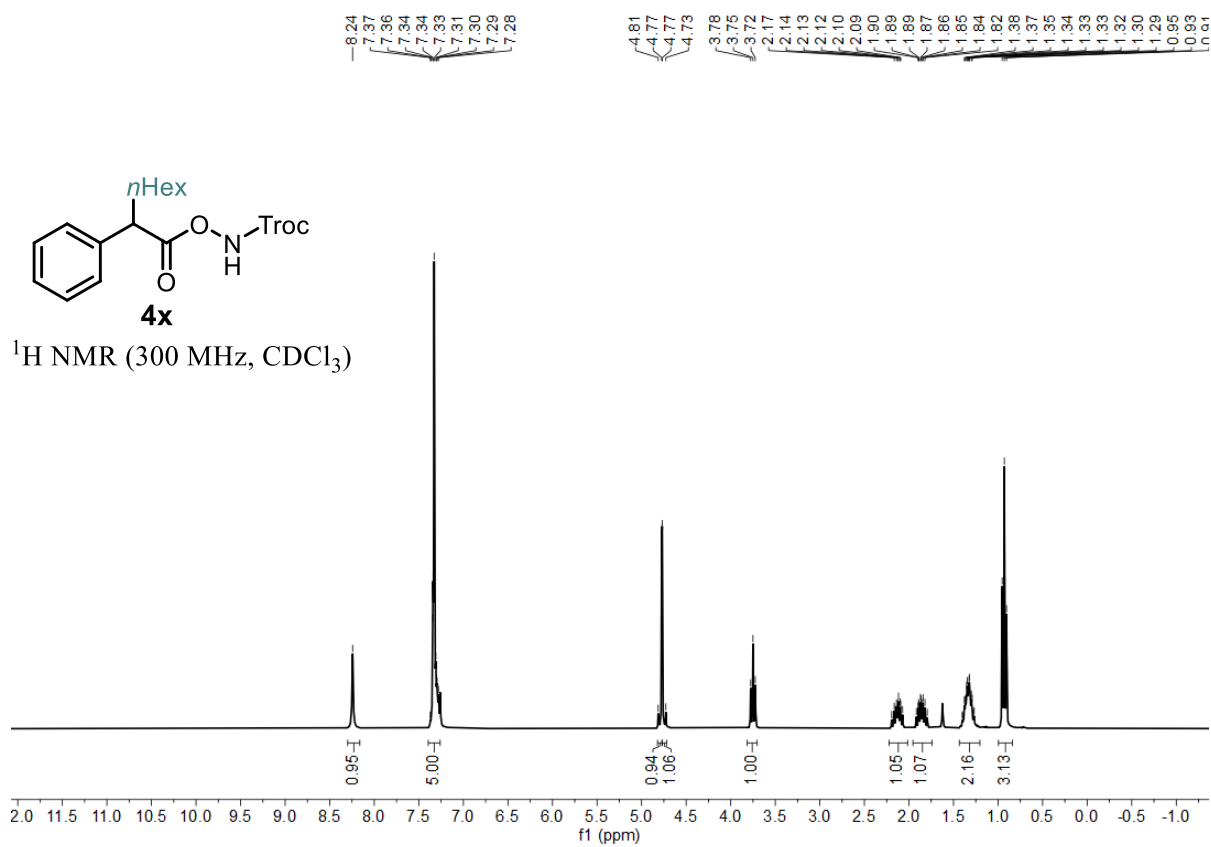
Statement



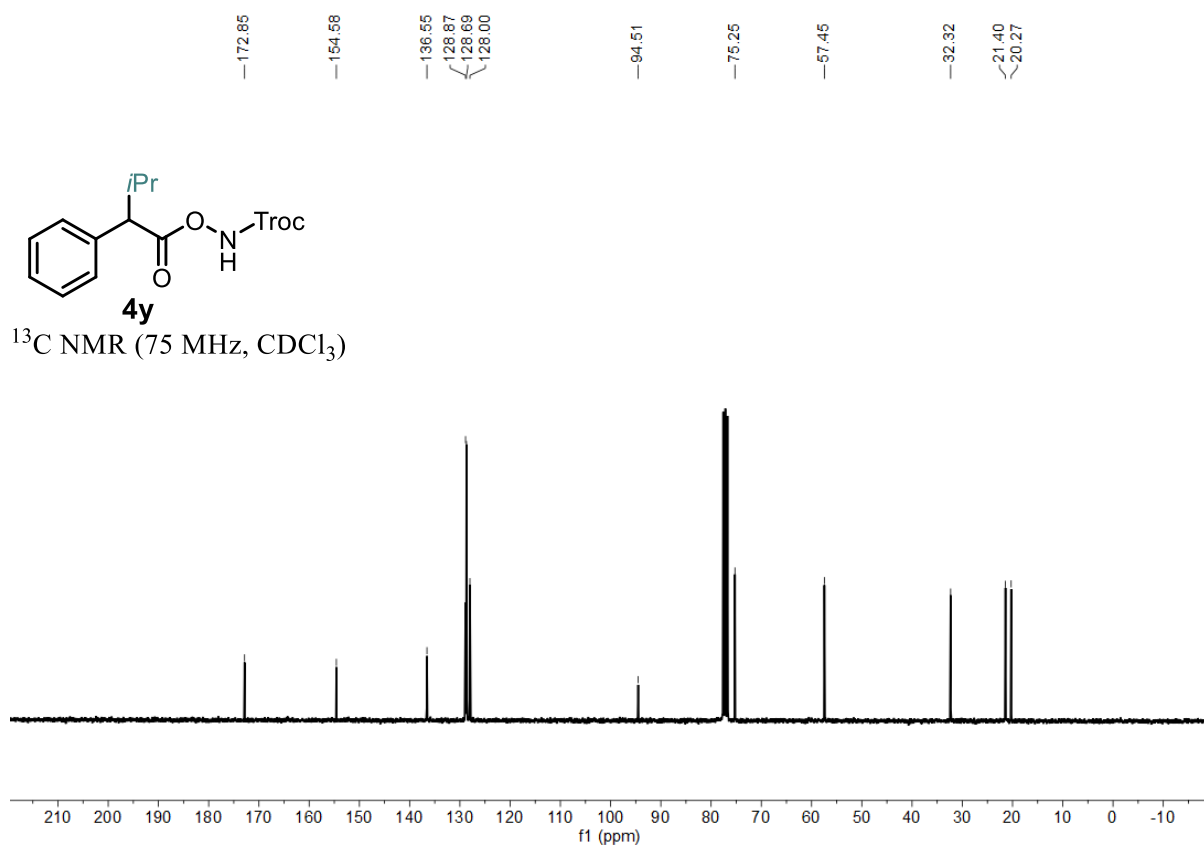
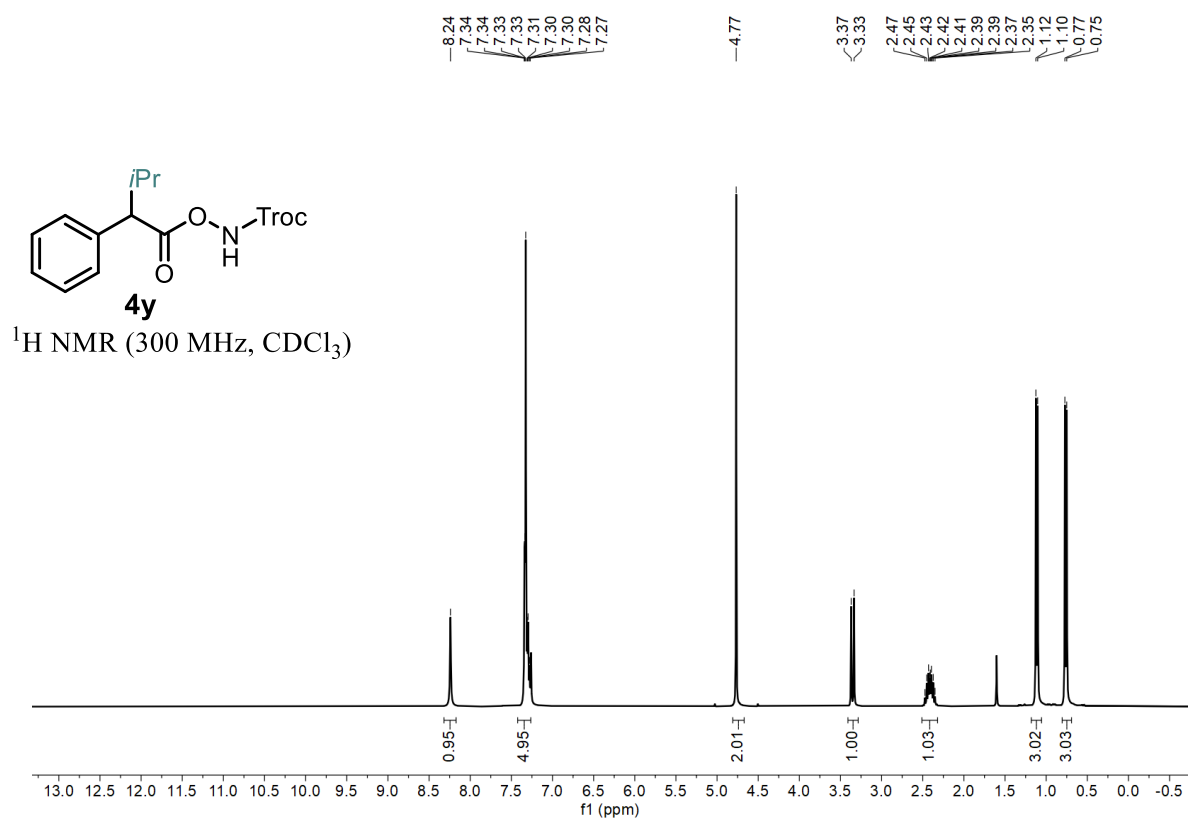
Statement



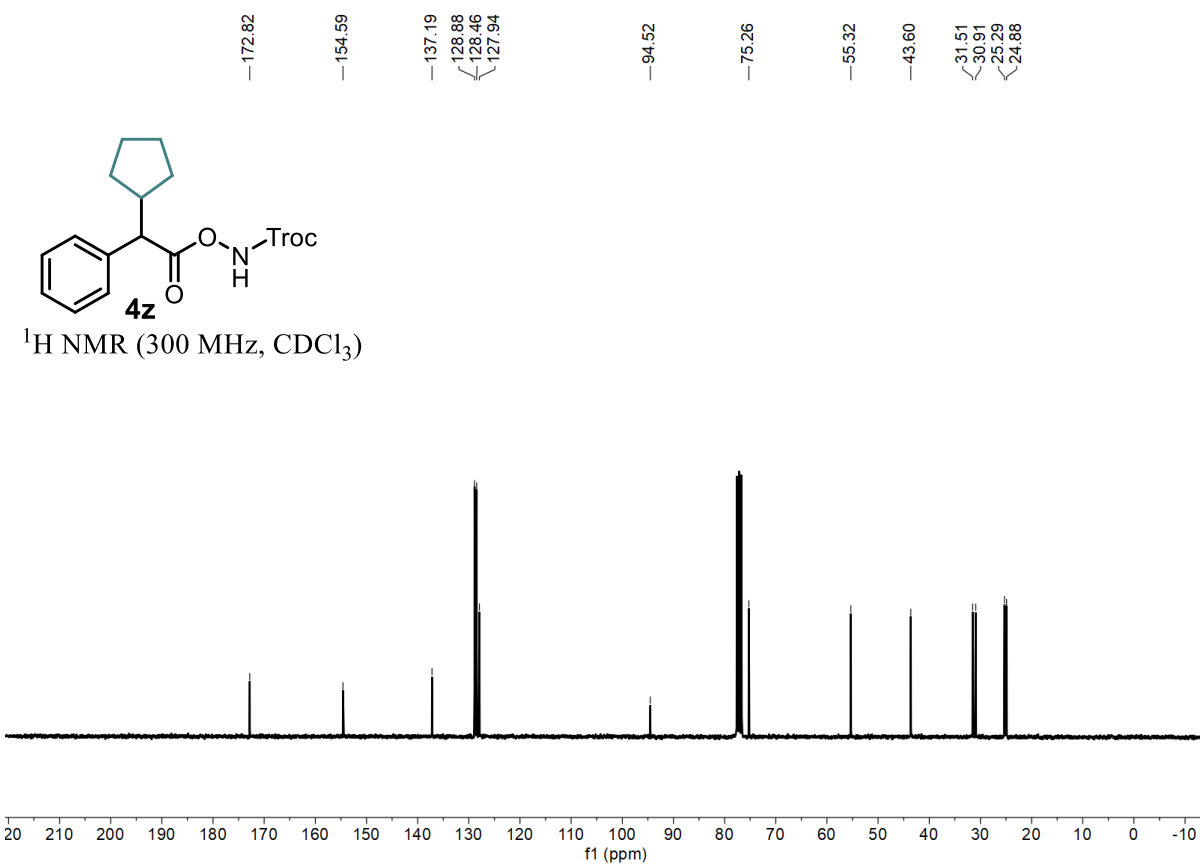
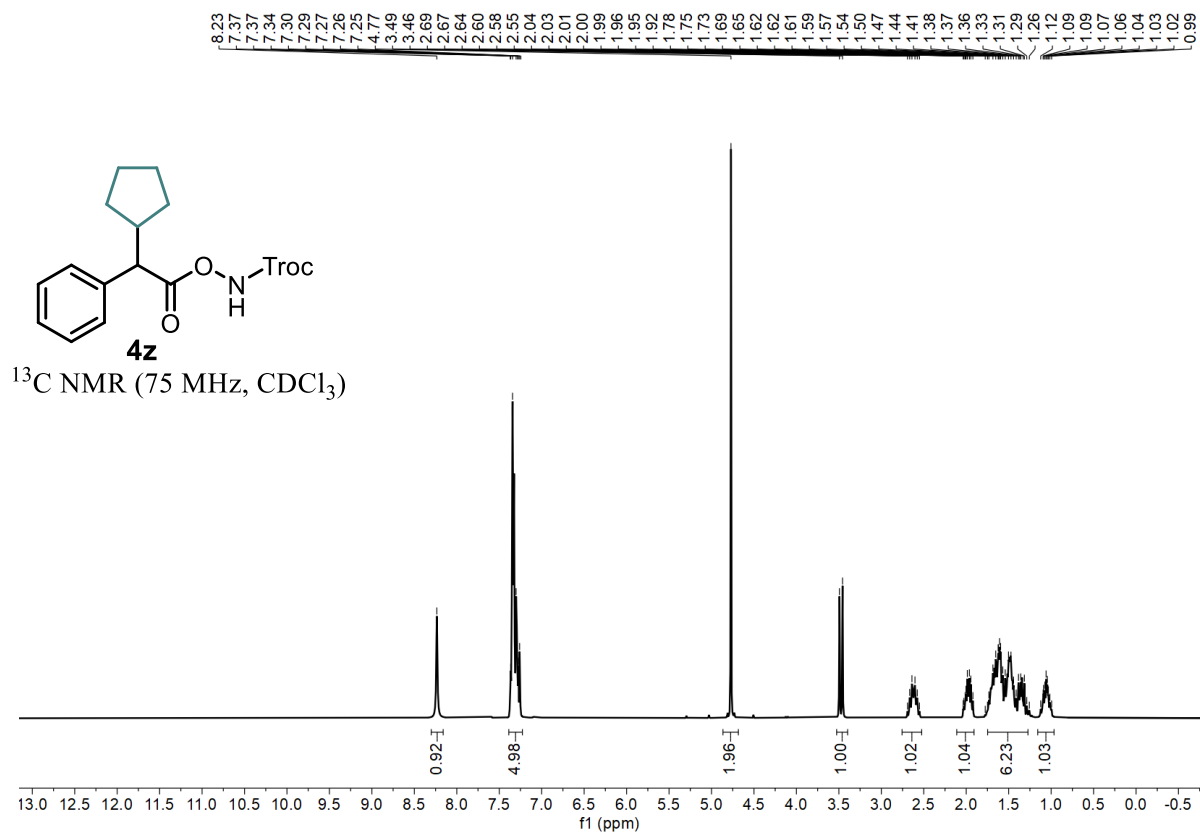
Statement



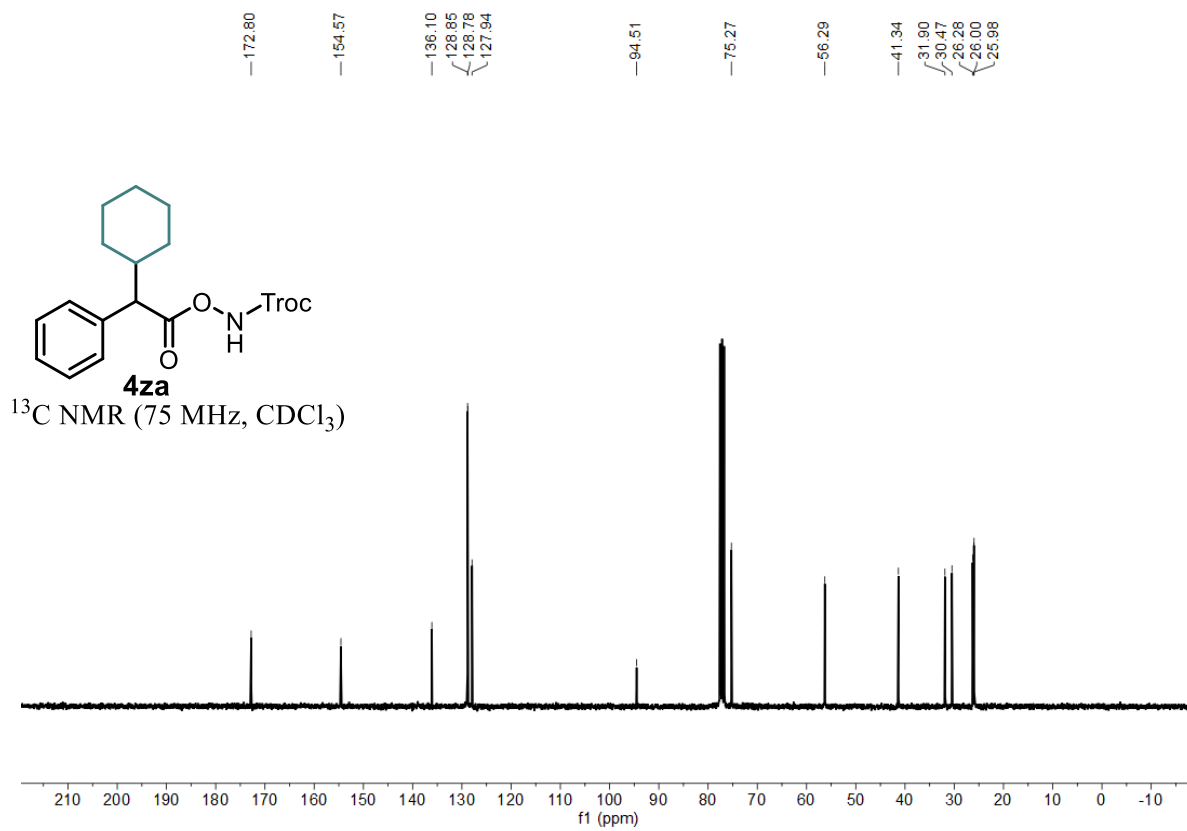
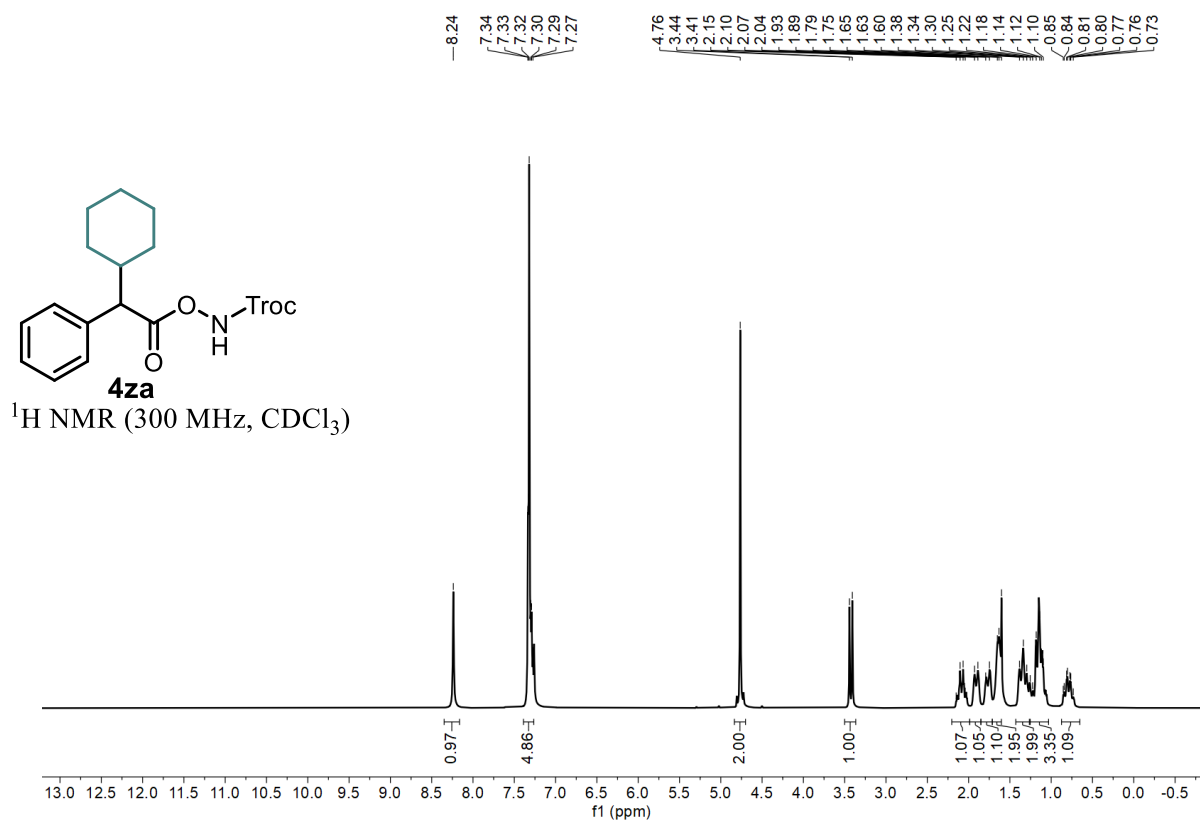
Statement



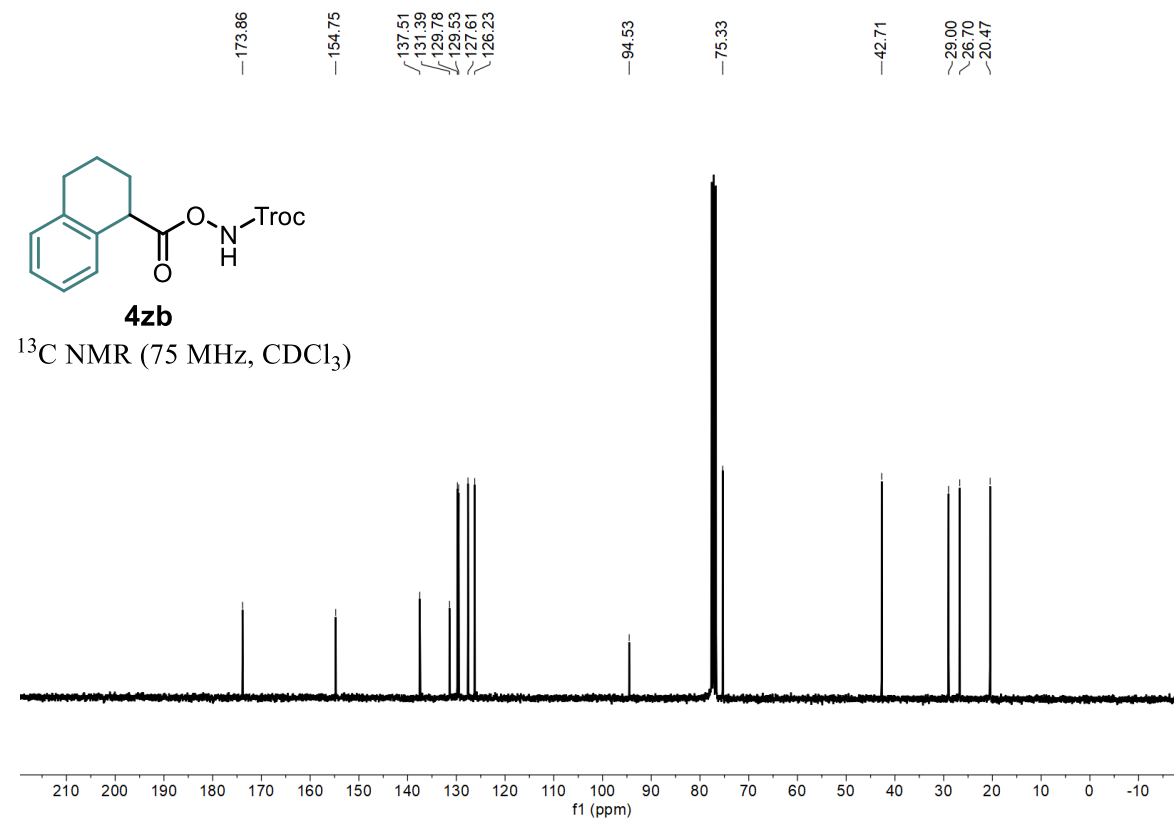
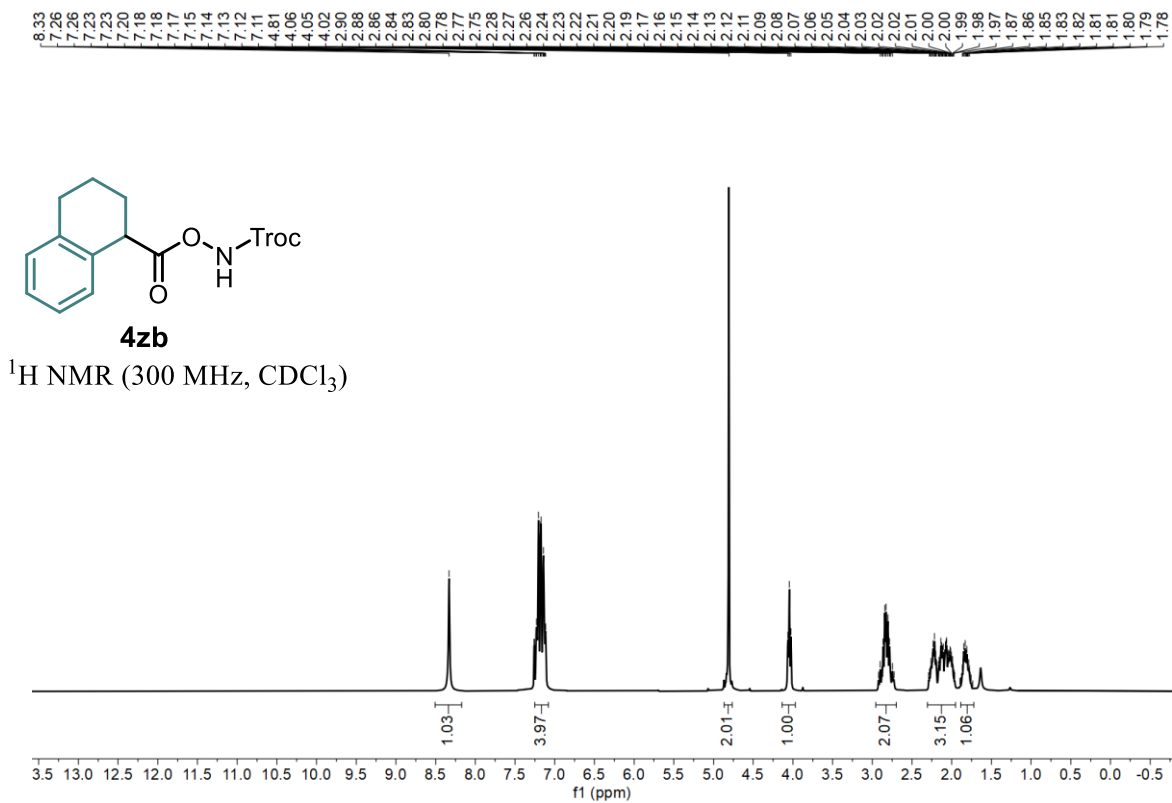
Statement



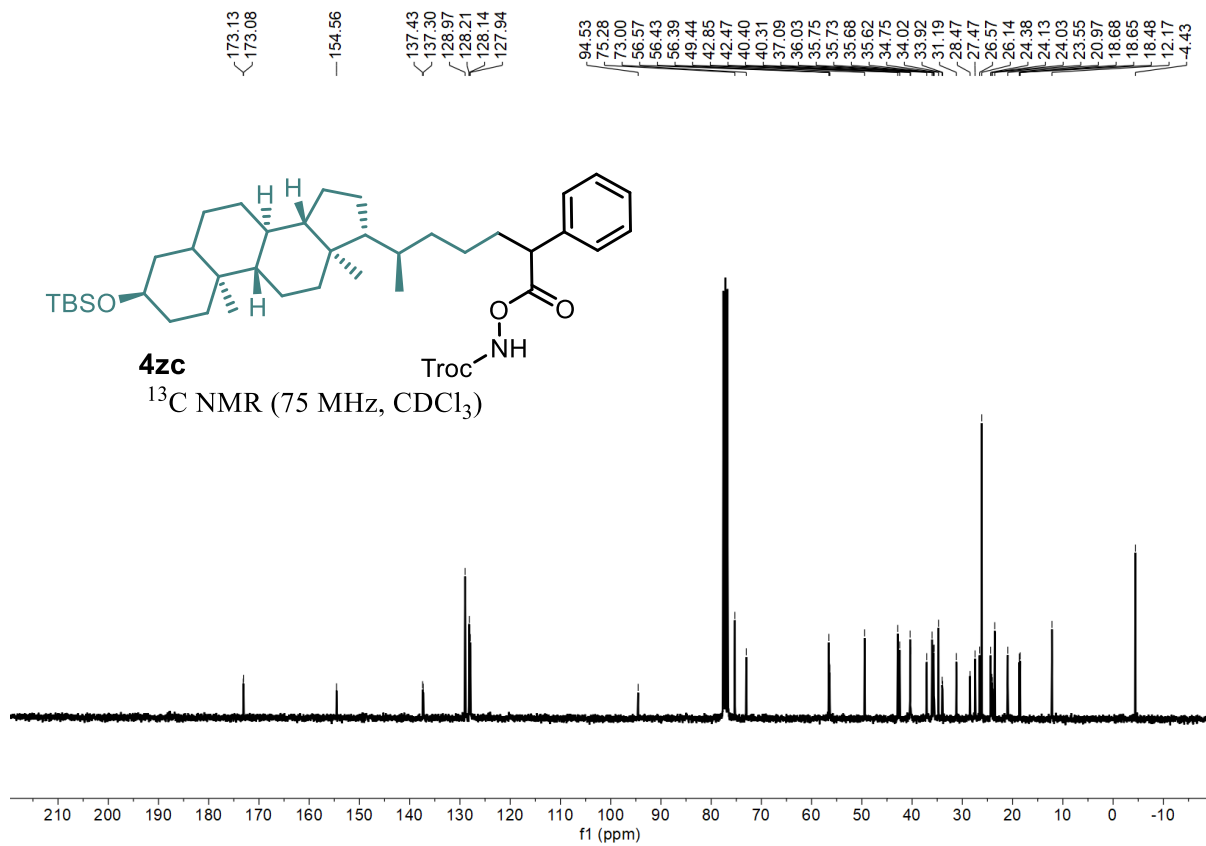
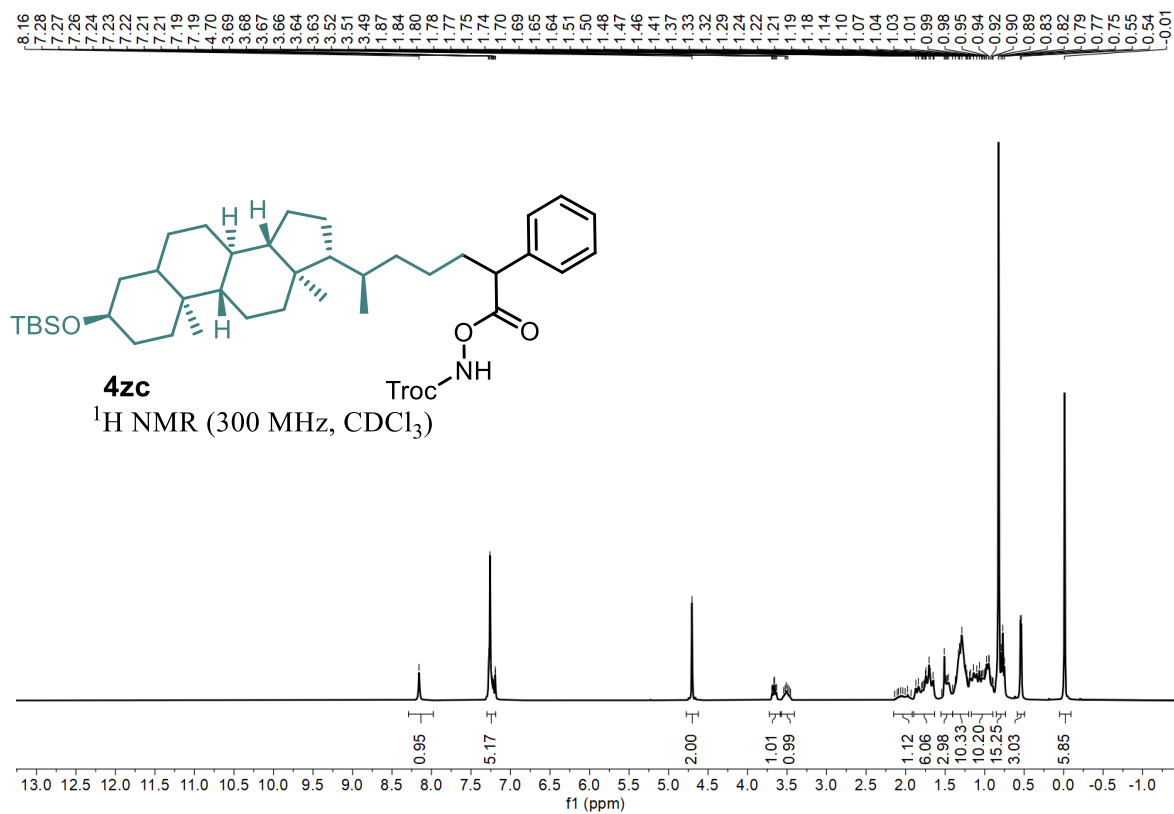
Statement



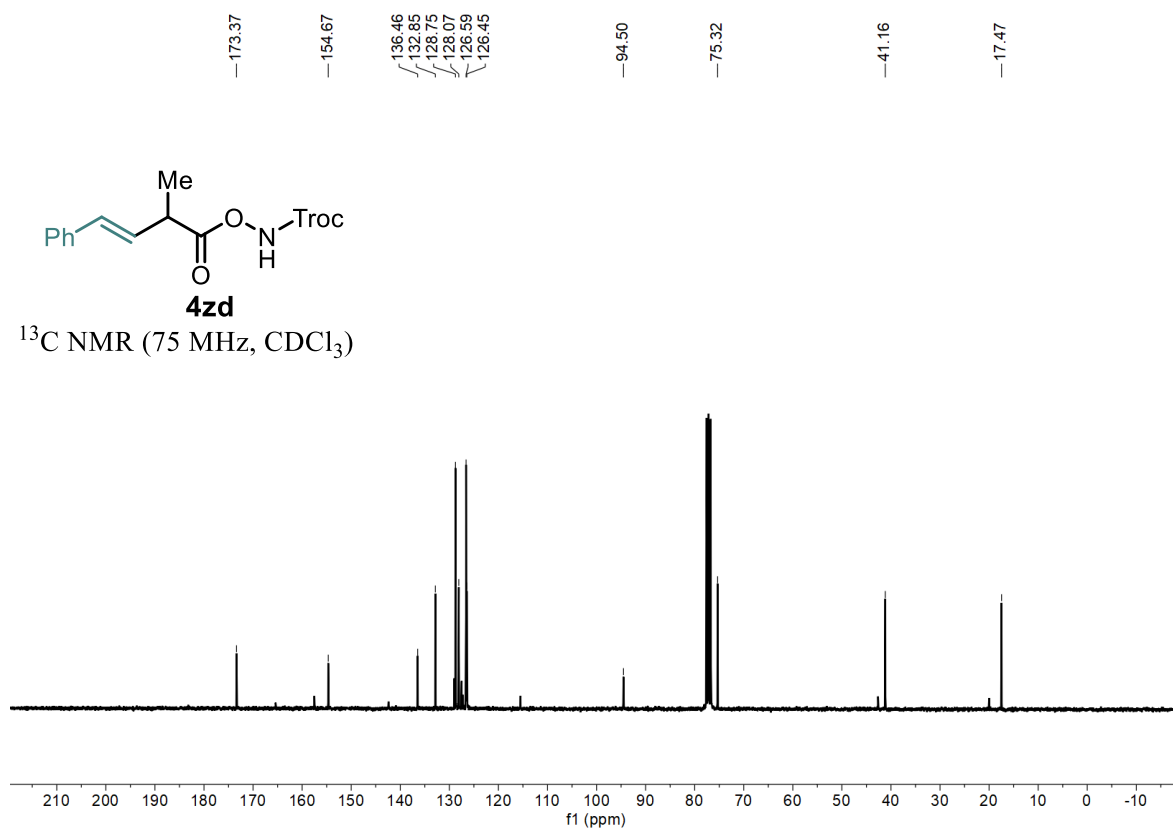
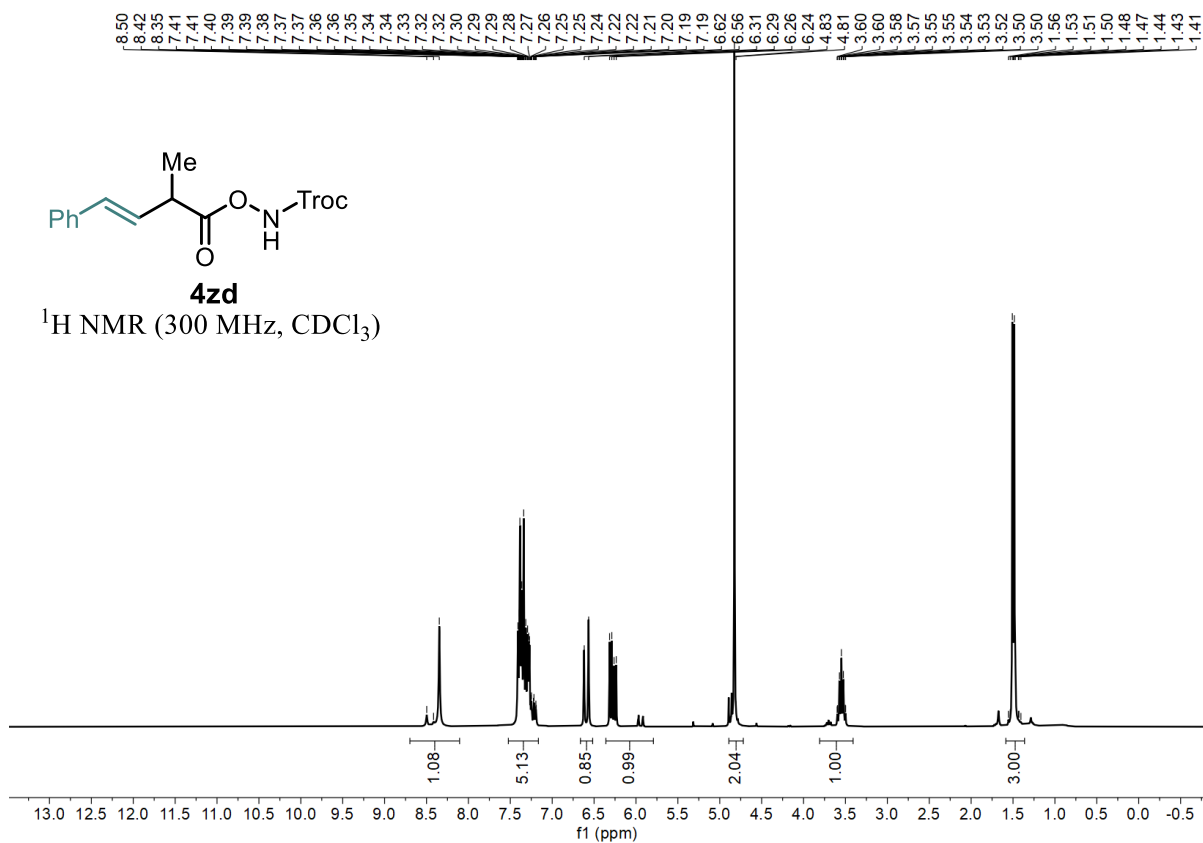
Statement



Statement

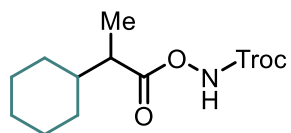


Statement



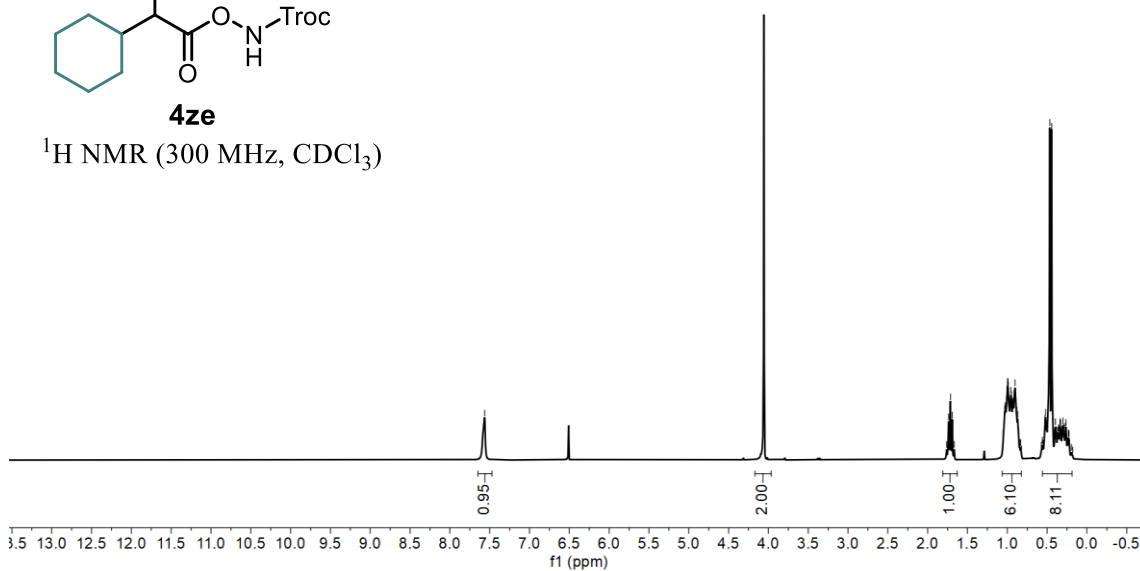
Statement

7.56
4.06
1.76
1.74
1.71
1.69
1.67
1.05
1.04
1.03
1.02
1.01
1.00
1.00
0.99
0.99
0.98
0.96
0.95
0.95
0.93
0.93
0.92
0.91
0.90
0.89
0.88
0.87
0.86
0.84
0.83
0.57
0.56
0.55
0.53
0.53
0.52
0.51
0.50
0.49
0.48
0.47
0.44
0.43
0.43
0.41
0.40
0.39
0.37
0.37
0.36
0.34
0.34
0.33
0.32
0.31
0.30
0.30
0.29
0.27
0.26
0.25
0.24
0.23
0.22
0.19

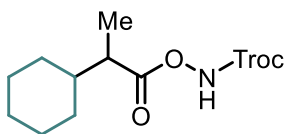


4ze

^1H NMR (300 MHz, CDCl_3)

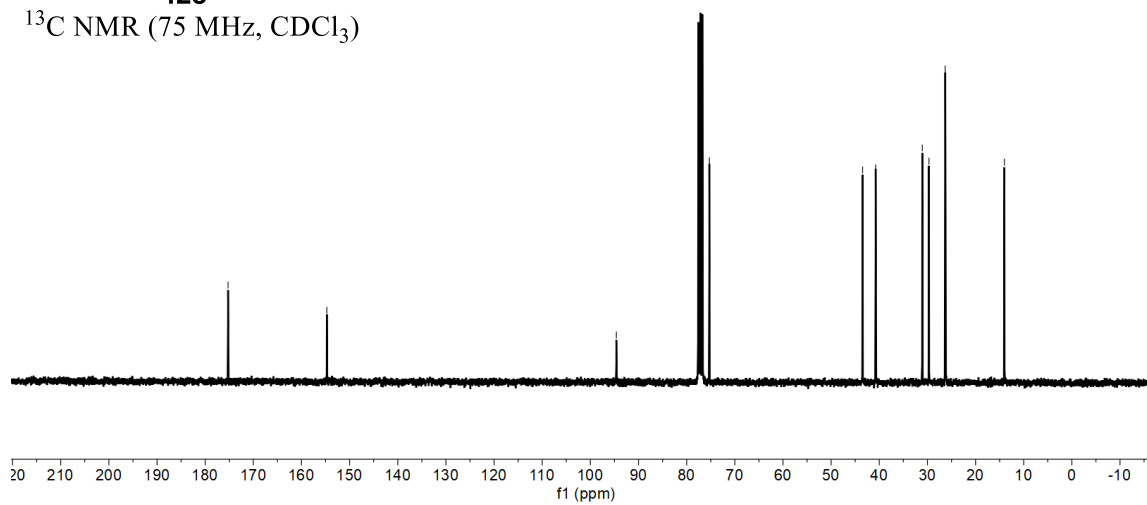


175.25
154.74
94.60
75.29
43.46
40.75
31.06
29.68
26.31
14.01

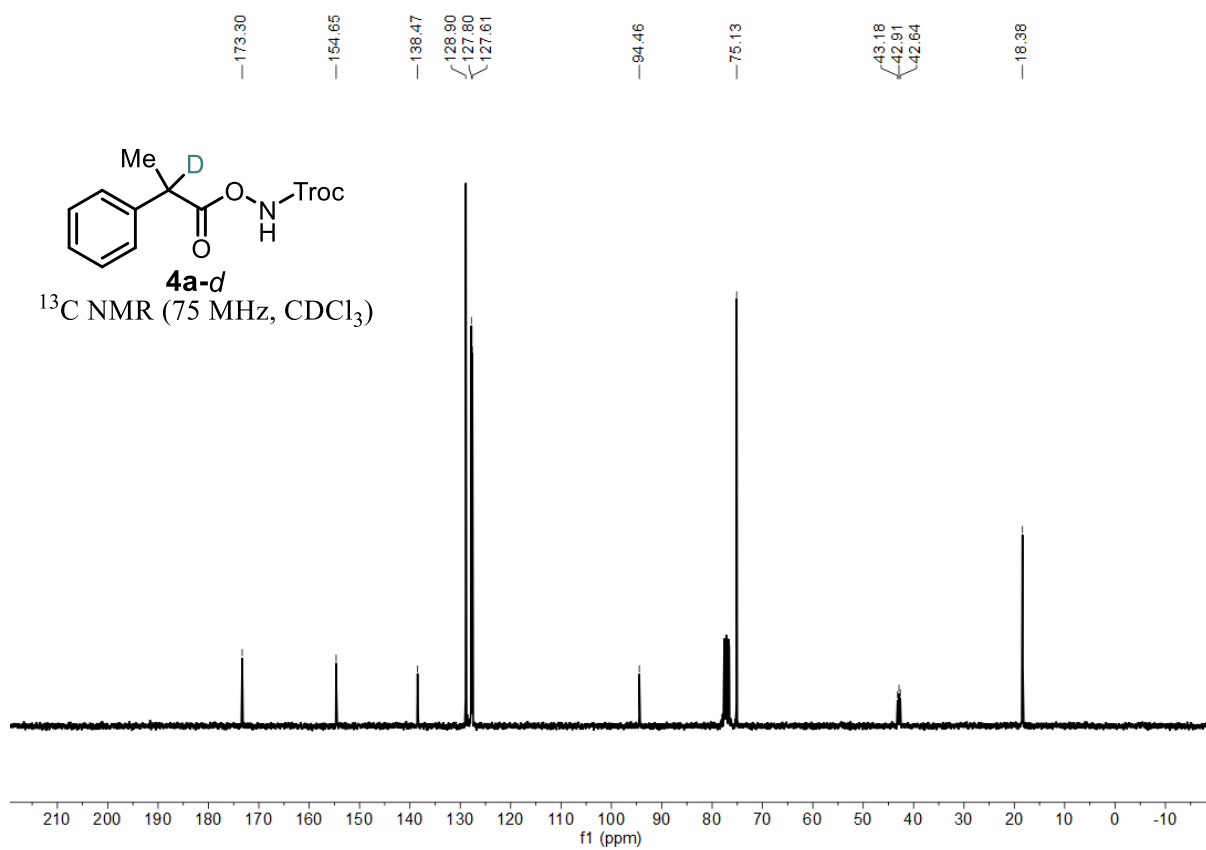
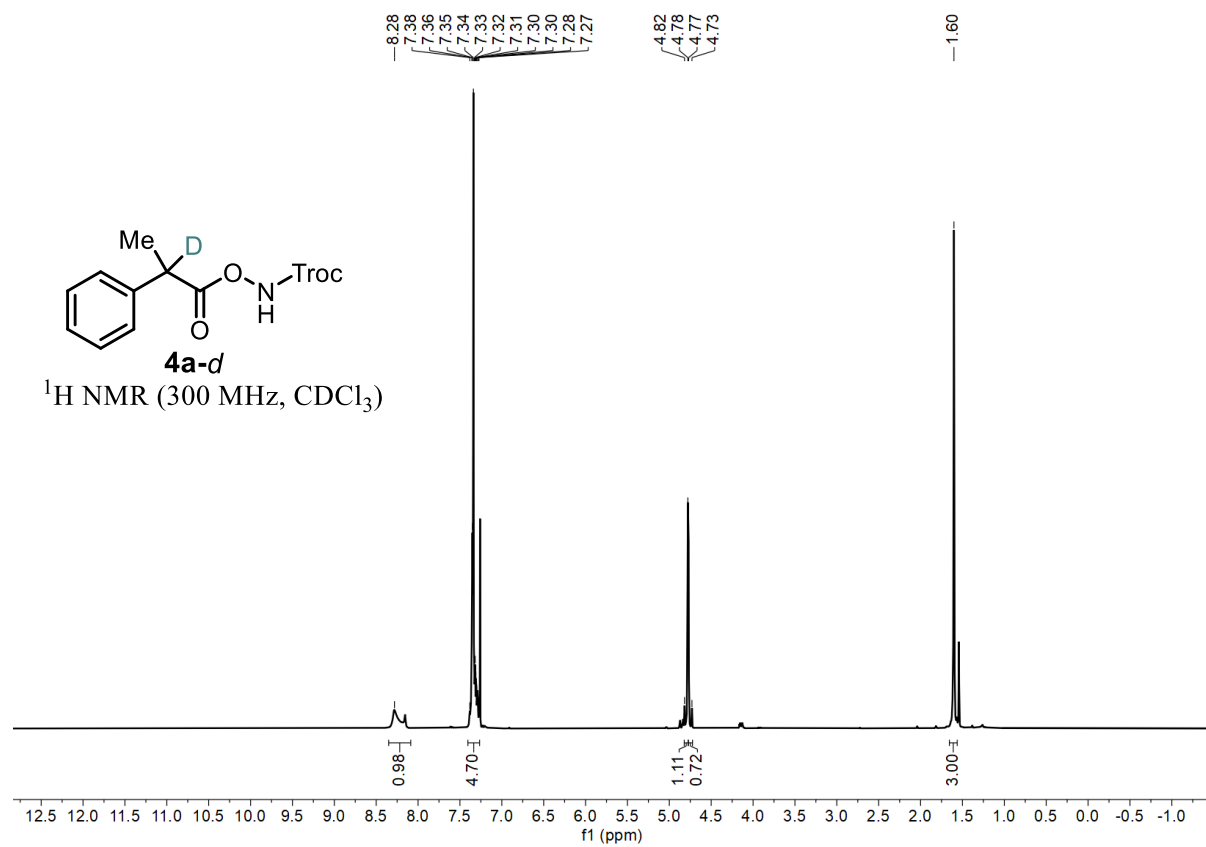


4ze

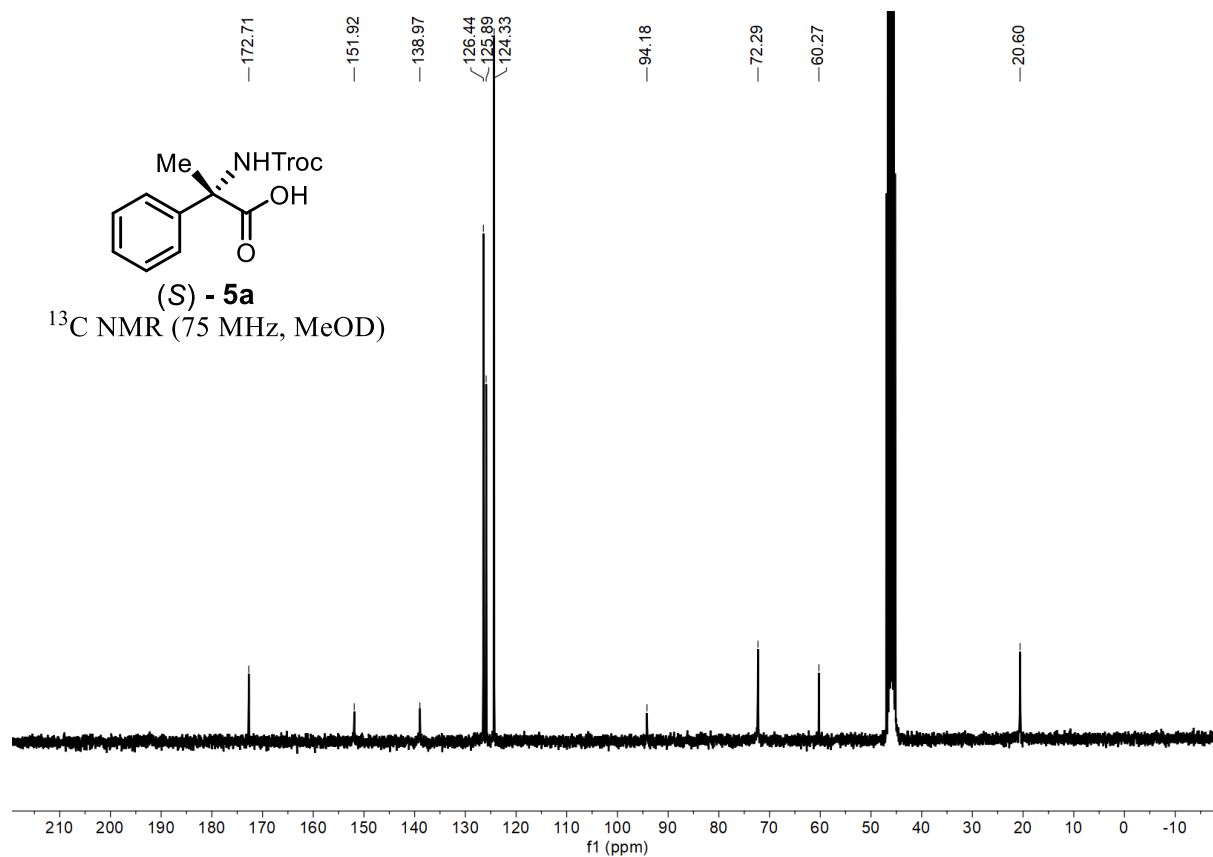
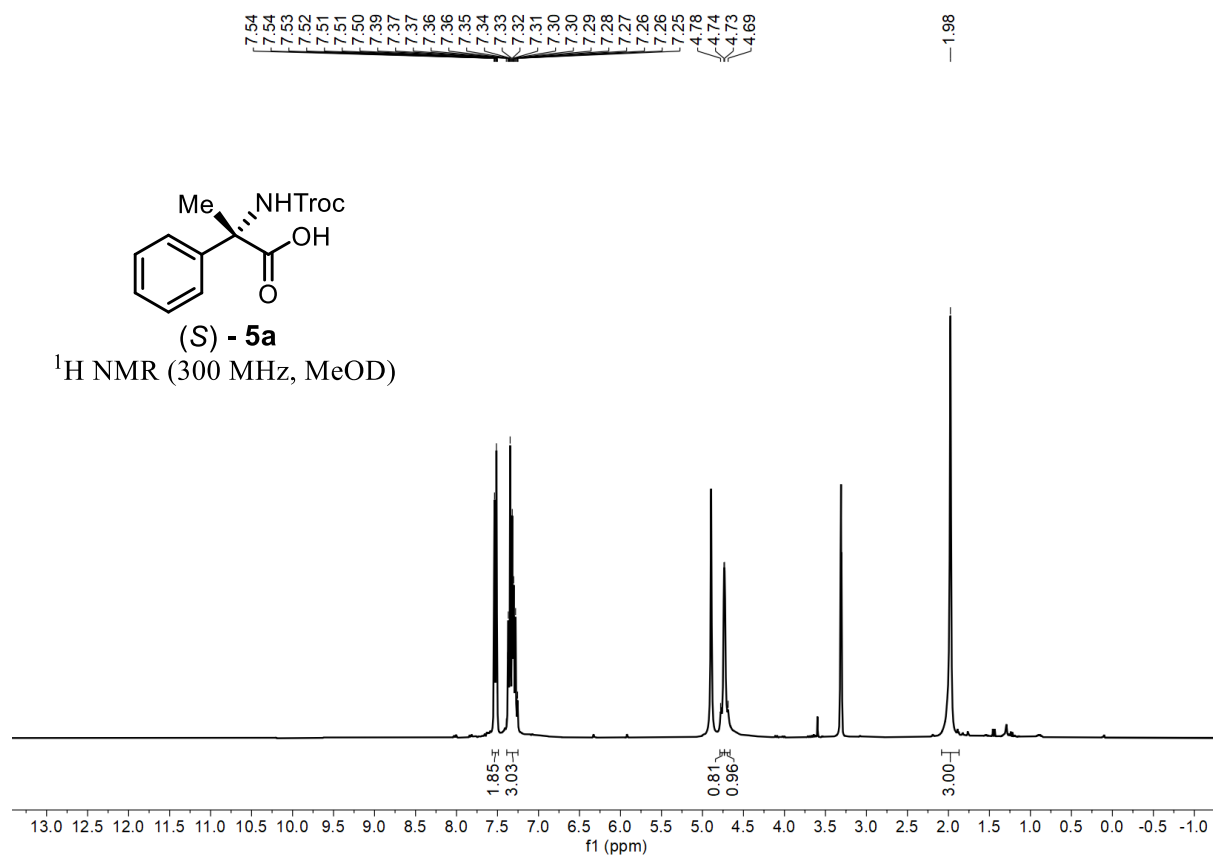
^{13}C NMR (75 MHz, CDCl_3)



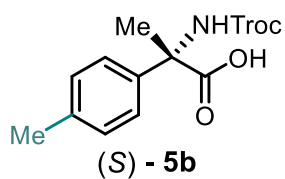
Statement



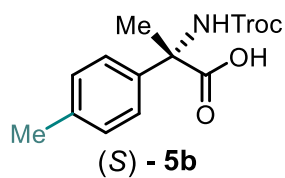
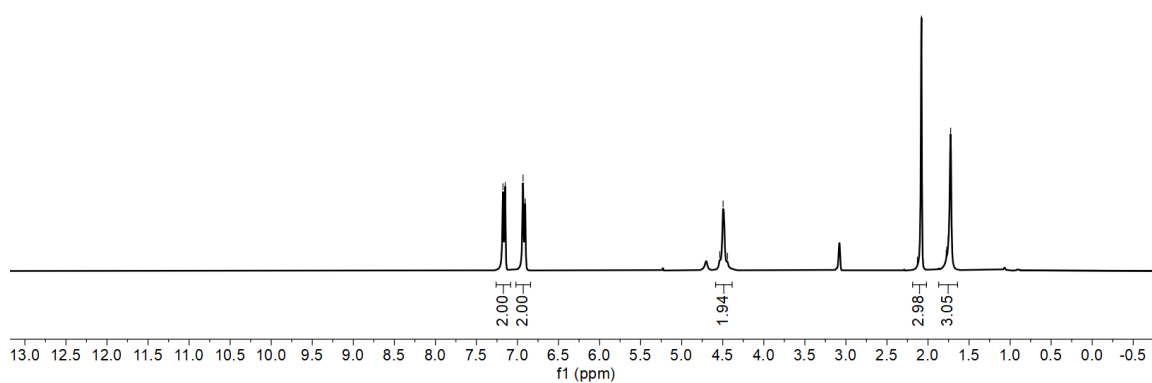
Statement



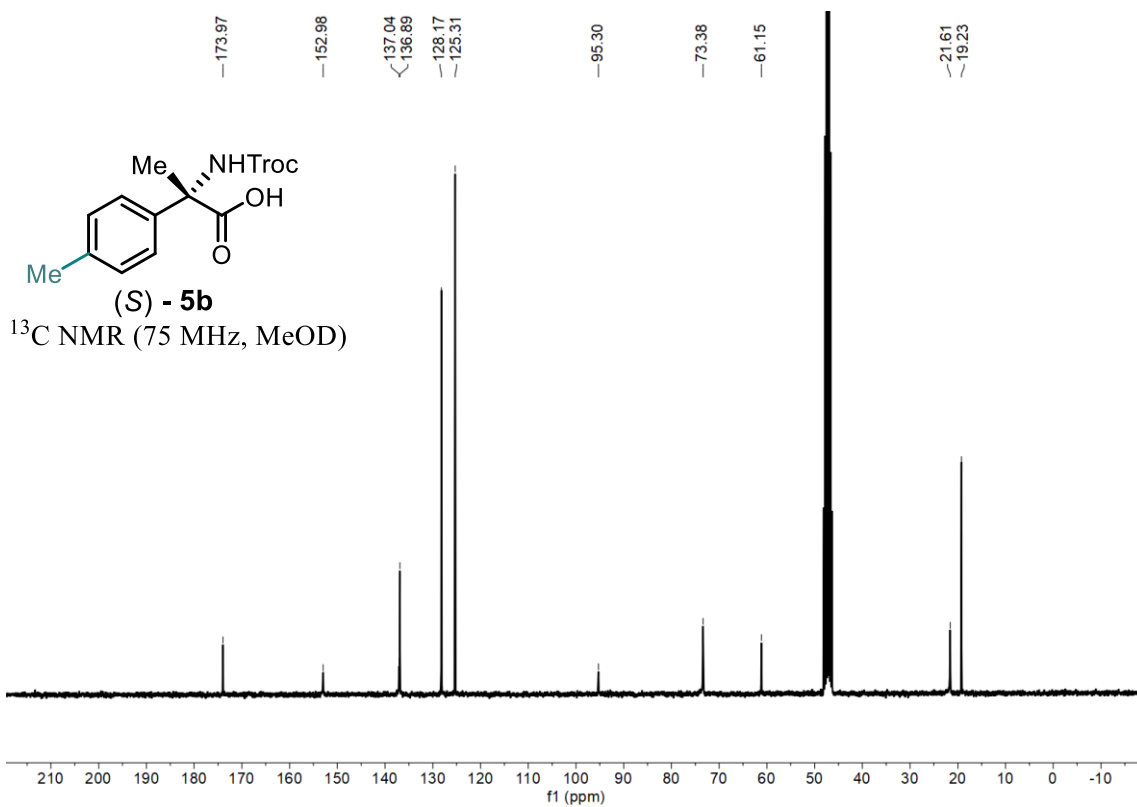
Statement



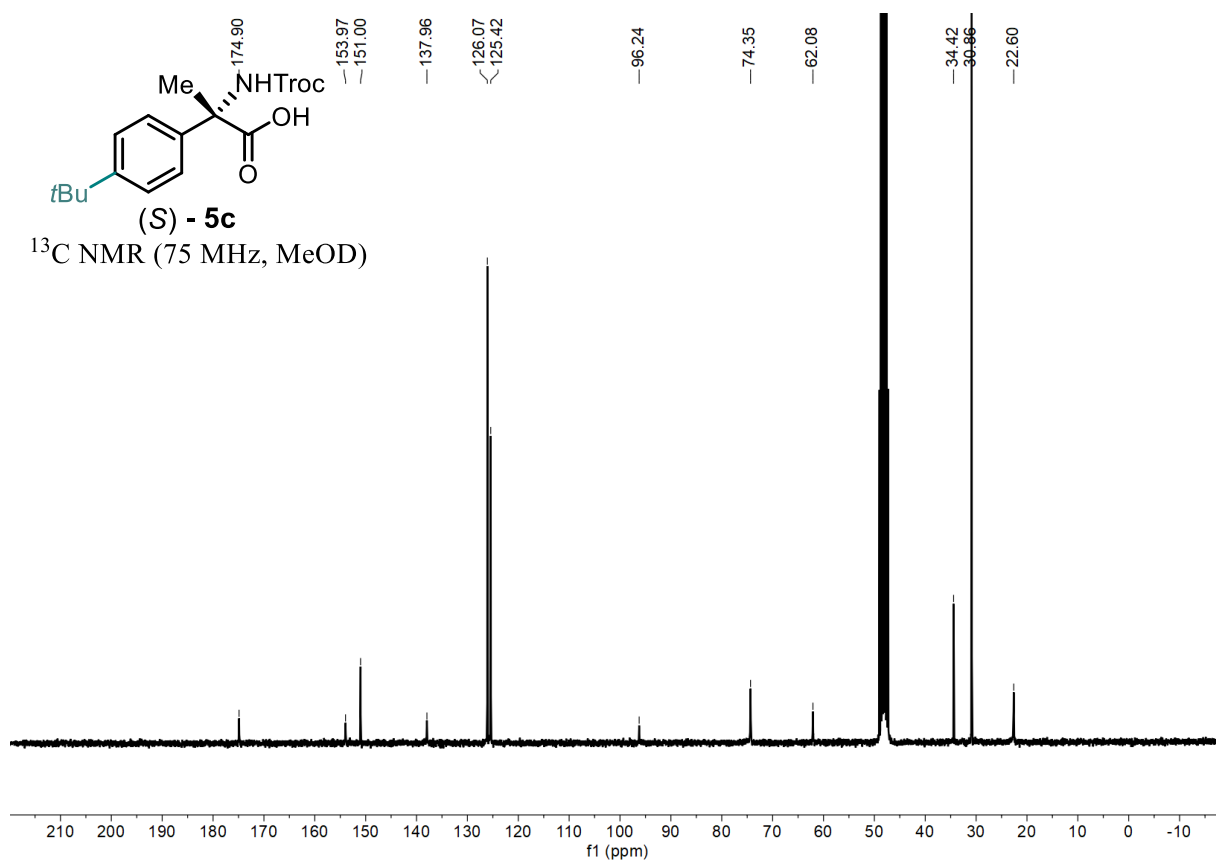
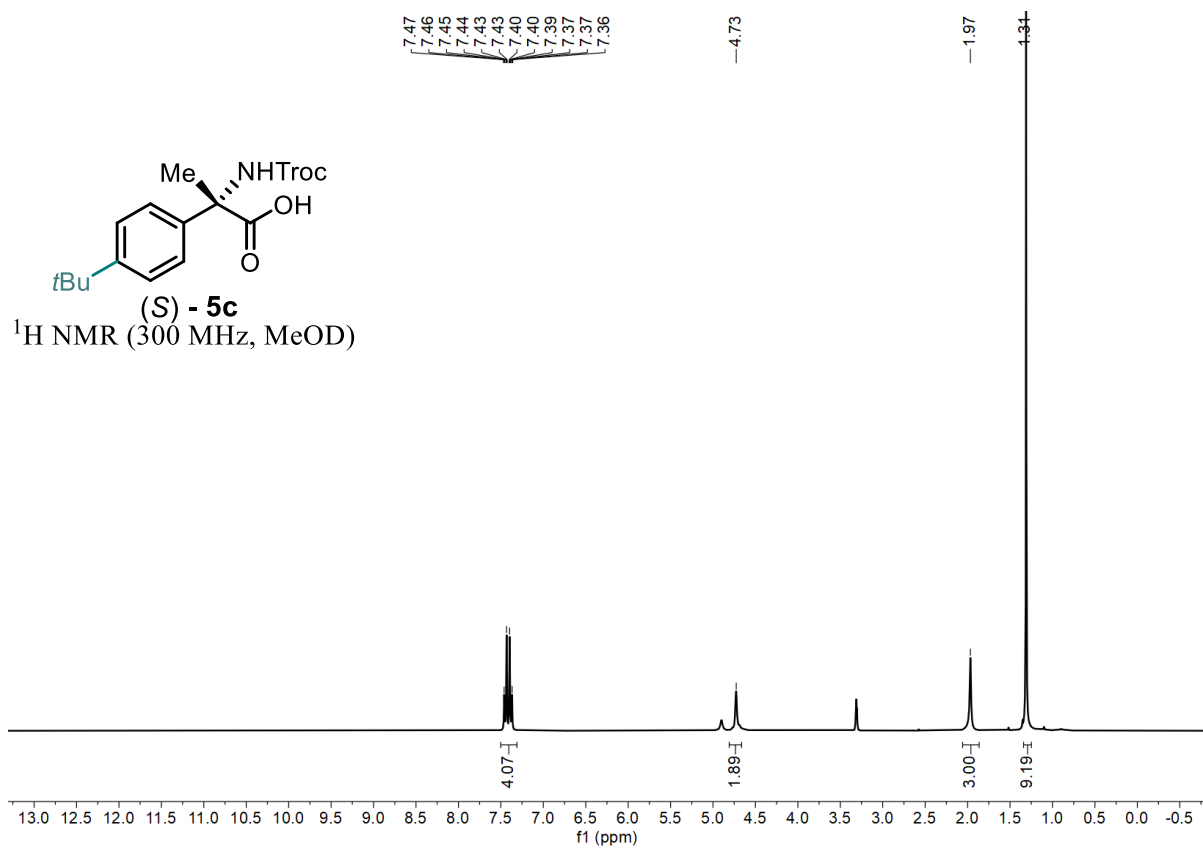
¹H NMR (300 MHz, MeOD)



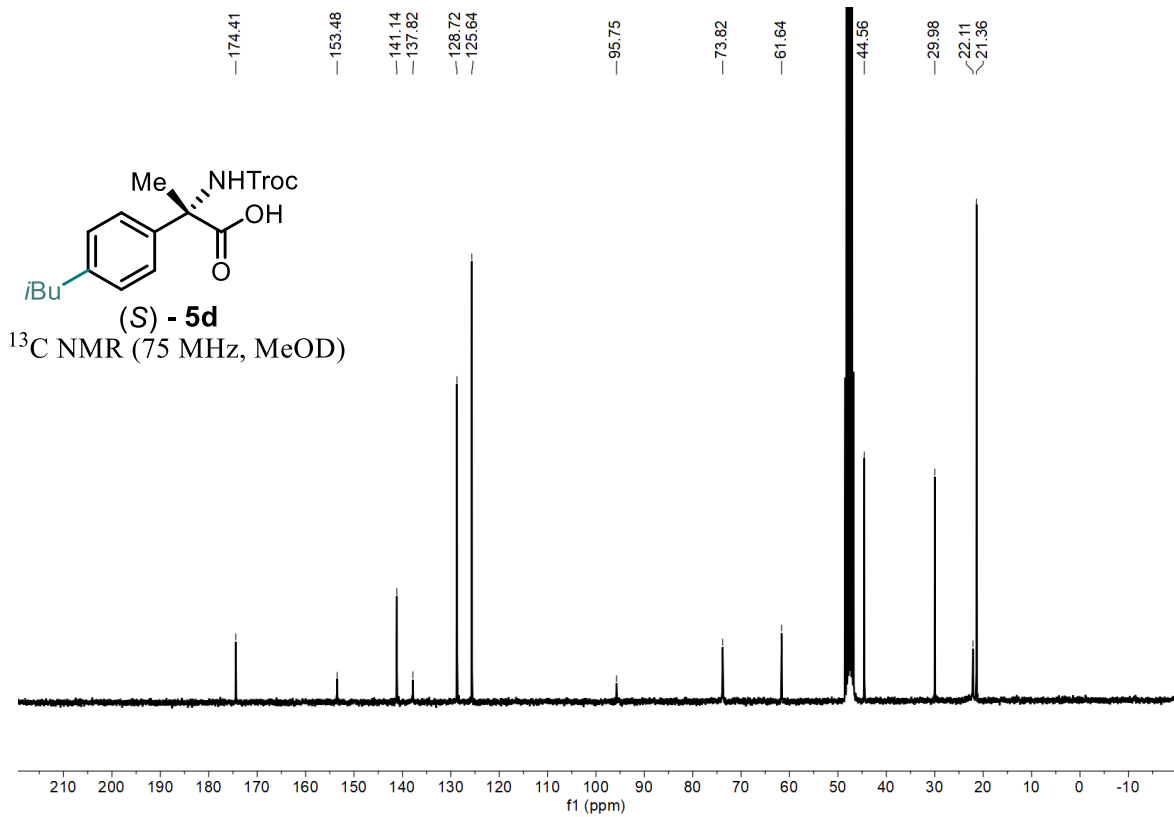
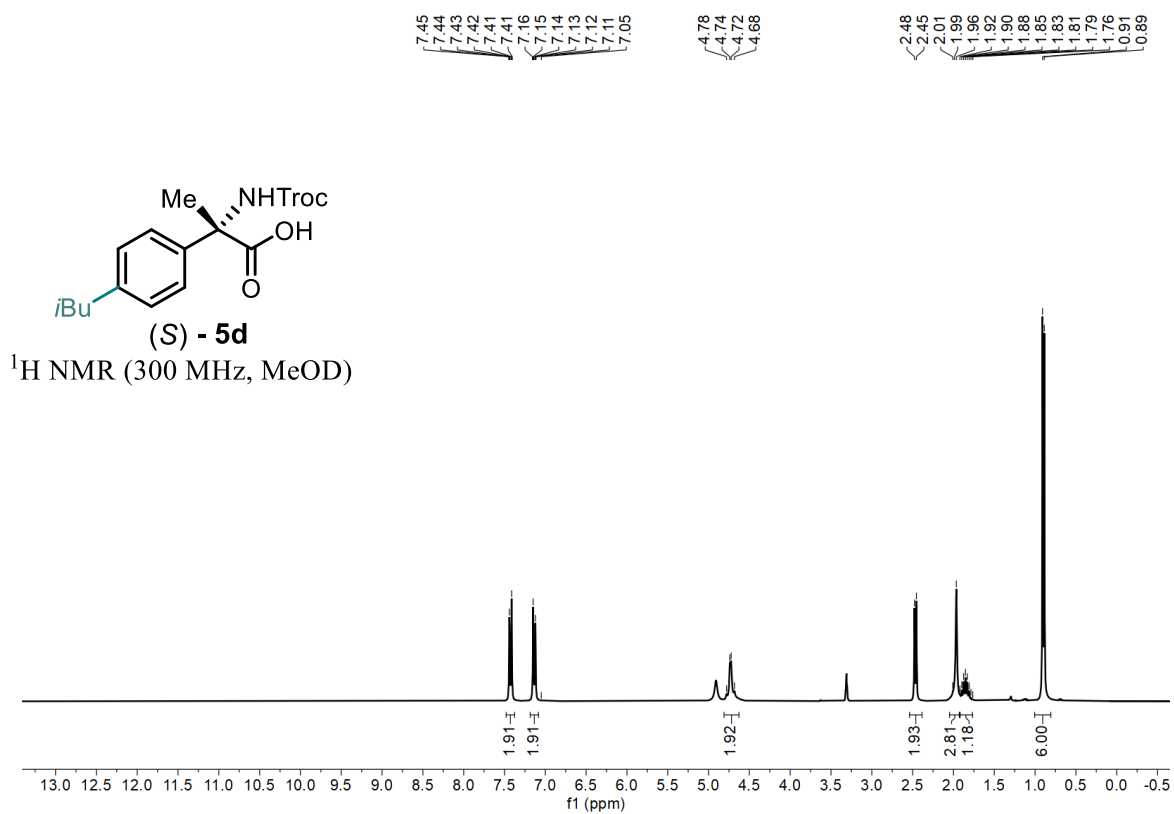
¹³C NMR (75 MHz, MeOD)



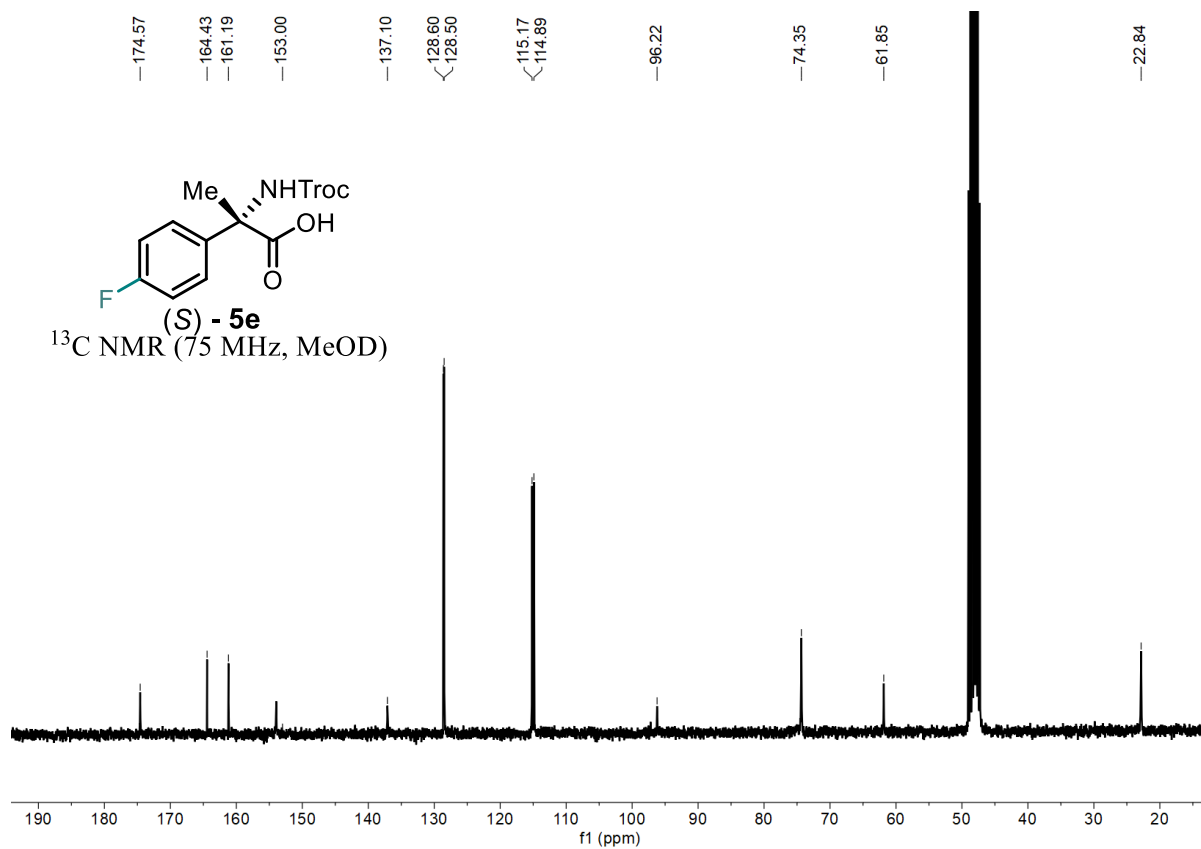
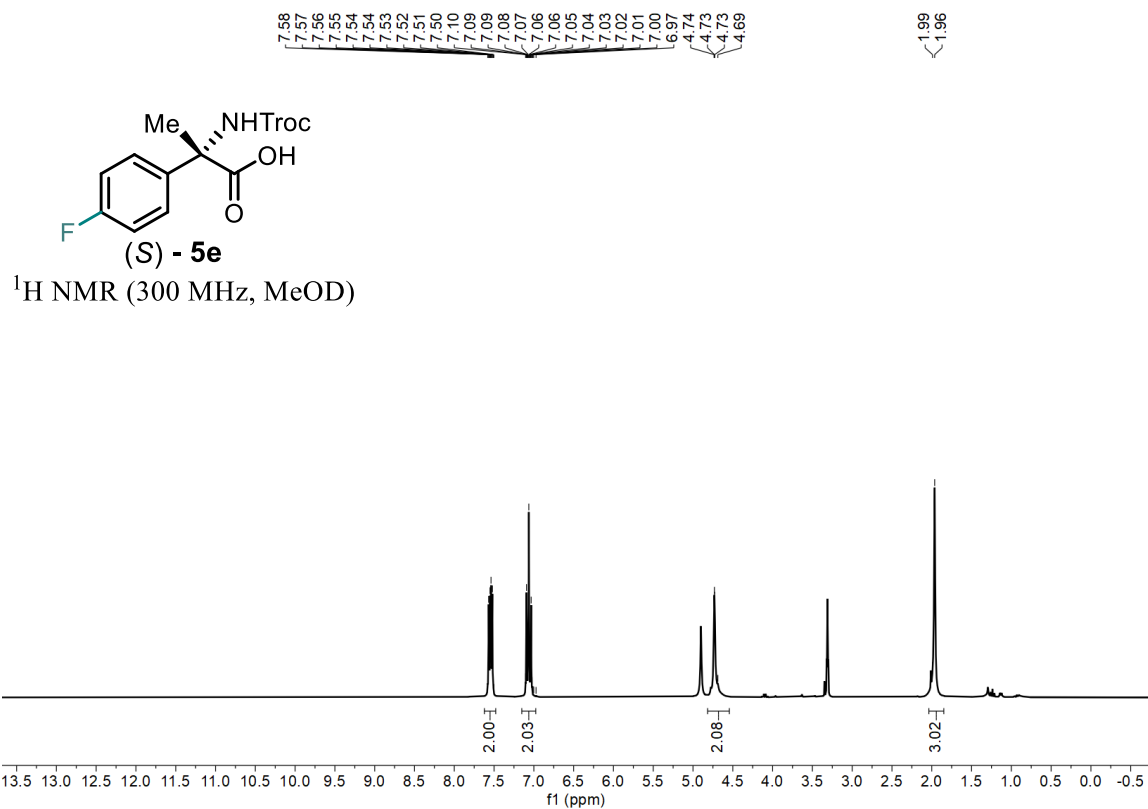
Statement



Statement

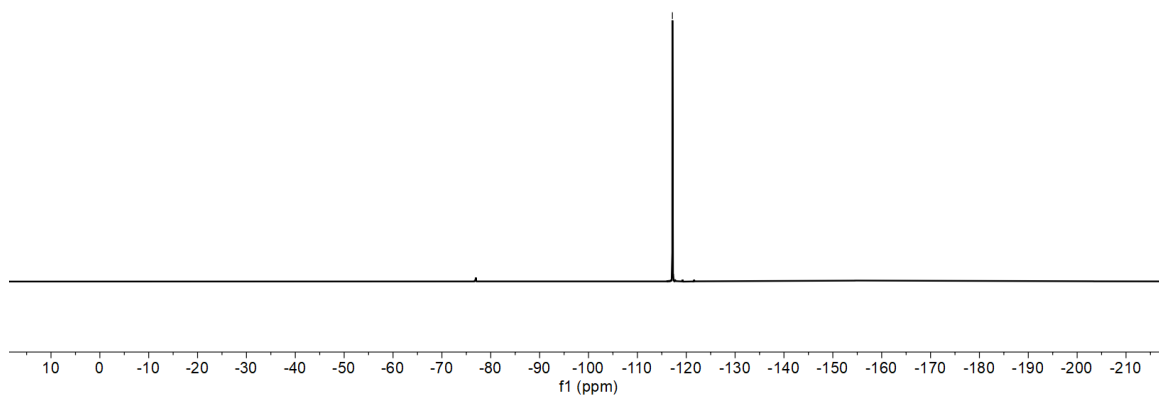
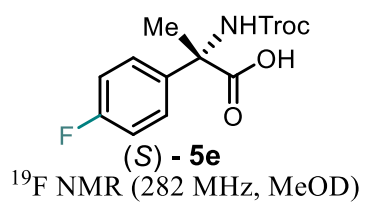


Statement

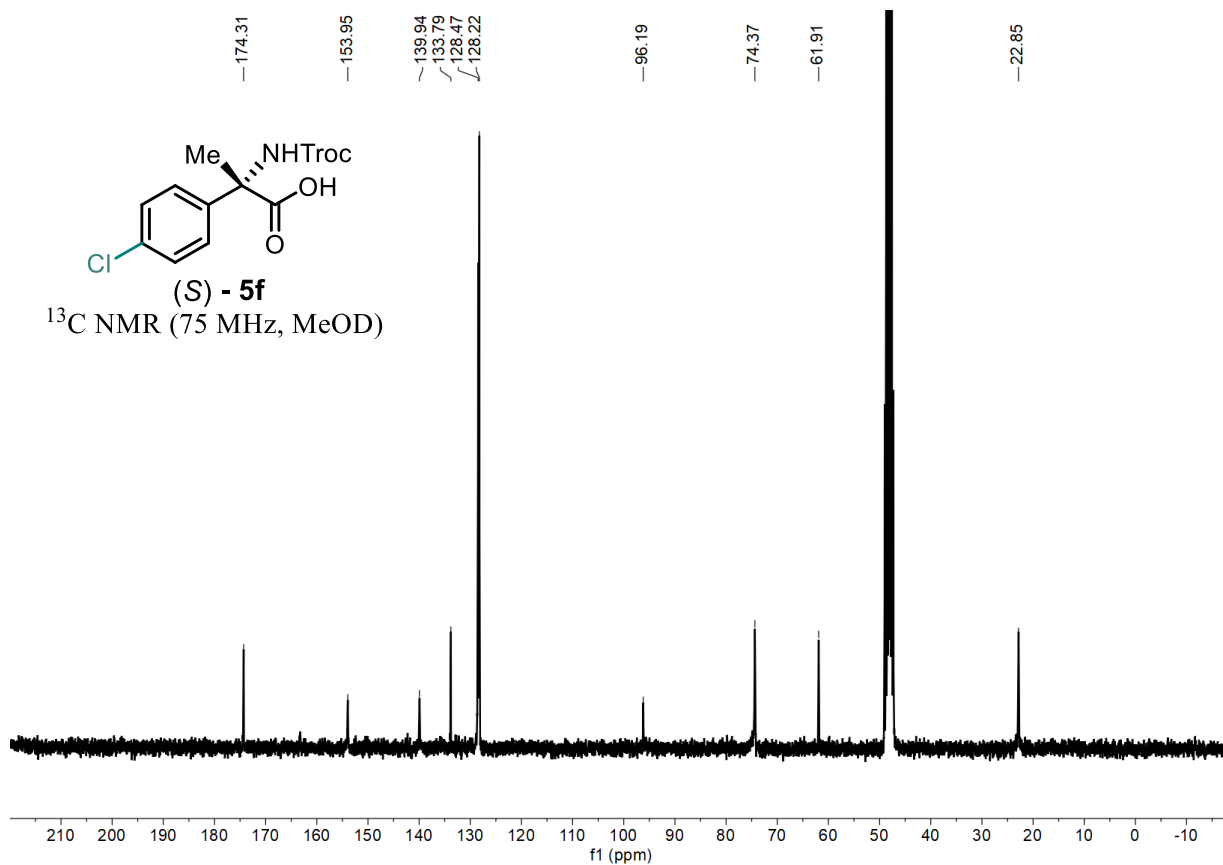
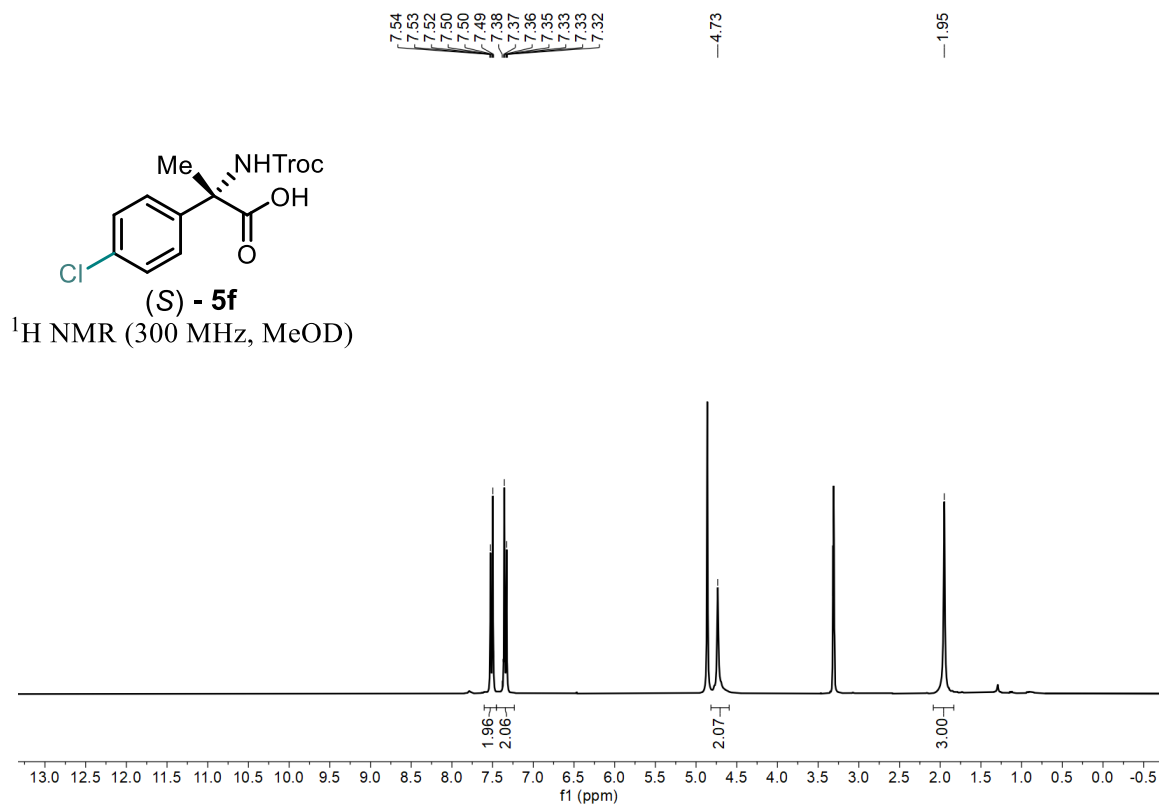


Statement

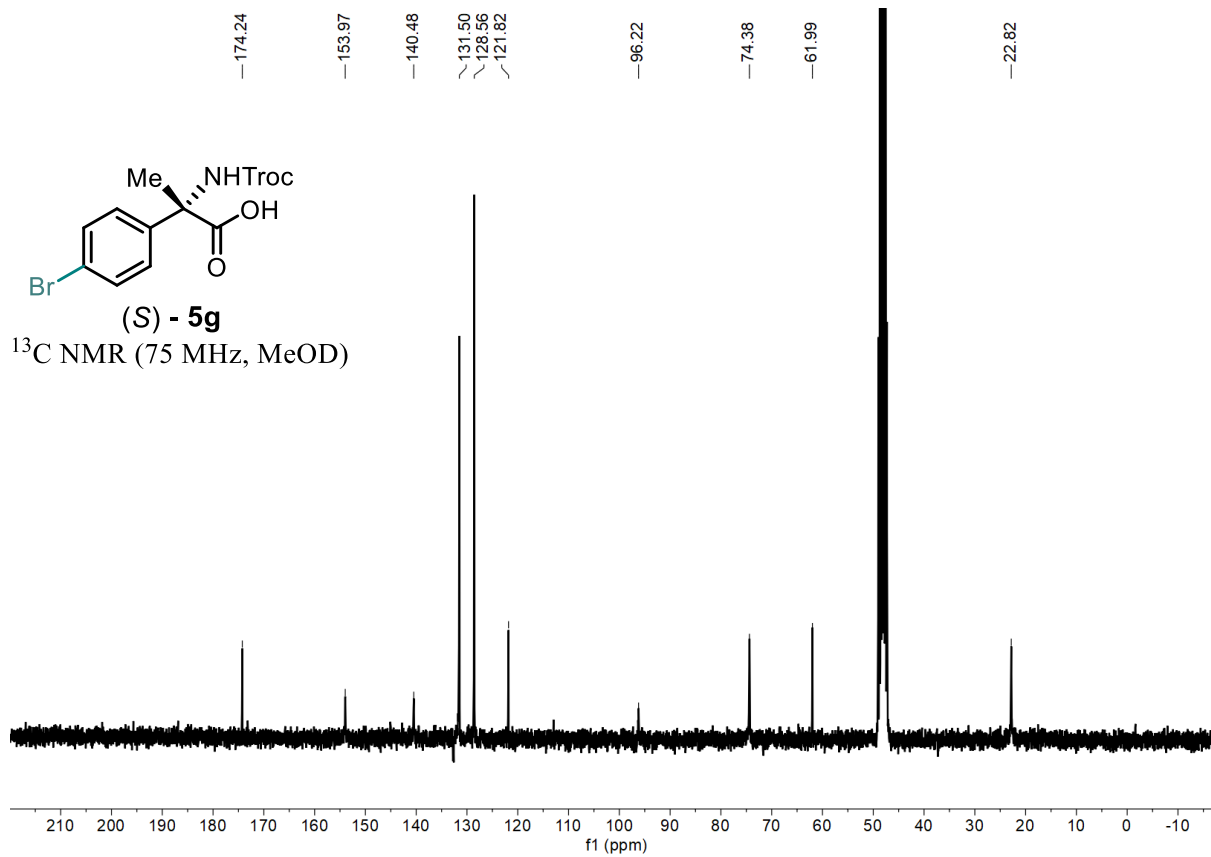
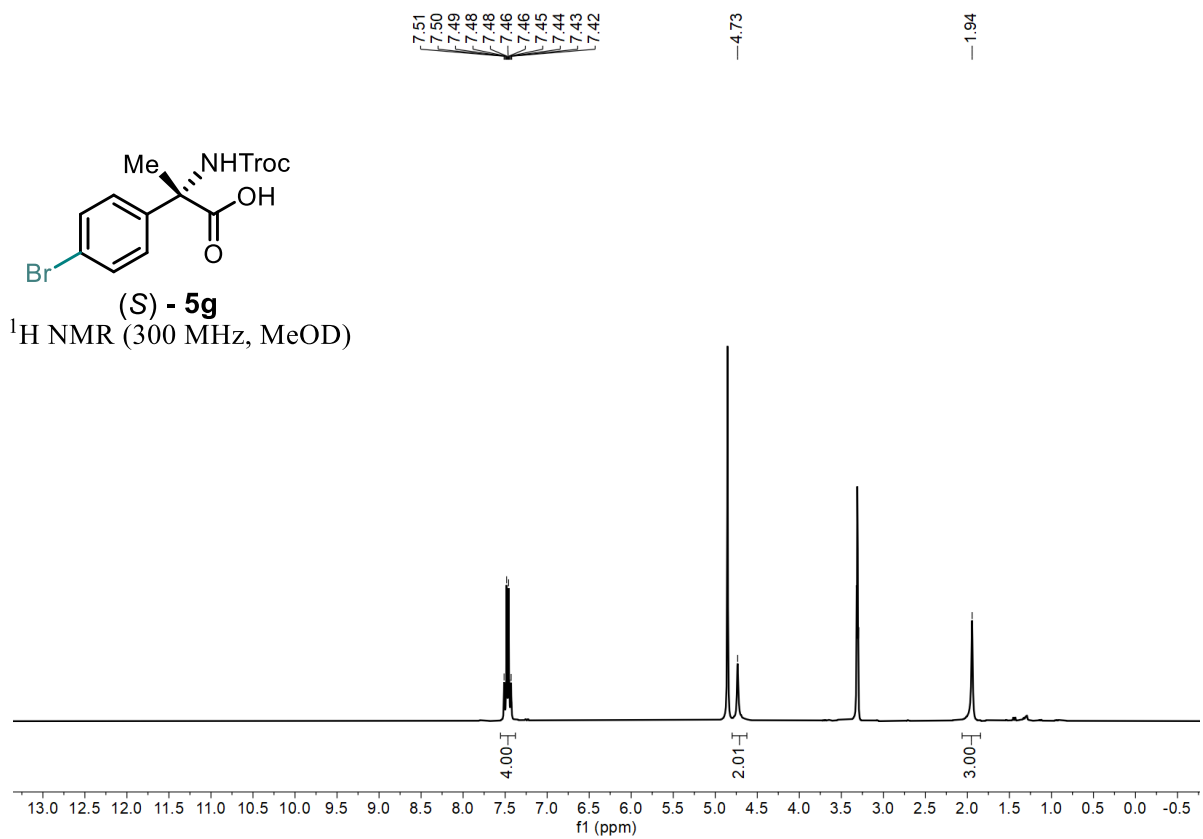
--117.17



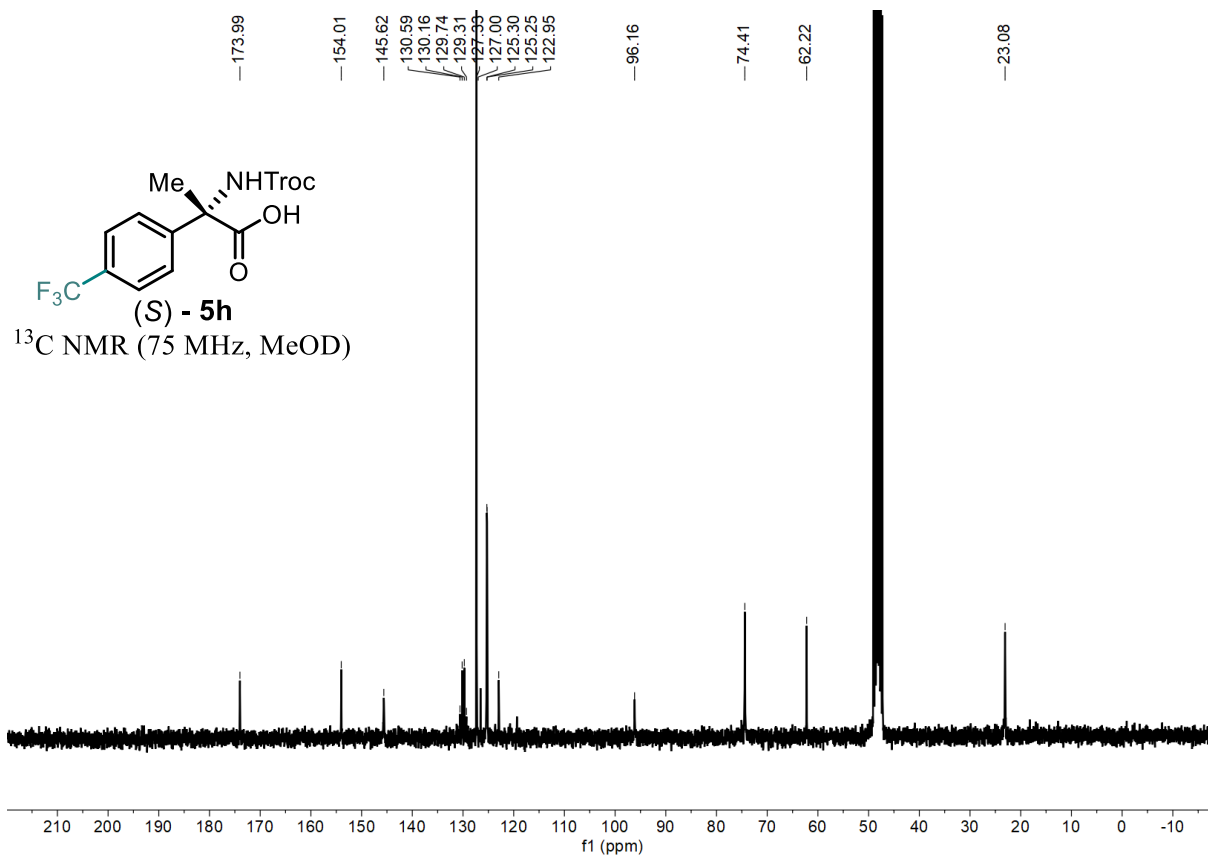
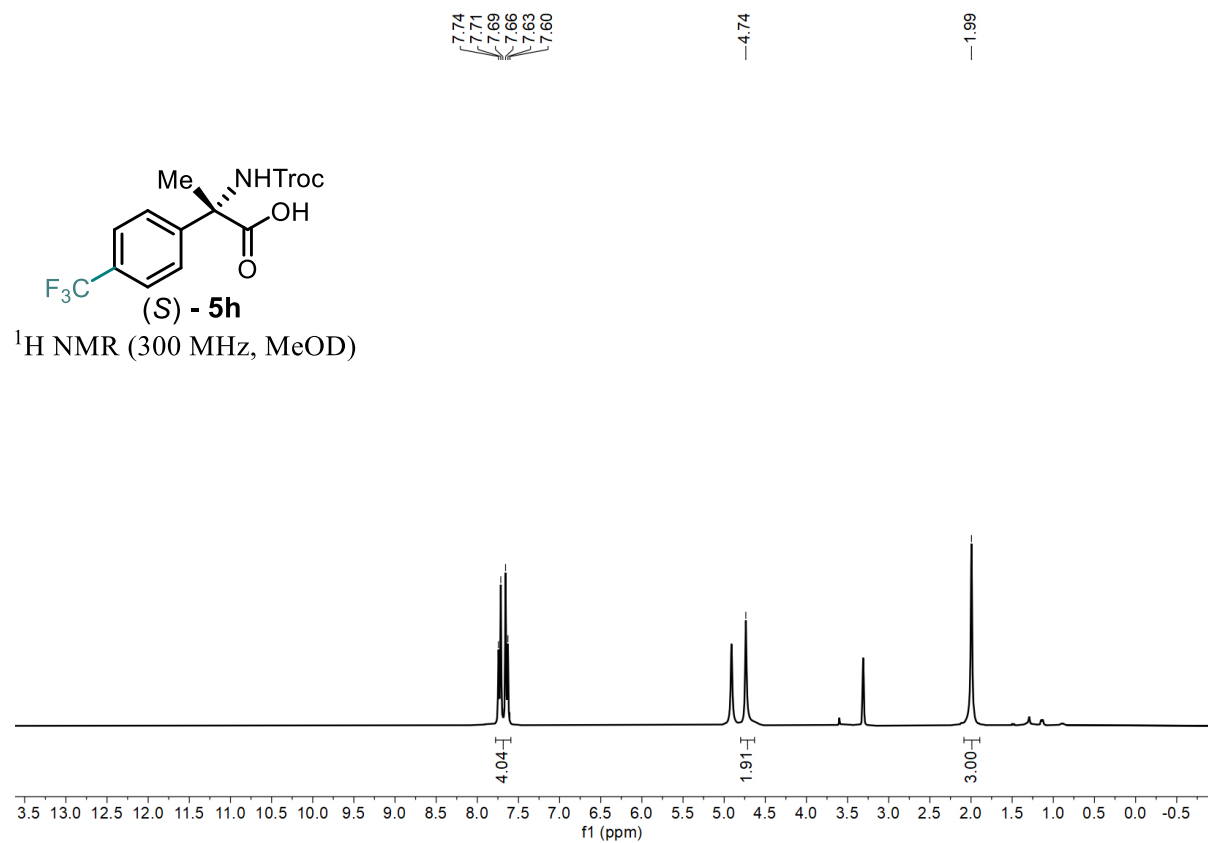
Statement



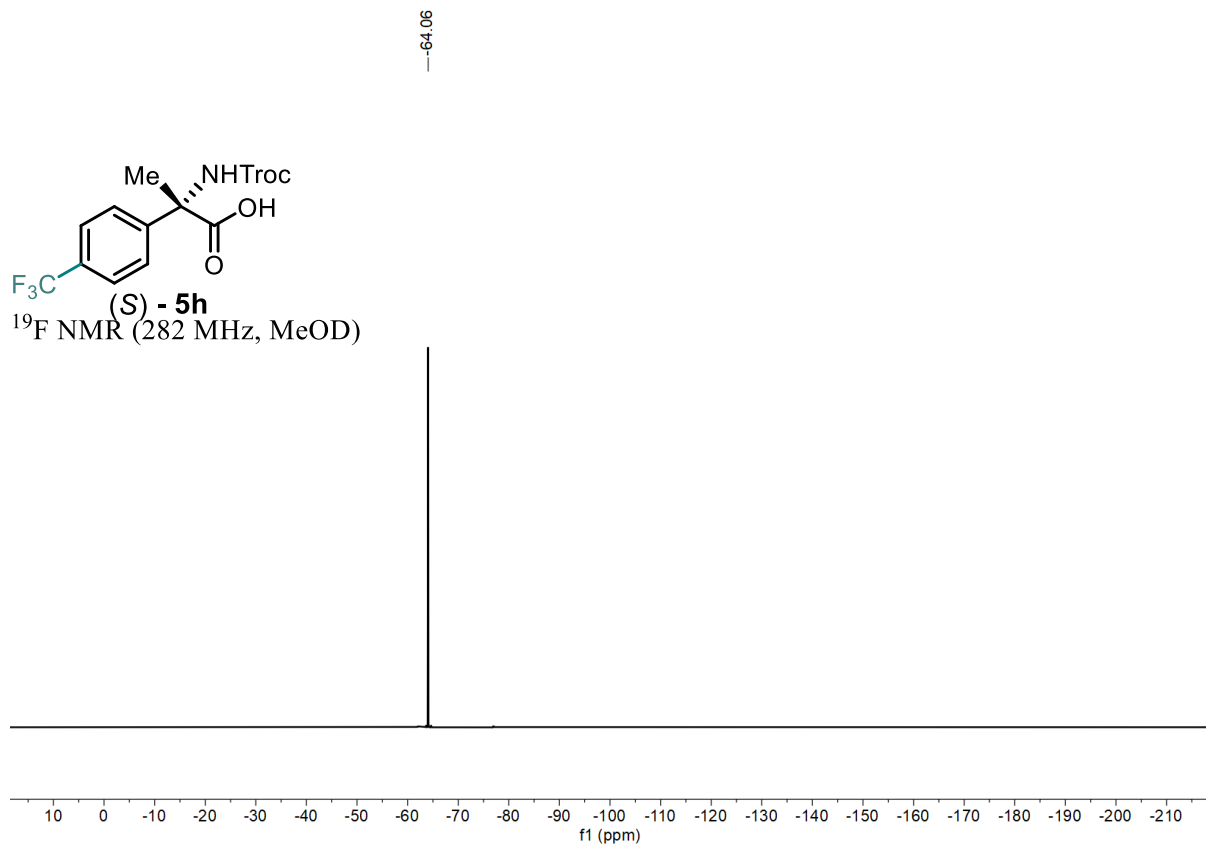
Statement



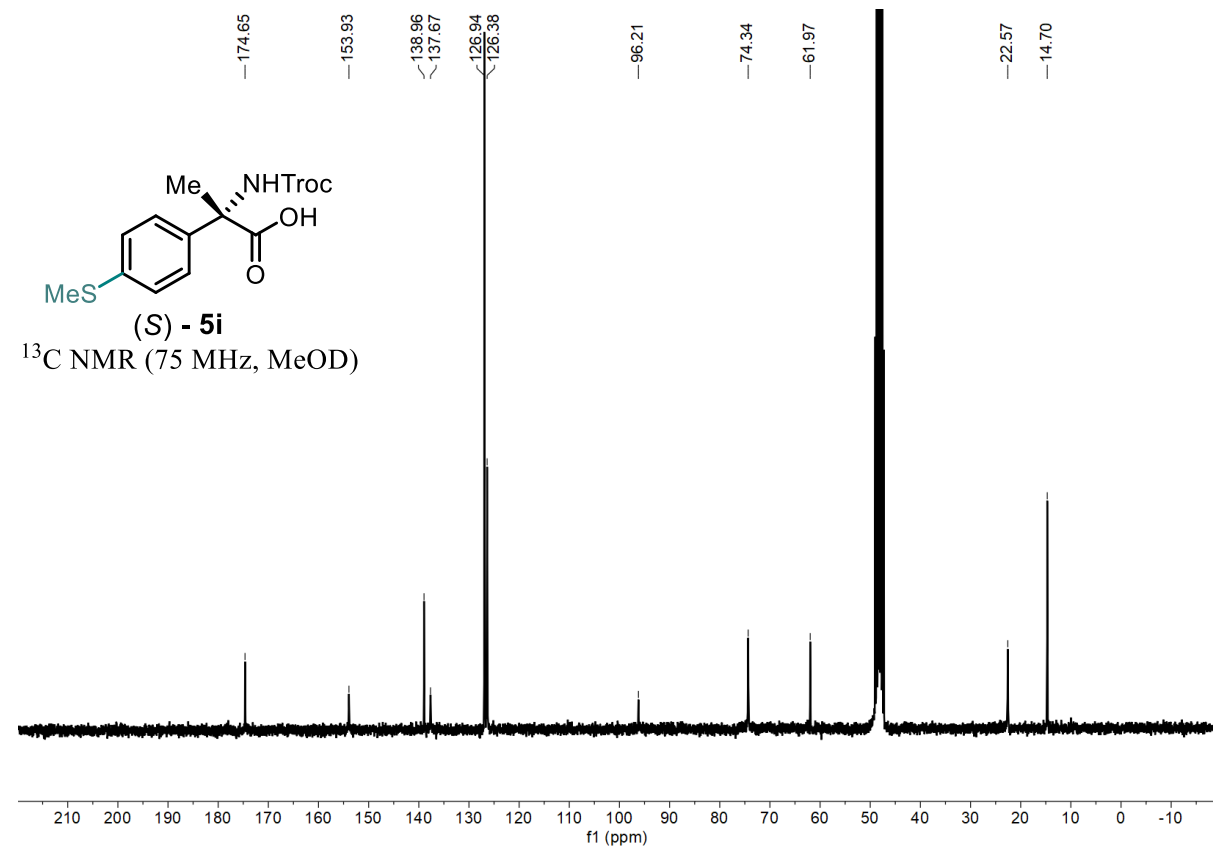
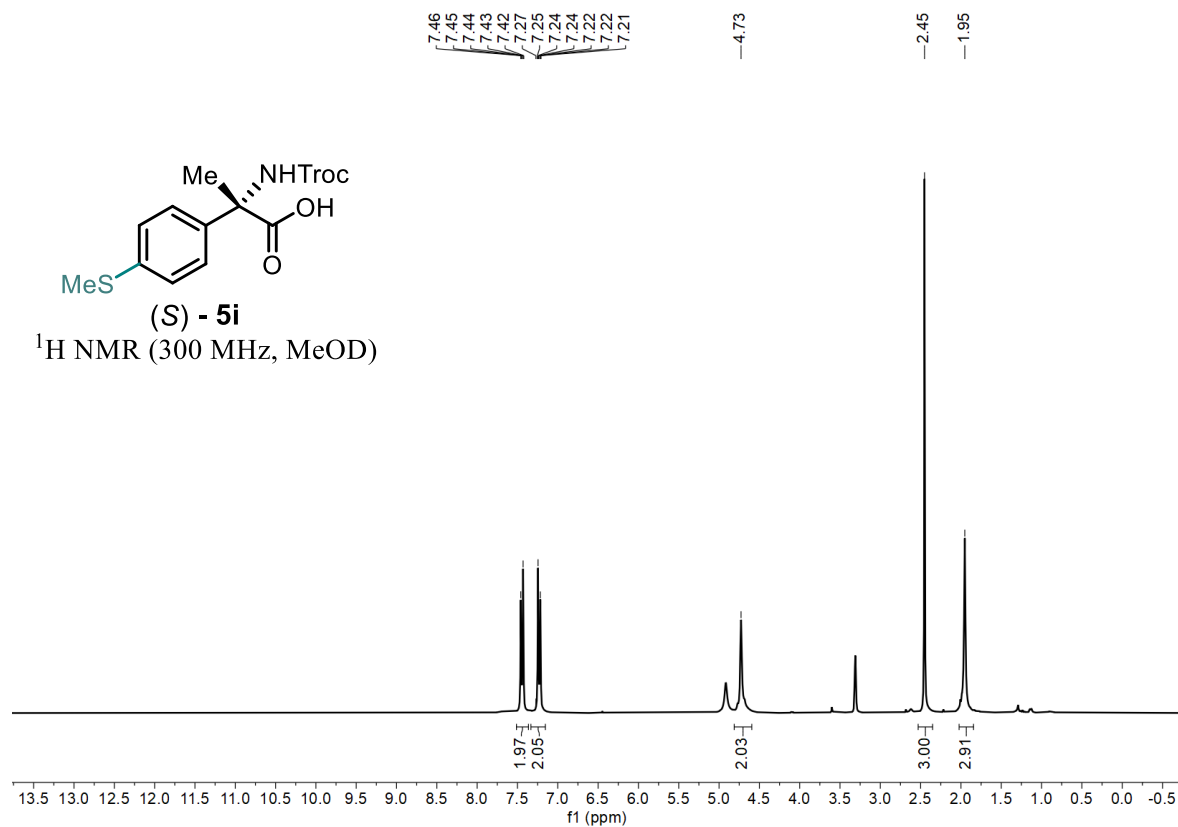
Statement



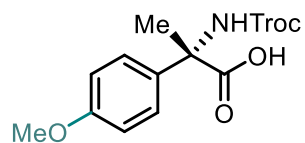
Statement



Statement

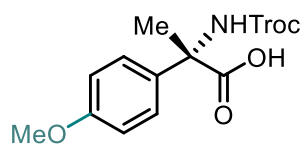
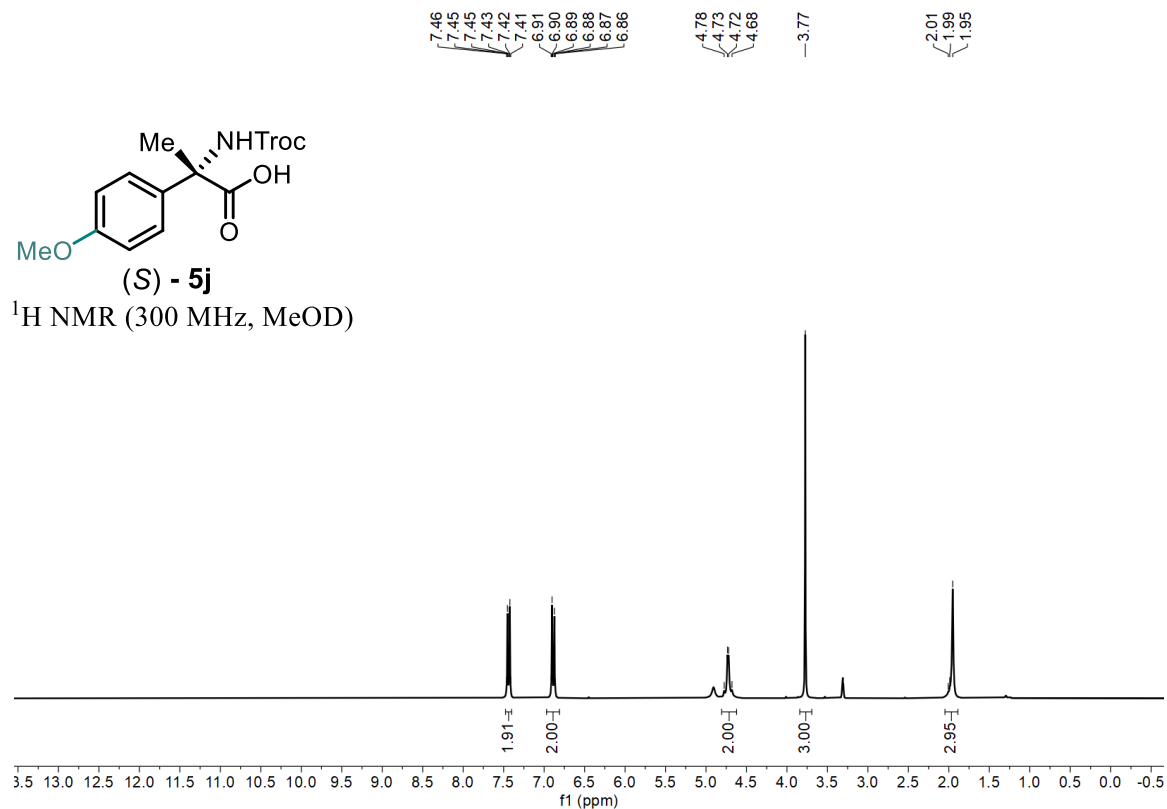


Statement



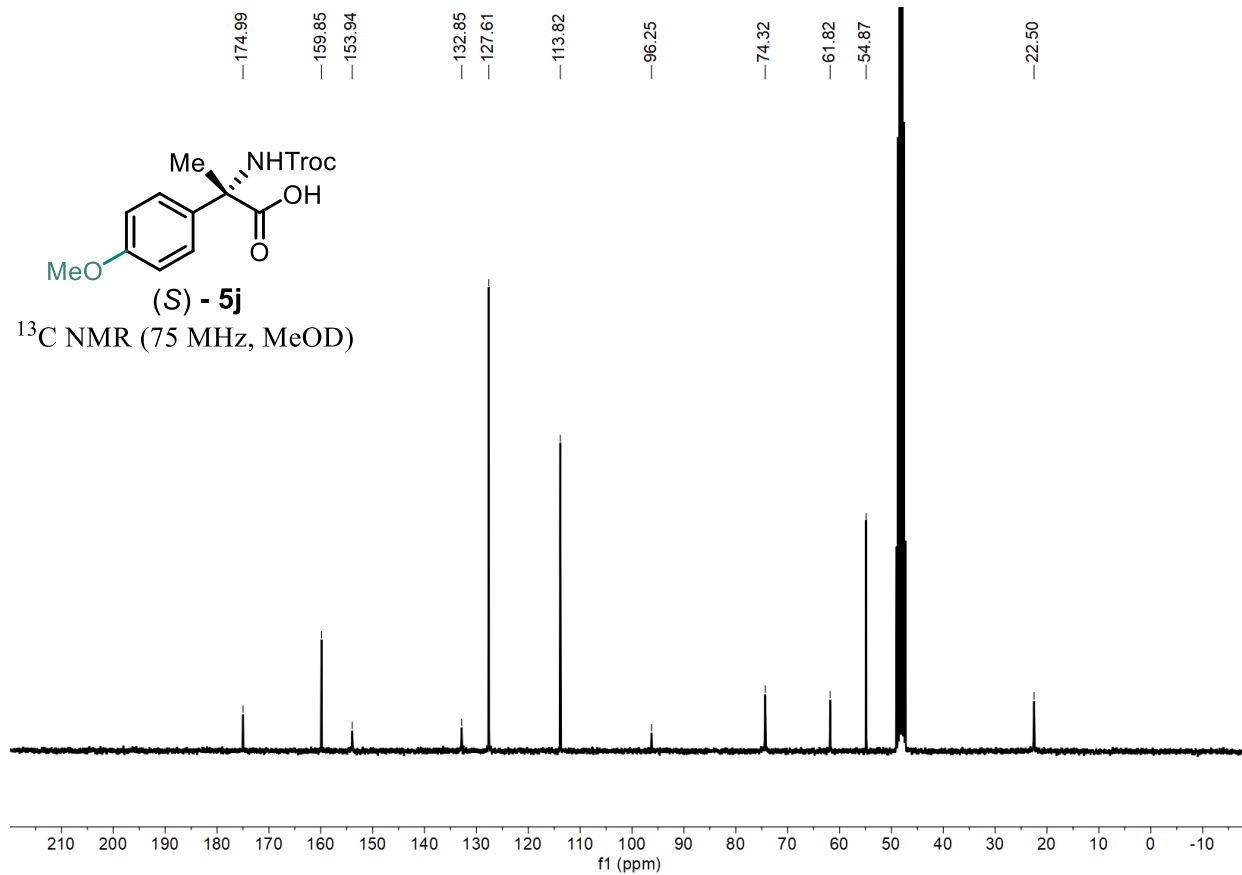
(S) - 5j

¹H NMR (300 MHz, MeOD)

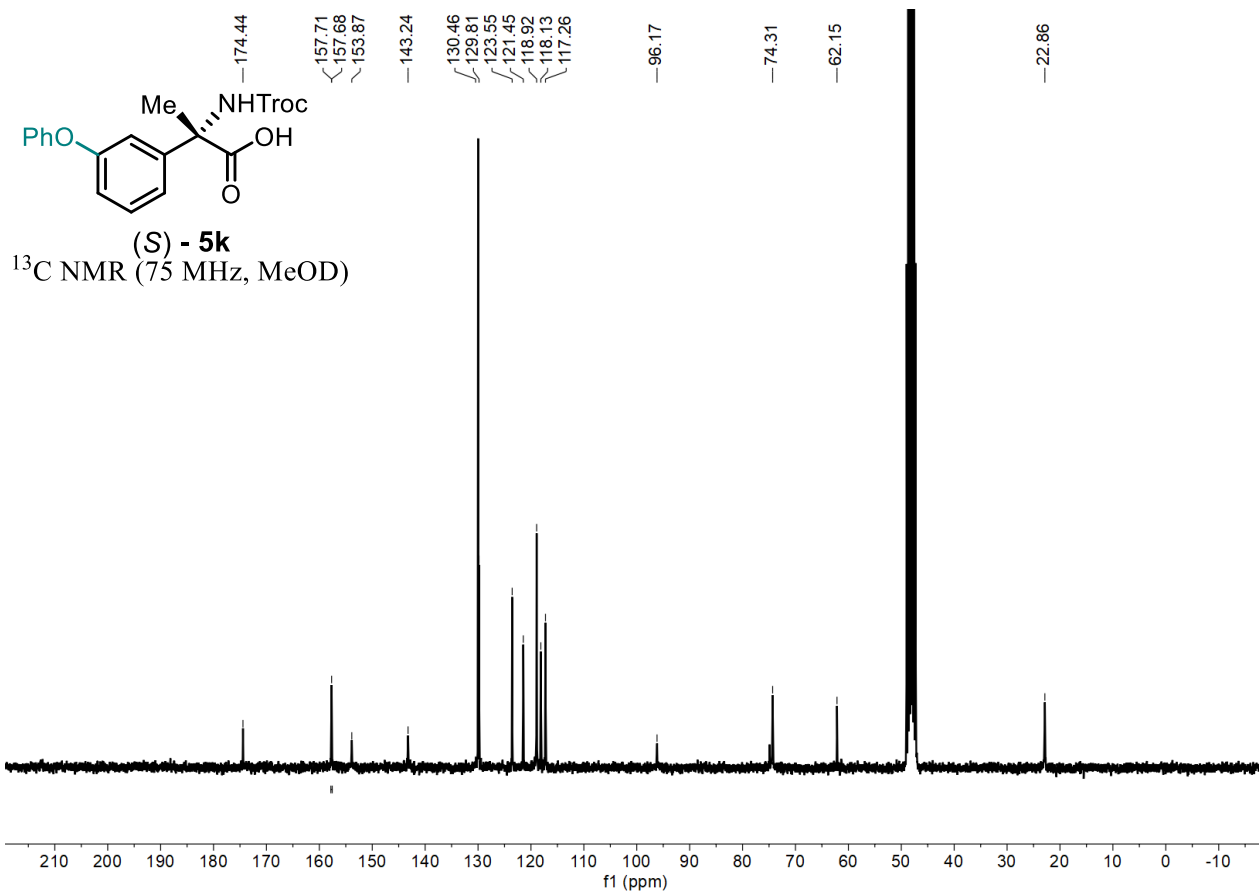
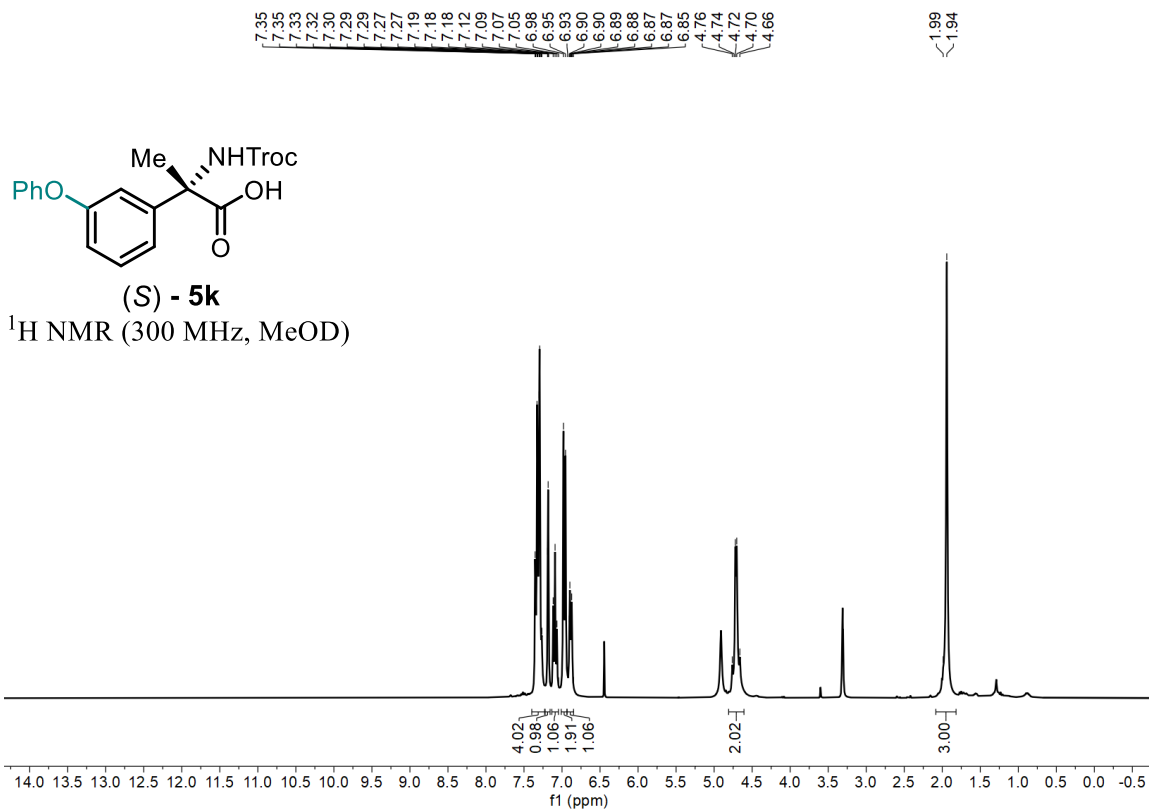


(S) - 5j

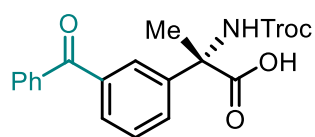
¹³C NMR (75 MHz, MeOD)



Statement

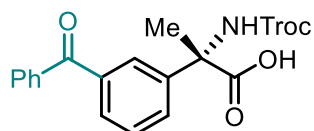
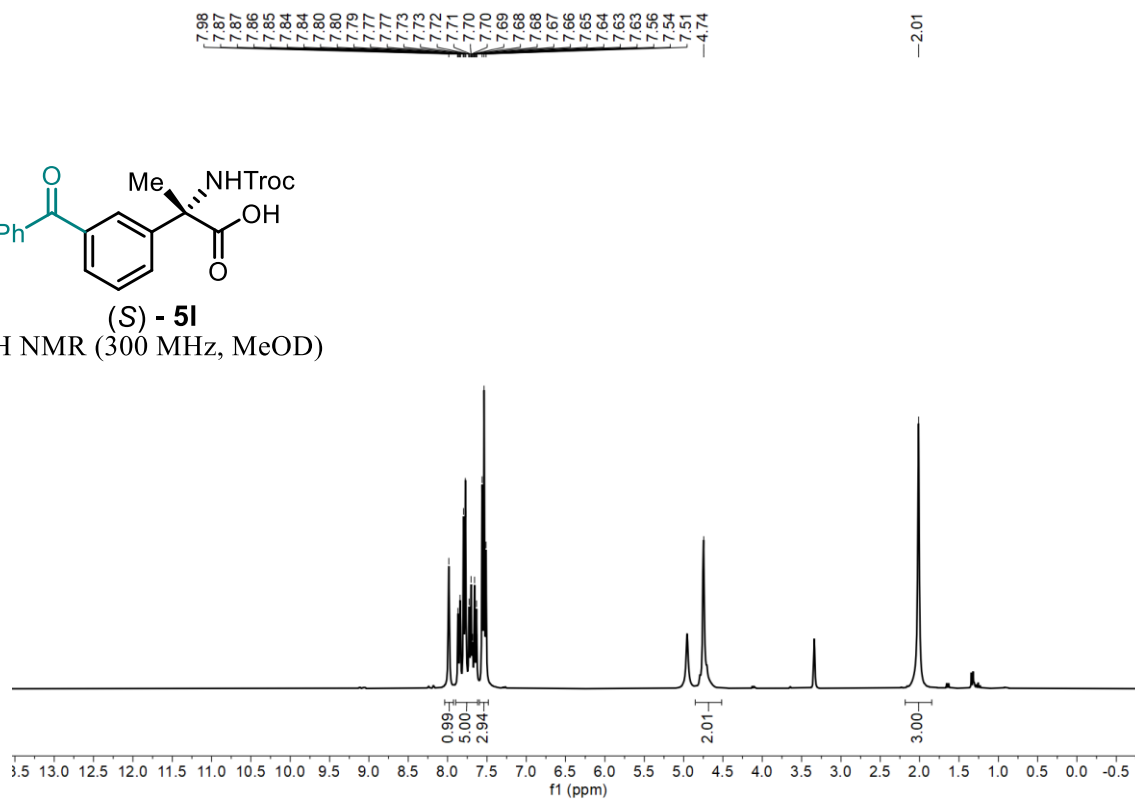


Statement



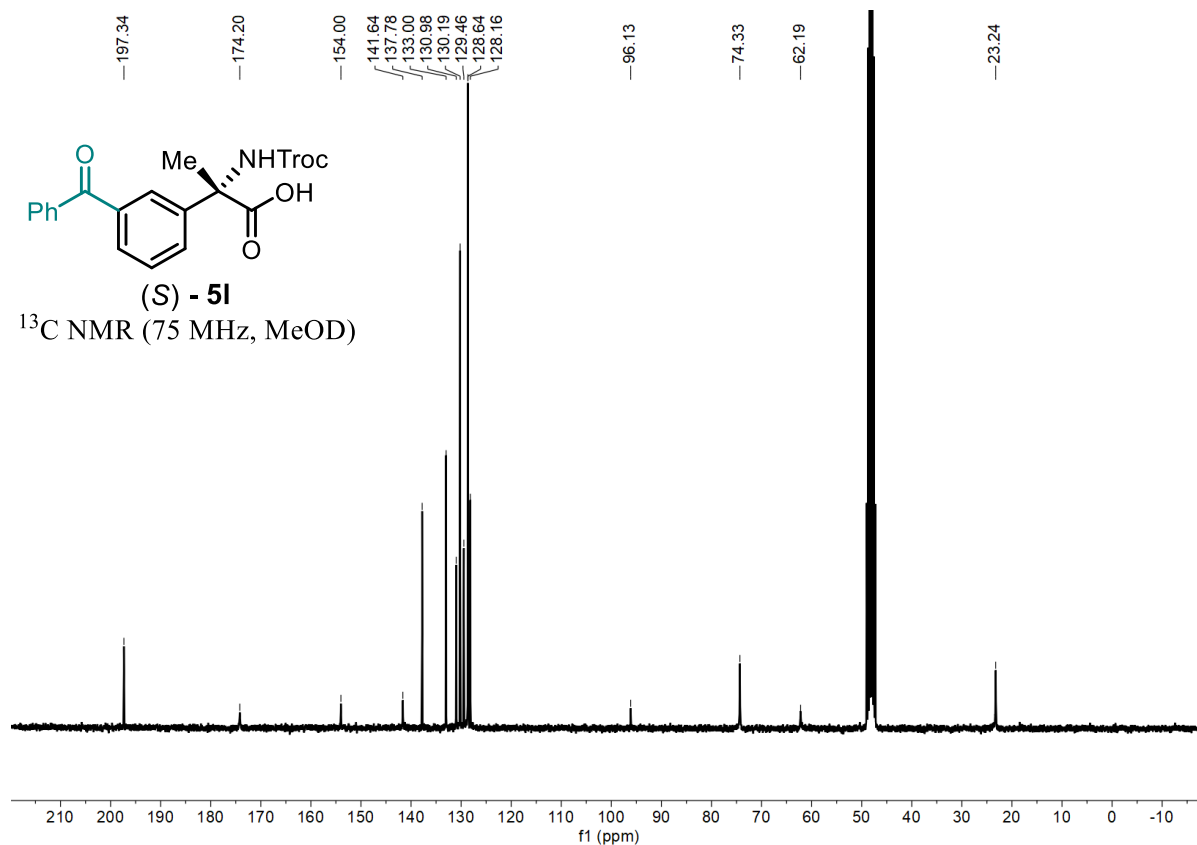
(S) - 5I

^1H NMR (300 MHz, MeOD)

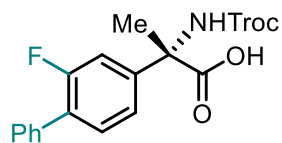


(S) - 5I

^{13}C NMR (75 MHz, MeOD)

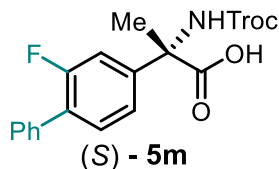
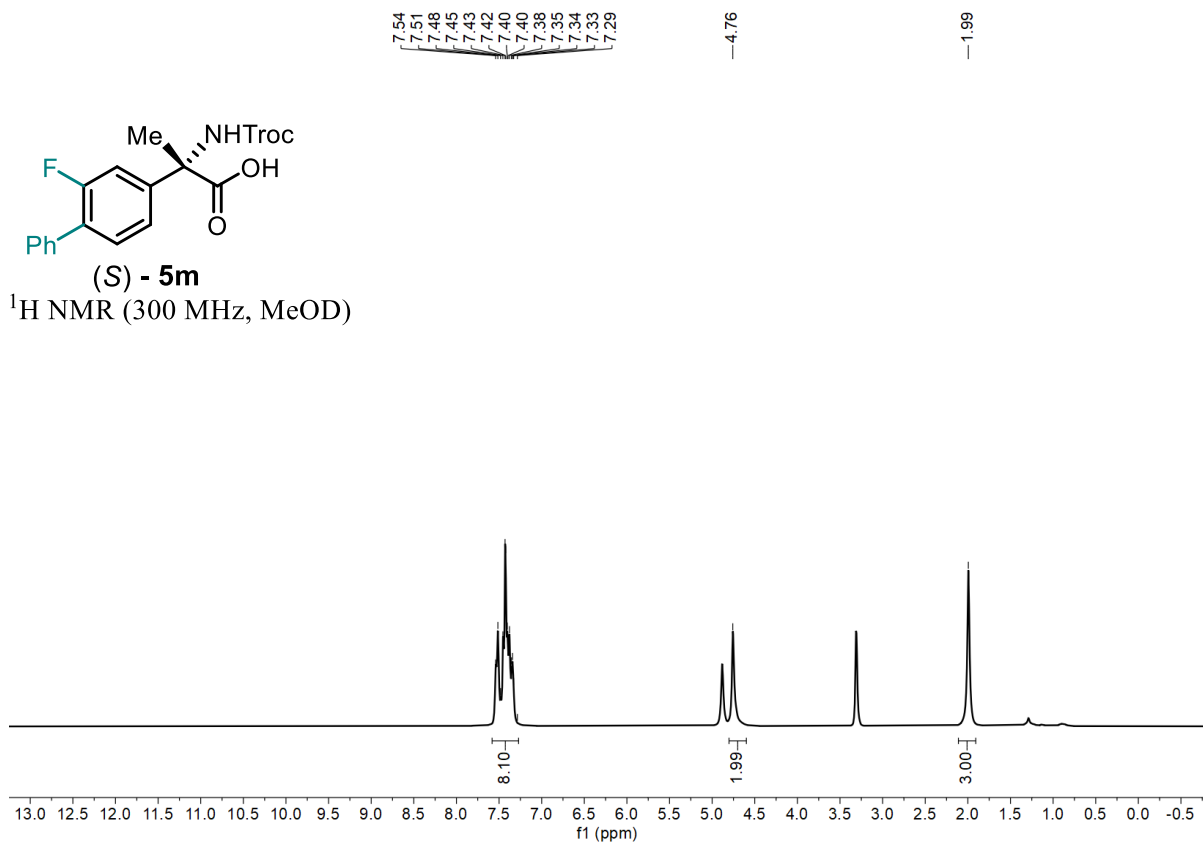


Statement



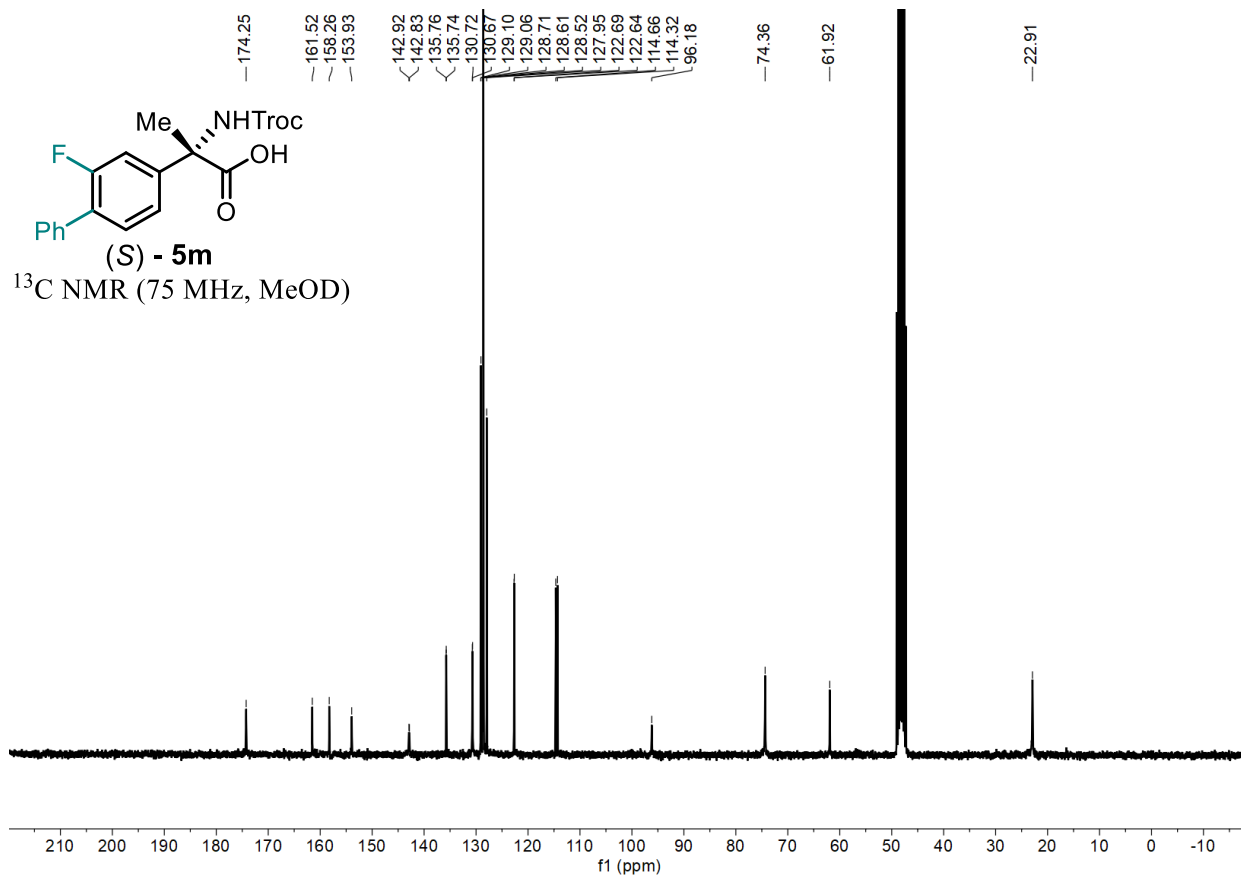
(S) - 5m

¹H NMR (300 MHz, MeOD)



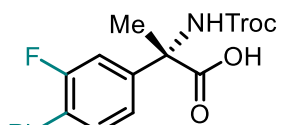
(S) - 5m

¹³C NMR (75 MHz, MeOD)

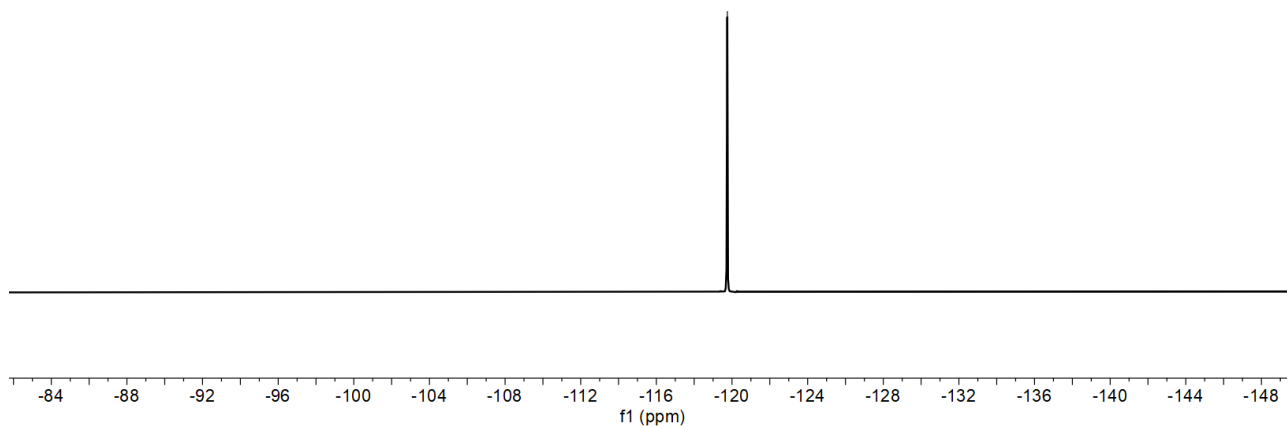


Statement

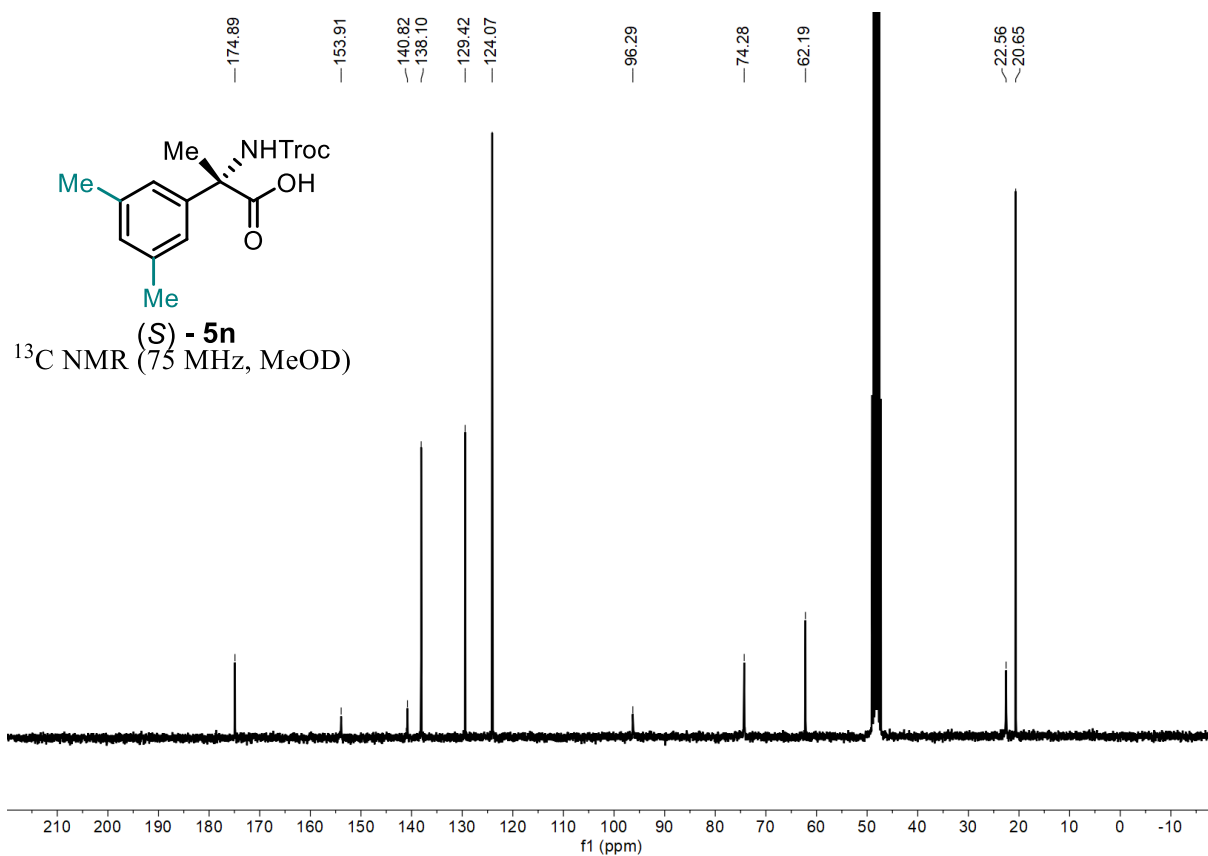
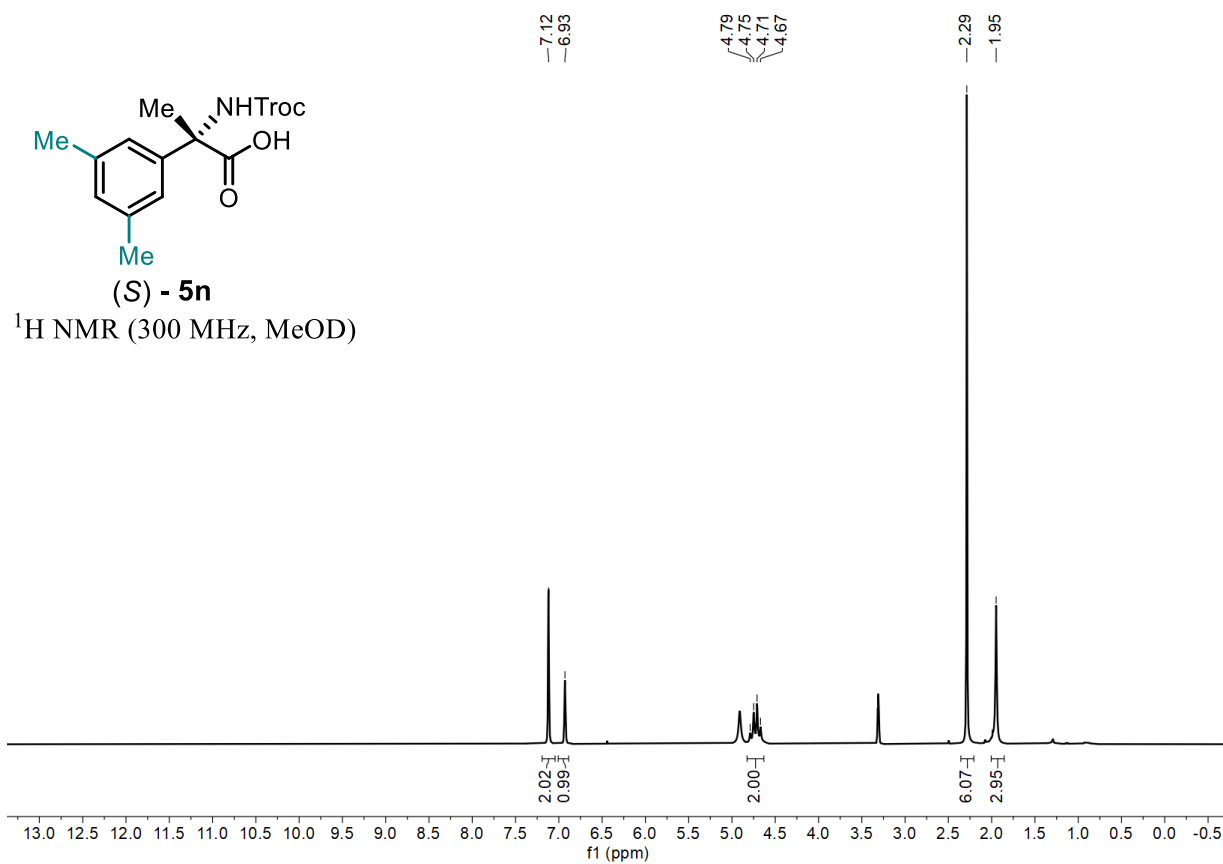
-119.76



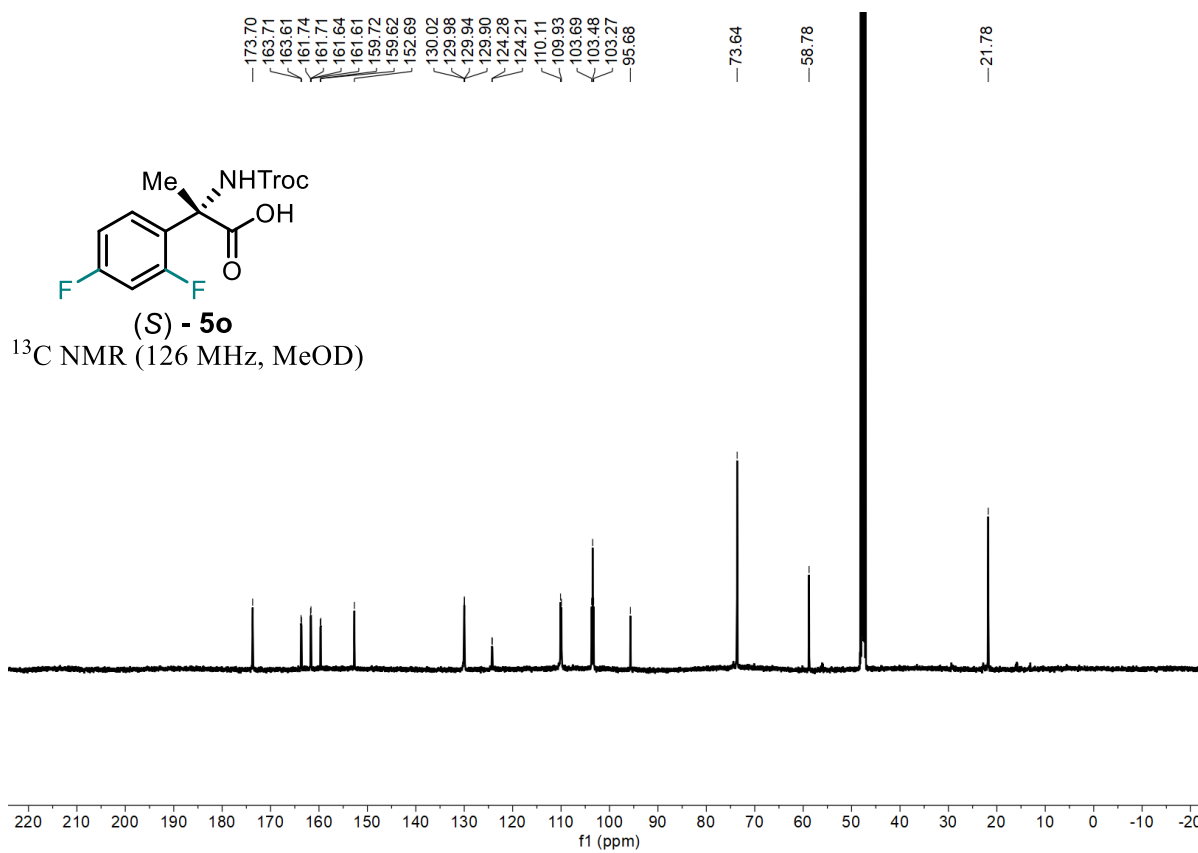
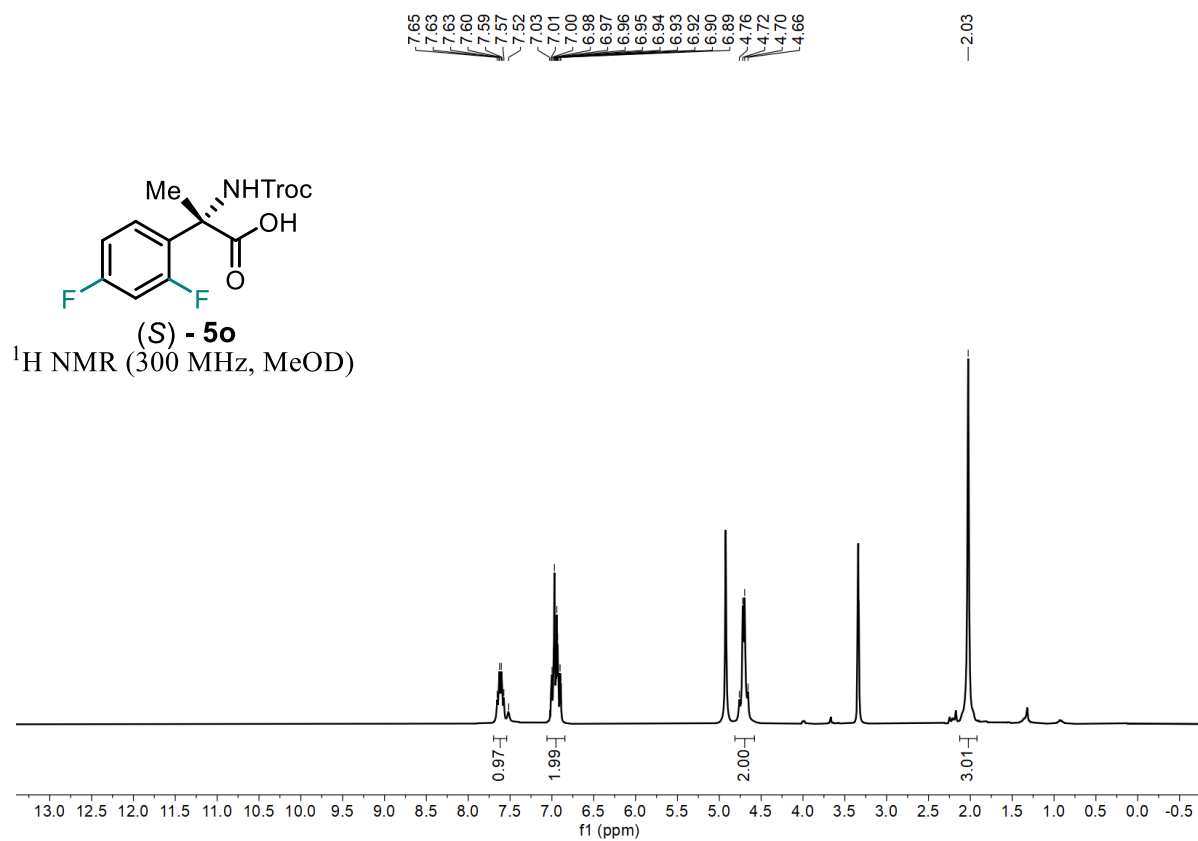
(S) - 5m
¹⁹F NMR (282 MHz, MeOD)



Statement



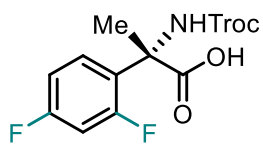
Statement



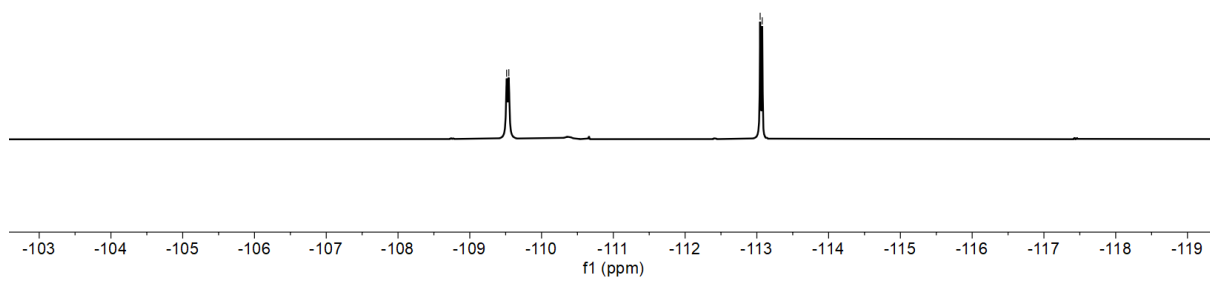
Statement

-109.51
-109.54

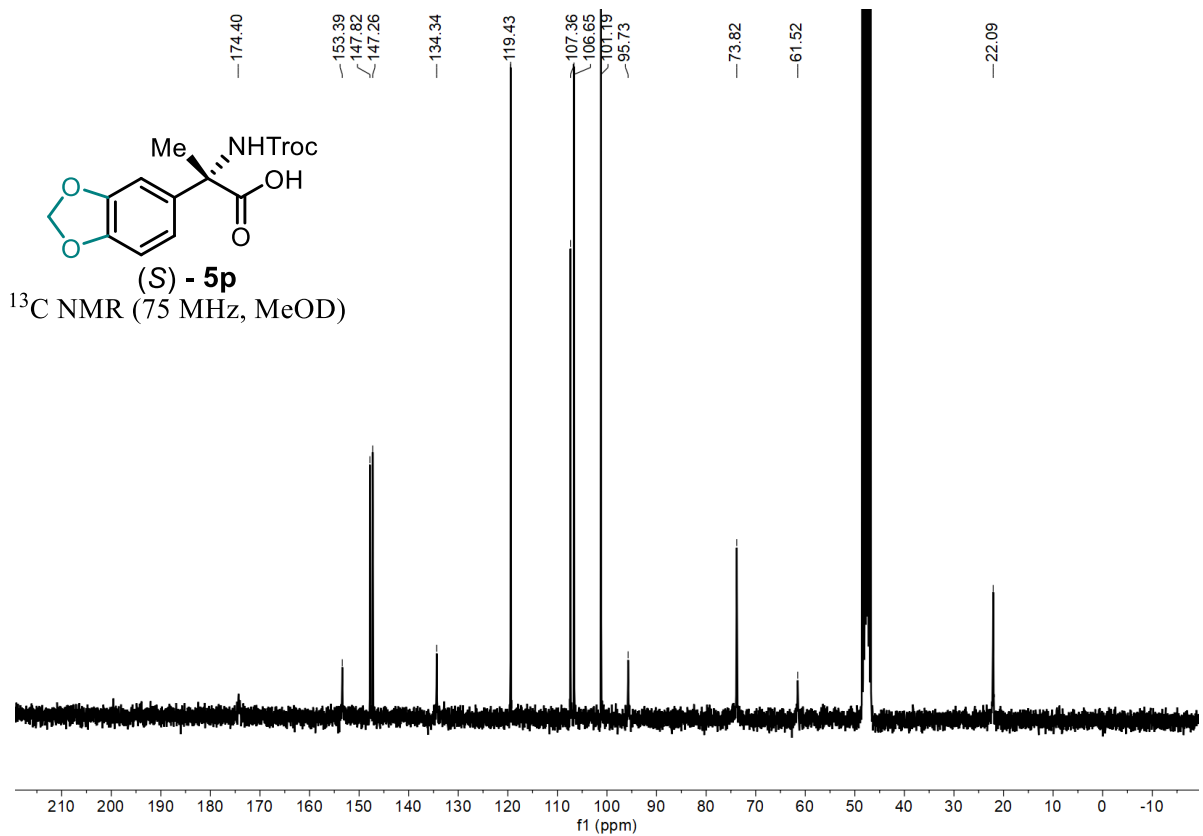
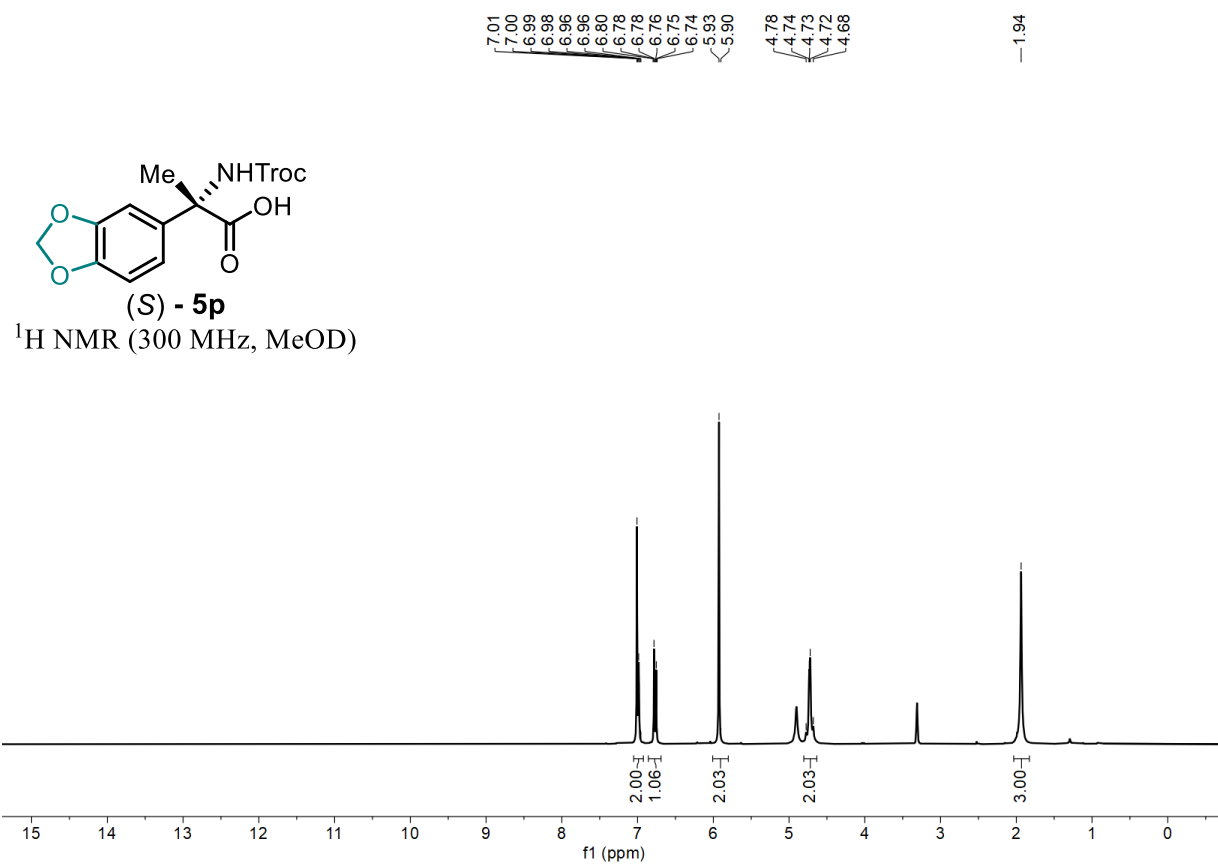
-113.05
-113.07



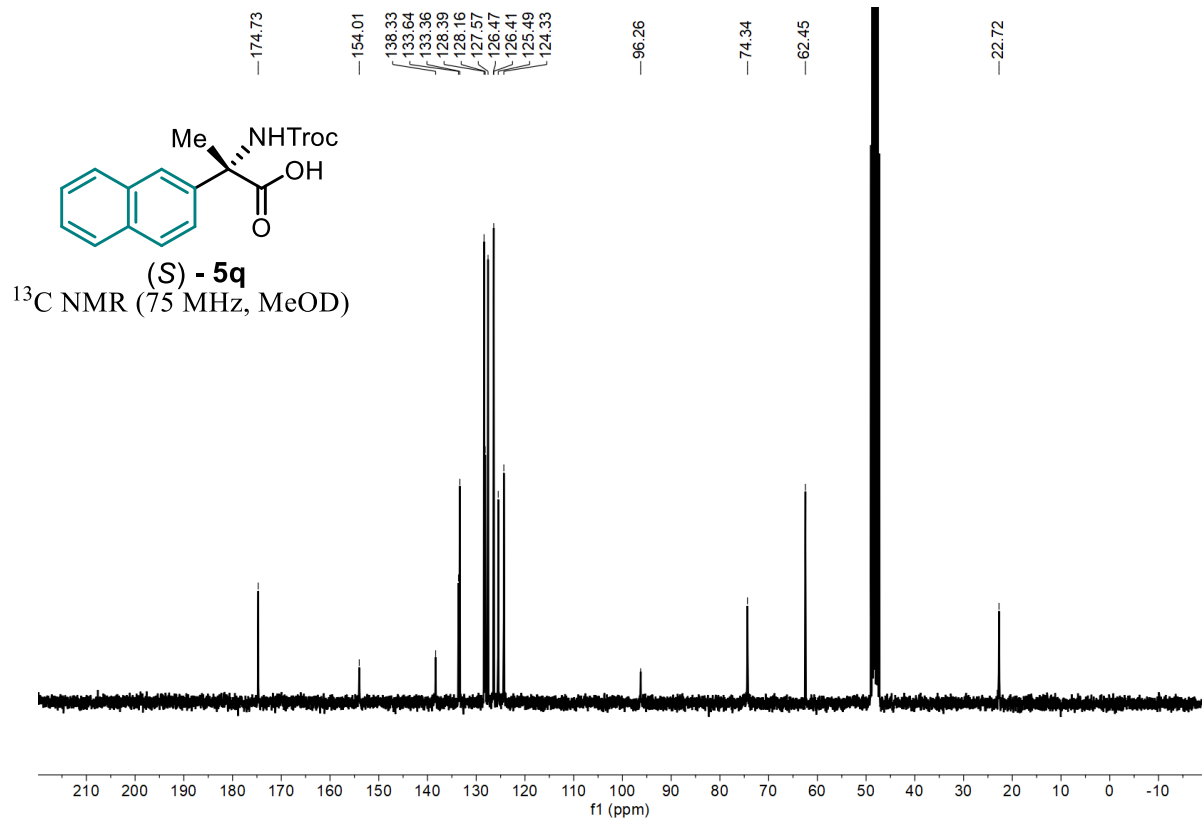
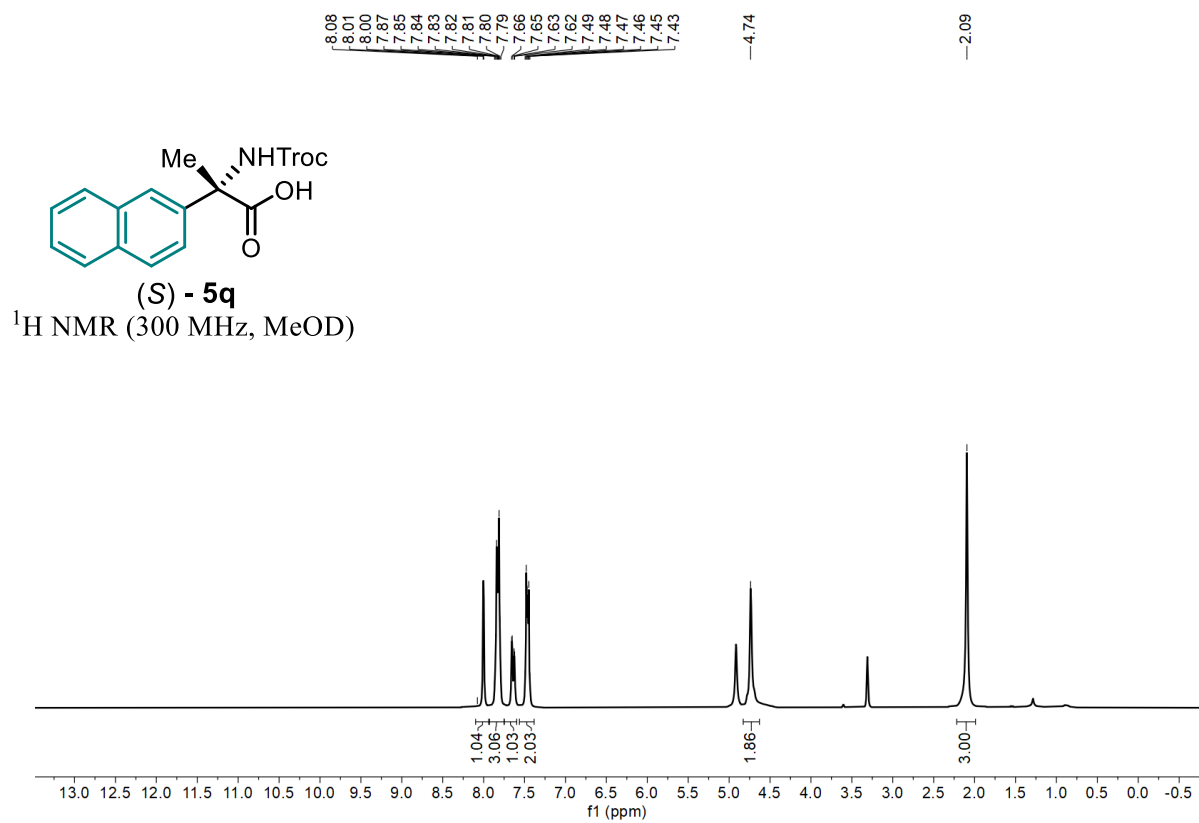
(S) - **5o**
¹⁹F NMR (282 MHz, MeOD)



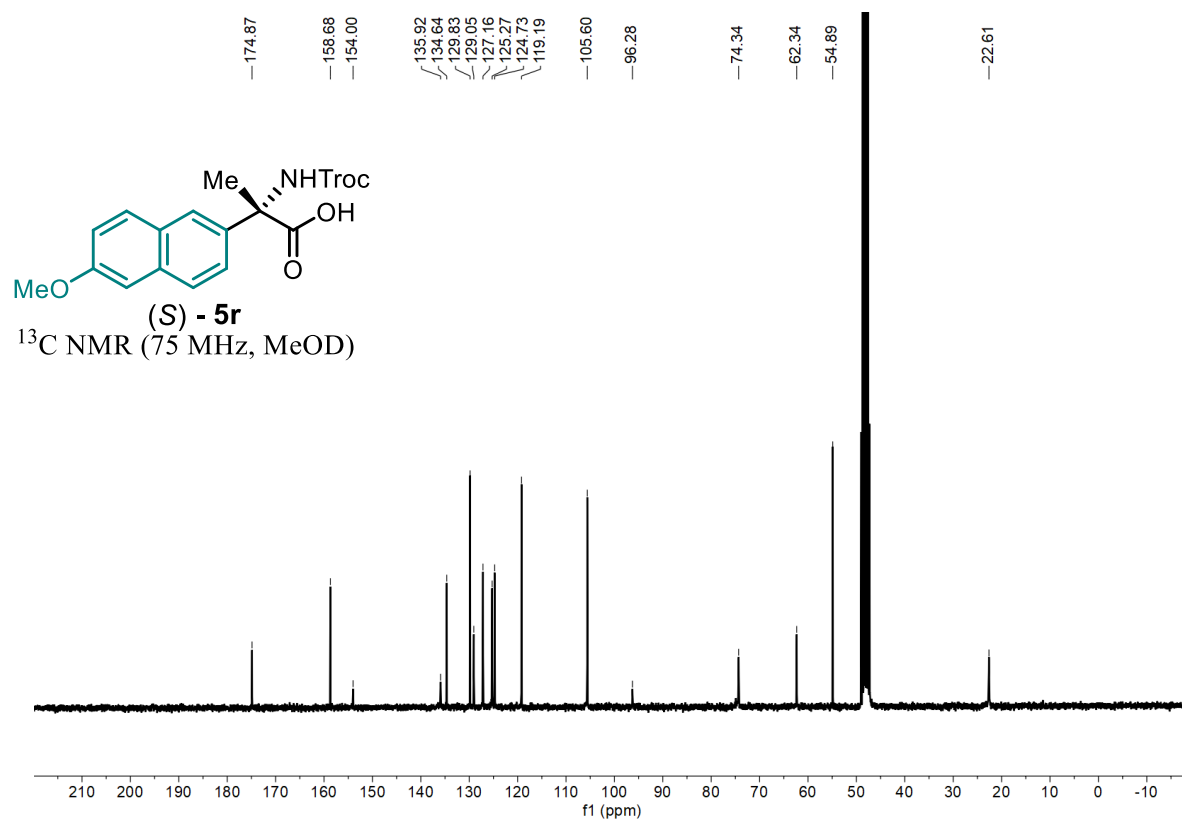
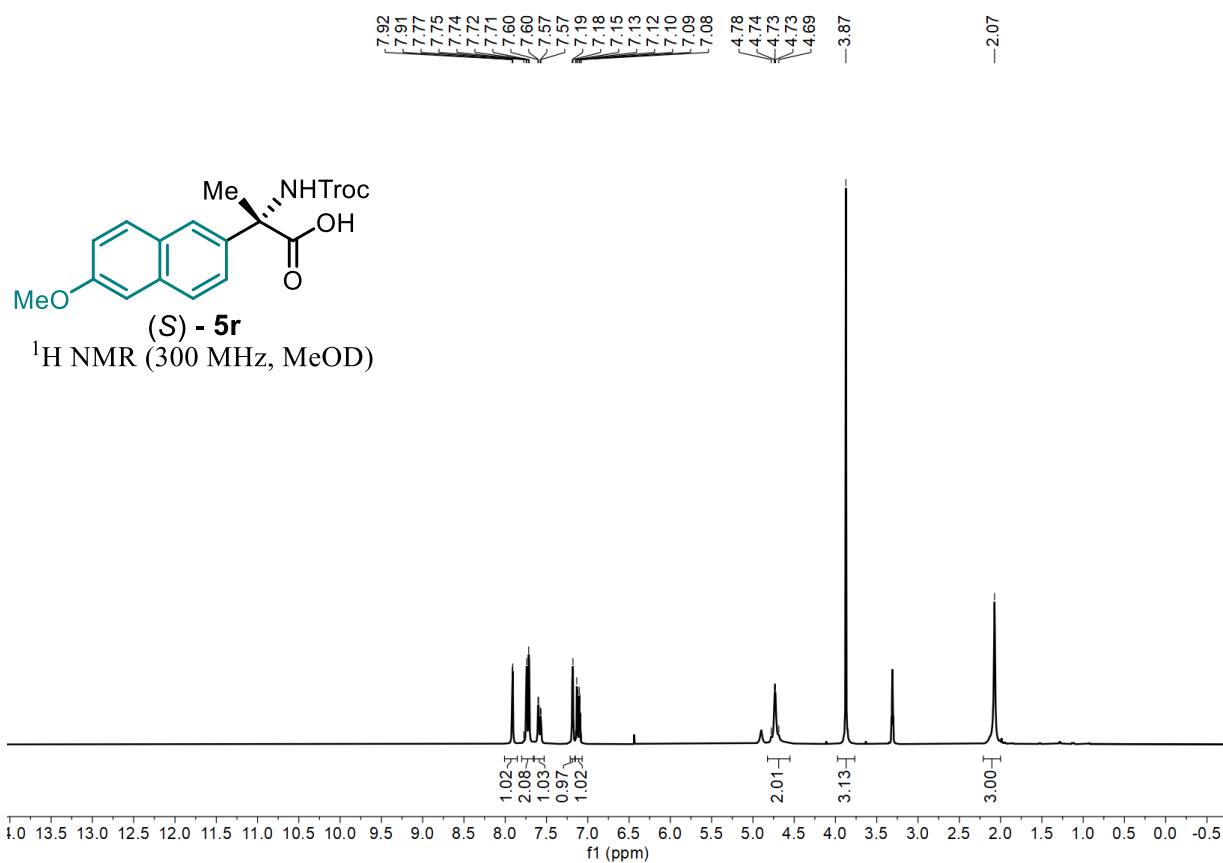
Statement



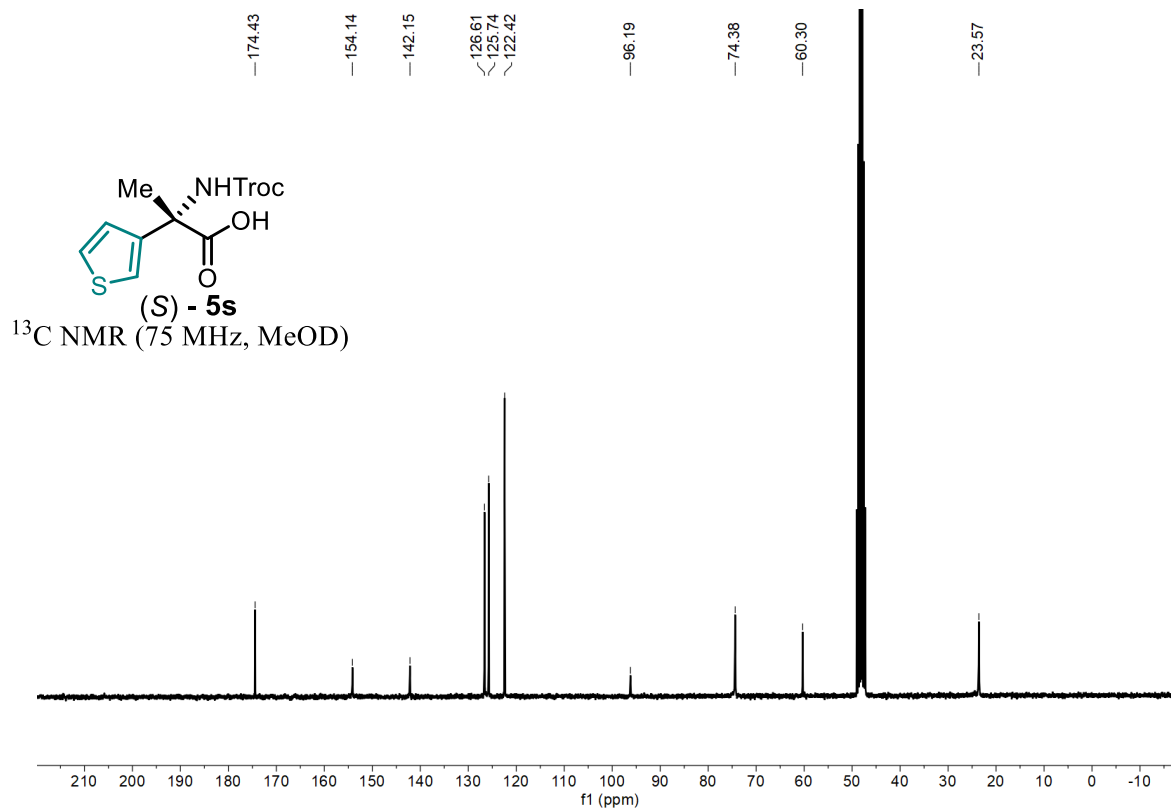
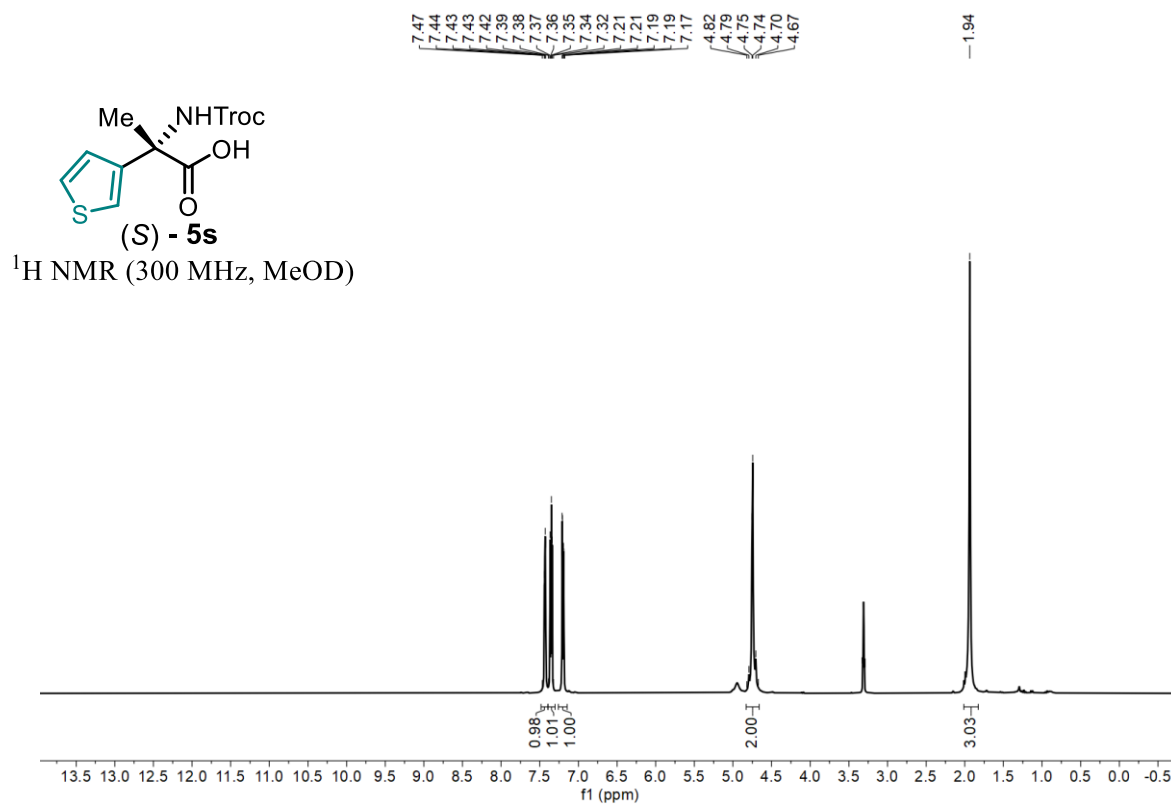
Statement



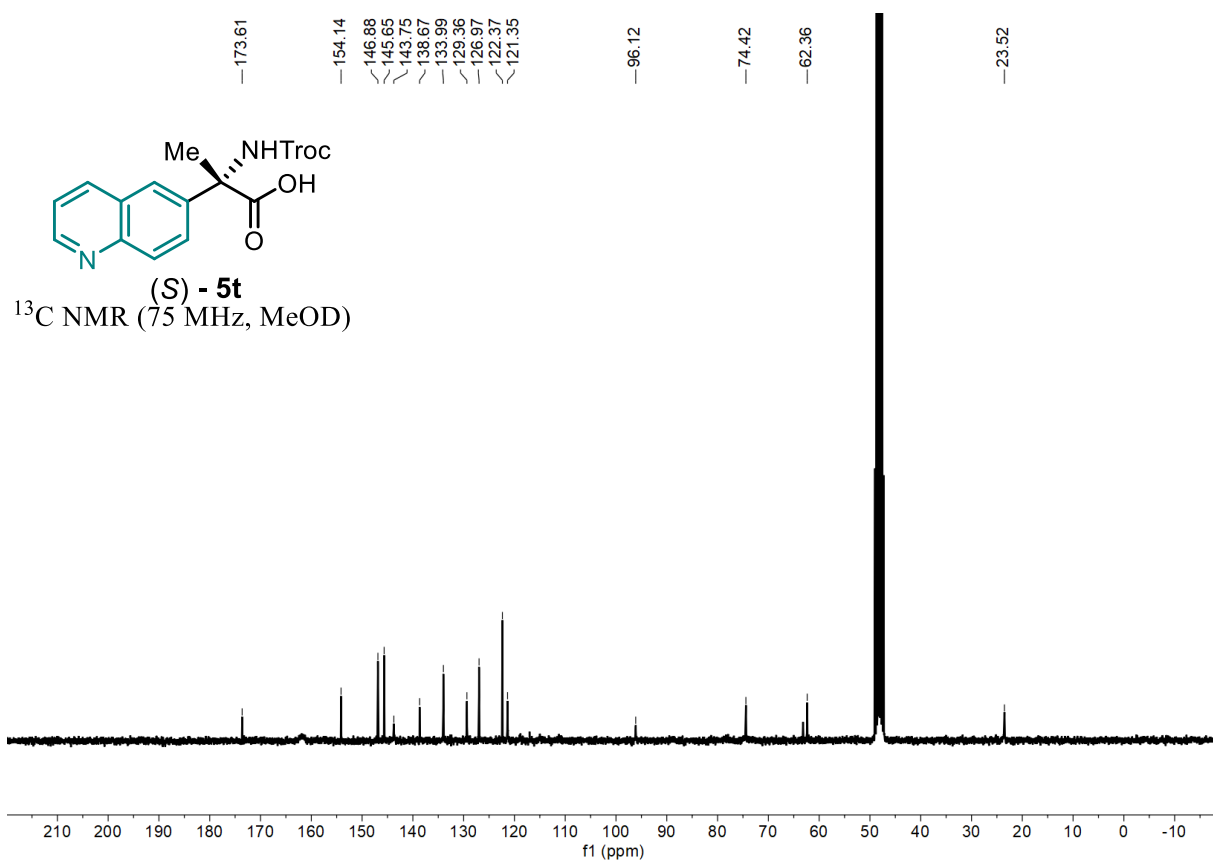
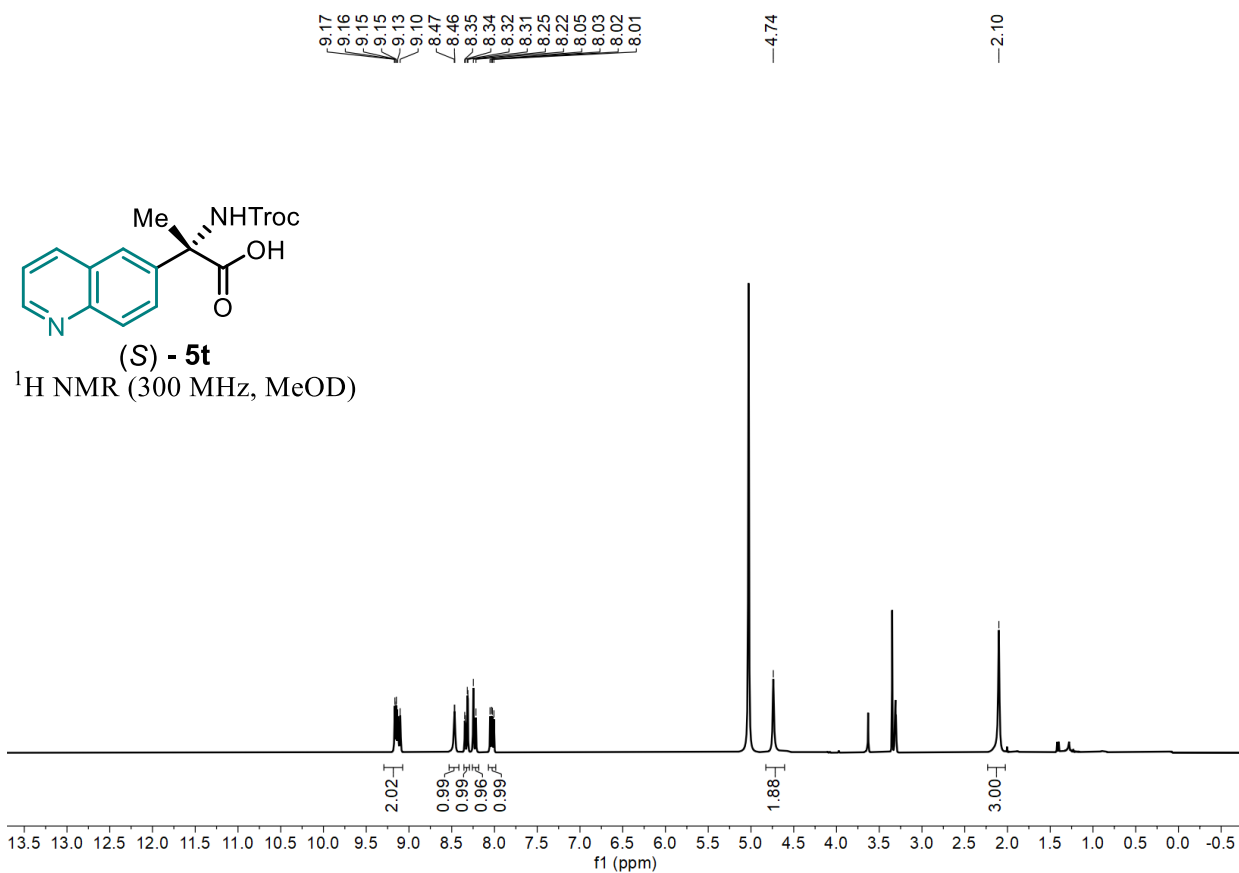
Statement



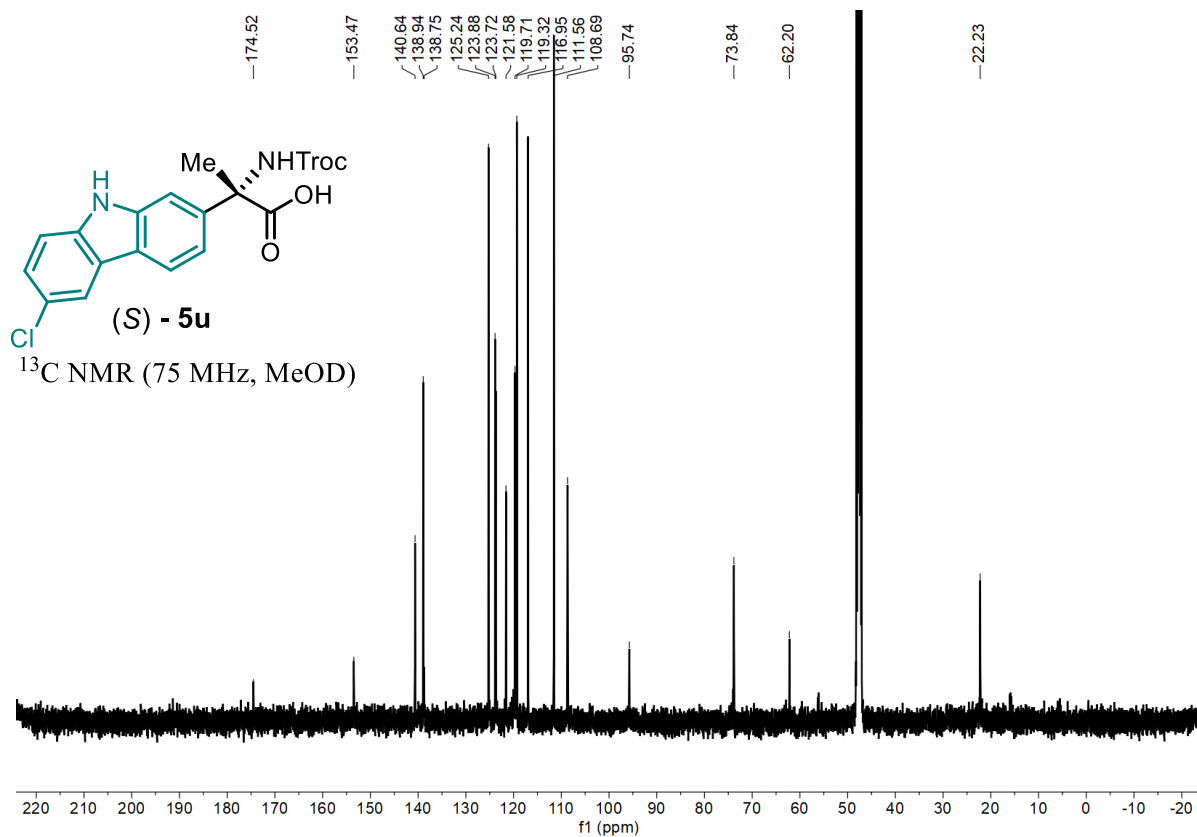
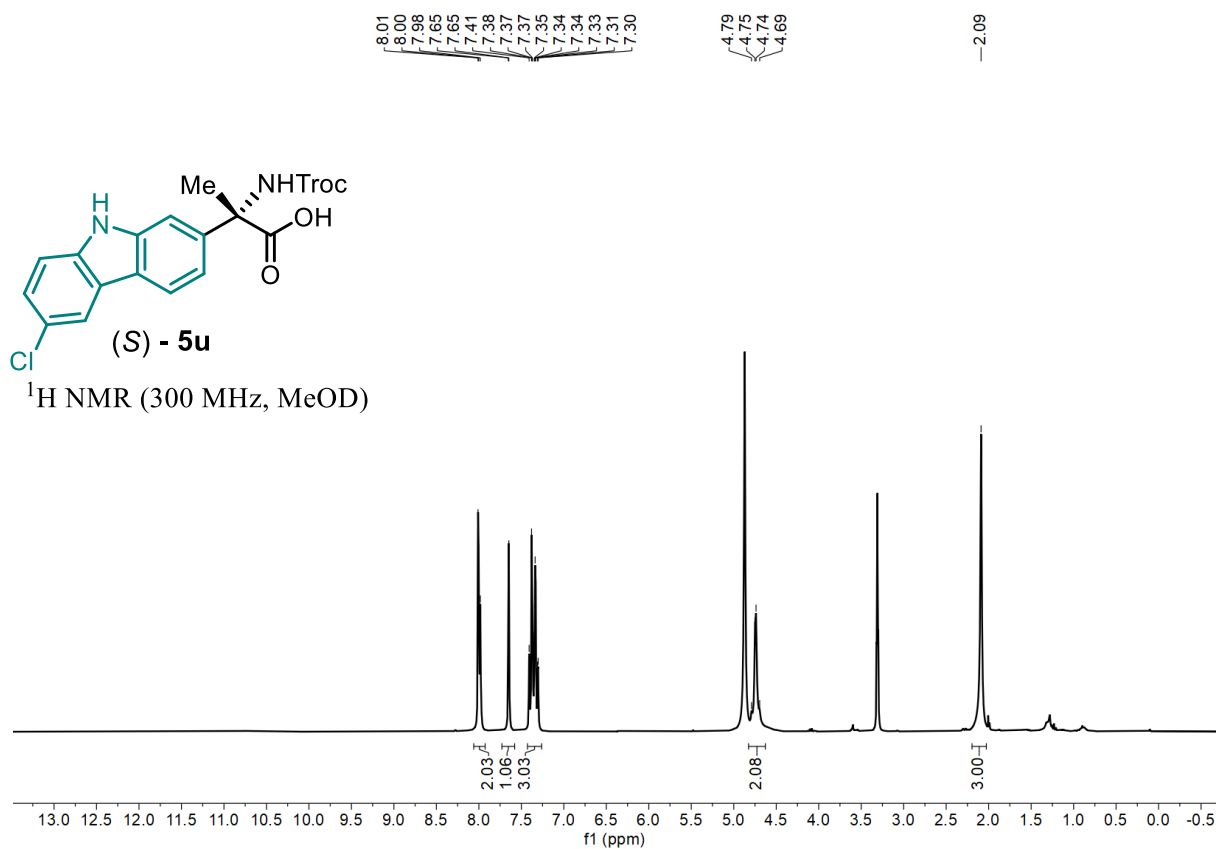
Statement



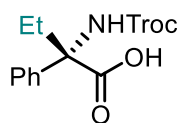
Statement



Statement

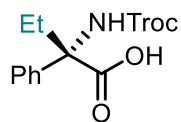
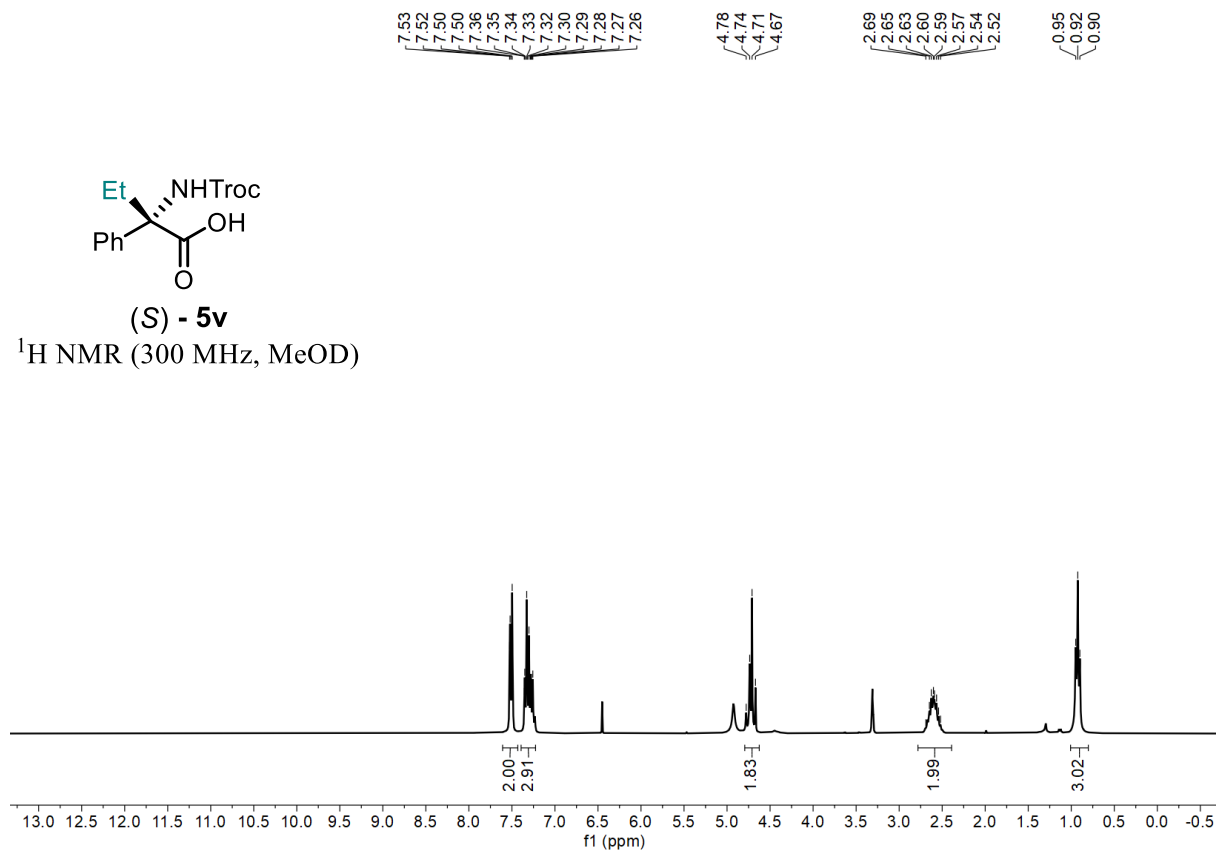


Statement



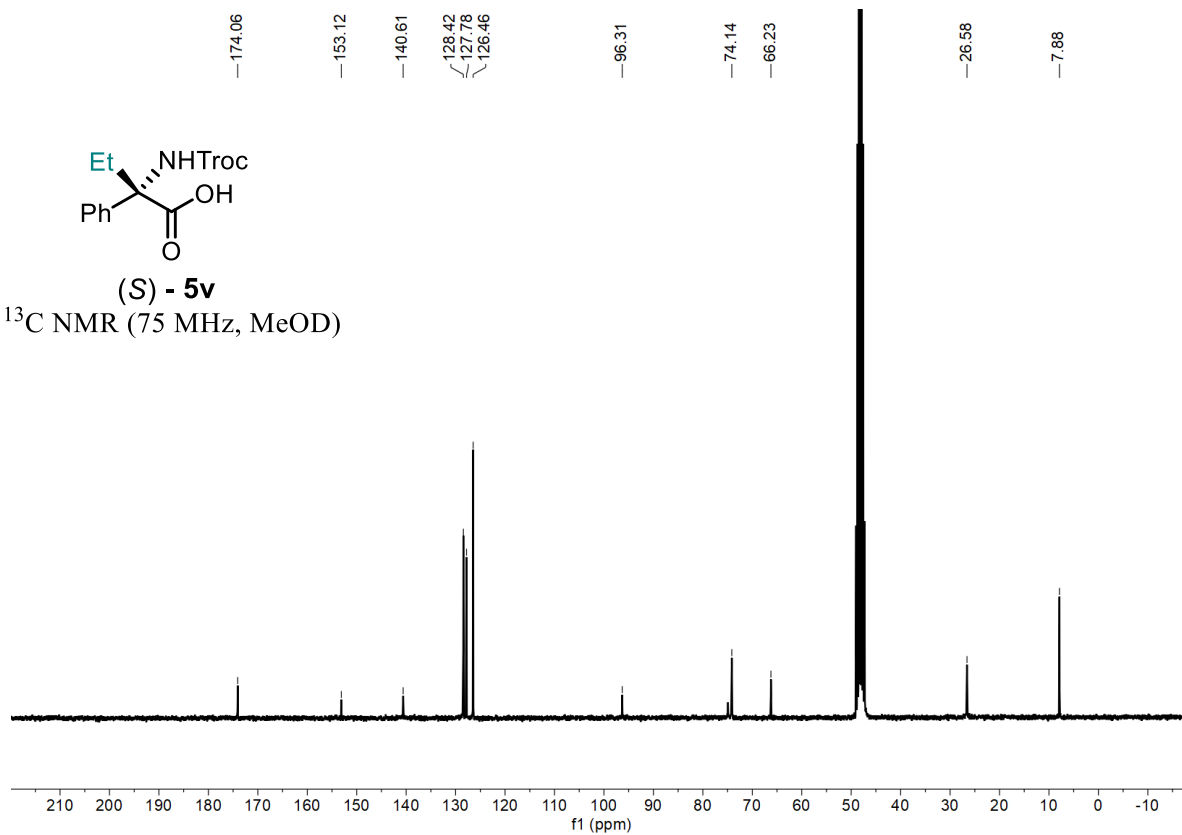
(S) - 5v

^1H NMR (300 MHz, MeOD)



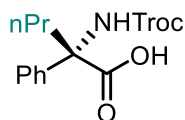
(S) - 5v

^{13}C NMR (75 MHz, MeOD)



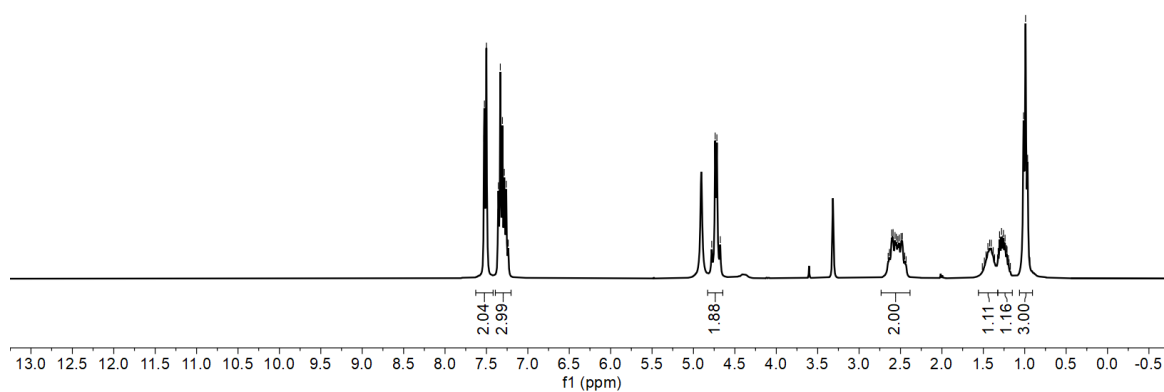
Statement

7.53
7.52
7.50
7.36
7.33
7.33
7.31
7.28
7.26
7.25
7.24
4.78
4.74
4.72
4.68
2.65
2.63
2.61
2.59
2.57
2.55
2.53
2.51
2.49
2.48
2.45
2.45
1.51
1.49
1.47
1.44
1.42
1.40
1.38
1.36
1.33
1.32
1.30
1.30
1.28
1.26
1.26
1.24
1.22
1.21
1.20
1.19
1.17
1.01
0.99
0.97
0.94

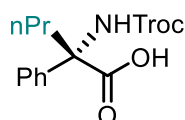


(S) - 5w

^1H NMR (300 MHz, MeOD)

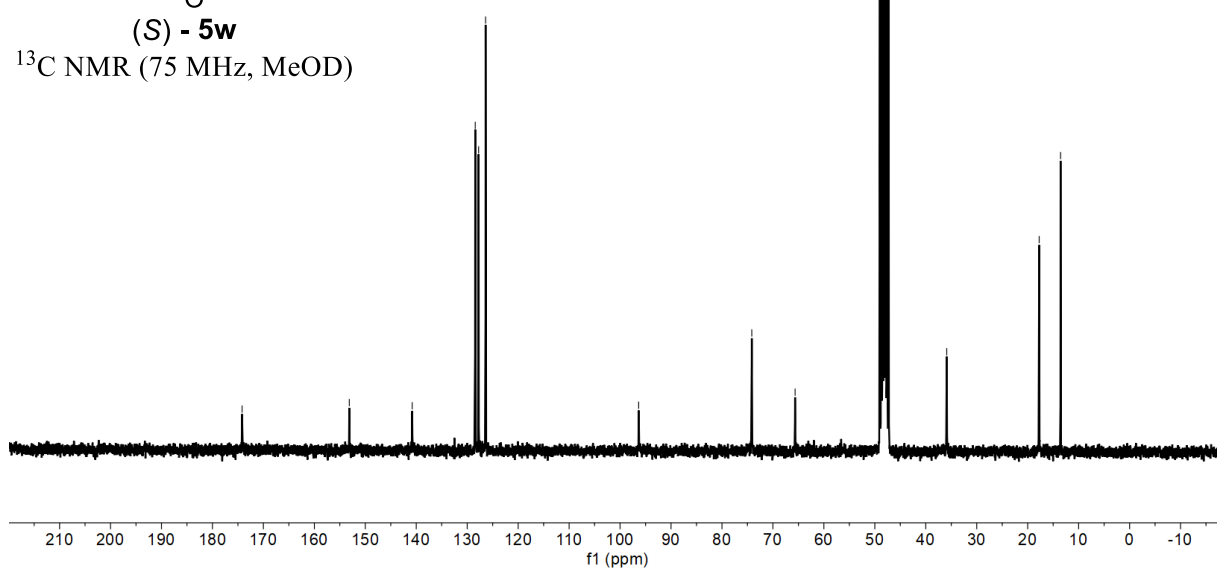


—174.18
—153.14
—140.80
128.42
127.77
126.39
—96.34
—74.15
—65.65
—35.88
—17.74
—13.54

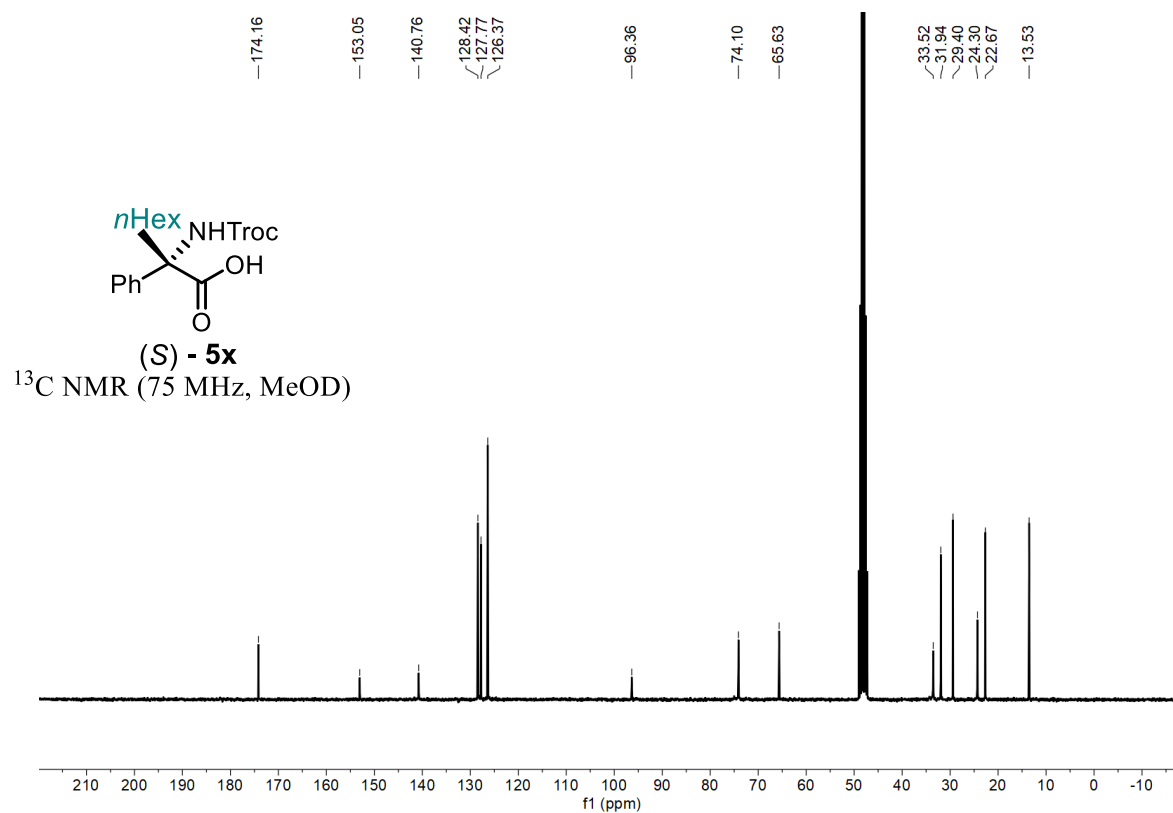
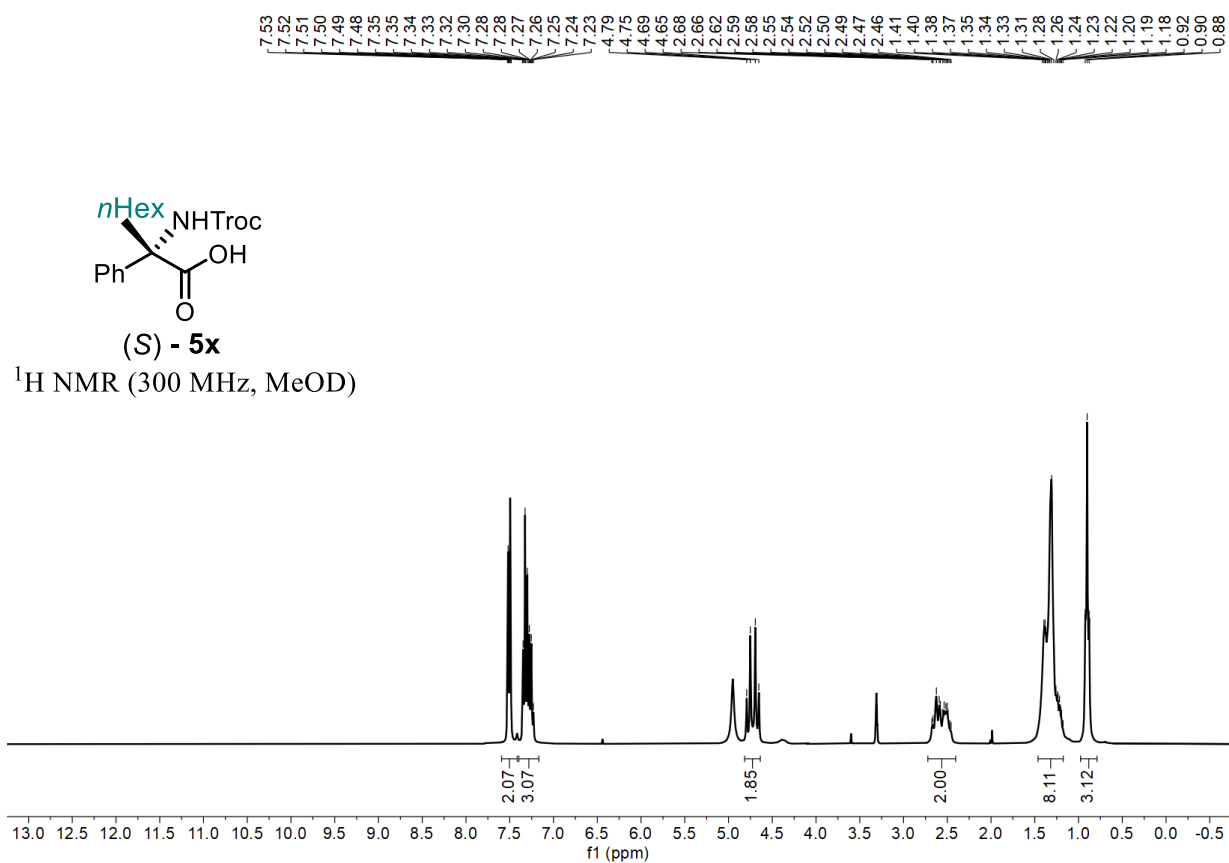


(S) - 5w

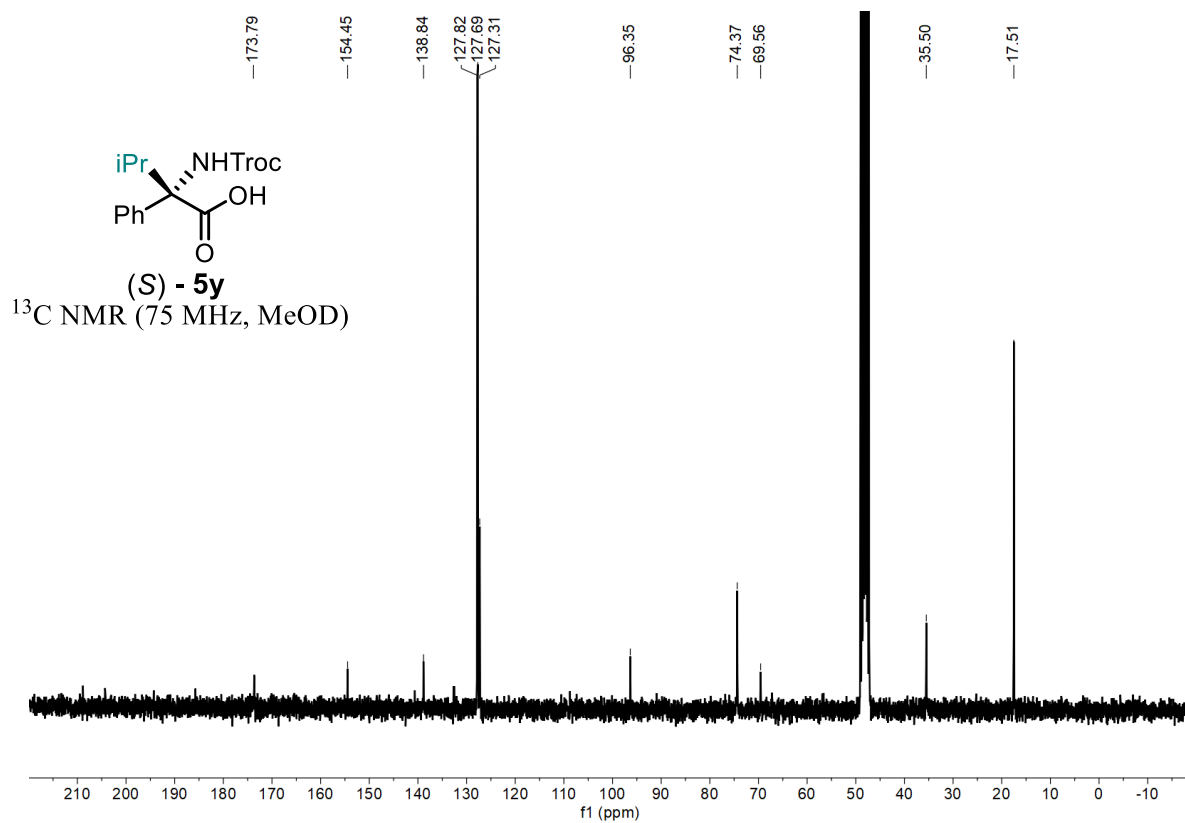
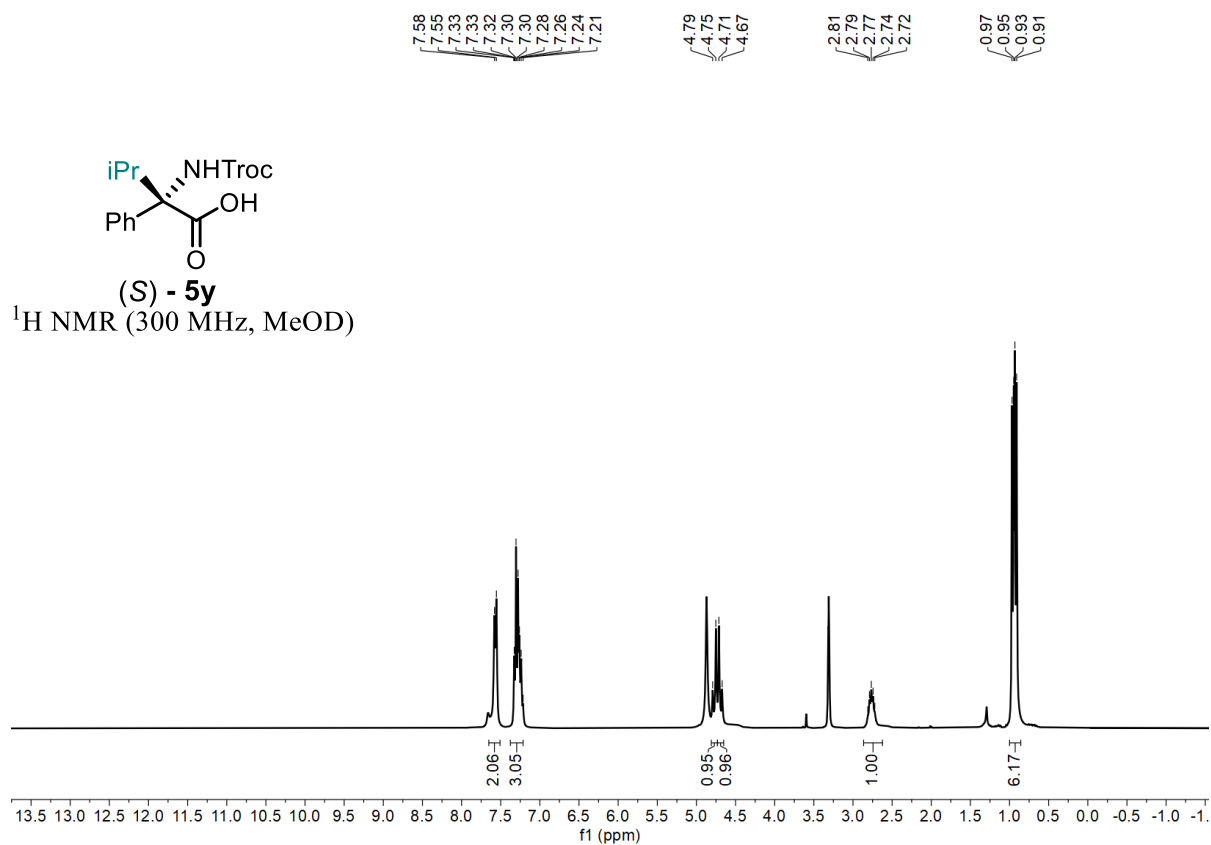
^{13}C NMR (75 MHz, MeOD)



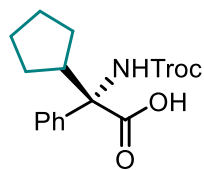
Statement



Statement

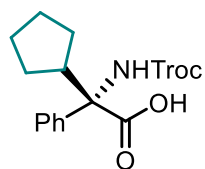
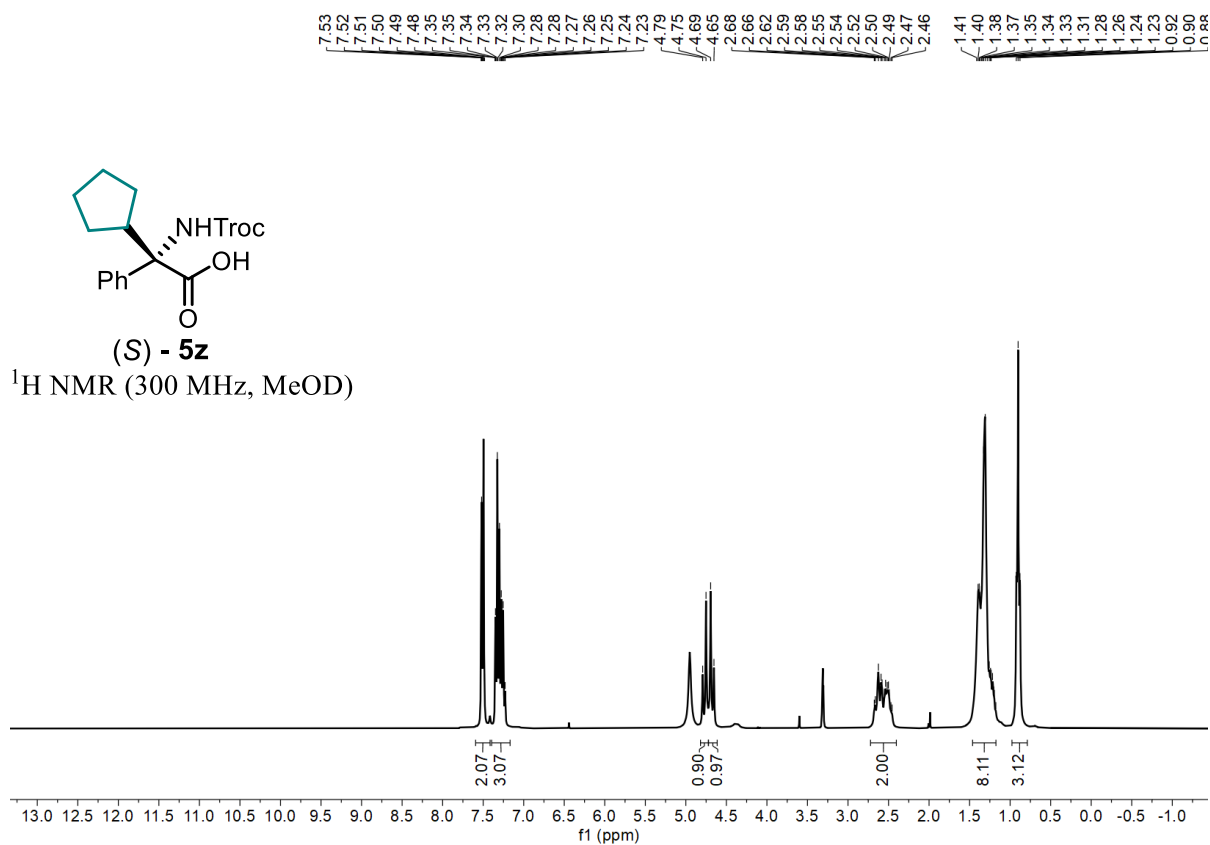


Statement



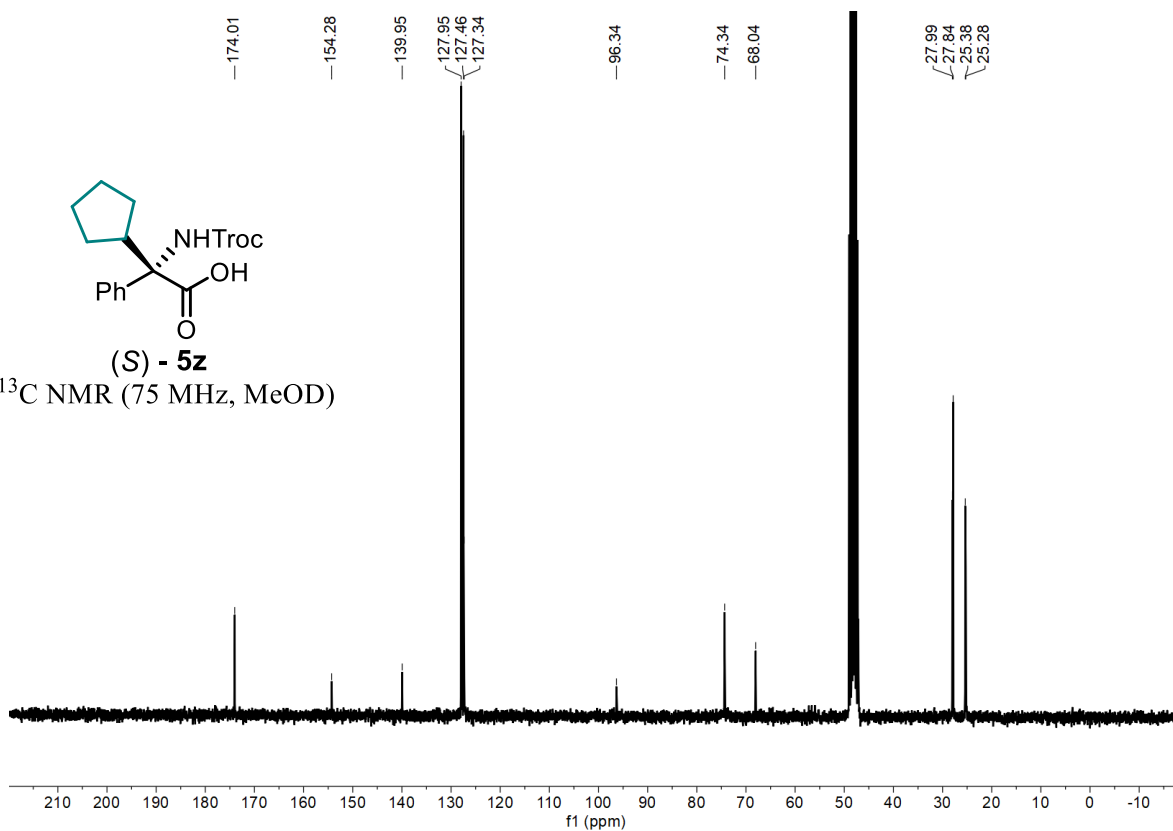
(S) - **5z**

^1H NMR (300 MHz, MeOD)

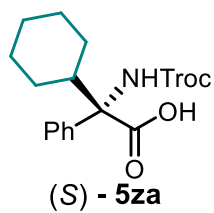


(S) - **5z**

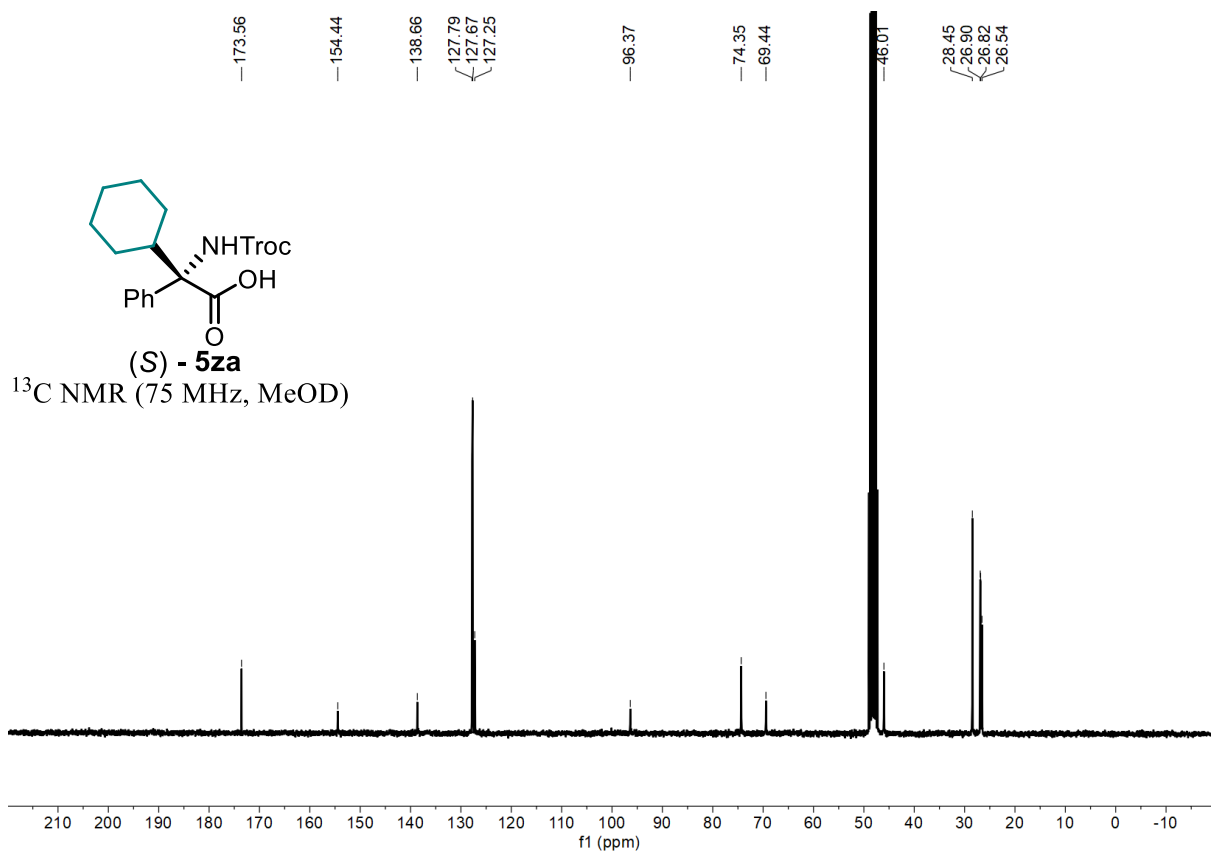
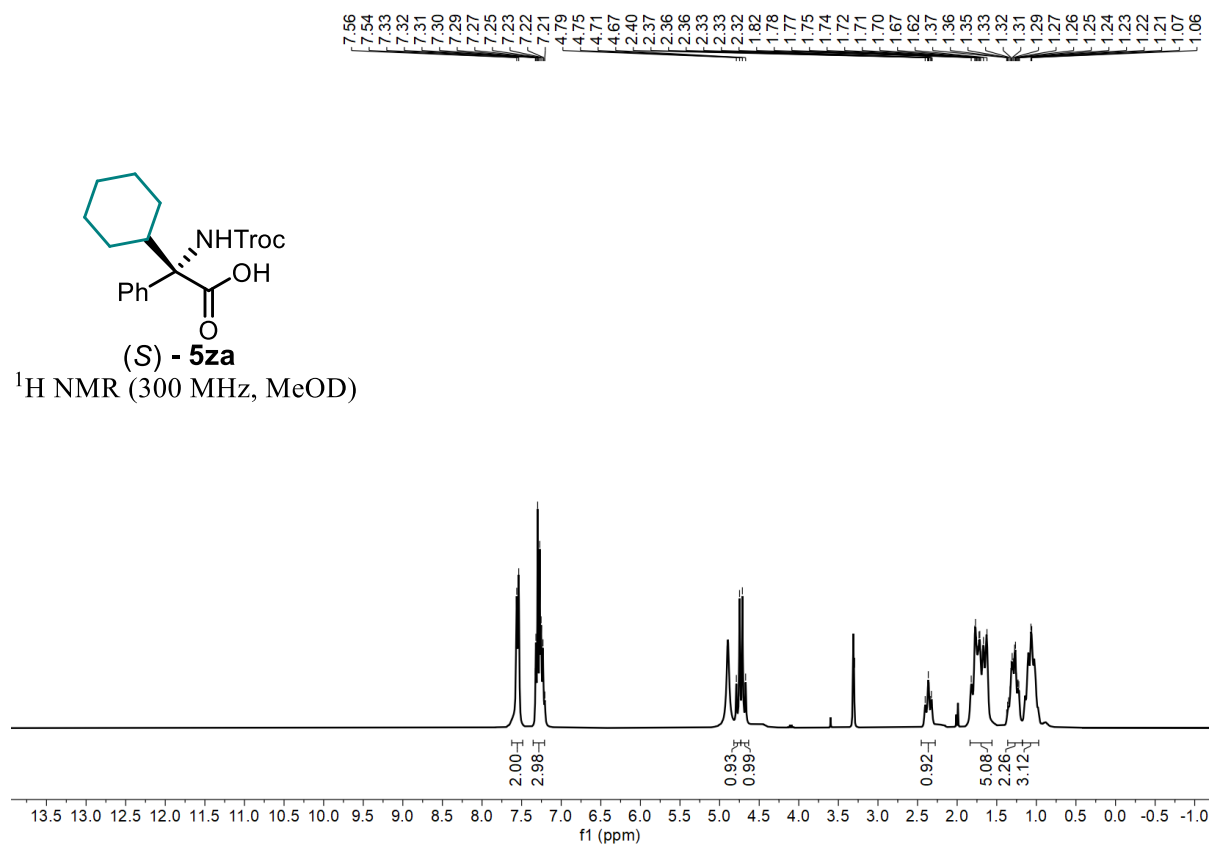
^{13}C NMR (75 MHz, MeOD)



Statement

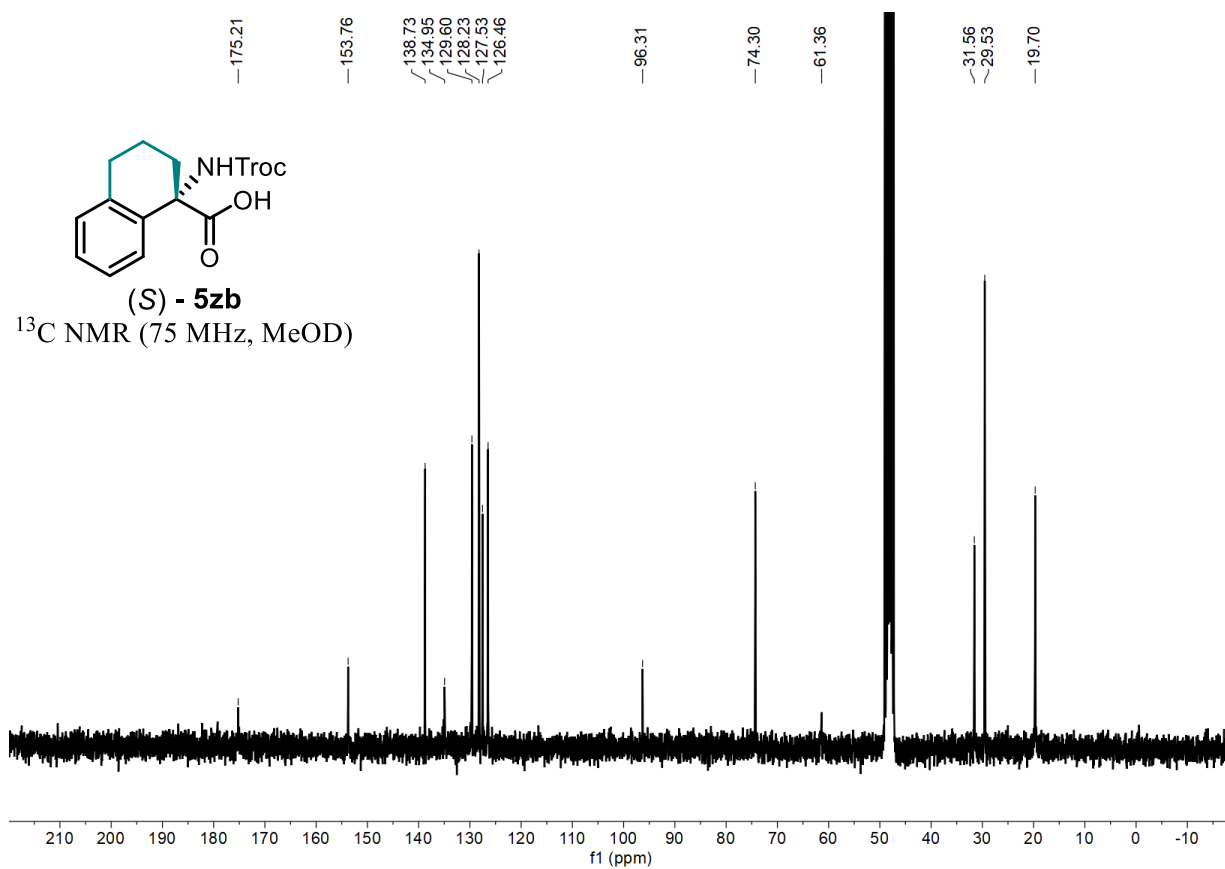
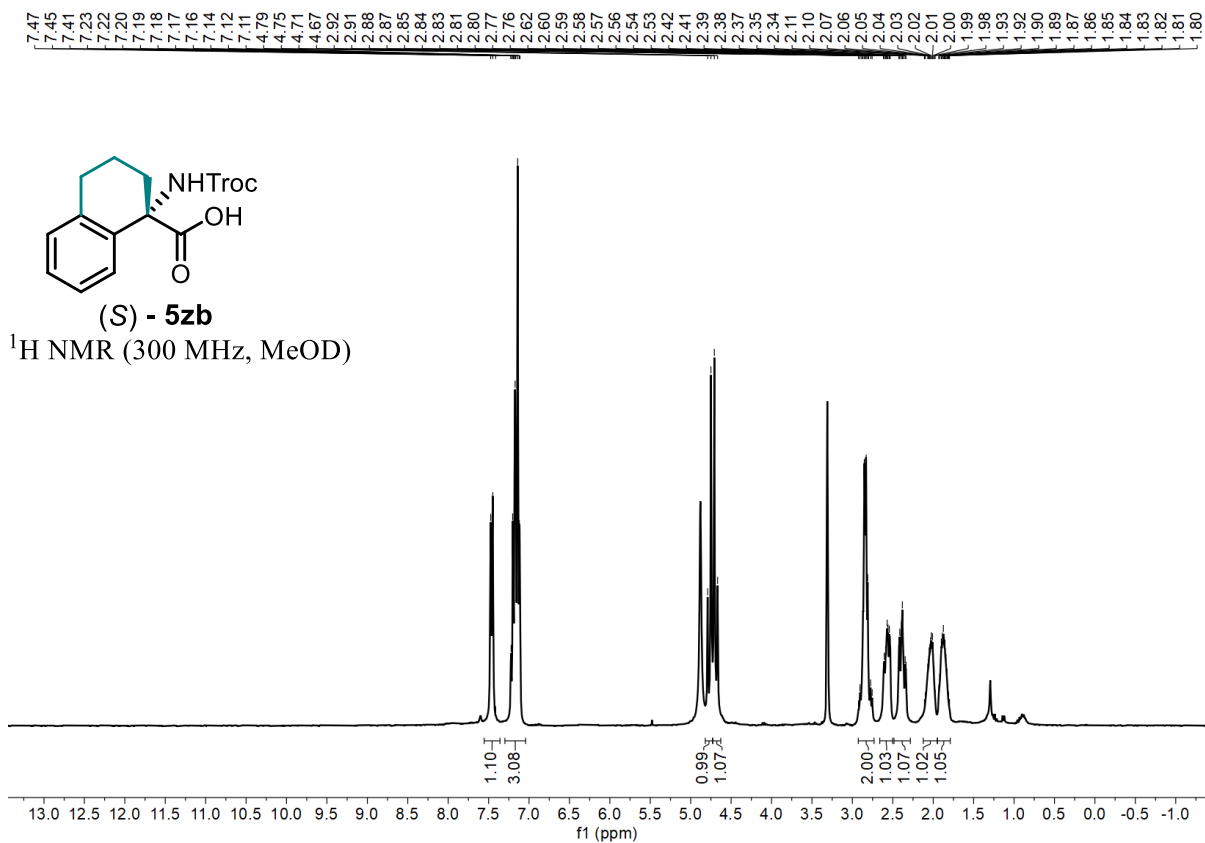


¹H NMR (300 MHz, MeOD)

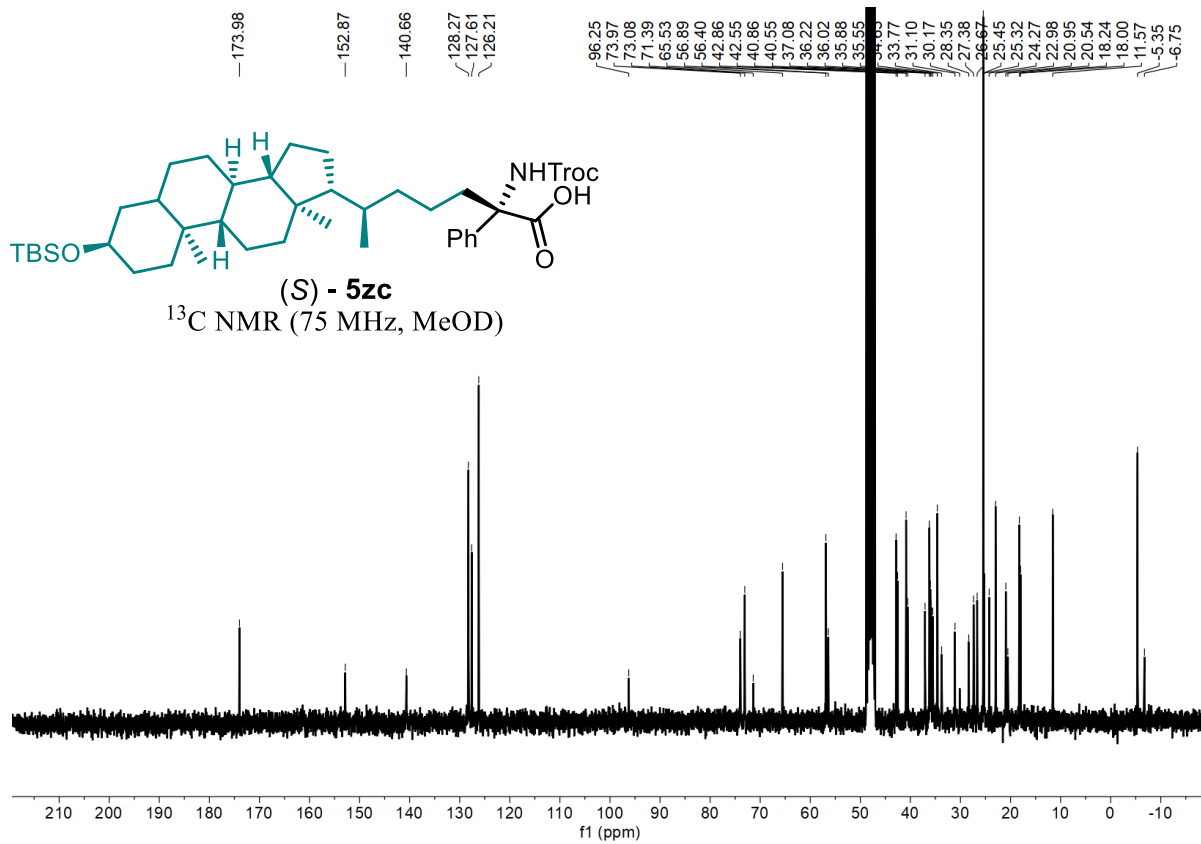
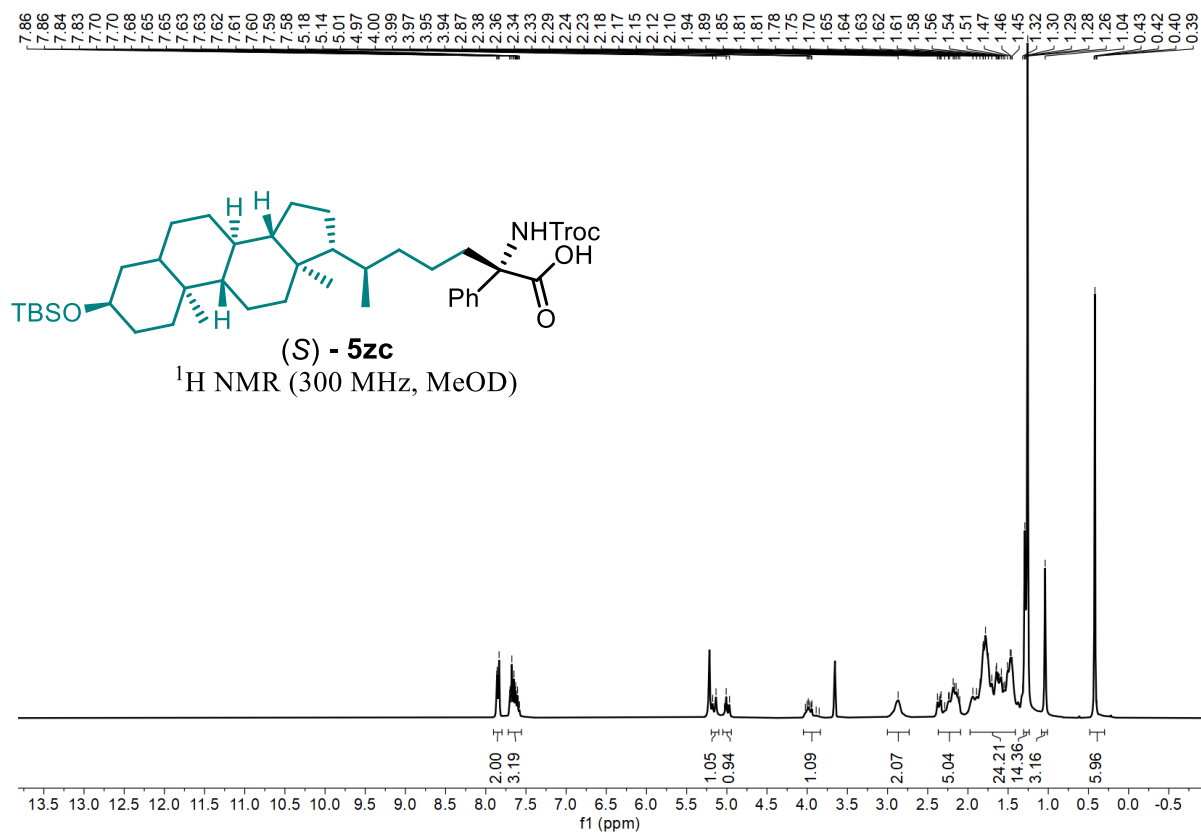


¹³C NMR (75 MHz, MeOD)

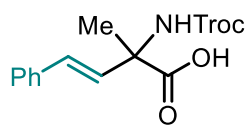
Statement



Statement



Statement

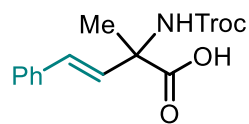
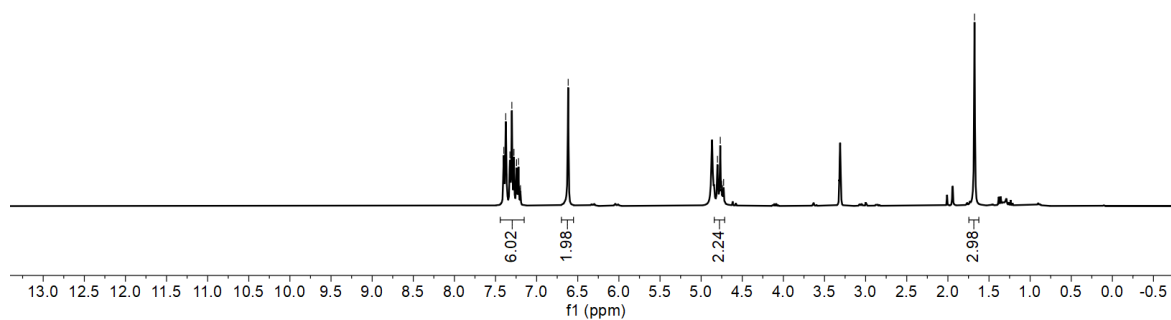


7.40
7.40
7.39
7.38
7.38
7.37
7.36
7.36
7.33
7.32
7.31
7.31
7.30
7.30
7.28
7.28
7.25
7.24
7.24
7.23
7.22
7.21
7.20
7.19
-6.62

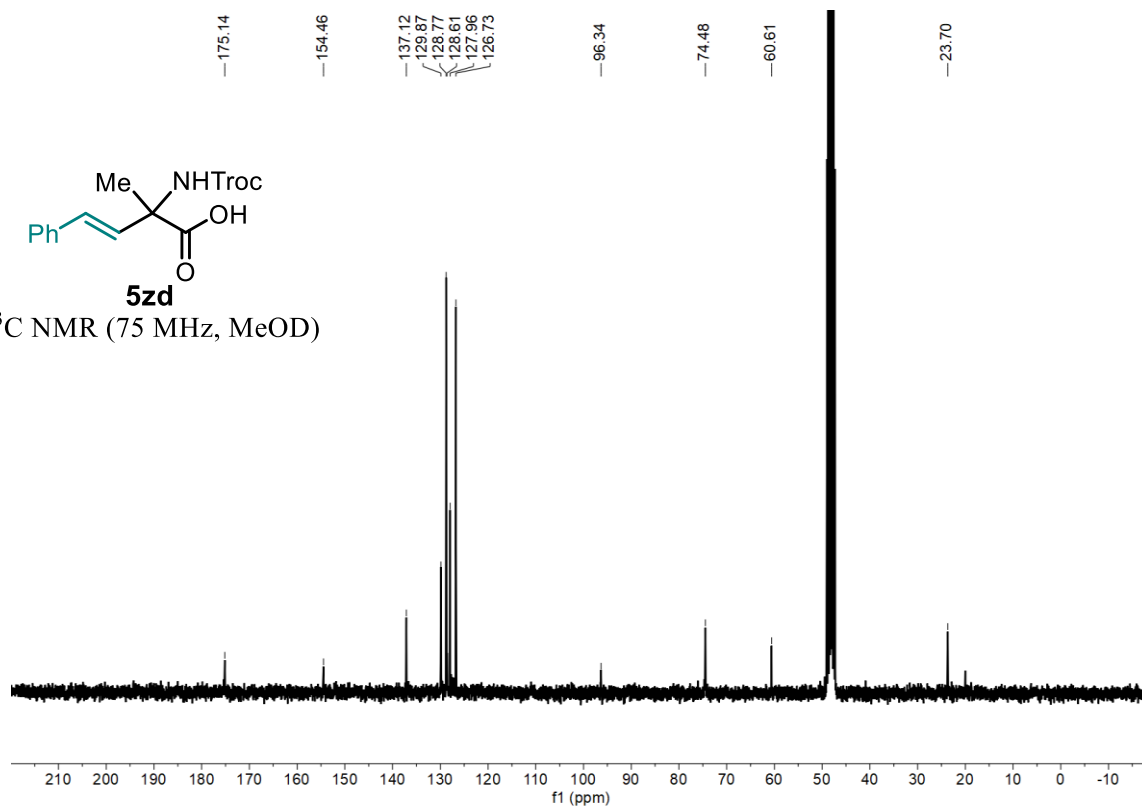
4.80
4.78
4.77
4.75
4.74
4.73

-1.68

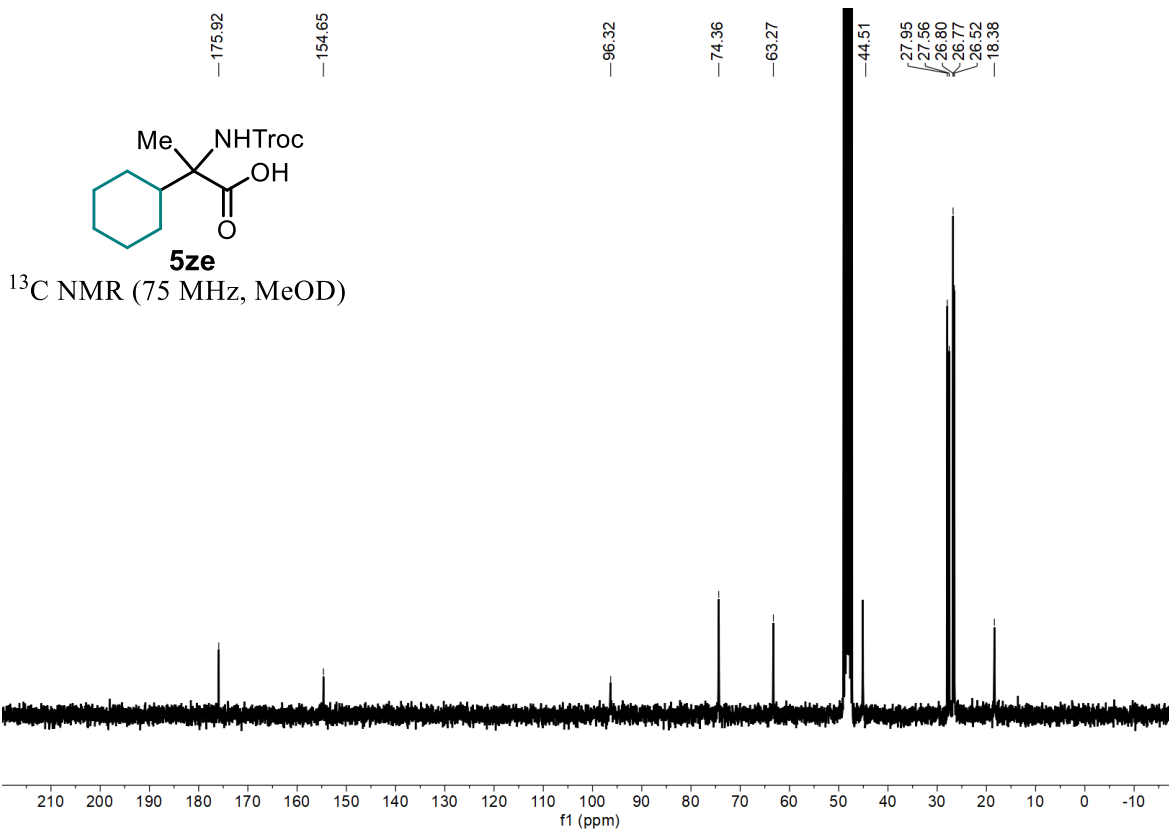
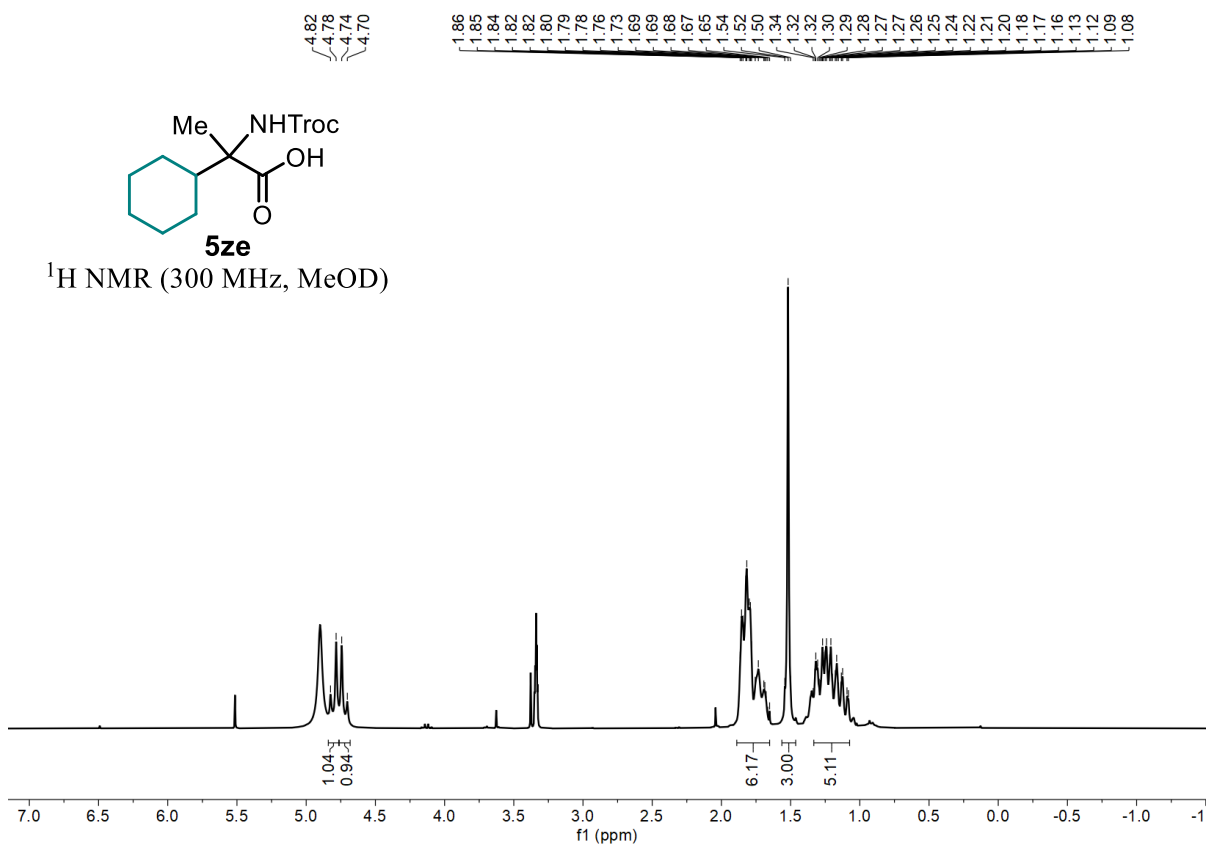
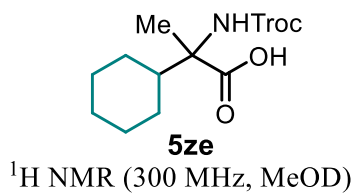
¹H NMR (300 MHz, MeOD)



¹³C NMR (75 MHz, MeOD)



Statement



Statement

gemäß § 10, Abs. 1 der Promotionsordnung der mathematisch-naturwissenschaftlichen Fachbereiche und des Medizinischen Fachbereichs für seine mathematisch-naturwissenschaftlichen Fächer der Philipps-Universität Marburg vom 09. Jul.2009

Ich erkläre, dass eine Promotion noch an keiner anderen Hochschule als der Philipps-Universität Marburg, Fachbereich Chemie, versucht wurde und versichere, dass ich meine vorgelegte Dissertation

Chiral Iron-N4-Complexes for Asymmetric C-H Aminations

selbst und ohne fremde Hilfe verfasst, nicht andere als die in ihr angegebenen Quellen oder Hilfsmittel benutz, alle vollständig oder sinngemäß übernommenen Zitate als solche gekennzeichnet sowie die Dissertation in der vorliegenden oder ähnlichen Form noch bei keiner anderen in- oder ausländischen Hochschule anlässlich eines Promotionsgesuchs oder zu anderen Prüfungszwecken eingereicht habe.

Xiang Shen

Marburg, den 09.Mar.2020

Curriculum Vitae

Xiang Shen

Male, born Dec 21, 1991 in Hubei, P. R. China

Email: xiangshen6@gmail.com

Education

- 09/2018–present *Ph.D.* Organic Chemistry, University of Marburg, Germany
Supervisor: Prof. Dr. Eric Meggers
- 2015/09–2018/07 *M.Sc.* Organic Chemistry, Xiamen University, China
Supervisor: Prof. Dr. Eric Meggers and Prof. Dr. Lei Gong
- 2011/09–2015/07 *B.S.* Applied Chemistry, Hubei Polytechnic University, China
Supervisor: Prof. Dr. Yong Zhang

Research Experiences

Ph.D. study: Chiral Iron-N4-Complexes for Asymmetric C-H Aminations

Publications:

1. **X. Shen**, M. Hemming, Z. Zhou, S. Ivlev, E. Meggers, *to be submitted*.
2. C.-X. Ye*, **X. Shen***, S.-M. Chen, E. Meggers, *Nat. Chem.* **2022** accepted. (*Equal contribution)
3. Z. Zhou, Y. Tan, **X. Shen**, S. Ivlev, E. Meggers, *Sci. China Chem.* **2020**, *64*, 452.
4. G.-H Wang, Z. Zhou, **X. Shen**, S. Ivlev, E. Meggers. *Chem. Commun.* **2020**, *56*, 7714.

M.Sc. study: A Chiral Nickel DBFOX Complex as a Bifunctional Catalyst for Visible-light-Promoted Asymmetric Photoredox Reactions

Publications:

1. **X. Shen**, Y. Li, Z. Wen, S. Cao, X. Hou, L. Gong, *Chem. Sci.* **2018**, *9*, 4562. (Cover paper)
2. W. Xu, **X. Shen**, Q. Ma, L. Gong, E. Meggers, *ACS. Catal.* **2016**, *6*, 7641.
3. Y. Li, K. Zhou, Z. Wen, S. Cao, **X. Shen**, M. Lei, L. Gong, *J. Am. Chem. Soc.* **2018**, *140*, 15850.